Mousa Kareem, Mohanad (2013) *Novel redox active building blocks for the creation of functional macromolecules.* PhD thesis.

https://theses.gla.ac.uk/4453/

Novel redox active building blocks for the creation of functional macromolecules

Mohanad Mousa Kareem

BSc, MSc

Submitted in the Fulfilment of the Requirements for the Degree of Doctor of Philosophy

June 2013

School of Chemistry

University of Glasgow

Abstract

This thesis describes an investigation into a wide range of potential materials for organic photovoltaic (PV) devices. Chapter 1 provides a general introduction relating to donor - acceptor systems and conjugated polymers with photovoltaic applications. Chapter 2 describes the design, synthesis and characterisation of new organic super-acceptors based on an NDI core. An investigation of their optical and redox properties is described. Chapter 3 describes the synthesis of new flavin-functionalised dithienylpyrrole systems. In addition, preliminary polymerisation studies are described, together with a study of their chemical and physical properties. Chapter 4 describes the synthesis and characterisation of new ferrocene and NDI functionalised polymers by ATRP and RAFT techniques. Chapter 5 describes the synthesis of new bis-acceptor systems based on NDI and TCAQ and a brief study their chemical and physical properties. Chapter 6 describes the synthesis of conjugated polymers featuring NDI units. Chapter 7 describes the synthesis and characterisation of novel substituted metal phthalocyanines featuring NDI units. Chapter 8 provides the experimental details and characterisation of all the compounds prepared in this thesis. Finally, chapter 9 provides the appendices and additional information.

Acknowledgements

In the name of Allah, the most gracious and the most merciful, Alhamdulillah, all praises to Allah for the strengths and his blessing in completing this thesis.

I would like to give grateful acknowledgements to the following people and institutions that have enabled me to pursue and complete this work. This thesis would not have been possible unless the Ministry Of Higher Education and Scientific Research/Iraq (MOHESR) and the Babylon University who had provided the necessary funding to carry out my research work.

To my supervisor, Prof. Graeme Cooke, I am profoundly indebted. I express my gratitude to Prof. Graeme Cooke, for all his time, advices, constant encouragement and support concerning my research. In addition I would especially like to express my deep appreciation to him for the kindness, patience and his understanding shown to me when I have gone through difficult times during the four year period.

To all the current and former colleagues in the Cooke group goes my gratitude. Special thanks to Dr. Brian Fitzpatrick for the numerous feedback and suggestions and his help in the DFT modelling work. Also, thanks for Dr. Stuart Caldwell, Dr. Catherine MacLean, Dr. Nada Zainalabdeen and Mrs Helen Smith for all their help. I also wish to thank Dr. Deliang Long for X-ray, Mr. Jim Tweedie and Mr. Harry Jackson for mass spectroscopic analysis, Dr. David Adam for NMR analysis, and Mr. Stuart Mackay for his help. My thanks go to the many research students and staff who I have met at the University of Glasgow.

I would like to express my gratitude to Professor Peter Skabara and his Ph.D Student Dr. Saadeldin Elmasly, Department of Chemistry, University of Strathclyde, for his assistance in the electrochemical polymerisation.

Never could I have done alone without those people around me, my family and friends, who have provided considerable support, especially those in Iraq and UK for their encouragements for me. To those who indirectly contributed in this research, your kindness means a lot to me. Thank you very much.

Mohanad

Dedication

To my parents, sisters and brothers

To my wife and my children (Yazen, Banan, Mustafa, Almuntadhar)

To my homeland Iraq

Declaration:

I hereby declare that the substance of this thesis has not been submitted, nor is currently submitted in candidature for any other degree. I also declare that the work presented in this thesis is the result of my own investigations and where the work of other investigators has been used, this has been fully acknowledged within the text.

Mohanad Mousa Kareem

Contents

Abbreviations

A	Acceptor
Abs	Absorbance
MeCN	Acetonitrile
Ac	Acetyl
a.u	Arbitrary unit
ATRP	Atom transfer radical polymerisation.
Å	Angstrom
BHJ	Bulk heterojunction
bpy (or bipy)	2,2'-Bipyridine
CT	Charge transfer
CI	Chemical ionisation
δ	Chemical shift
cm	Centimetre
CP	Conjugated polymer
CV	Cyclic Voltammetry
°C	Degrees Celsius
DNA	Deoxyribonucleic acid
Dec	Decomposed
DAP	Diamidopyridine
DMAP	4-(Dimethylamido) pyridine
DCM	Dichloromethane
DMF	Dimethylformamide
DMSO	Dimethylsulfoxide
NiCl2(dppp)	Dichloro(1,3bis(diphenylphosphino)propane)nickle
DSSCs	Dye sensitized solar cells
D	Donor
DCC	*N,N'*-Dicyclohexylcarbodiimide
d	Doublet
DLS	Dynamic light scattering
η	Efficiency
EI	Electron ionization
eV	Electron volt
E	Energy
EtOH	Ethanol.
EDCI	1-Ethyl 3-(3-dimethylaminopropyl) carbodiimide
EDG	Electron donating group
EDOT	3,4- Ethylenedioxythiophene
EWG	Electron withdrawing group
Eg	Bandgap energy
Ev	Electron volt
ESR	Electron spin resonance
hv	Electromagnetic radiation
Et	Ethyl

eq	Equivalents
eq	Equation
S*	Excited singlet state
FAD	Flavin adenine dinucleotide
Fc	Ferrocene
FMN	Flavin mononucleotide
FT-IR	Fourier transform infrared
FF	Fill Factor
C_{60}	Fullerene
GPC	Gel Permeation Chromatography
g	Gram
ΔG	Gibbs free energy
$E_{\frac{1}{2}}$	Half wave potential
HH	Head to head
HT	Head to tail
Δ	Heat
HRMS	High resolutions mass spectroscopy
HOMO	Highest occupied molecular orbital.
h	Hour
ITO	Indium tin oxide
IR	Infrared
Lit	Literature
L	Litre
LUMO	Lowest unoccupied molecular orbital.
Me	Methyl
MeOH	Methanol
MMA	Methyl methacrylate
mV	Millivolt
mL	Milliliter
min	Minute
M	Molar(Mol per litre)
NBS	*N*-bromosuccinimide
DCC	*N,N'*-Dicyclohexylcarbodiimide
nm	Nanometer
NPs	Nanoparticles
NDI	1,4,5,8-Naphthalenediimide
NADH	Nicotinamide adenine dinucleotide
NMR	Nuclear magnetic resonance
NLO	Nonlinear optics
NREL	National Renewable Energy Laboratory
Mn	Number average molecular weight
VOC	Open Voltage Current
OPVs	Organic Photovoltaics
Pd(C)	Palladium (on carbon)
ppm	Parts per million

PA	Polyacetylene
PDI	Poly dispersion index
PEC	Photoelectrochemical cell
PCBA	Phenyl-C_{61}-Butyric Acid
PCBM	Phenyl-C61-Butyric Acid Methyl Ester
PEDOT	Poly(3,4-ethylenedioxythiophene)
P3HT	Poly(3-hexylthiophene)
PSS	Poly(styrenesulfonate)
Pcs	Phthalocyanines
h	Planck constant
h^+	Positive hole
PCE	Power conversion efficiency
RAFT	Reversible Addition-Fragmentation chain Transfer
k	Rate constant
RT	Room temperature
s	Singlet
JSC	Short circuit current
SHE	Standard hydrogen electrode
TBAPF$_6$	Tetrabutylammonium hexafluorophosphate
TCB	1,2,4-Trichlorobenzene
TCNE	Tetracyanoethylene
TCNQ	7,7,8,8-Tetracyano-p-quinodiméthane
TCNAQ	Tetracyano-*p*-anthraquinodimethane
OFETs	Thin Film Effective Transistors
TLC	Thin layer chromatography
Et$_3$N	Triethylamine
PCBM	Phenyl-C_{61}-Butyric Acid Methyl Ester
PPV	Poly Phenylene Vinylene
P3HT	Poly(3-phenyl thiophene-2,5-diyl)
UV/Vis	Ultraviolet/Visible light
Vs^{-1}	Volts per second
Ʌ	Wavelength
Mw	Weight average molecular weight
ZnPc	Zinc-Phthalocyanine

1. Chapter 1

General introduction

1.1. Molecular electronics

Molecular electronics (ME) (often referred to as moletronics) is a multidisciplinary field that includes chemistry, physics, materials, micro/nanoelectronics, computer science, biology and medicine. From the chemists' point of view the design and synthesis of new model compounds which have a controllable function is a major aim. Molecular building blocks have been used for the fabrication of passive (current rectifiers, resistive wires) and active (switching, sensing) electronic devices.[1] Molecular electronics is an important field in nanoscience, involving the investigation of the electronic level structure, response and transport. Molecular electronics includes single molecules, molecular arrays and molecular networks attached to other electronic components.[1]

Mulliken *et al.* advanced a study of charge transfer in so-called "donor-acceptor" systems in the 1940s and developed the study of charge transfer and energy transfer in molecules. The first concrete idea for an electronic component was described by Aviram and Ranter[2] in 1974 and developed in 1982 by Carter.[3] They constructed a very simple electronic device based on the use of a single organic molecule **1**. The molecule consists of a donor π-system (tetrathiafulvalene (TTF)) and an acceptor π-system (7,7,8,8-tetracyanoquinodi-methane (TCNQ)), separated by a sigma bonded (methylene) tunnelling bridge. This molecule was shown to have rectifying properties when placed between two electrodes (Figure 1-1). Later, Aviram and Ratner detailed a single-molecule field-effect transistor in 1988.[4]
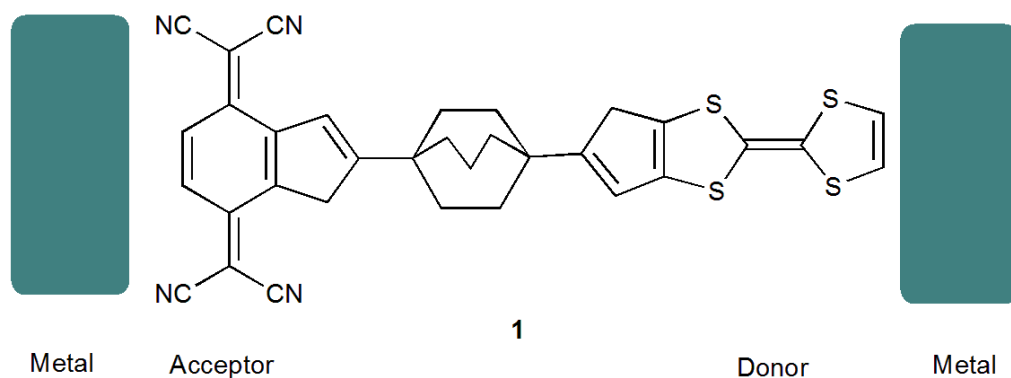
Figure 1-1. Donor-acceptor rectifier system between two metal electrodes.

In the mid-seventies molecular electronics was further developed from the experimental discovery of conducting polymers. Previously, organic molecules were considered

insulating or weakly conducting semiconductors. McGinness *et al.*[5] reported the first molecular electronic device by using melanin for voltage-controlled switch and an oxidized mixed polymer of polyacetylene, polypyrrole, and polyaniline. This switch exhibited extremely high conductivity.

In 1977, Heeger *et al.*[6] discovered the high conductivity of oxidized ("doped") poly-acetylene, producing a passive highly-conductive form of polyacetylene. Subsequently, the conductance of conjugated polymers was improved. These discoveries helped the development of plastic electronics and optoelectronics in extensive commercial application (Figure 1-2).

Nowadays molecular electronics technology is used in major electronics applications, such as sensors, interconnects, transistors, displays, switches, rectifiers, smart materials, di-electrics, nonlinear components, molecular motors, memory devices, and photovoltaics. More recently the importance of molecules in device applications that have ability to bind to one another and assemble into larger structures has been shown.[1]

Electrical conductivity
Conductivity approaching that of copper
Chemical doping induces solubility
Transparent electrodes,antistatics
EMI shielding, conducting fibers

Control of electrochemical potential
Electrochemical batteries
Electrochromism an "smart windows"
Light-emitting electrochemical cells

Chemical

Electrochemical

Doping of Conjugated Polymers

Photochemical

Interfacial

High-performance optical materials
1-d nonlinear potical phenomena
Photoinduced electron transfer
Photovoltaic devices
Tunable NLO properties

Charge injection without counterions
Organic FET circuits
Tunneling injection in LEDs

Figure 1-2. Doping mechanisms of conjugated polymers and their applications.

Molecular electronics is currently a very active research field. Basically all electronic processes in nature occur in molecular structure starting from the photosynthesis to signal transduction. Electronics applications have four major advantages:[7]

1) **Size.** The size scale of molecules is between 1 and 100 nm, which permit functional nanostructures with accompanying advantages in efficiency, cost, and power dissipation.

2) **Self-assembly**. Intermolecular interactions can be exploited to form structures by nanoscale self-assembly. Also, molecular recognition can be used to provide both switching and sensing capabilities on the single-molecule scale.

3) **Stereochemistry.** Many molecules have multiple distinct stable geometric structures or isomers. Such geometric isomers can have distinct optical and electronic properties, for example, retinal molecules switch between two stable structures, a process that transduces light into a chemoelectrical pulse and allows vision.

4) **Synthetic flexibility**. Synthetic tuning permits extensive variation of a molecule's transport, binding, optical, and structural properties.

Molecules have disadvantages such as instability at high temperature and when exposed to oxygen and UV light. However, the aforementioned four advantages render molecules ideal for electronics applications.

1.2. Organic conjugated polymers

Generally, polymers are considered good insulators. However conjugated polymers (CPs) are classified as organic semiconductors (Figure 1-3).[8] Conjugated polymers contain a back bone consisting of alternating single and double bonds between carbon-carbon or carbon-nitrogen atoms. Conjugated polymers have linear or rigid rod structures; however they are twisted along their back bones because they are not completely straight and flat.
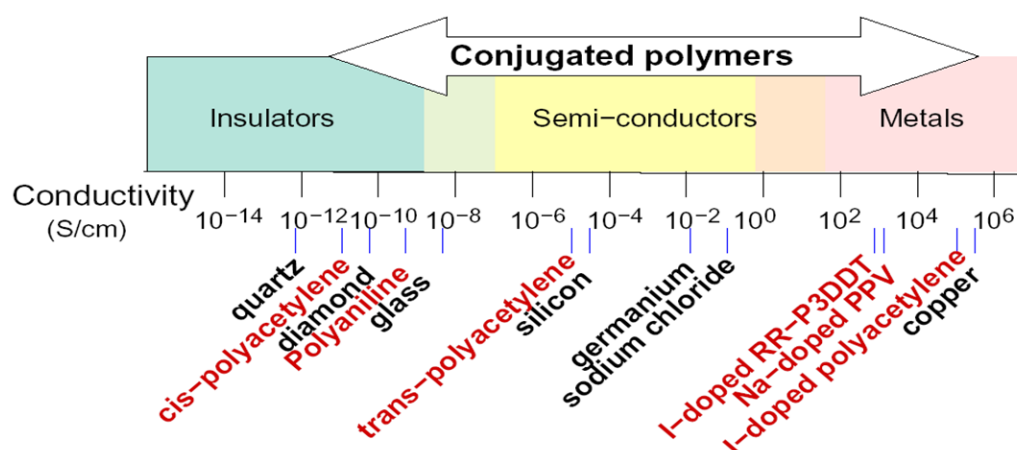
Figure 1-3. Conductivity of conductive polymers compared to those of other materials, from quartz (insulator) to copper (conductor).

Conjugated polymers have been investigated since Shirakawa and co-workers[9] synthesised the very first example of a semiconducting polymer. They discovered that the conductivity of polyacetylene could be increased by a factor of ten million by bromine doping. Also, the

addition of the phenyl ring into the polyacetylene backbone increases the conductivity and changes the absorption and emission spectra. The simplest example of a conjugated polymer is polyacetylene $(CH)_n$, however conjugated polymers exist in a variety of structures as shown in (Figure 1-4).
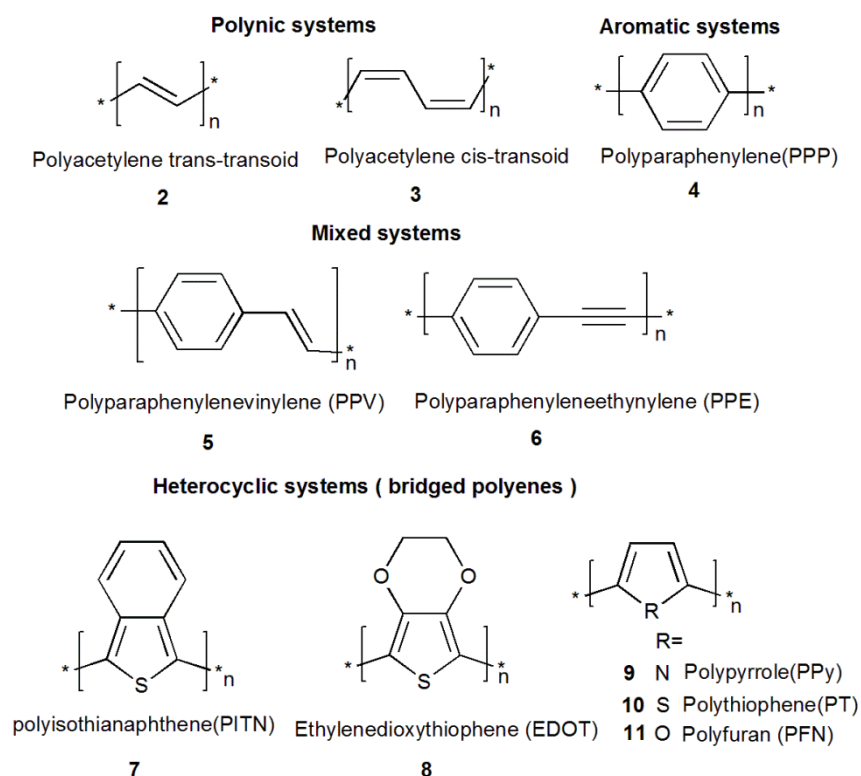
Figure 1-4. Polynic, aromatic, mixed and heterocylclic polymers systems.

Polymer chains consist of sp^2-hybridized carbons and π-electrons. These π-electrons form a delocalized π-system, which gives rise of semi-conducting properties of polymer. The π-electron system along the conjugated polymer backbone make the charged species formed upon doping able to move along the carbon chain (delocalization) allowing electron transport and thus giving an electronically conductive material. As shown in Figure 1-5 the *cis* and *trans*-polyacetylene structures should have the same band gap but don't because the conjugation yields an energy/unit length which is minimized with increasing backbone planarity. Also it has been shown that the rotation breaks the conjugation.[10]
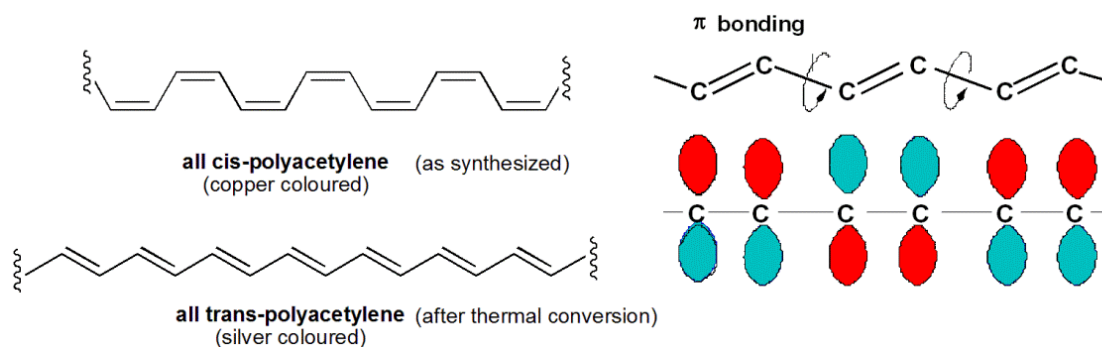
Figure 1-5. *Cis* and *trans* polyacetylene.

Solitons, polarons and bipolarons were proposed in part to understand the conduction mechanism of conjugated polymers. A polaron is a radical cation (or radical anion) that is partially delocalized over some polymer segment as a result of cleavage of a double bond in the polymer backbone by oxidation (or reduction). A bipolaron has two charges associated with the localized polymer segment. Therefore, low oxidation produces polarons, while bipolarons are formed at higher oxidation potentials. Solitons can be classified into three categories: neutral, positive and negative. Neutral solitons have spin with no charge however charged solitons have no spin. Positively charged solitons are obtained by the insertion of acceptor band or removal of an electron from a neutral soliton by oxidation. However, negatively charged solitons are formed when an electron is inserted by reduction. Polarons are formed from the combination of a neutral and a charged solitons on the same polymer chain.[10, 11]
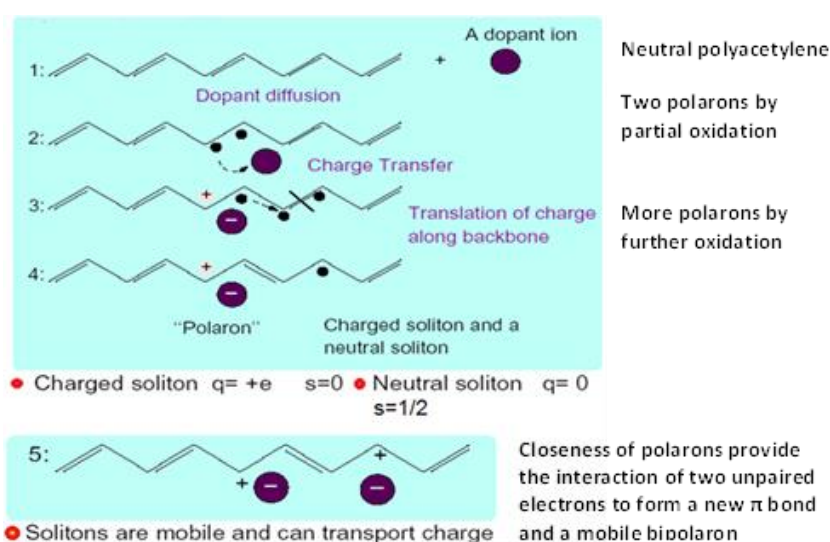
Figure 1-6. Formation of polaron and bipolaron for polyacetylene.

Conjugated polymers (CPs) have undergone significant advances in order to increase their conductivity, make them soluble and alter their optical and electrical properties. Most of

the current research aims to prepare new materials as viable alternatives to silicon. Currently, CPs are very important materials and used widely in industry for the development of devices such as light emitting diodes, sensors, thin film transistors, photodiodes, nonlinear optical systems, plastic lasers, and photovoltaic cells. Figure 1-7 shows some applications of CPs.[12]
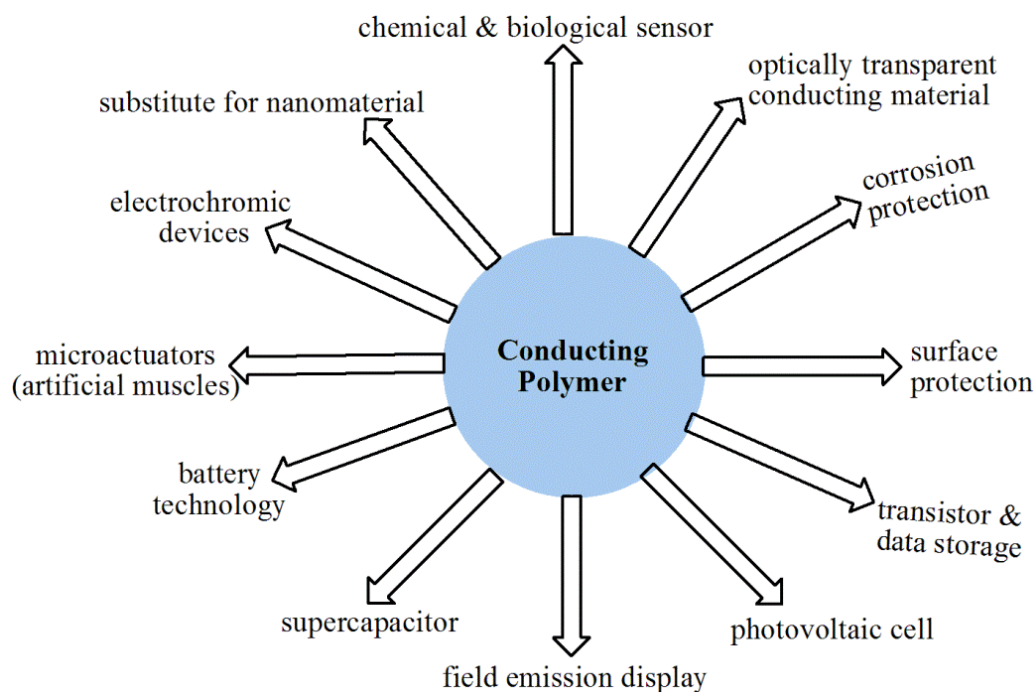
Figure 1-7. Applications of conducting polymers

There are many benefits that characterize polymer based electronics over conventional inorganic semiconducting materials:[13]

1) Lower material cost due to low temperature deposition and processing. Furthermore, simpler fabrication steps and less stringent purity requirements.

2) Flexibility: Organic polymers can be designed to be flexible whereas inorganics are not.

3) Lightweight and large area: Organic polymers are more lightweight than inorganics and it could have extremely large areas with little structural support needed.

4) Semiconducting organic materials are able to absorb light in the ultraviolet-visible part of the solar spectrum and transport electric current.

1.3. Photovoltaics (PV)

In the modern world there are many sources of energy; these include oil, coal, gas and other such forms of non-renewable energy which are depleting rapidly and hence there is a need to develop renewable sources of energy like that form the sun, wind, and biomass etc.

Due to the growing environmental issues and the need for alternative non-polluting energy and consequently, research in the manufacture of solar cells has increased during recent years. Solar power is predicted to become a strong viable alternative to fossil fuel energy, however, the fabrication cost of conventional photovoltaic devices is still too high. Photovoltaic energy conversion is a process where incoming solar radiation is directly converted into electricity without emission of any hazardous by products. The potential of using sunlight is vast and essentially unlimited.[14] Table 1-1 lists some of advantages and disadvantages of photovoltaics.[15]

Table 1-1. Advantages and disadvantages of photovoltaics

Advantages of photovoltaics	Disadvantages of photovoltaics
- Fuel source is vast and essentially infinite. - No emissions, no combustion or radioactive fuel for disposal. - Low operating cost (no wear) - No moving part (no wear) - No high temperature corrosion or safety issues. - High reliability in modules (>20 years) - Modular (small or large increments) - Quick installation - Can be integrated into new or exciting building structures. - Can be installed at nearly any point-of-use. - Daily output peak match local demand. - Excellent safety record.	- High, no competitive costs of generated energy. - Fuel source is diffuse (sun light is relatively low density energy) - Poorer reliability of auxiliary elements including storage. - Lack of widespread commercially available system integration and installation so far. - Lack of economical efficient energy storage.

1.3.1. Historical aspects

In 1839, Becquerel[16] reported a photocurrent when a silver coated platinum electrode was illuminated in aqueous solution; this was seen as the discovery of the photovoltaic effect. Then, in 1873 and 1876, respectively, Smith[17] and Adams[18] reported the first experiments with selenium. At this time the first solid state photovoltaic devices were constructed from a rectifying junction formed between a semiconductor and a metal.

Photoconductivity was discovered in anthracene by Pochettino[19] and Volmer[20] in 1906 and 1913 respectively. Between 1950s and 1960s the possibility of using organic materials as photoreceptors in imaging systems was recognized. In the early 1960s, the semiconducting properties of methylene blue and many common dyes were discovered which later considered among the first organic materials to exhibit the photovoltaic effect.[21]

In 1954, the first fabricated inorganic solar cell at Bell Laboratories was reported by using a crystalline silicon solar cell with p-type (hole conducting) and n-type (electron conducting) junctions, which converted sunlight into electric current with an efficiency of 6%, which was six times higher than the best previous attempt. Now, the efficiency of crystalline silicon cells has reached more than 38% in a laboratory setting.[22]

A photovoltaic effect was created by using a cell based on magnesium phthalocyanine (MgPc) which had a photovoltage of 200 mV was reported in 1958. Also, Ghosh *et al.*[23] investigated an Al/MgPc/Ag cell, and obtained photovoltaic efficiency of 0.01%. Thereafter, PV cells made of from cadmium sulphide, gallium arsenide, cadmium telluride, and indium phosphide appeared.[24] In the 1970s, amorphous silicon or microcrystalline silicon was used to reduce the production costs of thin film technologies. The current PV technologies and the efficiencies reached are presented in Table 1-2. [24, 25]

Table 1-2. Current photovoltaic technologies and their efficiencies[24, 25]

Technology	Photovoltaic device	Conversion efficiencies and notes
Monocrystalline solar cells	Silicon solar cells	24.7% Laboratory efficiency; 20.1% commercial module efficiency.
	Galium arsenide(GaAs)	25.1% Laboratory efficiency.
Thin-film technologies	Thin-film silicon (TFSi)	9.5% (a-Si); 12% (tandem a-Si/^{l}c-Si); 13% (triple junction using SiGe alloys). All these are laboratory efficiencies.
	Cu(In, Ga)(S, Se)$_2$ and related I-III-VI compounds (CIGS)	19.9% Laboratory efficiency;13.4%commercial module efficiency.
	Cadmium telluride (CdTe)	16.5% Laboratory efficiency; 10.7% commercial module efficiency.
	GaAs	24.5%
Organic-based solar cells	Bulk-heterojunction solar cells	6.5% Laboratory efficiency
	Dye-Sensitized cells (Graetzel cell)	10.4% Laboratory efficiency
Novel PV technologies :Novel active layers	Quantum wells, Quantum wires, Quantum dots, Nanoparticle inclusion in host semiconductor	Theoretical efficiency limits are 50-60%.
Novel PV technologies: Boosting the structure at the periphery of the device	Up-down converters	>10% Efficiency improvement relative to baseline should be demonstrated in the coming decade.
	Exploitation of plasmonic effects	> 10% Efficiency improvement relative to baseline should be demonstrated in the coming decade
Concentrator photovoltaic technologies (CPV)	Si concentrator cells, III-V multi-junction cells	Laboratory efficiencies: 26.8%, 96 suns (Si cells); 40.7%, 240 suns (III-V cells)

1.3.2. Photovoltaic Device Operation

There are several processes that solar cells require for operation. These are light absorption (A), exciton formation (B), exciton transport leading to charge separation (C) and finally charge transport to the electrodes (D) as shown in Figure 1-8. Briefly, light is absorbed through a transparent electrode (anode, ITO) and then a photoexcited state is created consisting of the electron and the 'hole' it left behind which is called an exciton. The exciton then diffuses through the active layer until the charges separate or recombines. Finally, the separated charges then drift to the relevant electrodes, creating a flow of charge.[26]
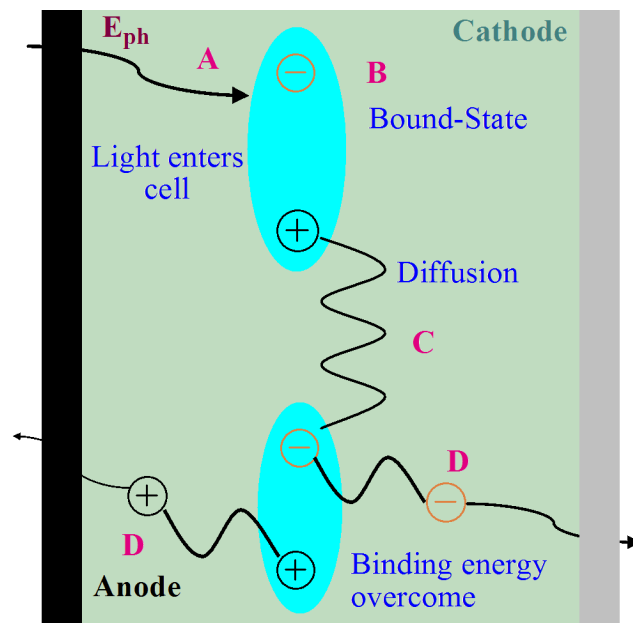
Figure 1-8. Schematic showing the stepwise operation of a solar cell.

A photon excites an electron from the valence band to the conduction band. Electrons and holes are separated before they can relax by a built-in asymmetry to produce an external current through the load, resulting in electrical power generation. The power output of the solar cell is the product of the flow of photo-excited carriers which is the current, and the driving force for the flow is directly related to the potential difference.

1.3.3. Device characteristics

Figure 1-9 shows the typical current-voltage characteristics of a solar cell. The maximum power point (**MPP**) of a solar cell is characterized by its open circuit voltage (V_{oc}), short circuit current density (J_{sc}) and the fill factor (**FF**) according to:[27]

$$MPP = V_{oc} \times J_{sc} \times FF \qquad \ldots\ldots\ldots\ldots(1\text{-}1)$$

$$FF = \frac{V_{max} \times J_{max}}{V_{max} \times J_{max}} \qquad \ldots\ldots\ldots\ldots\ldots(1\text{-}2)$$

Where V_{max} and J_{max} are the voltage and current at the maximum power point.

The efficiency of a solar cell is the ratio of the electrical power it delivers to the load, to the optical power incident on the cell, the estimated efficiency (η_{est}) can be calculated by:

$$\eta_{est} = \frac{MPP}{P_{in}} \qquad \ldots\ldots\ldots\ldots..(1\text{-}3)$$

Where P_{in} is the incident light power density
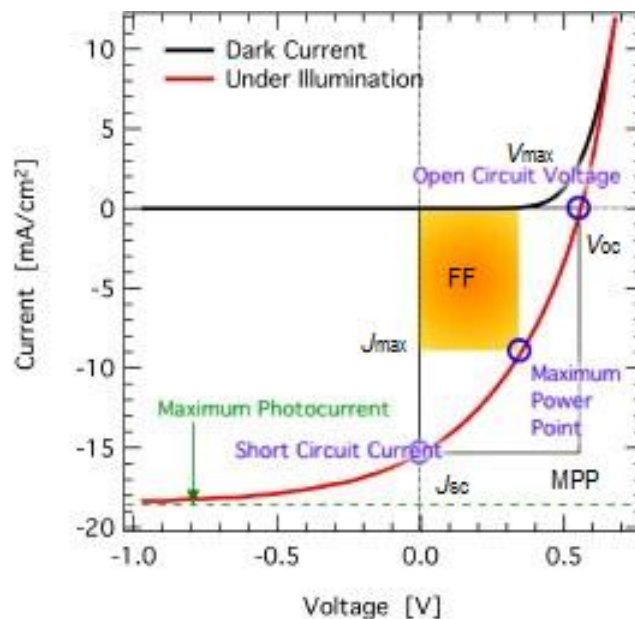
Figure 1-9. Typical Current-Voltage plot of a solar cell.[27]

1.3.4. Organic solar cells

Organic solar cells are a less expensive alternative to inorganic solar cells. Organic photovoltaics can be classified into three categories: small molecule, dye-sensitized and polymer based solar cells. The discovery of polyacetylene led to the development of electronic applications like field-effect transistors (FETs), light-emitting diodes (LEDs), and photovoltaics (PV). Organic materials can possess all the essential electronic features like light absorption and emission, charge generation and transport. The absorption of a quantum of energy in the form of light of an appropriate wavelength ($\Delta E = E_{LUMO} - E_{HOMO}$), results in an electron in the HOMO being promoted into the LUMO. The material with highest LUMO level is called donor and the semiconductor with the highest electron affinity the acceptor. After excitation, the electron is transferred from the donor to the acceptor and electron transfer from the HOMO level of the donor to the HOMO level of the excited acceptor takes place. The separation between HOMO and LUMO is considered the band gap of organic electronic materials and the band gap is usually in the range of 1- 4 eV (Figure 1-10).[28]
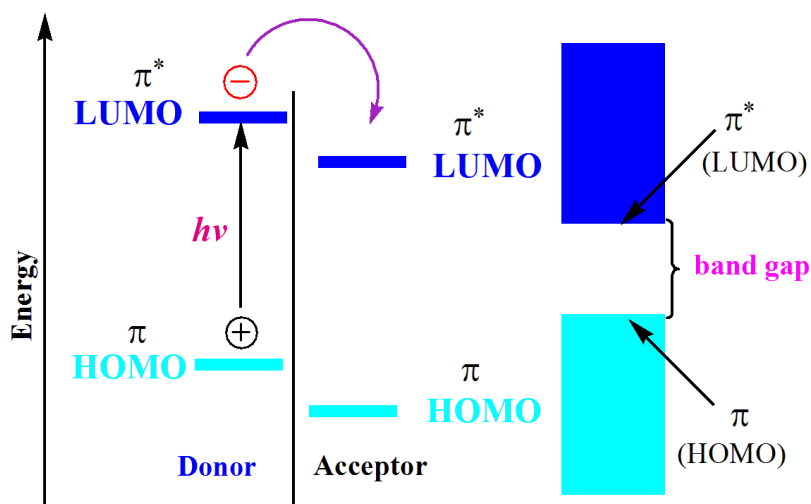
Figure 1-10. Schematic energy diagram of two semiconductors with different LUMO levels.

The energy required to promote an electron from the HOMO-LUMO is defined by Equation 1-4.

$$\Delta E = E_{LUMO} - E_{HOMO} = h\nu = h\ (c/\lambda) \ \text{.......(1-4)}$$

Where (E) corresponds to the energy of the photon, (h) is Planck's constant, and v refers to the frequency. The frequency of light (v) is equal to the speed of light (c) divided by the particular wavelength of light (λ).

Figure 1-11 shows a Jablonski diagram which can be used to explain at the molecular level and what occurs upon the absorption of light. The absorption of light promotes a ground state molecule (S_0) into the first excited singlet state (S_1). Singlet excited states (higher energy) are also available, depending on the excitation energy, and are noted as S_n ($n = 2$, 3…). The triplet state (T_1) is a different excited state, occurs when the two unpaired electrons have the same spin quantum numbers. The S_1 state can relax to the S_0 state in multiple ways: vibrational relaxation, internal conversion and a radiationless process known as intersystem crossing. The excited state can also relax to the S_0 state with the emission of a photon by a process known as fluorescence, with rate constants in the range 10^9-10^{12} s^{-1}. The triplet state T_1 can be excited and then relax to S_0 either with the emission of a photon by phosphorescence process, or by intersystem crossing, both occur with rate constants ~10^2 s^{-1}. Fluorescence and phosphorescence are collectively known as luminescence.[28, 29]
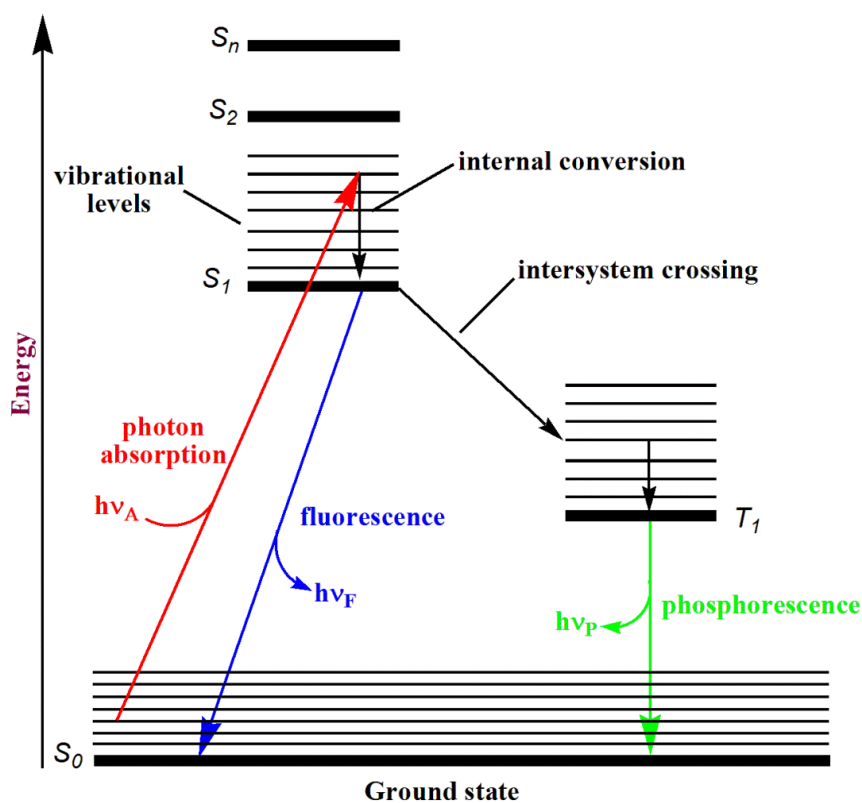
Figure 1-11. Simplified Jablonski diagram

1.3.5. Device architectures of organic photovoltaic cell

There are three main device architectures of organic photovoltaic cells:

1.3.5.1. Single layer organic photovoltaic cell

These types of organic photovoltaic cells are the simplest form among various organic photovoltaic cells. They are made by a layer of organic electronic materials between two metallic conductors (sandwich); generally a layer of indium tin oxide (ITO) with high work function and a layer of low work function metal such as Al, Mg and Ca, as shown in Figure 1-12.[29]
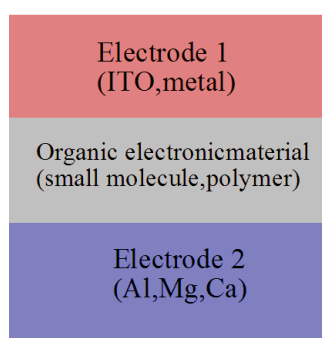
Figure 1-12. A representative basic structure of a single layer organic photovoltaic cell.

Conjugated polymers were used in this type of photovoltaic cell. Polyacetylene as organic layer and Al and graphite as electrodes were used to fabricate a cell by Weinberger and co-workers.[30] The fabricated cell had an open circuit voltage of 0.3 V and quantum efficiency of 0.3%. Another cell constructed from Al/poly (3-ethyl-thiophene)/Pt was reported by Glenis and co-workers.[31] This cell had an external quantum yield of 0.17%, and an open circuit voltage of 0.4 V. Single layer organic photovoltaic cells have low power conversion efficiencies (~0.1%), to resolve this problem, the multilayer organic photovoltaic cells were developed.

1.3.5.2. Bilayer (donor/acceptor) organic photovoltaic cell

This type of organic photovoltaic cell contains two different layers of materials (having differences in electron affinity and ionization energy) in between the conductive electrodes (Figure 1-13). The electron acceptor layer has a higher electron affinity and ionization potential and the other layer is the electron donor, so the local electric fields are strong.
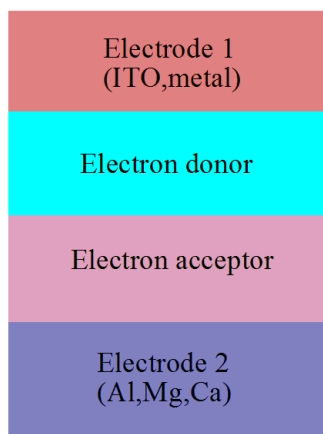
Figure 1-13. A representative basic structure of a double layer organic photovoltaic cell.

C_{60} was used in this type of photovoltaic cells, as it has high electron affinity. Sariciftci and co-workers[32] fabricated a C_{60}/MEH-PPV double layer cell with a power conversion efficiency of 0.04%. The double layer cell of PPV/C_{60} reported by Halls and co-workers[33] had a power conversion efficiency of 1%. The diffusion length of excitons in organic electronic materials is 10 nm. Typically a polymer layer needs a thickness of at least 100 nm to absorb enough light. Therefore, only a small fraction of the excitons can reach the heterojunction interface. To deal with this problem, a new type of heterojunction photovoltaic cells has been developed.

1.3.5.3. Bulk heterojunction organic photovoltaic cell (BHJ)
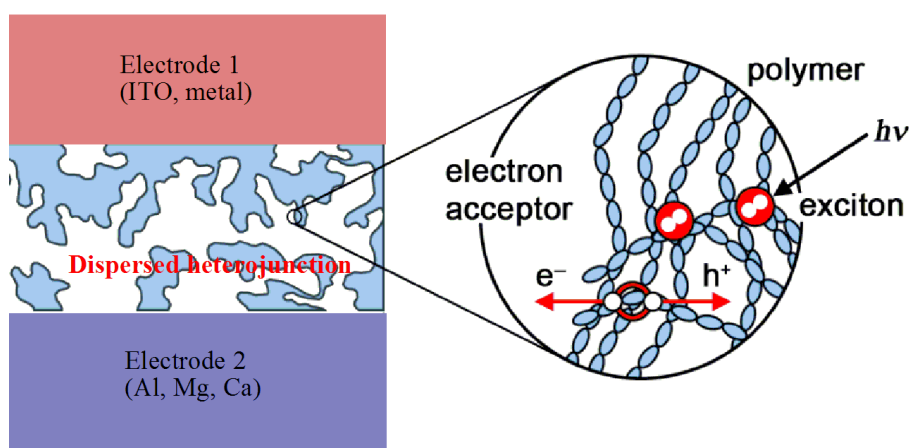
Figure 1-14. A representative blend dispersed heterojunction organic photovoltaic cell.

In dispersed heterojunction photovoltaic cells, the electron donor and acceptor are mixed together, forming a polymer blend (Figure 1-14). The mechanism involves the electrons moving to the acceptor domains where they are carried through the device and collected by one electrode. The holes are pulled in the opposite direction and collected at the other side.

C_{60} **20** and its derivatives are used as electron acceptor in these cells. Yu and co-workers[34] have fabricated a cell from the blend of poly[2-methoxy,5-(2'-ethyl-hexyloxy)-*p*-phenylene vinylene] (MEH-PPV) or poly[2-methoxy,5-(3',7'-dimethyloctyloxy)-*p*-phenylene vinylene] (MDMO-PPV) (as donor) and C_{60} derivative (as acceptor). This cell showed a power conversion efficiency of 2.9%.

Heeger and co-workers[35] reported a device that experienced photo-induced electron and hole mobility between a polymer donor and fullerene acceptor. The efficiency has been greatly improved since Heeger's first device was fabricated. The reported efficiency was increased in 2005 to 5% for devices using P3HT **13** and PCBM **19** in BHJ solar cells. The morphology of the BHJ can influence the device's efficiency and many parameters can direct the morphology of the active layer such as donor acceptor composition, spin cast solvent, chemical structure, solution concentration, controlled phase separation and induced crystallization.

Recently, Liang and co-workers reported efficiencies of 7.4% for solar cells made from PTB7 and phenyl-C_{71}-butyric acid methyl ester.[36] The highest documented efficiencies were set by Solarmer at 7.9% (National Renewable Energy Laboratory NREL 0.1 cm^2), Heliatec and Iapp at 7.7% (Fraunhofer Institute for Solar Energy Systems in Freiburg (1.1 cm^2)) with the current world record by Konarka in 2010 at 8.3% (NREL 1.0 cm^2).

1.3.6. Donor/ Acceptor for PV

There are essential requirements for a material to be useful for organic photovoltaic applications such as high broadband light absorption, efficient charge transport, solubility and low fluorescence. Therefore, researchers have attempted to incorporate functionalisation into the organic molecules to remedy insolubility in organic solvents (Figure 1-15). The solubility in the same organic solvent is essential to intimately blend the acceptor and donor together. The compatibility between the acceptor and donor materials is important for efficient phase separation and can increase the device efficiency. The donor and acceptor must be chemically inert from one another and the polymeric components should create a crystalline lattice for diffraction and device purposes.[29]

Organic solar cells can be classified depending on the type of donor-acceptor materials employed and include polymer-polymer, polymer-fullerene, and hybrid solar cells. The

polymers in OPVs are generally conjugated and possess delocalized electrons that can absorb photons. Polymers serve as the acceptor and donor material; however, fullerenes are used exclusively as highly effective electron acceptors. The incorporation of metal oxide nanoparticles into the organic active materials has resulted in hybrid solar cells.[37]
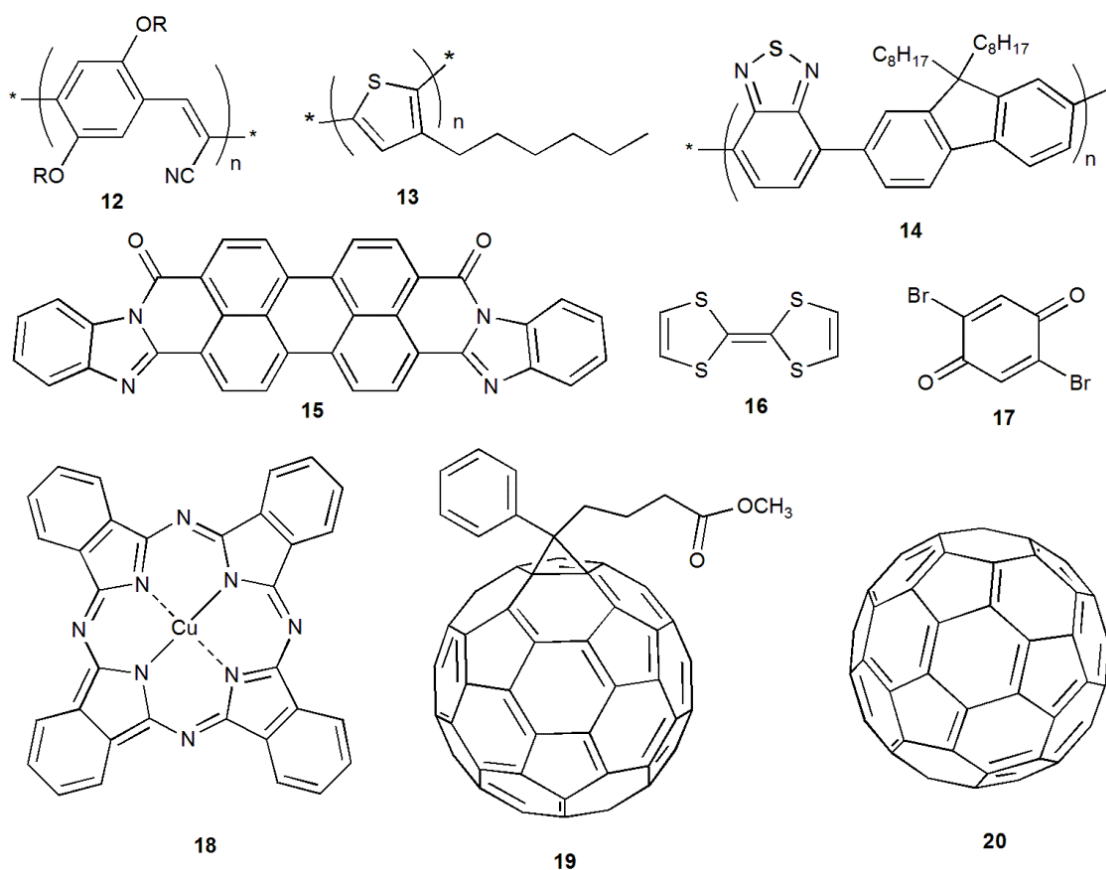
Figure 1-15. Some of organic materials used in BHJ solar cells.

1.3.6.1. Donors for PV

1.3.6.1.1. Polythiophene

Thiophene and its derivatives are far more reactive than their phenyl equivalents. It has relatively acidic protons, when compared with benzene. The α-protons are the most acidic ones and the most reactive positions on the thiophene molecule. Therefore the most transformations take place exclusively on the α-carbon. Thiophene is usually polymerised through the 2-C and 5-C positions and every time a monomer is incorporated in the growing polymer chain it can add with the head (2-position) or the tail (5-position) first. The band gap energy for thiophene polymers can be decreased by increasing the quinoid

character of the π-electron conjugated backbone or adding an electron donating group in the thiophene ring.[38]

Poly (thiophene) itself is rather insoluble and difficult to process, but by incorporating soluble side groups such as alkyl tails along the backbone the polymer can be dissolved and processed from organic solvents. Thiophene polymers have been extensively studied and used as electrodes because of their good conductivity. Conjugated polythiophenes have a wide range of applications in electronics, batteries, nonlinear optical and photovoltaics devices. Poly (3-hexylthiophene-2,5-diyl) (P3HT) **13** is one of the most studied conjugated polymers. It exhibits exceptionally long conjugation lengths and high electrical conductivity and mobility. Specific to OPVs, P3HT acts as the electron donor and possesses a band gap (1.9 eV). It is compatible with the electron acceptor phenyl-C_{61}-butyric acid methyl ester (PCBM) **19**.[39]

Worfolk and co-workers[40] reported the optoelectronic and photophysical properties of four regioregular poly[3-(carboxyalkyl)thiophene-2,5-diyl] (P3CAT) with different carboxy-alkyl chain lengths. P3CAT is combined with [6,6]-phenyl-C_{61}-butyric acid methyl ester to form the photoactive bulk heterojunction layer for organic photovoltaic devices. OPV devices were fabricated and the highest power conversion efficiency of 2.6% obtained. Also, poly(3,4-ethylenedioxythiophene) (PEDOT) is very attractive for many applications including hole injection layers in anti-static coating, OLED, and solar cells due to their high conductivity, low oxidation potential, and moderate band gap. Many conjugated copolymers have been synthesised and tested as donor material in bulk heterojunction organic solar cells. These polymers consist of electron rich and electron poor units such as thiophenes, fluorenes, carbazoles or benzothiazoles **14**. The optical and electronical properties of the resulting polymer can be controlled by combining these building blocks.

1.3.6.1.2. Tetrathiafulvalene

Tetrathiafulvalene (TTF) is an organosulfur compound and has been extensively investigated as strong electron-donating unit in charge-transfer complexes. TTF may be oxidized in two steps to the radical cation **16-a** and dication **16-b** sequentially and reversibly at low potentials (Figure 1-16). Although the neutral TTF unit is a planar 14π-electron system, it is nonaromatic according to the Hückel definition because the 14π-electrons lack cyclic conjugation. In contrast to the neutral TTF unit, both cations are

aromatic in the Hückel sense as a result of the 6π- electron heteroaromaticity of the 1,3-dithiolium cation. This makes TTF a suitable candidate as an alternative redox mediator for dye-sensitized nanocrystalline (DSC) solar cells. In addition, TTF has key properties which make it an interesting building block into a number of molecular and supramolecular systems, such as cyclophanes, macrocycles, cage molecules, rotaxanes catenanes, dendrimers, and polymers.[41, 42]
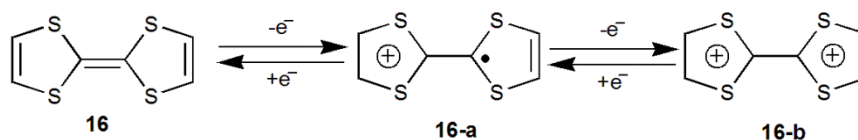
Figure 1-16 Sequential and reversible oxidation of TTF **16** affords stable cationic species **16-a** and **16-b**.

The oxidation potentials can be tuned by attachment of electron-donating or electron-withdrawing substituents. The TTF radical cations are thermodynamically stable species, and the UV-vis absorption spectra of the neutral TTF unit and both cations are distinctly different from one another. Also, TTF derivatives can form dimers, highly ordered stacks or two-dimensional sheets, which are stabilized by intermolecular π-π interactions and non-bonded sulfur-sulfur interactions. The influence from 6π-electron heteroaromaticity in the 1,3-dithiolium cations explains the relatively low oxidation potentials for the parent TTF.[41]

The TTF molecule has been modified by different strategies, which has led to a wide range of functionalized TTF derivatives. The aim is to control the energies of the HOMO-LUMO gap. Two different synthetic approaches have been used to achieve this modification, extending π-conjugation in the molecule, and construction of molecular Donor-spacer-Acceptor systems. Many TTF-spacer-Acceptor systems exhibit lower HOMO-LUMO gaps due to their functionalization with electron-donating groups (EDG) and electron-withdrawing groups (EWG). A variety of π-conjugated oligomers, polymers and TTF-spacer-A systems have been synthesised, and their electrochemical properties for potential applications in materials chemistry have been explored. A wide range of functionalized TTF moieties covalently linked to a π-acceptor moiety through σ or π-bonded bridges possess intramolecular charge-transfer (ICT) properties. Electron acceptors include TCNQ, electron-deficient aryl, quinone, phthalocyanine, pyridinium, bipyridinium, fullerene, ester, thiocarbonyl, conjugated carbonyl, and related acceptor groups. They can be divided into

several groups according to their structural characteristics: nonconjugated TTF-σ-A systems; conjugated TTF-π-A systems; and π-extended TTFs.[43, 44]

Roncali and co-workers reported the electropolymerisation of TTF-derivatized thiophene monomers (Figure 1-17).[45] Polythiophenes **21** and **22** displayed interesting electrochemical properties with a much lower electro-polymerisation potential than their precursors.
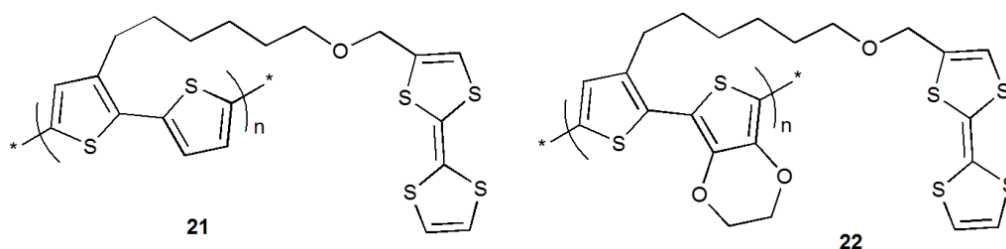
Figure 1-17. Structures of compounds **21** and **22**.

Wenger and co-workers[42] have successfully demonstrated photovoltaic energy conversion with a new class of stable tetrathiafulvalene derivatives-sensitized solar cells. These compounds show an up to 300 mV more negative oxidation potential, in comparison with standard ruthenium-complex sensitizers. They observed highly efficient regeneration of the photo-oxidized tetrathiafulvalene sensitizers, which were attached to a mesoporous TiO_2 film, by a redox mediator in the pores (iodide/tri-iodide). The measured driving force for regeneration was only ~150 mV.
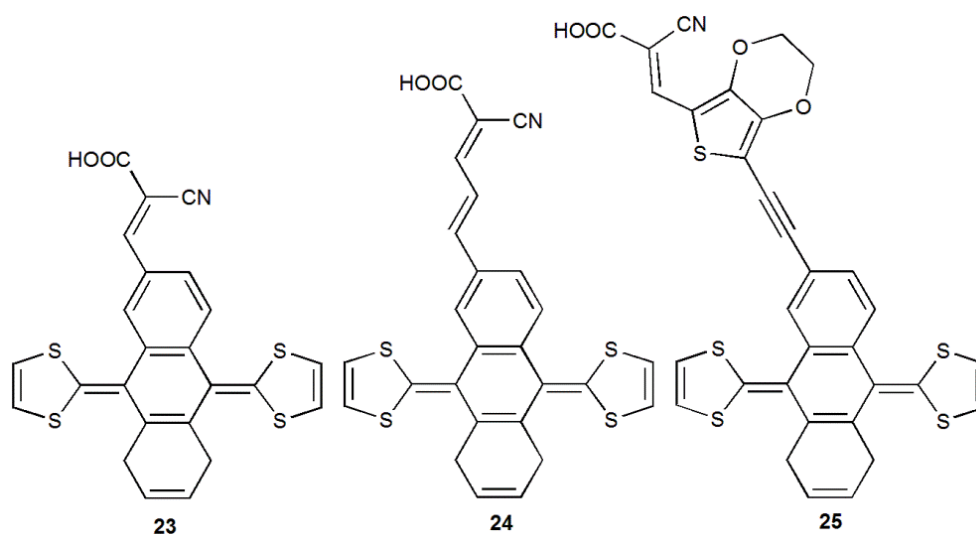
Figure 1-18. Molecular structures of functionalized TTF sensitizers **23**, **24**, and **25**.

1.3.6.2. Acceptors for PV

1.3.6.2.1. Fullerenes (C$_{60}$ PCBM)

Fullerenes are carbon allotropes like diamond and graphite. However unlike these other forms, fullerenes are the only soluble allotrope of carbon. Fullerenes are spherically shaped and consist of hexagonal and pentagonal rings, each fullerene contains $2(10 + M)$ carbon atoms corresponding to exactly 12 pentagons and M hexagons. The smallest stable structure made entirely of carbon atoms is C$_{60}$ **20**, called Buckminsterfullerene. The whole class of fullerenes which proceeds with the higher fullerenes are C$_{70}$, C$_{74}$, C$_{76}$, C$_{78}$, C$_{80}$, C$_{82}$, C$_{84}$ and so on. Fullerenes, especially C$_{60}$ **20**, are known for their unique chemical and physical properties. They are strong electron acceptors and capable of accepting up to 6 electrons. Fullerenes are excellent electron conductors due to their low reorganization energy. Furthermore, their solubility in organic solvents and easy functionalisation makes fullerenes interesting for applications in photovoltaics and non-linear optics, xerography or holographic imaging.[46]

C$_{60}$ **20** is an excellent electron acceptor and hence lends itself to being used in polymer blends. It is not readily soluble in many of the solvents used for conjugated polymers. However, the development of soluble C$_{60}$ derivatives such as [6,6]-Phenyl C$_{61}$ butyric acid methyl ester (PCBM) **19** has allowed bulk heterojunctions to be designed. Over the past years many different polymers were synthesised, developed and used as donor materials in organic solar cells, but PCBM **19** as acceptor material is still extensively used. Many attempts were made to replace PCBM **19** by other fullerene derivatives, however, these have generally proved to be less successful. PCBM **19** shows similar crystal-packing as C$_{60}$ **20**, which results in a higher electron mobility, compared to other fullerene derivatives. It still remains the n-type material of choice in organic solar cells. However, C$_{60}$ **20** is more and more replaced by PCBM **19** which has similar electronic properties but a significantly higher absorption coefficient especially at shorter wave lengths. However, it still lacks absorption in the blue-green part of the solar spectrum.[47]

Recently, Murthy and co-workers[48] have investigated the mechanism of mobile charge carrier generation in blends of conjugated polymers and fullerenes (P3HT with PCBM or bis PCBM) using the time-resolved microwave conductivity technique (TRMC) (Figure 1-19). They found the quantum yields of P3HT:PCBM blends for mobile charge

generation on excitation in the visible and NIR are very similar, and the yield is independent of temperature ranging between 88 and 300 K. The realization that photoexcitation to the CT state does not significantly contribute to the optical absorption of the blend is important for photovoltaic applications.
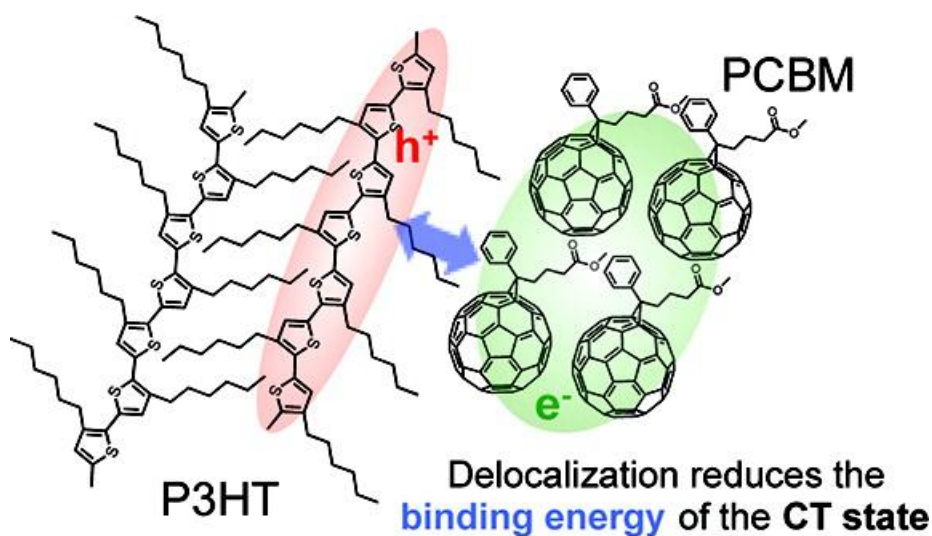
Figure 1-19. Charge carrier photogeneration for P3HT:PCBM (reprinted with permission from ref.[48] Copyright (2012) American Chemical Society).

Improving the device performance compared to benchmark devices comprising P3HT:PCBM either consists of raising the efficiency through improved current or voltage obtained from a cell or by extending the lifetime of the cell. Methods to increase the lifetime of devices mostly consist of improving their resistance to both air and water, or by increasing the thermal stability of the active layer morphology. Kim and co-workers[49] reported tandem solar cells with power-conversion efficiencies of more than 6% at illuminations of 200 milliwatts per square centimetre (Figure 1-20). It was constructed from two solar cells with different absorption characteristics that are linked to use a wider range of the solar spectrum. They were fabricated with each layer processed from solution with the use of bulk heterojunction materials comprising semiconducting polymers and fullerene derivatives. A transparent layer of titanium oxide (TiOx) separates and connects the front cell and the back cell. The TiOx layer works as an electron transport and collecting layer for the first cell and as a stable foundation that enables the fabrication of the second cell to complete the tandem cell architecture. The low band-gap polymer-fullerene composite has been used as the charge-separating layer in the front cell and the high band-gap polymer composite as the back cell.
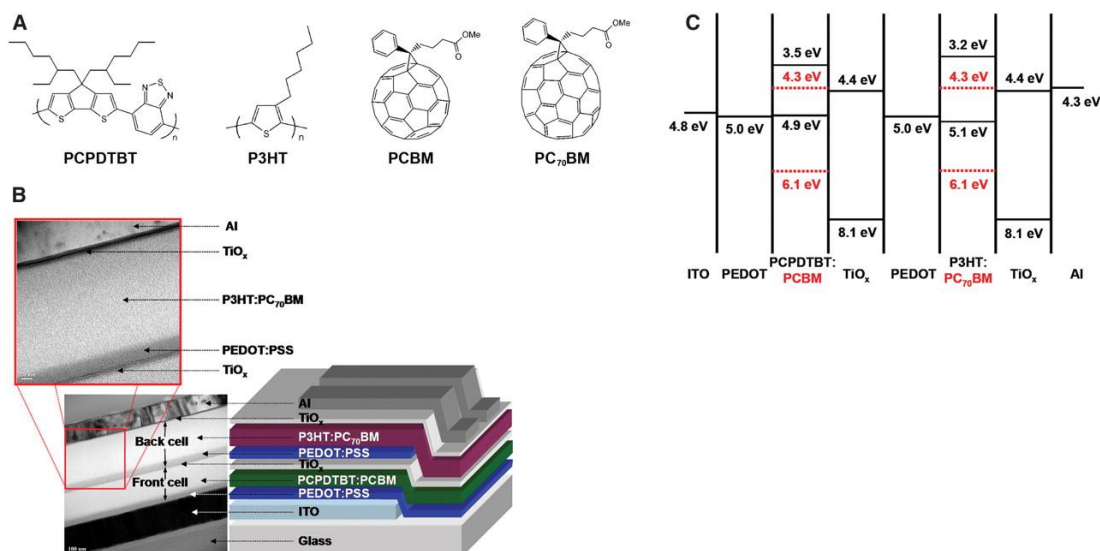
Figure 1-20. (A) Molecular structures of the active materials: PCPDTBT, P3HT, PCBM, and PC$_{70}$BM. **(B)** The device structure (right) and TEM cross-sectional image (left) of the polymer tandem solar cell. Scale bars, 100 nm (lower image) and 20 nm (upper image). ITO, indium tin oxide. **(C)** Energy-level diagram showing the HOMO and LUMO energies of each of the component Materials. (reprinted with permission from ref.[49] Copyright The American Association for the Advancement of Science).

Organic solar cells incorporating two active donor-acceptor heterojunctions consisting of two donor materials, CuPc and SnPc, and a single C$_{60}$ acceptor have been fabricated with power conversion efficiency of 2.9%.[50] The NIR absorbing material, tin (II)-phthalo-cyanine (SnPc), is grown into nanocrystalline islands using organic vapour phase deposition. Recently, organic photovoltaic (OPV) devices based on an optimal metal-phthalocyanine/fullerene (C$_{60}$) planar heterojunctions have been reviewed.[51] Recently, nanocrystals CuMePc were incorporated into P3HT:PCBM bulk heterojunction photo-voltaic cells to increase the carrier mobility and photon harvesting.[52] The cell featuring a weight ratio of P3HT:CuMePc = 1:1 exhibited the best photovoltaic performance with a PCE of 5.3%.

2. Chapter 2

Synthesis and characterisation of new naphthalene diimide-based acceptors

2.1. Introduction

2.1.1. Outline

The interaction between conjugated electron-deficient molecules (acceptors) and electron-rich molecules (donors) has been used to construct interesting supramolecular structures and sensors because of the favourable electrostatic interactions that exist between them.[53] However, in organic-based devices such as photovoltaic cells, donor and acceptor molecules need to be assembled into segregated structures for high electrical conductivity[54, 55] and efficient organic photovoltaic cells.[56, 57] This alternating hetero-stacked assembly is most commonly observed in solids[58, 59] and solutions.[60]

2.1.2. 1,4,5,8-Naphthalenediimides (NDI)

The development of n-type semiconductors so far has focused on the introduction of electron-accepting groups such as 1,4,5,8-naphthalenediimides (NDIs) **26** (also known as naphthalene carbodiimides) (Figure 2-1).[61] NDIs have attracted much attention due to their large conjugate planes, special electronic properties and tendency to form n-type over p-type semiconductor materials.[62, 63] They are a compact, neutral, planar, chemically robust, and electron deficient class of aromatic compound capable of self-organisation and incorporation into larger multicomponent assemblies.[62, 64]
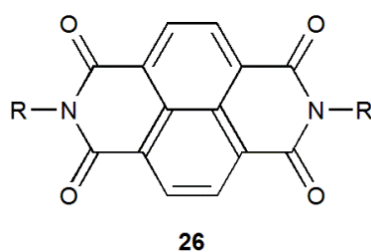
Figure 2-1. 1,4,5,8-naphthalenediimides (NDIs) **26**.

There are two functionalization sites within naphthalenediimides, either through the diimide nitrogen sites or via substitution on the naphthalene core. This produces different analogues which have been designed and applied in both the organic and inorganic metal, organic supramolecular and material chemistry fields. NDIs display variable absorption and emission properties which depend on the functional groups present. Substitution on the diimide nitrogens, with aromatic functional groups produces non-fluorescent or weakly fluorescent compounds, whilst alkyl groups at the same positions produce fluorescence.[65]

On the other hand, core substituted NDIs produce attractive strategy to create highly colourful and conducting functional materials with different absorption and emission properties compared with non-core unsubstituted NDIs.[61, 65]

Naphthalenediimides were synthesised and developed by Vollmann *et al.*[66] in the early 1930s, and have found popularity in the 20th Century due to the their ability to form covalent and noncovalent functional supramolecular materials such as catenanes and rotaxanes, and as gelators for sensing aromatic systems.[61, 62, 67] Furthermore, they are widely used as electron acceptor units in artificial photosynthetic systems for solar energy conversion.[68] Most of the modulations and modifications of the optical nature and the physical properties such as redox properties of these materials have been as a result of aromatic electron donor-acceptor interactions. Core-unsubstituted NDIs show absorption only in the UV region. Figure 2-2 shows the absorption and emission properties of N, N-di-alkyl-substituted NDIs in CH_2Cl_2.[69, 70] It displays absorptions below 400 nm, and a weak emission at λ_{ex}= 348 nm with a 7 nm Stokes shift. The absorption at λ_{max}= 476 nm for the stable radical anion of NDI can be generated by chemical and electrochemical reduction (Figure 2-3).[71, 72]
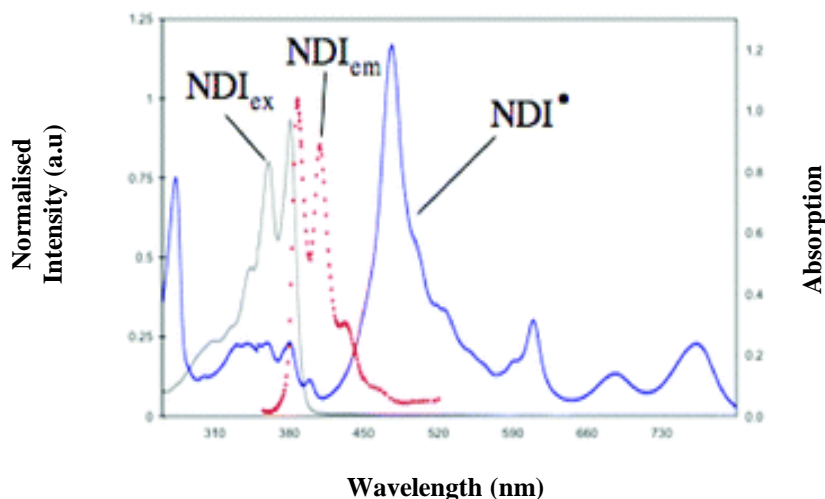
Figure 2-2. Absorption and emission spectra of *N,N*-dialkyl-substituted NDIs in CH_2Cl_2.[61]

The naphthalenediimides undergo single reversible one-electron reduction (chemically and electrochemically) at modest potentials E^1_{red}= -1.10 V vs. Fc/Fc$^+$ in CH_2Cl_2. Consequently, NDIs are considered as attractive redox-active units because of their electronic comple-mentarity to ubiquinones (E^1_{red} trimethylbenzoquinone= -1.20 V vs. Fc/Fc$^+$ in CH_2Cl_2), thereby making them excellent components for studying photoinduced electron transfer.[73]
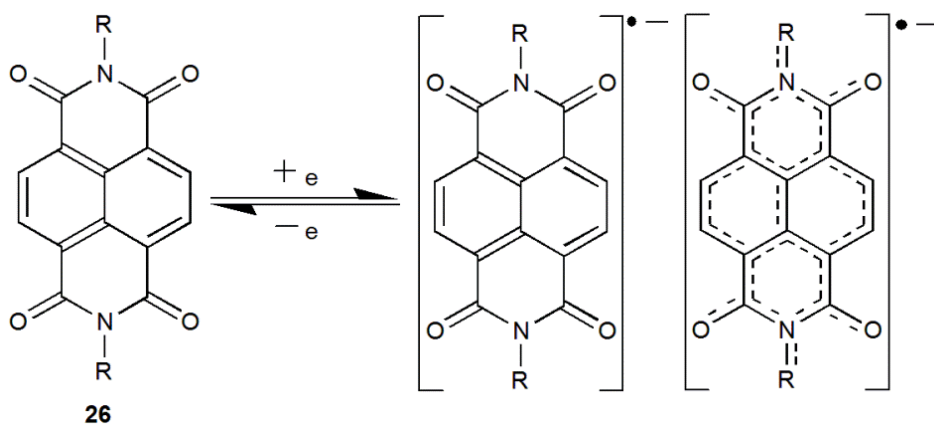
Figure 2-3. Reduction of NDIs **26** leads to radical anion which is delocalised over the core naphthalene structure.

Naphthalenediimides generally have higher solubilities in low polarity lipophilic solvents (e.g. toluene, DCM, chloroform) and polar aprotic solvents (e.g. acetonitrile, DMF, DMSO). This is because they contain a lipophilic naphthyl core, four polar carbonyl groups, and the substituents on the imide nitrogens.[74] Furthermore, naphthalenediimides exhibit π-stacking in the solid-state, due to their planar aromatic nature. The nature of the imide substituents is useful handle to control the assembly of NDI in solution and the solid phase. Figure 2-4, shows the reduction of the diimides with dithionite in aqueous solution leads to mainly dimers, whereas extended and highly ordered π-stacks result when cationic structures generated through peripheral pyridinium groups are induced.[75]
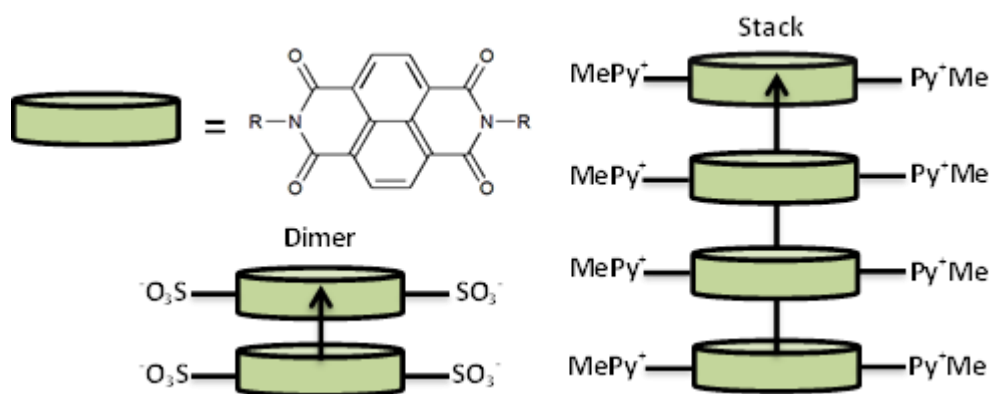
Figure 2-4. Self-assembly of NDI units

2.1.3. Synthesis of naphthalenediimides

A variety of NDI acceptors with different side chains have been synthesised from the commercially available starting material "naphthalene dianhydride **27**". Several functional groups can be introduced at the imides using simple and efficient one step procedures in

the synthesis of symmetric NDI compounds. For example 1,4,5,8-naphthalenetetra-carboxylic dianhydride can be condensed with the appropriate primary amine in DMF to afford high yields of the corresponding diimide **26** (Scheme 2-1).

Recently, microwave conditions were used to synthesise NDIs **28** by reaction of naphthalenedianhydride **27** with urea in refluxing 1,3,5-trichlorobenzene at 205 $^{\circ}$C in 5 min. (Scheme 2-1).[76] In 2005, Ghadiri prepared NDIs **30** by a sophisticated method which required control of the pH 6.2 (Scheme 2-1).[77]
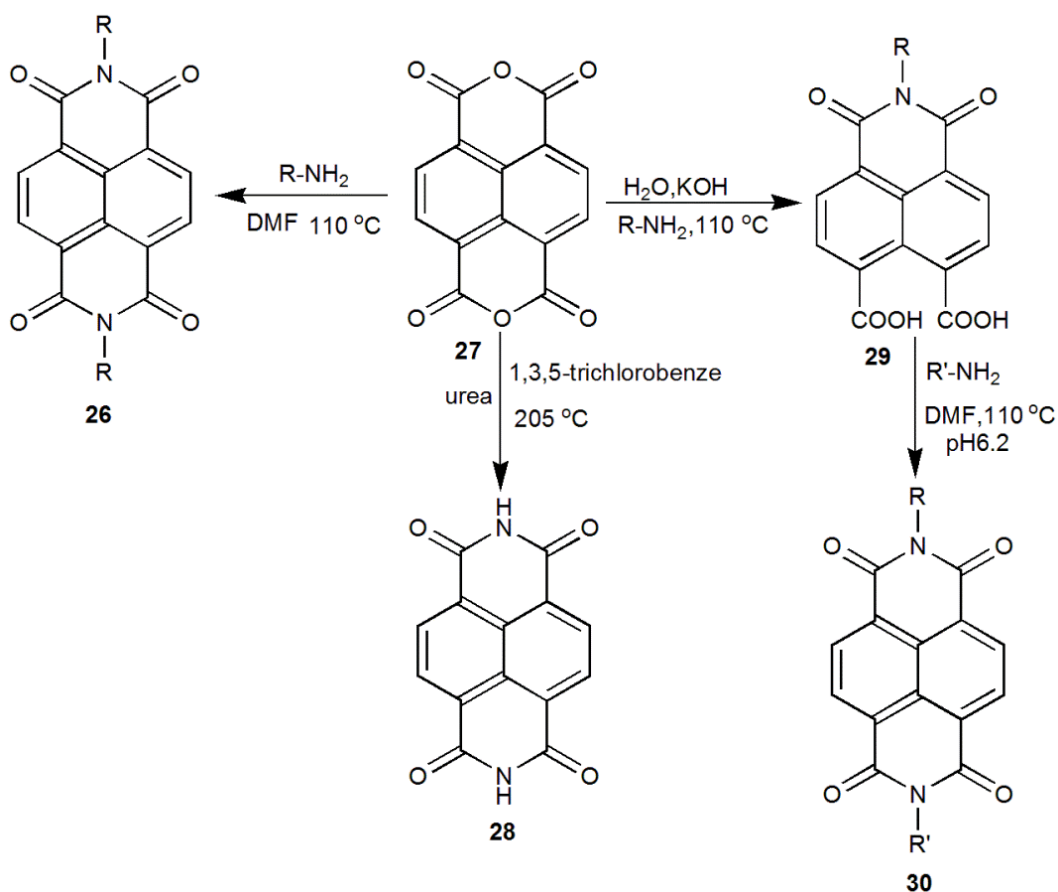
Scheme 2-1. General synthetic methods for preparing symmetric and *N,N'*-disubstituted NDIs.

NDI derivatives (Figure 2-5) were synthesised from amines and 1,4,5,8-naphthalene-tetracarboxylic dianhydride **27** upon heating in quinoline in the presence of zinc acetate (as catalyst).[62] NDIs with perfluorinated alkyl chains were first published as air-stable arylene derivatives in organic field-effect transistors (OFETs).[78] However, the perfluorinated octyl group resulted in lowered mobility compared to that of the parent fluorine-free hydrocarbon.[79] Furthermore, these compounds do not have a significant visible absorption due to their wider band gap (~3.0 eV). However, they exhibited high electron mobility, environmental stability, and solution processability.[78]

R= H   31
$CH_2C_3F_7$ 32
$CH_2C_7F_{15}$ 33
C_8H_{17} 34
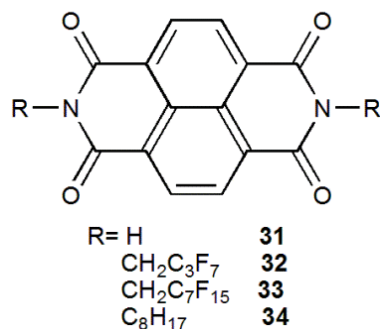
Figure 2-5. NDI derivatives.

Politi and co-workers[80] found that the fluorescence quantum yield of the *N,N'*-dibutyl derivative of naphthalenediimide was very weak due to the n–π* character of the lowest excited states (Figure 2-6). *N,N'*-Bis-aryl(alkyl)1,4,5,8-naphthalenediimides were prepared by the condensation of 1,4,5,8-naphthalenedianhydride **27** with the appropriate amine derivative in m-cresol/isoquinoline at high temperatures (>200 °C) for 4-6 h.[69]

Ar
35 Phenyl
36 *o* -Chlorophenyl
37 *p* -Tolyl
38 α -Naphthyl

R
39 *n*-Butyl
40 *n*-Dodecyl
41 Cyclohexyl
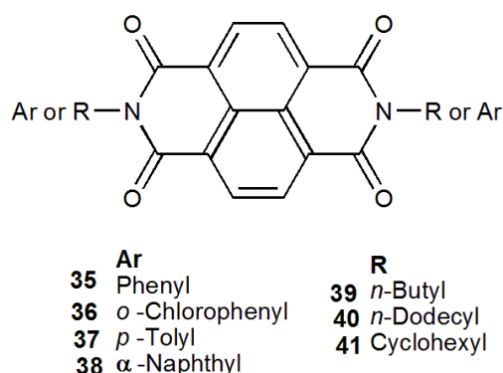
Figure 2-6. *N,N'*-Di-aryl (alkyl) derivative of naphthalenediimides.

2.1.3.1. Materials chemistry of NDIs

Naphthalene diimides derivatives have been used in the study of electron-transfer processes,[81, 82] as liquid crystalline and photorefractive materials,[83, 84] as photosynthetic model compounds,[85] and for opto-electronic applications.[86]

Politi and co-workers[87] constructed photoactive thin films of NDI derivatives that indicated the electrochemical reduction of 20-layer films resulted in the formation of stable *N,N'*-bis(2-phosphonoethyl) naphthalene-1,8:4,5-dicarboximide (NDI-BP) radical anions and dianions. NDI-BP/ZP (zirconium phosphonate) were grown on gold substrates in a layer-by-layer fashion to form multilayer thin films, which was achieved by exposing the phosphonate-rich modified surface to solutions of $ZrOCl_2$ and NDI-BP, respectively (Figure 2-7).
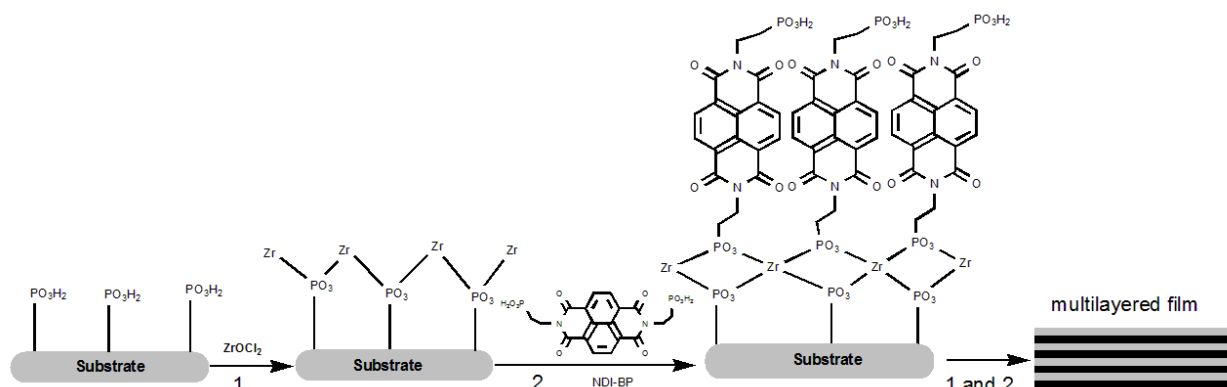
Figure 2-7. Layer-by-layer growth of NDI/Zr thin films on gold electrodes leads to multilayers.

Takenaka and co-workers[88] succeeded in DNA sensing by using ferrocenyl naphthalene-diimide **42** coupled with a probe DNA-immobilized electrode (Figure 2-8). Also, they have designed and synthesised novel ferrocenyl naphthalene diimide carrying ferrocene moieties at the end of linker chains from the naphthalene diimide skeleton (Figure 2-8).[89] This ligand has methylene moieties instead of the carbonyl in compound **42** which provides a lower oxidation potential to that of compound **43** and reduced the measuring time. Furthermore, the ferrocenyl ligands were applied to form a multi-electrode gene sensor as an electrochemical DNA chip, which could bind to the DNA•RNA hetero duplex more strongly than to the DNA homo duplex, and therefore could be easily used in mRNA expression analysis which is important in the post genome research.
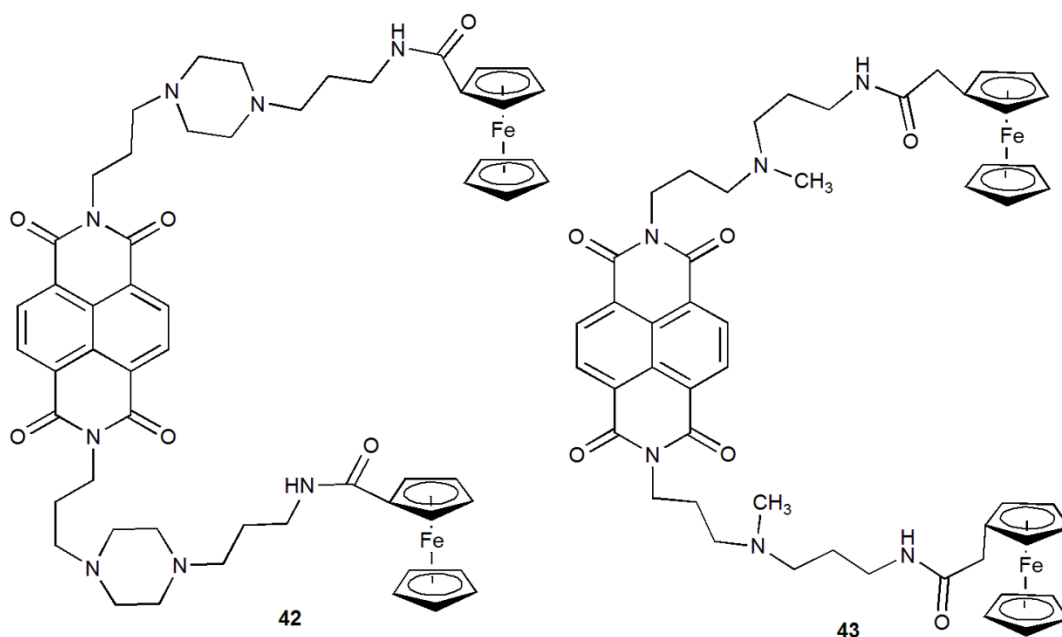
Figure 2-8. Ferrocenyl naphthalenediimide ligands.

Two rod-shaped compounds were designed (e.g. **44**), which incorporated a naphthalene diimide core and two terminal carboxylic acids units (Figure 2-9).[90] These molecules are able to aggregate and self-organize into supramolecular arrays in aqueous solution on the surface of solid substrates. The hydrogen bonds between the carboxylic acid groups and hydrophobic contacts between naphthalene diimide cores were responsible for the aggregation of these compounds into cylindrical microstructures (Figure 2-10).
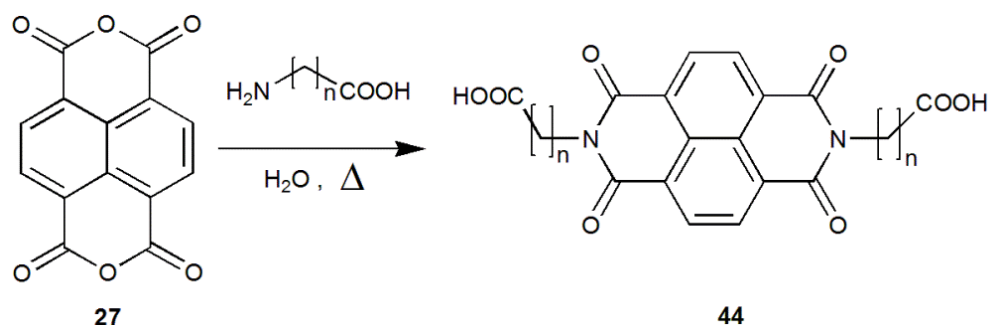
Figure 2-9. Synthesis of the naphthalene diimides **44** where n=1 or 2.
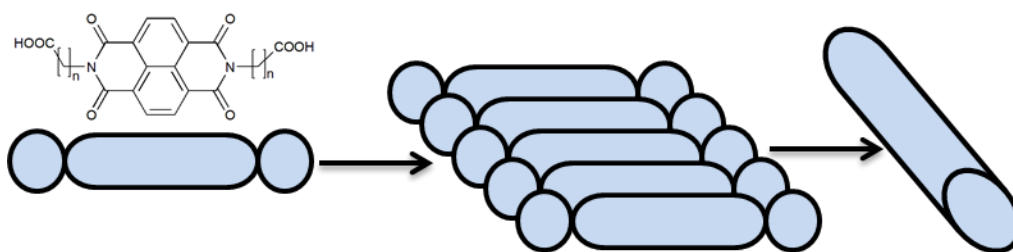
Figure 2-10. Self-assembly of naphthalene diimides into cylindrical microstructures.

The structural and chemical properties such as their electron deficient nature, aromatic, planar structure along with the ability to be functionalized with a wide variety of side groups make NDIs ideal candidates for host-guest interactions in particular donor–acceptor charge transfer type complexes. Naphthalenediimides have been studied with respect to host-guest systems such as intercalation, foldamers, ion channels, catenanes and rotaxanes.[61] In 1987 Nobel Laureate Jean-Marie Lehn highlighted the ability of NDA **27** in this area by formation of the cyclophane **45** through face-to-face aromatic interactions with electron donors including two NDI units linked by two alkyl chains. The structure of the macrocycle was confirmed by crystallographic analysis of a crystal grown from nitro-benzene **46** (Scheme 2-2).[91]
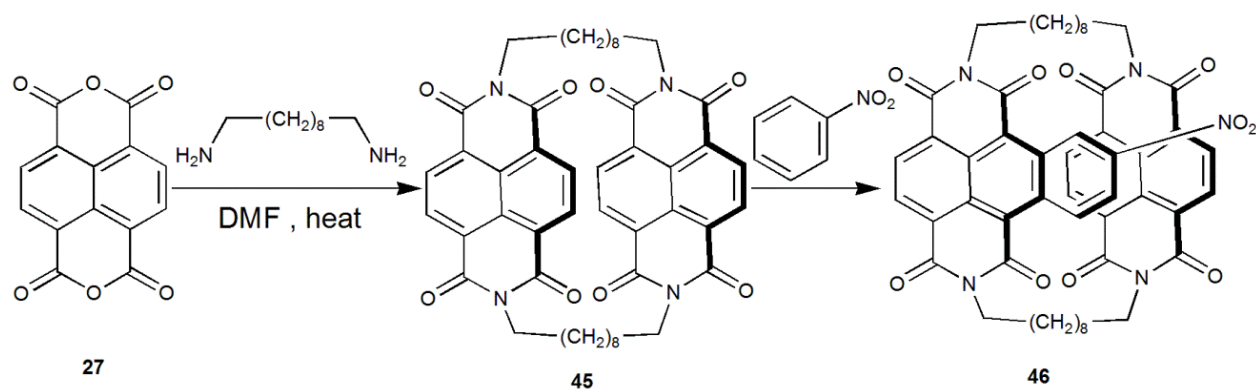
Scheme 2-2. Synthesis and inclusion properties of Lehn's NDI macrocycle.

A novel [2]catenane **47** that exhibited unusual solid-state behavior was synthesised from NDI (Figure 2-11).[92] The strategy for forming the interlocked supramolecular structure was based upon templation effects between the electron rich macrocycle and the newly formed NDI-based catenane.
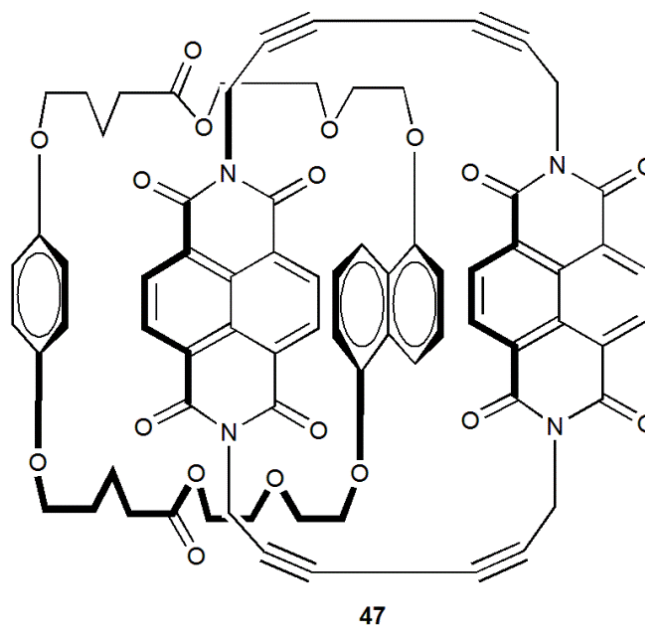
Figure 2-11. Novel [2]catenane from NDI.

Recently, the first example of a Donor-spacer-Acceptor based system featuring a naphthalene-diimide acceptor and a molybdenum-ene-1,2-dithiolate unit as the donor has been synthesised (Figure 2-12). Garner and co-workers[93] prepared this dye **48** from a new pro-ligand containing a protected metal-ene-1,2-dithiolate bound through a phenyl linkage to a naphthalenetetracarboxylic diimide group to form a donor-spacer-acceptor configuration. The photophysical properties were investigated and the electron para-magnetic resonance (EPR) spectra proved that the highest occupied molecular orbital (HOMO) is located over the ene-metalladithiolene moiety, and the lowest unoccupied

molecular orbital (LUMO) is diimide based. This system is capable of electron transfer, leading to separated electron/hole pair with a lifetime about 15 ns in CH_2Cl_2 at room temperature.
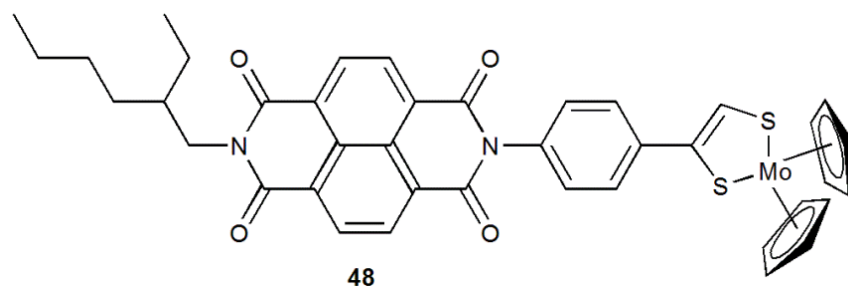
Figure 2-12. Structure of [Cp$_2$Mo(SC(H)C(C$_6$H$_4$−NDI)S)] **48**.

In 2009, Wasielewski and co-workers[94] synthesised series of donor-bridge-acceptor (D-B-A) triads (Figure 2-13(**b**)). The donor 3,5-dimethyl-4-(9-anthracenyl)julolidine and the acceptor naphthalene-1,8,4,5-bis(dicarboximide) are linked by p-oligophenylene bridging units. Recently, they have developed the previous system into (D−B−A) systems in which a 3,5-dimethyl-4-(9-anthracenyl)julolidine chromophore and a naphthalene-1,8:4,5-bis(di-carboximide) acceptor are linked by oligomeric 2,7- fluorenone bridges (Figure 2-13(**a**)).[95] The fluorenone oligomers bridges are useful because their reduction potentials change only modestly as n increases (-1.27, -1.14, and -1.08 V vs. SCE for n= 1-3), respectively.
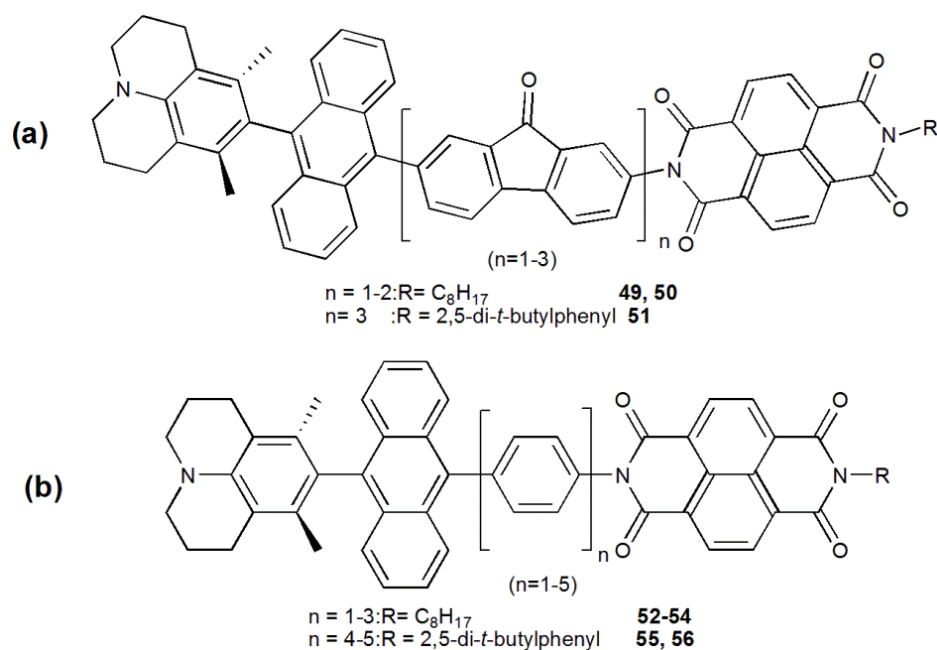
Figure 2-13. (a) D−Bridge−A molecules were studied recently and compared to the **(b)** analogous molecules which were studied previously.

Complex **59** is the first example of a Pt(II)-diimine-diimide dyad and was synthesised in 2008 by Sazanovich and co-workers[96] (Scheme 2-3). Imide substituted ligands have been successfully incorporated into numerous metal complexes, and the physical and chemical studies of electrochemically generated anions confirmed that the lowest unoccupied molecular orbital (LUMO) in this system is localized on the NDI acceptor group.
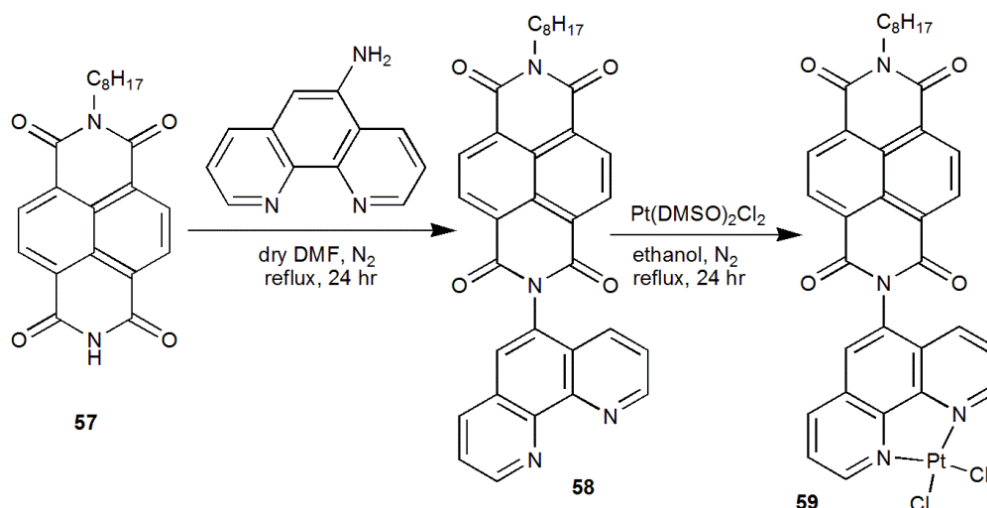
Scheme 2-3. Synthesis of the Pt(phen-NDI)Cl$_2$ Complex **59**.

2.1.4. Tetracyanoethene (TCNE) and 7,7,8,8-Tetracyanoquino-dimethane (TCNQ) as acceptor units

Tetracyanoethene (TCNE) and 7,7,8,8-tetracyanoquinodimethane (TCNQ) are important molecules, containing multiple cyano (CN) groups, and as a consequence are strong organic electron acceptors (Figure 2-14). These powerful electron acceptors were reported in the early 1960s.[97] Due to their low energy π^* orbitals, the four cyano groups with their π systems conjugated with the central C=C (phenyl ring) double bond, then give rise to an excellent acceptor.
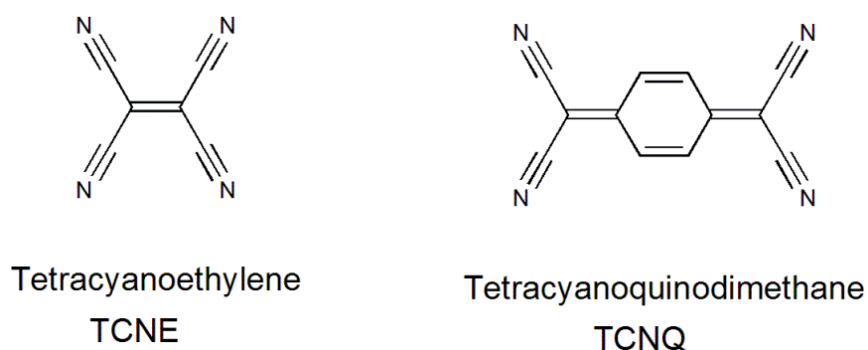
Figure 2-14. TCNE and TCNQ structures.

The high electron affinity of TCNQ (2.8+0.1 eV) can be explained by the occurrence of two electron-withdrawing dicyanomethylene groups in the molecule. The presence of quinonoid ring moiety in TCNQ structure provides stabilization of the anionic system because it allows a more efficient charge delocalization.[98] TCNE moiety has the same two electron-withdrawing dicyanomethylene groups but not the quinonoid ring, thus, the electron affinity obtained for TCNE is 3.17+0.2 eV.[99] When the stable strong electron acceptors (TCNE or TCNQ) are conjugated to strong donors, the resulting push–pull chromophores undergo efficient intermolecular charge transfer (CT) interactions and can display high third-order optical non-linearities and exceptional electron storage capacities.[100]

Diederich *et al.*[61] reported that the thermal [2+2] cycloadditions of tetracyanoethene and 7,7,8,8-tetracyanoquinodimethane to *N,N*-dimethylanilino substituted (DMA-substituted) alkynes afforded a new class of stable, strong organic super-acceptors (Figure 2-15).
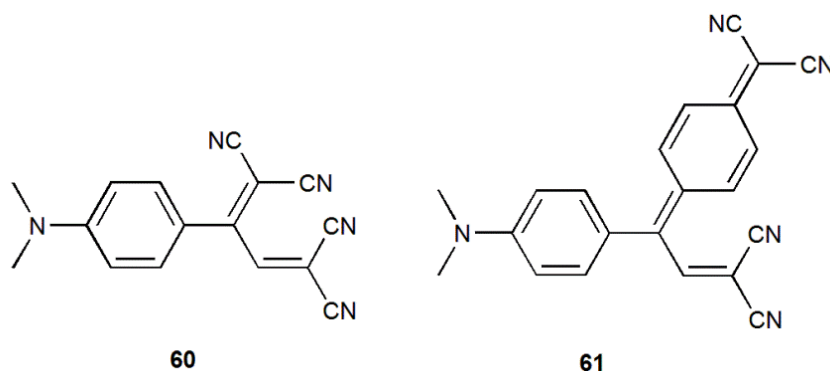
Figure 2-15. Anilino donor-substituted acceptors.

In early 1981,[101] the [2+ 2] cycloaddition of TCNE or TCNQ with electron-rich metal acetylides, followed by retro-electrocyclisation gave organometallic 1,1,4,4-tetracyano-buta-1-3-diene TCDB derivatives (Scheme 2-4).[102] The corresponding reaction with electron-rich organodonor-substituted alkynes has only been systematically explored in the last decade.
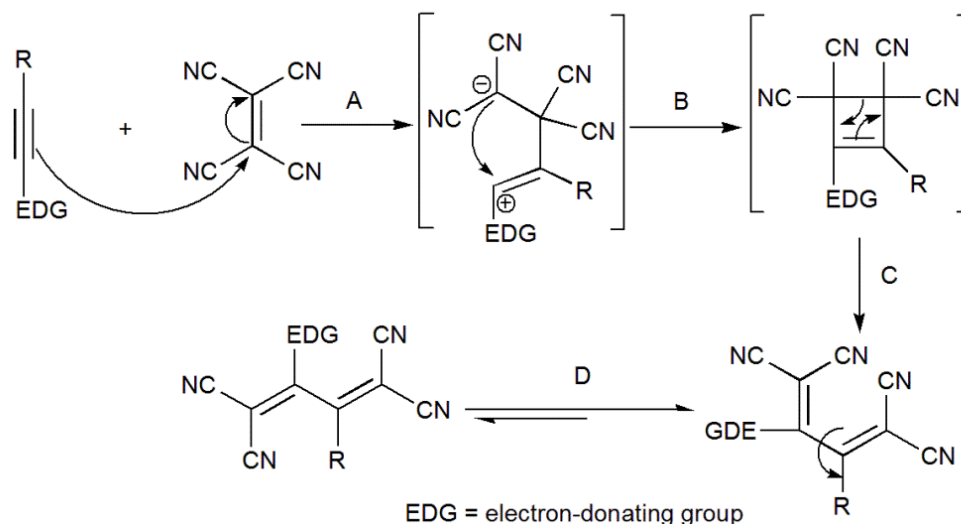
Scheme 2-4. Proposed mechanism for the reaction of EDG-based alkynes with TCNE.

2.2. The aim of the project
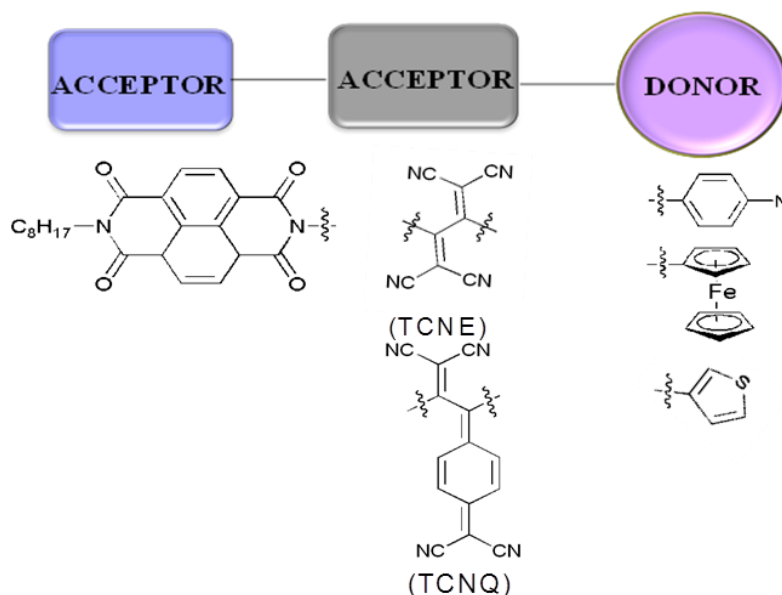
Figure 2-16. New push-pull systems based on NDI.

The aims of this project have been to synthesise a range of new, stable, strong organic super-acceptors based on an NDI core and study their chemical and physical properties. This chapter describes our efforts to utilize the naphthalene diimide (NDI) as primary acceptor. In addition, to increase the lifetime of the charge-separated (CS) state in donor-acceptor arrays, two strategies have been used, the separation between the donor and the acceptor has been increased and a reduction gradient between D and A has been introduced by insertion of additional electroactive moieties.[103, 104] The target molecules are an attractive target for fabricating photovoltaic devices because of the extensive redox

chemistry and photochemical properties of NDI, acceptors, and donors. In particular these energy and electron transfer donor-acceptor molecular systems could afford a broader range of LUMO energies which may allow the investigation of a wider range of complementary donor polymers. In addition, by synthesising these kinds of compounds, we can modulate the absorption of light towards the near-IR region and enhance third-order optical non-linearities of the push-pull chromophores.

2.3. Results and Discussion

2.3.1. Synthesis and characterisation of new NDI push-pull systems 64 and 65 using dimethylaniline as the donor unit

The general methodology for the synthesis of **64** and **65** is shown in Scheme 2-5. These compounds were synthesised via a [2 + 2] cycloaddition of tetracyanoethene (TCNE) or 7,7,8,8-tetracyanoquinodimethane (TCNQ) and electron-rich NDI-acetylene-dimethyl-aniline.

Scheme 2-5 shows the synthesis of naphthalenediimides (NDI) from 1,4,5,8-naphthalene-tetracarboxylicdianhydride (NDA) **27** in one step with octylamine and 4-iodoaniline at 140 $^\circ$C under N_2. This one-pot process affords a better yield (64%) of compound **62** than that reported for a similar two step route.[105] The condensation reaction of the naphthalene with a primary amine is usually accompanied by a change in colour. Usually when heat is applied, the reaction will proceed from a dull colour (yellow) corresponding to the naphthalene dianhydride to a bright violet colour.

The first synthetic approach to afford at the newly designed donor-acceptor chromophores started with the coupling of commercial 4-ethynyl-*N,N*-dimethylaniline with phenyl iodide-NDI **62** under modified palladium catalysed Sonogashira cross-coupling reactions (Scheme 2-6).[106] This reaction occurred at 80 °C using Pd/C, Ph$_3$P, and CuI in a ratio of 1:4:2 and 2.5 equivalents of K_2CO_3 overnight under N_2 atmosphere. The cross-coupling of 4-ethynyl-*N,N*-dimethylaniline with **62** afforded **63** in high yield (88%).

Compound **63** was used as a building block to create the new acceptors **64** and **65**. The addition of 1.2 equivalent of TCNE to a THF solution of **63** at 60 °C yielded molecule **64**

in 66% yield. On the other hand, the reaction of 1 equivalent of TCNQ with **63** yielded molecule **65** in 64% yield (Scheme 2-5).
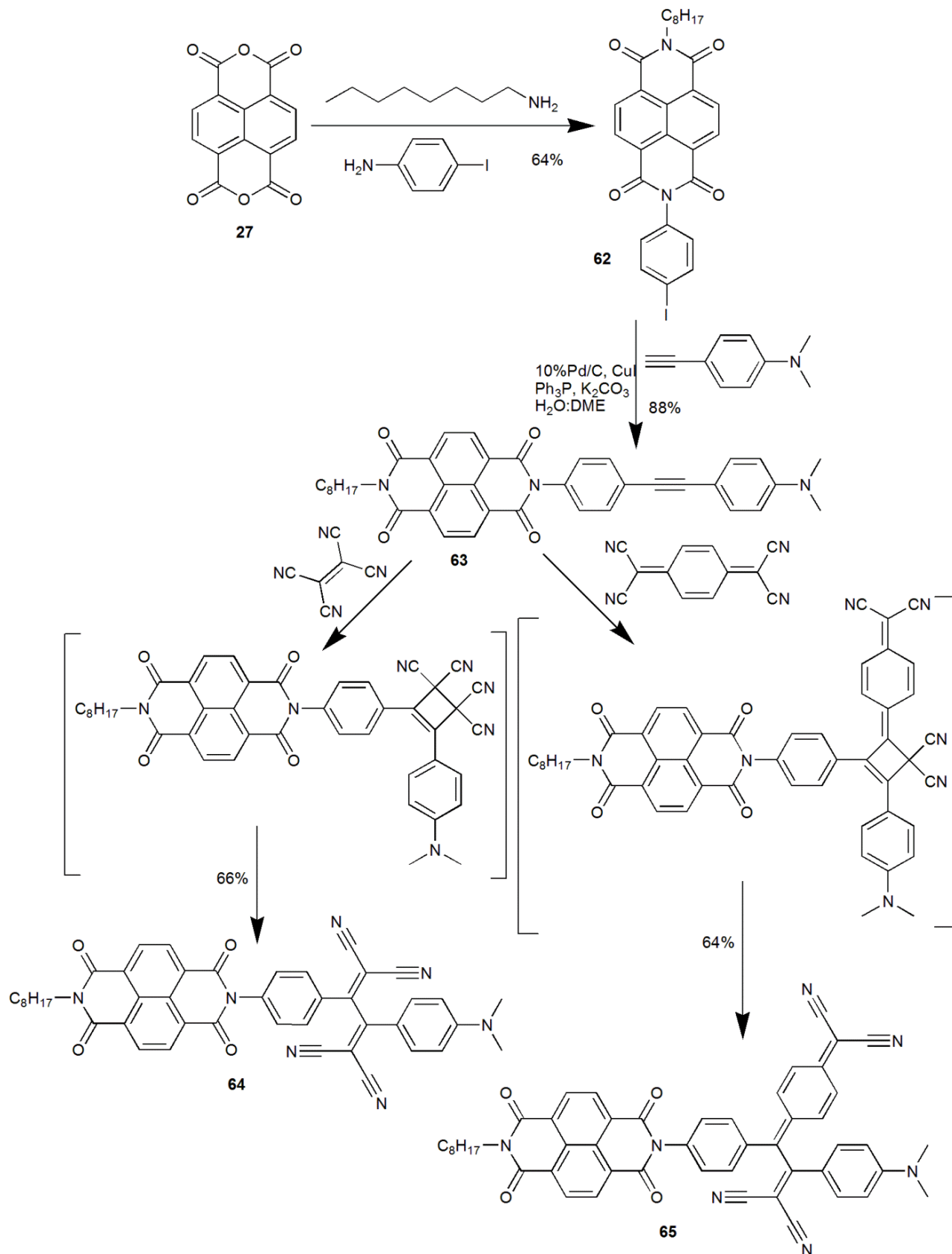
Scheme 2-5. Synthesis push-pull NDI-based super acceptors **64** and **65**.
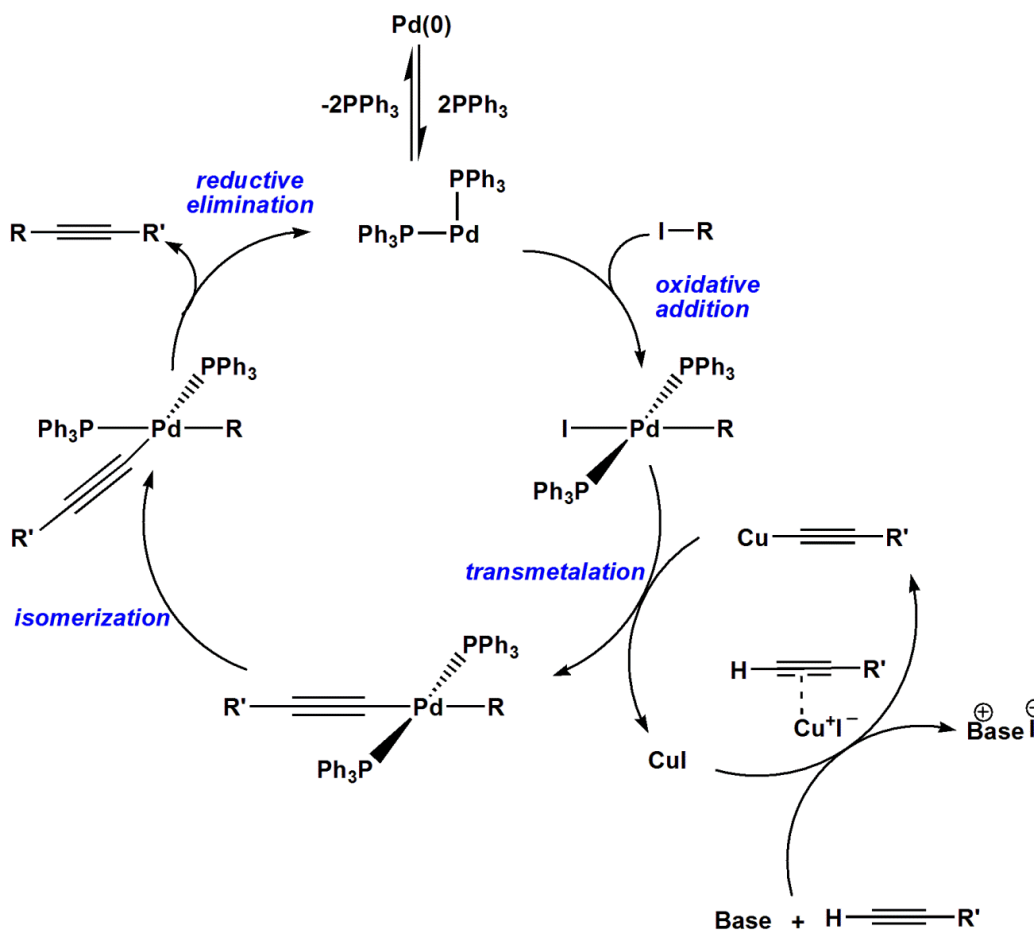
Scheme 2-6. Reaction mechanism of the modified palladium catalysed Sonogashira cross-coupling reactions.

2.3.1.1. Spectroscopic studies of 64 and 65

^{1}H, ^{13}C NMR, mass spectrometry, and FTIR spectra, were consistent with the structures of **64** and **65**. The ^{1}H NMR and ^{13}C NMR displayed the expected signals for **64** and **65**.

The absorption properties of the compounds **63**, **64**, and **65** were studied by UV-vis spectroscopy. The UV-vis spectra of **64** and **65** in CH$_2$Cl$_2$ displayed broad CT bands with end-absorptions reaching into the near infrared (Figure 2-17). Compound **63** has an absorption band in the 300-400 nm region with a maxima for the π-π* transition at λ_{max} = 383 nm (3.24 eV) and at λ =361 nm, in addition to weak absorption at 351 nm.
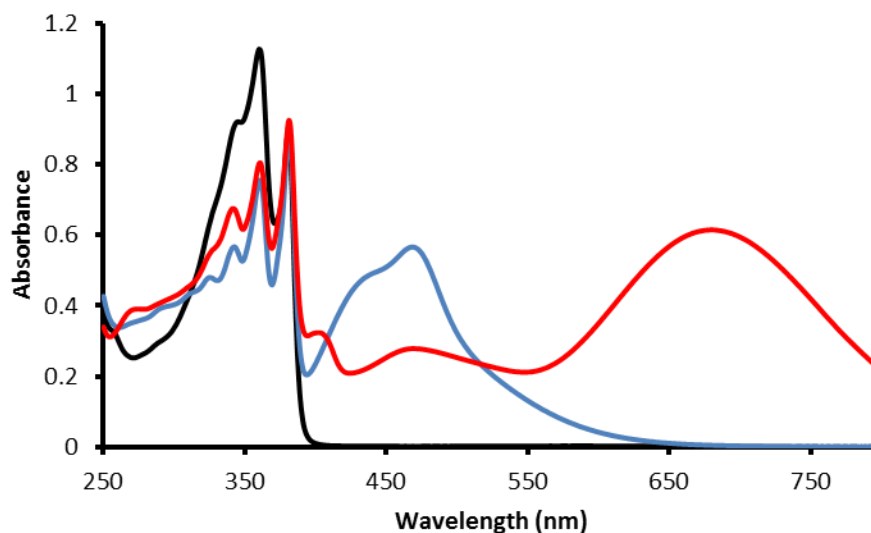
Figure 2-17. UV-vis spectra of compounds **64** (blue line), **65** (red line), and **63** (black line) recorded in CH_2Cl_2 (1×10^{-4} M).

Compound **64** has additional absorption peaks corresponding to the NDI-acetylene entity that are observed at λ_{max} = 476 nm (2.60 eV) and a shoulder at 443 nm. Compound **65** displayed similar peak profile to λ_{max} of **64** at 476 nm, however it exhibits an additional absorption peak at λ_{max} = 690 nm (1.80 eV) and a weak absorption at 409 nm, reflecting the effective conjugation. This trend retained after TCNE and TCNQ addition. It is worth noting that the onset wavelength of also compounds **64** and **65**, shown in Figure 2-17, corresponds to an optically determined band gap energy (Eg^{opt} = 1242/ λ_{onset}) (Table 2-1).

Table 2-1. UV-visible spectra data of compounds **64**, **65**, and **63** recorded in CH_2Cl_2 (1×10^{-4} M). Where the λ_{abs} is absorption wavelength (nm), λ_{Max} is maximum absorption wavelength (nm), and Eg^{opt} optically determined band gap energy (eV).

Compounds	λ_{abs1} (nm)	λ_{abs2} (nm)	λ_{abs3} (nm)	λ_{abs4} (nm)	λ_{abs5} (nm)	λ_{abs6} (nm)	λ_{abs7} (nm)	Band gap (eV)
63	351	361	383	---	---	---	---	3.24
64	319	350	362	383	443	476	---	2.60
65	331	345	362	382	409	476	690	1.80

Figure 2-18 illustrates the UV-vis spectra of compound **64** in three organic solvents: dichloromethane, dimethylsulfoxide, and acetonitrile, respectively. As detailed in Figure 2-18, each of the spectra was recorded at the same concentration (1 x 10^{-4} M) and any spectral change, therefore, must have arisen from the solvent. Compound **64** in DCM

displayed λ_{max} at 469 nm and small red shift was observed with CH_3CN (3 nm), whereas in DMSO the λ_{max} = 485 nm which is bathochromically shifted by16 nm.
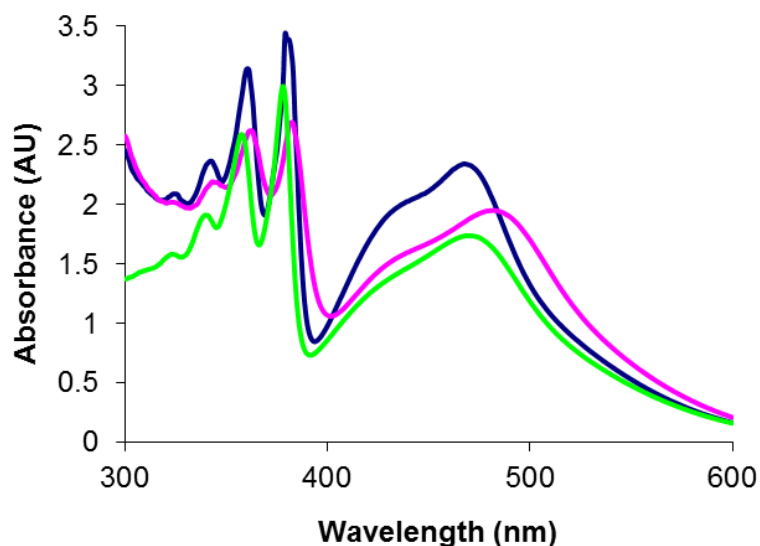
Figure 2-18. UV-visible spectra of compound **64** recorded in CH_2Cl_2 (blue line), DMSO (purple line), and CH_3CN (green line) (1×10^{-4}M).

The photophysical behavior was investigated by fluorescence spectroscopy recorded in 10^{-5} M solution in dichloromethane. It can be seen that the TCNE and TCNQ units play an important role in modulating the fluorescence properties of the NDI-acetylene unit **63**. As shown in Figure 2-19, the fluorescence emission of **64** and **65** are quenched strongly compared to NDI-acetylene-DMA **63**.
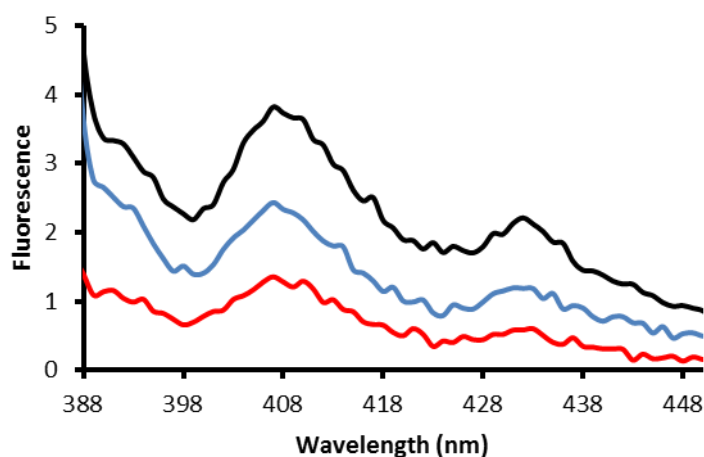
Figure 2-19. Fluorescence spectra recorded for compounds **64** (blue line), **65** (red line), and **63** (black line) in CH_2Cl_2 (1×10^{-5} M) at excitation wavelength = 381 nm.

2.3.1.2. Electrochemical Studies of 63, 64 and 65

The redox properties of the new chromophores **63**, **64** and **65** were investigated by cyclic voltammetry (CV) using tetrabutylammonium hexafluorophosphate (n-Bu$_4$NPF$_6$) as a supporting electrolyte and ferrocene (Fc$^+$/Fc) as internal reference in CH$_2$Cl$_2$. All three compounds **63**, **64** and **65** were reduced in well-defined reversible one-electron reduction steps, with the first reduction occurring at E$_{1/2}$= -1.06 V for **63**, E$_{1/2}$= -0.90 V for **64**, and E$_{1/2}$= -0.68 V for **65** (Figure 2-20, Table 2-2).
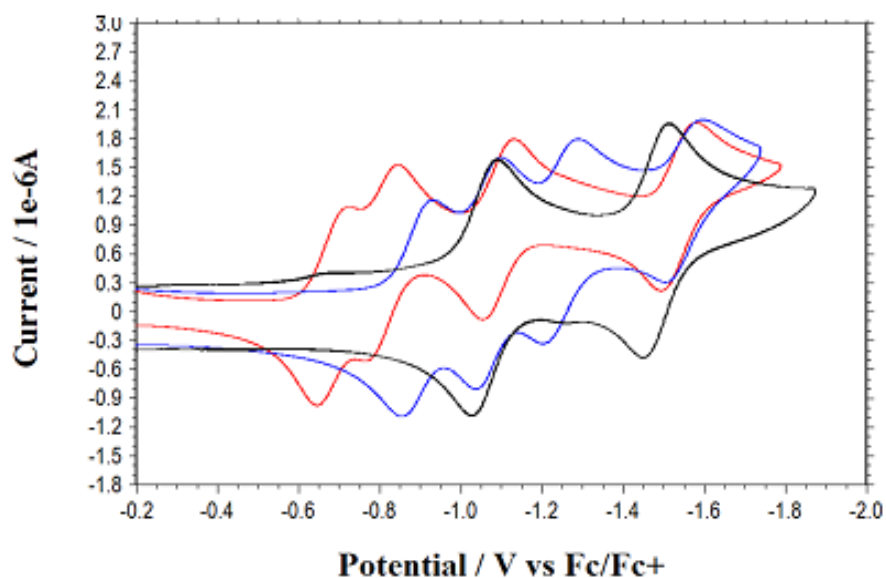
Figure 2-20. Cyclic voltammogramms of compounds **64** (blue line), **65** (red line), and **63** (black line) recorded using a glassy working electrode, an Ag wire as a reference electrode and a Pt wire as a counter electrode. Recorded in CH$_2$Cl$_2$ (1x10^{-4} M) with 0.1M (n-Bu$_4$NPF$_6$) as a supporting electrolyte at 20 ºC, and a scan rate of 0.1 Vs^{-1}.

Compound **63** displayed two reversible redox waves at E$_{1/2}$= -1.06 V and E$_{1/2}$= -1.48 V for the two electron reduction of NDI-acetylene moiety. This corresponds to a LUMO energy of E$_{LUMO}$= -3.74 eV. On the other hand, it displayed irreversible peak potential at +0.40 V, this corresponds to a HOMO energy of E$_{HOMO}$= -5.2 eV, resulting in an electrochemically determined band gap of E$_{gap}$= 1.46 eV. Compound **64** displayed two reversible redox waves at E$_{1/2}$= -0.90 V and E$_{1/2}$= -1.25 V for the two electron reduction of NDI-TCNE moiety. This corresponds to LUMO energy of E$_{LUMO}$= -3.90 eV. Compound **65** displayed two reversible redox waves at E$_{1/2}$ = -0.68 V and E$_{1/2}$= -0.80 V for the two electron reduction of NDI-TCNQ moiety. This corresponds to a LUMO energy of E$_{LUMO}$= -4.12 eV (Table 2-2).

Table 2-2. Electrochemical data (CV) of compounds **64**, **65**, and **63** recorded in CH_2Cl_2 (+0.1M n-Bu_4NPF_6) vs.Fc+/Fc at scan rate v = 0.1 V s^{-1}.

Compounds	$E^1_{1/2}$ [V]	$E^2_{1/2}$ [V]	$E^3_{1/2}$ [V]	$E^4_{1/2}$[V]	E LUMO eV	E HOMO eV	E gap eV
63	-1.06	-1.48	-----	-----	-3.74	-5.2	1.46
64	-0.90	-1.07	-1.25	-1.55	-3.90	-----	-----
65	-0.68	-0.80	-1.08	-1.53	-4.12	-----	-----

2.3.1.3. X-ray structure of 64

Single crystals of **64** suitable for X-ray crystallographic analysis were obtained by slow diffusion of methanol into CH_2Cl_2 solution at 25 °C. This provided crystals of sufficient quality for X-ray structure determination. The X-ray structure of **64** is shown in Figure 2-21 and clearly proves NDI-TCNE formation.
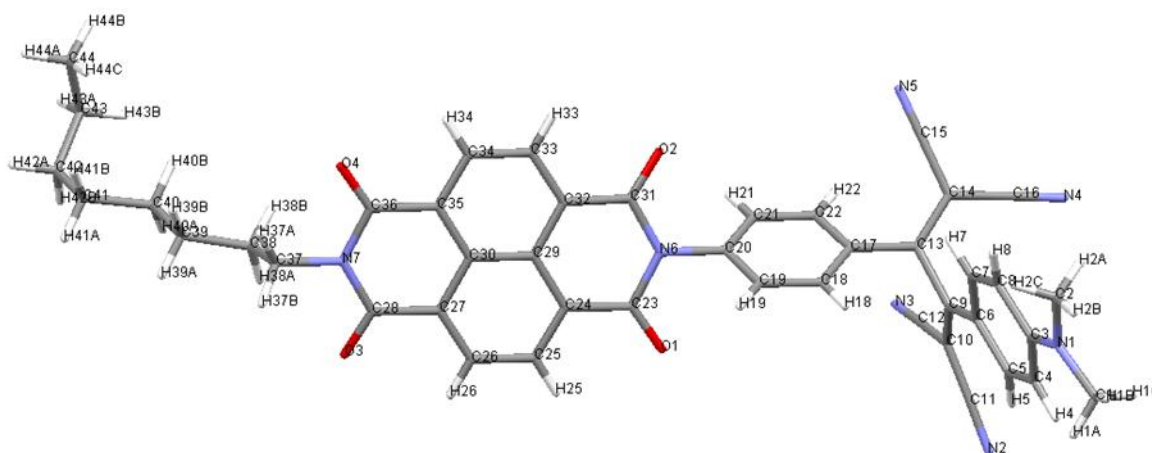
Figure 2-21. X-ray crystal structure of **64**.

The NDI core portion of the molecule adopts a roughly planar configuration and the considerable nonplanarity was observed in the expanded NDI-TCNE acceptor moiety. The torsion angles of C(17)-C(13)-C(9)-C(6) and C(10)-C(9)-C(13)-C(14) are 116.8(2)° and 120.1(3)°, respectively. The distance between the dicyanomethylene carbons C(10) and C(14), is 4.23 Å, and there is no bonding between them.

2.3.1.4. Molecular Modelling of 64 and 65

We calculated the electron distribution in the molecular structure using density functional theory (DFT) in order to study the electron delocalization in molecule **64**. In order to get the simplification of the calculation, the long alkyl chain (octyl) was replaced by a CH_3 group in the molecules. The MO electron density plots reveal that the LUMO is completely delocalized across the naphthalenediimide core and the computed LUMO energy for **64** is E_{LUMO} = -3.57 eV (Figure 2-22).
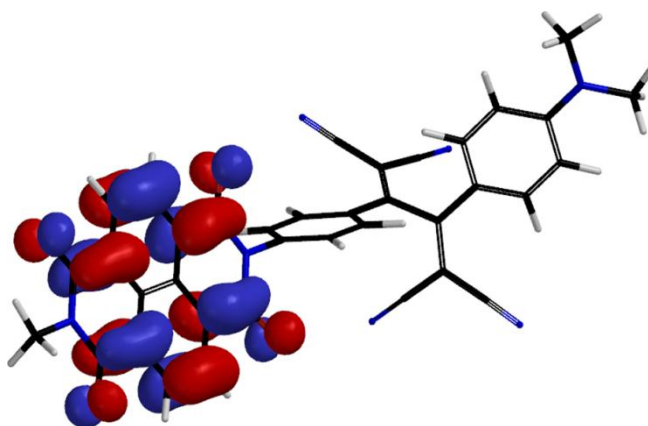
Figure 2-22. DFT B3LYP 6-311G calculation of **64** showing LUMO location.

Inspection of the HOMO densities for this system shows that π-orbitals are delocalized along the dimethylaniline unit and the computed HOMO energy for **64** is E_{HOMO}= -5.99 eV (Figure 2-23).
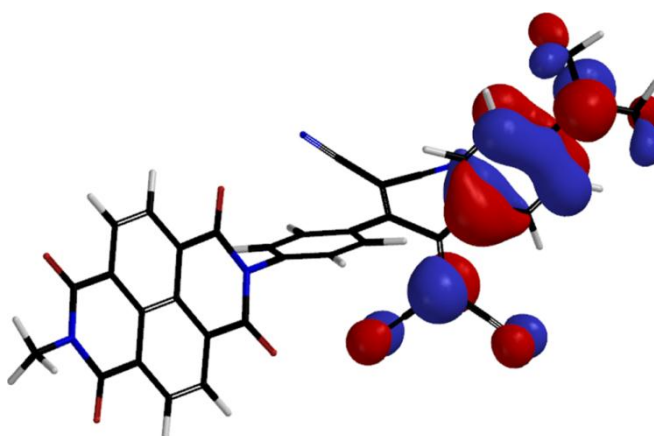
Figure 2-23. DFT B3LYP 6-311G calculation of **64** showing HOMO location.

2.3.2. Synthesis and characterisation of new NDI push-pull systems 67 and 68 using ferrocene as the donor system

The general methodology for the synthesis of **67** and **68** is shown in Scheme 2-7. These compounds were synthesised via a [2 + 2] cycloaddition of tetracyanoethene or 7,7,8,8-tetracyanoquinodimethane and compound **66**. There are only a few reports where the ferrocenyl group is attached to the NDI derivatives. In the current research work, the ferrocene was linked to the naphthalenediimide unit via a ferrocenethynyl bond. We were interested to explore the photophysical, and electrochemical properties of these compounds.

The naphthalenediimide-ferrocene conjugates were synthesised using Sonogashira cross-coupling reactions (Figure 2-23). This reaction occurred at 80 °C using CuI/10% Pd/C and Ph$_3$P as the catalyst affording **66** in 79% yield (Scheme 2-7). This material was used as the building block to synthesise the TCNE and TCNQ adduct **67** and **68**, respectively (Figure 2-23).

The addition of 1.2 equivalents of TCNE to a CH$_2$Cl$_2$ solution of **66** led to a colour change from green to blue at 20°C when the reaction was left overnight gave rise to compound **67** in 93%. On the other hand, addition of 2 equivalent of TCNQ to a 1, 2-dichloroethane solution of **66** led to a colour change from green to brown at 70 °C for 72 hours, yielding compound **68** in 78% (Scheme 2-7). We have also attempted reactions using different organic solvents such as THF, DMF, and toluene but these solvents failed to give the required products.
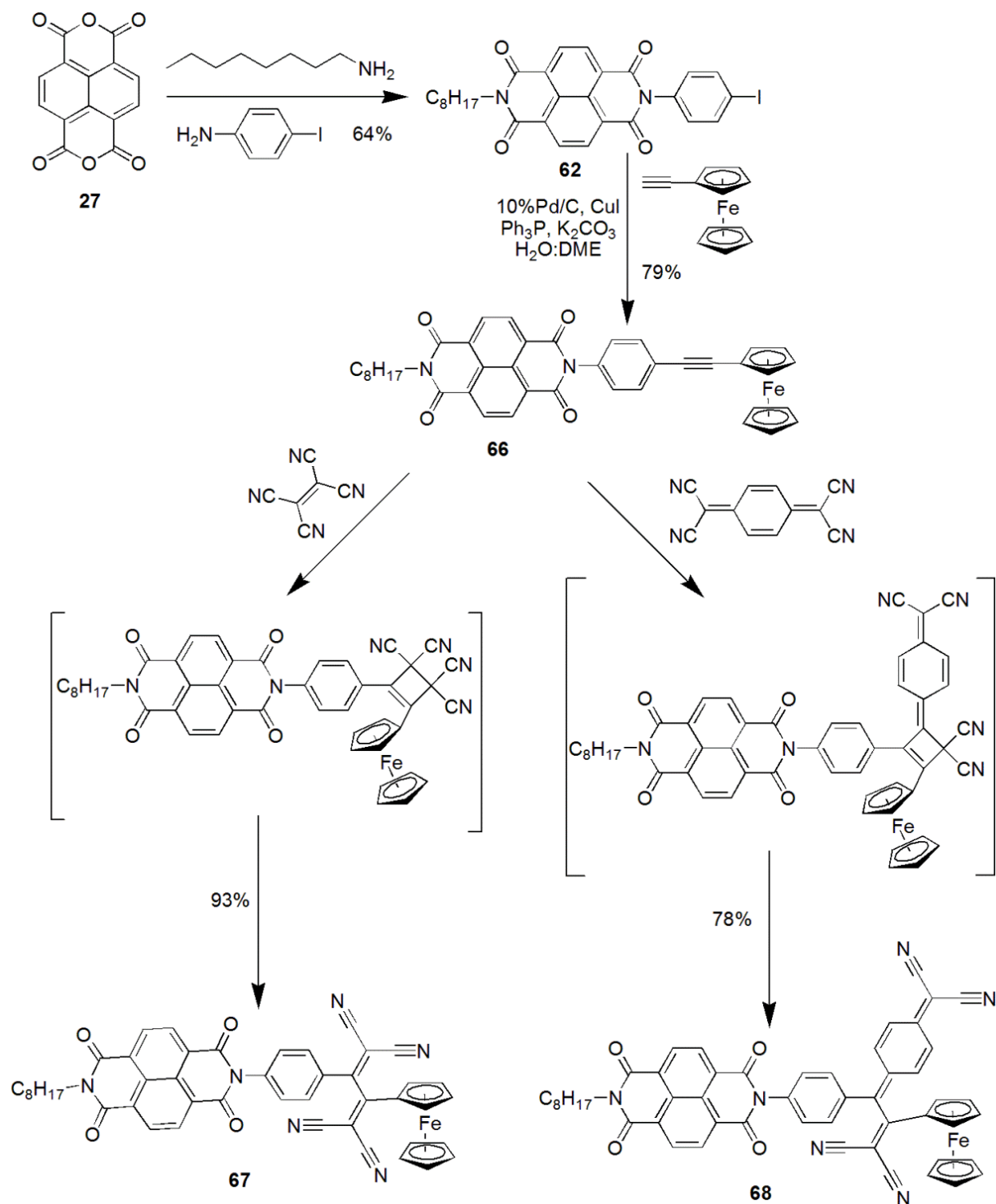
Scheme 2-7. Synthesis of push-pull NDI-based acceptors **67** and **68**.

2.3.2.1. Spectroscopic studies of 67 and 68

^{1}H, ^{13}C NMR, mass spectrometry, and FTIR spectroscopy were used to characterise the main target molecules **67** and **68**. The ^{1}H NMR and ^{13}C NMR displayed the expected signals for **67** and **68**. The relative integration of these peaks was useful in confirming the identity of the **67** and **68**. The absorption properties of the compounds **66**, **67** and **68** were

investigated by UV-vis spectroscopy. The UV-vis spectra of **67** and **68** in CH_2Cl_2 displayed broad CT bands with end absorptions reaching into the near infrared region (Figure 2-24, Table 2-3). Compound **66** has an absorption band in the 298-440 nm region with a maxima for the π-π* transition at λ_{max}= 440 nm in addition to absorption at 380 nm, 361 nm and weak absorption at 340 nm.
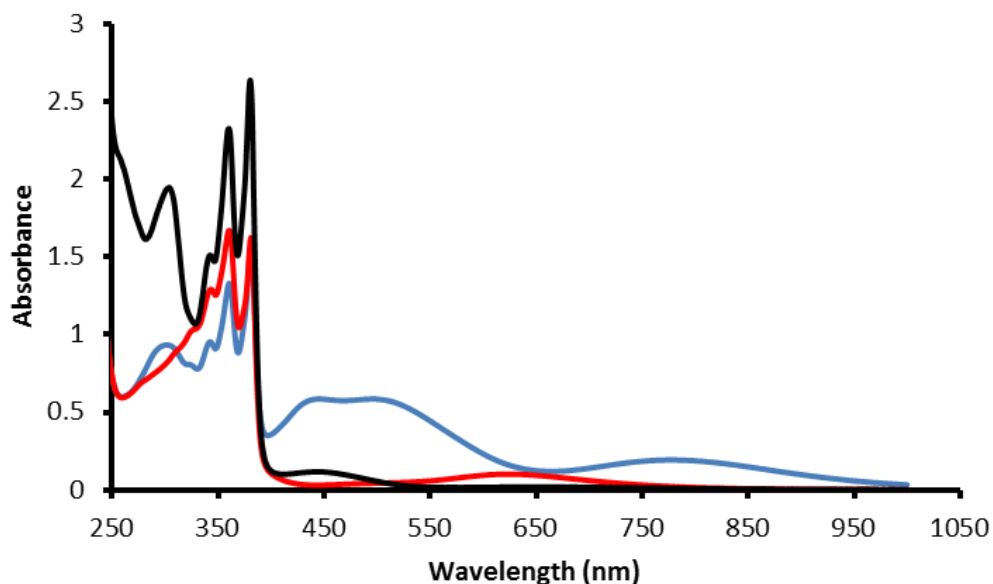
Figure 2-24. UV-visible spectra of compounds **67** (blue line), **68** (red line), and **66** (black line) recorded in CH_2Cl_2 (1×10^{-4} M).

Compound **67** has additional absorption peaks corresponding to the NDI-acetylene entity that are observed at λ_{max}= 636 nm (1.95 eV). Compound **68** displayed similar peak profile to **66** providing a λ_{max} of 445 nm (2.79 eV). This compound exhibited an additional absorption peak at 506 nm and maxima λ_{max}= 791 nm (1.57 eV), reflecting the effective of conjugation to the TCNE and TCNQ units. It is worth noting that the onset wavelength of these compounds (Figure 2-24), corresponds to an optically determined band gap energy (Eg^{opt}= 1242/ λ_{onset}) (Table 2-3).

Table 2-3. UV-visible spectra data of compounds **66**, **67**, and **68** recorded in CH_2Cl_2 (1×10^{-4} M). Where the λ_{abs} is absorption wavelength (nm), λ_{Max} is maximum absorption wavelength (nm), and Eg^{opt} optically determined band gap energy (eV).

Compounds	λ_{abs1} (nm)	λ_{abs2} (nm)	λ_{abs3} (nm)	λ_{abs4} (nm)	λ_{abs5} (nm)	λ_{abs6} (nm)	λ_{abs7} (nm)	λ_{abs7} (nm)	Band gap (eV)
66	298	340	361	380	440	---	---	---	2.82
67	237	343	360	381	636	---	---	---	1.95
68	237	301	343	360	381	445	506	791	1.57

The photophysical behaviour was investigated by fluorescence spectroscopy recorded in 10^{-5} M solution in DCM. It can be seen that the TCNE and TCNQ units played an important role in modulating the fluorescence properties of the parent unit **66**. As shown in Figure 2-25, the fluorescence of **67** and **68** are quenched strongly compared to NDI-acetylene-ferrocene **66**.
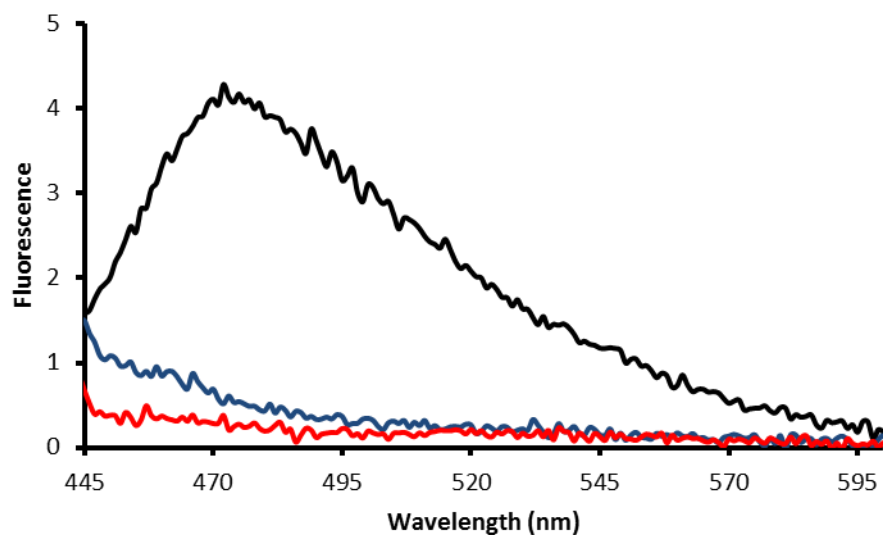
Figure 2-25. Fluorescence spectra recorded for compounds **67** (blue line), **68** (red line), and **66** (black line) in CH_2Cl_2 (1×10^{-5} M) at excitation wavelength = 360 nm.

2.3.2.2. Electrochemical Studies of 67 and 68

The redox properties of the new chromophores **66**, **67** and **68** were investigated by cyclic voltammetry (CV) using tetrabutylammonium hexafluorophosphate (n-Bu_4NPF_6) as a supporting electrolyte and ferrocene (Fc^+/Fc) as internal reference in CH_2Cl_2. All three compounds **66**, **67** and **68** were reduced in well-defined reversible one-electron reduction steps, with the first reduction occurring at $E_{1/2}$= -1.08 V for **66**, $E_{1/2}$= -0.91 V for **67**, and $E_{1/2}$= -0.74 V for **68** (Figure 2-26, Table 2-4).
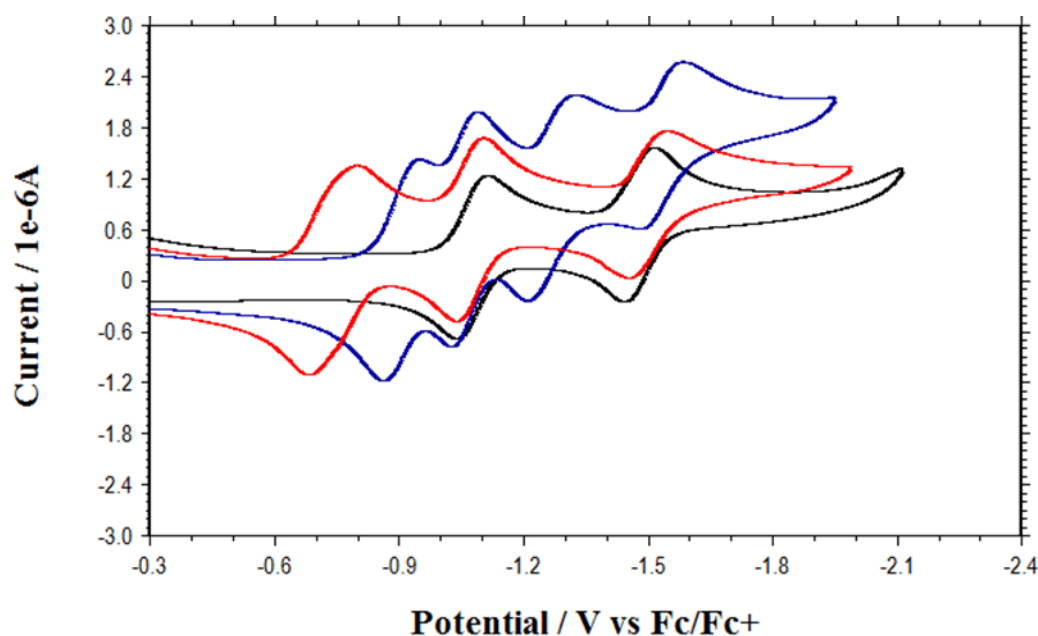
Figure 2-26. Cyclic voltammogramms of compounds **67** (blue line), **68** (red line), and **66** (black line) recorded using a glassy working electrode, an Ag wire as a reference electrode and a Pt wire as a counter electrode. Recorded in CH_2Cl_2 (1×10^{-4} M) with 0.1M (n-Bu_4NPF_6) as a supporting electrolyte at 20 °C, and a scan rate of 0.1 Vs^{-1}.

Compound **66** displayed two reversible redox waves at $E_{\frac{1}{2}}$= -1.08 V for the reduction of NDI moiety. This corresponds to a LUMO energy of E_{LUMO}= -3.72 eV. Compound **66** displayed irreversible oxidation peaks at +0.14 and +0.50 V, this corresponds to a HOMO energy of E_{HOMO}= -4.94 eV, resulting in an electrochemically determined band gap energy of E_{gap}= 1.22 eV. Compound **67** displayed two reversible redox waves at $E_{\frac{1}{2}}$= -0.91 V for the reduction of NDI-TCNE moiety and this corresponds to a LUMO energy of E_{LUMO}= -3.89 eV. This process displayed irreversible oxidation peaks at +0.48 V, this corresponds to a HOMO energy of E_{HOMO}= -5.28 eV, resulting in an electrochemically determined band gap energy of E_{gap}= 1.39 eV. Compound **68** displayed a reversible redox wave at $E_{\frac{1}{2}}$= -0.74 V. This represents a reduction of NDI-TCNQ moiety corresponding to a LUMO energy of E_{LUMO}= -4.06 eV. Moreover, it displayed an irreversible oxidation peak at +0.34 V, corresponding to a HOMO energy of E_{HOMO}= -5.14 eV and an electrochemically determined band gap energy of E_{gap}= 1.08 eV (Table 2-4).

Table 2-4. Electrochemical data (CV) of compounds **66**, **67**, and **68** recorded in CH_2Cl_2 (+0.1M n-Bu_4NPF_6) vs.Fc^+/Fc at scan rate v = 0.1 V s^{-1}.

Compounds	$E^1_{1/2}$ [V]	$E^2_{1/2}$ [V]	$E^3_{1/2}$ [V]	$E^4_{1/2}$ [V]	E LUMO eV	E HOMO eV	E gap eV
66	-1.08	-1.48	-----	-----	-3.72	-4.94	1.22
67	-0.91	-1.06	-1.27	-1.54	-3.89	-5.28	1.39
68	-0.74	-1.08	-1.50	-----	-4.06	-5.14	1.08

2.3.2.3. Molecular Modelling of compounds 66, 67, and 68

The electron distribution was calculated using density functional theory (DFT) in order to study the electron delocalization on molecules **66**, **67** and **68**. In order to simplify the calculation, the long alkyl chain (octyl) was replaced by a methyl group in the molecules. The MO electron density plots reveal that the LUMO is completely delocalized across the naphthalenediimide core and the computed LUMO energy for **66** was E_{LUMO}= -3.40 eV (Figure 2-27). Inspection of the HOMO densities for this system showed that π-orbitals were delocalized along the ethynyl ferrocene and the computed HOMO energy for **66** was E_{HOMO}= -5.30 eV (Figure 2-28).
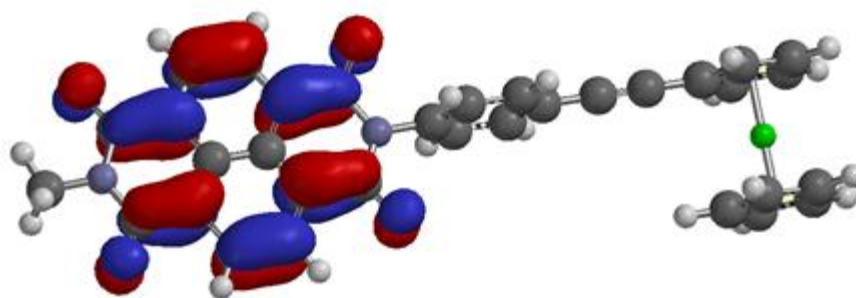
Figure 2-27. DFT B3LYP 6-311G calculation of **66** showing LUMO location
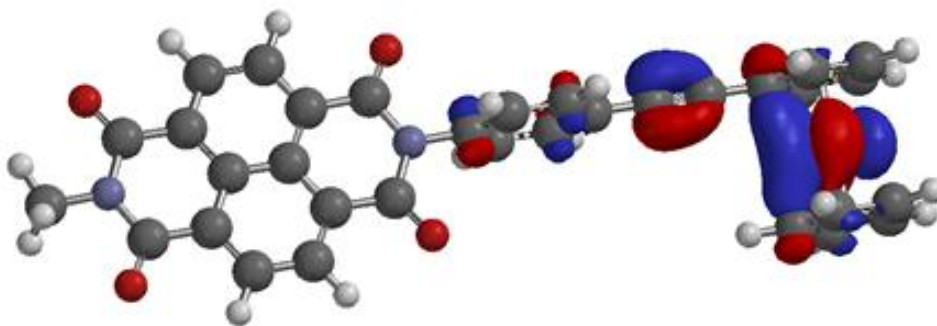
Figure 2-28. DFT B3LYP 6-311G calculation of **66** showing HOMO location

The MO electron density plots revealed that the LUMO was completely delocalized across the naphthalenediimide core and the computed LUMO energy for **67** was E_{LUMO}= -3.80 eV (Figure 2-29). Inspection of the HOMO densities for this system showed that π-orbitals were delocalized along the ferrocene unit and the computed HOMO energy for **67** was E_{HOMO}= -6.0 eV (Figure 2-30).
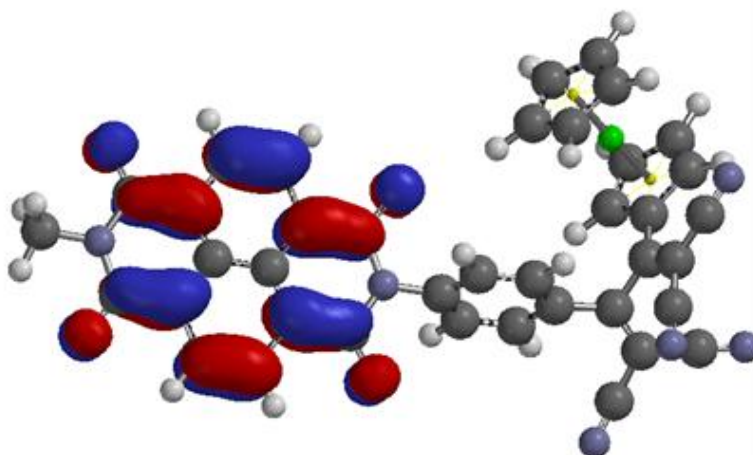
Figure 2-29. DFT B3LYP 6-311G calculation of **67** showing LUMO location
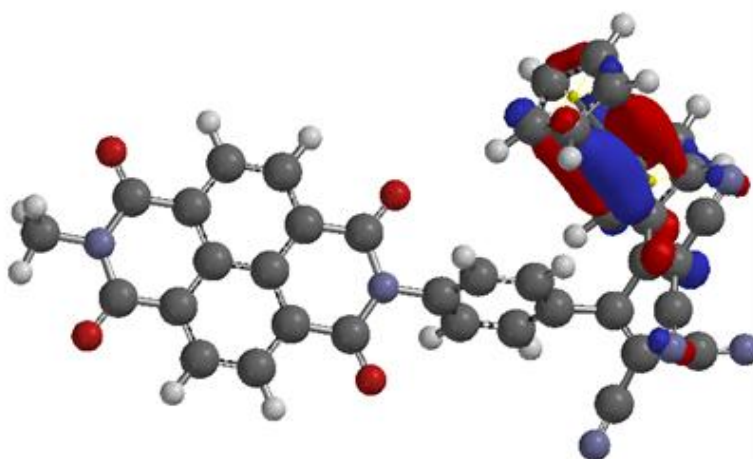
Figure 2-30. DFT B3LYP 6-311G calculation of **67** showing HOMO location

The MO electron density plots revealed that the LUMO was completely delocalized across the naphthalenediimide core and the computed LUMO energy for **68** was E_{LUMO}= -3.80 eV (Figure 2-31). Inspection of the HOMO densities for this system showed that π-orbitals were delocalized along the ferrocene unit and the computed HOMO energy for **68** was E_{HOMO}= -6.1 eV (Figure 2-32).
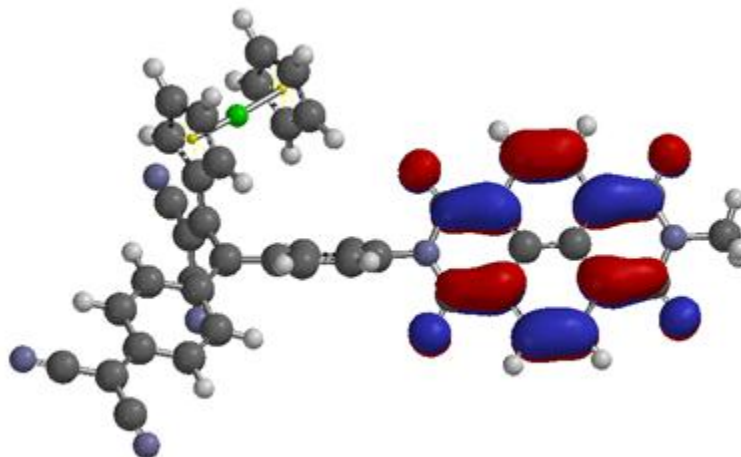
Figure 2-31. DFT B3LYP 6-311G calculation of **68** showing LUMO location
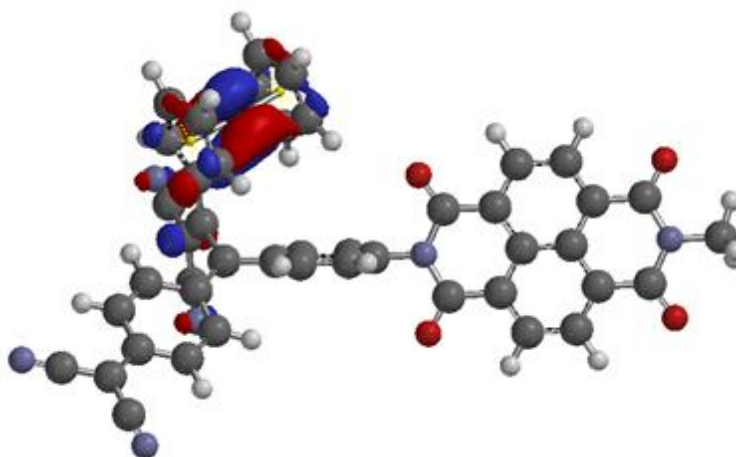
Figure 2-32. DFT B3LYP 6-311G calculation of **68** showing HOMO location

2.3.3. Synthesis and characterisation of thienyl-NDI derivatives

2.3.3.1. Synthesis of compound 69

Compound **69** was synthesised using the same cross-coupling method used for the synthesis of compounds **63** and **66**. The newly designed donor-acceptor chromophore was prepared from coupling of commercially available 3-ethynylthiophene with **62** at 80 ºC using CuI/10%Pd/C and Ph₃P as the catalyst to afford **69** in high yield (61%) (Scheme **2-8**). Different methods were attempted using different organic solvents (e.g. DCM, THF, DMF, and toluene) to add TCNE and TCNQ to compound **69**. Unfortunately the attempts to synthesise **70** and **71** were unsuccessful (Scheme 2-8).
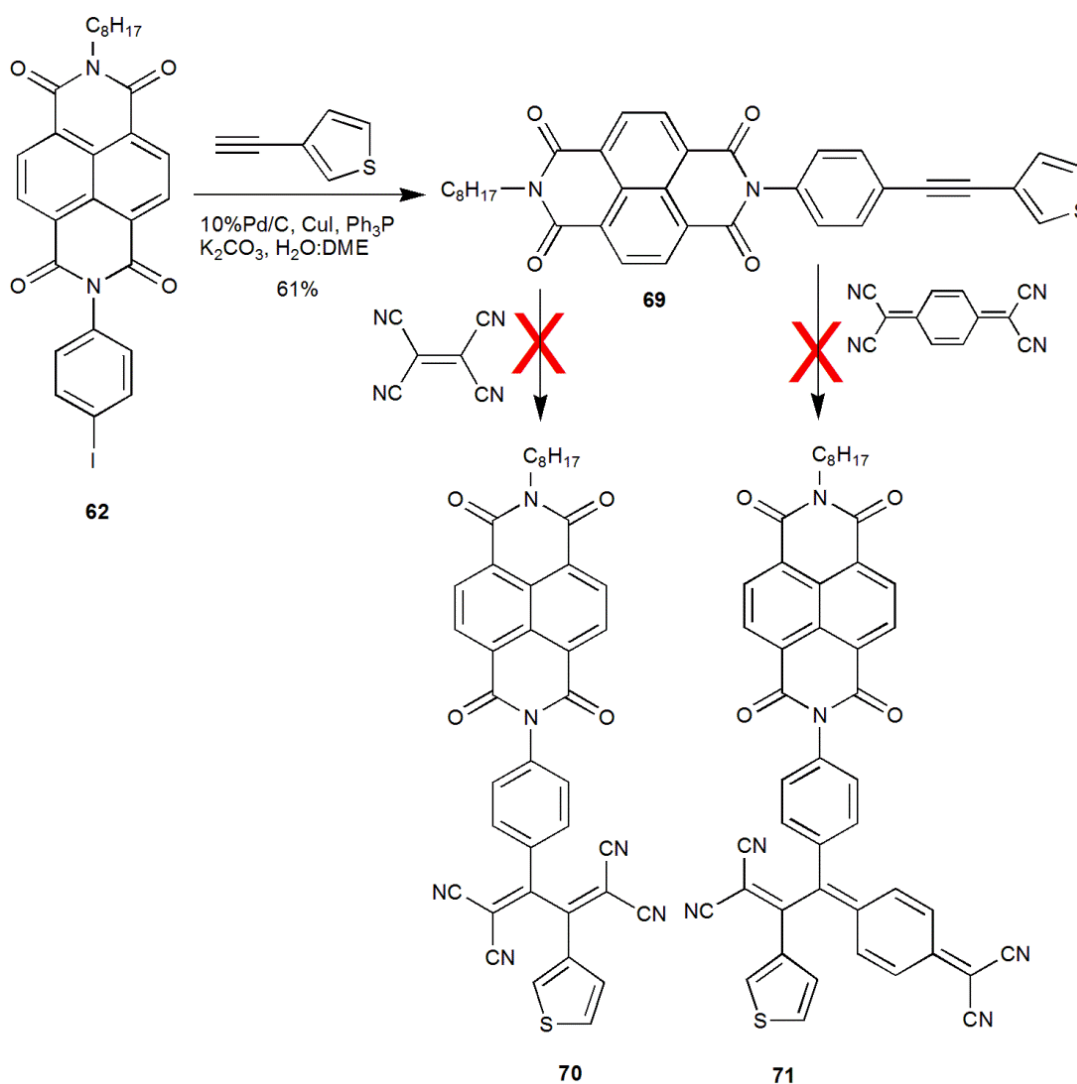
Scheme 2-8. Synthesis of compound **69**.

2.3.3.2. Polymerisation of 69

The thiophene unit can play an important role in a chromophore, where the acetylene is conjugated with the sulphur atom effectively providing aromatic stability and the acetylene helps in the extension of the conjugation. The design of macromolecules (like compound **69**) consisting of NDI, acetylene and thiophene moieties is interesting because such polythiophenes could have good thermal and chemical stability and relative ease of functionalization. Furthermore, polyconjugated chains can exhibit third-order non-linear behaviour. In view of these characteristic the functionalization of polythiophenes with non-linear optical chromophores may be of interest in the attempt to combine different interesting properties in one material and to achieve multifunctional polymers. Generally, the non-linear optical chromophore chemically attached to the backbone of polymer seems to be very promising for these purposes.

In this chapter we report the polymerisation using 4 equivalents of $FeCl_3$ and two different thiophene monomers: (a) compound **69** (1 equivalent) and (b) 4 equivalents of the commercially available 3-hexylthiophene (3HT) **72**. The polymerisation was achieved using a mixture of nitromethane/carbon tetrachloride to afford polymer **73** in high yield (95%) (Scheme 2-9). Soxhlet extraction after polymerisation with polar solvents (methanol, acetone, and DCM) was found to effectively fractionate the polymer and remove residual catalyst.
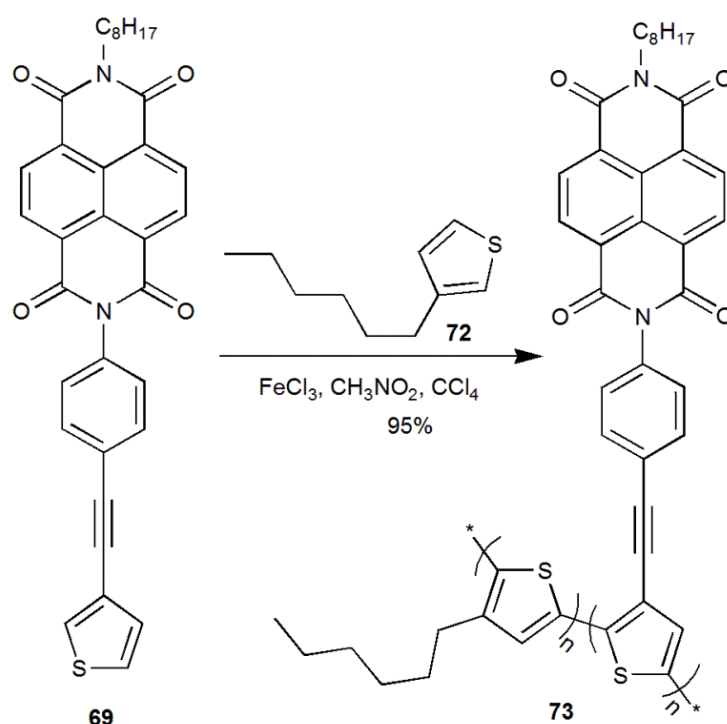
Scheme 2-9. Chemical polymerisation of monomer **69**.

The average molecular weight was determined by gel permeation chromatography in THF using polystyrene as reference. This provided an average molecular weight *(Mw)* = 24972 g/mol and the polydispersity index (*PDI*) = 2.49 (Figure 2-33).
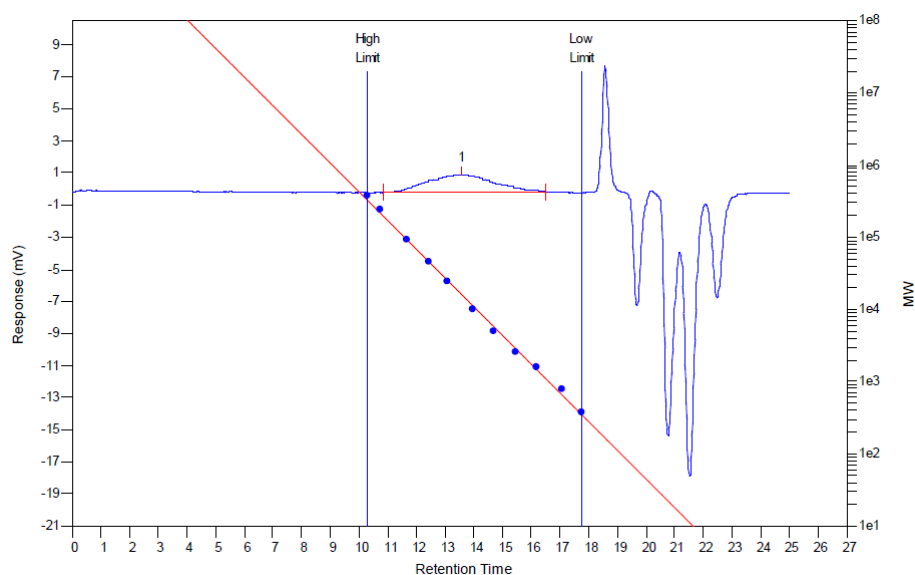
Figure 2-33. Molecular weight determination of polymer **73** by GPC.

2.3.3.3. Spectroscopic studies of 69, 72 and polymer 73

The ^{1}H NMR and ^{13}C NMR spectra displayed the expected signals for **69**. The ^{1}H NMR of the polymer **73** displayed the expected broad signals peaks and the relative integration of these peaks was useful in confirming the identity of the polymer **73**. The absorption spectra of the compounds **69,73**, and **72** was studied by UV-vis spectroscopy in CH_2Cl_2 (Figure 2-34, Table 2-5). Compound **72** has a maxima for the π-π* transition at 237 nm while compound **69** displayed absorption band in the 237-380 nm region with a maxima for the π-π* transition at λ_{max}= 380 nm and at 359 nm. Polymer **73** UV-vis spectra displayed a broad band at λ_{max}= 430 nm.
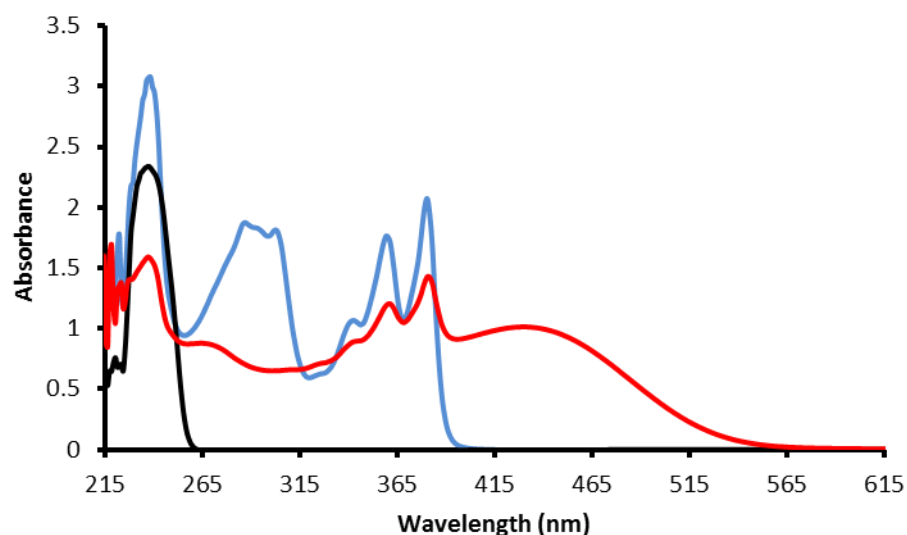
Figure 2-34. UV-visible spectra of compounds **69** (blue line), polymer **73** (red line), and **72** (black line) recorded in CH_2Cl_2 ($1x10^{-4}$ M).

Table 2-5. UV-vis spectra data of compounds **69**, **73**, and **72** recorded in CH_2Cl_2 ($1x10^{-4}$ M). Where the λ_{abs} is absorption wavelength (nm), λ_{Max} is maximum absorption wavelength (nm), and Eg^{opt} optically determined band gap energy (eV).

Compounds	λ_{abs1} (nm)	λ_{abs2} (nm)	λ_{abs3} (nm)	λ_{abs4} (nm)	λ_{abs5} (nm)	λ_{abs6} (nm)	Band gap (eV)
72	237	---	---	---	---	---	5.24
69	237	286	302	341	359	380	3.27
73	237	269	342	361	381	430	2.89

2.3.3.4. Electrochemical Studies of 69, 72, and polymer 73

The redox properties of the new chromophores **69** and **73** were investigated using cyclic voltammetry (CV) using tetrabutylammonium hexafluorophosphate (n-Bu$_4$NPF$_6$) as a supporting electrolyte and ferrocene (Fc$^+$/Fc) as internal reference in CH_2Cl_2.

Compounds **69** and **73** were reduced in well-defined reversible one-electron reduction steps (Figure 2-35, Table 2-6). Compound **69** displayed two reversible redox waves at $E_{1/2}$= -1.06 V and $E_{1/2}$= -1.46 V for the two one-electron reduction of **69** moiety and this corresponds to a LUMO energy of E_{LUMO}= -3.74 eV. Polymer **73** displayed two reversible redox waves at $E_{1/2}$= -1.09 V and $E_{1/2}$= -1.47 V for the two one-electron reduction, this corresponds to a LUMO energy of E_{LUMO}= -3.70 eV. On the other hand, it displayed

irreversible oxidation peaks at +0.31 corresponding to a HOMO energy of E_{HOMO}= -5.11 eV, resulting in an electro-chemically determined band gap energy of E_{gap}= 1.41 eV.
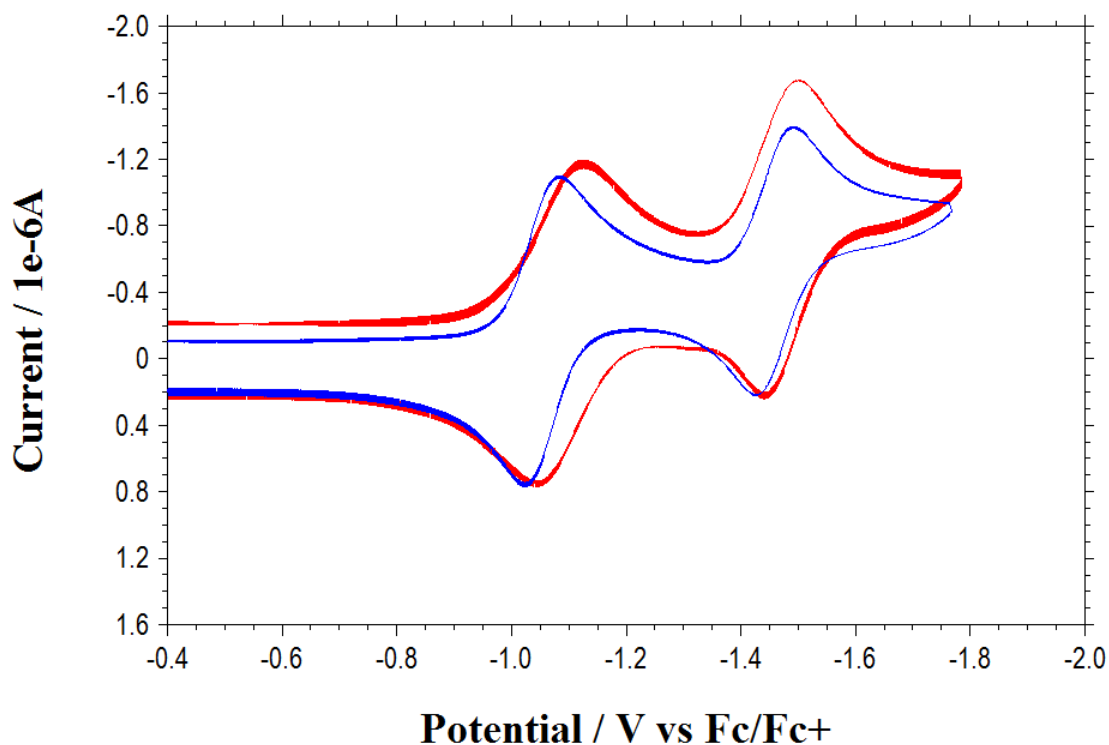
Figure 2-35. Cyclic voltammogramms of compounds **69** (blue line), and **73** (red line) recorded using a glassy working electrode, an Ag wire as a reference electrode and a Pt wire as a counter electrode. Recorded in CH_2Cl_2 ($1x10^{-4}$ M) with 0.1M (n-Bu$_4$NPF$_6$) as a supporting electrolyte at 20 °C, and a scan rate of 0.1 Vs^{-1}.

Table 2-6 Electrochemical data (CV) of compounds **69** and **70** recorded in CH_2Cl_2 (+0.1M n-Bu$_4$NPF$_6$) vs.Fc$^+$/Fc at scan rate v = 0.1 V s^{-1}.

Compounds	$E^{1}_{\frac{1}{2}}$ [V]	$E^{2}_{\frac{1}{2}}$ [V]	E_{LUMO} eV	E_{HOMO} eV	E_{gap} eV
69	-1.06	-1.46	-3.74	----	----
70	- 1.09	- 1.47	-3.70	-5.11	1.41

2.3.3.5. Attempted electrochemical polymerisation of 69
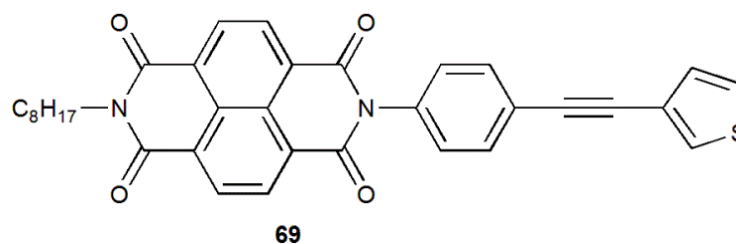
Figure 2-36. Structure of compound **69**.

We have tried to electrochemically polymerise **69** on a glassy carbon working electrode surface (Figure 2-36). Compound **69** displayed two reversible redox waves at $E_{1/2}$= - 0.76 V and $E_{1/2}$= -1.20 V for the two one-electron reduction of the **69** moiety on a glassy carbon working electrode, in acetonitrile 10^{-4} M. This corresponds to a LUMO energy of E_{LUMO}= - 4.04 eV. Also, it is displayed irreversible oxidation peaks at +0.31 and +0.68 corresponds to a HOMO energy of E_{HOMO}= -5.11 eV, resulting in an electrochemically determined band gap energy of E_{gap}= 1.07 eV. The reduction peak of this compound showed reversible peaks as shown in the Figure 2-37. Many attempts were made to polymerize **69** in solution by electrochemical methods using different parameters, however no evidence for polymerisation was observed (Figure 2-38).

a)

b)
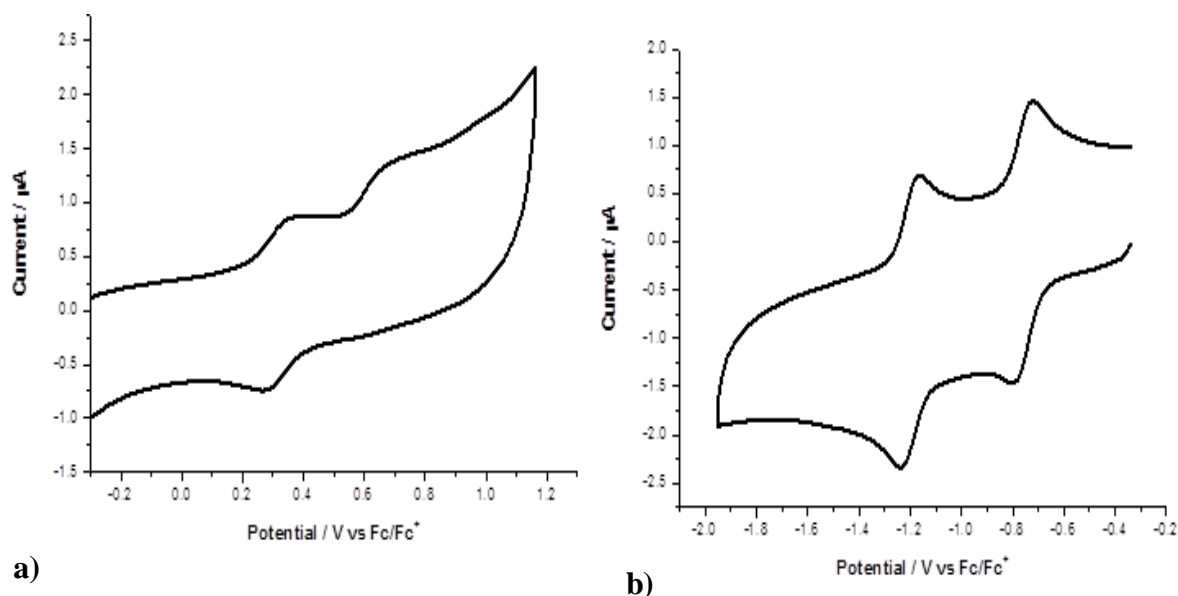
Figure 2-37. a) Oxidation and b) reduction of compound **69** on a glassy carbon working electrode, in acetonitrile 1×10^{-4}M, with 0.1 M TBAPF$_6$ as supporting electrolyte. Using an Ag wire as a reference electrode and Pt as a counter electrode, at scan rate of 100 mV s^{-1} and ferrocene (Fc$^+$/Fc) as internal reference.
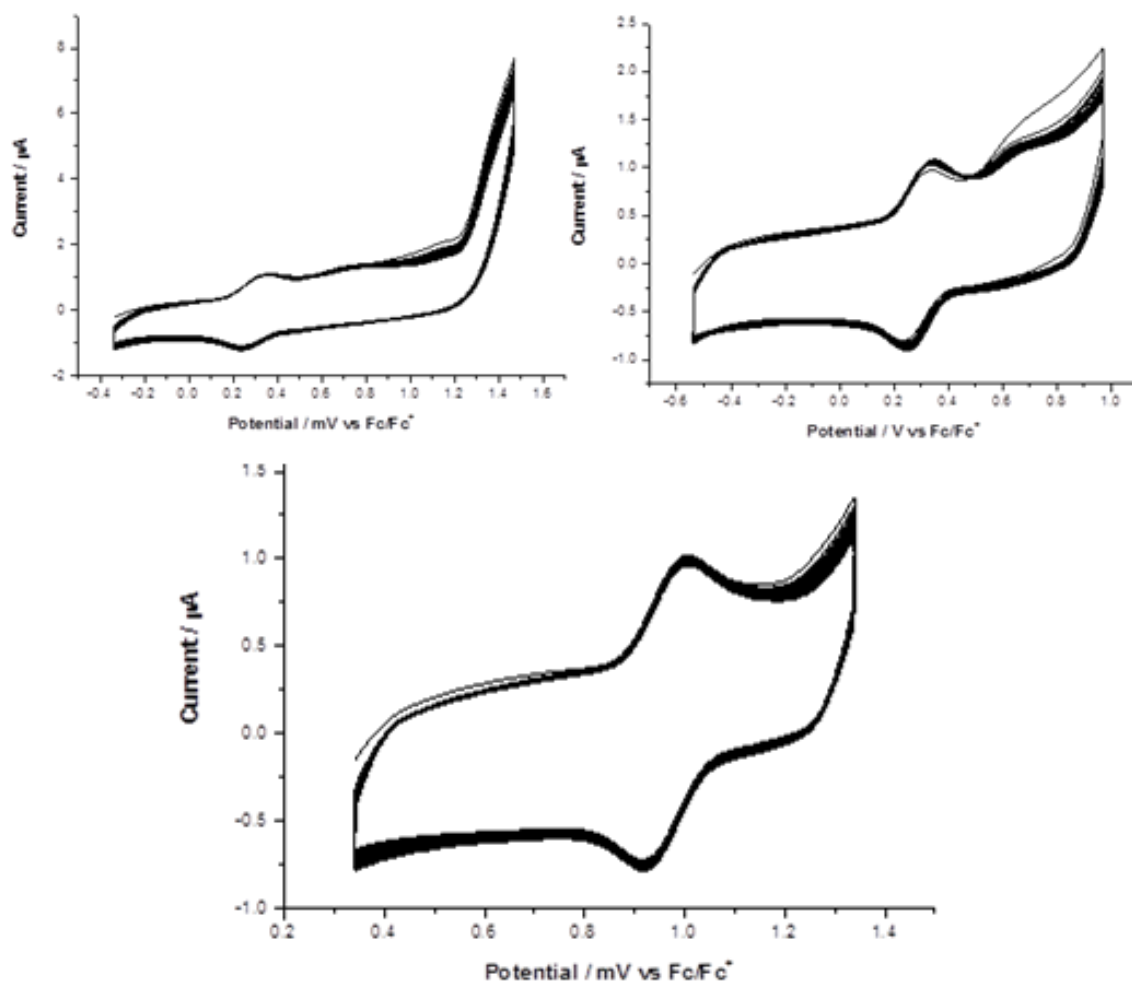
Figure 2-38. Attempts to electropolymerise **69.**

2.4. Conclusion

A range of new push-pull systems have successfully been synthesised based on an NDI core incorporating TCNE, TCNQ, dimethylaniline, ferrocene and thiophene functionalities. They were characterised using different techniques ^{1}H NMR, ^{13}C NMR, I.R, Mass, Fluorescence, UV-vis, and UV-vis-NIR spectroscopies, in addition to cyclic voltammetry, X-ray and DFT modelling.

We have shown that it was possible to polymerised compound **69** bearing an NDI side-chain substituent with 3-hexylthiophene in high yield (95%) and molecular weight (24972 g/mol). For future work, compound **64** is currently under investigation at St. Andrews University where they are fabricating the solar cells.

3. Chapter 3

Synthesis and characterisation of new flavin-functionalised dithienyl pyrroles

3.1. Introduction

3.1.1. Flavins

Flavins are yellow-coloured compounds with the basic structure of 7,8-dimethyl-10-alkylisoalloxazine units, that have a substituent on the 10 position. Flavins are redox active compounds ubiquitously found in nature and take part in many biochemical reactions such as coenzyme in enzymes and as cofactor in photoreceptors. In 1879, Riboflavin (RF) was first reported as lactochrome, a bright yellow pigment isolated from cow milk which is considering the precursor of all the biologically important flavins.

In the early 1930s, yellow pigments with bright greenish fluorescence were isolated from different sources, RF is the most abundant flavin compound found in nature. RF is found in milk, yeast, meat, beans, and peas.[107] Flavins are broadly distributed in tissues, but little is present as free riboflavin. The majority is found in flavocoenzymes, mainly as flavin adenine dinucleotide (FAD), and in lesser amounts as riboflavin-5´-phosphate, commonly called flavin mononucleotide (FMN) (Figure 3-1).[108]

In 1935, Theorell[109] demonstrated the biochemical basis for the requirement of RF as a vitamin and its role as precursor of the FMN cofactor in enzyme catalysis (coenzyme). FMN contains a ribityl chain and a phosphate group. FMN plays an important role as a cofactor in the plants, which are the blue light sensitive photoreceptors responsible for phototropism, and many other functions.[110] Krebs[111] and Warburg[112] have showed the FMN role as precursor of FAD cofactors. FAD contains a flavin moiety conjugated with an adenosine diphosphate. It is found as a redox cofactor in many enzymes which are involved in several important reactions in metabolism. However, Lumichrome and Lumiflavin are the photoproduct of photodegradation of FAD, FMN and riboflavin.

Flavins are capable of inducing one- and two-electron transfer processes. They play an important role in coupling the two-electron oxidation of most organic substrates to the one-electron transfers in the aerobic chain. Also, they can function as electrophiles and nucleophiles.[113]
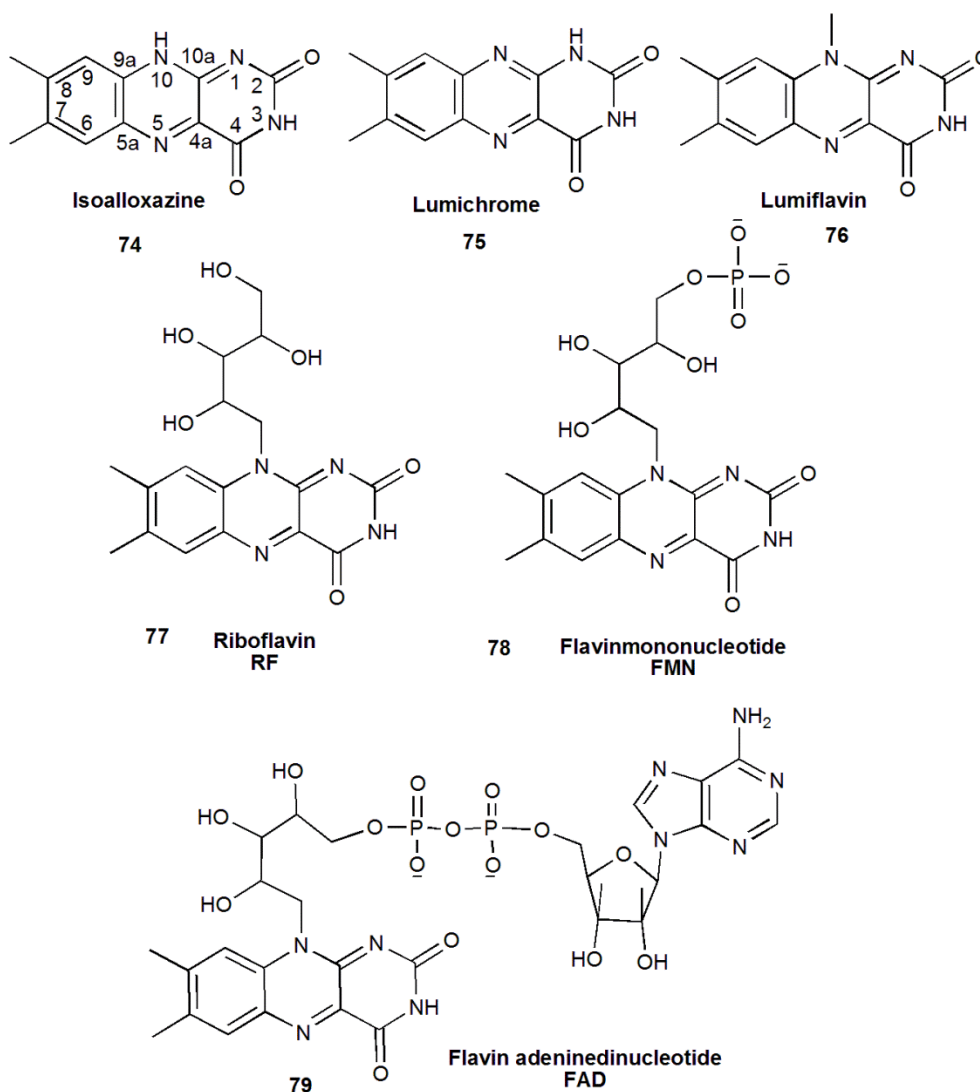
Figure 3-1. Chemical structures of riboflavin (RF), flavin mononucleotide (FMN), flavin adenine dinucleotide (FAD), lumichrome and lumiflavin along with the isoalloxazine moiety structure.

3.1.1.1. Physical and chemical properties of flavins

The chemical entity responsible for the varied biological activity of flavins is the isoalloxazine moiety. RF and its derivatives FMN and FAD have been recognized by their ability to participate in both one- and two-electron transfer processes. The isoalloxazine ring promotes the absorption in the visible wavelength region, with two main absorption maximum at ~ 360-390 nm and at ~ 440-470 nm. The absorption spectrum of RF in aqueous solution consists of four peaks at 446 nm, 375 nm, 265 nm, and 220 nm, respectively, which possess high molar extinction coefficients ($> 10^4$ M^{-1} cm^{-1}) indicative of π-π* transitions. In FAD, the adenine also contributes to the absorption spectrum in the UV spectral region. The absorption spectra of RF, FAD, FMN, Lumichrome and Lumiflavin are shown in Figure 3-1. In the visible region, free FMN absorbs maximally at

373 nm and 445 nm (ε= 10,400 and 12,500 M^{-1} cm^{-1}, respectively). Free FAD has maxima at 375 nm and 450 nm (ε= 9300 and 11300 M^{-1} cm^{-1}, respectively). The high values of molar absorptivities of riboflavin indicate that the molecule undergoes a π-π* electronic transition. Generally, symmetry and/or overlap restrictions make the n-π* transitions low probability; however, they are possibly intense in flavins due to the lack of molecular symmetry. The environment of flavin chromophore (e.g. pH, solvent, hydrogen bonding) may influence the position of the absorption maxima and the associated molar absorptivities.[114]

(a)   (b)
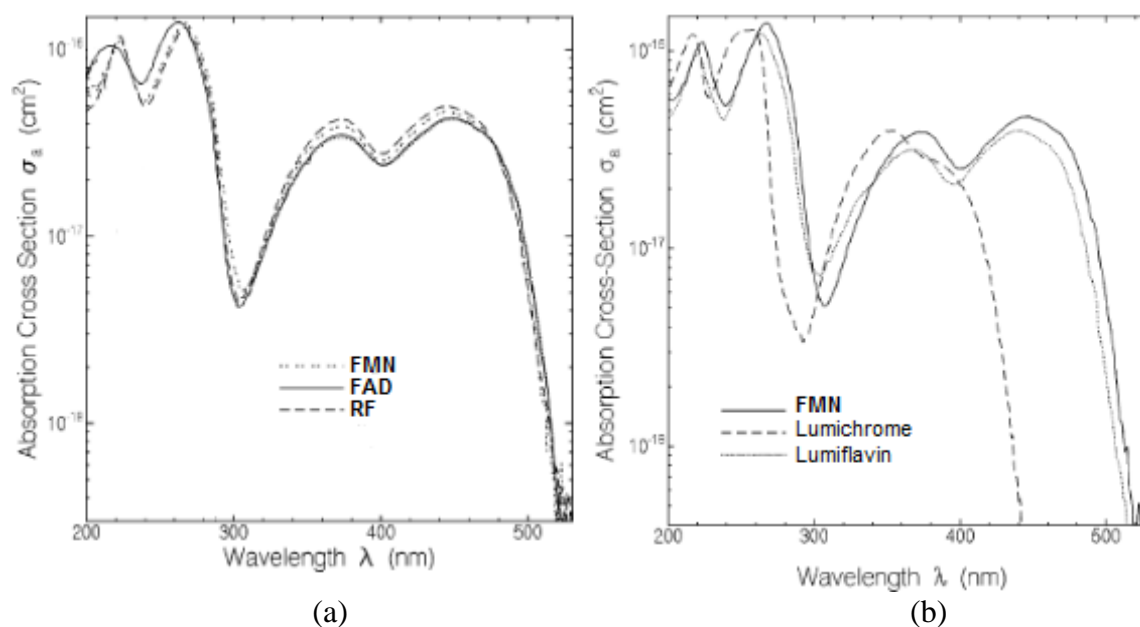
Figure 3-2. Absorption spectra for RF, FAD, FMN, lumiflavin in aqueous solutions at pH 7 and lumichrome in bi-distilled water.(a) FMN, FAD, and RF(b)FMN, lumichrome, and lumiflavin.[115, 116]

Figure 3-3 shows the normalized fluorescence quantum distributions of RF, FAD, FMN, lumiflavin and lumichrome in aqueous solution. The fluorescence quantum yields in aqueous solution buffered to pH 8 are about 0.26 (RF), 0.27 (FMN), 0.032 (FAD), 0.235 (lumiflavin) and 0.049 (lumichrome).[115, 116]

The absorption and fluorescence characteristics of riboflavin have indicated three different forms for this molecule exist in aqueous solution. At low pH (pKa= 0.4), an equilibrium has been observed between the cationic form (RF$_{ox}$H$_2$$^+$) and the neutral form (RF$_{ox}$H). At high pH (pKa= 7.5), an equilibrium has been observed between the neutral form and the anionic form (RF$_{ox}$$^-$). The neutral dipolar form of riboflavin is fluorescent only and the cation and anion are non-fluorescent. Flavins exhibit an intense yellow green fluorescence at λ_{max}= 520 nm in aqueous solution. The emission maximum is shifted to shorter wave-

lengths in solvents that are less polar than water. It exhibits an orange-red phospho-
rescence with a maximum at 615 nm.
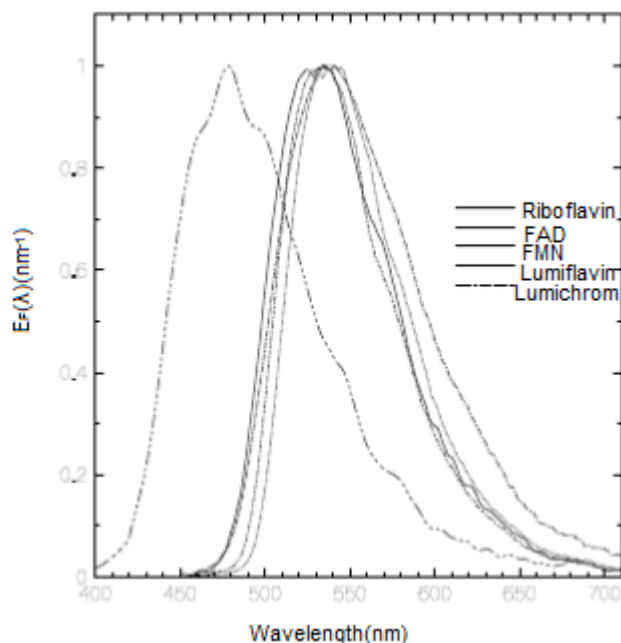
Figure 3-3. Normalized Fluorescence quantum distribution of RF, FMN, FAD, Lumichrome in aqueous solution at pH 8 and FAD in pH 7.[115, 116]

3.1.1.2. The redox system of flavin

Flavin adenine dinucleotide (FAD) and flavin mononucleotide (FMN) are important redox co-factors in many enzymes. Several variables can effect their redox properties (UV absorption and reactivity), such as substitution, non-covalent interactions (for example hydrogen bonds), and the nature of the surrounding protein. For each redox state of flavins; oxidized, one-electron reduced (semiquinone) and two electron reduced (flavohydroquinone), they can exist in various protonation forms depending on the pH as schematized below (Scheme 3-1).[117]
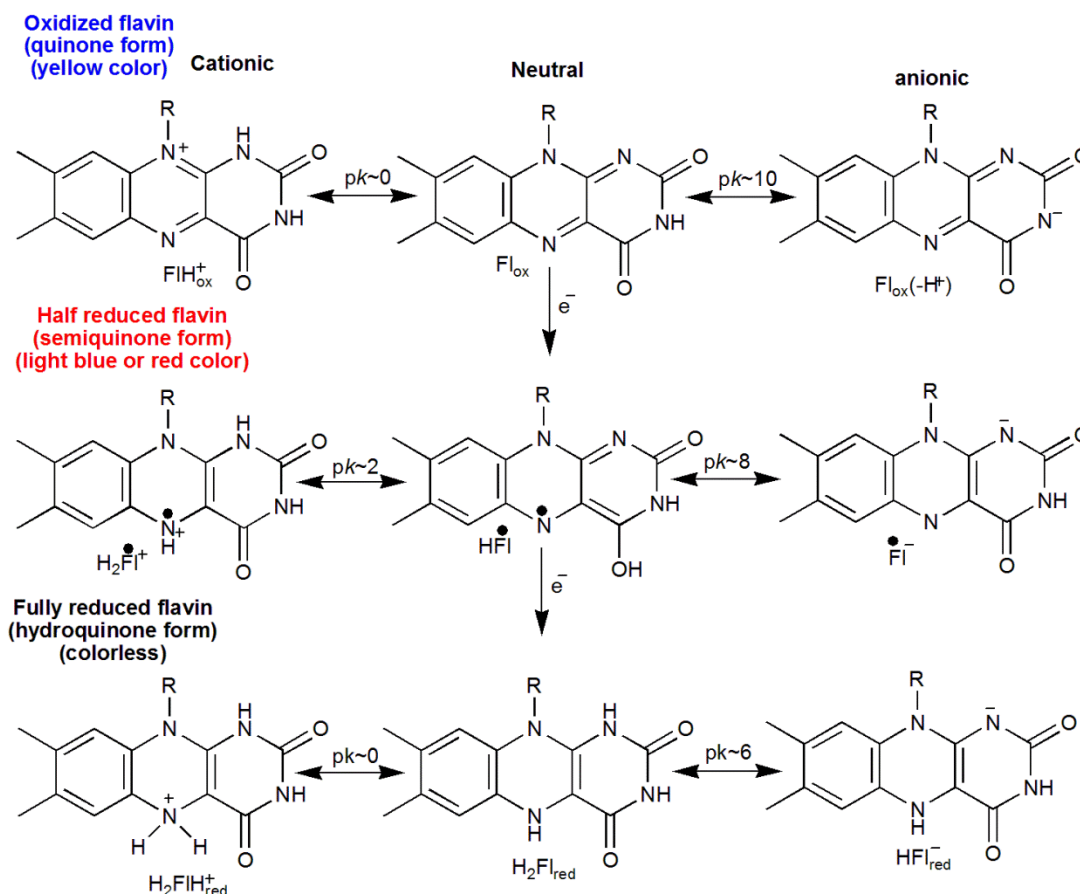
Scheme 3-1. The structures of the neutral, anionic and cationic flavin species in the three redox states.

The ability of flavin to participate in one-electron transfer reactions indicates the existence of semiquinone-type oxidation states. In free solution, that is when not enzyme-bound, a mixture of oxidized flavins and reduced flavins very rapidly leads to equilibrium, containing also flavin radicals. For free flavins, the equilibrium is shifted to the left and only 5% of the radical form is present in an equimolar mixture of oxidized and reduced flavins at pH 7.

The neutral state exists at pH between 1 and 9, however, at pH > 10, the proton at (N3) is deprotonated and it forms a cation at pH < 1. The oxidized state of flavin can be reduced to a semiquinone by one electron reduction. Furthermore, at pH=2 the semiquinone protonates to form a cationic semiquinone and it is converted to an anionic form at pH=8. Flavohydroquinone produced by the two electron reduction of the oxidized flavin, which protonates at pH > 0 at (N5) and deprotonates at pH=6.7 to produce the cationic and anionic form respectively. Important spectral differences exist between the various flavin oxidation states, which are used to monitor the events occurring in enzyme catalysis using the flavin itself as a reporter (Figure 3-4).[118]
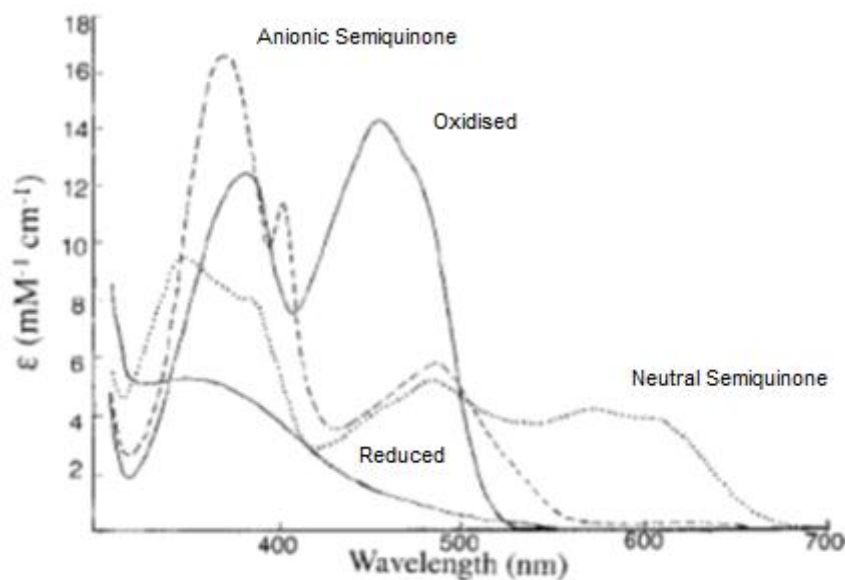
Figure 3-4. Absorption spectra of various flavin oxidation states.[119]

In addition to the redox and ionic forms, there are other electronic states, known as charge-transfer states that flavins can adopt. Charge-transfer interactions are important in catalysis, which was well documented as early as in the 1970s[120] and has been observed in many flavoenzymes. Charge-transfer states are novel electronic states that do not belong to any of the three redox states but those in which partial charge is transferred to or from one of the three redox states. Flavoenzymes catalyse electron transfer processes associated with flavin, and electron transfer occurs via the transfer of electron(s) from the HOMO of an electron donor to the LUMO of an electron acceptor. The value of redox potentials for all redox transitions of free flavins at neutral pH about -200 mV, as compared to a value of range from -500 mV to +80 mV for the protein-bound flavin cofactors.

3.1.1.3. Flavin electrochemistry

Scheme 3-2 shows the common redox and protonation states of the flavin cofactor.[121] Reduction of oxidized flavin (Fl_{ox}) in a two-electron process directly to the flavohydro-quinone anion ($Fl_{red}H^-$) can occur. Reduction can also occur sequentially in either the anionic (Fl_{rad}^-) or neutral ($Fl_{rad}H$) form via two one-electron processes involving the flavosemiquinone radical. Flavoenzymes are able to control the redox pathways that the cofactor follows, tolerating catalysis of both one- and two-electron redox processes.
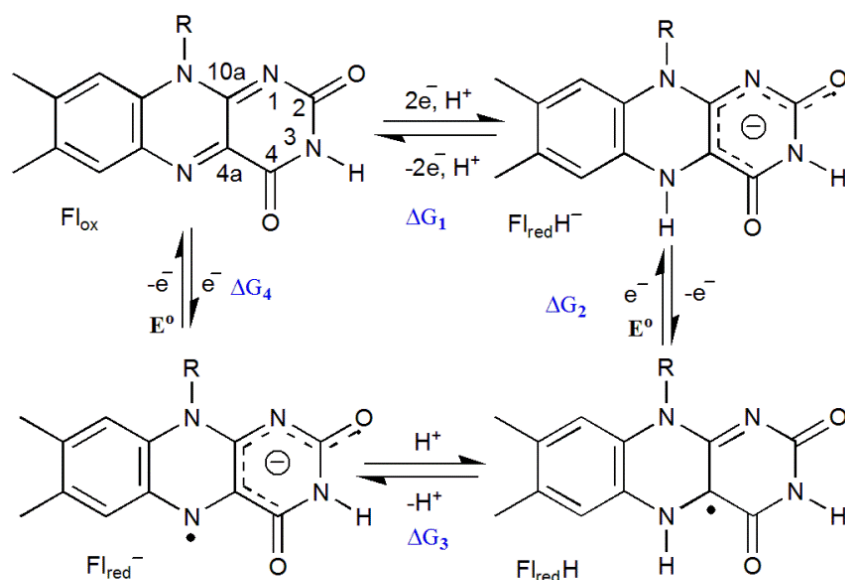
Thermodynamic cycle: $\Delta G_1 + \Delta G_2 = \Delta G_3 + \Delta G_4$

ΔG and E^o are related by the Nernst equation

$$\Delta G^o = -nFE^o = -\frac{RT}{nF} \ln K_{eq} \qquad \text{---------------3-1}$$

n = number of electrons

F = Faraday constant = 23.063 Kcal.V^{-1}.eq^{-1}

= 96.542 KJ.V^{-1}.eq^{-1}

Scheme 3-2. Common redox and protonation states of the flavin cofactor.

Rotello and co-workers[122] established that the coupled electrochemical and chemical reactions (Scheme 3-3) occurred due to the intermolecular proton transfer of the acidic imide proton of oxidized flavin Fl_{ox}, which is reduced to the radical anion Fl_{rad}^- at the electrode. The neutral radical $Fl_{rad}H$ was produced by protonation of portion of the anionic species by the imide of Fl_{ox} in bulk solution. $Fl_{rad}H$ is instantly reduced to $Fl_{red}H^-$, because it has a less negative reduction potential than Fl_{ox}, by an electrochemical-chemical-electrochemical (ece) process. This process gives rise to only one reduction wave in the cyclic voltammogram (Scheme 3-3-b). Fl_{rad}^- is oxidized at more negative potential than $Fl_{red}H^-$ during the reoxidation process, resulting in the two oxidation waves observed. The $Fl_{ox} \rightarrow Fl_{rad}^-$ couple is basically reversible; therefore the ΔG can be deduced from the half-wave potential $E_{\frac{1}{2}}$ between the reduction and the first oxidation wave via the Nernst equation (equation 3-1, Scheme 3-2).
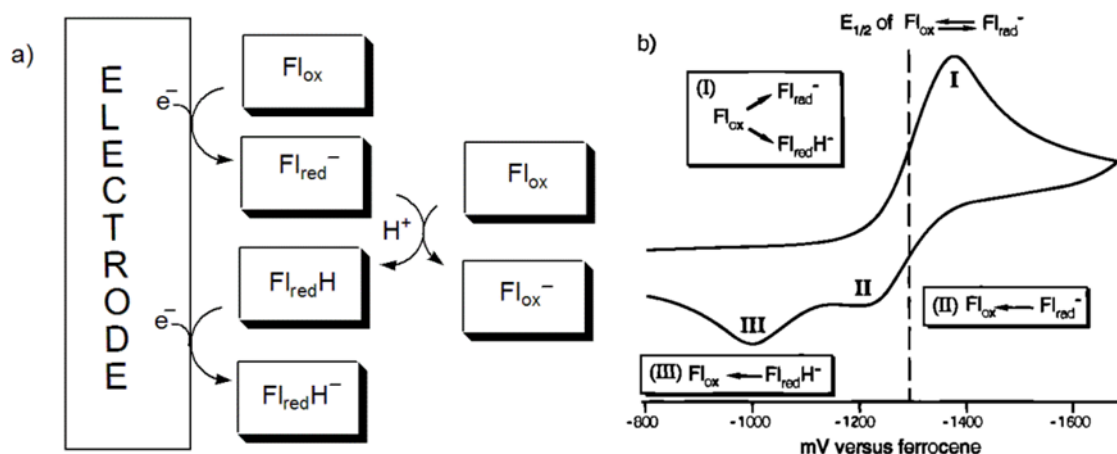
Scheme 3-3. (a) Schematic representation of the ece pathway for two-electron reduction of flavins in aprotic media and (b) cyclic voltammogram of flavin.

3.1.1.4. Flavin structure

The chromophoric part of the flavin is 7,8-dimethylisoalloxazine moiety, is an amphoteric molecule in that its xylene aromatic ring is lipophilic, while the pyrimidine subnucleus of flavin is hydrophilic (Figure 3-5).[123] The pyrimidine ring undergoes specific interactions (hydrogen bonding) with protein functional groups. The approach of such interactions and the accessibility of the pyrimidine moiety have been probed in various ways:

1. Position N(3)-H can be altered by alkylation, and the size and properties of the N(3)-substituent can be varied. Generally, most flavoproteins do not appear to accommodate substantial changes at the isoalloxazine N(3) position.

2. The carbonyl oxygen at the 2 position has been replaced with =N-R and =S. The stronger electronegativity of the sulphur can compensate for the weaker H-bonds that it forms. Also, the thiocarbonyl function is a much better nucleophile and electrophile compared to the essentially unreactive C=O group. Thus, 2-thioflavins will react with a variety of alkylating agents and are prone to oxidation. The C=S group can also easily be substituted with amines and other nucleophiles.

X	Reactant
1. S⁻	H⁺
2. Cl	S⁻², RS⁻
3. N₃	light, amino acids
4. N₂⁺	nucleophiles

Z	Reactant
1. SCN	RS⁻, MMTS, NEM, H₂O₂, Peracids
2. OH	H⁺
3. N⁻H₂	H⁺
4. N₃	light, amino acids
5. N₂⁺	nucleophiles
6. S⁻	H⁺

Reactants
1. MMTS
2. H₂O₂
3. Peracids
4. NH₂OH
5. Amines
6. RS⁻
7. SO₃⁻³
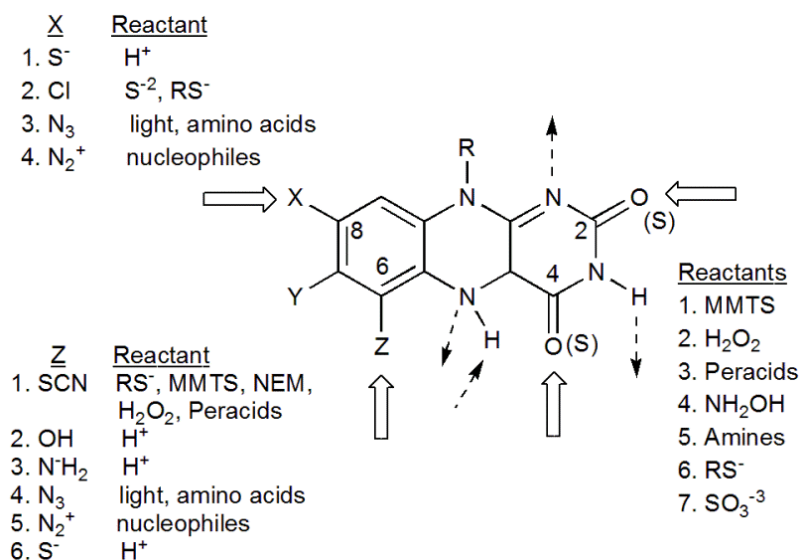
Figure 3-5. Overview of the functional groups on the flavin ring that are amenable to chemical analysis by either modification or substitution.

3. The carbonyl at the C(4) position, is more labile, than the C(2) position. The reduced species of 4-thio-flavins exhibit well defined absorption spectral bands with the maxima at 485 nm for the neutral forms and at 425 nm for the anionic forms. In contrast, the difference between the neutral and the anionic forms of reduced flavins bound to various enzymes is very difficult to determine due to the lack of particular features and the spectral similarity of both forms.

The pyrazine ring middle of the flavin system consists of the main positions of chemical reactivity. These positions are C(4a)-N(5), which are involved in electron donation and acceptance. The accessibility of the C(4a) position appears to promote formation of reactive oxygen hydroperoxides. The xylene ring is unreactive, because there are no cases in which chemical events resulting from interaction with substrate have been found.

The potential alterations can be predicted by the inductive influence of the substituent on the lowest unoccupied molecular orbital (LUMO) of the oxidized flavin or on the highest occupied molecular orbital (HOMO) of the reduced flavin. Alterations of these energies and the distribution of electron densities about the flavin ring can provide important evidence for the reaction mechanism. The modifications at all positions of the flavin ring will affect the redox potential. The chemistry and interactions of the flavin is considerably affected by the substitutions in the pyrimidine moiety.[123]

The incorporation of flavins into thiophene and their derivatives as materials for organic photovoltaic cells can offer a number of possible advantages: (1) flavins will allow increased π overlap between neighboring chains due to their planar structure, (2) it is possible to carefully fine tune the optical and electronic properties of the material by careful synthetic alteration of the structure, and (3) flavins are easy to synthesise. The combination of flavin and dithienylpyrrole rings into alternating donor acceptor copolymers will allow modulation of the band gap, and may lead to a range of highly efficient organic semiconductors suitable for use in OPV cells.[124]

3.1.2. 2,5-Di (2-thienyl) pyrroles

2,5-Di(2-thienyl)pyrroles (SNS) **83** contain thiophene and pyrrole rings interconnected through their α-positions and are of interest in the preparation from them of conductive materials (Figure 3-6).[125] SNS derivatives have been synthesised from 1,4-di(2-thienyl)-butane-1,4-dione in two steps.[126] In the first step, thiophene **80** undergoes Friedel-Crafts acylation with succinyl chloride **81** and aluminium chloride to form the di-ketone **82**. The Paal-Knorr synthesis was then undertaken by refluxing the di-ketone in ammonium acetate in glacial acetic acid and acetic anhydride to give the SNS derivatives (Scheme 3-4).[127]
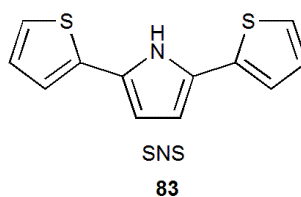
Figure 3-6. Structure of 2,5-di(2-thienyl)pyrroles (SNS) **83**.
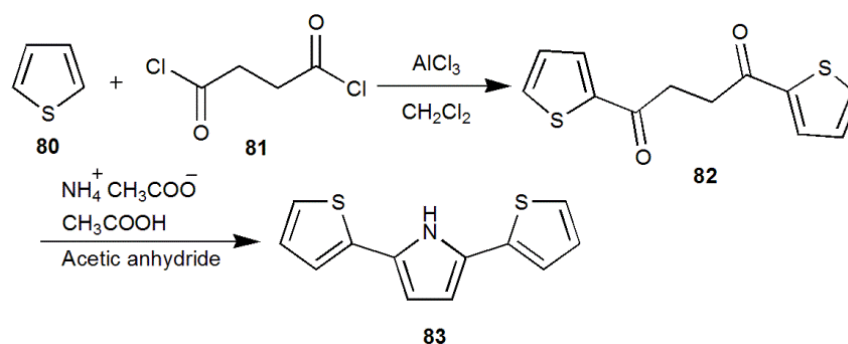
Scheme 3-4. Synthesis of SNS **83** in two steps starting from thiophene.

In 1991, Amarnath *et al.*[128] investigated the mechanism for the synthesis the pyrrole. The reaction is usually run under protic or Lewis acidic conditions, with a primary amine. The proposed mechanism suggested that the protonated carbonyl is attacked by the amine to form the hemiaminal. The other carbonyl was attacked by amine of the aminal to form a 2,5-dihydroxytetrahydropyrrole derivative which undergoes dehydration to give the corresponding substituted pyrrole (Scheme 3-5).
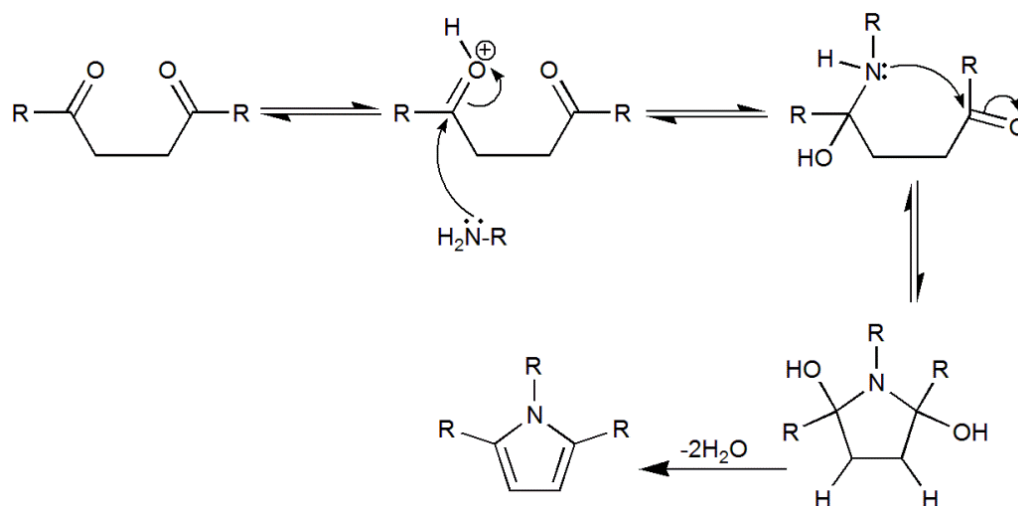
Scheme 3-5. Mechanism for the Paal-Knorr synthesis of the pyrrole.

3.1.3. 2,5-Di (2-thienyl) pyrrole derivatives

Copolymers offer an attractive strategy for obtaining novel conducting and structural properties. Copolymers can be prepared by polymerizing heterogeneous monomer units such as 2,5-bis(2-thienyl)pyrrole (SNS) (Figure 3-6).[129] The methodology of using symmetrical monomer units such as SNS facilitated the control of polymer structure and periodicity upon polymerisation of the heterogeneous monomer units. The system rises the HOMO residing on pyrrole and lowers the LUMO on thiophene, and that leads to a decrease of the band gap.[130]

There are several reasons why 2,5-di-(2-thienyl)-pyrrole derivatives are chosen for polymerisation:

1. They are easily synthesised and functionalized unit by use of the Paal-Knorr pyrrole condensation reaction, an attractive one-step procedure for introducing various bridges into the monomer.[131]

2. They are cheaper and more easily processable than terthiophene derivatives

3. They have oxidation potentials lower than the terthiophene derivatives (about +0.7 V vs SCE) and facile electrochemical polymerisation and attractive electrochromic abilities.[132]

4. The conducting polymer obtained from 2,5-bis(2-thienyl)pyrrole monomers have given rise to low band gap, easily processable, stable and highly conducting polymer.

5. Good quality film thickness of Poly-[2,5-di(2-thienyl)-pyrrole] can easily be fabricated with different solvents (such as acetonitrile, ethanol, propylene carbonate, and tetrahydrofuran) on platinum electrode and para-toluene sulphonate and lithium perchlorate ($LiClO_4$) as the supporting electrodes.[133]

A mechanism of electrochemical polymerisation proposed the existence of three resonance structures for the radical-cation formed on the basis from the molecule of the *N*-R-substituted 2,5-(2-thienyl)pyrrole. The positive charge is localized at the nitrogen atom of the pyrrole unit of the molecule and the unpaired radical electron is placed on three different carbon atoms on rings α, β', and β'' respectively (Scheme 3-6).

Connecting these radical-cations leads to the formation of either a linear structure (α–α coupling) or several branched structures (α–β', α–β'', β'–β', β''–β'', β'–β'' couplings).[134] The ratios between such structures determine the properties of the obtained polymer. The dimerization occurs with the formation of a protonated dimer, but the reaction between the radical cation and the neutral monomer is insignificant.

The obtained protonated dimer must lose two protons for continued chain growth; this process occurs more slowly than the formation of the C–C bond. This means, the formation of the new C–C bond by the pairing of two radical-cations occurs initially and is then followed by deprotonation.
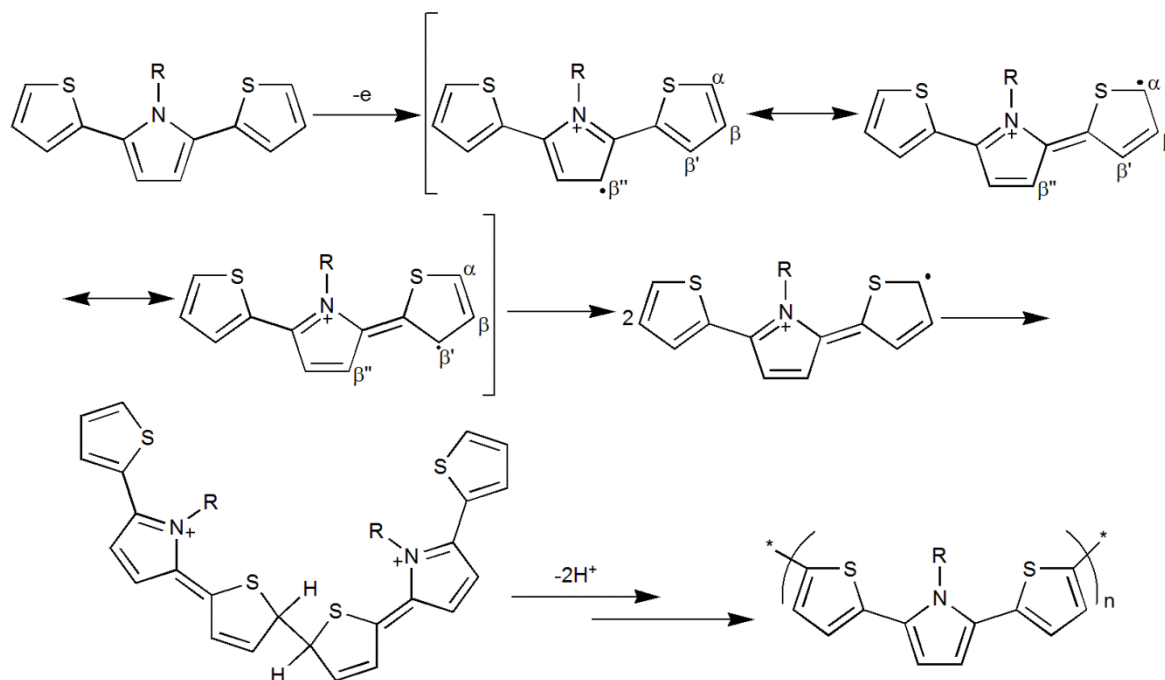
Scheme 3-6. Resonance structures of *N*-substituted-SNS and a possible electrochemical polymerisation mechanism.

Table 3-1 shows that poly(SNS) **84** exhibits the highest conductivity and poly(SSS) **85** films are within a factor of 5 compared to polythiophene, whereas poly(SMS) **87** is two orders of magnitude less conductive (Figure 3-7). In poly(N-methyl-pyrrole), the steric interactions between the hydrogens of methyl group and the adjacent rings, prevents the ring from attaining planarity in the oxidized state.[135]

X = N	SNS	**84**
S	SSS	**85**
O	SOS	**86**
-NCH₃	SMS	**87**
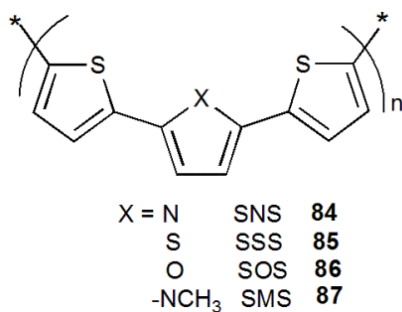
Figure 3-7. Structure of poly(SNS),(SSS),(SOS),and (SMS).

Table 3-1. Electrical conductivity of poly(SXS) films (S cm^{-1}). [135]

System	Conductivity (S cm^{-1})
Poly(SNS)	280
Poly(SMS)	1
Poly(SOS)	0.3
Poly(SSS)	20
Polythiophene	> 100
Furan	80
N-methyl pyrrole	< 0.001

Poly-SNS was used the first time in 1987 by Ferraris and Skiles [136] as a production of well-defined copolymers through oxidative copolymerisation of monomer mixtures. However, since the monomer oxidation potentials and reaction kinetics vary with heteroatom substitution the degree of polymerisation varies significantly. SNS and its polymerised form plays a key role in many areas including photovoltaic cells, electroluminescent (EL) devices, light emitting diodes, electro-chromic devices, biological and voltammetric sensors. [137-139]

Entezami *et al.*[140, 141] have studied the effects of SNS on the electropolymerisation and electrochemical behaviour of pyrrole. The resulting poly (Py-SNS)(100:1 mole ratio) **88** displayed a considerable increase in the electroactivity, conductivity, and the rate of polymerisation in comparison to polypyrrole alone (Figure 3-8).

88
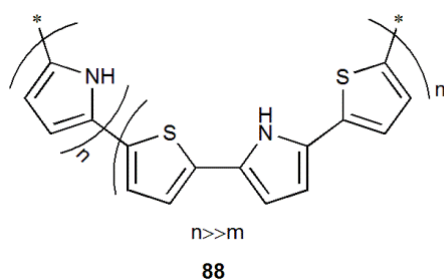
Figure 3-8. Structure of poly(Py-SNS) **88**.

Brillas *et al.*[142] reported that the electrogenerated poly(SNS) film is soluble in MeOH, acetone, THF and partially soluble in acetonitrile and insoluble in LiClO$_4$-acetonitrile couple. While the electrochemically reduced poly (SNS) is soluble in LiClO$_4$-acetonitrile couple. Kim *et al.*[143] electrochemically polymerised the conductive poly-DPB **91** from a newly synthesised 2,5-di(2-thienyl)-*1H*-pyrrole-1-yl-1-*p*-benzoic acid (DPB) **90** monomer in dichloromethane (Scheme 3-7). Poly-DPB **91** film exhibited optically determined band-

gap energy (E_g) of 2.16 eV and good stability therefore could be used in electron transporting materials and a promising candidate for both electrochromic devices and the construction of conducting polymer biosensors.
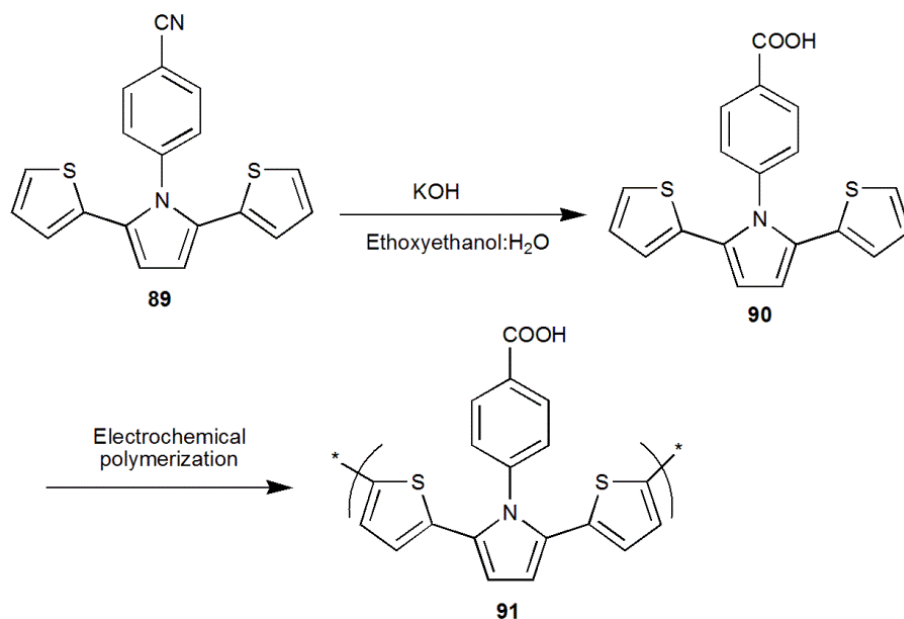
Scheme 3-7. Synthesis of DPB-polymer**.**

Recently, Camurlu and Gültekin[144] disclosed the utilization of conducting homopolymer and copolymers **93**, **94**, **95**, and **96** based on SNS **92** in electrochromic devices (ECDs) (Scheme 3-8). Four different dual type complementary colored devices were assembled in a glass/ITO/ poly(SNS-R)/PEDOT/ITO/glass configuration (Figure 3-9). The introduction of a ferrocene group on to polymer chain was found to be an effective strategy to enhance coloration efficiency. The switching speeds and stability of ECDs having the copolymers as the active layer were found to be better than the devices of corresponding homo-polymers. Also, devices assembled with homopolymers exhibited superior optical memory, and all the ECDs have good redox stability, esthetically pleasing colors and they could be operated between 0.0 V and 1.2 V.
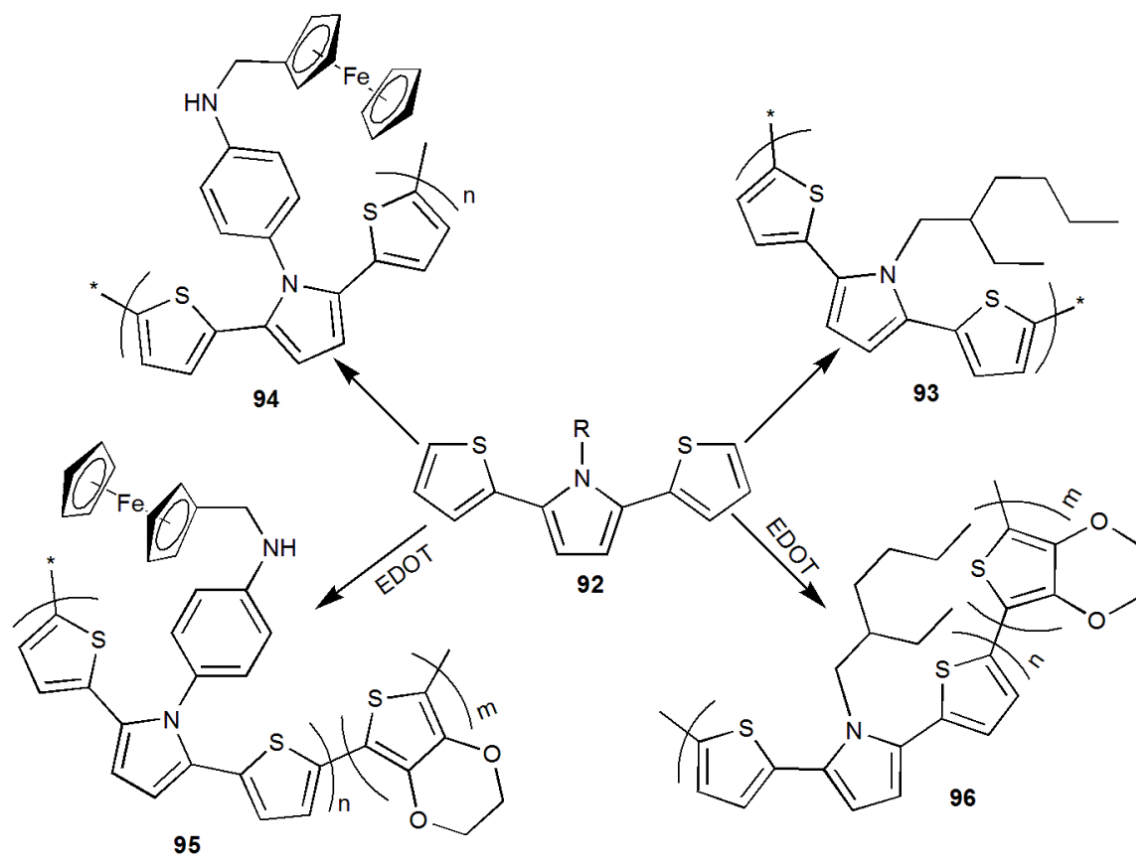
Scheme 3-8. Structures of the electrochromic polymers.
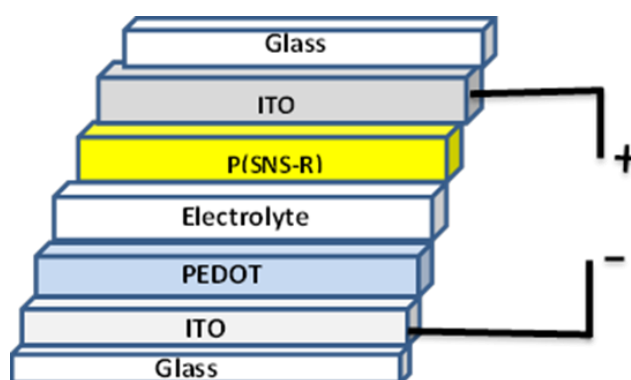
Figure 3-9. Configuration of electrochromic device.

The synthesis of Poly(SNS) derivatives as an electroactive polymeric material for ion sensing purposes has been reported.[145] These materials show clear and reversible voltammetric response towards alkali metal cations (Li^+, Na^+ and K^+) in both neat water and organic media (ethanol). Benzo-SNS-15-crown-5(SNS-Crown) **97** was electro-polymerised in TBAClO$_4$/ethanol solution to yield its corresponding polymer **99** (Scheme 3-9).
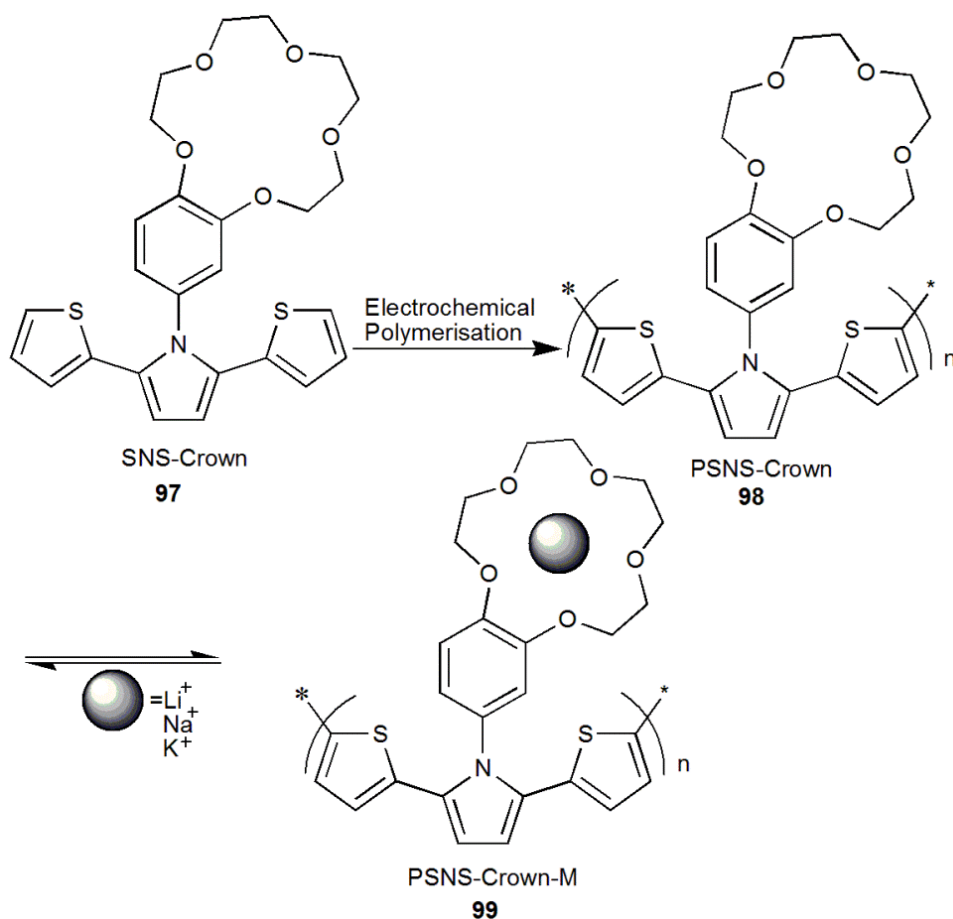
Scheme 3-9. Electrochemical polymerisation of compound **97** and ion recognition by the PSNS-Crown film to give PSNS-Crown-M.

Poly (*N*-dodecyl-2,5,-bis(2′-thienyl)pyrrole-2,1,3-benzothiadiazole) (PTPTB) **100** and P3HT **13** have been used as the energy-acceptor and energy-donor materials respectively (Figure 3-10). In energy-acceptor materials for the improvement exciton harvesting in organic-inorganic hybrid photovoltaic cells via resonance energy transfer (Figure 3-11).[146] The ability of PTPTB **100** to accept excitons from P3HT **13** was determined using a layer of PTPTB **100** inserted between the P3HT **13** and glass substrate in FTO/TiO$_2$/ PTPTB/ P3HT/Ag device (Figure 3-11).
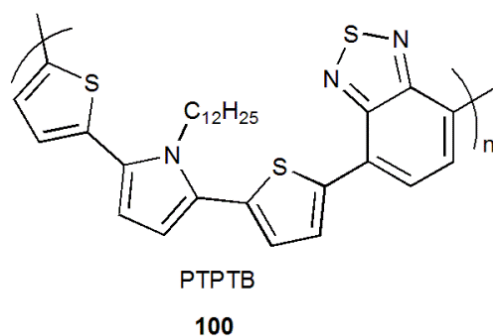
Figure 3-10. Chemical structure of PTPTB **100**.
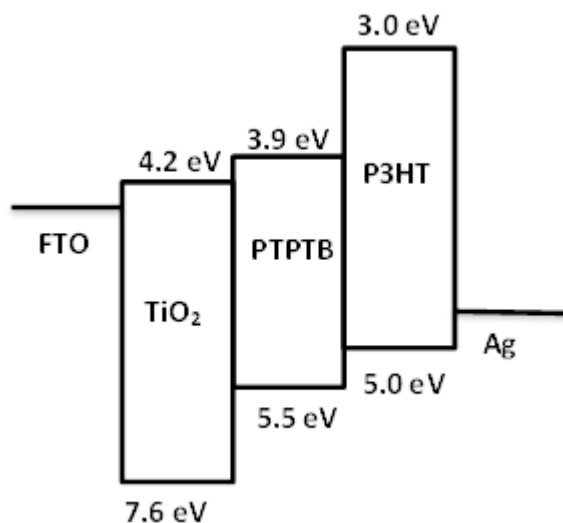
Figure 3-11. Device structure.

Cooke and co-workers[147] synthesised a dithienylpyrrole-stoppered rotaxane **101** and reported its electrochemical polymerisation onto a platinum working electrode (Figure 3-12). The cyclobis (paraquat-p-phenylene) based rotaxane was electropolymerised onto an electrode surface, showing that the tetracationic cyclophane moiety of **101** does not impair electropolymerisation of this derivative.
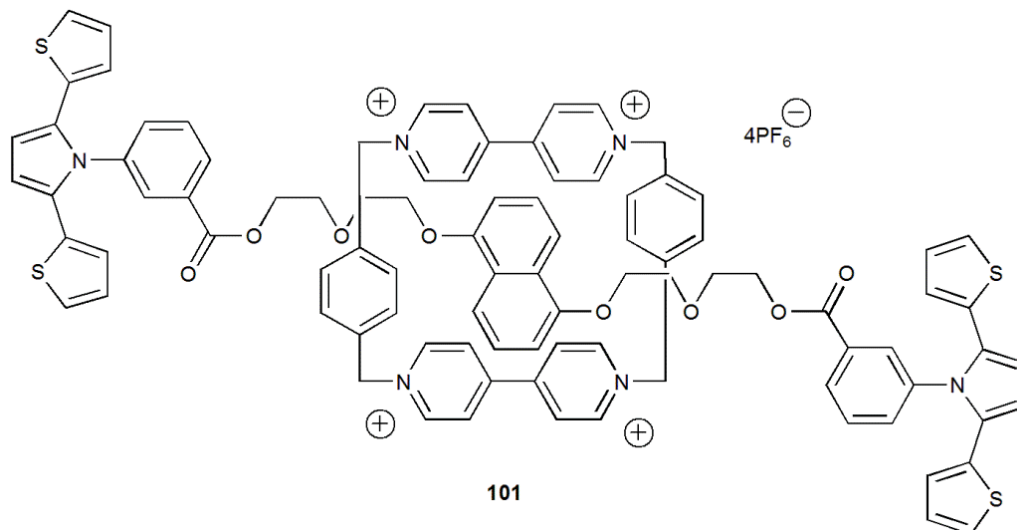
Figure 3-12. Cyclobis(paraquat-p-phenylene) and SNS based rotaxane structure.

3.1.4. 2,5-Di (2-thienyl) pyrrole-flavin based derivatives

The recent studies regarding SNS derivatives bearing *p*-substituted benzene as well as fluorescent mainly focused on the investigation of both electrochemical and optical pro-perties of these polymers for possible use in light emitting diodes, electrochromic devices and biosensors. Flavins are attractive species to attach to SNS-systems due to their

interesting redox and fluorescent properties. The electrochemically tuneable recognition properties between an electropolymerised flavin derivative and 2,6-diethylamidopyridine **102** was reported by Cooke and co-workers (Figure 3-13).[148] The flavin functionalised electrode was fabricated by electropolymerising SNS moiety, and these combined effects of the SNS + flavin provide an encouraging precedent for the development of the advanced materials and nanotechnological applications of systems of this type.
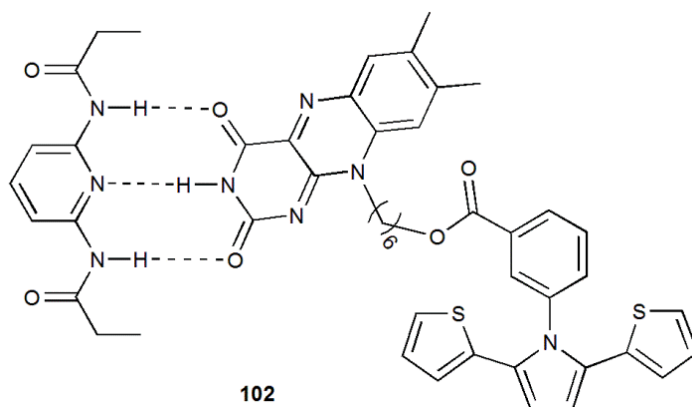
Figure 3-13. SNS-flavin structure **102**.

Cooke *et al.*[149] also described a new class of electrochemically tunable rotaxanes incorporating a flavin moiety and SNS **103** (Figure 3-14). The electrochemical reduction of the flavin unit results in significant stabilization of the flavin radical anion state of the axle moiety in the solution state, and to a lesser extent at the solid-liquid interface of an electropolymerised thin film.
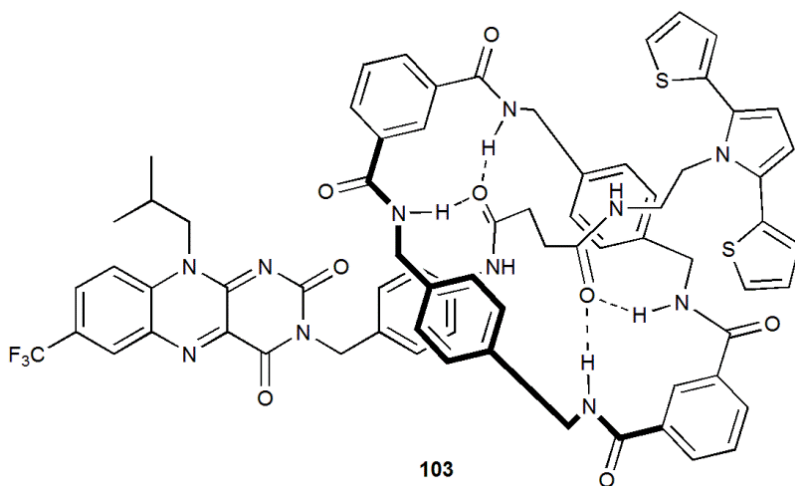
Figure 3-14. Rotaxane **103** structure.

3.2. The aim of project

The aim of the work described this chapter was to synthesise and characterise new flavin-functionalised SNS systems and conduct polymerisation to give new conjugated polymers (Figure 3-15). The main goal for synthesizing these materials was to design low band gap polymers featuring an electron-rich chain and an electron-deficient flavin in the side chain. The combination of flavin and dithienylpyrrole rings into polymers of this type could allow modulation of the band gap, leading to a range of highly efficient organic semiconductors suitable for use in organic photovoltaic cells (OPV).
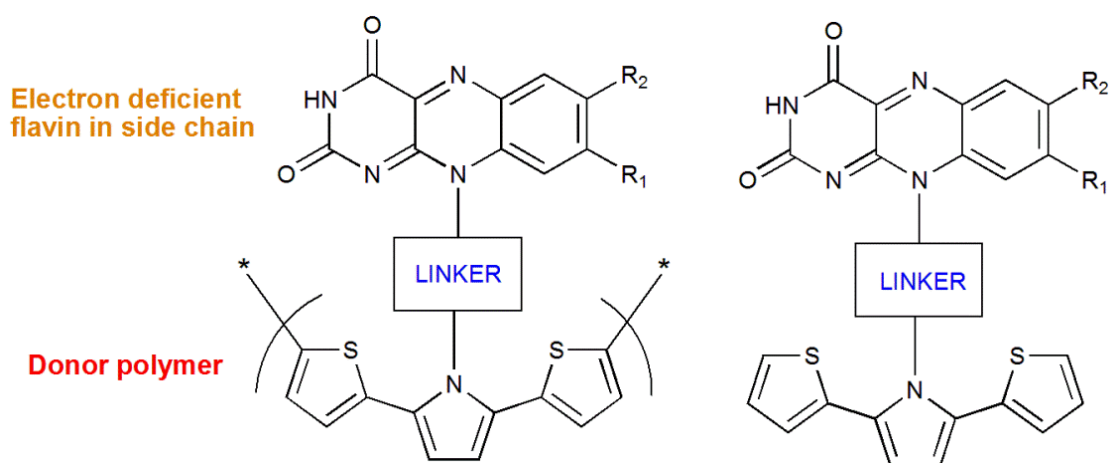
Figure 3-15. Flavin-functionalised dithienyl-pyrroles systems.

3.3. Results and Discussion

3.3.1. Synthesis

3.3.1.1. Synthesis of precursors[148]

3-(2,5-Di(thiophen-2-yl)-*1H*-pyrrol-1-yl)benzoic acid **104** was synthesised in two steps. Firstly, compound **82** was synthesised. Merz *et al.*[150] synthesised compound **82** by a double Friedel-Crafts reaction. Thiophene **80** and succinyl chloride **81** were reacted in the presence of aluminium chloride as the Lewis acid catalyst. This method provided **82** in good yield (80%) (Scheme 3-10).

The Paal-Knorr route was then followed to synthesise compound **104**. Compound **82** and 3-aminobenzoic acid **103** in the presence of *para*-toluenesulfonic acid (PTSA) was heated

under reflux using a Dean-Stark apparatus for 12 hours to yield the target compound **104** in (28%) (Scheme 3-10). The mechanism of this reaction was shown in Scheme 3-5.
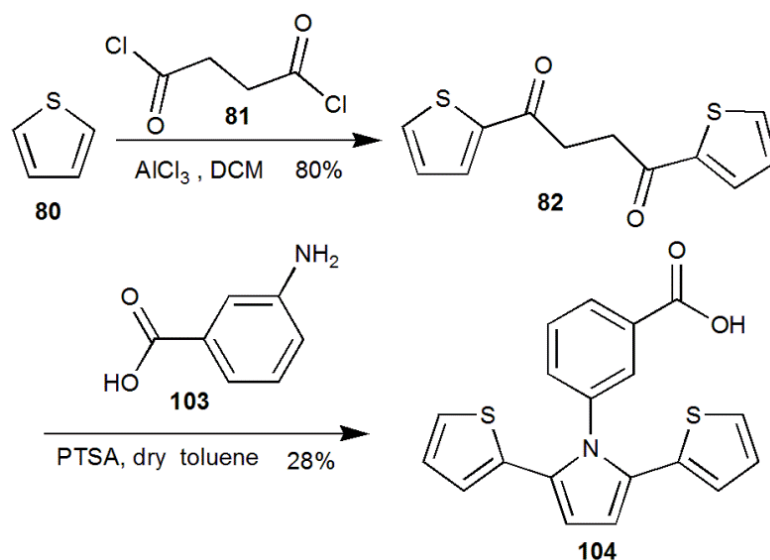
Scheme 3-10. Synthesis of compounds **82** and **104**.

The synthesis of flavin-functionalised SNS derivatives was carried out through preparation of compound **108** which was synthesised using the following synthetic scheme shown in Scheme 3-11.[151] Compound **106** was synthesised in 40% yield by a nucleophilic aromatic substitution reaction between ethanolamine and compound **105** in the presence of triethylamine. Due to the presence of strong electron withdrawing groups in the *para* and *ortho* positions to the -Cl group in the aryl ring, the nucleophilic substitution reaction was facilitated. Afterwards, the nitro group in compound **106** was reduced to amine group using palladium on carbon as a catalyst in the presence of ammonium formate as the hydrogen source to afford compound **107**. Due to the instability of compound **107**, the product was taken on immediately to react with alloxan monohydrate and boric anhydride in glacial acetic acid to afford flavin compound **108** as a yellow powder in 93% yield (Scheme 3-11).
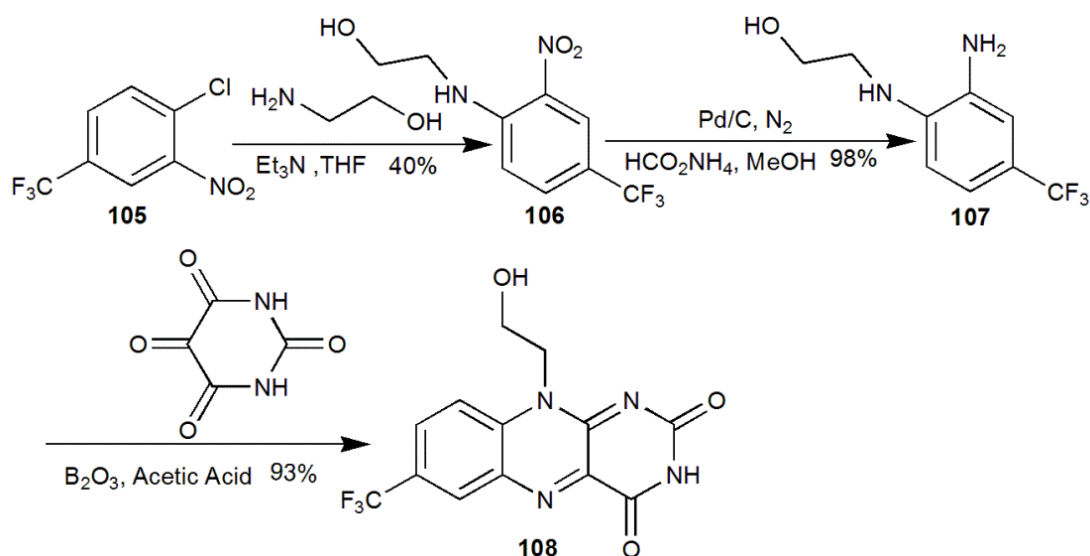
Scheme 3-11. Synthesis of flavin **108**.

The mechanism of this reaction involves the carbonyls in the alloxan structure becoming activated by coordinating with the boron atom. Once the carbonyls activated the ion pair of the amines can readily react with the activating carbonyl groups (Scheme 3-12). Finally, two molecules of water are eliminated leaving two new double bounds in the final structure of flavin. It is characteristically fluorescent in yellow colour, so detection within the reaction mixture as it forms is easily observed through a change in colour.
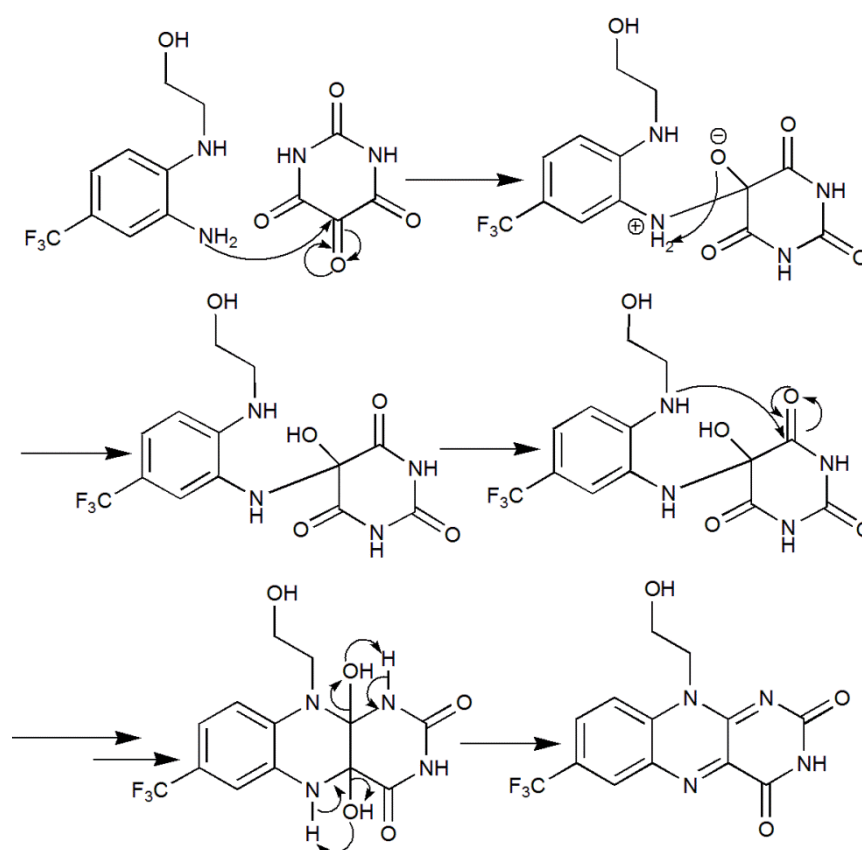
Scheme 3-12. Mechanism of alloxan with ortho-aromatic diamines.

3.3.1.2. Synthesis of SNS-flavin derivatives

Compound **109** was synthesised by reacting compound **104** with flavin **108** *via* Steglich esterification (Scheme 3-13). The reaction was undertaken in DMF at room temperature for three days, producing a satisfactory yield (64%) of the required ester **109**. 1-Ethyl–3-(3-dimethylaminopropyl) carbodiimide (EDCI) was used as coupling reagent and 4-dimethylaminopyridine (DMAP).

In order to increase the solubility of compound **109** a methyl group was added to the N3 of the flavin. The reaction took place in the polar solvent (DMF) in the presence of potassium carbonate at room temperature overnight producing a high yield (92%) of the methylated compound **112** (Scheme 3-13). The next step is the formation of the compound **113**. This was achieved by reacting the compound **112** and 2 equivalents of *N*-bromosuccinimide in DMF to give the product **113** in a 45% yield (Scheme 3-13).

Compound **110** was synthesised by the reaction of compound **109** with iodoheptane in the polar solvent (DMF) in the presence of potassium carbonate at room temperature overnight producing a moderate yield (42%) of compound **110** (Scheme 3-13). The heptyl group was added to the N3 of the flavin to increase the solubility of compound **110** in non-polar solvent.

Formation of compound **111** was the next step. This was achieved by reacting the compound **110** and 2 equivalents of *N*-bromosuccinimide in the DMF at 0 ^{o}C for 5hr under stirring to give the product **111** in a 58% yield (Scheme 3-13). *N*-(6'-Hydroxyhexyl) flavin **114** was reacted with acid **104** *via* a Steglich esterification to yield compound **115** (Scheme 3-13). The reaction was undertaken in DMF at room temperature for seven days, producing a good yield (74%) of the required ester **115**.
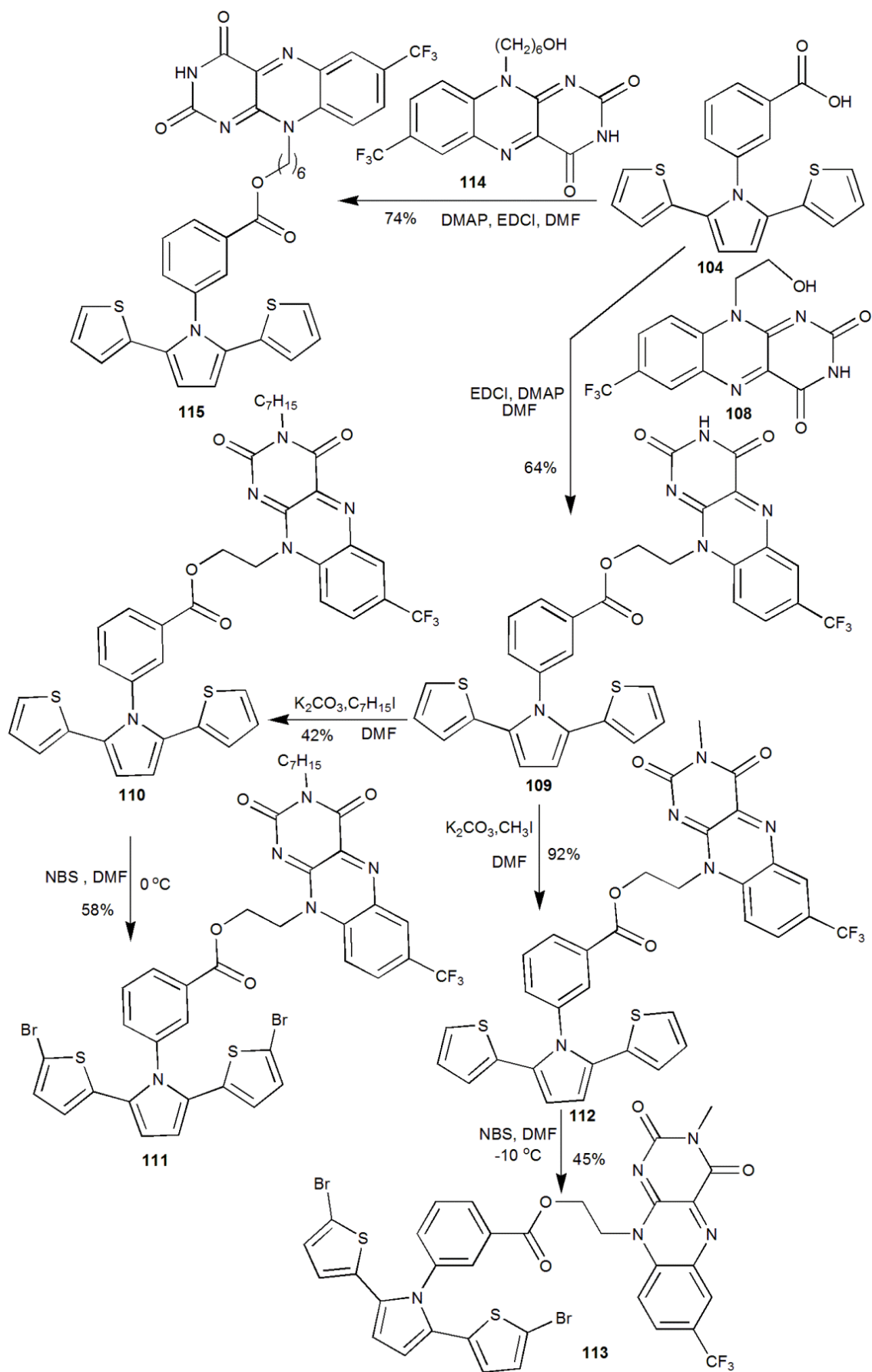
Scheme 3-13. Synthesis of SNS-flavin derivatives.

3.3.1.3. Synthesis of a SNS-flavin copolymer

The copolymerisation of 3-hexylthiophene (3HT) **72** with SNS-flavin **110** was next studied. A mixture of monomer **110** with T6H, in the mole ratio 1:4, was oxidatively chemically polymerised using iron(III)chloride as the oxidant in a mixture of nitro-methane/carbon tetrachloride under dry N_2 (Scheme 3-14). Soxhlet extraction after polymerisation with polar solvents (methanol, acetone, and DCM) was found to effectively fractionate the polymer **116** and remove residual catalyst. The average molecular weight was determined by gel permeation chromatography in THF using polystyrene standards as reference. This gave an average molecular weight (Mw) = 21351 g/mol and the poly-dispersity index (PDI) = 1.37 (Figure 3-16).
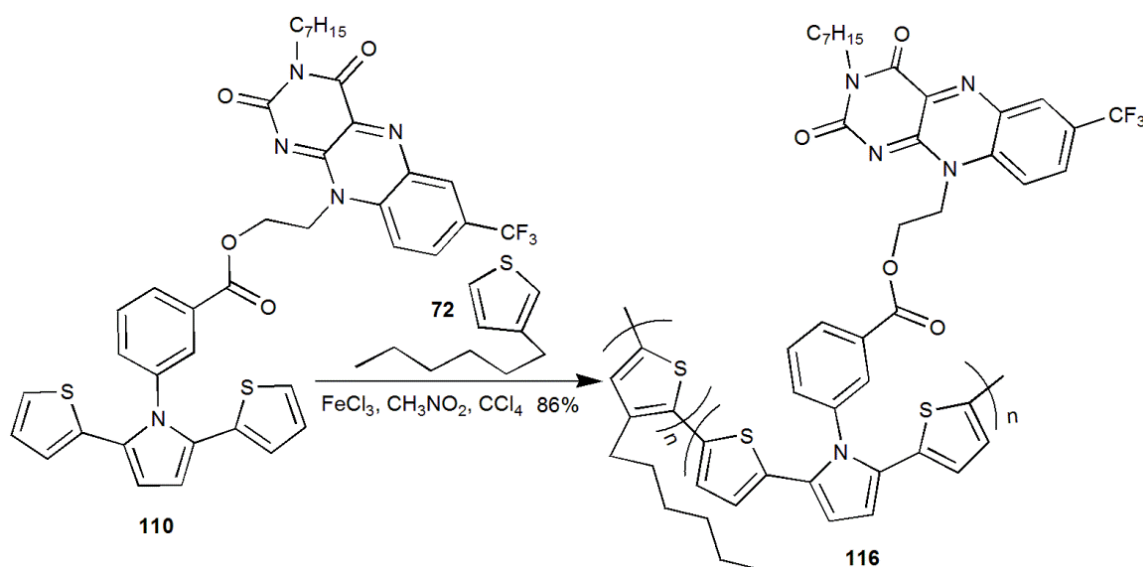
Scheme 3-14. Synthesis of copolymer **116**.
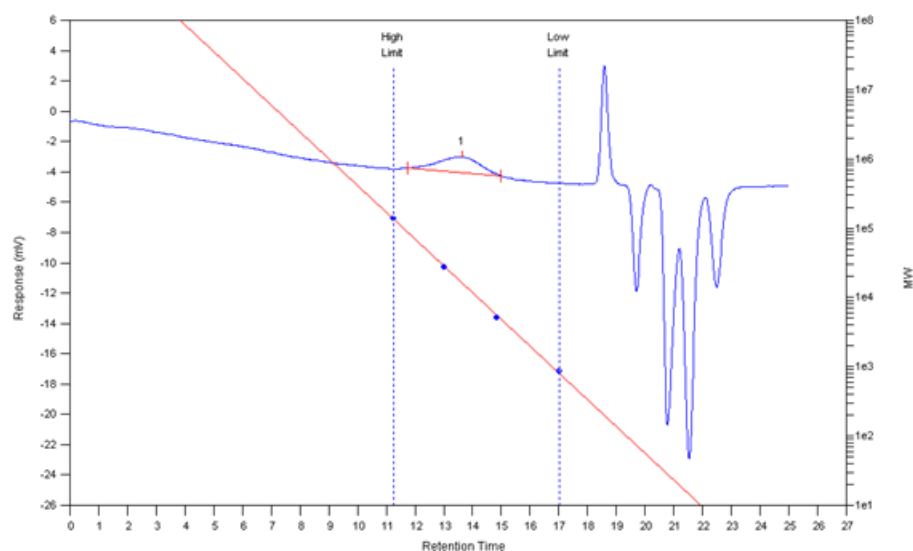
Figure 3-16. Molecular weight determination of polymer **116** by GPC.

3.3.2. Spectroscopic studies of SNS-flavin derivatives.

The spectroscopic data of all derivatives are compatible with the proposed structures. Compounds **109**, **115**, **117**, **118**, and **119** and the key precursor compounds were characterized by ^{1}H, ^{13}C NMR, mass spectrometry, and FTIR spectroscopy and they are in agreement with the proposed structures (Figure 3-17).
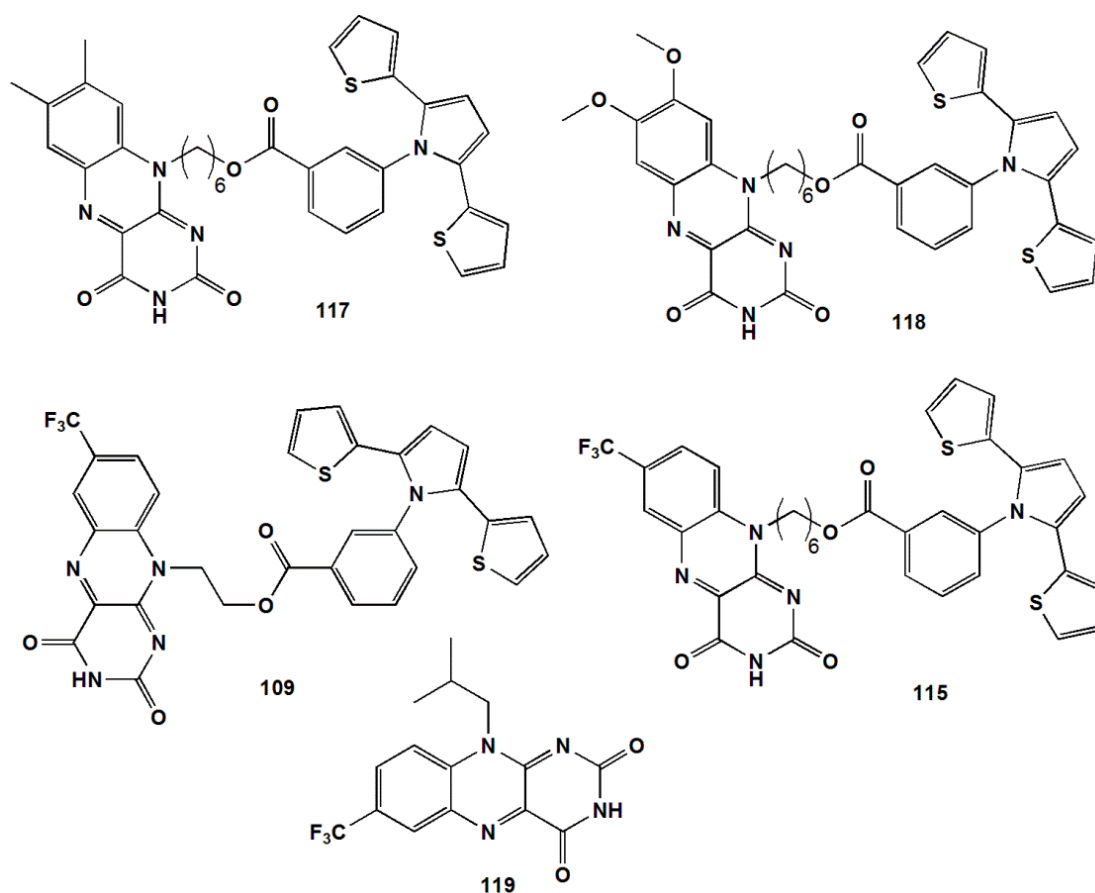
Figure 3-17. Structures of new 2,5-di(2-thienyl) pyrrole functionalised flavins.

The UV-vis spectra generally show a systematic change in the spectral range of absorption and energy gaps of the 2,5-di-(2-thienyl)pyrrole functionalised flavins (Figure 3-18). The UV-vis spectra of **109**, and **115** recorded in CH_2Cl_2 (1 x 10^{-4} M) displayed broad CT bands with end-absorptions reaching into the visible region. Compound **115** displayed the maximum absorption at λ_{max}= 458 nm and at onset wavelength at λ_{onset}= 480 nm with other absorptions at 431 nm, 409 nm, and 325 nm, respectively. Compound **109** displayed the same absorptions with a blue shift of 3 nm for all absorptions (Table 3-2).
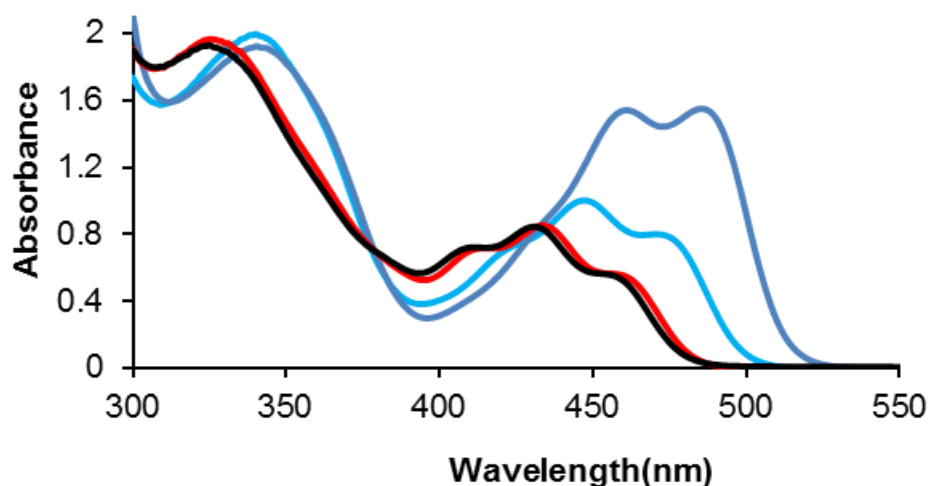
Figure 3-18. UV-vis spectra of compounds **117** (aqua line), **118** (blue line), **115** (red line) and **109** (black line) recorded in CH_2Cl_2 (1×10^{-4} M)

The UV-vis spectra of compounds **117**, **118**, **115**, and **109** are shown in Figure 3-18. Compounds **109** and **115** have very similar absorption spectra, however, compounds **117** and **118** have their main absorption shifted to higher wavelength (Table 3-2).

Table 3-2. UV-vis spectra data of compounds **117**, **118**, **115**, and **109** recorded in CH_2Cl_2 (1×10^{-4} M). Where the λ_{abs} is absorption wavelength (nm), λ_{onset} is end-absorption, λ_{Max} is maximum absorption wavelength (nm), and Eg^{opt} is optically determined band gap energy (eV).

Compounds	λ_{abs1} (nm)	λ_{abs2} (nm)	λ_{abs3} (nm)	λ_{max} (nm)	Band gap (eV)
117	340	420	444	471	2.63
118	340	430	458	484	2.56
115	325	409	431	458	2.71
109	322	406	428	455	2.85

The UV-vis spectroscopy suggests that there is some degree of through space electronic communication between the flavin moiety and the dithienylpyrrole moiety for compounds **115** and **109** when compared to the UV-vis spectra of **119**. In particular, all absorptions for the flavin unit are shifted between 4 and 6 nm to higher wavelength for compound **119** (Figure 3-19).
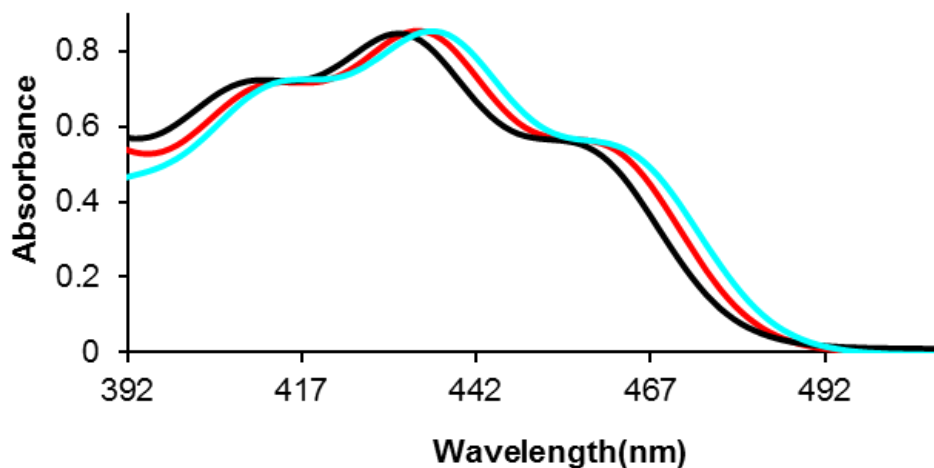
Figure 3-19. UV-vis spectra of compounds **109** (black line), **115** (red line) and **119** (aqua line) recorded in CH_2Cl_2 (1×10^{-4} M).

The fluorescence properties of compounds **109**, **115**, **117**, **118**, and **119** were investigated by fluorescence spectroscopy (recorded in 10^{-5} M solution in CH_2Cl_2). It can be seen that the dithienylpyrrole plays an important role in modulating the fluorescence properties of the flavin unit **119** as shown in Figure 3-20. The fluorescence of compounds **115** and **109** is significantly quenched compared to the non-functionalised flavin **119**, and compounds **117**, and **118**. This is presumably due to the electron rich dithienylpyrrole unit acting as a quencher for the flavin moiety.
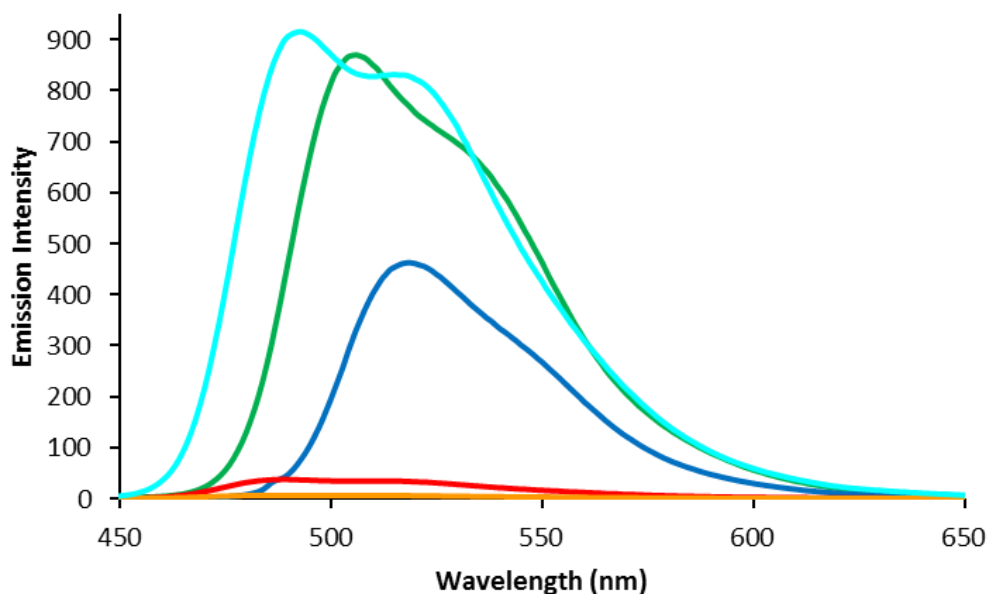
Figure 3-20 .Fluorescence spectra recorded for compounds **109** (orange line), **117** (green line), **118** (blue line), **115** (red line), and **119** (aqua line) in CH_2Cl_2 (1×10^{-5} M) at excitation wavelength = 450 nm.

3.3.3. Electrochemical Studies of SNS-flavin derivatives.

The redox properties of the new dithienylpyrrole-flavin **109**, **115**, **117**, **118**, and **119** were investigated by cyclic voltammetry (CV) using tetrabutylammonium hexafluorophosphate (n-Bu$_4$NPF$_6$) as a supporting electrolyte and ferrocene (Fc$^+$/Fc) as internal reference in CH$_2$Cl$_2$. As shown in Figure 3-21 the compounds were reduced in well-defined reversible one-electron reduction steps.
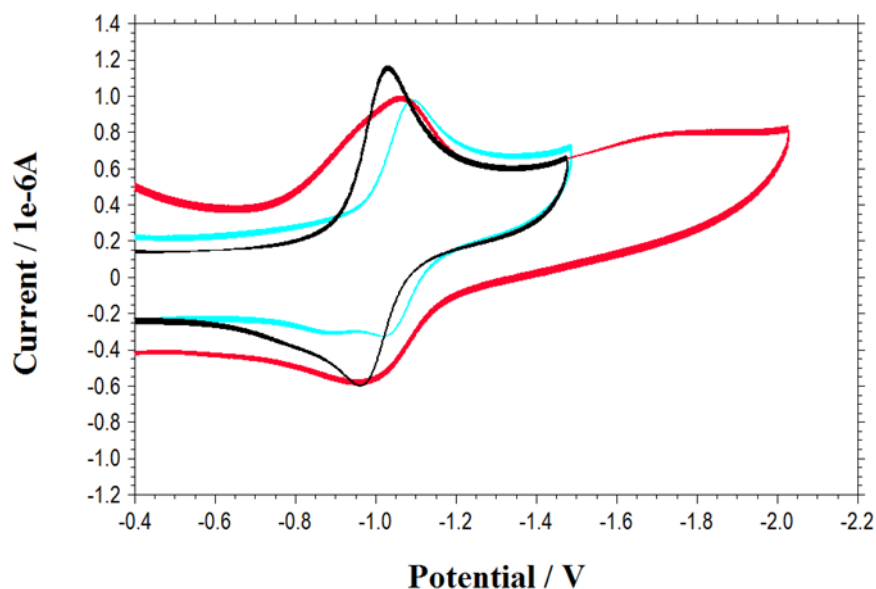
Figure 3-21. Cyclic voltammogramms of compounds **115** (red line), **109** (black line), and **119** (aqua line), recorded using a glassy carbon working electrode, an Ag wire as a reference electrode and a Pt wire as a counter electrode. Recorded in CH$_2$Cl$_2$ (1x10^{-4}M) with 0.1M (n-Bu$_4$NPF$_6$) as a supporting electrolyte at 20 °C, and a scan rate of 0.1 Vs^{-1}.

Compound **115** displayed a reversible redox wave at E$_{1/2}$= -1.04 V which corresponds to a LUMO energy of E$_{LUMO}$= -3.76 eV. Compound **109** displayed reversible redox wave at E$_{1/2}$= -1.0 V which corresponds to a LUMO energy of E$_{LUMO}$= -3.80 eV. Also, it displayed irreversible peak at +0.23 V, which corresponds to a HOMO energy of E$_{HOMO}$= -5.03 eV, resulting in an electrochemically determined band gap energy of E$_{gap}$= 1.23 eV. On the other hand, compound **119** displayed reversible redox wave at E$_{1/2}$= -1.06 V which corresponds to a LUMO energy of E$_{LUMO}$= -3.74 eV (Figure 3-21, Table 3-3). The data are consistent with the dithienylpyrrole unit having only a limited affect on to LUMO of the flavin unit.

Compound **117** displayed reversible redox wave at E$_{1/2}$= -1.28 V which corresponds to a LUMO energy of E$_{LUMO}$= -3.52 eV. Also, it displayed an irreversible peak at +0.34 V, which corresponds to a HOMO energy of E$_{HOMO}$= -5.14 eV, resulting in an electrochemically determined band gap energy of E$_{gap}$= 1.62 eV. Compound **118** displayed a

reversible redox wave at $E_{1/2}$= -1.34 V which corresponds to a LUMO energy of E_{LUMO} = -3.46 eV. Also, it displayed an irreversible peak at +0.38V, which corresponding to a HOMO energy of E_{HOMO}= -5.20 eV, resulting in an electrochemically determined band gap energy of E_{gap}= 1.72 eV (Figure 3-22, Table 3-3). The data are in accordance with the differing electron affinity of the flavin due to differing functionality in 7 and 8-position of the flavin nucleus.

Table 3-3 Electrochemical data (CV) of compounds **109**, **115**, **117**, **118**, and **119** recorded in CH_2Cl_2 (+0.1M n-Bu$_4$NPF$_6$) vs.Fc$^+$/Fc at scan rate v = 0.1 V s^{-1}.

Compounds	$E_{1/2}$ [V]	E_{LUMO} [eV]	E_{HOMO}[eV]	E_{gap} [eV]
115	-1.04	-3.76	----	----
109	-1.0	-3.80	-5.03	1.23
117	-1.28	-3.52	-5.14	1.62
118	-1.34	-3.46	-5.20	1.72
119	-1.06	-3.74	----	----
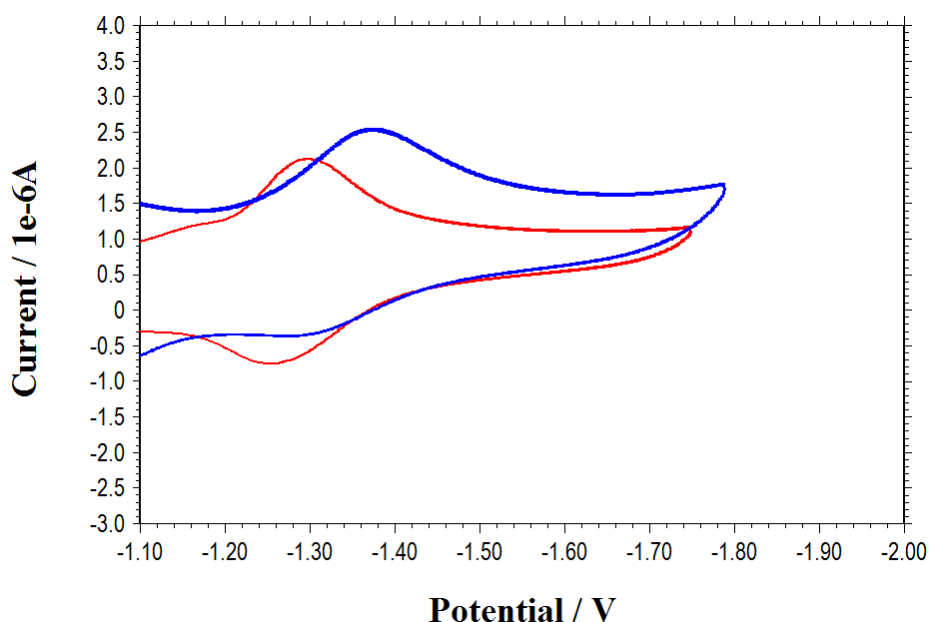
Figure 3-22. Cyclic voltammogramms of compounds **117** (red line), and **118** (blue line) recorded using a glassy carbon working electrode, an Ag wire as a reference electrode and a Pt wire as a counter electrode. Recorded in CH_2Cl_2 (1x10^{-4}M) with 0.1M (n-Bu$_4$NPF$_6$) as a supporting electrolyte at 20 ºC, and a scan rate of 0.1 Vs^{-1}.

3.3.4. X-ray structure of compound 109

Single crystals of **109** suitable for X-ray crystallographic analysis were obtained by slow diffusion of methanol into CH_2Cl_2 solution at 25 ^{o}C. This provided crystals of sufficient quality for X-ray structure determination. Intensity data were collected on a single crystal 0.20 x 0.10 x 0.03 mm^3. The X-ray structure of **109** is shown in Figure 3-23 and clearly proves SNS-flavin formation.

Figure 3-23 shows the crystal structure which belongs to the triclinic *P*-1 space group. Both thienyl rings are disordered. The disorder proportion for each thienyl ring on either side is not the same for the two conformations. However, to minimise the steric hindrance, the two thienyl rings significantly deviate from the planarity with respect to the pyrrole ring (N-C-C-S1=23° and N-C-C-S2=42.7°). The angle between the two thienyl planes is around 62°. The phenyl ring is oriented perpendicularly to the pyrrole ring (C8-N1-C13-C18=92.8°), and this is again to minimise the steric hindrance of the thienyl rings attached to the pyrrole.
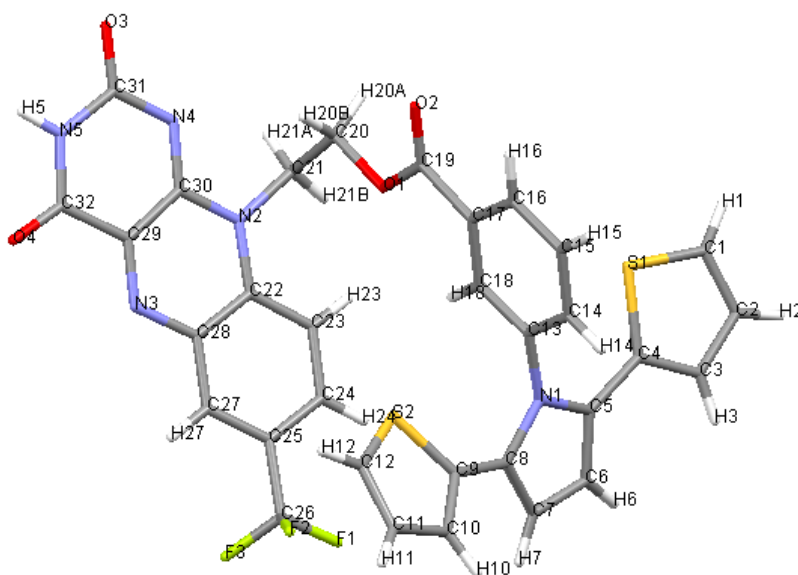
Figure 3-23. X-ray crystal structure of **109**.

Some important intermolecular interactions are shown in Figure 3-24. Molecular packing of the **109** in the unit cell as viewed along axis and arranged head to head. The molecular assembly is mainly due to C-H···π interactions which are widespread and responsible for the specific arrangement and orientation of the molecules in the crystal. The most prominent interaction is between H14 and H15 of phenyl group and the π electrons (C7-C8) of the pyrrole ring (with N1 atom) of an adjacent molecule. The two H atoms attached

to C7 atom are involved in the formation of C-H⋯π type interactions with two thiophene moieties on both side of the reference molecule at a distance of 2.866 Å and 2.896 Å, respectively. The H14 atom forms a short interaction with the C8 atom of an adjacent molecule at a distance of 2.791 Å. The fractional coordinates, bond angles, covalent bond lengths, and anisotropic thermal displacement parameters for the final model are listed in chapter 9 of this thesis.
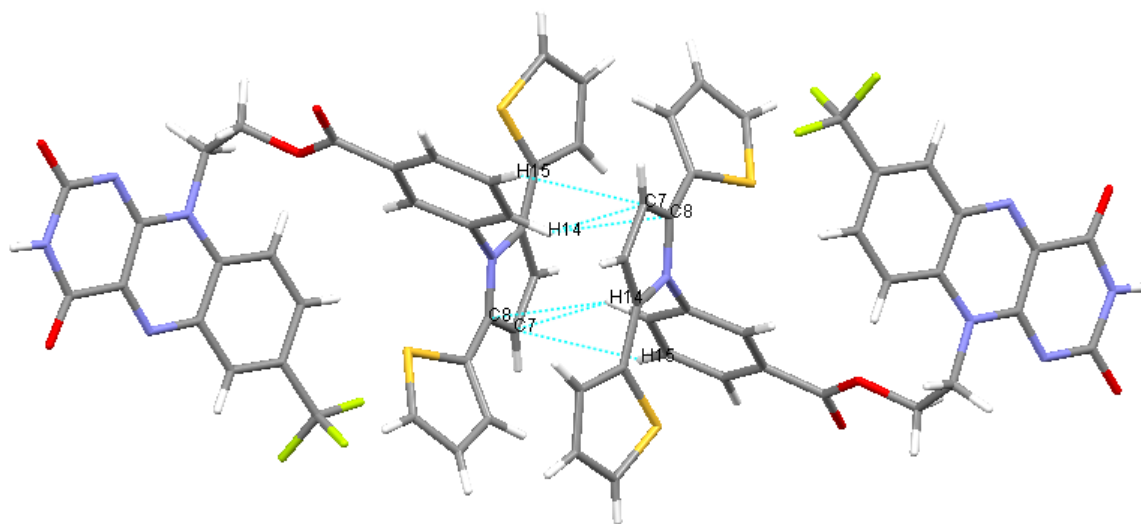
Figure 3-24. Molecular packing of **109** in the unit cell.

3.3.5. Spectroscopic and electrochemical studies of copolymer 116

The ^{1}H NMR displayed the expected broad signals for polymer **116**. The relative integration of these peaks was useful in confirming the relative ratio of the monomers in the polymer **116**. The polymer displayed the expected peaks of the functional groups. The UV-vis spectra of **110**, polymer **116**, and **72** were recorded in CH_2Cl_2 and are shown in Figure 3-25 and Table 3-4.

Table 3-4. UV-visible spectra data of compounds **110**, **116**, and **72** recorded in CH_2Cl_2 (1×10^{-4} M). Where the λ_{abs} is absorption wavelength (nm), λ_{onset} is end-absorption, λ_{Max} is maximum absorption wavelength (nm), and Eg^{opt} is optically determined band gap energy (eV).

Compounds	λ_{abs1} (nm)	λ_{abs2} (nm)	λ_{abs3} (nm)	λ_{abs4} (nm)	λ_{abs5} (nm)	λ_{abs6} (nm)	Band gap (eV)
72	237	---	---	---	---	---	5.24
110	267	275	326	411	433	460	2.70
116	267	274	333	437	---	---	2.84

Compound **72** has a maximum for the π-π* transition at 237 nm while compound **110** displayed absorption band in the 267-479 nm region with a maxima for the π-π* transition at λ_{max}= 460 nm and at 433 nm, in addition to absorptions at 411 nm, 326 nm, 275 nm, and 267 nm, respectively. The UV-vis spectrum of polymer **116** displayed a broad band at λ_{max} = 437 nm, in addition to absorptions at 333 nm and 274 nm.
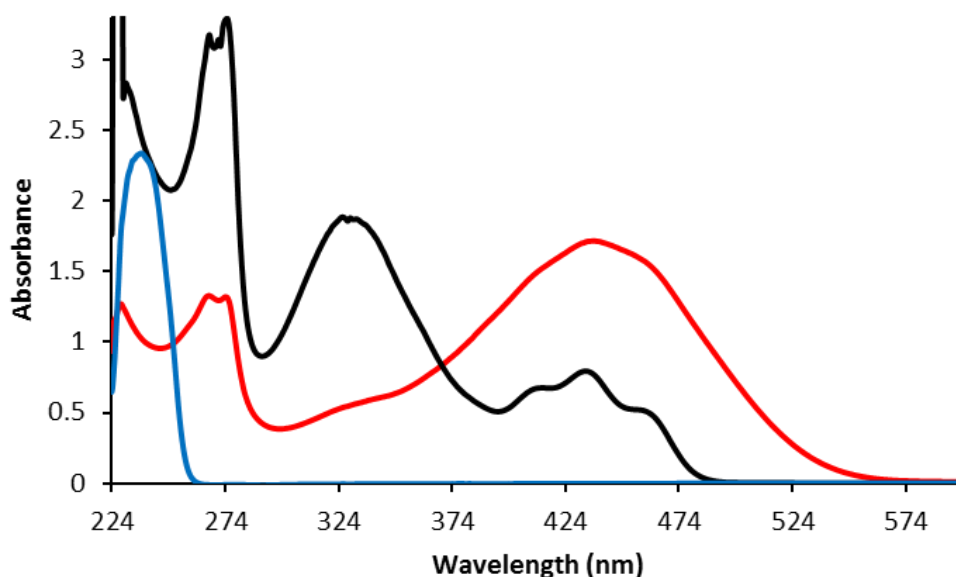
Figure 3-25. UV-vis spectra of compounds **72** (blue line), polymer **116** (red line), and **110** (black line) recorded in CH_2Cl_2 (1×10^{-4} M).

3.3.6. Electrochemical Studies of the 72, 110, and 116

Compounds **110** and **116** were reduced in well-defined reversible one-electron reduction steps (Figure 3-26, Table 3-5). Compound **110** displayed a reversible redox wave at $E_{1/2}$= -1.08 V which corresponds to a LUMO energy of E_{LUMO}= -3.72 eV. Also, it displayed an irreversible oxidation peak at +0.33V, which corresponds to a HOMO energy of E_{HOMO}= -

5.13 eV, resulting in an electrochemically determined band gap of E_{gap}= 1.41 eV. Polymer **116** displayed reversible redox waves at $E_{\frac{1}{2}}$= -1.06 V which corresponds to a LUMO energy of E_{LUMO}= -3.74 eV. Also, it displayed an irreversible peak at +0.30V, corresponding to a HOMO energy of E_{HOMO}= -5.10 eV resulting in an electrochemically determined band gap of E_{gap}= 1.36 eV.

The data indicate that the monomer **110** and polymer **116** have relatively similar band gaps, and LUMO and HOMO energies suggesting that the flavin and the polythienyl pyrrole units do not interact significantly in the polymer.
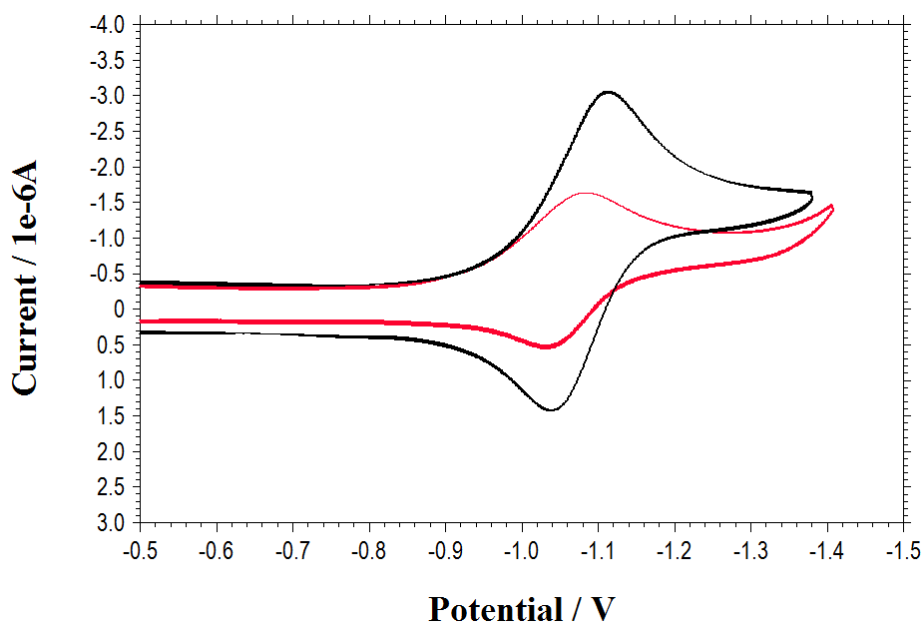
Figure 3-26. Cyclic voltammogramms of compounds **110** (black line), and **116** (red line) recorded using a glassy carbon working electrode, an Ag wire as a reference electrode and a Pt wire as a counter electrode. Recorded in CH_2Cl_2 (1×10^{-4}M) with 0.1M (n-Bu$_4$NPF$_6$) as a supporting electrolyte at 20 ^{0}C, and a scan rate of 0.1 Vs^{-1}.

Table 3-5. Electrochemical data (CV) of compounds **110** and **116** recorded in CH_2Cl_2 (+0.1M n-Bu$_4$NPF$_6$) vs.Fc$^+$/Fc at scan rate v = 0.1 V s^{-1}.

Compounds	$E_{1/2}$ [V]	E_{LUMO}[eV]	E_{HOMO}[eV]	E_{gap}[eV]
110	-1.08	-3.72	-5.13	1.41
116	- 1.06	-3.74	-5.10	1.36

3.3.7. Electrochemical polymerisation of compounds 115
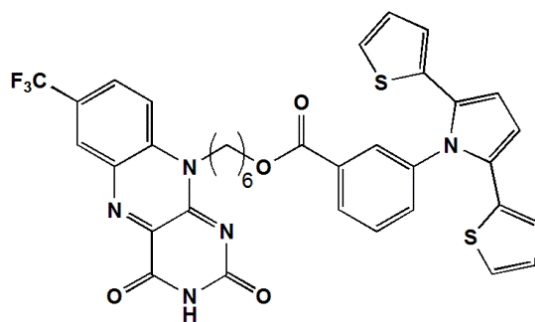
Figure 3-27. Structure of compound **115**.

The onset of the absorption edge of compound **115** (Figure 3-27) at 481 nm gives an optically determined band gap energy of 2.58 eV. The oxidation of monomer **115** shows a quasi-reversible wave at + 0.44 V and the reduction process gives clear reversible waves at -1.42 and at -2.38 V (Figure 3-28-a,b). Figure 3-28-c shows the onset of oxidation = +0.31 V which gives HOMO= -5.11 eV, and the onset of reduction = -1.35 V which gives LUMO= -3.45 eV (Table 3-6). The electrochemically determined band gap energy (1.66 eV) is lower than the optically determined band gap energy (2.58 eV) of the monomer **115**. This difference may be due to the experimental error and conditions such as humidity and oxygen.

Table 3-6. Electrochemical data (CV) of compound **115** recorded in acetonitrile (+0.1M n-Bu$_4$NPF$_6$) vs.Fc$^+$/Fc at scan rate v = 0.1 V s^{-1}.

Compounds	Onset of oxidation / V	Onset of reduction / V	E_{LUMO}[eV]	E_{HOMO}[eV]	E_{gap}[eV]
115	+0.31	-1.35	-3.45	-5.11	1.66
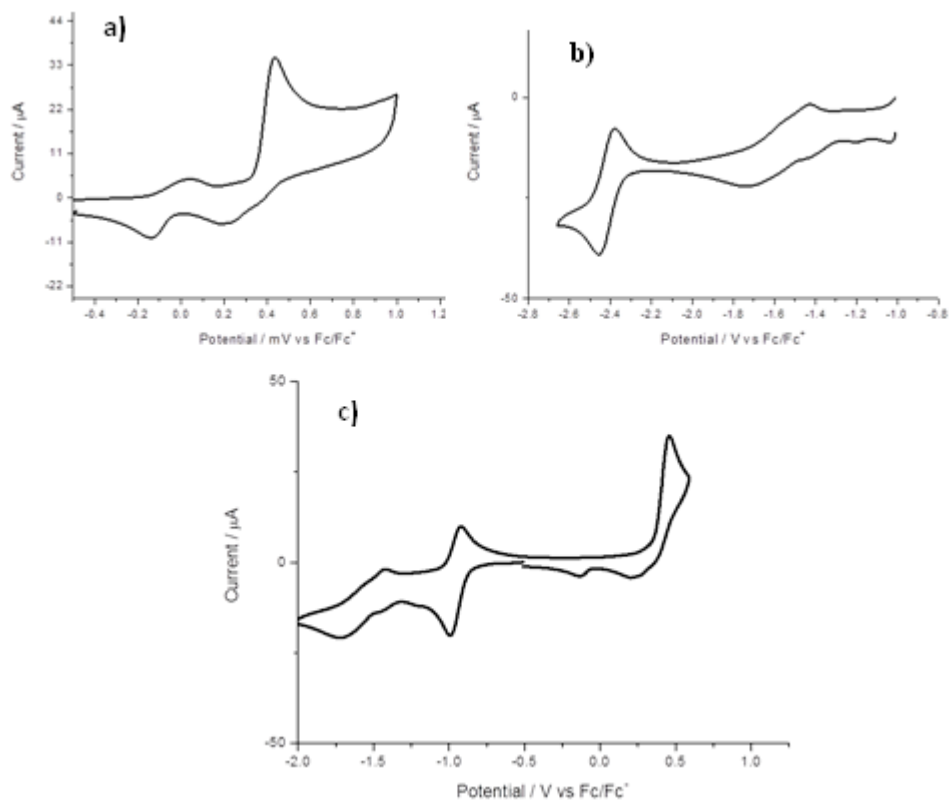
Figure 3-28. Showing (a) oxidation, (b) reduction, and (c) redox cyclic of compound **115** recorded using a glassy carbon working electrode, an Ag wire as a reference electrode and a Pt wire as a counter electrode. Recorded in acetonitrile (1×10^{-4}M) with 0.1M (n-Bu$_4$NPF$_6$) as a supporting electrolyte at 20 ºC, and a scan rate of 0.1 Vs^{-1}.

A number of attempts were made to find conditions for growing films of polymer **120** on large electrodes such as ITO coated glass. Best results for polymer growth were obtained by cycling over -0.4V to +1.2V is shown in the (Figure 3-29). The oxidation of polymer **120** displays reversible broad wave at + 0.22 V and the reduction process gives reversible wave at -1.0 V. The CV of polymer **120**, shows that the onset of oxidation = +0.03 V which gives a HOMO= -4.83 eV, and the onset of reduction = -0.82 V gives a LUMO= -3.98 eV. The electrochemically determined band gap energy = 0.85 eV (Figure 3-30, Table 3-7).

Table 3-7 Electrochemical data (CV) of polymer **120** recorded in acetonitrile (+0.1M n-Bu$_4$NPF$_6$) vs.Fc$^+$/Fc at scan rate v = 0.1 V s^{-1}.

Polymer	Onset of oxidation / V	Onset of reduction / V	E$_{LUMO}$[eV]	E$_{HOMO}$[eV]	E$_{gap}$[eV]
120	+0.03	-0.82	-3.98	-4.83	0.85
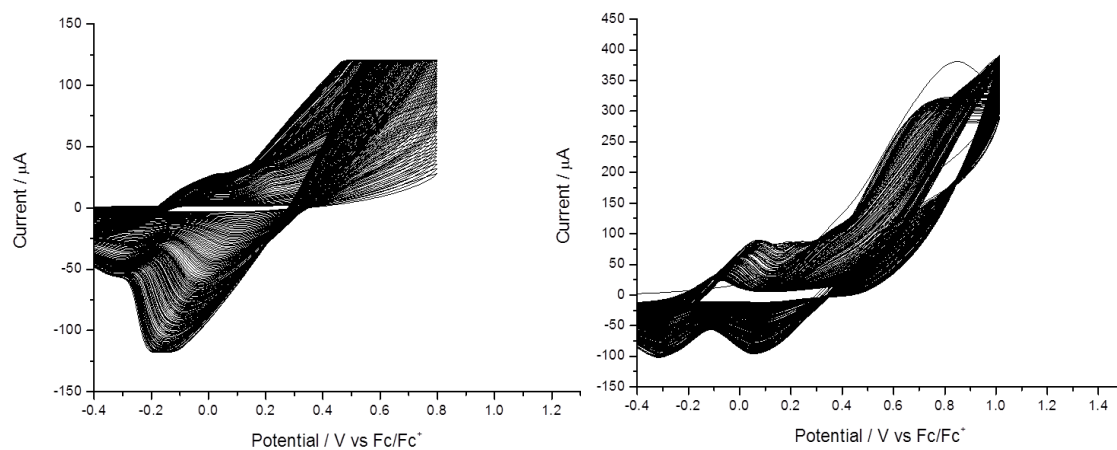
Figure 3-29. Polymer growth of compound **115** on ITO slides, an Ag wire as a reference electrode and a Pt wire as a counter electrode. Recorded in acetonitrile (1x 10^{-4} M) over 300 segments at scan rate 0.1 Vs^{-1}.
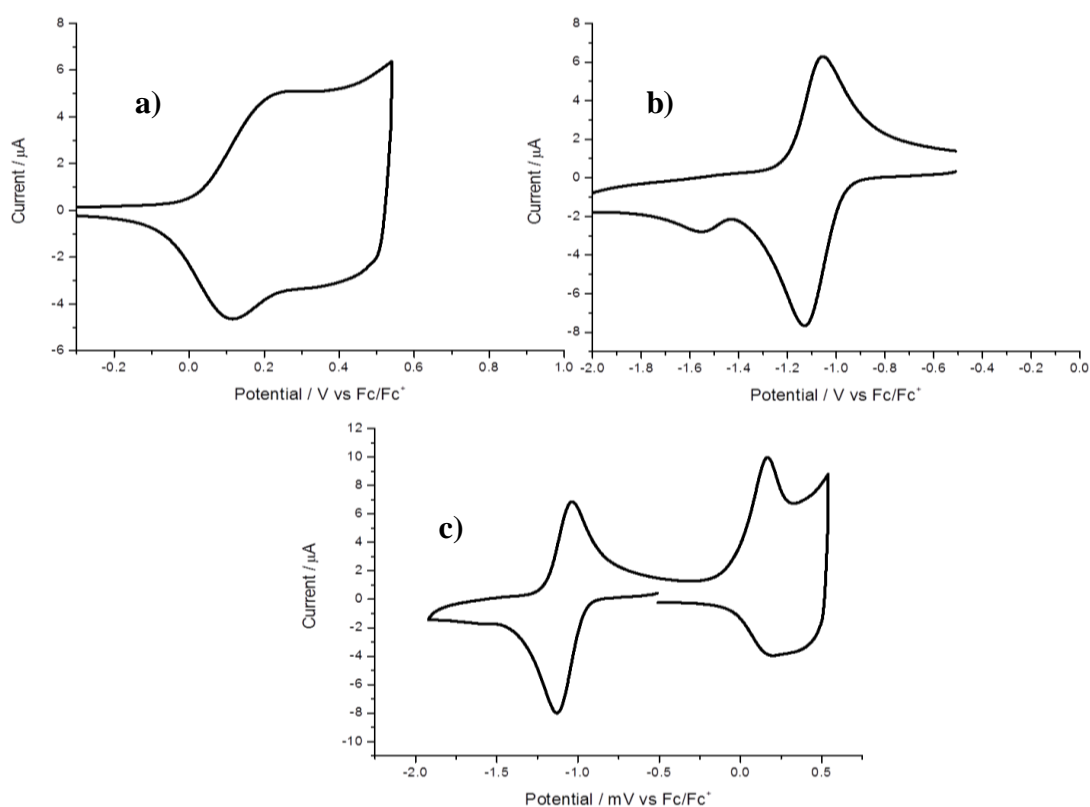
Figure 3-30. Showing a) Oxidation, b) reduction, and c) polymer cyclic of polymer **120** on ITO slides, an Ag wire as a reference electrode and a Pt wire as a counter electrode. Recorded in acetonitrile (1x 10^{-4} M) at scan rate 0.1 Vs^{-1}.

The difference between the HOMO and LUMO values gave an electrochemically determined band gap energy of E_{gap}= 0.85 eV, which is lower than the electrochemically determined band gap energy of the monomer **115** (1.66 eV). The stability of the polymer

120 films was investigated by repeating cycling over the first redox active peak using CV, which indicated that the polymer possessed good oxidative stability (Figure 3-31).
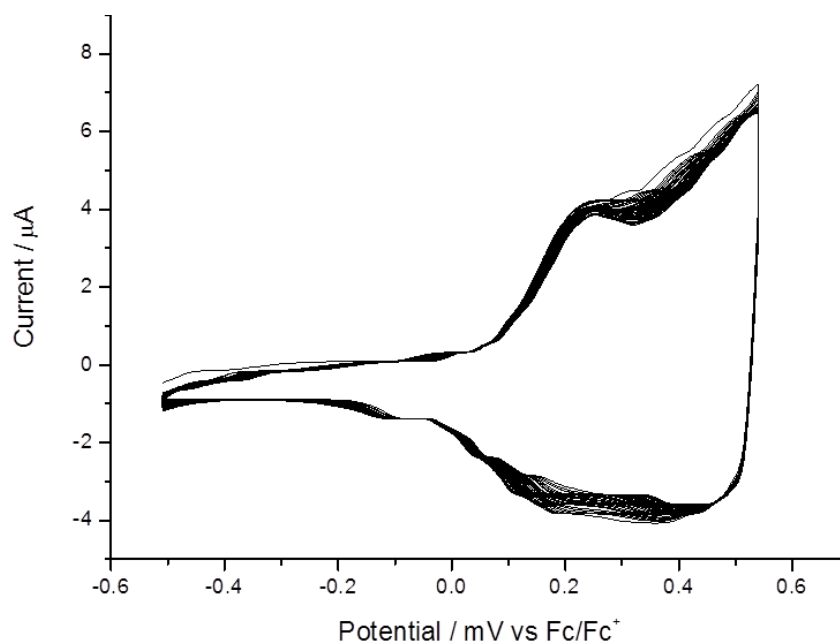
Figure 3-31. Oxidation stability of polymer **120** over 100 segments.

Figure 3-32 shows the peak current of the thin film of polymer **120** deposited on the electrode and was recorded in a monomer free MeCN. This showed that current varies linearly with change of the electrochemical scan rate between 25 mVs^{-1} and 500 mVs^{-1}. This behaviour is due to the polymer being strongly adsorbed onto the electrode.
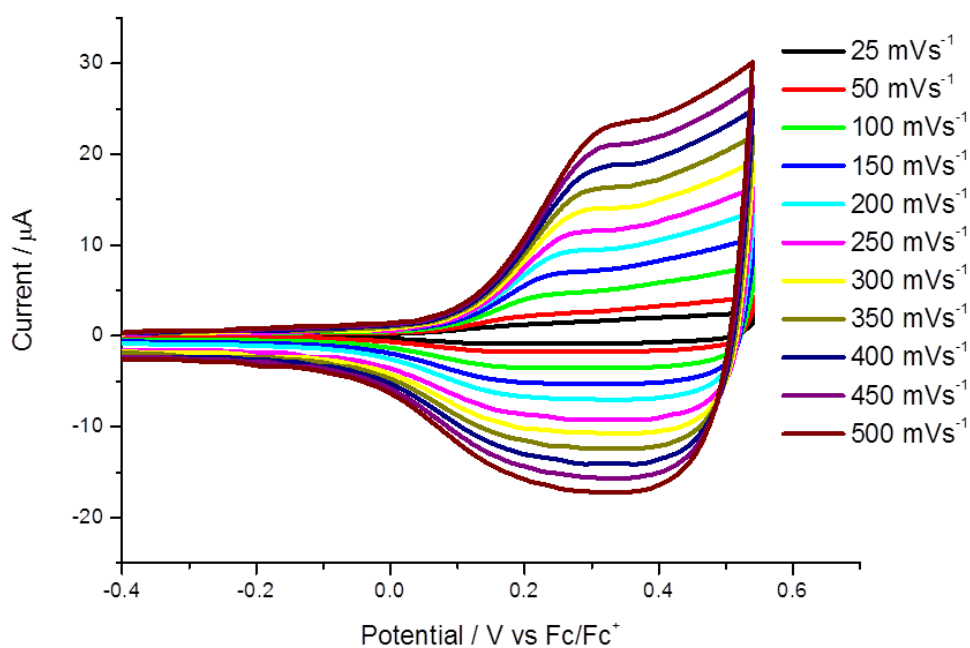
Figure 3-32. Scan rate of polymer **120** in MeCN at scan rates 25-500 mV s^{-1}.

The relationship of scan rate against peak currents of polymer **120** provides a straight line confirming the stability of the polymer **120** at the electrode/electrolyte interface in (Figure 3-33).
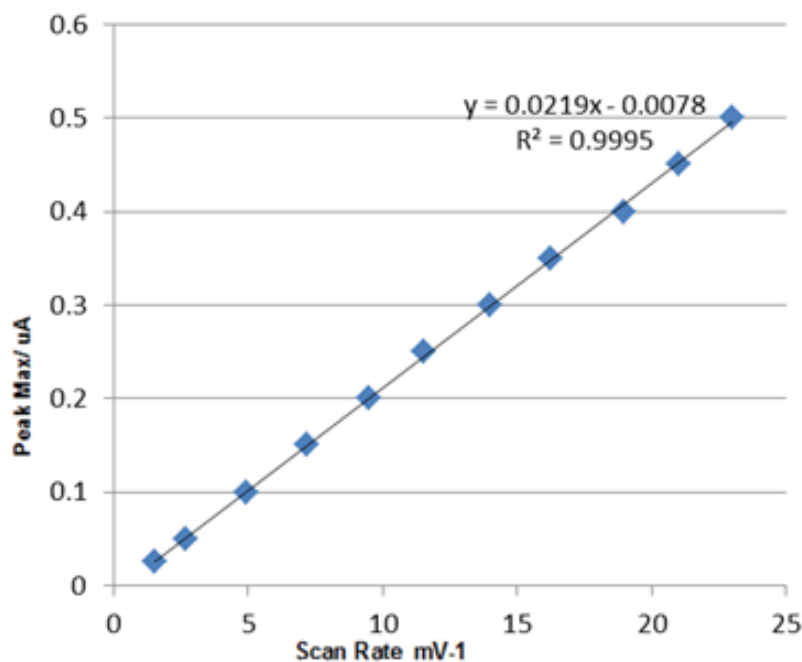
Figure 3-33. Plot of scan rate vs. peak current for polymer **120**.

The absorption spectroscopy of the polymer **120** provides information on the $\pi-\pi*$ transition which is normally associated with the band gap of polymer. It shows that the onset of the longest wavelength absorption band in polymer **120** shifted (59 nm) compared to the monomer **115** (Figure 3-34). The absorption spectra of polymer **120** display a λ_{max} at 420 nm. The onset of absorption edge (540 nm) of this polymer gives the optically determined band gap energy of 2.3 eV, which is higher than the electrochemically determined band gap energy (0.85 eV). This difference may be due to the experimental error and conditions such as humidity and oxygen. The reason for the red shift is probably due to the alternation of SNS donor polymer chain and the presence of the flavin acceptor moiety in the polymer side chain.
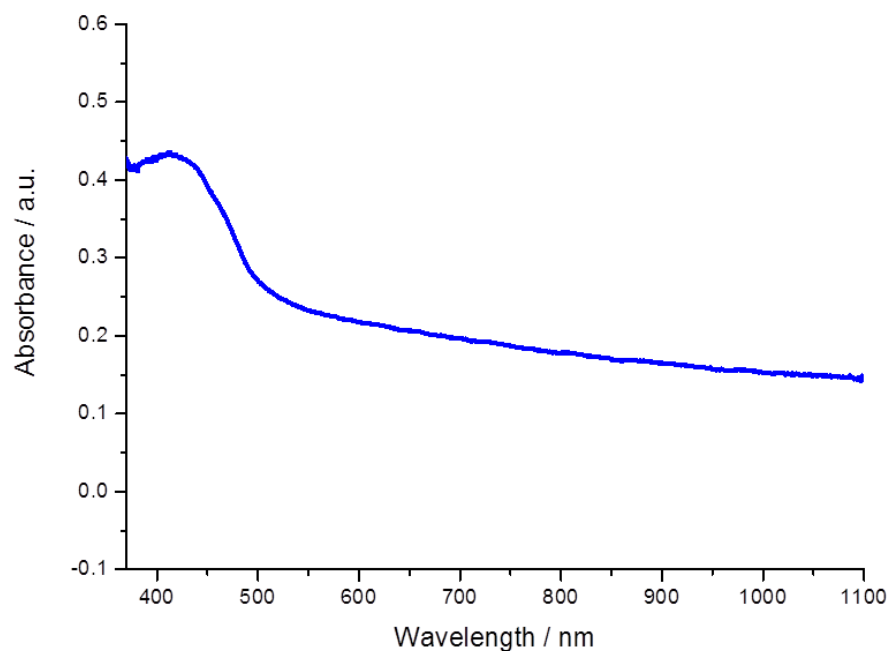
Figure 3-34. Absorption spectra of Polymer **120** after being de-doped in dichloromethane solution (-0.4 to -0.2 V)

3.3.8. Electrochemical polymerisation of compounds 109
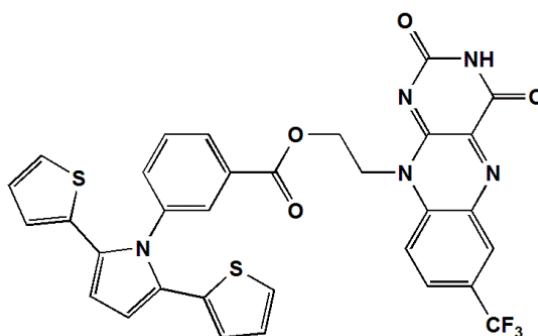
 Figure 3-35. Structure of compound **109**.

The onset of the absorption edge of compound **109** at 480 nm gives the optically determined band gap energy of 2.59 eV (Figure 3-35). The oxidation of monomer **109** shows a quasi-reversible wave at + 0.35 V and the reduction process gives two reversible waves at -1.50 and at -2.50 V (Figure 3-36-a,b). Figure 3-36-C shows the onset of oxidation = +0.21 V which gives HOMO = -5.01 eV, and the onset of reduction = -0.83 V which gives LUMO = -3.97 eV (Table 3-8). The electrochemically determined bandgap energy (1.04 eV) is lower than the optically determined band gap energy (2.59 eV) of the monomer **109**. This difference may be due to the experimental error and conditions such as humidity and oxygen.

Table 3-8. Electrochemical data (CV) of compounds **109** recorded in acetonitrile (+0.1M n-Bu$_4$NPF$_6$) vs.Fc$^+$/Fc at scan rate v = 0.1 V s^{-1}.

Compounds	Onset of oxidation / V	Onset of reduction / V	E $_{LUMO}$[eV]	E $_{HOMO}$[eV]	E $_{gap}$[eV]
109	+0.21	-0.83	-3.97	-5.01	1.04
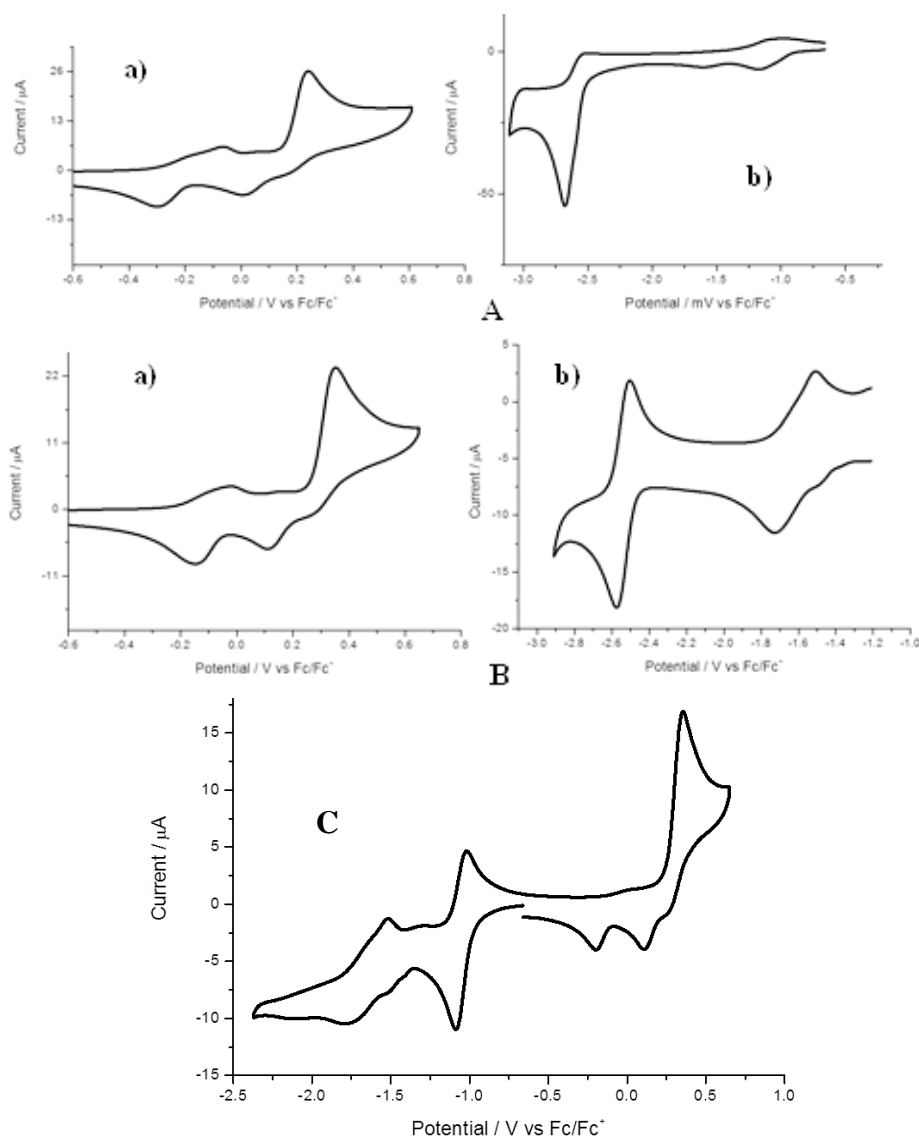
Figure 3-36. Showing (**a**) Oxidation, (**b**) reduction and **C** redox cyclic of compound **109** recorded using a glassy carbon working electrode, an Ag wire as a reference electrode and a Pt wire as a counter electrode. Recorded **A** in acetonitrile (1x10^{-4} M), **B** and **C** in acetonitrile: toluene solution (1:1) (1x10^{-4} M) with 0.1M (n-Bu$_4$NPF$_6$) as a supporting electrolyte at 20 $^{\circ}$C, and a scan rate of 0.1 Vs^{-1}.

A number of attempts were made to find conditions for growing films of polymer **121** on large electrodes such as ITO coated glass. The best results were obtained by cycling over -1.0V to +1.0V (Figure 3-37). The oxidation of polymer **121** displays reversible a broad wave at + 0.89 V and the reduction process gives reversible wave at -1.23V. The CV of

polymer **121**, shows that the onset of oxidation = +0.69 V which gives HOMO= -5.49 eV, and the onset of reduction= -1.45 V which gives LUMO = -3.35 eV. The electrochemically determined bandgap energy = 2.14 eV (Figure 3-38, Table 3-9).

Table 3-9. Electrochemical data (CV) of polymer **121** recorded in acetonitrile (+0.1M n-Bu$_4$NPF$_6$) vs.Fc$^+$/Fc at scan rate v = 0.1 V s^{-1}.

Polymer	Onset of oxidation / V	Onset of reduction / V	E $_{LUMO}$[eV]	E $_{HOMO}$[eV]	E $_{gap}$[eV]
121	+0.69	-1.45	-3.35	-5.49	2.14
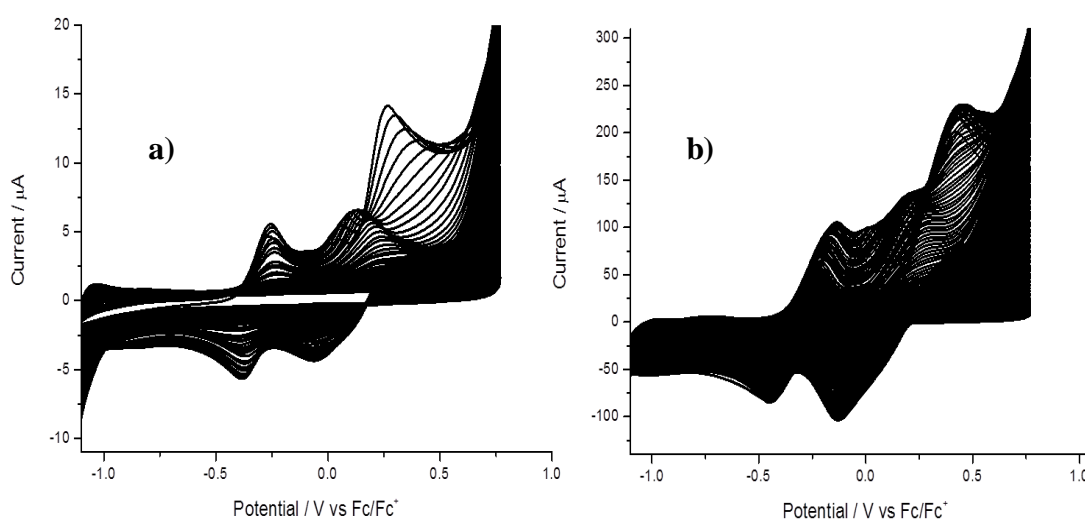
Figure 3-37. Polymer Growth of compound **109** on a) glassy carbon electrode b) ITO slides, an Ag wire as a reference electrode and a Pt wire as a counter electrode. Recorded in acetonitrile: toluene (1:1) (1x10^{-4} M) over 300 segments at scan rate 0.1 Vs^{-1}.
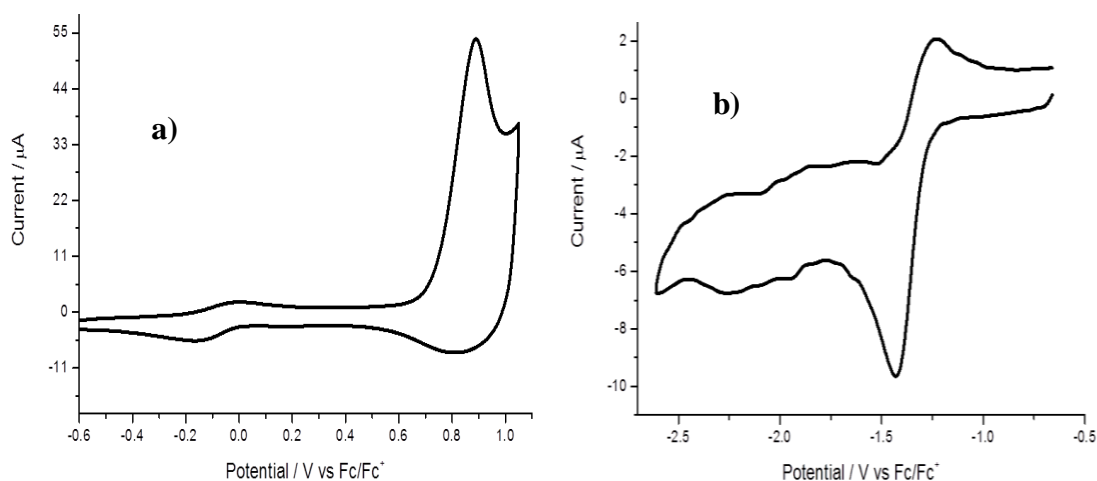
Figure 3-38. Showing a) oxidation and b) reduction of polymer **121** using glassy carbon electrode, an Ag wire as a reference electrode and a Pt wire as a counter electrode. Recorded in DCM (1x10^{-4} M) at scan rate 0.1 Vs^{-1}.

The difference between the HOMO and LUMO values gave an electrochemically determined bandgap energy = 2.14 eV, which is lower than the electrochemically determined bandgap energy of the monomer **109** (2.59 eV). The stability of the polymer **121** films was investigated by repeating cycling over the first redox active peak using CV, which indicated that the polymer possessed good oxidative stability (Figure 3-39).
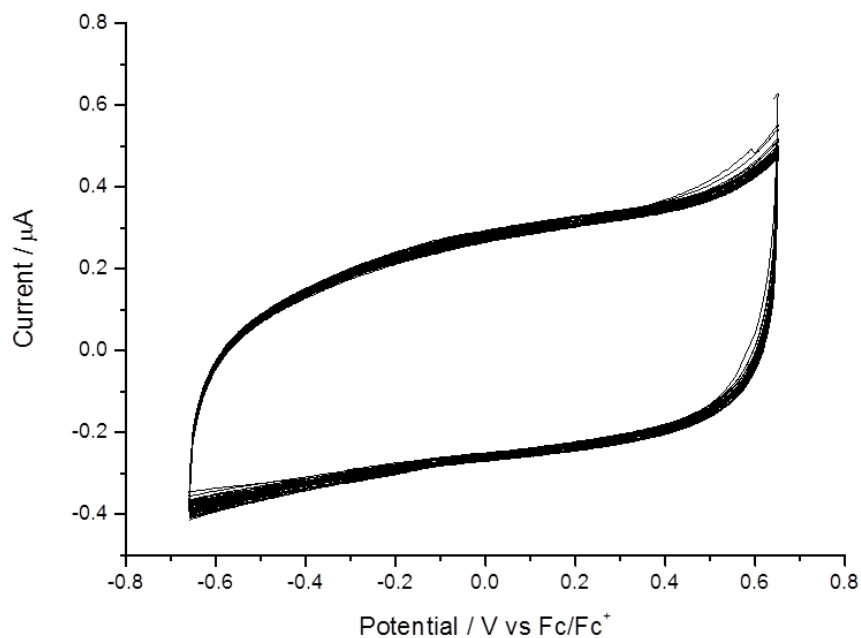
Figure 3-39. Oxidation stability of polymer **121** over 100 segments.

Figure 3-40 shows the peak currents of the thin film of polymer **121** deposited on the electrode (recorded in a monomer free MeCN). This showed that current varies linearly with change of the electrochemical scan rate between 25 mV s^{-1} and 500 mV s^{-1}. This behaviour is due to the strongly adsorbed electroactive species of polymer **121** onto the electrode.
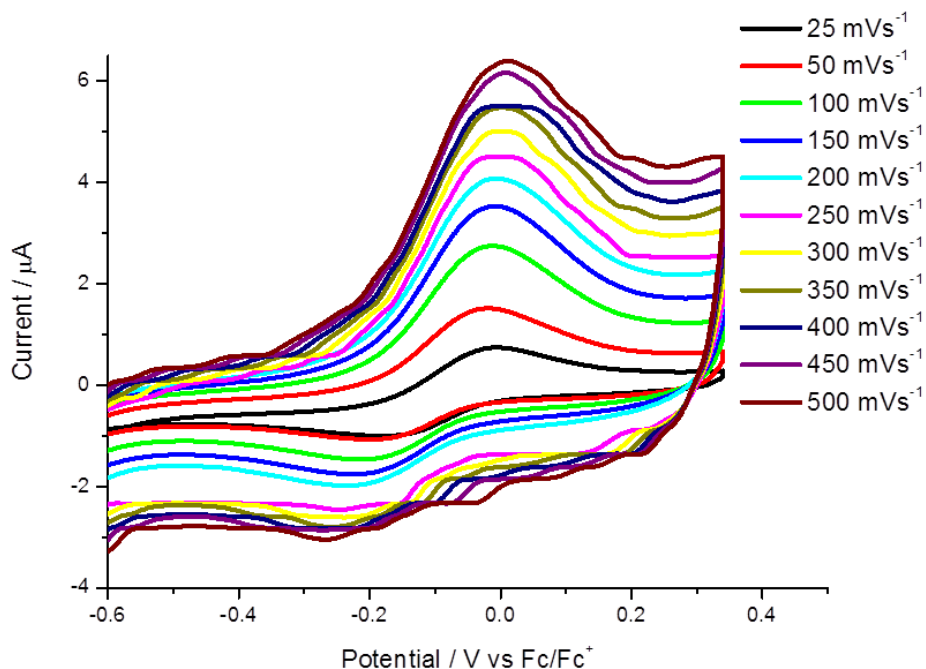
Figure 3-40. Scan rate of polymer **121** in MeCN at scan rates 25-500 mV s^{-1}.

The relationship of scan rate against peak currents of polymer **121** provides an approximately linear relationship confirming a satisfactory stability of the polymer **121** at the electrode/electrolyte interface as shown in Figure 3-41.
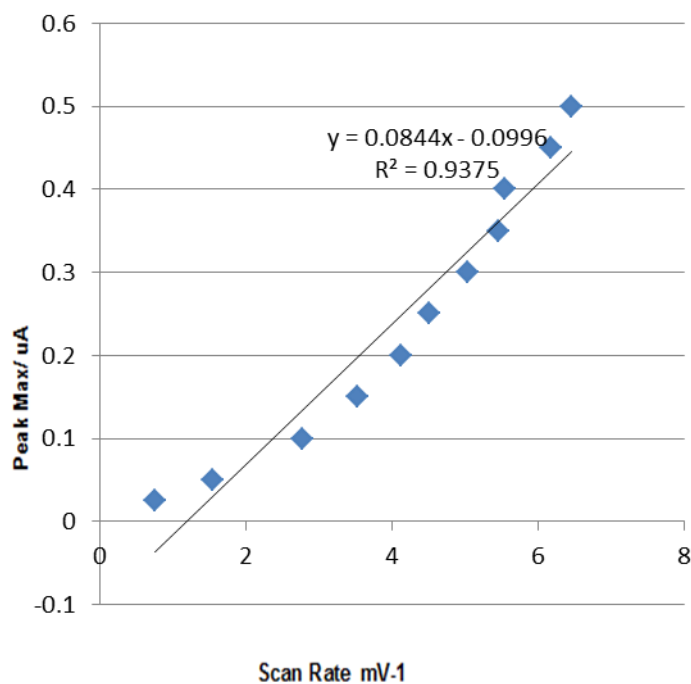
Figure 3-41. Plot of scan rate vs. peak current for polymer **121**.

The absorption spectroscopy of the polymer **121** provides information on the $\pi-\pi*$ transition which is normally associated with the bandgap of polymer. It shows that

the onset of the longest wavelength absorption band in polymer **121** shifted (80 nm) compared to the monomer **109** (Figure 3-42). The absorption spectra of polymer **121** display a λ_{max} at 425 nm. The onset of the absorption edge (560 nm) of this polymer gives the optically determined band gap energy of 2.22 eV, which is slightly higher compared to electrochemically determined band gap energy (2.14 eV). This difference may be due to the experimental error and conditions such as humidity and oxygen. The reason for the red shift is probably due to the alternation of SNS donor polymer chain and presence of the flavin acceptor moiety in the polymer side chain.
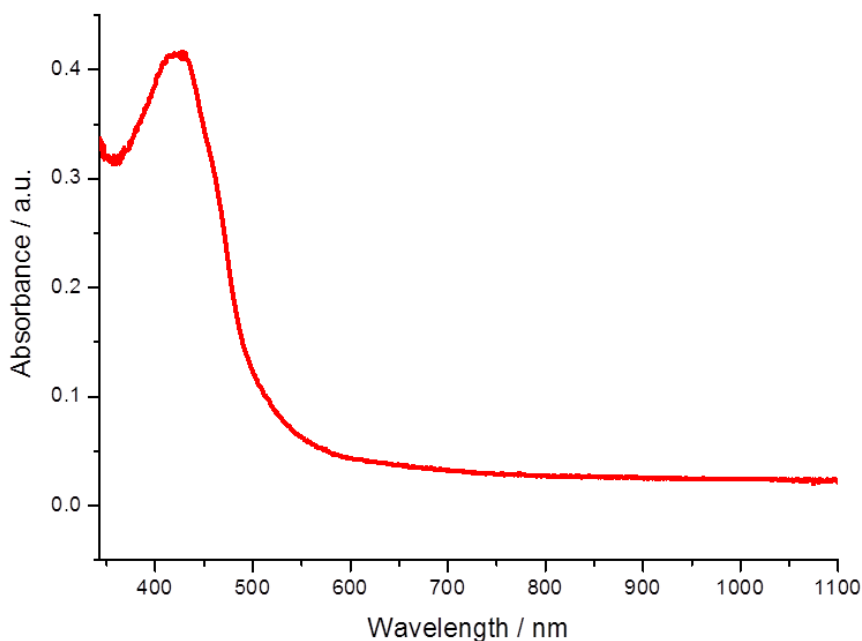
Figure 3-42. Absorption spectra of polymer **121** after de-doped in dichloromethane solution (-0.4 to -0.2 V).

Figure 3-43 shows the spectroelectrochemistry of polymer **121** recorded in DCM on ITO electrode as a thin film. The applied potential range from the neutral polymer **121** to the fully oxidized state of the polymer **121** was studied. The neutral polymer shows absorption band at around 350 nm. Upon increasing applied potential, a new peak at 400 nm appeared, which is related to the polaron states. Further increase in the applied potential leads to the appearance of new sharp peak absorption at around 750 nm. This absorption may be related to the bipolaron states.
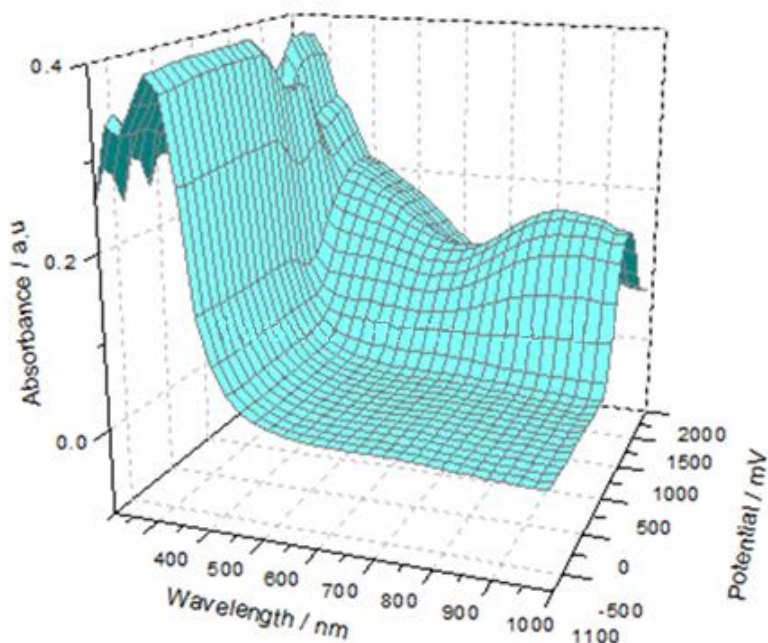
Figure 3-43. UV-vis spectroelectrochemical plot upon p-doping polymer **121**deposited on ITO in DCM in presence TBAPF$_6$ (0.1M)

3.3.9. Molecular Modelling of compound 109

Compound **109** was moddled using density functional theory (DFT). The electron density plots reveal that the LUMO is completely delocalized across the flavin moiety (E$_{LUMO}$= -3.3 eV and E$_{LUMO}$ (+1)= -1.8 eV) (Figure 3-44). While the inspection of the HOMO densities for this system showed that they were delocalized along the thiophene-pyrrole-thiophene unit (E$_{HOMO}$= -5.10 eV and E$_{HOMO}$ (-1)= -6.1 eV) (Figure 3-45).

E$_{LUMO}$ = -3.3 eV   E$_{LUMO}$ (+1) = -1.8 eV

a)   b)
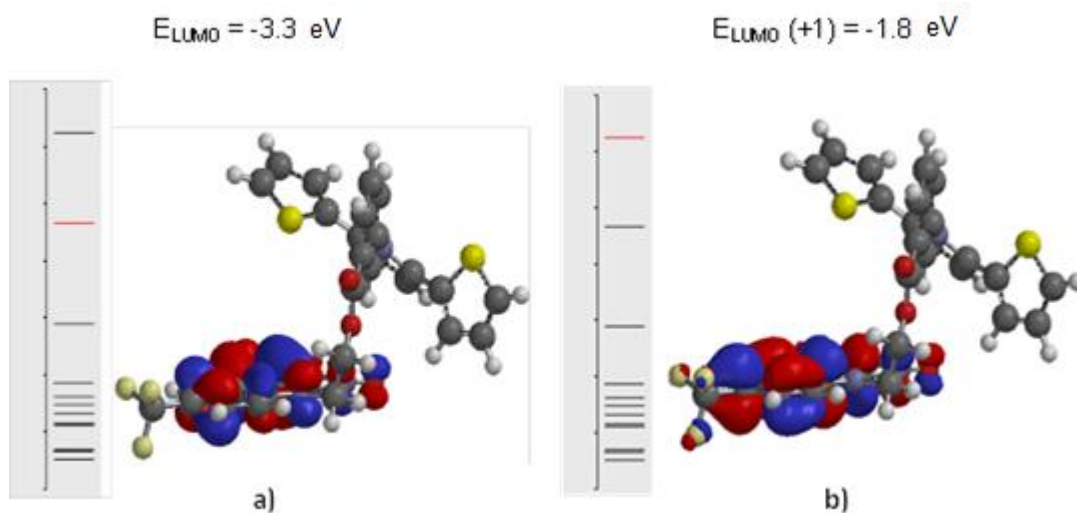
Figure 3-44. DFT B3LYP 6-311G calculation of **109** showing LUMO location.

$E_{HOMO} = -5.10$ eV

$E_{HOMO}(-1) = -6.1$ eV

a)

b)
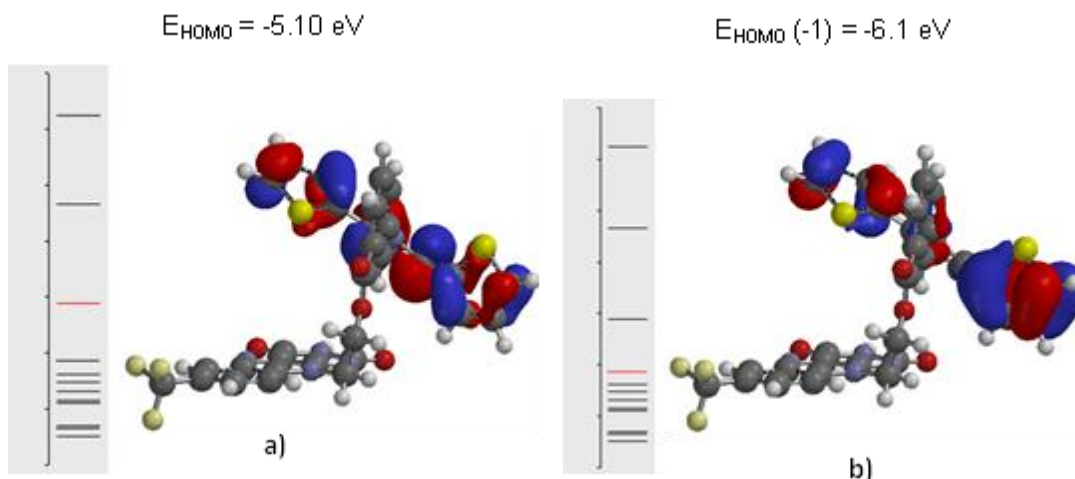
Figure 3-45. DFT B3LYP 6-311G calculation of **109** showing HOMO location.

3.4. Conclusion

A series of 2,5-di(2-thienyl) pyrrole functionalised flavins have been successfully synthesised as flavin appended SNS systems. A polymer has also been made from one of these systems. Optical analysis using UV-vis, UV-vis-NIR and fluorescence spectrometry showed they had strong absorption in the visible region. In addition, the fluorescence of **115** and **109** are quenched strongly compared to **119**. Also, compound **109** was characterised by X-ray and DFT modelling. The cyclic voltammetry showed a decrease in reduction potential to more negative values for 2,5-di(2-thienyl) pyrrole functionalised flavins, compared to that of the parent flavin moiety. This study paves the way for the synthesis of more elaborate derivatives, whereby functionality can be introduced to control the redox properties and reactivity of the SNS and flavin moieties. Polymer **116** has also been made from one of these systems in good yield (86%) and molecular weight = 21351 g/mol. Compounds **115** and **109** have successfully polymerised by electrochemical polymerisation.

4. **Chapter 4**

Synthesis and characterisation of new ferrocene and naphthalene diimide-containing polymers

4.1. Introduction

4.1.1. Radical polymerisation

Free radical polymerisation (FRP) is one of the most widely employed polymerisation techniques. FRP is a method to form a polymer by successive addition of free radical building blocks. It takes place via the breaking of a double bond of the monomer unit, converting it into an active propagating radical. Many different mechanisms exist for formation of free radical monomer units, usually involving separate initiator molecules. The polymer growing chain formed via the initiating free radical adds to (nonradical) monomer units.

Four distinct processes determine free radical polymerisation reactions.

1. *Initiation* is the first step, which includes the formation of the reactive site, thereby "initiating" the polymerisation.

2. *Propagation* is the second step. This is where the polymerisation is activated by an initiator, and monomer molecules are added one by one to the active chain ends in the propagation step and the reactive site is regenerated after each addition of monomer.

3. *Transfer*: This step involves active site transferring into an independent molecule such as an initiator, monomer, polymer, or solvent. This process occurs in both a terminated molecule and a new active site that is capable of undergoing propagation.

4. *Termination* is the final step, which includes the eradication of active sites to be "terminated," or inert, macromolecules. Termination processes result via coupling reactions of two active centres (termed combination), or atomic transfer between active chains (termed disproportionation) (Scheme 4-1)[152] where R'$^{\bullet}$ represents a free radical capable of initiating propagation; M denotes a molecule of monomer; Rm$^{\bullet}$ and Rn$^{\bullet}$ refer to propagating radical chains with degrees of polymerisation of *m* and *n*, respectively. Also, AB is a chain transfer agent; and $P_n + P_m$ represent terminated macromolecules.

Since the 1980s about 50% of synthetic polymers were obtained by free radical polymerisation processes. There are several reasons why radical polymerisation is so important. Firstly, many types of monomers can undergo free radical polymerisation and this led to a growing number of polymerisation techniques that have a high tolerance for many functional groups, including acid, hydroxyl, and amino groups. Secondly, facile copolymerisation can occur between various monomers. Furthermore, a convenient

temperature range and very minimal requirements for purification of monomers and solvents are required.[153]

$$\text{Initiator} \longrightarrow 2R'^{\bullet} \qquad \text{Initiation}$$

$$R'^{\bullet} + M \longrightarrow R_1^{\bullet} \qquad \text{Chain Initiation}$$

$$R_1^{\bullet} + nM \longrightarrow R_n^{\bullet} \qquad \text{Propagation}$$

$$R_n^{\bullet} + AB \longrightarrow R_nA + B^{\bullet} \qquad \text{Transfer}$$

$$R_m^{\bullet} + R_n^{\bullet} \longrightarrow P_{m+n} \qquad \text{Combination}$$

$$R_m^{\bullet} + R_n^{\bullet} \longrightarrow P_m + P_n \qquad \text{Disproportionation}$$

Termination
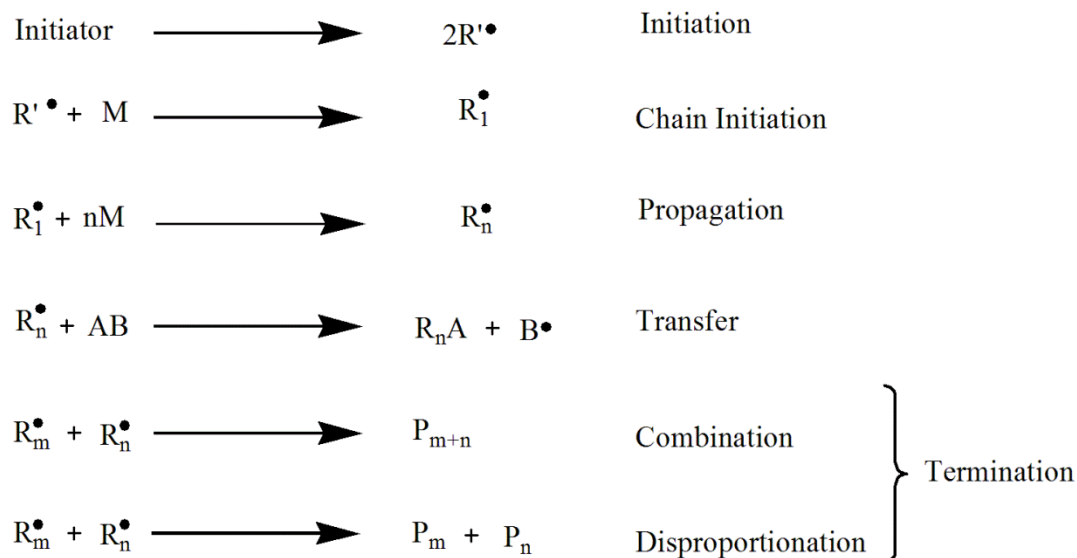
Scheme 4-1. General free radical polymerisation mechanism.

Free radical polymerisation has an important feature in that the partially polymerised mixture mainly consists of high molar mass polymer molecules and unreacted monomer molecules. A wide variety of different polymers and material composites has been obtained by free radical polymerisation. Free radical polymerisation along with anionic, cationic and coordination polymerisation represents a type of chain growth polymerisation (Figure 4-1).[154, 155] The poor control of the molecular weight, the molecular weight distribution, and the difficulty of preparing well-defined copolymers or polymers with a predetermined functionality are the common disadvantages related to the mechanism of free radical polymerisation.

4.1.2. 'Living' or controlled radical polymerisations (CRP)

In 1982, Otsu *et al.*[156] coined the term "living radical polymerisation" to free radical systems which use initiator-transfer-agent-terminators. This mechanism yields radicals that can initiate new chains throughout the course of the reaction and also shows significant loss of active end groups from the growing polymers.

'Living' or controlled radical polymerisation (CRP) techniques were developed based on either reversible deactivation of polymer radicals or a degenerative transfer process. The exchange process of CRP methods can be approached in several ways depending on the

structure of the dormant and deactivating species, the presence of the catalyst and the particular chemistry and mechanism of the exchange. Three methods of controlled radical polymerisations appear to be most efficient, atom transfer radical polymerisations (ATRP), reversible addition-fragmentation chain transfer polymerisation (RAFT), and stable free radical polymerisation (SFRP), best represented by nitroxide-mediated polymerisations (NMP) (Figure 4-1). These methods represent key strategies for the preparation of polymers with narrow molecular weight distributions. Each of these methods has relative advantages and limitations. They have four typical features including the range of polymerizable monomers, typical reaction conditions (temperature, time, sensitivity to impurities, etc.), the nature of transferable end groups/atoms and various additives such as catalysts, accelerators, etc.[157]
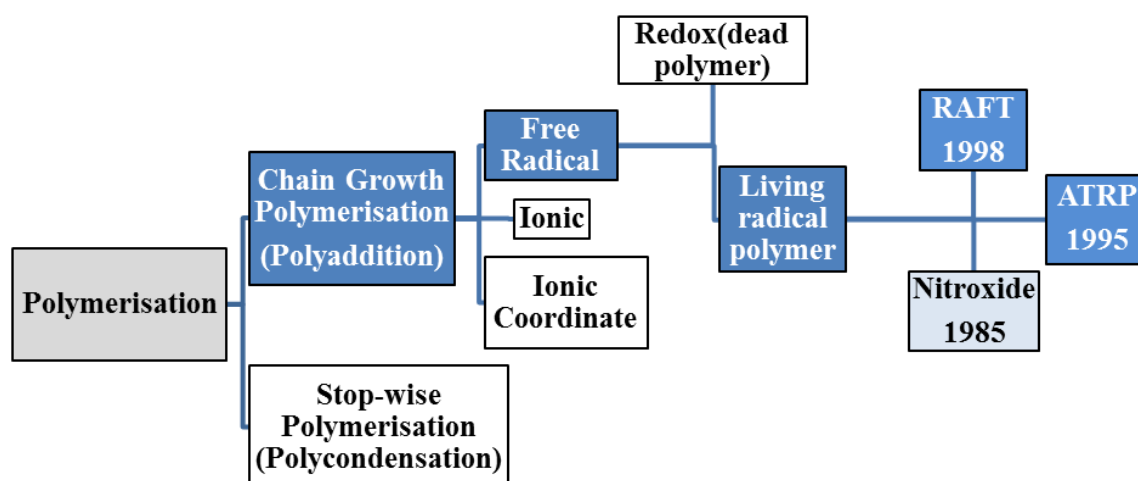
Figure 4-1. Development stages of controlled radical polymerisations.

Controlled radical polymerisations provide impressive control, leading to an unprecedented opportunity in materials design, including the ability to prepare bioconjugates, organic/inorganic composites, and surface-tethered copolymers. Due to the robustness of the polymerisation conditions, CRP enables a new level of materials design and is accessible to all levels of synthetic expertise. Also, CRP can be utilized with a broad range of vinyl monomers for a wide variety of applications (Figure 4-2).[158]
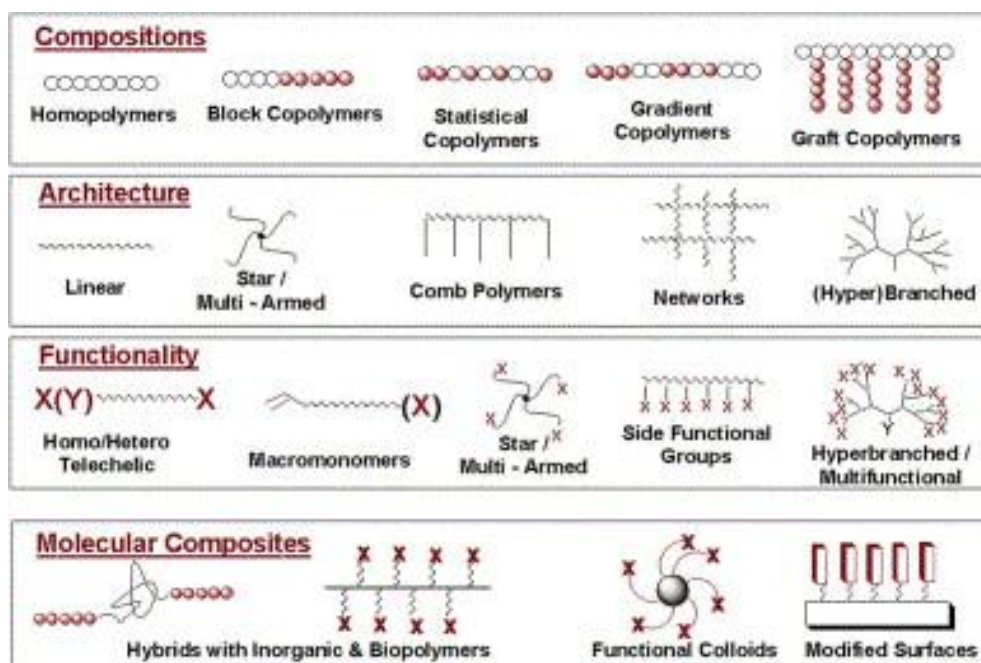
Figure 4-2. Examples of molecular structures attained through CRP.[158]

Controlled radical polymers are used in many applications, such as surface modification, applications which rely on tailored hydrophilicity, nanoparticle functionalization, and adhesive properties, commonly performed through ATRP. Moreover, block copolymers for bio-applications have enabled advancements in drug delivery, bio-mineralization, bio-compatibilization, and hydrogel applications, and are commonly performed through RAFT or ATRP. However, block copolymers generated from NMP are used in pigment dispersion, composite manufacturing, memory devices, and many others.[152, 158]

Scheme 4-2 shows some existing markets targeted by materials prepared by living radical polymerisation process. These methodologies open the door to a wide range of novel polymers with unique properties, regardless of the type of controlled radical polymerisation employed.[152]
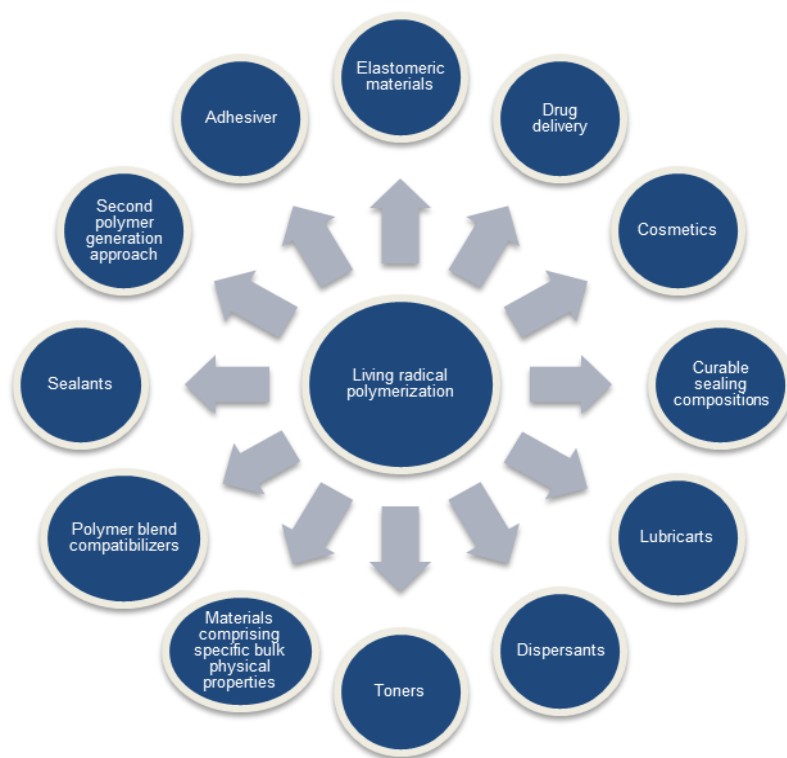
Scheme 4-2. Applications of Living radical polymerisation.

The free radical polymerisation limitations have been controlled as several procedures for controlled radical polymers have evolved based on an understanding and integration of chemistry developed in the fields of organic chemistry, conventional radical polymerisation, and living ionic polymerisation (Figure 4-3).[158]
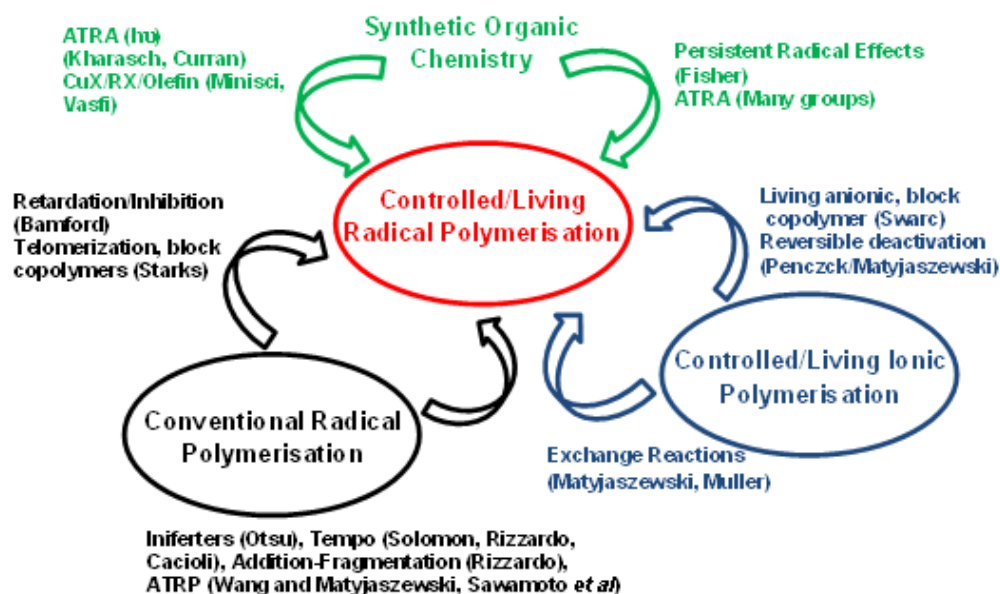
Figure 4-3. Development of CRP by integration of advances in several fields of chemistry.[159-167]

4.1.3. Atom transfer radical polymerisation (ATRP)

All controlled radical polymer techniques operate by rapidly establishing equilibrium between a small fraction of active polymerizing chains and a majority of dormant moieties. ATRP or transition metal mediated atom transfer addition (ATRA) reactions proceed by the transfer of an atom or molecule from the substrate to a transition metal complex generating radical intermediates. Further reactions for these radicals include intra- or inter-molecular addition to unsaturated group. In ATRP the substrates are chosen in such a way that the addition product is much less stable than the initiating radical. Thus it irreversibly adds to the oxidized transition metal complex acting as a persistent radical to give the required product molecule. It is possible to repeat the catalytic cycle for multiple additions of unsaturated monomers leading to a polymerisation reaction, when the starting and product radicals are of similar reactivity. ATRP has proved the most successful synthetic technique for the preparation of polymers. Their polymers have predetermined molecular weights, narrow distributions of molecular weight, and chain end functionality.[168-171]

Atom transfer radical polymerisation was independently reported by two research groups in 1995 as a controlled radical polymerisation technique. They were based on an efficient method of forming carbon- carbon bonds between organic halides and alkenes. Sawamoto *et al.*[172], reported for the first time the polymerisation of MMA initiated by CCl_4 by using $RuCl_2 (PPh_3)_3$/Al (O-*i*Pr)$_3$ as a catalyst.

Matyjaszewski *et al.*[171] reported a second system of polymerisation of styrene catalysed by CuCl/ 2,2'-bipyridyl (bpy) in the presence of 1-phenylethyl chloride as an initiator. After that, many reports using ATRP of styrene, acrylates, methacrylates, acrylonitrile, and dienes by using various transition metal complexes which include nickel, iron, palladium, and rhodium. ATRP considered as a very versatile and effective controlled radical polymerisation method, because of the ability of a metal complex to dictate the rate of monomer addition to the propagating polymer chain.

ATRP provides control in the polymerisation for wide range of monomers under different reaction conditions. Also, it makes possible to prepare polymers having a wide range of architectures including blocks, gradient copolymers, grafts, branched, hyper-branched, stars, and combs.[173]

The ATRP polymerisation is multicomponent and is composed of monomer, initiator, catalyst, ligand and solvent. Scheme 4-3 shows the equilibrium equation describing the mechanism of ATRP polymerisation. This polymerisation based on the reversible transfer of halogen atoms, between a dormant species (the initiator is alkyl halide R–X, where X = Cl or Br) and a transition metal catalyst Mt^n/L (L is a ligand) which has a lower oxidation state. The alkyl halides are reduced to active radicals $R^{\bullet}$ and transition metals are oxidized via an inner sphere electron transfer process. The higher oxidation state metal complex with a coordinated halide anion $X\text{-}Mt^{n+1}/L$ proceed with the rate constant k_{act} by activation process. Complex $X\text{-}Mt^{n+1}/L$ can transfer the halogen atom back to the radical to regenerate the alkyl halide and the lower oxidation state metal complex. Generating polymer with the rate constant of propagation K_P proceeds by reacting with the radicals with the monomer M. Also, these radicals can react with each other to terminate the reaction with a rate constant of termination k_t or with $X\text{-}Mt^{n+1}/L$ by deactivation processes with the rate constant k_{deact}. In the last step, two radical end-groups combine to terminate and kill the reaction (this is neither reversible nor desired), the halogen-terminated polymeric dormant state is reactivated by reaction with Mt^n/L.[171, 174]
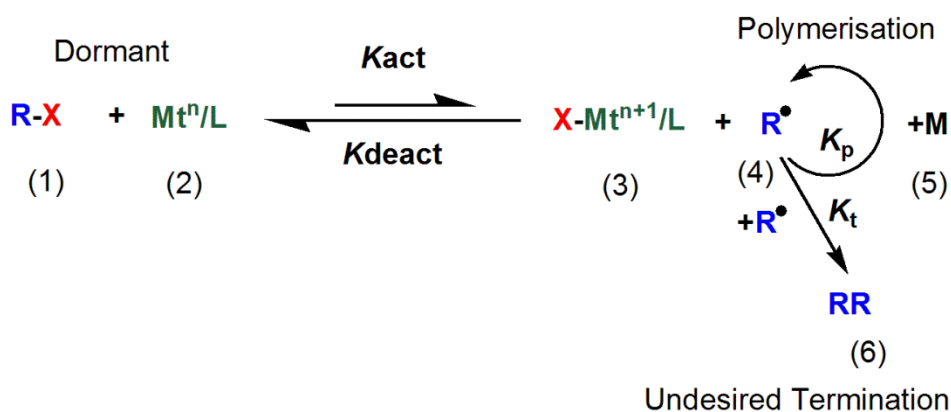
Scheme 4-3. ATRP mechanism, which resides predominantly to the left/ dormant side, includes dormant initiator R-X (1), catalyst composed of a transition metal Mt^n with ligand L (2), oxidized catalyst (3), active radical or active initiator R• (4), and monomer M (5) and terminated polymer RR (6). The reaction rates are labeled with k_x.

4.1.3.1. Components in ATRP

4.1.3.1.1. Catalysts

Several different transition metal catalysts based on copper, iron, cobalt, ruthenium, nickel, molybdenum, osmium, etc. have been used in ATRP (Figure 4-4).[175] Catalysts play an important role in ATRP for determining the position of equilibrium dynamics between active and dormant species. The catalyst must have several prerequisites to be an efficient catalyst in ATRP; these are: **a**) the metal centre must have at least two readily accessible oxidation states separated by one electron, **b**) the metal centre should have reasonable affinity towards a (pseudo) halogen atom, **c**) the metal should undergo relatively strong complexation with ligand and the (pseudo)halogen, **d**) expandable coordination sphere around the metal upon oxidation to accommodate a (pseudo) halogen.[175] However, oxidation of the catalyst to the higher oxidation state during reaction can be avoided by operating under inert conditions.

Copper is the most commonly used transition metal used in ATRP, due to its low cost and versatility. Copper mediated ATRP has been extensively studied with halides as counterions. Polymerisation of alkenes with radical stabilizing substituents such as styrene, methyl acrylate (MA), and methyl methacrylate (MMA) were accomplished successfully with a linear increase in the molecular weight range up to 100000 and molecular weight distributions (MWD) < 1.1 by using cuprous halides complexed with bipyridyl ligands.[176]

Counterions such as carboxylates, hexafluorophosphate, thiocyanate, triflate, and CuM (M= O, S, Se, Te) have been used in copper mediated ATRP. Moreover, addition of small amount of Cu(I) or Cu(II) halide to the polymerisation system, reduces the polydispersity and produces more well-defined products without sacrificing the rate of polymerisation.[177]

The ideal catalyst for ATRP should be highly selective for atom transfer and should not participate in other side reactions. It should have easily tunable activation rate constants to meet the particular requirement for specific monomers. Thus, very active catalysts with equilibrium constants for styrenes and acrylates $K > 10^{-8}$ are not suitable for methacrylates, while acrylamides require higher activities.[178]
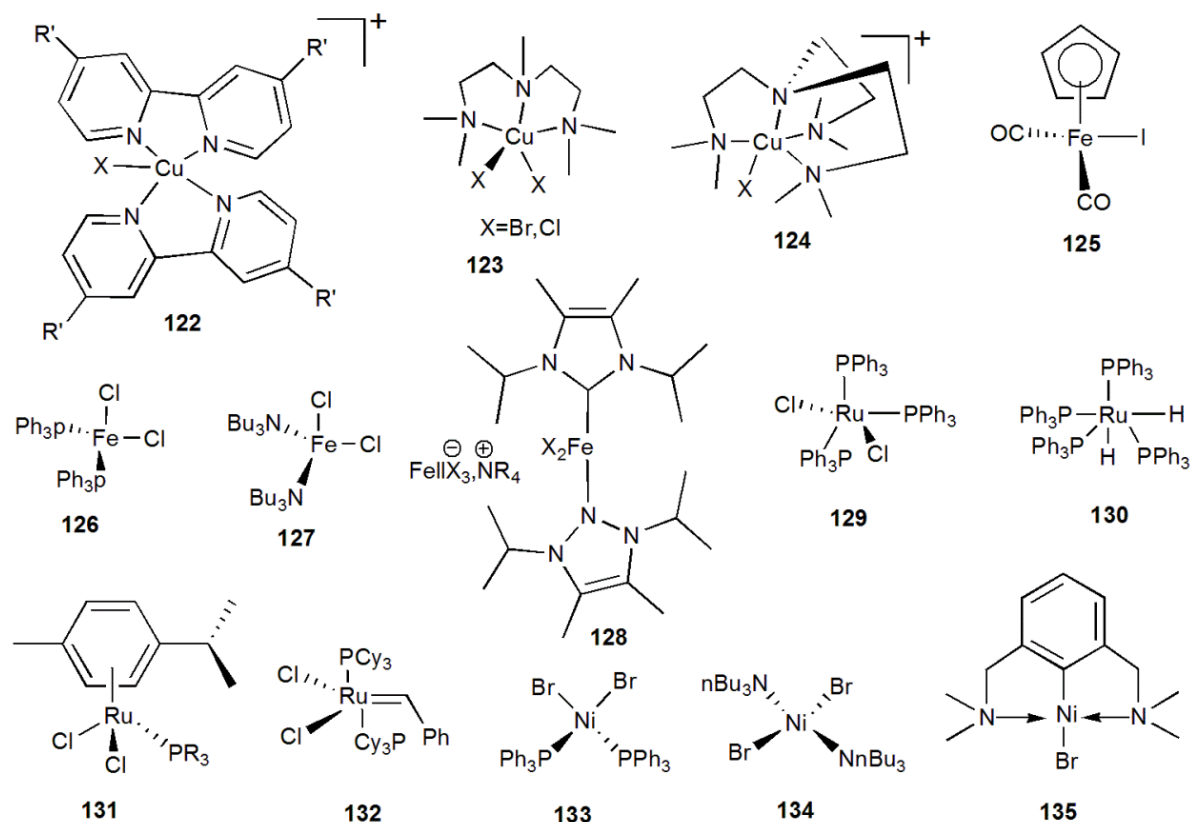
Figure 4-4. Examples of transition metal complexes used in ATRP.

4.1.3.1.2. Ligands

A large variety of ligands have been used in ATRP reactions, in conjunction with different transition metals. The role of the ligand in the ATRP catalyst system is three-fold. The primary role of the ligand in ATRP is to control the solubility of the complex in the reaction mixture which ensures stability of the complex in different monomers, solvents and temperatures.[179] Secondly, the ligand controls catalyst selectivity by steric effects and electronic factors. Finally, the redox potential of the metal center is adjusted by the ligand, thus, affecting the reactivity and equilibrium dynamics of the atom transfer process.[180]

The bidentate ligand 2,2'-bipyridine (bpy) was the first ligand used by Matyjaszewski.[178] Other multidentate nitrogen ligands proved to be superior in controlling the radical formation (Figure 4-5). Nitrogen-based ligands are used for copper-based ATRP, phosphorus based ligands are also used to complex other metals in ATRP reactions such as rhenium, ruthenium, rhodium, nickel and palladium. Also, iron ligated by phosphine base ligands such as tributylphosphine or triphenylphosphine but can also be used in conjunction with nitrogen based ligands.[178]
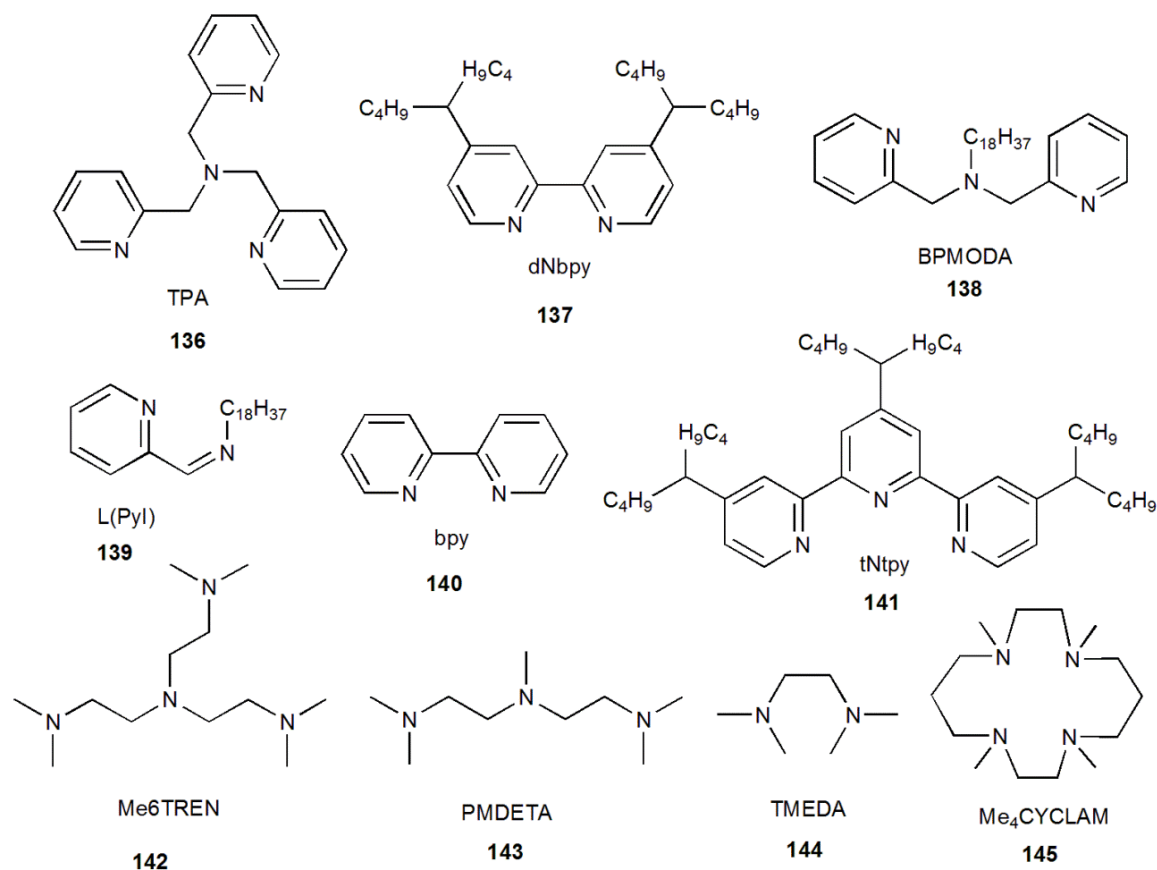
Figure 4-5. Examples of ligands used in ATRP.

4.1.3.1.3. Monomers

Monomers that have a functional group can stabilize the propagating radical in ATRP. A variety of monomers such as styrene, substituted styrenes, (meth)acrylates, (meth)-acrylamides, dienes, acrylonitrile etc. have been successfully used in polymerisation using ATRP (Figure 4-6).

In order to maintain polymerisation control, the concentration of propagating radicals and the rate of radical deactivation for each specific monomer need to be adjusted. Several variables can account for the influence of the monomer in ATRP reactions, including:[152]

a) The monomer solubility parameters and the effects in the complex formation will affect the polymerisation in a similar way as the solvent.

b) The polymerisation rate will be affected by the k_p of the monomer. Where there are multiple monomer additions per activation/deactivation step a broadening of the molecular weight distribution can occur.

c) The atom transfer equilibrium constant (K_{eq}) and the (de)activation constant will be influenced by each monomer used in a polymerisation.

d) Some halide containing polymer end-groups can have specific interactions with the copper species present in the reaction.

Each monomer possesses its own equilibrium constant ($K_{eq} = k_{act}/k_{deact}$) for active and dormant species in ATRP even with the same catalyst and conditions. The product of k_p and K_{eq} determines the polymerisation rate. Therefore, the polymerisation will occur very slowly if K_{eq} is too small, this could be the reasonable reason why polymerisation of less reactive monomers like olefins, halogenated alkenes and vinyl acetate are not yet successful. For this reason, ideal conditions for ATRP such as the catalyst type, ligand, solvent, additives, and temperature needs to be chosen carefully for each monomer.[178]
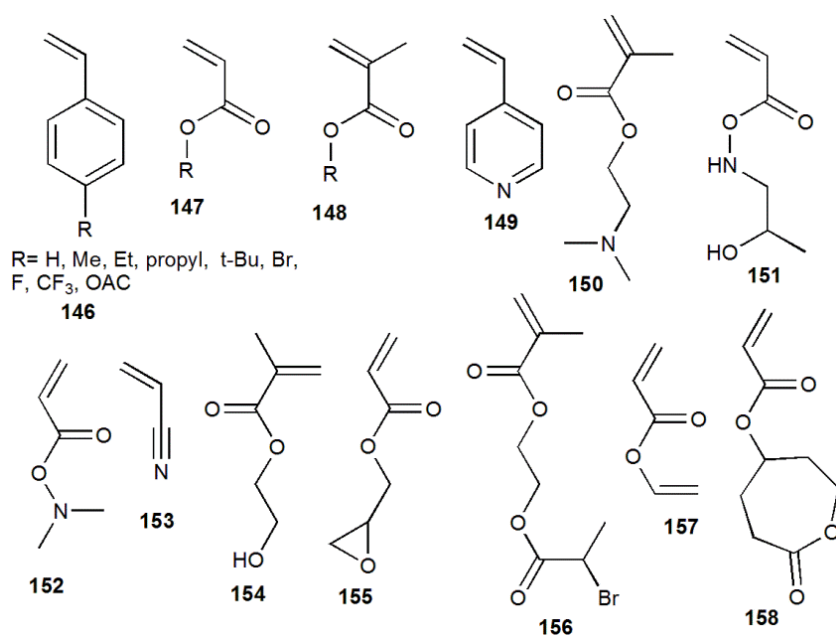
Figure 4-6. Examples of monomers with different functionalities.

Poly(MA) has been obtained with narrow MWD (1.10). whereas, methyl acrylate (MA) was polymerised using tris[2-(dimethylamino)ethyl]amine (Me6TREN) in conjunction with CuBr as the catalyst system in 1 h at ambient temperature.[181] Also, acrylates such as 2-hydroxyethyl acrylate, *t*-butyl acrylate, glycidyl acrylate, long chain alkyl acrylates, and fluorocarbon side chain acrylates have been successfully polymerised using ATRP methods.[182, 183] ATRP of MMA has been reported with different catalyst complexes such as copper, ruthenium, nickel, iron, palladium, and rhodium, due to their relative ease of activation of the dormant species and the high values of K_{eq}.[178] PMMA was obtained in a molecular weight range up to 180 000.

Other methacrylic esters such as 2-(dimethylamino)ethyl methacrylate, 2-hydroxyethyl methacrylate, *n*-butyl methacrylate, fluorinated methacrylic esters, and oligo(ethylene-oxide) substituent methacrylates were successfully polymerised using ATRP. Also, monomers such as acrylonitrile, (meth)acrylamides, 4-vinylpyridine was polymerised by ATRP.[178, 184]

4.1.3.1.4. Initiators

The role of the initiator is to determine the number of growing polymer chains. The faster initiation with a fewer terminations and transfers, more consistent the number of propagating chains leading to narrow molecular weight distributions.[178] Alkyl halides R-X (X= Cl, Br) are typically used as initiators in ATRP (Figure 4-7). The structure of the R group and halide atom X selected depending on the monomer and catalyst/ligand employed. In ATRP, a wide range of organic halogen containing compounds including alkyl halides with activated substituents on the α-carbon, benzylic halides, arenesulfonyl chlorides and polyhalogenated compounds have been used as initiators.[185, 186] Polymers prepared using ATRP, halogen containing polymers or halogen end functionalised polymers can also be employed as initiators.

The initiation rate can be affected by many factors, including:[187, 188]

a) Strength of the carbon-halide bond: The bond strength of alkyl bromides is generally lower than that of alkyl chlorides, thereby lowering the activation coefficient (ka).

b) The radical stability: The ease of formation and stability of the radicals increases proportionally with the number of alkyl side-groups on the radical center. Tertiary halides are better initiators than the secondary, which are better than the primary halides.

c) Formation of anions: When the initiators form very electron deficient radicals, outer sphere electron transfer (OSET) process could occur during activation, leading to radical anions susceptible for side reactions. Moreover, in outer sphere electron transfer processes there is no bonded complex between the transition metal center and dormant species, and transfer of the electron and the halogen occur sequentially.
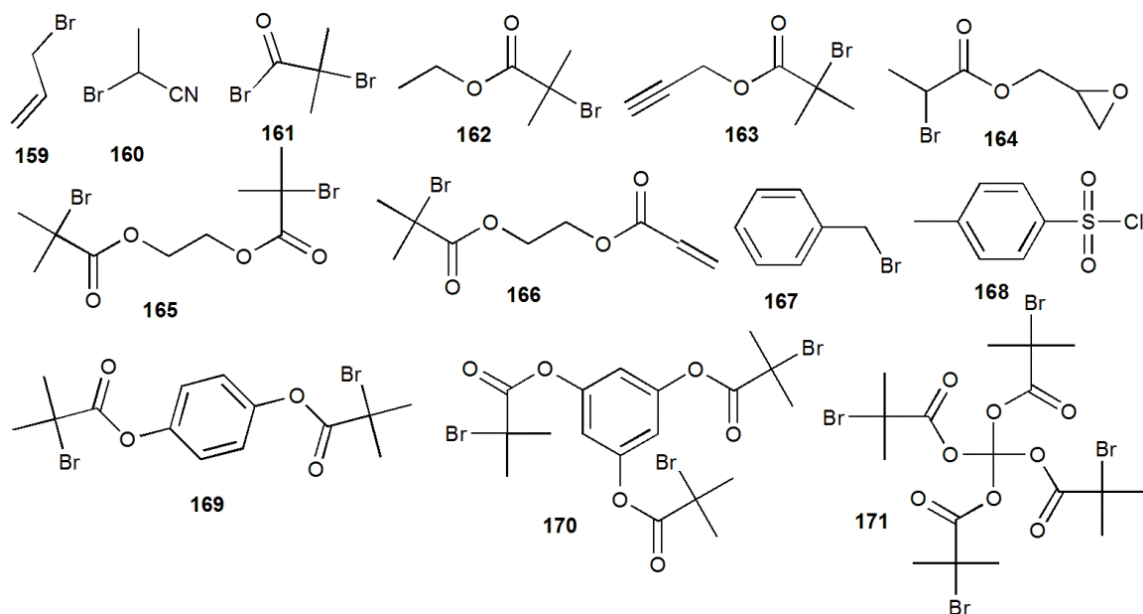
Figure 4-7. Some examples of ATRP initiator.

The number-average molecular weight (*Mn*) of polymers prepared by ATRP depends on the initial concentration ratio of monomer (M) to initiator as well as the monomer conversion (Equation 4-1):[171]

$$M_n = \frac{[M]_o}{[RX]_o} \text{ x Conversion of monomer x Molecular weight of monomer(M)}................4\text{-}1$$

The prepared polymer architectures in ATRP can be varied from linear, using alkyl halide initiators with a single halogen atom, to star-like or brush-like using multiple halogen atoms in the initiator. The advantages of using functional initiators in the synthesis of polymers via ATRP are that direct functionalisation (no post-polymerisation modification required), yields α-telechelic polymers, with multiple applicable functionalities (more than those attainable via nucleophilic substitution of ω-end halogen atom).

4.1.3.1.5. Solvents

ATRP can be carried out in bulk, solution, suspension or emulsion, thus the choice of the solvent is as important. The structure of the catalyst complex may change in different solvents, which influences the atom transfer equilibrium and the polymerisation reaction rate. Also, it is necessary to achieve good control over polymerisation, when the growing polymer complex is not soluble in the monomer. Several solvents such as benzene, xylene, toluene, anisole, diphenyl ether, ethyl acetate, acetone, DMF, alcohol, ethylene carbonate, water, carbon dioxide and others have been used in ATRP for various monomers.[189]

Several factors affect the solvent choice. One of the basic requirements for selecting a solvent is to minimize chain transfer to the solvent. Also, interactions between solvent and the catalytic system or other components in the ATRP system should be minimized. In addition, catalyst poisoning by the solvent (*e.g.* carboxylic acids or phosphines) in copper-based ATRP and solvent-assisted side reactions, should be minimized. The catalyst structure changes in different solvents, and solubility of the catalyst is better in polar solvents.[152, 178]

4.1.3.1.6. Temperature and Reaction Time

In general increasing the temperature in an ATRP affects the rate of polymerisation proportionally. With increasing temperature both the radical propagation rate constant (k_p) and the atom transfer equilibrium constant (K_{eq}) and k_p/k_t increases, thus giving better control in the polymerisation.

In general, the solubility of the catalyst increases at higher temperatures, also catalyst decomposition may occur as the temperature increases. Furthermore, the chain transfer and other side reactions become more pronounced at elevated temperatures. For these reasons, the optimal temperature for the reaction depends mostly on the monomer, the catalyst, and the targeted molecular weight.[178, 190]

The range from 20 °C to 150 °C is a useful reaction temperature range. Generally, the rate of propagation slows down considerably at high monomer conversions. The long reaction times leading to nearly complete monomer conversion may not increase the polydispersity of the final polymer but will induce loss of end groups. Thus, for obtaining polymers that have high end-group functionality or to synthesise block copolymers, conversion should not exceed 95% to avoid end-group loss.[178]

4.1.3.1.7. Additives

Additives are sometimes necessary for a successful ATRP. For example, Lewis acid additives such as aluminium and other metal alkoxides are needed for the controlled polymerisation of MMA catalysed by ruthenium or other catalyst systems.[172]

 In the absence of the Lewis acid activator no or very slow polymerisation was observed. These additives probably activate and stabilize the catalyst in a higher oxidation state. Polymerisation can be accelerating in the presence of very polar solvents such as water.

Moreover, the presence of strong nucleophiles such as phosphines may sometimes terminate the process.[189, 191]

The polymerisation is considerably accelerated by addition of zerovalent copper in copper based ATRP and iron powder in iron based ATRP without losing the control over molecular weight and MWD. This means the polymerisation may be carried out even without removing the oxygen traces and other inhibitors.[192] Also, various phenols and methyl hydroquinone have been used as additives in ATRP to improve the rate of polymerisation.

4.1.4. Reversible Addition-Fragmentation Chain Transfer Polymerisation (RAFT)

RAFT (Reversible Addition-Fragmentation Chain Transfer) polymerisation is a reversible deactivation radical polymerisation (RDRP) and one of the more versatile methods for providing living features to radical polymerisation. The first RAFT polymerisation using thiocarbonyl compounds was reported by the Commonwealth Scientific and Industrial Research Organization (CSIRO) in 1998.[193]

RAFT polymerisation, in comparison to other controlled polymerisations, has the following advantages:

1. The compatibility of the technique with a wide range of monomers, such as styrene, acrylates, methacrylates, (meth) acrylamides, acrylonitrile, styrenes, dienes, and vinyl monomers is the most significant advantage of the RAFT polymerisation over other CRP techniques.

2. Toleration of unprotected functionality in monomer and solvent (e.g., OH, COOH, NR_2, $CONR_2$, SO_3H). RAFT polymerisations can be carried out in aqueous or protic media conditions.

3. Compatibility of RAFT polymerisations with reaction conditions (e.g. bulk, organic and aqueous solution, mini-emulsion, emulsion, suspension).

4. Ease of application and inexpensive comparative to competitive technologies.

RAFT can be applied to form homopolymers or copolymers with a narrow molecular weight distribution and can be formed from most monomers amenable to radical polymerisation with a wide range of solvents and initiators. A variety of architectures including stars, blocks, microgel and hyperbranched structures, supramolecular assemblies

and other complex architectures are accessible. RAFT has an ability to form polymers with uniform compositions with the possibility of eliminating the low molecular weight "impurities" which can act as hole or electron traps in organic semiconductors. At the same time, it can target modest molecular weights that offer advantages in solubility, processing and film forming characteristics.[194]

An important current application of RAFT is to link non-conjugated to conjugated polymer. There are three main strategies to form block copolymers RAFT to conjugated polymers:[195]

1. Grafting to strategy: the post polymerisation involves coupling of a RAFT-synthesised polymer to a conjugated polymer segment.
2. Grafting through strategy: which involves RAFT polymerisation of a macro-monomer with pendant semiconductor functionality.
3. Grafting from strategy: in which macro-RAFT agents based on organic semiconductor or analogous oligomeric species are prepared by end-group modification of an organic semiconductor.

4.1.4.1. Classes of RAFT Agents

The RAFT process involves conventional free radical polymerisation of a substituted monomer in the presence of a suitable chain transfer agent (RAFT agent or chain transfer agent (CTA)). RAFT agents include thiocarbonylthio compounds such as dithioesters, dithiocarbamates, trithiocarbonates, xanthates, and phosphoryl esters (Figure 4-8). The choice of the RAFT agent is critical to synthesis polymers with a high degree of functionality and narrow distribution of molecular weights (referred to as a low poly-dispersity index (PDI)).
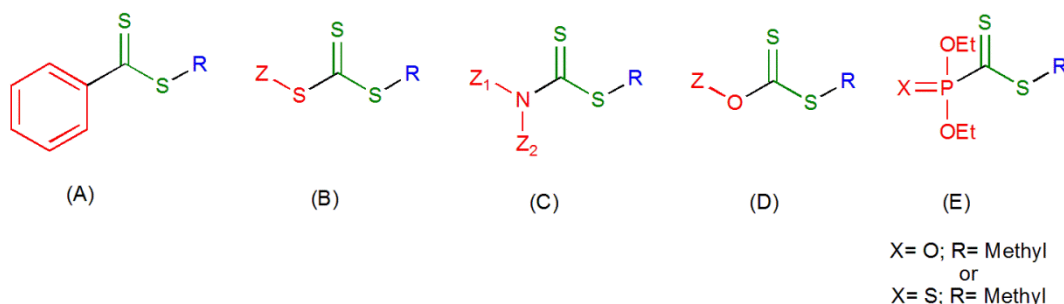
Figure 4-8. Four classes of RAFT agents: A) Dithiobenzoates, B) Trithiocarbonates, C) Dithio-carbamates, D) Xanthates, and Phosphoryl esters.

The thiocarbonylthio group (S=C-S) with substituents R and Z in a RAFT agent influences the polymerisation reaction kinetics and therefore, the degree of structural control. RAFT agent solubility and reactivity depends on the R and Z groups. A variety of RAFT agents are more suitable for specific classes of monomers (Figure 4-9). R is a free homolytic leaving group that is capable of re-initiating the polymerisation. Although the rates of polymerisation for reactions investigated did show a slight dependence on the Z group, the Z groups with electron withdrawing or donating substituents did not significantly affect the activity of RAFT agents.
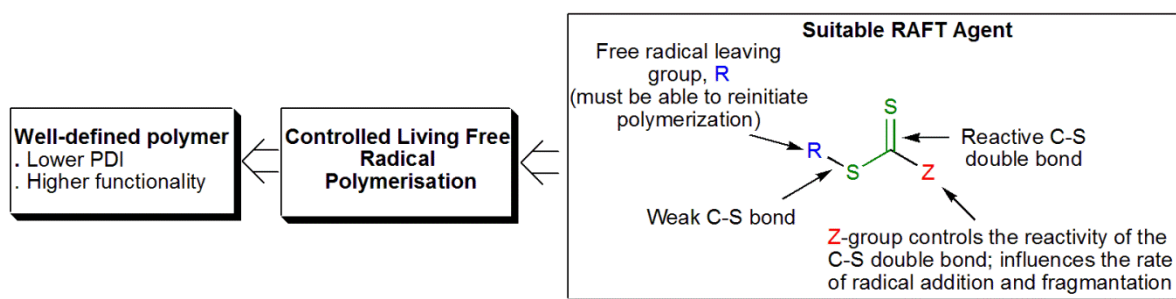
Figure 4-9. General structure of a RAFT agent, indicating the R and Z subtituents impact.

The main classes of RAFT agents are:

A) **Dithiobenzoates:** The dithioesters are one of most effective and have very high transfer constants. However they are prone to hydrolysis, and may cause polymerisation retardation under high concentrations. The role of the activating group is governed by the alkyl-, aryl-S-moiety.

B) **Trithiocarbonates:** They are effective RAFT agents and have high transfer constants. They are more hydrolytically stable than dithiobenzoates and cause less retardation. They are relatively simple to synthesise and easier to purify than other RAFT agents. The role of the activating group is governed by the alkyl-S-moiety.

C) **Dithiocarbamates:** The activity determined by substituents on N and are most effective with electron-rich monomers. The role of the activating group is governed by the R_1R_2-N-moiety.

D) **Xanthates:** They are easier to synthesise than dithiobenzoates, and have lower transfer constants in polymerisation of certain monomers such as styrene and methyl methacrylate. They are more effective with less activated monomers and made more active by electron-withdrawing substituents. The role of the activating group is governed by the alkyl-O-moiety.

E) **Phosphoryl-esters:** Phosphoryl moieties such as methyl diethoxyphosphoryl- and diethoxyphosphoryl-dithioformates have been used as new and efficient trapping agents. The role of the activating group is governed by the phosphonate moiety.[196]

4.1.4.2. Mechanism of RAFT

The first step of the RAFT mechanism[193] (Scheme 4-4) involves the chain transfer of an active species that reacts with propagating radical $P_n\cdot$, which is generated by initiator decomposition. The propagating radical $P_n\cdot$ adds to the dormant chain (**1**), and the resulting intermediate radical (**2**) fragments to a new polymeric thiocarbonylthio compound (**3**) and a new radical $R\cdot$.

a. Initiation:
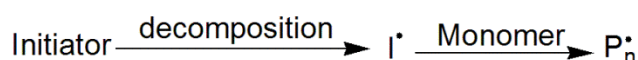
b. Chain transfer:
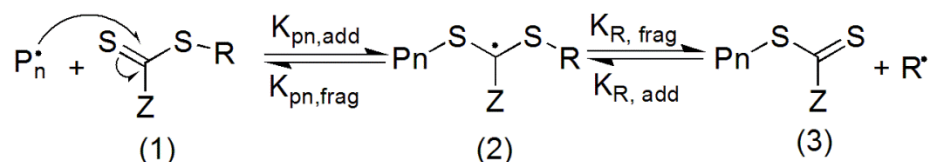
c. Reinitiation
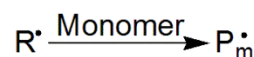
d. Chain equilibration:
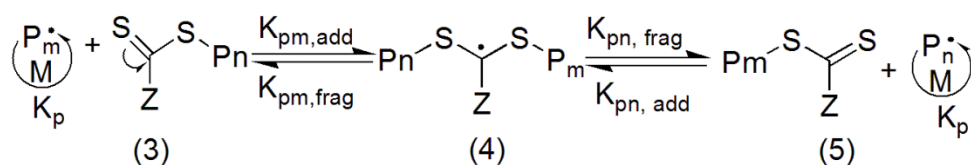
e. Termination

Scheme 4-4. Mechanism of RAFT.

The adduct radical (**2**) can fragment back to the original polymeric species (**1**) and $P_n\cdot$. Subsequently, in order to form the new propagating radical $P_m\cdot$, the new radical $R\cdot$ formed is added to a monomer M. Radical $P_m\cdot$ plays an important role in the RAFT polymerisation, as it makes the polymerisation proceed via formation of the intermediate

radical species (**4**). This radical can either undergo fragmentation to give a new dormant species (**5**), or fragment back to species (**3**) and $P_m\cdot$. Finally, once the dormant species (**1**) is consumed, the equilibrium is arrangement between propagating radicals and dormant species.

4.1.5. Comparison of ATRP and RAFT

Table 4-1 summarizes the main features of the two discussed systems.[157] It seems that ATRP may be especially well suited for low molar mass functional polymers due to the cost of end groups and easier removed of the catalyst. Also, it is very successful for the synthesis of block copolymers and some special hybrids with end functionalities. ATRP require catalyst recycling. However, it is able to withstand small amounts of oxygen, inhibitor and impurities. RAFT is successful for the polymerisation of many less reactive monomers and for the preparation of high molecular weight polymers. There is a need for new efficient transferable groups, due to some limitations of the sulphur containing compounds.

Table 4-1 Comparison of ATRP and RAFT

Feature	ATRP	RAFT
Monomers	All monomers with activated double bonds, except those poisoning the catalytic system acrylic acid and vinyl acetate.	Nearly all monomers.
Conditions	-Large range of temperatures (-30 to $150\ ^{\circ}C$) -Water-borne systems -Tolerance to O_2 and -Inhibitor with Mt°.	-Elevated temperatures for less reactive monomers. -Water-borne systems. -Sensitive to oxygen.
End Groups	**Alkyl (pseudo)halides** -Either S_N, E or radical chemistry for transformations. -Inexpensive & available. -Thermally and photostable. -Halogen exchange for enhanced cross-propagation.	**Dithioesters, iodides & methacrylates** -Radical chemistry for transformations -Relatively expensive. -Thermally and photo less stable. -Colour/odor.
Additives	-Transition metal catalyst/ligand used. -Should be removed /recycled. -Conventional radicals can also be used.	-Conventional radical initiator -May decrease end functionality -May produce too many new chains

4.1.6. Some examples of free radical polymerisation based on Ferrocene

The metallopolymer field has provided soluble and stable well-characterised high molecular weight metallopolymers in usable quantities. The properties, applications and a wide range of characterisation tools have been critical to the emergence of metallopolymers as functional materials. The incorporation of transition metals into polymeric structures has resulted in materials with some unusual and attractive characteristics including electrical, magnetic, preceramic, catalytic, and nonlinear optical properties. Metallopolymers have been utilized for applications such as biosensors, catalysts, lithography, and battery materials. [197]

Ferrocene has an iron centre which is usually assigned to the +2 oxidation state. Each cyclopentadienyl (Cp) ring allocated a single negative charge. The number of π-electrons on each ring is six electrons, and thus making them aromatic. These twelve electrons shared with the metal via covalent bonding. The complex attains an 18-electron configuration when combined these electrons with the six d-electrons on Fe^{2+}. The ability of ferrocene to undergo chemically reversible oxidation and reduction processes has been utilised in the preparation of polymers. Ferrocenyl groups have been incorporated into the polymers either as a side group or as a chain backbone unit.[198]

A number of ferrocene polymers with various functional groups have been prepared. It is relatively easy to introduce metal moieties as side groups as long as they are stable under free-radical polymerisation conditions. The copolymer **172** is a typical example of ferrocene-based polymers which is prepared by ATRP polymerisation (Figure 4-10).[199] Copolymer **172** is soluble in water at room temperature with Mw = 3.4-8.4 x 10^4.

172
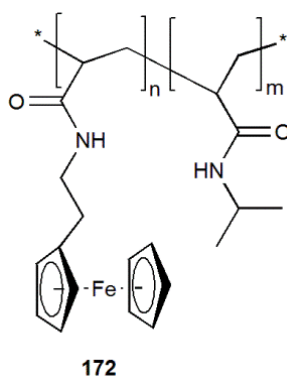
Figure 4-10. Structure of poly[(*N*-2-ferrocenylethylacrylamide)-co-(*N*-isopropylacrylamide)] co-polymer **172**.

Recently, a novel cobaltocenium and ferrocene-containing heterobimetallic diblock co-polymer **173** was prepared via RAFT polymerisation (Figure 4-11).[197] Solution self-assembly of the heterobimetallic diblock copolymer was studied in two different cosolvents (DMF/MeCN and DMF/THF), and in both solvent systems, the self-assembly of the block copolymers resulted in spherical micelles.
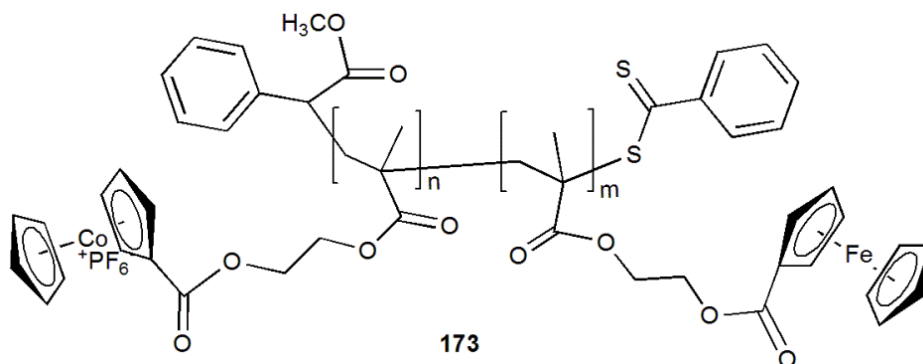
Figure 4-11. Structure of cobaltocenium and ferrocene-containing heterobimetallic diblock co-polymer **173**.

4.2. The aim of the project

The aim of the work described in this chapter was to synthesise and characterise new ferrocene and NDI functionalised polymers (Figure 4-12). The basic principles of ATRP and its application in the synthesis of homo and block (co)polymers of ferrocene were described. Also, RAFT principles and its application in the synthesis of NDI homopolymer are described. The main goal for synthesizing these materials was to design new non-conjugated polymers to develop donor and acceptor polymers with new electronics and self-assembly applications.
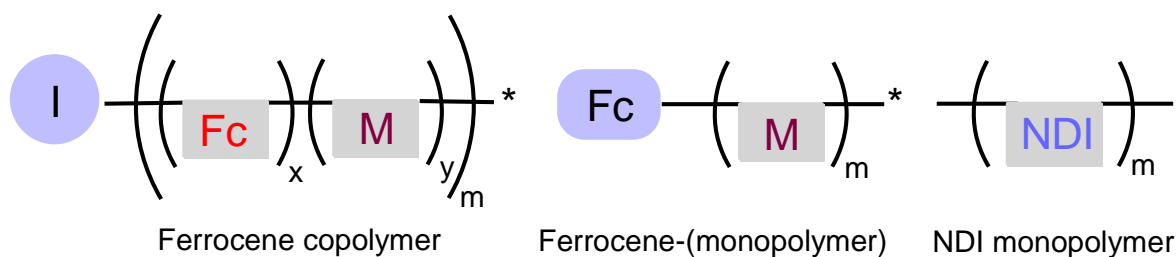
Figure 4-12. Ferrocene and NDI containing polymers.

4.3. Results and Discussion

4.3.1. Synthesis of compounds 178 and 179

The general methodology for the synthesis of compounds **175, 176** and **177** are shown in Scheme 4-5. These compounds were prepared according to the literature.[200] ^{1}H, ^{13}C NMR, mass spectrometry, and FTIR spectra, were consistent with the proposed structures of **175**, **176**, and **177**.
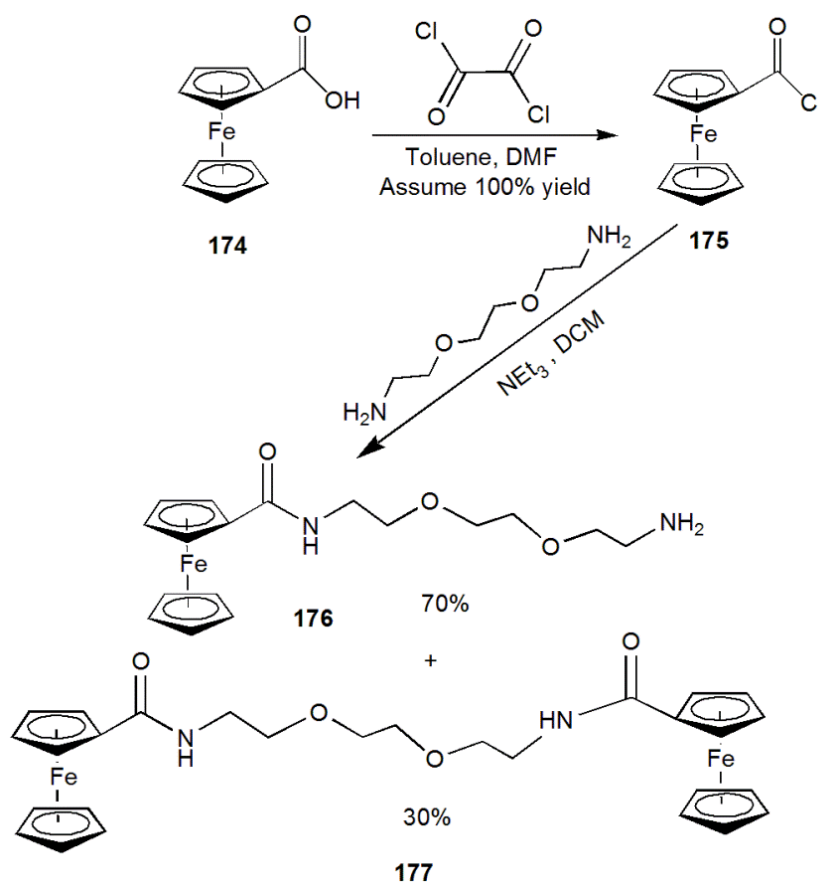
Scheme 4-5. Synthesis of compounds **175**, **176**, and **177**.

The first synthetic approach to afford monomer **178** started with the coupling of commercial methacryloyl chloride with ferrocene amine **176** to afford **178** in 44% yield (Scheme 4-6). The ferrocene initiator **179** was prepared by the coupling of commercial 2-bromo-isobutyryl bromide with ferrocene amine **176** to afford **179** in 49% yield (Scheme 4-6).
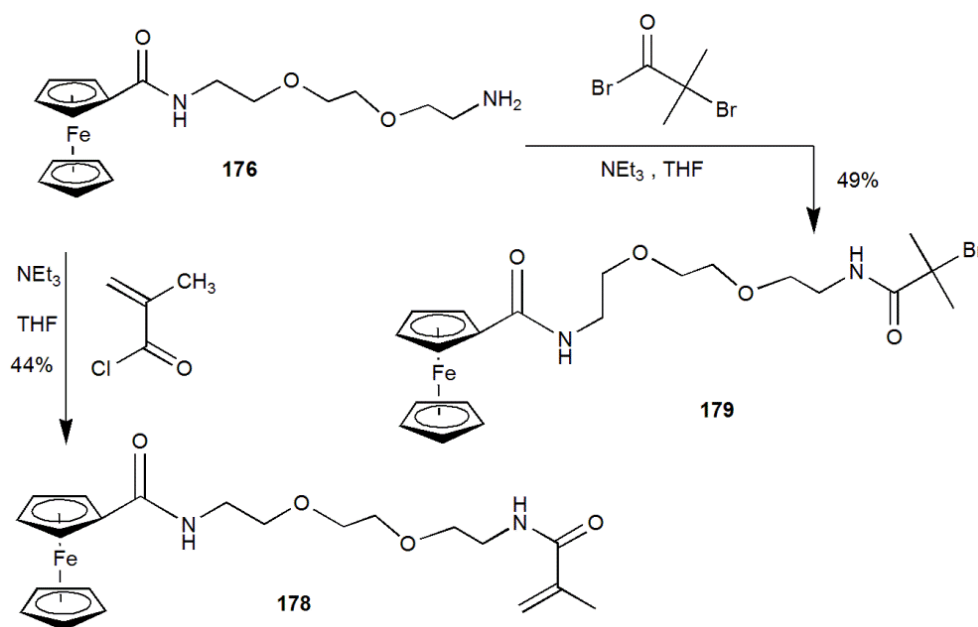
Scheme 4-6. Synthesis of compounds **178** and **179**.

4.3.2. Synthesis of ferrocene polymers 181,183, and 184 by ATRP

Compounds **178** and **179** were used for synthesis of three different polymers by ATRP. To prepare polymer **181**, ethyl 2-bromo-2-methylpropanoate (EBIB) was used as initiator, which was copolymerised with monomer **178** and polyethylene glycol methacrylate **180** in DMSO with pentamethyldiethylenetriamine (PMDETA) as ligand (Scheme 4-7). Copolymer **181** was produced in high yield (94%) (GPC: (THF, 40 ºC, 1mL/min), *Mw* = 11579 *g/mol*, *PDI* = 1.06 (Figure 4-13)).

During the ATRP synthesis the initiator and ferrocene monomer were combined in DMSO in one flask. The catalytic system (Cu(I), Cu(II) and ligand) was added to a second flask and dissolved also in DMSO. Both mixtures were purged of oxygen by the "freeze-pump-thawing" technique (3 cycles) and the reaction flask was immersed in an oil-bath at the reaction temperature. The Cu(I)/Cu(II)/ligand mixture was injected by syringe into the centre of the stirring reaction under a fast flowing nitrogen purge.
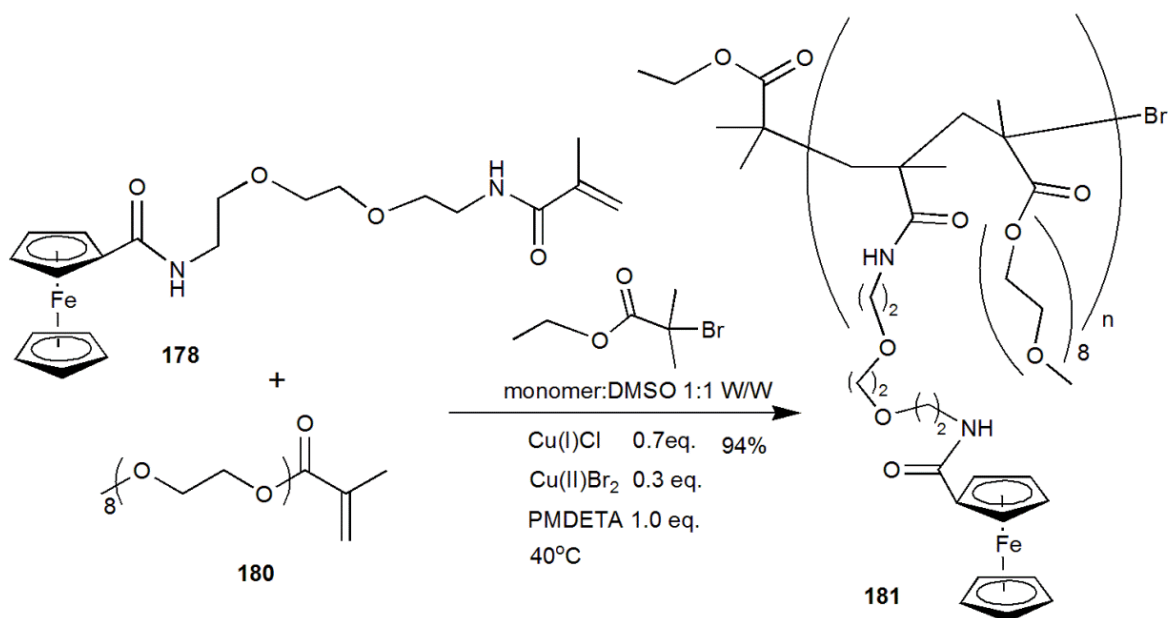
Scheme 4-7. Synthesis of polymer **181**.
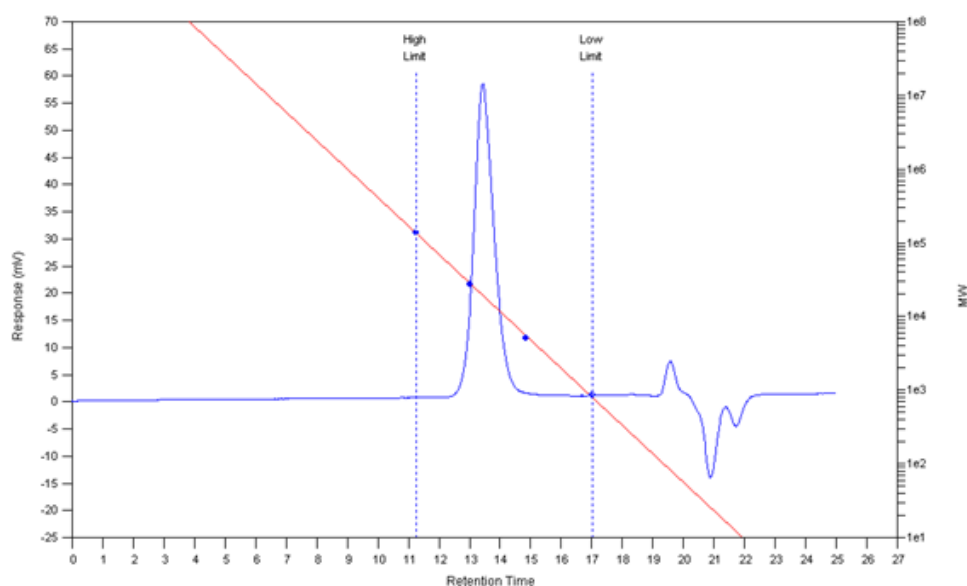
Figure 4-13. Molecular weight determination of polymer **181** by GPC.

The ATRP was terminated typically after 4 hours by slowly pouring the reaction mixture into conical flask of vigorously stirring diethyl ether (400 mL) for one hour which precipitated the polymer **181**. The resulting mixture was put in fridge overnight, the polymer was settled at the base of the flask then isolated by decanting and filtering. The polymer was then dissolved in in a minimum quantity of chloroform and passed through a short column of alumina oxide to remove the copper catalyst. The polymers were then re-precipitated in the same manner as before and after allowing settling for up to 1h were isolated by decanting and filtering.

Copolymer **183** was synthesised by using ethyl 2-bromo-2-methylpropanoate (EBIB) as initiator, monomer **178** and dimethylaminoethyl methacrylate (DMAEMA) **182** in DMSO with PMDETA as ligand (Scheme 4-8). Copolymer **178** was obtained in 97% yield (GPC: (THF, 40 °C, 1mL/min), *Mw* = 17127 *g/mol*, *PDI* = 1.00 (Figure 4-14)).

The ATRP was terminated typically after 2 hours by slowly pouring the reaction mixture into conical flask of vigorously stirred diethyl ether (400 mL) for one hour which precipitated the polymer **183**. The polymer was re-precipitated and collected in the same manner as for polymer **181** to provide the polymer **183** as bright yellow syrup.
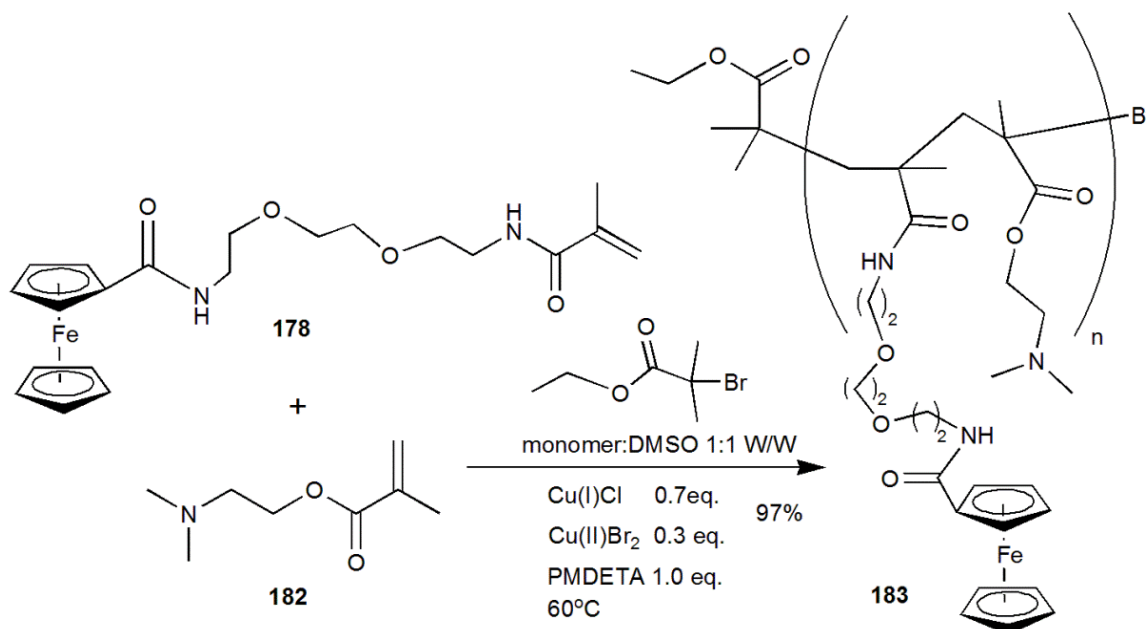
Scheme 4-8. Synthesis of polymer **183**.
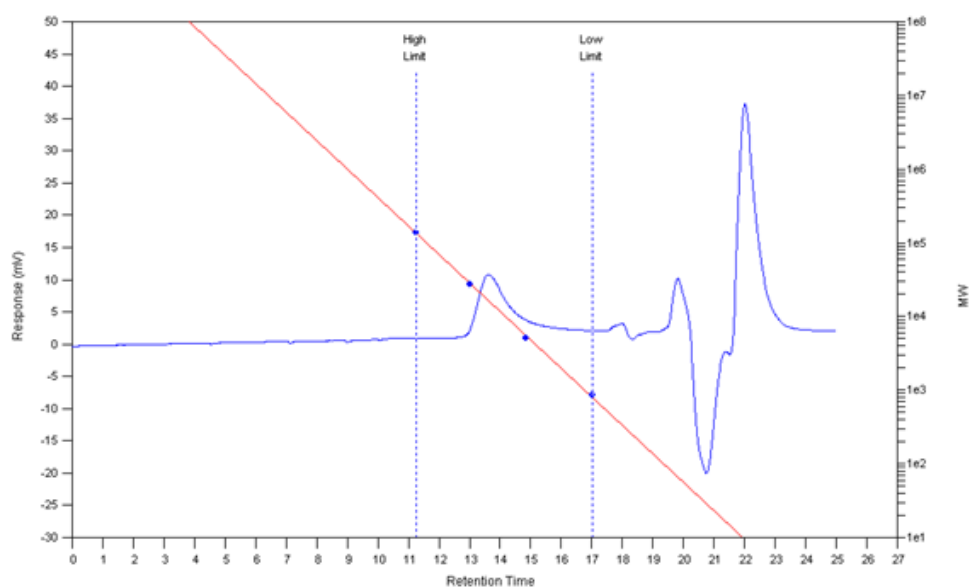
Figure 4-14. Molecular weight determination of polymer **183** by GPC.

Ferrocene derivative **179** was used as initiator in the synthesis of polymer **184**, with dimethylaminoethyl methacrylate (DMAEMA) **182** in DMSO and PMDETA as ligand (Scheme 4-9). Polymer **184** was synthesised in quantitative yield (GPC: (THF, 40 °C, 1mL/min), *Mw* = 33183 *g/mol*, *PDI* = 1.14 (Figure 4-15)).
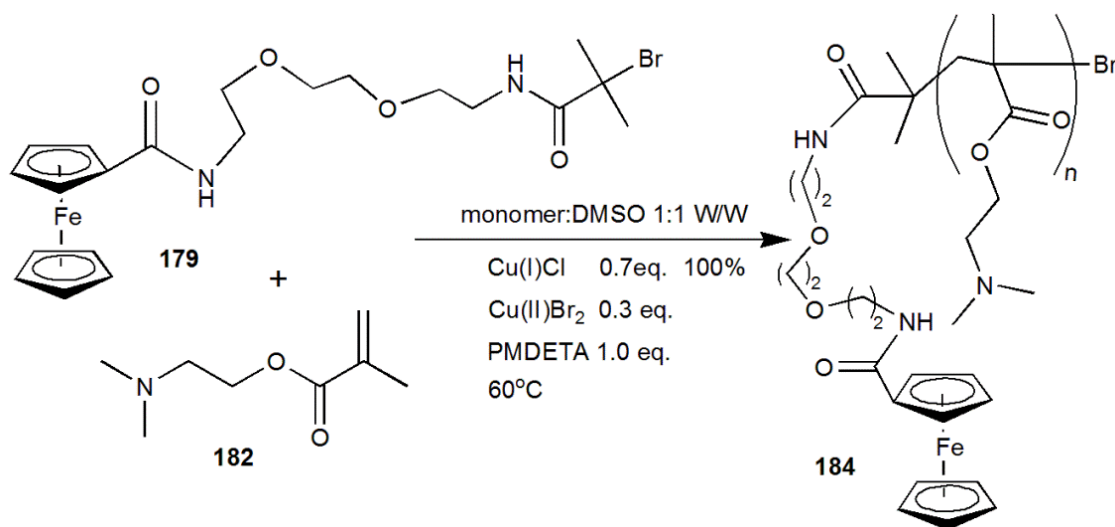
Scheme 4-9. Synthesis of polymer **184**.
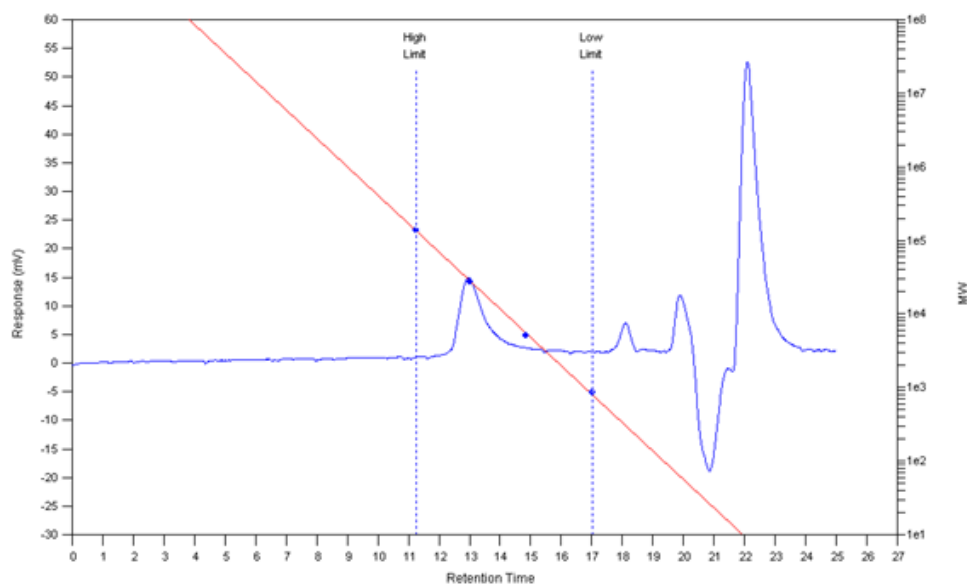
Figure 4-15. Molecular weight determination of polymer **184** by GPC.

The ATRP was terminated typically after 2 hours by slowly pouring the reaction mixture into conical flask of vigorously stirred hexane (400 mL) for one hour which precipitated the polymer **184**. The polymer was re-precipitated and collected in the same manner as before for polymers **181** and **183** to provide the polymer **184** as a clear red syrup.

4.3.3. Particle sizing of polymers 181,183 and 184 by dynamic light scattering (DLS)

The diameter of the polymer particles **181**, **183** and **184** was determined using dynamic light scattering (DLS) in THF (**A**) and water (**B**) as solvents (Figure 4-16). These results would seem to suggest that the size of the polymers is solvent dependent.
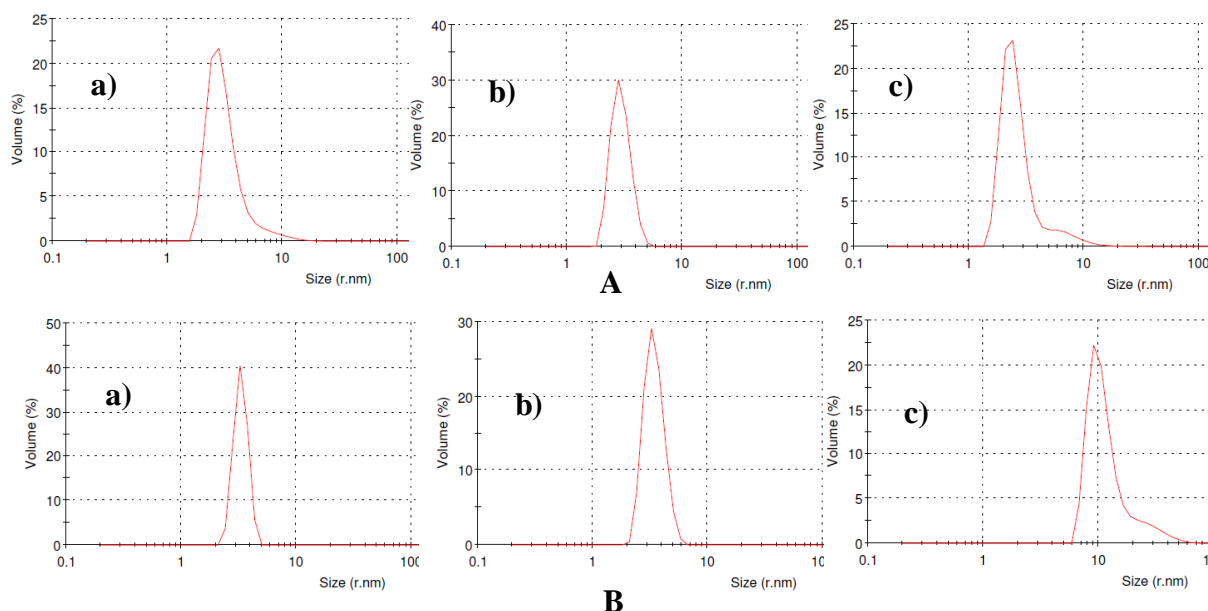
Figure 4-16. Dynamic Light Scattering (DLS) for polymers **a)** **181**, **b)** **183** and **c)** **184**, represent the size distribution by volume in THF (**A**) and water (**B**) as a solvents.

Table 4-2 provides a comparison between the molecular weights obtained by GPC and the particle diameter in THF and water for all polymers. The polymers **183** and **184** form the smallest particle size (2.97 nm diameter) in THF, while the particle size diameter of polymer **184** in water 12.72 nm. The molecular weight obtained by GPC also shows the polymer **184** to have the higher value (33183 g/mol). These observations may suggest that polymer backbone has a determining effect on particle size, a behaviour that may also be solvent dependant. However due to time constraints this was not investigated further.

Table 4-2. Comparison of polymers **181**,**183**, and **184** particle size obtained using dynamic light scattering (DLS) in THF and water with results for the polymer molecular weight *Mw* obtained by GPC.

Polymer	Polymer particle size diameter (nm) in THF	Polymer particle size diameter (nm) in water	GPC results *Mw* (*g/mol*)
181	3.31	3.32	11579
183	2.97	3.46	17127
184	2.97	12.72	33183

4.3.4. Spectroscopic studies of polymers 181,183, and 184

The ^{1}H NMR and ^{13}C NMR spectra displayed the expected signals for **181**,**183** and **184**. The ^{1}H NMR of the polymers **181**,**183** and **184** displayed the expected broad signal peaks and the relative integration of these peaks were useful in confirming the identity of the polymers **181**,**183** and **184**. The UV-vis spectra polymer **181** displayed a broad band at λ_{max}= 270 nm and this corresponds to an optically determined band gap energy E_{gap}= 4.6 eV (Figure 4-17).
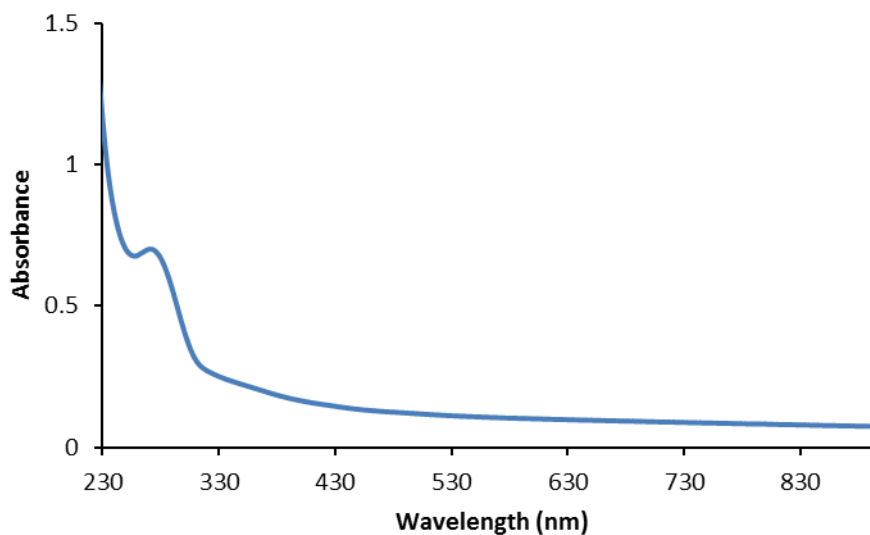
Figure 4-17. UV-visible spectra of polymer **181** recorded in CH_2Cl_2 (1×10^{-4} M).

The UV-vis spectra of polymer **183** displayed a broad band at λ_{max}= 435 nm which corresponds to an optically determined band gap energy E_{gap}= 2.86 eV (Figure 4-18, Table 4-3).
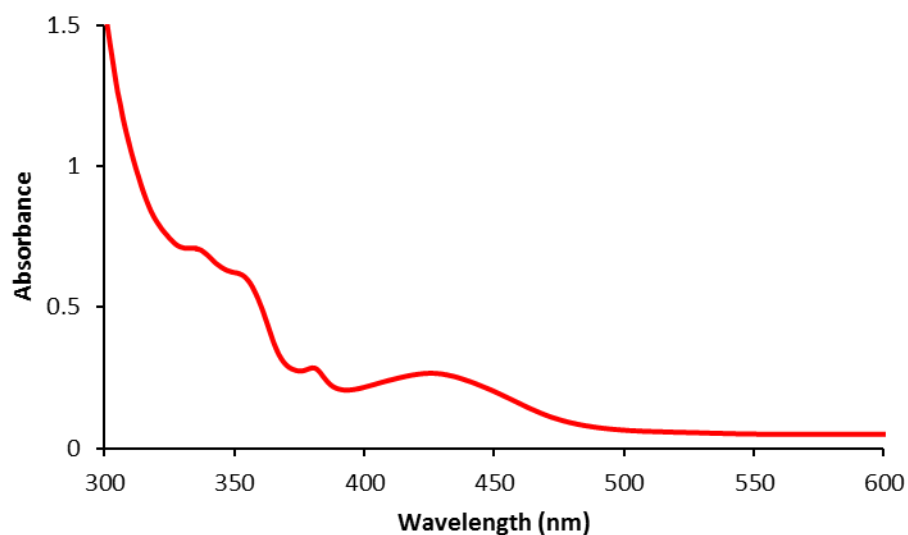
Figure 4-18. UV-visible spectra of polymer **183** recorded in CH_2Cl_2 (1×10^{-4} M).

Table 4-3. UV-vis spectra of polymer **183** recorded in CH_2Cl_2 (1×10^{-4} M). Where the λ_{abs} is absorption wavelength (nm), λ_{Max} is maximum absorption wavelength (nm), and Eg^{opt} optically determined band gap energy (eV).

Compounds	λ_{abs1} (nm)	λ_{abs2} (nm)	λ_{abs3} (nm)	λ_{max} (nm)	Band gap (eV)
183	341	357	384	435	2.86

The UV-vis spectra of polymer **184** displayed a broad band at λ_{max}= 499 nm which corresponds to an optically determined band gap energy E_{gap}= 2.49 eV (Figure 4-19, Table 4-4).
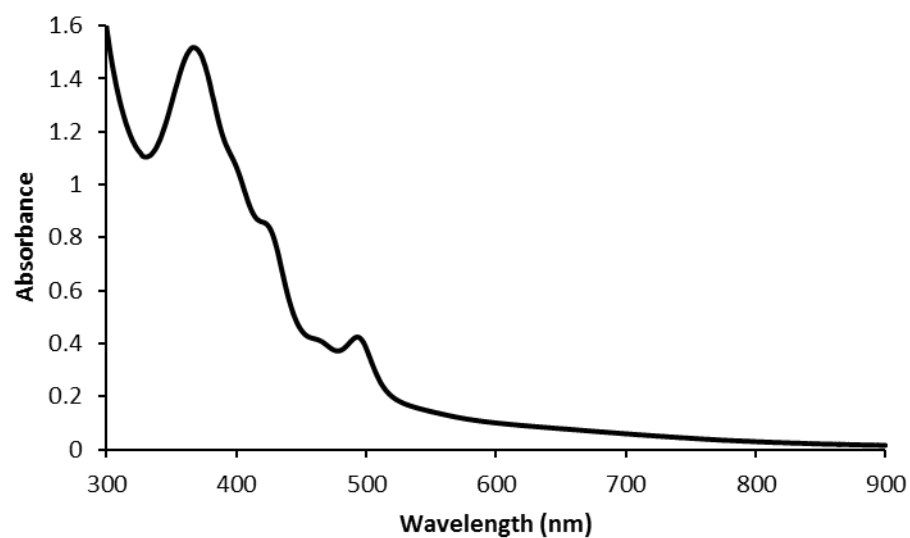
Figure 4-19. UV-visible spectra of polymer **184** recorded in CH_2Cl_2 (1×10^{-4} M).

Table 4-4. UV-vis spectra of polymer **184** recorded in CH_2Cl_2 (1×10^{-4}) M Where the λ_{abs} is absorption wavelength (nm), λ_{Max} is maximum absorption wavelength (nm), and Eg^{opt} optically determined band gap energy (eV).

Compounds	λ_{abs1} (nm)	λ_{abs2} (nm)	λ_{abs3} (nm)	λ_{max} (nm)	Band gap (eV)
184	372	426	470	499	2.49

4.3.5. Electrochemical Studies of polymers 181,183 and 184

The electrochemical properties of the ferrocene polymers **181,183** and **184** was investigated by CV using H_2O as a solvent in the presence of NaCl as a supporting electrolyte and a glassy carbon electrode, Pt counter electrode and Ag/AgCl as reference electrode at ambient temperature (Figure 4-20). Polymers **181,183** and **184** displayed one redox wave at $E_{1/2}$= 0.50 V, $E_{1/2}$= 0.49 V, and $E_{1/2}$= 0.49 V respectively, corresponding to a one-electron oxidation process. Polymer **184** shows the reduction peak current that is slightly smaller than the oxidation current, suggesting that oxidation is not reversible in this solvent.
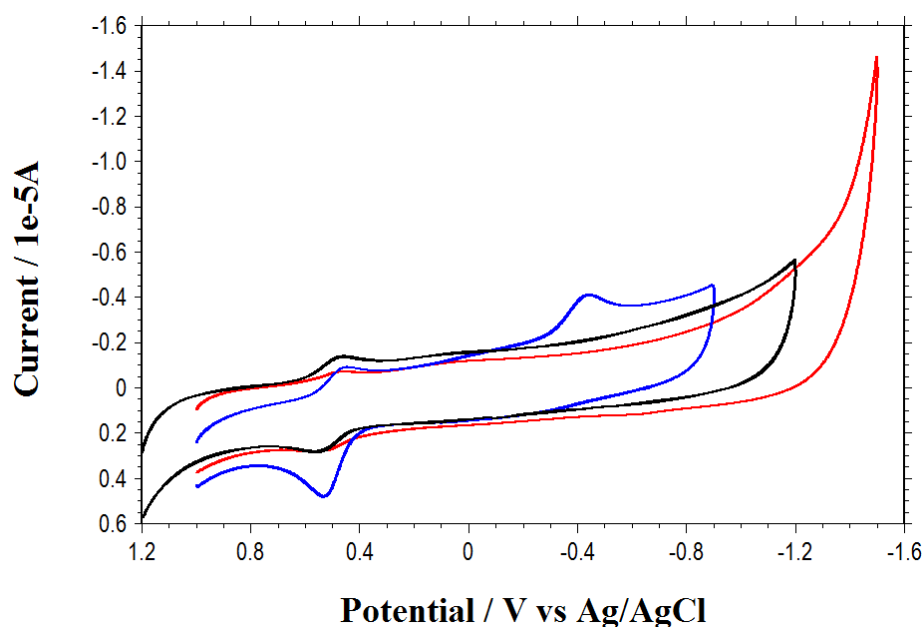
Figure 4-20. Cyclic voltammogramms of polymers **181** (black line), **183** (red line), and **184** (blue line) recorded using a glassy working electrode, and a Pt wire as a counter electrode. Recorded in water with 0.1M (NaCl) as a supporting electrolyte at 20 ºC, and at a scan rate of 0.1 Vs^{-1}.

4.3.6. Synthesis of NDI polymer 188 by RAFT

NDI was used as monomer for synthesis of polymer **188** by the RAFT technique. Compound **185** was synthesised from 1,4,5,8-naphthalene-tetracarboxylicdianhydride (NDA) **27** in one step with octylamine and 3-amino-1-propanol at 140 °C under N_2. This one-pot process affords a 28% yield of compound **185** (Scheme 4-10).
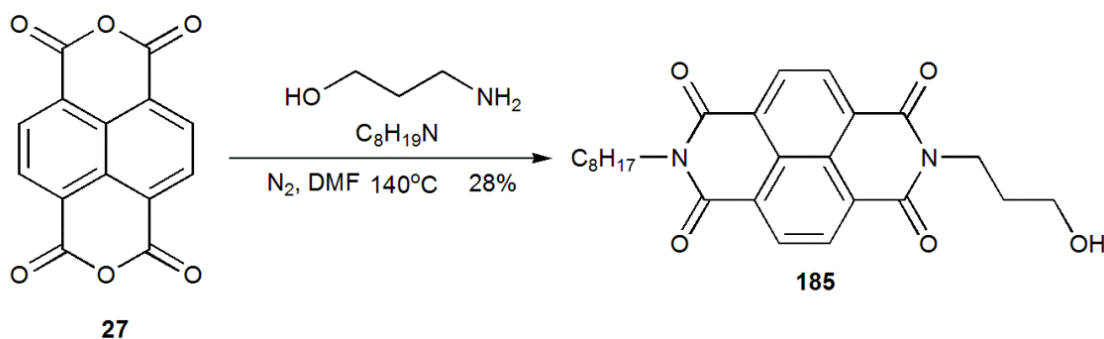
Scheme 4-10. Synthesis of compound **185**.

Compound **187** was synthesised in a 65% yield by the reaction of **185** with methacryloyl chloride *via* Steglich esterification (Scheme 4-11). Compound **186** was prepared by two routes. The first synthetic route involved the reaction of **185** with acrylic acid to afford **186** in a 22% yield. Acryloyl chloride was also used for synthesis **186** by reacting with **185** in presence of DMAP and triethylamine to afford **186** in 57% yield (Scheme 4-11).
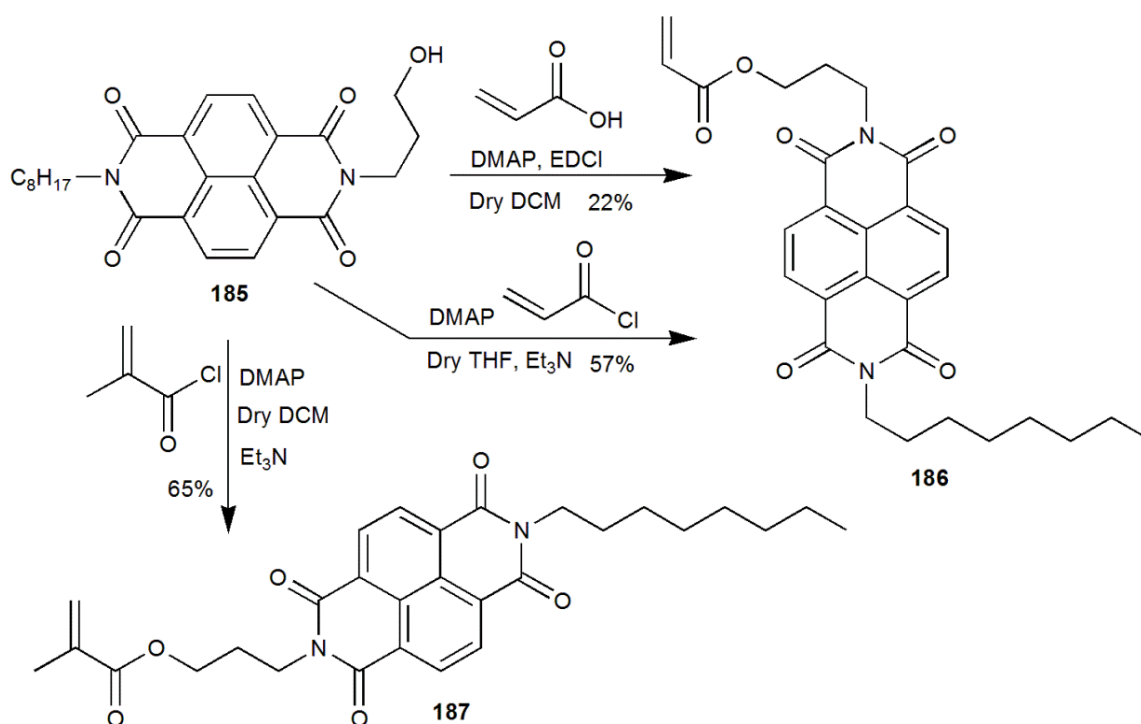
Scheme 4-11. Synthesis of compounds **186** and **187**.

To prepare polymer **188** used azobisisobutyronitrile (AIBN) as initiator, monomer **187** and 2-cyano-2-propyl benzodithioate as a RAFT agent (Scheme 4-12). The reaction was terminated after 1.5h by precipitation into vigorously stirred methanol (250 mL). Polymer **188** was synthesised in high yield (84%) (GPC: (THF, 40 $^\circ$C, 1mL/min), Mw = 10785 g/mol, PDI = 1.08 (Figure 4-21).
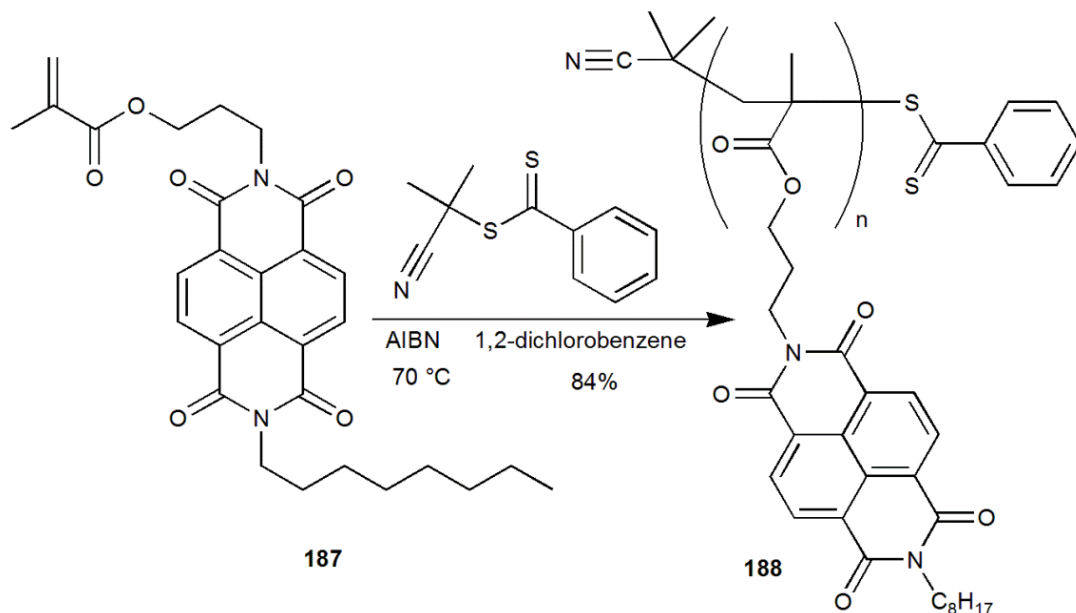
Scheme 4-12. Synthesis of polymer **188**.
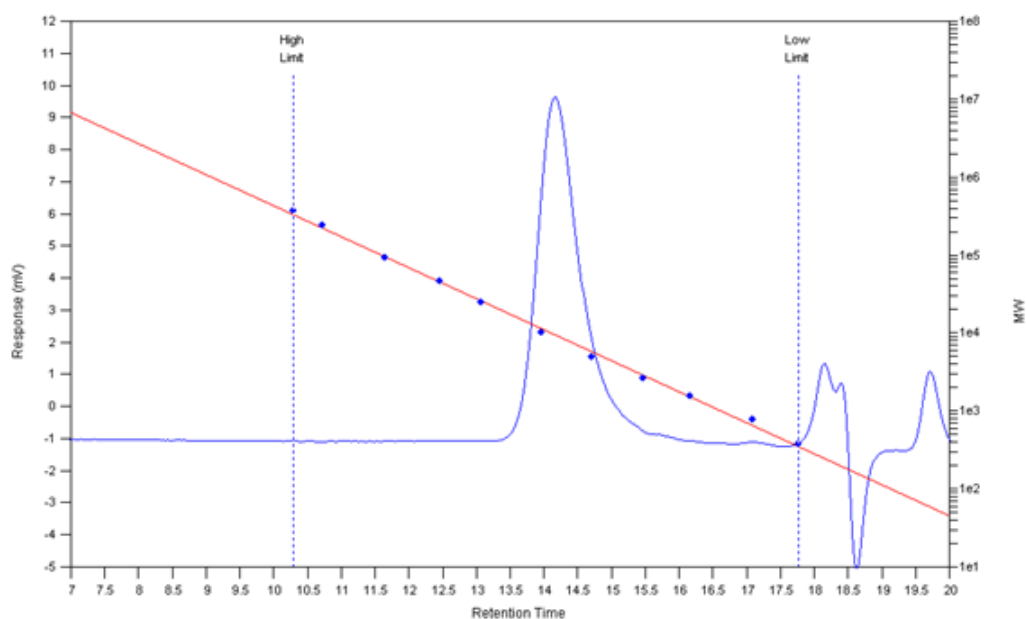
Figure 4-21. Molecular weight determination of polymer **188** by GPC.

4.3.7. Spectroscopic studies of 185, 186, 187 and polymer 188

The ^{1}H NMR and ^{13}C NMR of the **185**,**186**, and **187** displayed the expected signals peaks and the relative integration of these peaks was useful in confirming the composition of **185**,**186**, and **187**. The ^{1}H NMR of the polymer **188** displayed the expected broad signals peaks and the relative integration of these peaks was useful in confirming the identity of the polymer **188**.

The absorption spectra of the compound **187**, and polymer **188** was studied by UV-vis spectroscopy in CH_2Cl_2. Compound **187** displayed absorption bands in the 240-380 nm region with a maxima for the π-π* transition at λ_{max}= 380. The UV-vis spectra of polymer **188** displayed absorption bands in the 236-381 nm region with a broad band at λ_{max}= 381 nm (Figure 4-22, Table 4-5).
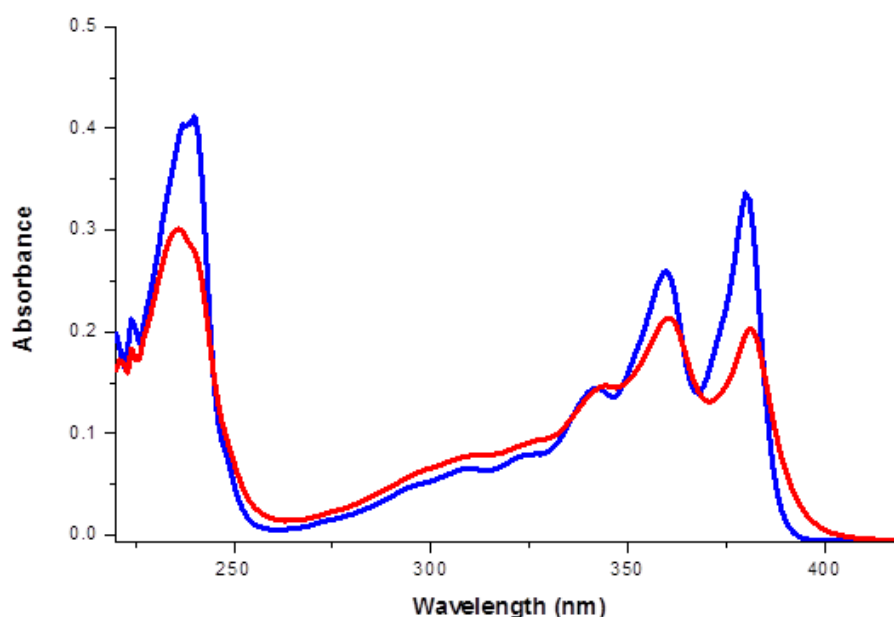
Figure 4-22. UV-visible spectra for **187** (blue) and polymer **188** (red) recorded in CH_2Cl_2 (1x10^{-5} M).

Table 4-5. UV-vis spectra data of compounds **187**, and **188** recorded in CH_2Cl_2 (1x10^{-5} M) Where the λ_{abs} is absorption wavelength (nm), λ_{Max} is maximum absorption wavelength (nm), and Eg^{opt} optically determined band gap energy (eV).

Compounds	λ_{abs1} (nm)	λ_{abs2} (nm)	λ_{abs3} (nm)	λ_{abs4} (nm)	Band gap (eV)
187	240	341	360	380	3.27
188	236	344	361	381	3.26

The photophysical behavior of **187** (blue) and polymer **188** (red) was investigated by fluorescence spectroscopy recorded as a 10^{-5} M solution in CH_2Cl_2 (excitation wavelength = 360 nm) (Figure 4-23). The emission intensity peak of polymer **188** was over 20 times that observed for the monomer **187**. This increase in emission plus a large stokes shift (140 nm) suggests a capacity for the NDI polymer **188** to exist in a stabilized photoexcited state.
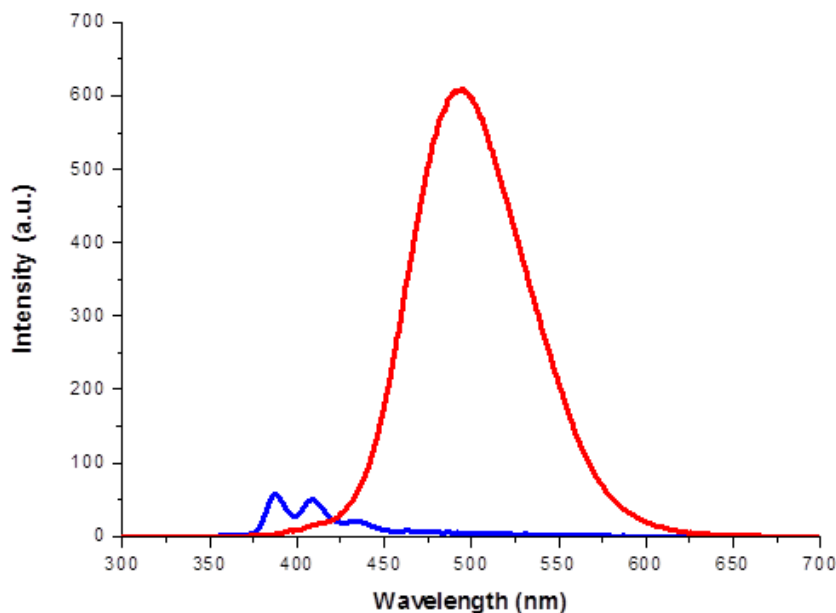
Figure 4-23. Emission spectra for **187** (blue) and polymer **188** (red) recorded in CH_2Cl_2 (1×10^{-5} M) at excitation wavelength = 360 nm.

4.3.8. Electrochemical Studies of 187 and 188

The redox properties of the **187** and polymer **188** were investigated using cyclic voltammetry (CV). Compound **187** and polymer **188** were reduced in well-defined reversible one-electron reduction steps (Figure 4-24, Table 4-6). Compound **187** displayed two reversible redox waves at $E_{1/2}$= -1.06 V and $E_{1/2}$= -1.46 V which corresponds to a LUMO energy of E_{LUMO}= -3.74 eV. Polymer **188** displayed two reversible redox waves at $E_{1/2}$= -1.30 V and $E_{1/2}$= -1.77 V which corresponds to a LUMO energy of E_{LUMO} = - 3.50 eV.

Table 4-6. Electrochemical data (CV) of compounds **187** and **188** recorded in CH_2Cl_2 (+0.1M n-Bu_4NPF_6) vs.Fc+/Fc at scan rate v = 0.1 V s-1.

Compounds	$E^1_{1/2}$ [V]	$E^2_{1/2}$ [V]	E_{LUMO} eV
187	-1.06	-1.46	-3.74
188	- 1.30	- 1.77	-3.50
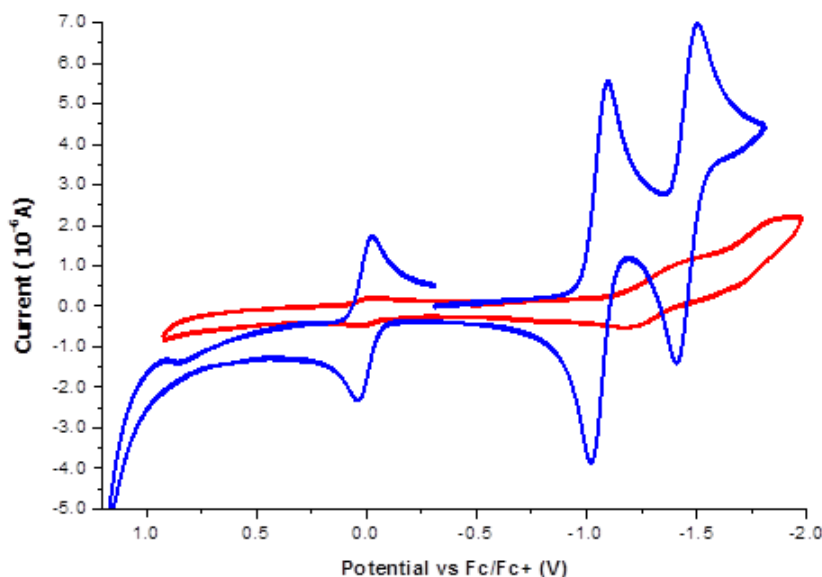
Figure 4-24. Cyclic voltammogramms of compounds **187** (blue line), and polymer **188** (red line), recorded using a glassy working electrode, an Ag wire as a reference electrode and a Pt wire as a counter electrode. Recorded in CH_2Cl_2 (5×10^{-4} M) with 0.1M (n-Bu$_4$NPF$_6$)

4.4. Conclusion

Three polymers **181**, **183** and **184** were synthesised successfully by ATRP. Ferrocene derivatives were used as either initiator or monomer in the synthesis of these polymers. Copolymers of **178** and PEG-methacrylate or DMAEMA yielded **181** and **183** with good results exhibiting low polydispersity and a linear evolution of molecular weights with conversion. Ferrocene initiator **179** was used to polymerise the DMAEMA to yield polymer **184** in high molecular weight. The number-average molecular weight increased linearly with conversion and the polydispersity at lower conversions was good (<1.2). Also, the diameter of these polymer particles was determined by dynamic light scattering (DLS) in THF and water solvents. The polymer backbone has a determining effect on particle size, a behaviour that may also be solvent dependant.

NDI- methylmethacrylate **187** was used as a monomer for the synthesis of polymer **188** via RAFT polymerisation. A good molecular weight resulted with a low polydispersity (<1.1) using a 2-cyano-2-propyl benzodithioate -based macro chain transfer agent. In present work the Cooke group in collaboration with Prof. Woisel's group at Lille University-France use these monomers for synthesis of more polymers either by ATRP or RAFT polymerisation. Also, in future work polymers **181, 183** and **184** will be complexed with β-cyclodextrin and analysis of these polymers to participate in on/off redox binding will be investigated.

5. **Chapter 5**

Synthesis and characterisation of new quinone functionalised naphthalene diimide derivatives

5.1. Introduction

5.1.1. Anthraquinone

Anthraquinone (AQ) **189** is a three-ringed aromatic organic compound. It is planar and usually forms monoclinic crystals. It exists usually as a yellowish to light tan powder. On treatment of anthracene-9,10-dione with various reagents the attack can take place at 6 sites. The nucleophile is able to attack the carbon of the carbonyl function (positions 3, 4). The carbon position 1, carbon position 2, and two oxygen atoms of carbonyl positions 5, 6 are able to attack electrophiles (Figure 5-1).[201]
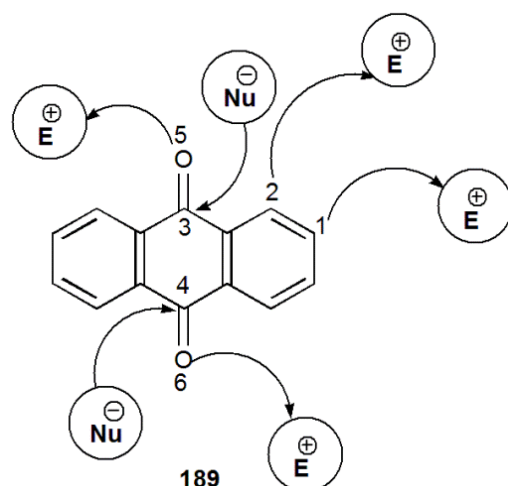
Figure 5-1. Anthraquinone **189** with binding sites label.

Anthraquinone **189** is an important and widely used raw material for the dye industry. Anthraquinones are a class of water-insoluble dyes that can easily be reduced to a water-soluble form for colouring fibres and textiles. Major uses of anthraquinone are seed dressing, seed treatments, a pesticide, a bird repellent, and as an additive in chemical alkaline pulp processes in the paper industry.[202]

Anthraquinone derivatives have been the subjected of much research because of their low cost, high temperature-stability, ambient conditions stability, reversible two-electron redox reactions, and because they tend to form liquid crystalline phases with appropriate substitution patterns.

5.1.2. 11,11,12,12-Tetracyano-9,10-anthraquinodimethane (TCAQ)

Several research groups have studied introducing either one or two dicyanomethylene groups to the anthraquinone core for different applications including, electrical conductors, molecular rectifiers, photoinduced electron transfer processes, optoelectronic devices and electrochiroptical materials (Scheme 5-1).[203-208]
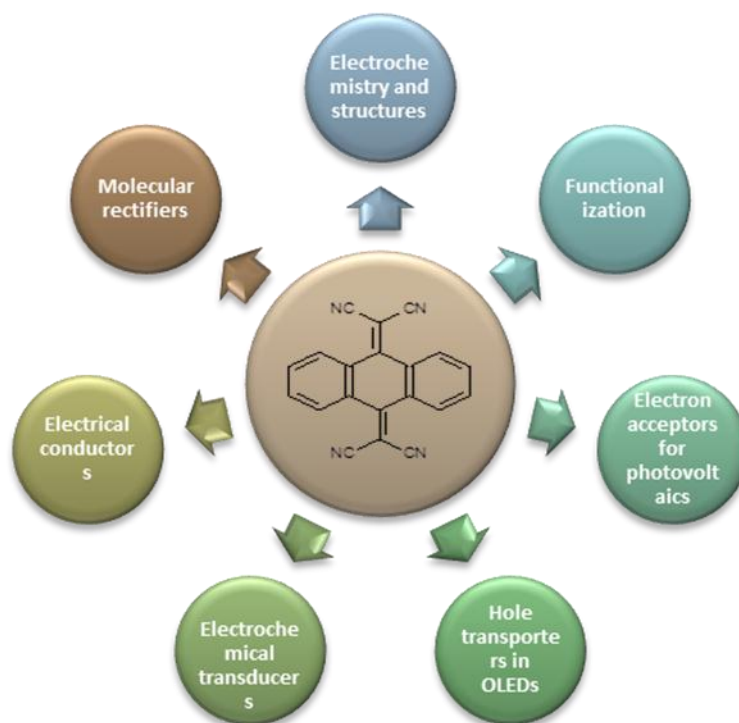
Scheme 5-1. Different applications for TCAQ.

11,11,12,12-Tetracyano-9,10-anthraquinodimethane (TCAQ) **190** (Figure 5-2) is a molecule that has interesting electronic properties that have challenged the creativity and inventiveness of chemists in areas such as organic, polymer, supramolecular and materials chemistry. It has attracted special attention due to its potential in areas such as photoinduced electron transfer, molecular rectifiers, and transport layers in organic optoelectronic devices or electrochiroptical materials.[209-214]
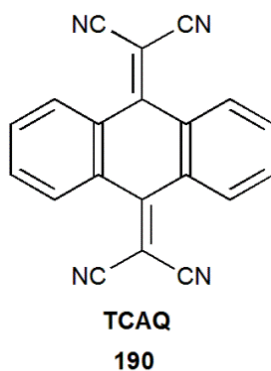
Figure 5-2. TCAQ **190** structure.

The structure of TCAQ **190** has been investigated by X-ray crystallography and theoretical calculations indicate that the neutral form adopts a folded boat-type structure, and the dicyanomethylene units can rotate freely allowing the anthracene core to become planar (Scheme 5-2).

In order to enhance the conducting properties, the extension of the π system in TCAQ derivatives was thought to be of great importance to reduce the intramolecular electron repulsion and it should lead to more stable radical anions. The electrochemical investigations of TCAQ showed that the extension of the π-conjugated system does not necessarily result in an improvement of the acceptor properties. It exhibits a more negative reduction potential and a great stability compared to the parent TCNQ but the electron affinity of TCAQ is lower. The first report showed that TCAQ exhibits a reversible two-electron reduction (Scheme 5-2) at -0.24 V *vs.* SCE (in acetonitrile, Pt as working electrode)[215] in 1984 by Aumuller and Hunig. Later, Kini and co-workers performed an in-depth electrochemical investigation of the TCAQ system.[207,208]
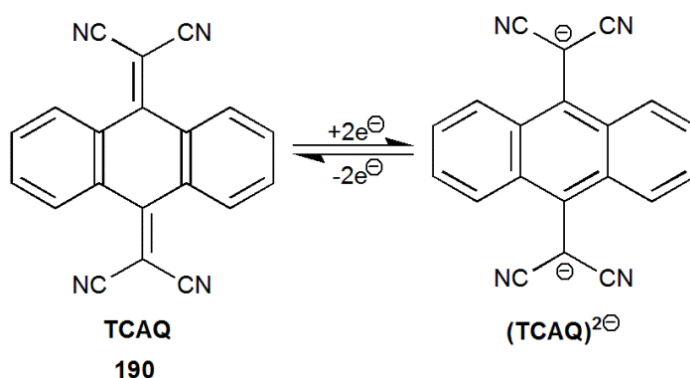
Scheme 5-2. TCAQ exhibit a reversible two-electron reduction.

Figure 5-3 shows the cyclic voltammogram of TCAQ in acetonitrile, at room temperature.[207,208] The first and the second reversible redox waves were observed at

potentials $E_{1/2}$= -0.29 V and $E_{1/2}$= -2.06 V *vs.* the Ag/Ag$^+$ reference electrode. The peak intensities are twice that for the former than for the latter wave moreover, the separation of their anodic and cathodic peaks amounts to 0.03 and 0.06 V, respectively. This electrochemical behavior is consistent with a two-electron process for the wave at higher potentials ($E_{1/2}$= -0.29 V) and a one-electron process for the other one ($E_{1/2}$= -2.06 V). In addition, there is irreversible wave with a cathodic peak at - 2.58 V was observed. All three reduction waves were confirmed by polarography under the same experimental conditions. For this reason, TCAQ is a good example of an electro active system in which the gain of a second electron takes place more easily than the first one (E^o_1- E^o_2< 0). TCAQ and other systems in which a significant structural change is associated with one or both electron-transfer steps has been normally observed like this behavior.[216]
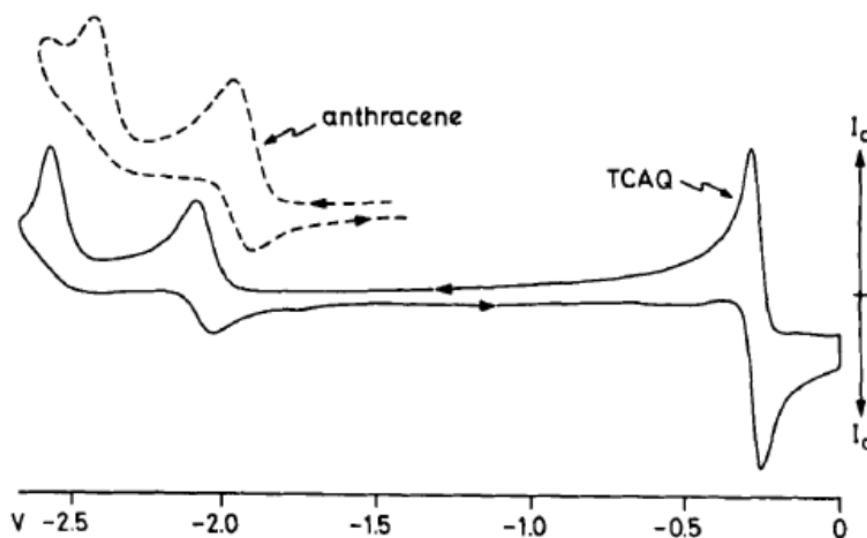
Figure 5-3. Cyclic voltammograms of TCAQ **190** and anthracene: solvent, acetonitrile; supporting electrolyte, Et$_4$N$^+$BF$_4^-$; temperature, 298 K; reference electrode, Ag/AgCl /KCl 3 M; working electrode, hanging mercury drop; sweep, 200 mV/s^{-1}; I_c cathodic current, I_a, anodic current (reprinted with permission from ref.[208] Copyright 1985 American Chemical Society).

5.1.3. Synthesis of TCAQ and derivatives

There are different synthetic routes for the preparation of TCAQ and derivatives that have been developed by different research groups due to the high interest of the TCAQ system. Misumi's group was first to report the preparation of TCAQ by following the synthetic route as shown in Scheme 5-3.[205] Dicyanomethylation of substituted naphthoquinone **191** was achieved by reacting with a large excess (40 eq.) of malononitrile in the presence of β-

alanine as a base in DMF to give the TCAQ **190** in 1% yield (Scheme 5-3). Under the same conditions 27% yield of TCAQ could be obtained by dicyanomethylenation of **192** (Scheme 5-3).[205] The groups of Ong[206] and Hunig[215] reported independently on the use of Lewis acid titanium (IV) chloride (TiCl₄) as an effective reagent for the promotion of this condensation as it can coordinate with oxygen atoms, thus promoting the nucleophilic attack of the malononitrile to the carbonyl group.

Aumuller and Hunig[215] succeeded in 1984 in the direct conversion of 9,10- anthraquinone **189** with good yields to TCAQ, by condensation with malononitrile in the presence of TiCl₄ and pyridine (Lehnert's reagent) (Scheme 5-3).[217]The condensation of anthraquinone with malononitrile is a synthetic challenge due to the steric crowding of the final product; however, this route gave rise to reasonable yields.[206]
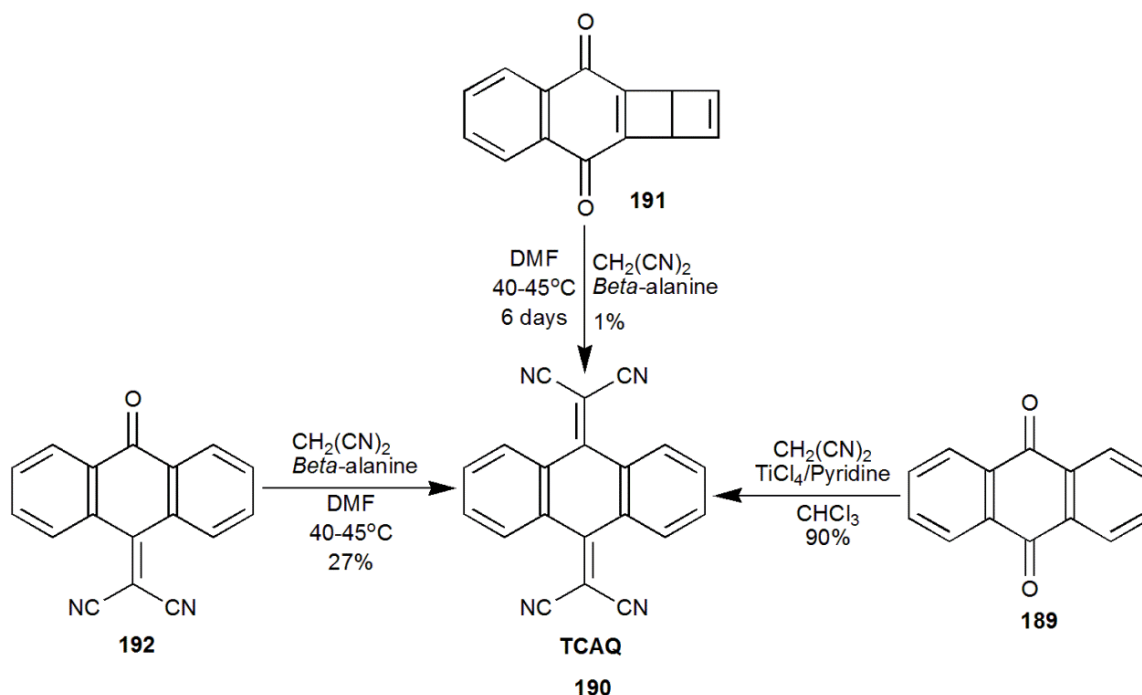
Scheme 5-3. Synthetic routes towards the preparation of TCAQ **190**.

2-Methyl-TCAQ, 2,3-dimethyl-TCAQ and 1,5-dichloro-TCAQ were synthesised following a similar synthetic procedure from the corresponding anthraquinone derivatives.[215] Ong and Keoshkerian have described the synthesis of TCAQ in a 87% yield and that of 2-tert-butyl-TCAQ in a 57% yield from the parent quinone precursors using the same procedure.[206] Cowan and co-workers developed another strategy which may be applicable to other cyanocarbons with extended π-systems, starting from 9,10-bis(cyanomethyl) anthracene that proceeds via the dicyano and tricyano analogs of TCAQ (Scheme 5-4).[207]
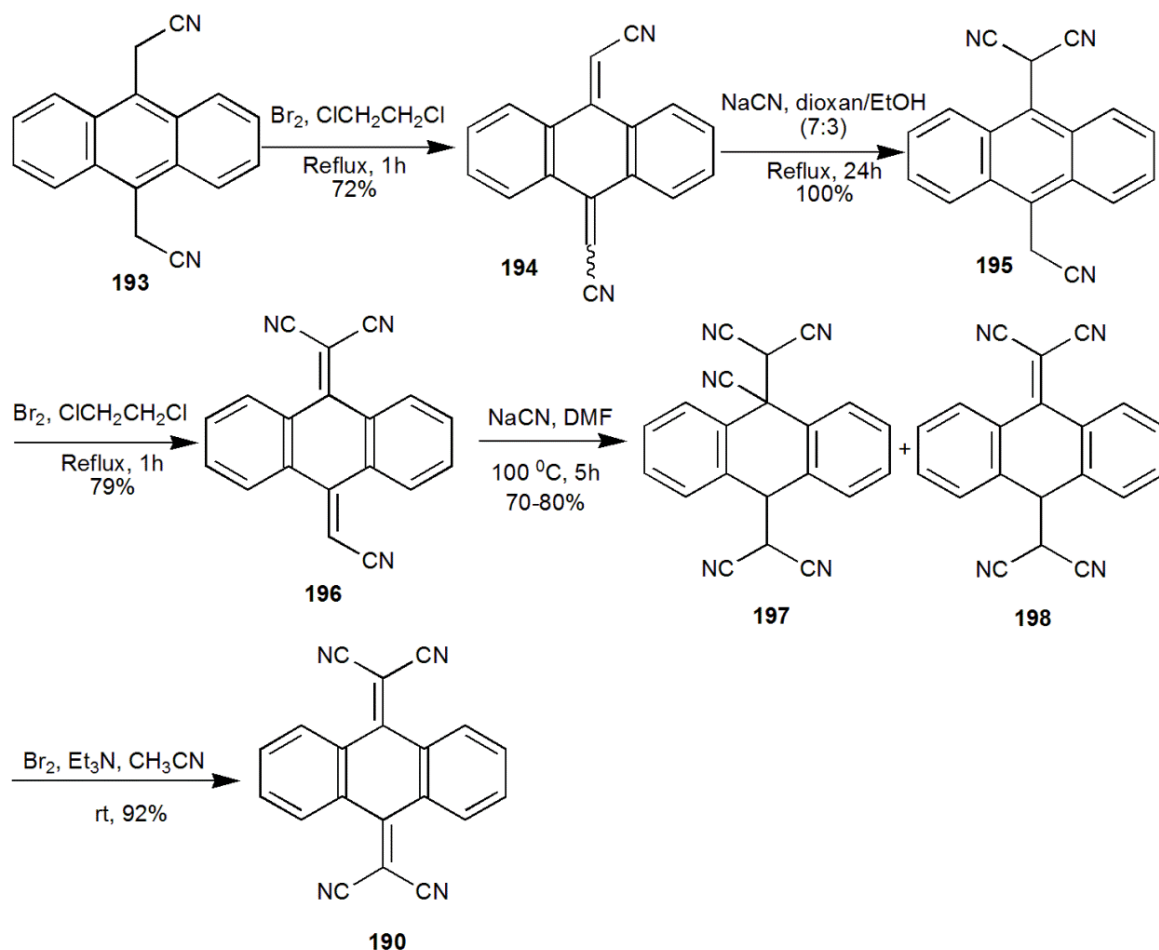
Scheme 5-4. Synthetic routes towards the preparation of TCAQ via the dicyano and tricyano-analogs.

Synthesis of surfactant TCAQ (Scheme 5-5) with different hydrophilic groups such as amino, sulfonyl and carbonyl into the head of a long-chain substituent can improve the molecular spreading on water subphases and increases the electron affinity of the molecule.[218,219]
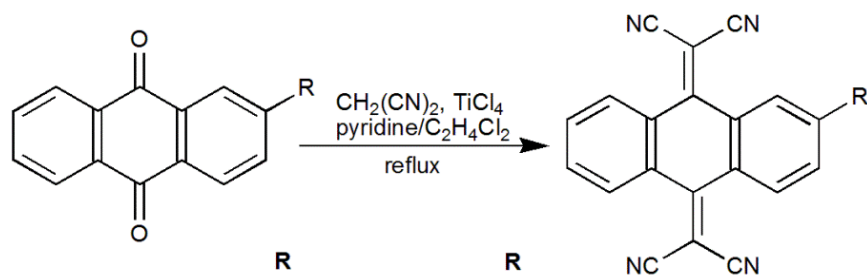
R	R
199 $NHCO_{15}H_{31}$	207 CH_3
200 $NHCOC_{19}H_{39}$	208 C_2H_5
201 $CONHC_{18}H_{37}$	209 Cl
202 $SO_2NHC_{18}H_{37}$	210 CO_2CH_3
203 $SO_2OC_{17}H_{35}$	211 CN
204 $CO_2C_{17}H_{35}$	212 NO_2
205 $CO_2C_{12}H_{25}$	213 $NH\text{-}COCH_3$
206 $CO_2C_8H_{17}$	214 $N(CH_3)_2$

Scheme 5-5. Some examples of substituted TCAQ derivatives.

In 1997, Martin and co-workers[220] reported the synthesis of the novel dimeric TCAQ acceptor **216** in a one-step procedure from 2,2′-oxydianthraquinone **215** and malononitrile in the presence of Lehnert's reagent in 45% yield (Scheme 5-6). The electrochemical behaviour of the dimer showed that both of the TCAQ moieties behave independently and therefore a four electron single reduction wave ($E_{1/2} = -0.34$ V, 4 e⁻) was observed indicating the simultaneous reduction of both TCAQ units to TCAQ⁻².
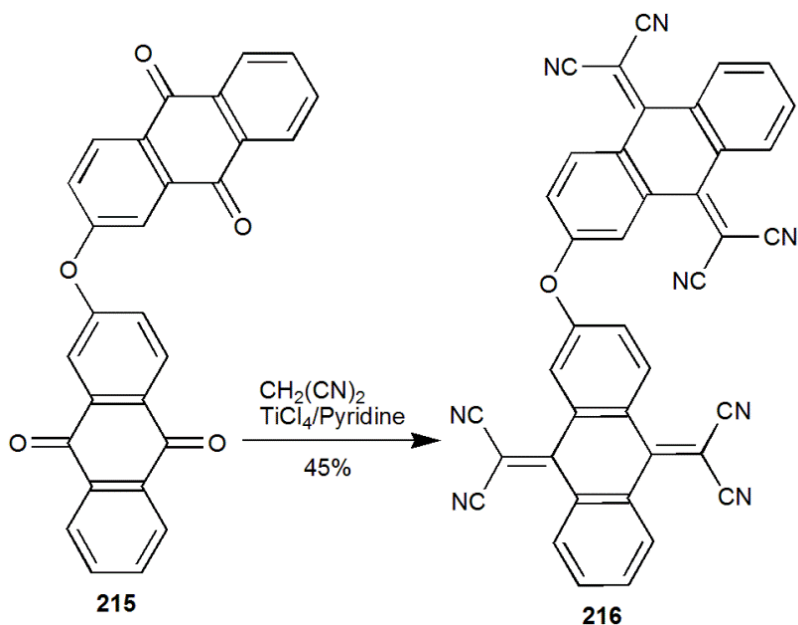
Scheme 5-6. Synthesis of the dimeric TCAQ acceptor.

An alternative dimer of TCAQ **219** is depicted in Scheme 5-7. The synthesis of dimer **219** was carried out in two steps from 2-hydroxymethyl-9,10-anthraquinone **217** by reaction with Lehnert reagent[221] by following Hunig's procedure.[222] Dimer **219** was obtained from TCAQ derivative **218** by reaction with malonyl dichloride at 0 ℃ in the presence of pyridine in a 69% yield. Dimer **219** represents an interesting building block, due to the presence of the reactive methylene group which makes it suitable for further chemical transformations.
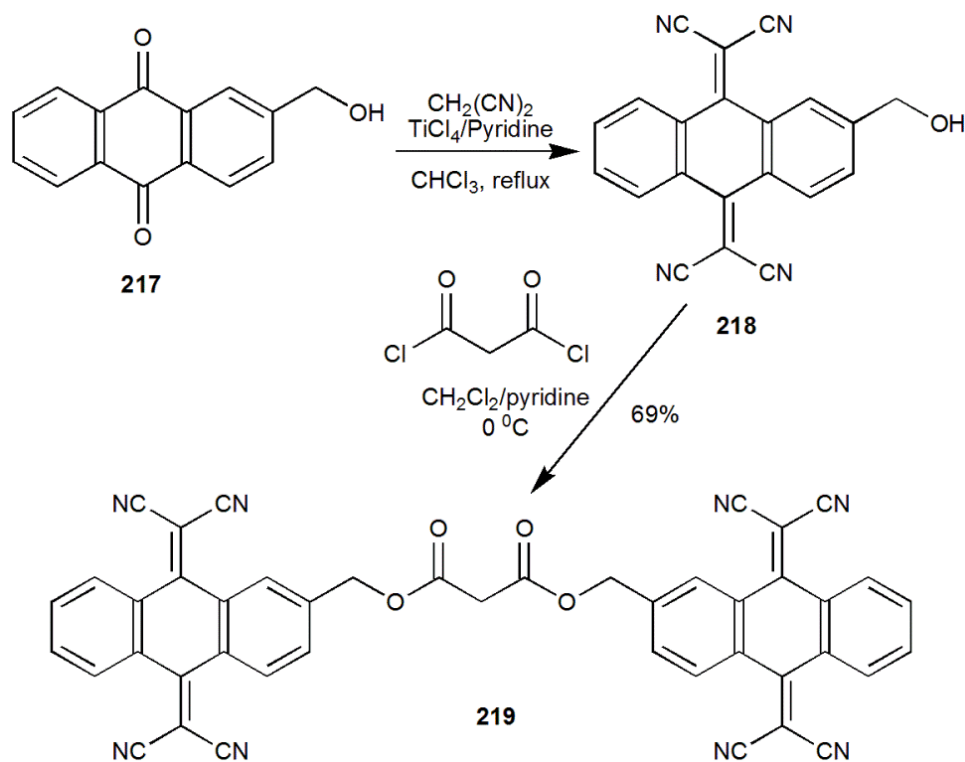
Scheme 5-7. Synthesis of new dimer of TCAQ **219**.

TCAQ has been linked to C_{60} to afford new acceptor-acceptor systems displaying multi-electron accepting properties as **221**,[223] and **222**,[224](Scheme 5-8). In these systems cyclo-addition reactions[225, 226] have played an important role in their synthesis. For example, Martın and co-workers synthesised using a 1,3-dipolar cycloaddition reactions of the N-trityl-protected fulleropyrrolidine produced **221** in 27% yield by treatment of 2-formyl-TCAQ **220** with N-tritylglycine to fullerene moiety.[223]

Seoane and co-workers have reported the synthesis of fulleropyrrolidine **224** in 20% by reaction of N-methylglycine with aldehyde **220** in the presence of C_{60} (Scheme 5-8). For the preparation of **224**, the reaction of aldehyde **220** with hydroxylamine hydrochloride afforded the corresponding oxime **223** which reacted with N-chlorosuccinimide yielded a nitrile oxide which undergoes a [3 + 2] cycloaddition reaction to the fullerene moiety to afford compound **224** in a 16% yield (Scheme 5-8).[223]
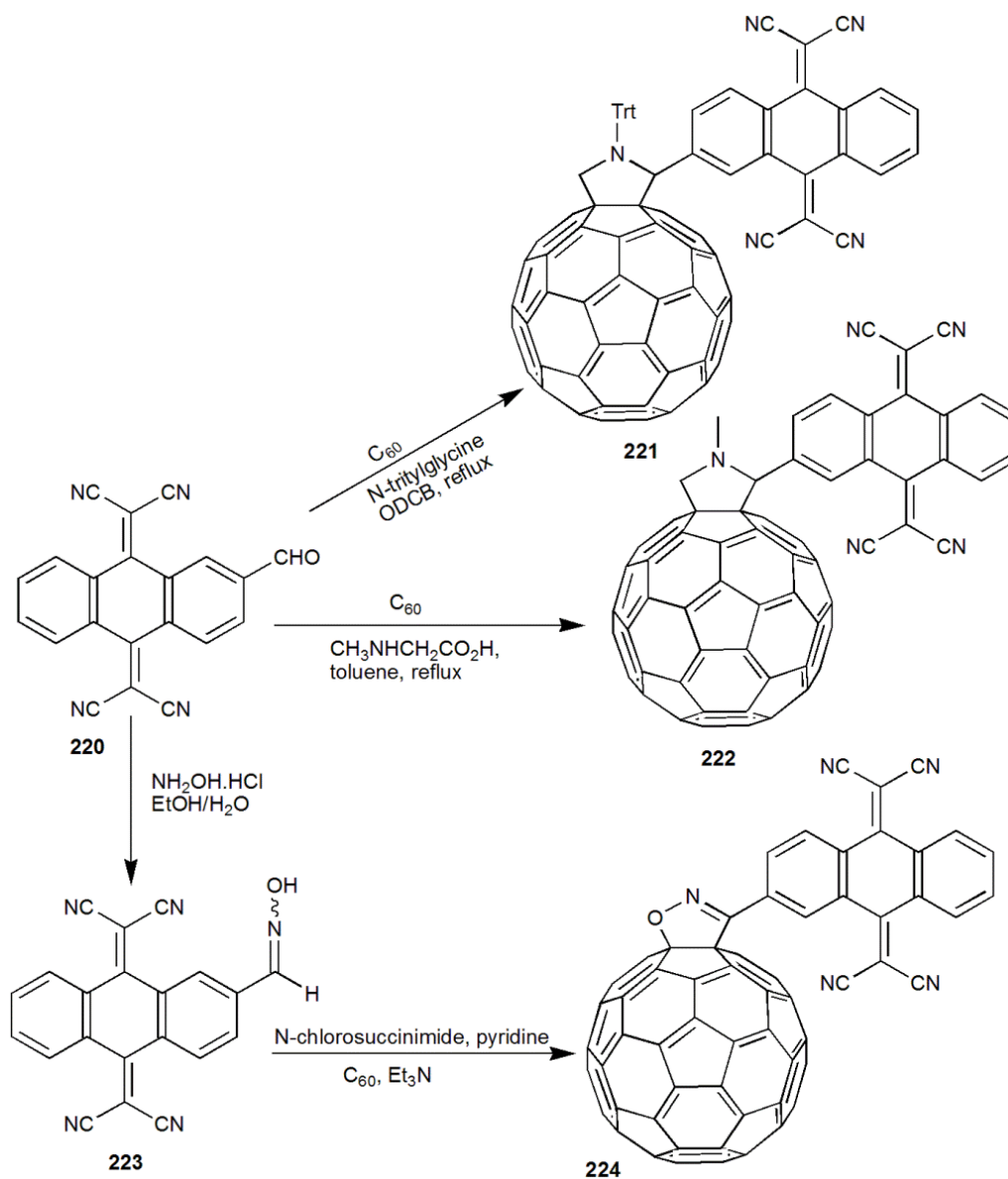
Scheme 5-8. TCAQ moiety as precursors for novel C$_{60}$-based organic metals.

5.1.4. TCAQ as sublayers in optoelectronic devices

Cao *et al.*[227] have used TCAQ as a hole transporting layer in electroluminescent devices (Figure 5-4). In this application, while the metal electrode injects electrons into the electroluminescent material, the TCAQ layer injects holes into the conduction band of the electroluminescent material, which barely meet any energy barriers. Therefore, the driving voltage of the device is lower than that of a similar device without the TCAQ layer.
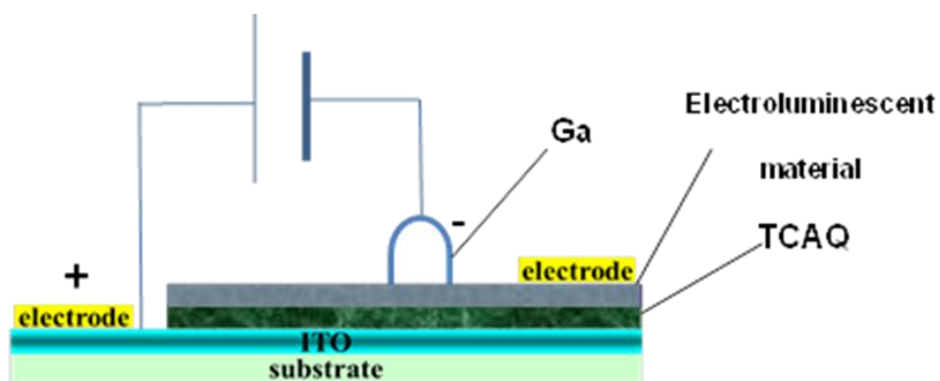
Figure 5-4. Schematic setup of a light emitting diode with TCAQ-based hole conducting layer.

A fullerene-TCAQ **225** derivative was prepared and tested in a bulk-heterojunction device (Scheme 5-9).[214,228,223] The power conversion efficiency of ITO/PEDOT:PSS/MDMO-PPV/TCAQ-C_{60}/Al cells was roughly one tenth of that of the ones made with PCBM. The low power conversion was explained by an ohmic contribution to the diode, probably due to small shunts which resulted from the immiscibility between MDMO-PPV and TCAQ-C_{60}. TCAQ derivatives have been shown to be very important substances used in the investigation of both inter- and intramolecular photoinduced electron transfer processes. However, the application of TCAQ derivatives in photovoltaic devices seems to be limited by the poor charge carrier transport in the amorphous blends.
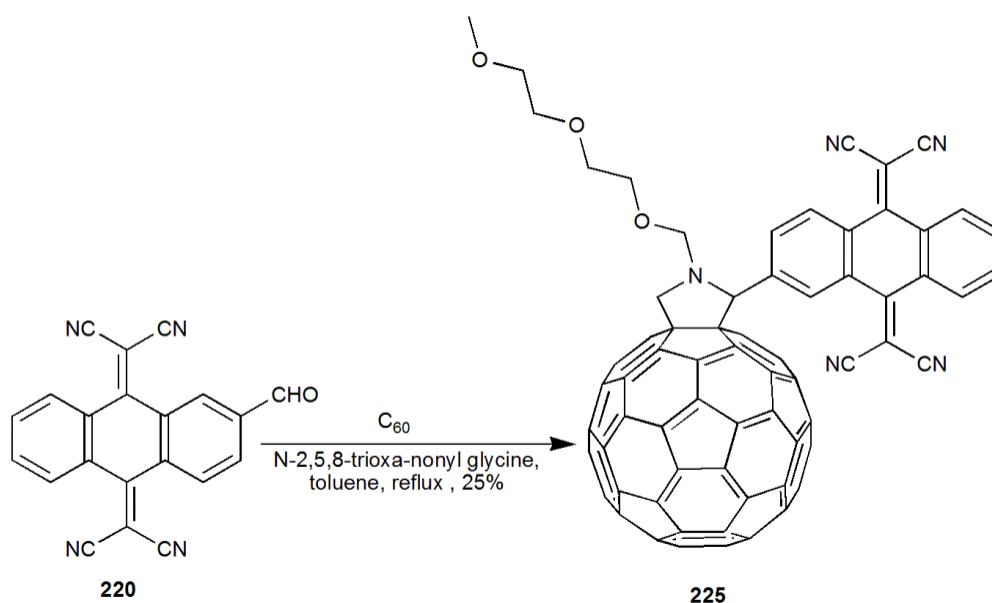
Scheme 5-9. Synthesis of TCAQ-C_{60} **225**.

5.2. The aim of the project
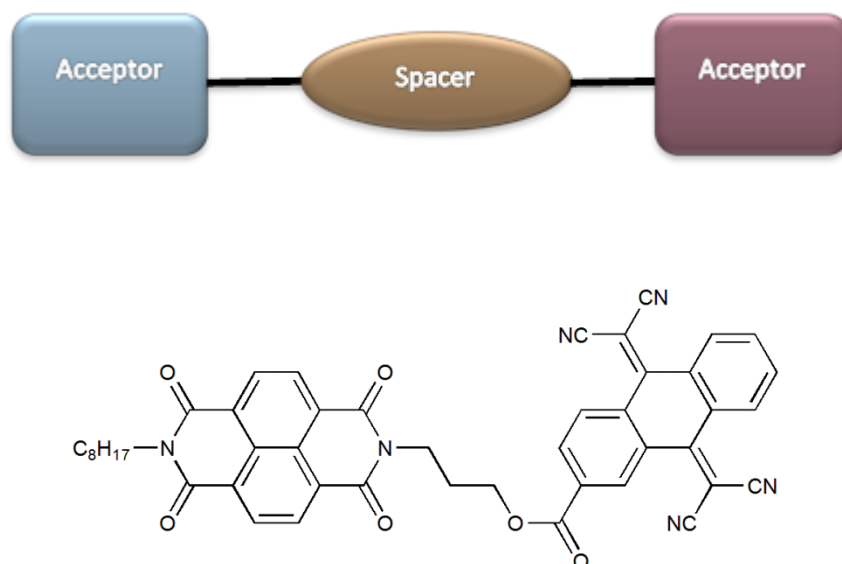
Figure 5-5. New bis-acceptor systems based on NDI and TCAQ.

The aim of this project is the synthesis of new bis-acceptor systems based on NDI and TCAQ and to study their chemical and physical properties. These compounds can be an attractive target in fabricating of photovoltaic devices because of the extensive redox chemistry and photochemical properties of NDI and TCAQ. These acceptor–acceptor molecular systems could afford a broader range of LUMO energies which may allow the investigation of a wider range of complementary donor polymers.

5.3. Results and Discussion

5.3.1. Synthesis

5.3.1.1. *N*-Octyl-*N'*-anthraquinone-naphthalenediimide 227

Thus, a new route was to devise a synthesis for compound **227** by reaction of naphthalene-1,4,5,8-tetracarboxylic dianhydride **27** with octylamine and 2-aminoanthraquinone **226** in a one-pot, two-step reaction in DMF at 180 °C under N_2 (Scheme 5-10). However, the obtained yield **227** was very low (1%), and this route was abandoned.
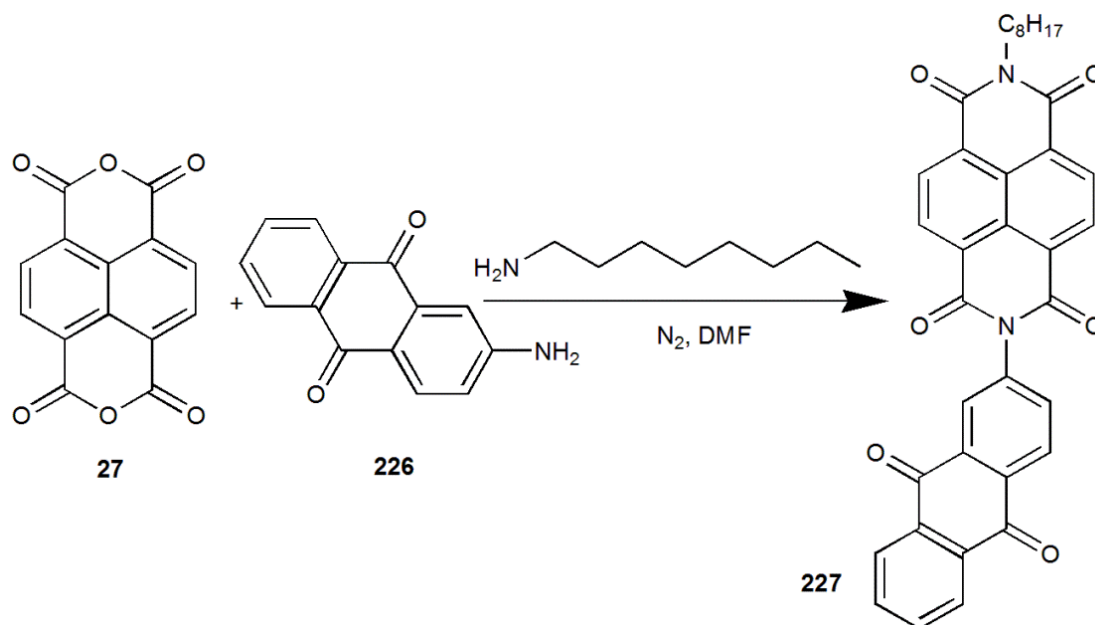
Scheme 5-10. Synthesis of compound **227**.

5.3.1.2. *N*-Octyl-*N'*-anthraquinonecarboxylate-naphthalenediimide 229

Two routes were undertaken to synthesise compound **229**, the first one involved reaction of *N*-octyl-*N'*-(propan-1-ol) naphthalene-1,4,5,8-tetracarboxylic acid diimide **185** which is previously prepared in chapter four with anthraquinone 2-carboxylic acid *via* Steglich esterification (Scheme 5-11).

The reaction was undertaken in DMF at room temperature for seven days, producing a satisfactory yield (55%) of the required ester **229**. 1-Ethyl–3-(3-dimethylaminopropyl) carbodiimide (EDCI) was used as coupling reagent and 4-dimethylaminopyridine (DMAP) as a catalyst (Scheme 5-12).
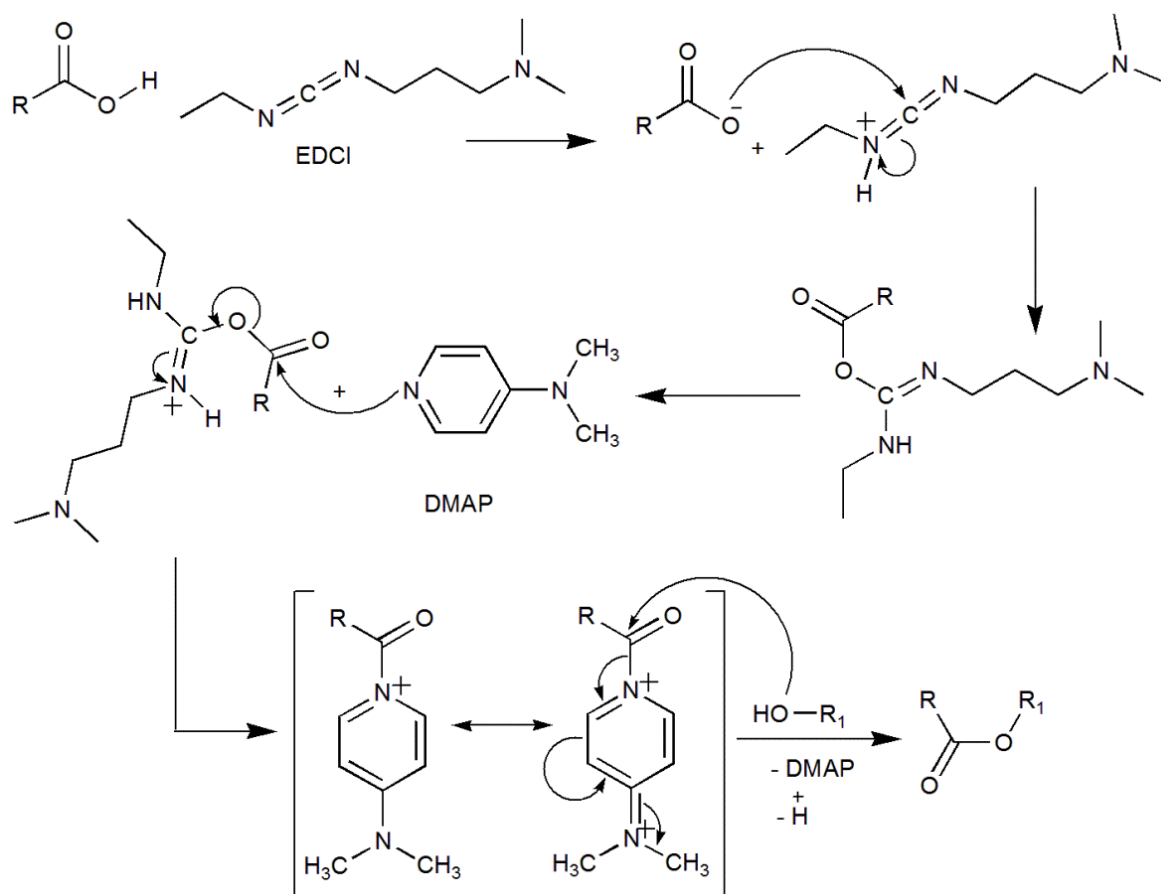
Scheme 5-11. Illustration of the Steglich esterification reaction used to form an ester bond between the carboxylic acid moiety and an alcohol.
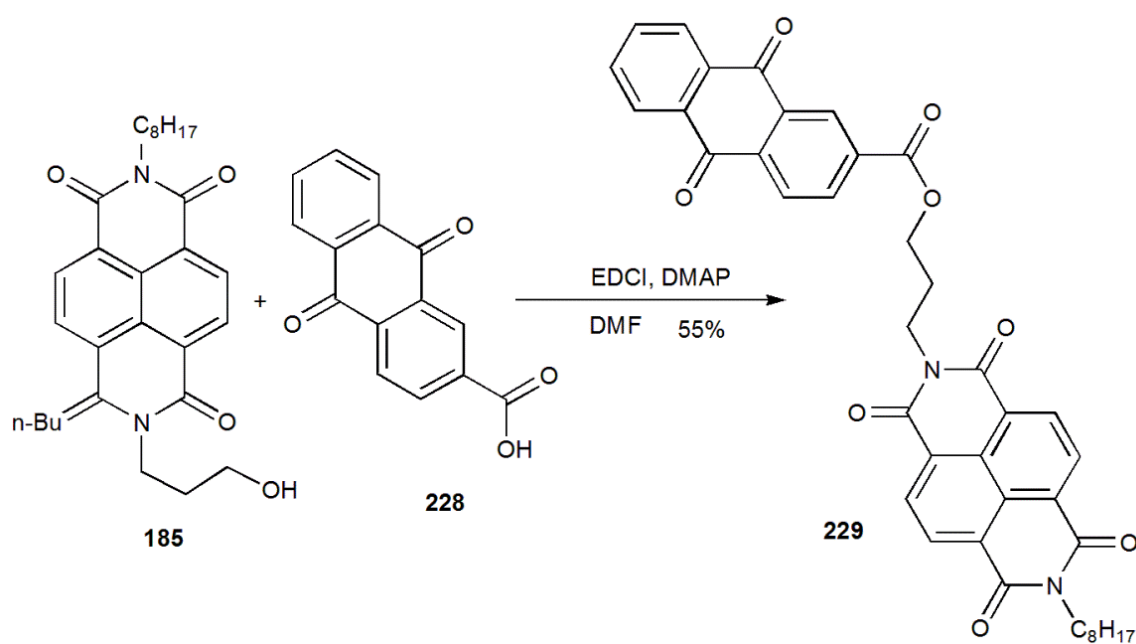
Scheme 5-12. Synthesis of compound **229**.

This synthetic route was successfully used to synthesise the *N*-octyl-*N'*-(propan-1-anthraquinonecarboxylate) naphthalene-1,4,5,8-tetracarboxylic acid diimide **229**, starting in turn from synthesis of 9,10-dioxo-9,10-dihydro-2-anthracenecarbonyl chloride **231** from the commercially available 2-carboxy-9,10-anthraquinone **230** by reaction with thionyl chloride (Scheme 5-13).[229]
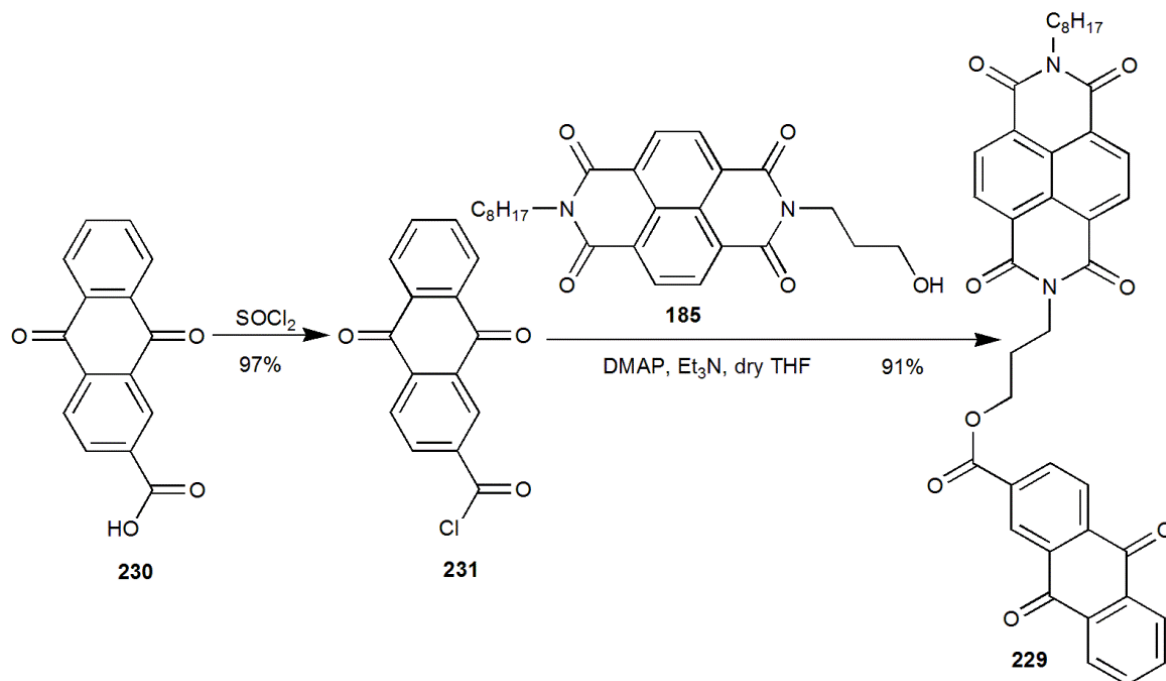
Scheme 5-13. Synthesis of compounds **231** and **229**.

N-Octyl-*N'*-(propan-1-anthraquinonecarboxylate) naphthalene-1,4,5,8-tetracarboxylic acid diimide **229** was synthesised in a 91% yield through the reaction of the previously reported **185** and the previously synthesised 9,10-dioxo-9,10–dihydro-2-anthracene-carbonyl chloride **231** *via* Steglich esterification (Scheme 5-11).

5.3.1.3. *N*-Octyl-*N'*-tetracyano-anthraquinonecarboxylate-naphtha -lene diimide 232

The synthesis of the novel acceptor molecules **232** was carried out by Knoevenagel condensation of **229** and Lehnert's reagent (TiCl$_4$, malononitrile, and pyridine) in presence of CH$_2$Cl$_2$ (Scheme 5-14).
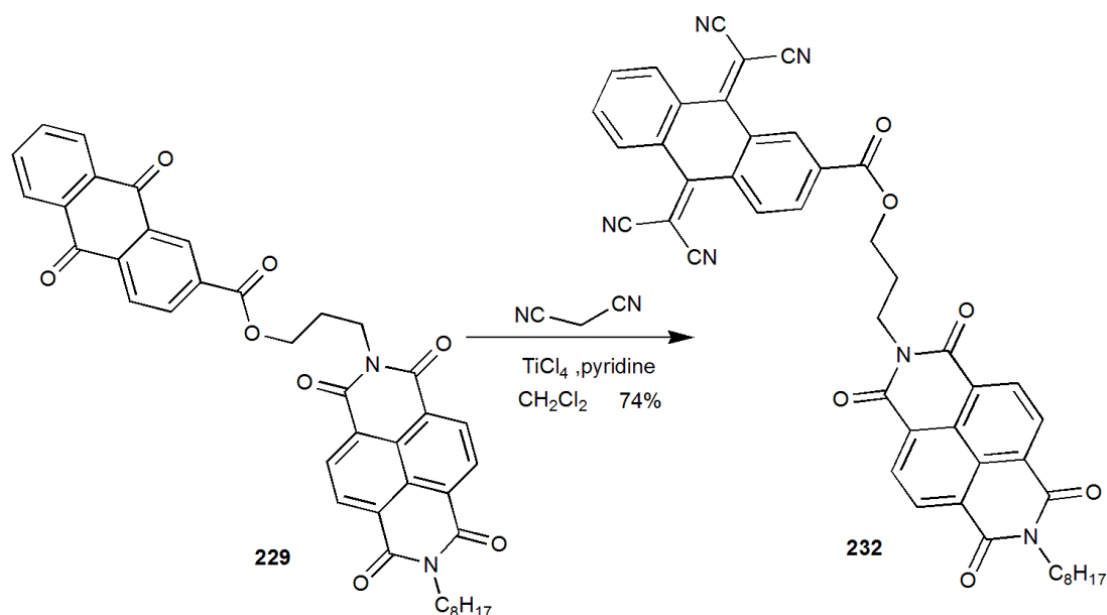
Scheme 5-14. Synthesis of compound **232**.

The condensation reaction of anthraquinone with malononitrile was expected to the challenging due to the steric crowding of the final product. However, use of TiCl$_4$, as a Lewis acid facilitated reasonable yields (74%).

5.3.2. Spectroscopic studies

Compounds **229** and **232** and the key compounds that lead to their synthesis were characterized by ^{1}H, ^{13}C NMR, mass spectrometry, and FTIR spectroscopy. In addition, a series of analytical studies involving cyclic voltammetry, fluorescence, and UV-visible were used to characterise **229** and **232**.

The ^{1}H NMR displayed the expected signals for **229** and **232**. ^{13}C NMR displayed the expected signals for (-CN) at 84.3 and 112.6 ppm for compound **232**. Moreover, the infrared spectra data for compound **232** showed the (C≡N) absorption at 2357 cm^{-1}.

Photophysical characterization of the **229** and **232** was performed using UV-Vis spectroscopy and fluorescence emission spectroscopy. Absorption spectra of the **229**, **232** and **185** are shown in Figure 5-6. The UV-Vis spectra of **229**, **232** and **185** recorded in CH$_2$Cl$_2$ (1 x 10^{-4} M) displayed broad CT bands with end-absorptions reaching into the visible region. Compound **185** does not have an absorption band above 400 nm. The maximum absorption occurred at λ_{max}= 380 nm with other absorptions at 359 nm and at 340 nm. Compound **229** has additional absorption peaks corresponding to the NDI-

anthraquinone entity that are observed at 257 nm and a shoulder at 272 nm. All TCAQ derivatives feature strong absorption between 250 and 380 nm which are transitions involving the anthraquinodimethane. For this reason NDI-TCAQ displayed strong absorption bands at around 379 nm and 284 nm which are characteristic of π-π* transitions located on the NDI and TCAQ subunits (Figure 5-6, Table 5-1).
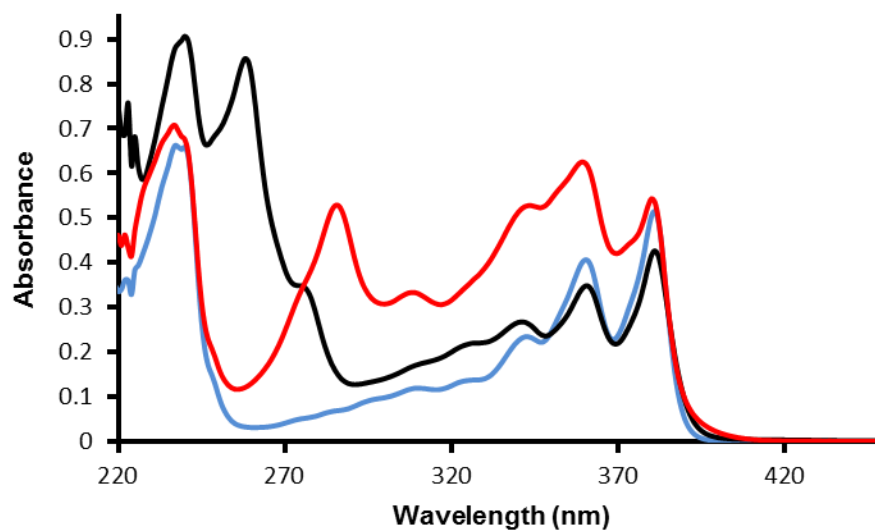
Figure 5-6. UV-vis spectroscopy recorded for compounds **185** (blue line), **229** (black line), and **323** (red line) in CH_2Cl_2 (1×10^{-4} M).

It is worth noting that the onset wavelength of the synthesised compounds, shown in Figure 5-6, corresponds to an optically determined band gap energy ($E_g^{opt} = 1242/ \lambda_{onset}$) (Table 5-1).

Table 5-1 UV-visible spectra data of compounds **185**, **229**, and **232** recorded in CH_2Cl_2 (1×10^{-4} M). Where the λ_{abs} is absorption wavelength (nm), λ_{Max} is maximum absorption wavelength (nm), and Eg^{opt} is optically determined band gap energy (eV).

Compounds	λ_{abs1} (nm)	λ_{abs2} (nm)	λ_{abs3} (nm)	λ_{abs4} (nm)	λ_{abs5} (nm)	λ_{abs6} (nm)	λ_{abs7} (nm)	λ_{abs8} (nm)	Band gap (eV)
185	238	306	320	340	359	380	---	---	3.27
229	239	257	272	307	321	338	358	380	3.27
232	236	284	305	341	357	379	---	---	3.28

The UV-Vis-NIR spectroscopy of compounds **185**, **229**, and **232** in CH_2Cl_2 (1 x 10^{-4} M) shows no absorption at near IR regions was obtained.

The photophysical behavior was investigated by fluorescence spectroscopy (recorded in 10^{-5} M solution in CH_2Cl_2). It can be seen that the TCAQ plays an important role in modulating the fluorescence properties of the **185** unit as shown in Figure 5-7. The fluorescence of compounds **229** and **232** is significantly quenched compared to the non-functionalised precursor alcohol **185.**
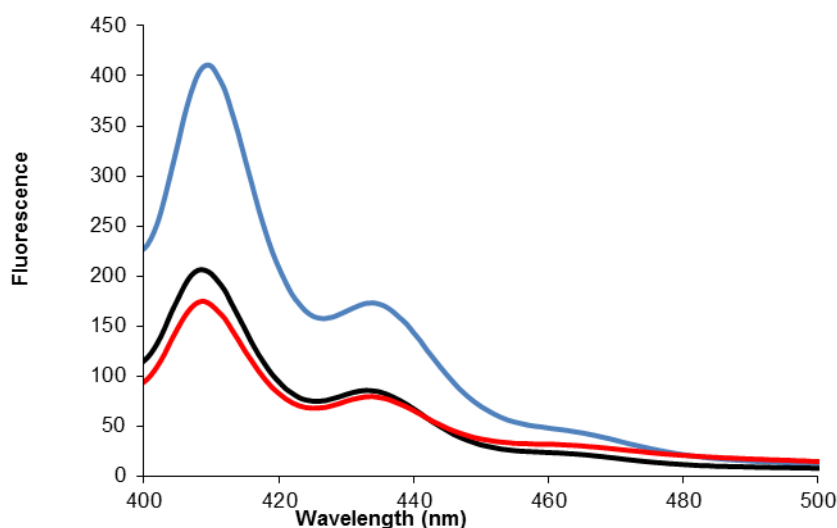
Figure 5-7. Fluorescence spectra recorded for compounds **185** (blue line), **229** (black line), and **232** (red line) in CH_2Cl_2 (1x10^{-5} M) at excitation wavelength = 380 nm.

5.3.3. Electrochemical Studies

The redox properties of the new compounds **185**, **229** and **232** were investigated by cyclic voltammetry (CV) using tetrabutylammonium hexafluorophosphate (n-Bu_4NPF_6) as a supporting electrolyte and ferrocene (Fc^+/Fc) as internal reference in CH_2Cl_2. As shown in Figure 5-8, compounds **185**, and **229** were reduced in well-defined reversible one-electron reduction steps whereas TCAQ **232** was reduced in a single reversible two-electron step.
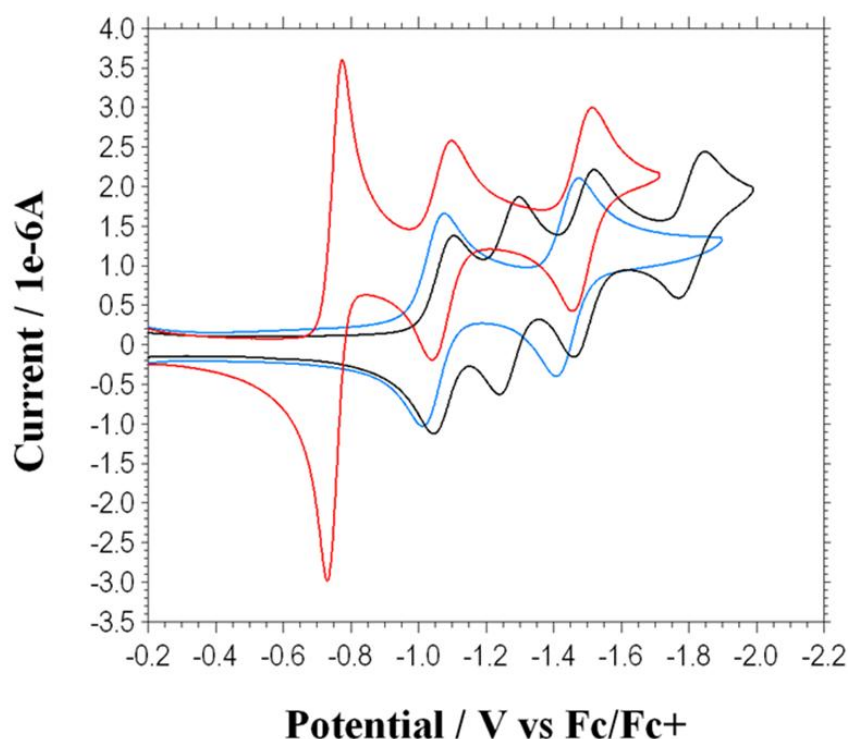
Figure 5-8. Cyclic voltammogramms of compounds **185** (blue line), **229** (black line), and **232** (red line) recorded using a glassy working electrode, an Ag wire as a reference electrode and a Pt wire as a counter electrode. Recorded in CH_2Cl_2 (1×10^{-4} M) with 0.1M (n-Bu$_4$NPF$_6$) as a supporting electrolyte at 20 ºC, and a scan rate of 0.1 Vs^{-1}.

Compound **185** displayed two reversible redox waves at E$_{1/2}$= -1.05 V and E$_{1/2}$= -1.44 V for the two electron reduction of NDI moiety. This corresponds to a LUMO energy of E$_{LUMO}$ = -3.75 eV. Compound **229** displayed two reversible redox waves at E$_{1/2}$= - 1.08 V and E$_{1/2}$ = -1.81 V for the two electron reduction of NDI-AQ moiety. This corresponds to a LUMO energy of E$_{LUMO}$= -3.72 eV. Compound **232** displayed one reversible redox waves at E$_{1/2}$= -0.75 V for the two electron reduction of TCAQ moiety. This corresponds to a LUMO energy of E$_{LUMO}$= -4.05 eV (Figure 5-8, Table 5-2). The peak characteristics are in agreement with a normal ordering of the two overlapping one-electron reduction steps, indicative of two almost independent redox centers.

Table 5-2. Electrochemical data (CV) of compounds **185**, **229**, and **232** recorded in CH_2Cl_2 (+0.1M n-Bu$_4$NPF$_6$) vs. Fc$^+$/Fc at scan rate v = 0.1 V s^{-1}.

Compounds	$E^1_{1/2}$ [V]	$E^2_{1/2}$ [V]	$E^3_{1/2}$ [V]	$E^4_{1/2}$ [V]	E_{LUMO} [eV]
185	-1.05	-1.44	-----	-----	-3.75
229	-1.08	-1.27	-1.50	-1.81	-3.72
232	-0.75	-1.07	-1.50	-----	-4.05

5.3.4. Molecular Modelling

Unfortunately, all attempts to crystallise **229** and **232** for X-ray analysis proved unsuccessful. We calculated the electron distribution in the molecular structure using density functional theory (DFT) in order to study the electron delocalization of **229** and **232**, which are formed from two acceptor units. In order to get the simplification of the calculation, long alkyl chain (octyl) was replaced by a CH_3 group in the molecule. The calculated electron density distributions of HOMO and LUMO for compound **229** are shown in Figure 5-9.
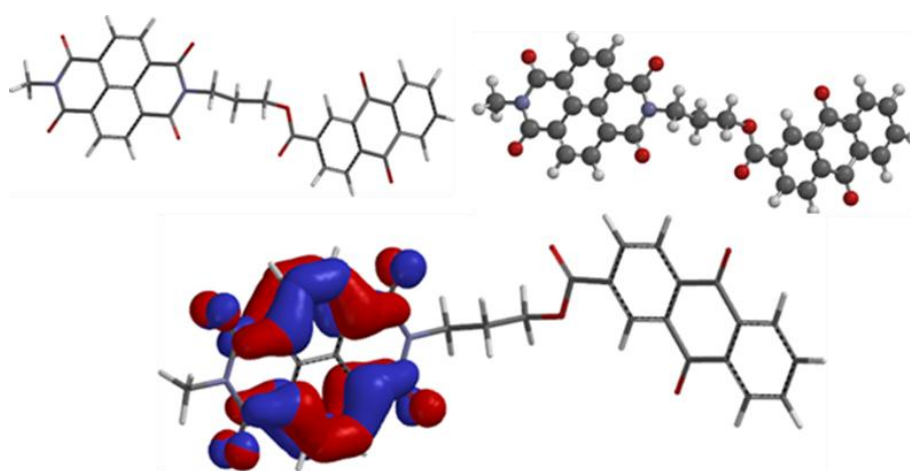
Figure 5-9. DFT B3LYP 6-311G calculation of **229** showing LUMO and HOMO location.

Inspection of the HOMO densities for this system shows that π-orbitals are delocalized along the NDI unit and the computed HOMO energy for **229** is E_{HOMO}= -7.08 eV (Figure 5-10).
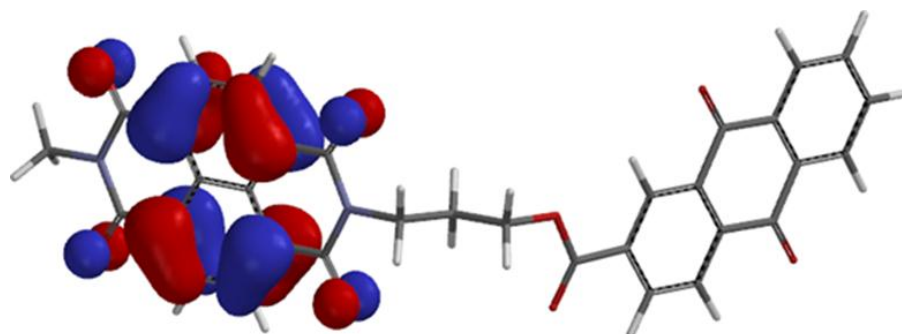
Figure 5-10. DFT B3LYP 6-311G calculation of **229** showing HOMO location.

The plots reveal that the LUMO is completely delocalized across the naphthalenediimide core and the computed LUMO energy for **229** is E_{LUMO}= -3.45 eV (Figure 5-11).
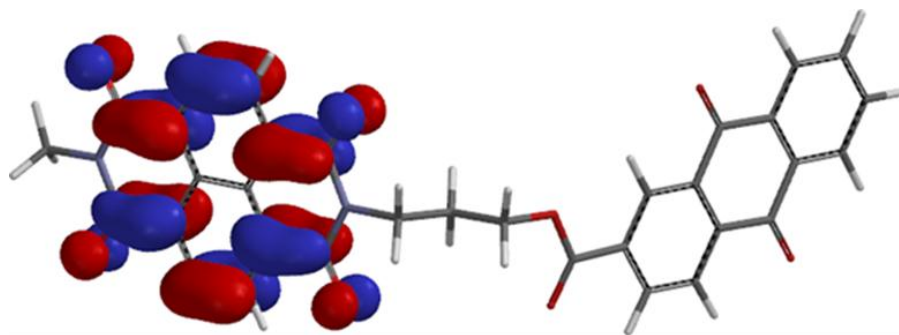
Figure 5-11. DFT B3LYP 6-311G calculation of **229** showing LUMO location.

The molecular orbital energies and contours were calculated for **232**. The plots reveal that the HOMO and LUMO are completely delocalized across the naphthalenediimide and tetracyanoanthraquinone subunits (Figure 5-12).
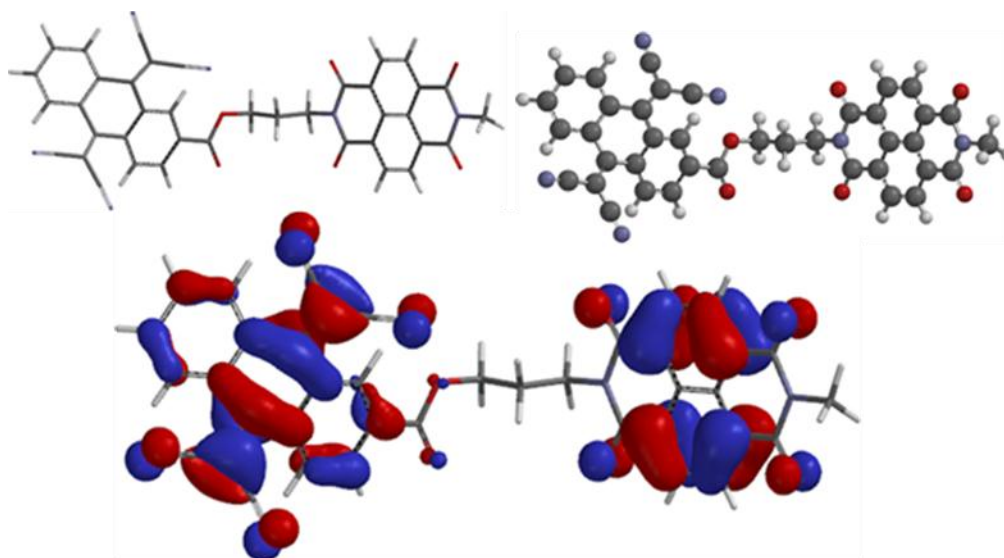
Figure 5-12. DFT B3LYP 6-311G calculation of **232** showing LUMO and HOMO location.

The computed HOMO energy for **232** is E_{HOMO}= -7.07 eV, the HOMO is completely delocalized across the naphthalenediimide core (Figure 5-13).
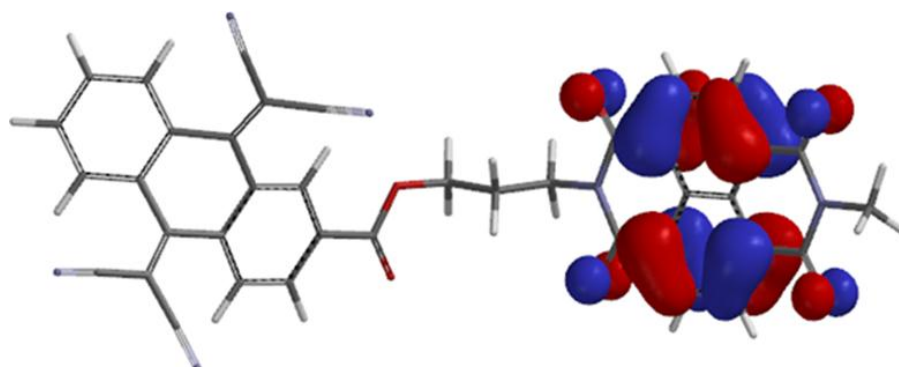
Figure 5-13. DFT B3LYP 6-311G calculation of **232** showing HOMO location.

The computed MABS show that the LUMO is completely delocalized across the tetracyanoanthraquinone core, and the computed LUMO energy for **232** is E_{LUMO}= -3.85 eV (Figure 5-14).
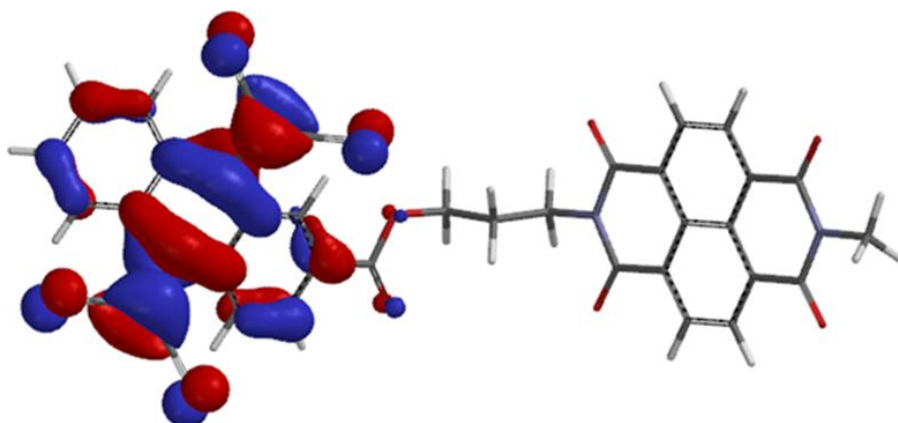
Figure 5-14. DFT B3LYP 6-311G calculation of **232** showing LUMO location.

5.4. Conclusion

Compound **232** has been successfully synthesised as a new electron acceptor-acceptor based on NDI and characterised via ^{1}H NMR, ^{13}C NMR, I.R, mass, fluorescence, UV-vis and UV-Vis-NIR spectroscopies, cyclic voltammetry, and DFT modelling. Optical analysis using UV-vis, UV-Vis-NIR and fluorescence spectrometry showed that strong absorption between 250 and 380 nm is due to the TCAQ moiety. In addition, the fluorescence of **229** and **232** are quenched strongly compared to **185**. The electrochemistry observed via cyclic voltammetry showed a decrease in reduction potential to more negative values for **232**, compared to that of the **229** and **185**. This study paves the way for the synthesis of more elaborate derivatives, whereby functionality can be introduced to control the redox properties and reactivity of the NDI and TCAQ moieties. Compounds **229** and **232** are currently under investigation at St. Andrews University where they are fabricating the solar cells.

6. **Chapter 6**

Design and synthesis of new naphthaleneamidinemono-imide-fused systems

6.1 Introduction

6.1.1 Conductivity of polythiophenes

Intramolecular and intermolecular delocalization of π-electrons is important for the structural, electrical, and optical properties of conjugated polymer systems. To obtain materials with excellent properties, high π-electron mobility is required, and intramolecular mobility depends on the effective conjugation length. The through conjugation is interrupted by mis-couplings between adjacent rings such as the meta coupling in benzene or the α-β-coupling in thiophene (Figure 6-1). The steric repulsions of groups attached to the rings force the rings to adopt a non-planar conformation (Figure 6-1).[230]
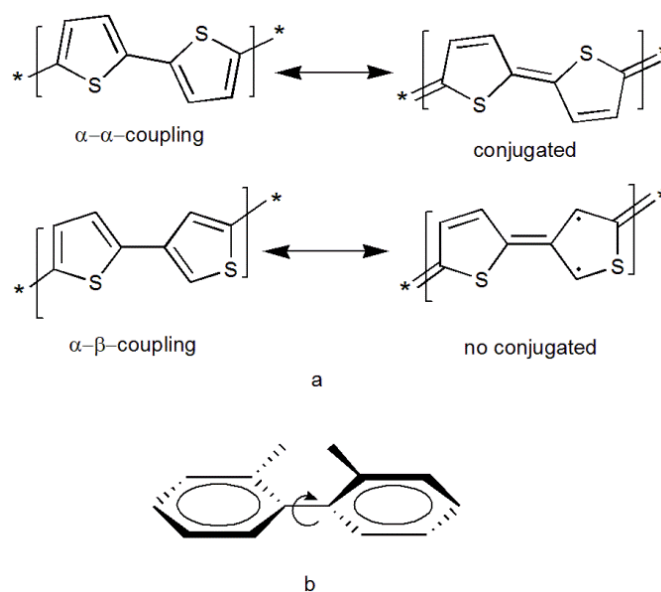
Figure 6-1. (a) α- and β-coupling in thiophene (b) meta coupling in benzene.

Alternation of electron-rich and electron-deficient units along the polymer chain leads to a successful and flexible strategy to design small band gap polymers. In order to design small band gap polymers for photovoltaics, ways of decreasing the band gap need to be taken into account. This is achieved by either lowering the lowest unoccupied molecular orbital (LUMO) or raising the highest occupied molecular orbital (HOMO) of the polymer, or both.[129]

The field of electrical conducting polymers is an important modern research field with scientific and technological importance. Polymers of this type can be synthesised by

chemical polymerisation or electropolymerisation. Electropolymerisation offers several advantageous features, such as:[231-234]

(i) No requirement for a catalyst.

(ii) Direct formation of the doped polymer film on the electrode surface.

(iii) Easy control of the film thickness.

(iiii) The possibility of performing in situ characterization of the deposited film by electrochemical and other techniques.

Conductive polymers such as polyacetylene, polypyrrole and polythiophene, possessing low band gaps (1.5, 2.5, and 2.1-2.2 eV), allow the transfer of electrons through the material, due to their π-conjugated nature.[235] Polythiophenes are the most extensively investigated classes of conjugated materials. These materials have chemical stability in various redox states and excellent electronic and charge transport properties. They are candidates for many applications such as electrical conductors, polymer LEDs, nonlinear optical devices, solar cells, electrochromic or smart windows, antistatic coatings, photoresists, sensors, electromagnetic shielding materials, batteries, artificial noses and muscles, electrodes, new types of memory devices, microwave absorbing materials, nanoswitches, optical modulators and valves, nanoelectronic, imaging materials, polymer electronic interconnects, light-emitting diodes (OLEDs) or lasers, field-effect transistors (OFETs), integrated circuits and optical devices.[236, 237]

The preparation of electrical conductive polythiophenes started at the beginning of the 1980s by two groups.(i) Yamamoto's[238] synthesis, using the Grignard type coupling of 2,5-dibromothiophene with Mg in tetrahydrofuran in the presence of nickel(bipyridine) dichloride, and (ii) Lin and Dudek[239] who also used magnesium in THF with a series of acetylacetonate catalysts (Scheme 6-1). These condensation reactions are propagated and eventually low molecular weight polythiophene is formed. Later, important progress has been made in the chemistry of polythiophene, due to the stability of neutral polythiophene. The polymerisation based on the organometallic coupling of thiophene monomers is now by far the most interesting method, because the properties of regioregular 3-substituted polythiophenes were improved.
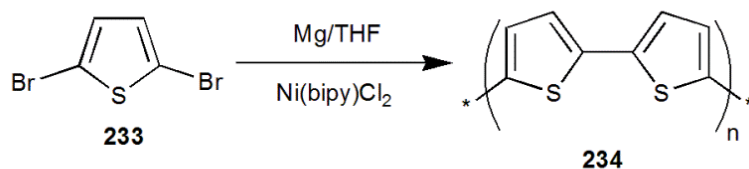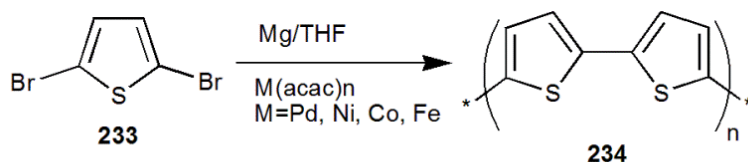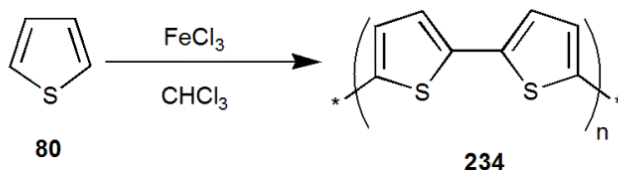
Scheme 6-1. The first chemical synthesis of polythiophene.

Conducting polythiophenes formed by the oxidation of thiophene or bithienyl with arsenic (V) fluoride, and reduced with ammonia clearly displays that polymerisation has occurred.[240] This method is not very practical because the arsenic (V) fluoride has poisonous properties. Sugimoto *et al.* have developed a more convenient method, by using iron (III) chloride as oxidizing agent and chloroform as solvent (Scheme 6-1). The reaction is easily carried out with good yields, and this method has now widely been employed in the synthesis of polythiophenes from thiophene with different substituents.[241, 242]

The oxidative coupling of thiophenes provides materials with higher molecular weights than the organometallic coupling route. The polymers obtained by the iron (III) chloride oxidation of 3-substituted thiophenes exhibit a regiorandom structure. The polymerisation of 3-(4-octylpheny1) thiophene by using a modified procedure has produced a polymer with a high degree of regioregularity. However, this high regioregularity is a result of the phenyl substituent and modified procedure.[243]

In 1981, Diaz[244] described the synthesis of polythiophenes by electrochemical oxidation. The polymerisation mechanism is proposed to proceed through the coupling of two thiophene radical cations, formed by the oxidation of the thiophene monomer as is shown in Scheme 6-2.[245] The dihydro dimer rearomatisation is the driving force for the coupling.

The dimer, which is more easily oxidized than the monomer, undergoes further coupling. Electropolymerisation proceeds then through deposition of polymer in its oxidized, and hence conducting, form onto the electrode.

235
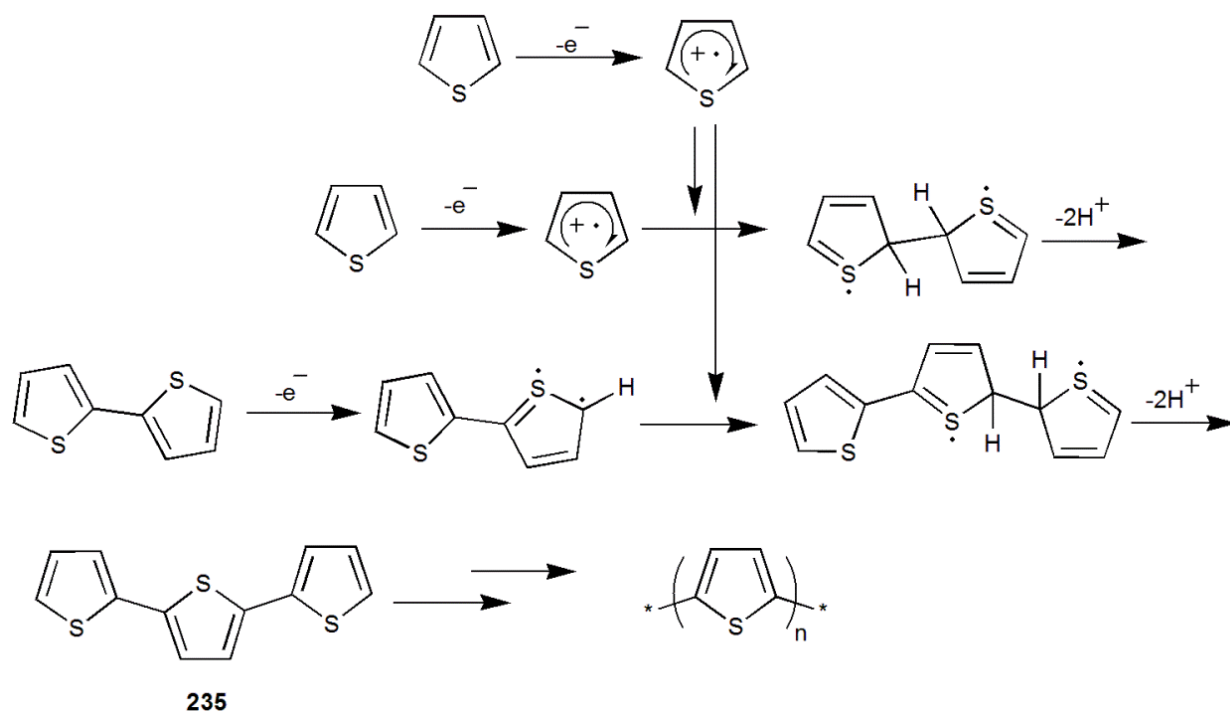
Scheme 6-2. Electrochemical polymerisation of polythiophene.

This method has the advantage that stable films are formed during the polymerisation. Electrochemical polymerisation has been used for the synthesis of unsubstituted polythiophene[246] and substituted polythiophenes[247] and these polymers possess a regiorandom structure.

The monomer 3,4-ethylenedioxythiophene (EDOT) **236** plays a fundamental role in oligo-thiophene and polythiophene chemistry. A new polythiophene derivative called poly(3,4-ethylenedioxythiophene) (PEDOT) **237** was developed by the scientists at the Bayer AG research laboratories in Germany.[248] The polymer poly(3,4-ethylenedioxythiophene) was derived directly from monomer EDOT **236** by chemical and/or electrical oxidation. PEDOT **237** shows interesting properties, including relatively good electrochemical and thermal stability as compared with that of other polythiophenes (Figure 6-2).

Figure 6-2. Chemical structure of EDOT and PEDOT.

PEDOT **237** is insoluble in many common solvents and unstable in its neutral state, as it oxidizes rapidly in air. Polyelectrolyte solution (e.g. polystyrenesulphonate (PSS)) **238** can be added to improve the processability of PEDOT **237** by acting as a counter ion, for PEDOT in its oxidized state. The PSS monomer has one acidic SO_3H (sulphonate) group on each phenyl ring, and sodium persulphate ($Na_2S_2O_8$) is used as the oxidizing agent. Polymer chain of PSS **238** is cross-linked to the PEDOT polymer chain **237** below, and they are connected by a valence, or weak bond connection (Scheme 6-3).[249] The resulting composite has highly conductive, transparent, and mechanically durable properties. Poly (3,4-ethylenedioxythiophene) was found to have many interesting features such as a conductivity of 300 Scm^{-1}, transparent in thin oxidized films, and behaviours of an intrinsic p-type organic semiconductor.

Scheme 6-3. Chemical structures of the species of PEDOT: PSS present in the film.

Co-monomers will introduce control of the optical absorption spectrum and additional electronic states in the corresponding copolymers that will tune the band gap and allow

multicolored products. EDOT and alkylenedioxythiophene derivatives have been used as structural units in diad and triad polymers in various approaches to A-B-A-type (A) and A-B-type (B) poly(BEDOT-arylenes) (Figure 6-3).[250]

A = 239, 240, 241, 242, 243, 244, 245   **B = 246, 247, 248, 249, 250, 251, 252**
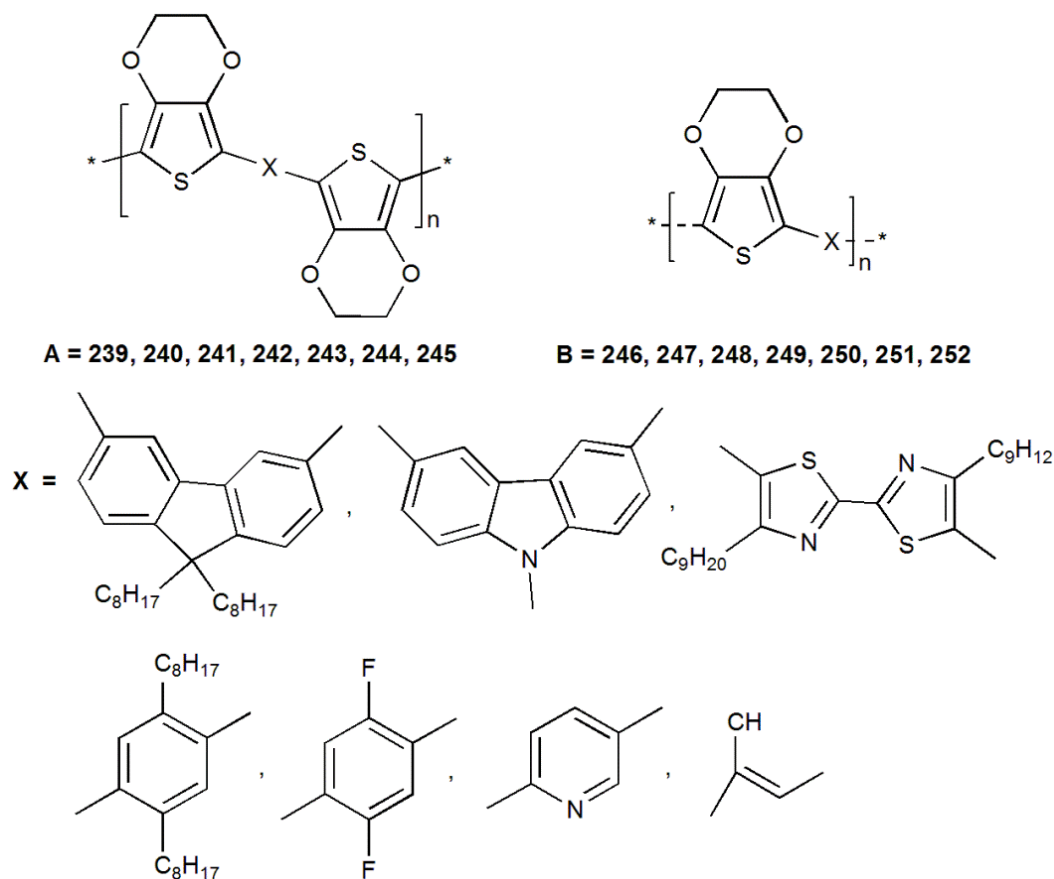
Figure 6-3. Chemical structures of A-B-A-type(**A**) and A-B-type (**B**) poly(BEDOT-arylenes).

Conjugated polymers, such as polyfluorenes, can be designed and synthesised with different properties for a wide variety of applications.[251] They are currently being investigated for use in many organic electronic applications such as solar cells, light-emitting diodes, and field-effect transistors. Conjugated polymers tend to be planar, and can aggregate; therefore, the bulky side chains are added to the 9 position of fluorene to increase the solubility of the polymer. Figure 6-4, shows the structure of a common low band-gap polyflourene derivative.[252] These polymers consist of fluorene and thiophene (electron donating groups), and benzothiadiazole (electron withdrawing group) from monomers which allow for a reduced band gap.

253
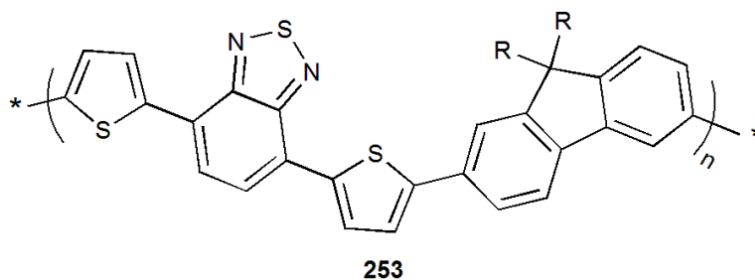
Figure 6-4. Structure of a common low band-gap polyflourene derivative.

6.1.2 Naphthaleneamidinemonoimide derivatives

Decreasing the LUMOs of electron-deficient organic semiconductors is an important target for researchers to improve the band gap. Increasing the electron mobility of n-type semiconductor classes has usually been at the expense of air stability.[253] Therefore, creating and learning to manipulate the properties of new n-type materials are essential to achieve the stability and processability goals imposed by the new organic electronics era.[254]

Imidazole derivatives are stable compounds, many of them are resistant to acids and bases. Also, they are not readily attacked by oxidizing reagents and they have high melting points and are stable at elevated temperatures (430-645 °C).[255] A most versatile and practical synthesis of benzimidazoles is provided by the reaction of an o-phenylenediamine with a carboxylic acid.[256] The resistance to thermal and oxidative degradation is observed in imidazole polymers. The introduction of blocks of imidazole structure into the copolymer increased its thermal stability. Aromatic polybenzimidazoles are high molecular weight materials with superior properties such as stability, retention of stiffness, and toughness at elevated temperatures.[257]

Imide-functionalized naphthalene derivatives have proven to be interesting candidates for use as electron-accepting units in a variety of device architectures. There are several reasons to investigate the use of imide-functionalized naphthalene derivatives as building blocks for polymers: **a**) tune the band structures of polymers over a large range to achieve polymers with low band gap for solar cell applications and OFETs, **b**) polymers with low-lying LUMO levels for n-type semiconductors; and polymers with increased ionization potentials for p-type semiconductors with enhanced device stability, **c**) intramolecular sulphur oxygen contact and intermolecular interaction between donor and acceptor units in the polymer backbone leading to controlled supramolecular self-assembly, **d**) the

introduction of halogenation of these compounds improving the electronic properties make them very favourable coupling partners for electron-rich aryl stannanes in the Stille coupling, **e**) the possibility of alkylation of the nitrogen atom on the imide groups to provide of polymers with better solubility and higher molecular weight.[258-260]

Polymers functionalized with electron withdrawing groups such as fluorine atoms usually leads to low solubility. Jenekhe *et al.*[261] reported a ladder-like n-type polymer **254** and non-ladder polymer **255** with excellent electron mobility (~ 0.1 cm^2 V s^{-1}) (Figure 6-5).

254

255
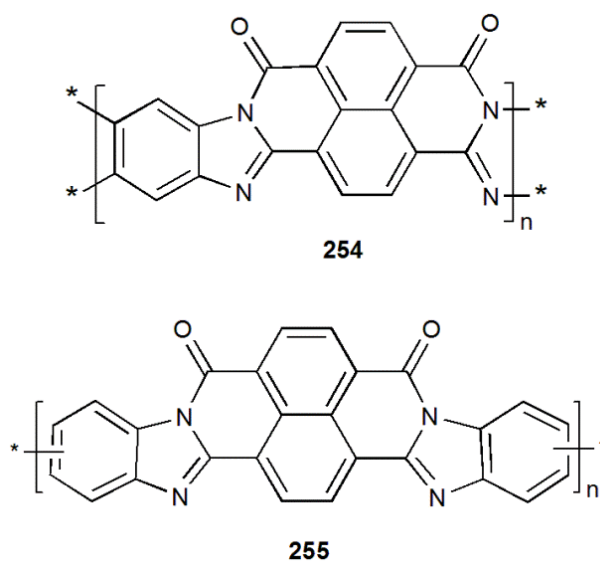
Figure 6-5. The molecular structures of ladder **254** and non-ladder **255** polymer semiconductors.

Jaschke and Langhals[262] synthesised derivatives of naphthalene-1,4,5,8-tetracarboxylic acid with amidine structures (Scheme 6-4). Bis-imide derivatives show light absorption in the UV region was shifted to the visible for the amidine imides, together with a large Stokes shift in their fluorescence spectra.

Scheme 6-4. Synthesis of naphthalene bisamidines **256** and **257** and naphthalene iminoimides.

Duff *et al.*[263] reported new photoconductive compounds comprising mono/dihydride-mono/dibenzamidazoleperinone chloride derivatives as shown in Figure 6-6. These materials were used for photoconductive and photoresponsive applications and exhibited excellent photosensitivity to blue light irradiation.
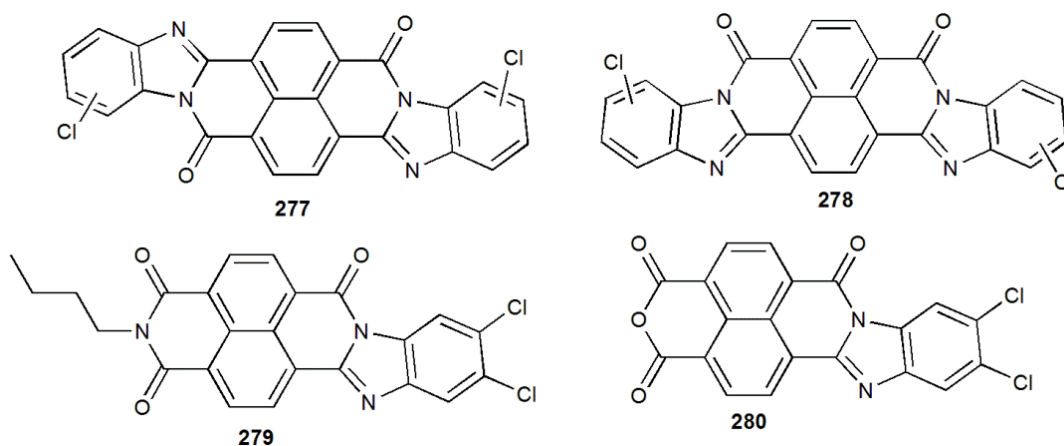
Figure 6-6. Structures of mono/dihydride-mono/dibenzamidazoleperinones chloride.

Tozlu *et al.*[264] described the first phototransistor based on naphthalene bis-benzimidazole **281** in a field effect transistor (Figure 6-7). Polyvinyl alcohol (PVA) was used as polymer

dielectric material, and gave rise to semiconductor material showing 10^{-5} cm^2 V^{-1} s^{-1} electron mobility, and a 10^2 I_{ON}/I_{OFF} ratio.

281
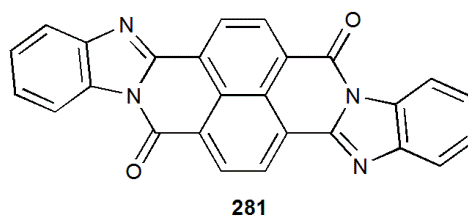
Figure 6-7. Molecular formula of organic semiconductor **281**.

Recently, 1,8-naphthoylene(trifluoro-methylbenzimidazole)-4,5-dicarboxylic acid imide derivatives were synthesised by Deng *et al.*[265] through condensation reactions between 4-(trifluoromethyl)benzene-1,2-diamine and corresponding naphthal-imide-dicarboxylic acid anhydrides (Scheme 6-5). These materials possessed low-lying LUMO energy levels of -3.92 to -3.95 eV and moderate band gaps of -2.56 eV. The organic field-effect transistors devices based on these materials presents typical n-type OFET behavior and exhibited electron mobilities of 10^{-3}-10^{-1} cm^2 V^{-1} s^{-1} in vacuum with good bias stress stability.

282 a: R=C$_{12}$H$_{25}$, R$_1$=CF$_3$, R$_2$=H
283 b: R=C$_{12}$H$_{25}$, R$_1$=H, R$_2$=CF$_3$
284 c: R=C$_8$H$_{17}$, R$_1$=CF$_3$, R$_2$=H
285 d: R=C$_8$H$_{17}$, R$_1$=H, R$_2$=CF$_3$
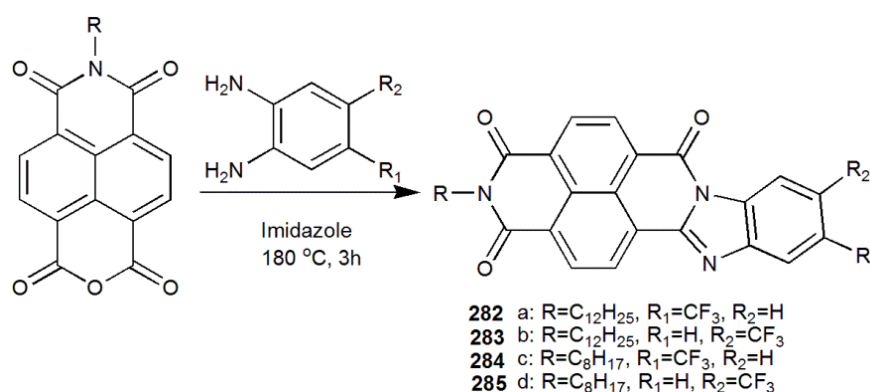
Scheme 6-5. Synthesis of 1,8-naphthoylene(trifluoromethylbenzimidazole)-4,5-dicarboxylic acid imide derivatives.

6.1.3 Naphthaleneamidinemonoimide-thiophene derivatives

A new family of arylenediimide-thiophene semiconductors (Figure 6-8) for n-channel OTFTs was synthesised by Segura *et al.*[260, 266] These materials exhibited field-effect mobilities as high as ~0.35 cm^2 V^{-1} s^{-1} and I_{ON}/I_{OFF} ratio = 10^6 when measured under vacuum.

The effects of oligothiophene backbone catenation, phenylene group introduction in the oligothiophene backbone, and naphthalenediimide vs. perylenediimide core interchange on thin film transistor performance have been studied. The catenation of the oligothiophene backbone decreases the electrical performance due to skeletal distortions, while substitution of the naphthalenediimide fragment enhanced the electron mobility. Also, the phenylene group in the oligothiophene backbone enhanced electron mobility via denser molecular packing. On the other hand, compound **287** exhibits well defined oxidation and reduction processes in solution. Naphthalene-amidinemonoimide modified poly-thiophene displays a p-doping process with anion exchange and its electrochemical reduction with cation exchange during potential cycling. The stored specific charge for the polymer reduction was 38 mAh g^{-1}, while 13 mAh g^{-1} for its oxidation.[267] These polymers have a low charge trapping effect and able to store high specific charges. These results strongly suggest that the polymer is a good material for supercapacitors, batteries, artificial muscles, smart membranes or any electrochemical devices.
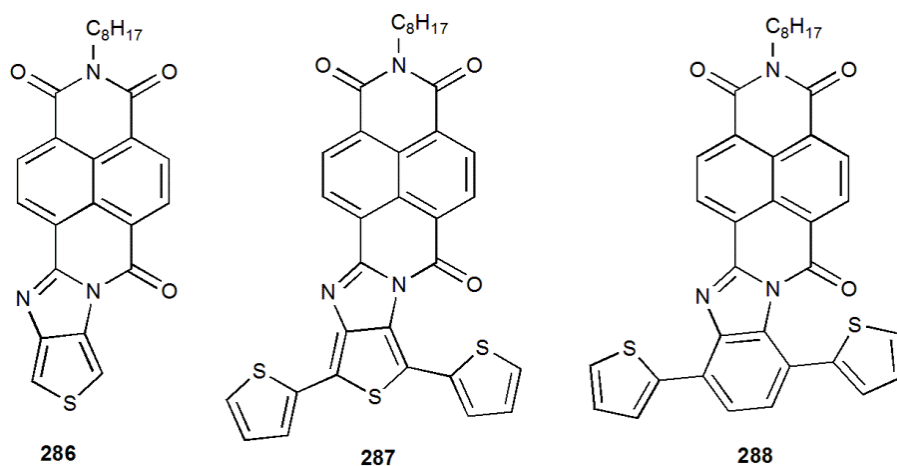
Figure 6-8. Chemical structures of the naphthalenediimide-thiophene semiconductors.

Recently, Segura *et al.*[268] reported a new series of naphthaleneamidinemonoimide-fused oligothiophene semiconductors (Figure 6-9), designed for facile charge transport in organic field-effect transistors. These thiophene-naphthalene semiconductor series have planar skeletons that induce high degrees of crystallinity and hence good charge-transport properties. The length of the oligothiophene fragment controls the carrier charge transport properties. The solution-processed films of **292** exhibited the highest FET performance. Also, it displayed the optimized film mobilities of 2 x 10^{-2} cm^2 V^{-1} s^{-1} for electrons, and 0.7 x 10^{-2} cm^2 V^{-1} s^{-1} for holes.
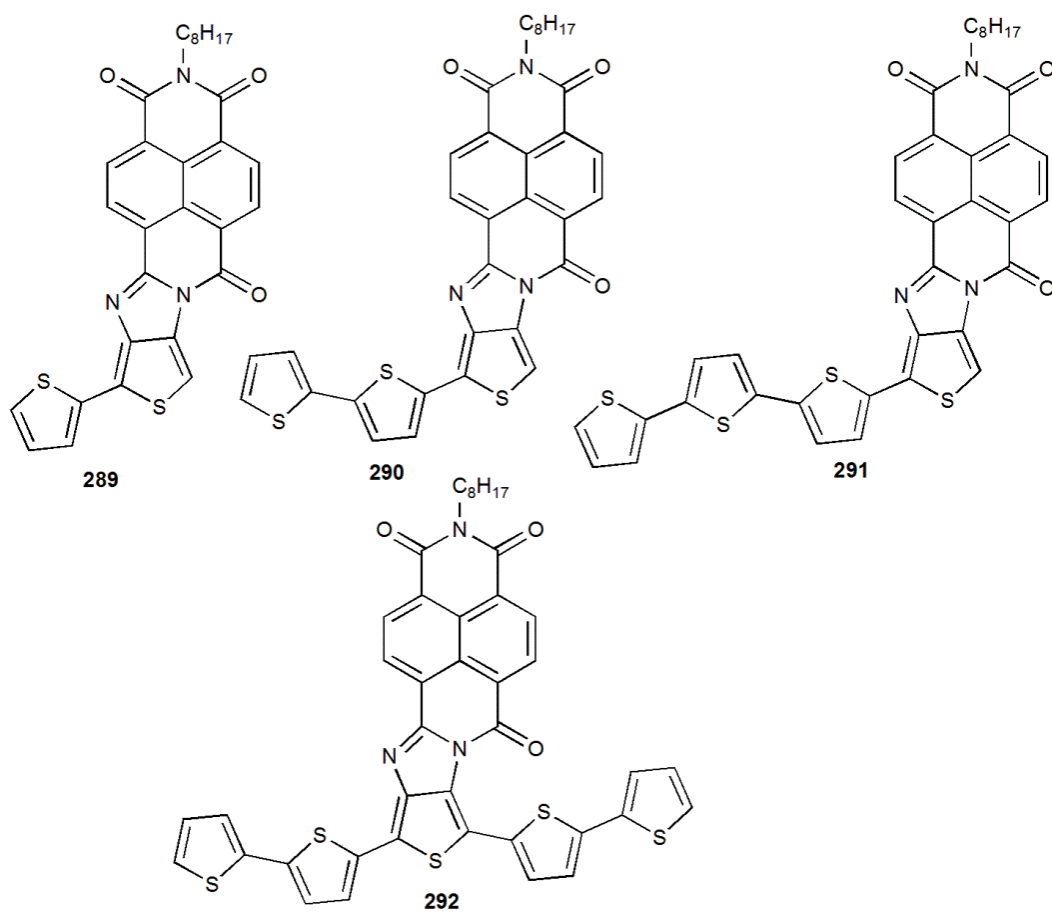
Figure 6-9. Chemical structures of naphthaleneamidinemonoimide-fused oligothiophene semi-conductors.

6.2 The aim of project
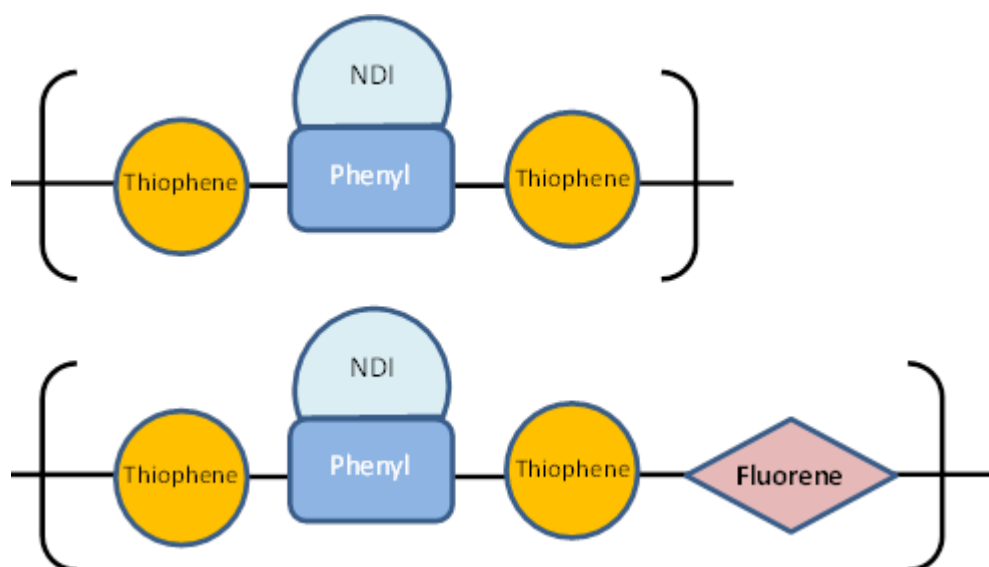
Figure 6-10. New polymers based on NDI described in this chapter.

The main aim of this project is to achieve low band gap polymers with alternating electron-rich and electron-deficient units along the conjugated polymer chain (Figure 6-10) and also to design conjugated polymers with low-lying LUMO levels for n-type semiconductors and increased ionization potentials for p-type semiconductors to enhance resulting device stability. Imide-functionalized naphthalene derivatives were synthesised and used as the building blocks for polymers with donor/acceptor architectures. Also fused rings have a quinoid resonance structure which minimized the bond length alternation between the repeating units which should decrease the band gap. These polymers are attractive targets for fabricating photovoltaic devices.

6.3 Results and Discussion

6.3.1 Synthesis

6.3.1.1 Naphthaleneamidinemonoimide-functionalised fused rings

A series of n-type semiconductors have been synthesised. In the initial stages of the work, compounds **293** and **294** were synthesised by reacting one equivalent each of the dianhydride and 1-aminooctane with 1,4,5,8-tetracarboxynaphthalene **27** followed by chromatographic separation of the monoimide **293** in 29% (Scheme 6-6).[269]
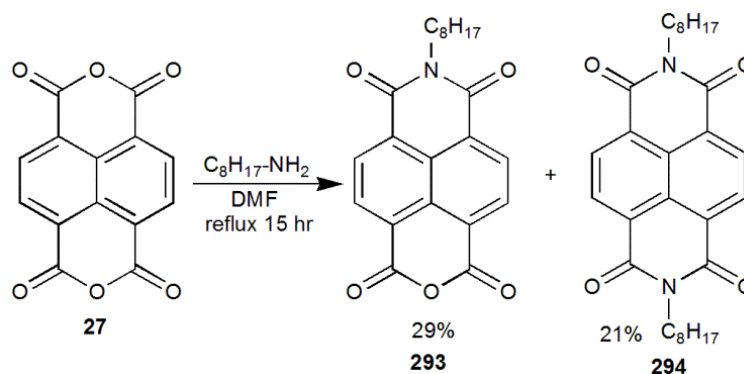
Scheme 6-6. Chemical structures of the *N*-(n-octyl)-naphthalene-1,8-dicarboxyanhydride-4,5-di-carboximide .

N-(*n*-Octyl)-naphthalene-1,8-dicarboxyanhydride-4,5-dicarboximide **293** was reacted with different diamine molecules such as 1,2-diaminoanthraquinone; diaminomalonitrile; 3, 6-dibromo-1,2-phenylenediamine; and 4-bromo-1, 2-diaminobenzene respectively, to yield a series of naphthalenediimide-fused rings.

Firstly, several attempts were made to prepare a naphthaleneamidinemonoimide-anthraquinone target **296**. Naphthalenemonoimide **293** was reacted with 1,2-diamino-anthraquinone **295** in presence of imidazole at 180 °C under N_2 to yield **296** in 59% (Scheme 6-7). Compound **296** is an attractive target in fabricating materials for making photovoltaic devices. The acceptor–acceptor molecular systems could afford broader range of LUMO energies, due to the extensive redox chemistry and photochemical properties of the associated species. This molecule could react with malononitrile by a condensation reaction to produce the novel acceptor molecules.
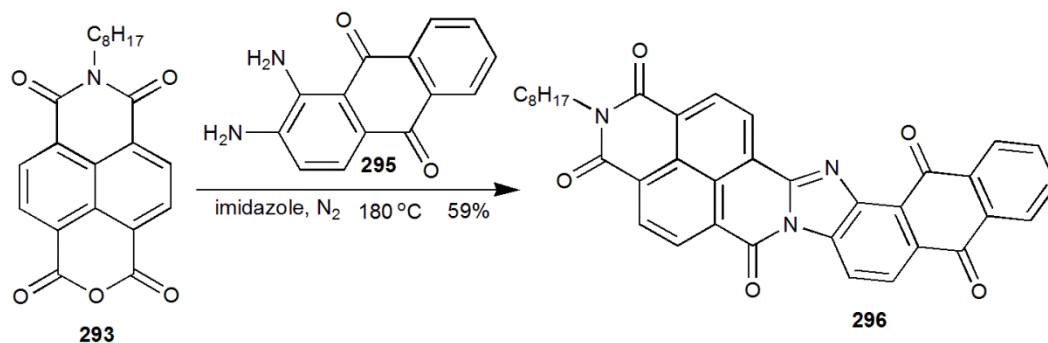
Scheme 6-7. Synthesis of compound **296**.

Compound **297** was synthesised by reacting diaminomalonitrile with naphthalene-monoimide **293** in presence of imidazole at 180 °C under N_2 (Scheme 6-8). However, the obtained yield of **297** was very low (5%), and this route was abandoned.
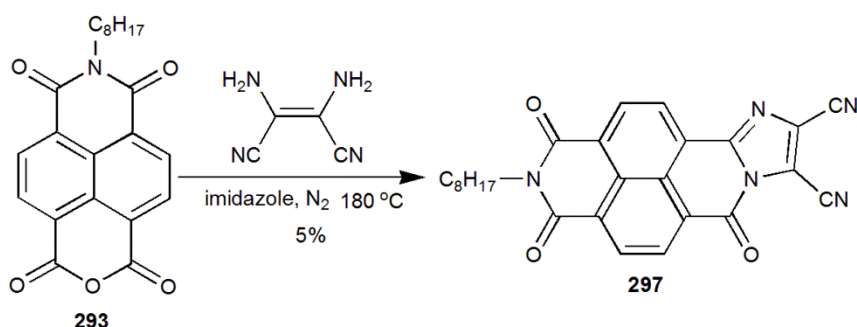
Scheme 6-8. Synthesis of compound **297**.

The naphthalenemonoimide-benzimidazole monomers bearing two thiophenes **302** or two 3,4-ethylenedioxythiophene (EDOT) **305** were targeted as potential precursors for the formation of the new polymers.

The synthesis of compound **301** a precursor to **302** is shown in Scheme 6-10. The reagents 2,1,3-benzothiadiazole **298**,[270] 4,7-dibromo-2,1,3-benzothiadiazole **299**[270] and 3,6-dibromo-1,2-phenylenediamine **300**[271] were prepared according to the literature. Synthesis of **300** starts by synthesis of 2,1,3-benzathiadizole **298** and bromination to form 4,7-dibromo-2,1,3-benzothiadizole **299** which can be reduced to dibromo-*o*-phenylenediamine **300** by the action of reducing agent like Zn in acetic acid. Scheme 6-9 shows the proposed mechanism of synthesis compound **299**.
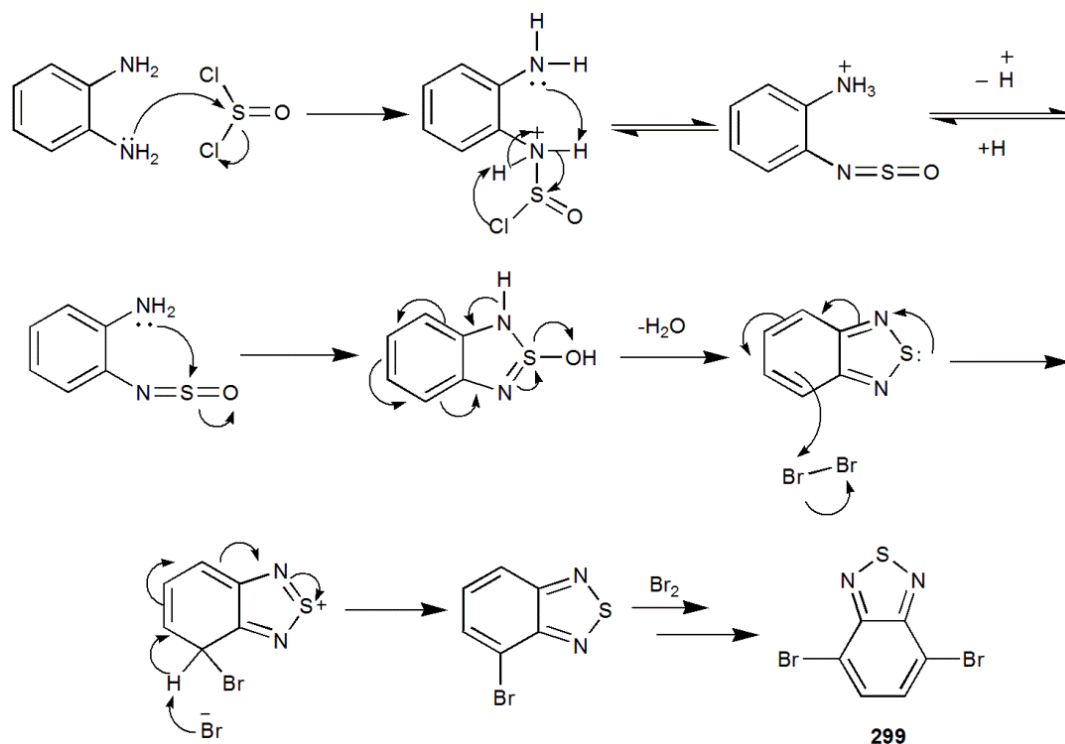
Scheme 6-9. Mechanism of the formation of 4,7-dibromo-2,1,3-benzothiadiazole **299**.

Several attempts were made to prepare a naphthaleneamidinemonoimide-8,11-dibromo-benzimidazole target **301** by using different organic solvents such as DMF, toluene, and 4-butan-1-ol. However, each method proved to be unsuccessful.

The reaction was attempted by heating compound **293**, 3,6-dibromo-1,2-phenylene-diamine **300**, imidazole, and solvent under reflux. Unfortunately, the TLC, mass spectrum, and ^{1}H NMR showed no reaction and this route was abandoned.

However, compound **301** was synthesised under melt conditions according to the literature.[260] A mixture of 3,6-dibromo-1,2-phenylenediamine **300**, *N*-(n-octyl)-naphthalene-1,8-dicarboxyanhydride-4,5-dicarboximide **293**, and imidazole was heated at 180 °C for 2 h under an N_2 atmosphere to yield **301** as an orange solid in 45% (Scheme 6-10).
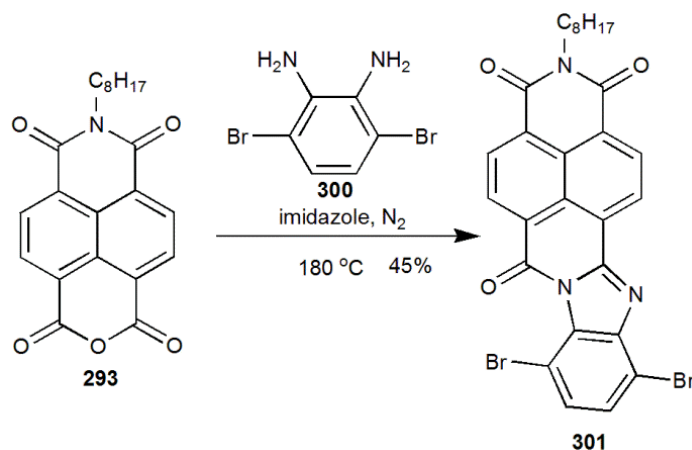
Scheme 6-10. Synthesis of compound **301**.

Compound **301** was synthesised according to the literature.[260] Compound **301** was converted to naphthaleneamidinemonoimide-8,11-dithien-2yl-benzimidazole target **302** *via* a Stille cross-coupling reaction, using of 2 equivalents of 2-(tributylstannyl)-thiophene with palladium(II)bis(triphenylphosphine) dichloride (2 mol%). The product was purified *via* flash column chromatography to afford **302** as a deep brown solid in 73% yield (Scheme 6-11).
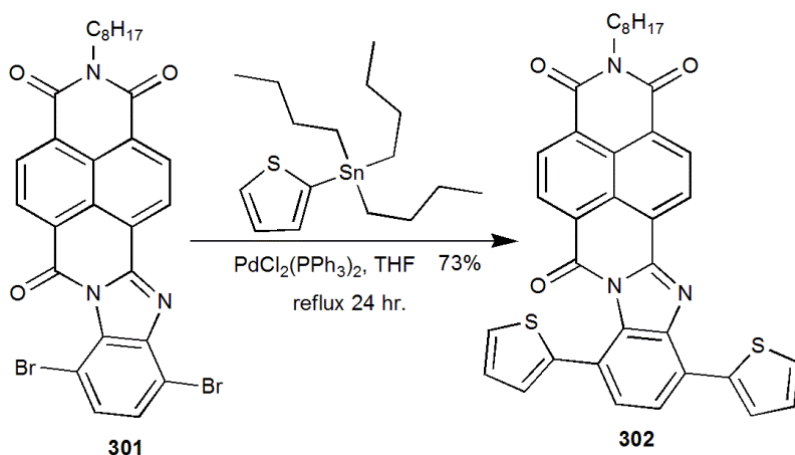
Scheme 6-11. Synthesis of compound **302**.

The Stille cross-coupling reaction was performed under inert nitrogen atmosphere using dry and degassed THF solvent. Scheme 6-12 shows the mechanism of the Stille cross-coupling reaction.[272] The reduction of the palladium catalyst (**A**) to the active Pd° species (**B**) is the first step in this catalytic cycle. The oxidative addition of the organohalide (**C**) gives a cis intermediate, which isomerizes to the trans intermediate (**D**). In the final step the transmetalation with the organostannane (**E**) forms intermediate (**G**), which produces the desired product (**H**). The active Pd(0) species (**B**) after reductive elimination was

produced. The oxidative addition and reductive elimination plays an important role to retain the stereochemical configuration of the respective reactants.
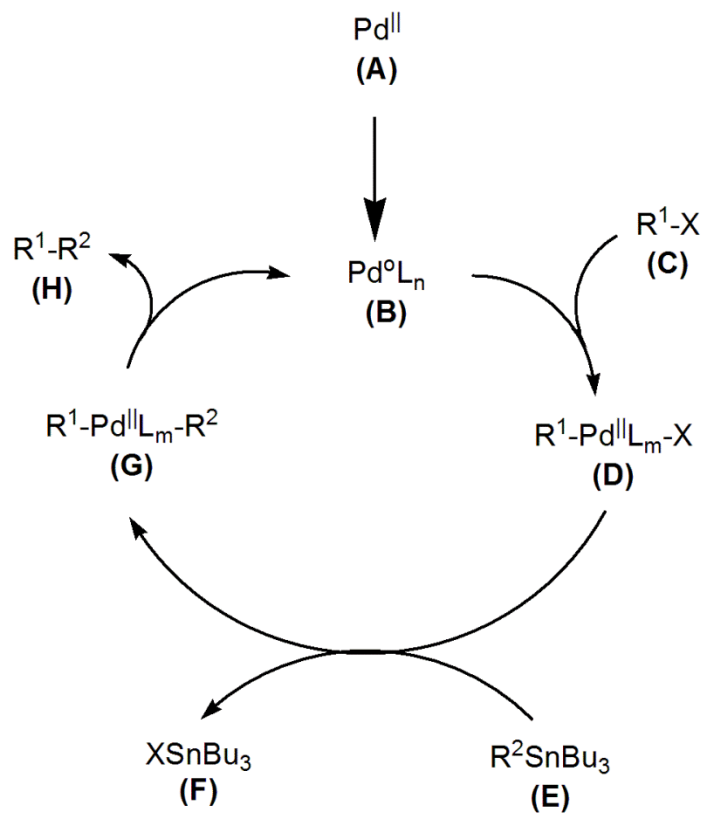
Scheme 6-12. Mechanism of the Stille cross-coupling reaction.

Compound **302** was brominated to form **303** using NBS and dry THF. The addition was undertaken under reflux overnight, and in dark to avoid further bromination. This afforded **303** as a dark red solid in 97% yield (Scheme 6-13).
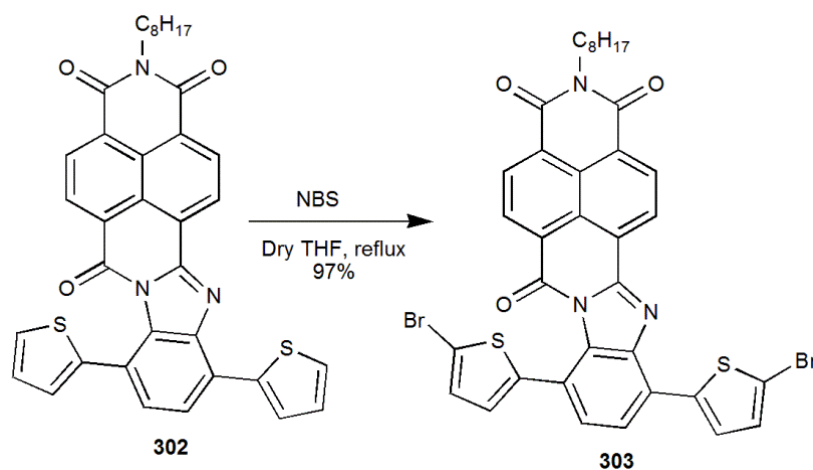
Scheme 6-13. Synthesis of compound **303**.

In order improve the donor properties, compound **303** was reacted with 2-(tributylstannyl)-EDOT in dry DMF. The reaction mixture was heated at 100 °C under N_2 overnight.

Unfortunately, the TLC, mass spectrum, and ^{1}H NMR showed no reaction occurred, and this route was abandoned.

Also, several attempts were made to prepare a naphthaleneamidine-monoimide-8,11-di-3,4-ethylenedioxythiophene-benzimidazole **305** under different conditions and using different organic solvents such as dry DMF, THF, and toluene. Unfortunately, the TLC, mass spectrum, and ^{1}H NMR showed no reaction, presumably due to steric hindrance (Scheme 6-14).
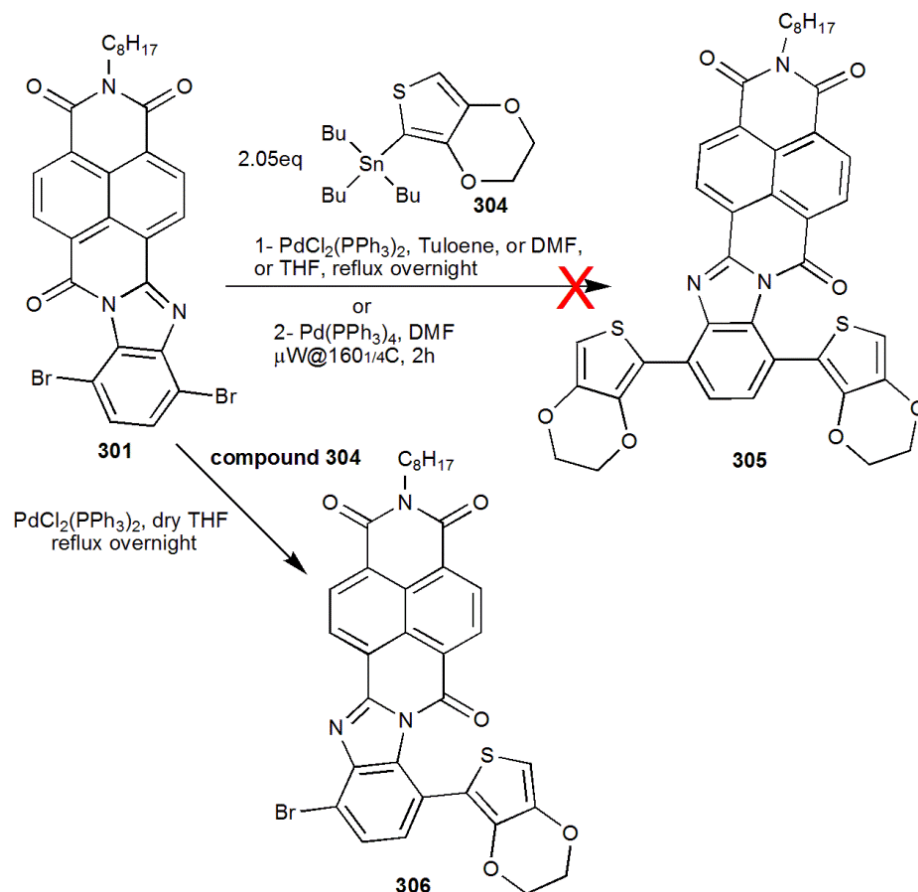
Scheme 6-14. Attempts to synthesise of compound **305,** and compound **306** synthesised.

Fortunately, naphthaleneamidinemonoimide-8-mono-bromo-11-mono-3,4-ethylenedioxy thiophene-benzimidazole **306** was obtained, while trying to prepare compound **305**. The synthesis was performed *via* Stille cross-coupling reaction, by means of 2.5 equivalents of 2-(tributylstannyl)-EDOT with palladium(II)bis(triphenylphosphine) di-chloride (2 mol%) as catalyst in dry THF. The product was purified *via* flash column chromatography to afford **306** as a brown solid in 14% yield (Scheme 6-14).

Other examples of compounds of naphthalenediimide-fused rings were prepared. Both isomers **307** and **308** were synthesised by reacting 4-bromo-1,2-diamino-benzene, *N*-(n-

octyl)-naphthalene-1,8-dicarboxyanhydride-4,5-dicarboximide **293**, and imidazole upon heating at 180 ℃ for 2 h under an N$_2$ atmosphere to yielded **307** as an yellow solid in 8% and **308** as an orange solid in 10% (Scheme 6-15).
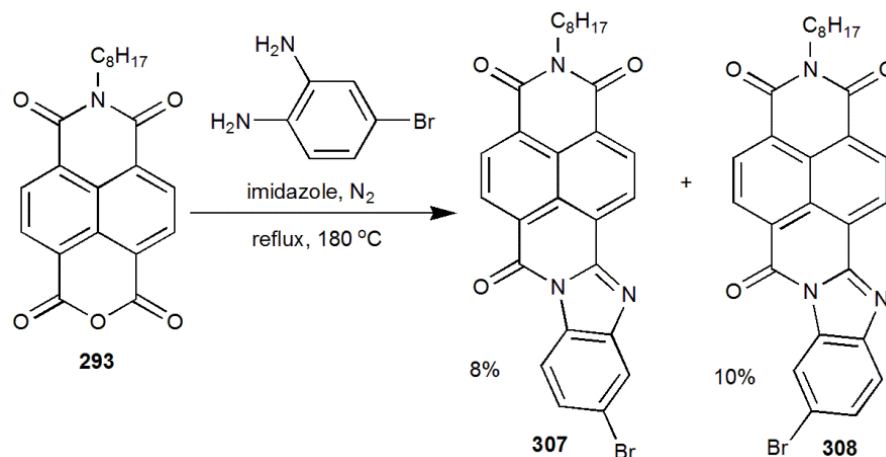
Scheme 6-15. Synthesis of compounds **307** and **308**.

In order to produce donor-acceptor chromophores we attempted the coupling of 4-ethynyl-*N,N*-dimethylaniline separately with **307** and **308** using palladium catalysed Sonogashira cross-coupling reactions. The reaction was attempted at 80 °C using Pd/C, Ph$_3$P, and CuI in a ratio of 1:4:2 and 2.5 equivalents of K$_2$CO$_3$. However, the TLC, mass spectrum, and ^{1}H NMR showed no reaction occurred, and this route was abandoned.

6.3.1.2 Poly-((2,'2-(5,'5-(phenylene-naphthalenediimide)thienyl-lene))-2, 7-(9,'9-dioctylflurene)) (311)

Several attempts were made to synthesise a copolymer **310** via Suzuki cross coupling reactions, by reacting naphthaleneamidinemonoimide-8,11-dibromo-benzimidazole **301** and boronic ester **309**. These reactions were attempted under different conditions and using different organic solvents such as dry DMF, THF, and toluene (Scheme 6-16). Unfortunately, the GPC and ^{1}H NMR showed polymerisation did not occur, and this route was abandoned.
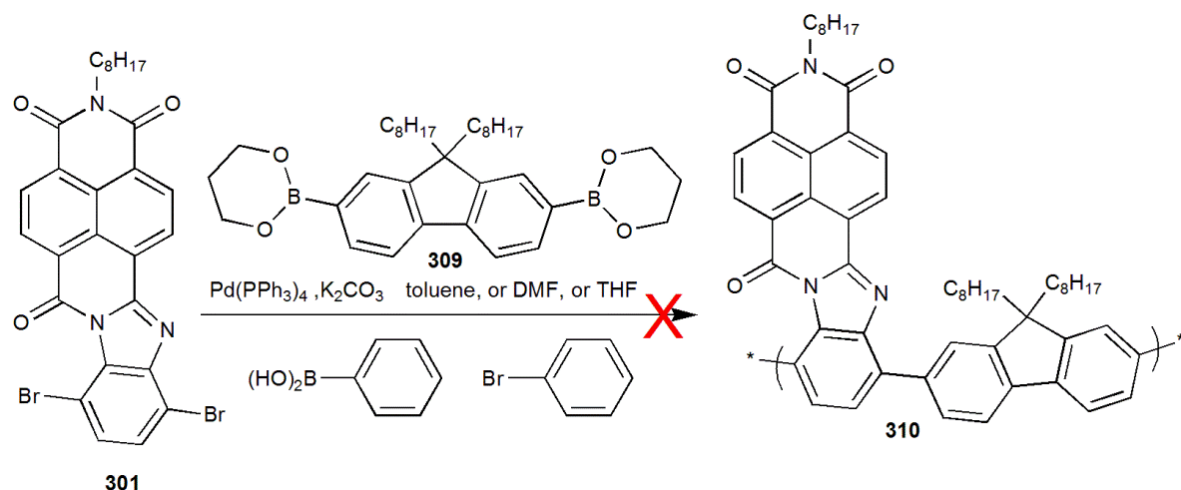
Scheme 6-16. Attempts to synthesise copolymer **310**.

Also, several attempts were made to synthesise copolymer **311** via Suzuki cross coupling reactions, by reacting **303** and boronic ester **309**. These reactions were attempted under different conditions and using different organic solvents such as dry DMF, THF, and toluene (Scheme 6-17 (2)). The end capping of polymer of bromide groups and boronic ester was carried out by the addition of phenyl boronic acid and the bromobenzene. Unfortunately, the GPC and ^{1}H NMR showed no reaction, and this route was abandoned.

The co-polymer **311** was synthesised via Suzuki cross coupling reactions of naphthaleneamidinemonoimide-8,11-dithien-2yl-benzimid-azole-dibromide **303** and the boronic ester **309**. The reaction mixture was deoxygenated by nitrogen bubbling and the reaction was carried out in the presence of palladium triphenylphosphine, aqueous sodium carbonate, and a mixture of n-butanol, toluene, and THF. The resulting polymer **311** was isolated as a green solid in 17% yield (Scheme 6-17 (1)). The mechanism for the formation of polymer **311** is illustrated in Scheme 6-18.[273]
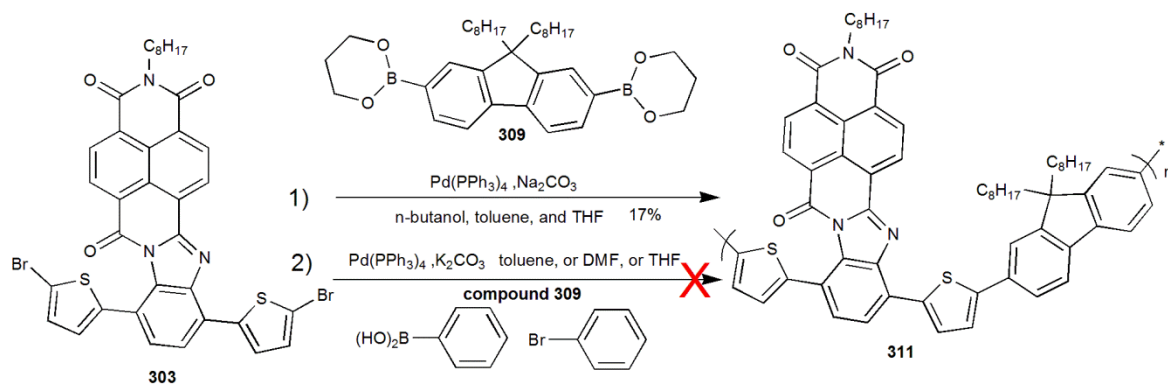
Scheme 6-17. (1) Synthesis and (2) attempts to synthesis copolymer **311**.

The first step in this mechanism is the oxidative addition of palladium to the halide to form the organopalladium species (R_2-Pd^{II}-X). Reaction of R_2-Pd^{II}-X with the base gives the intermediate R_2-Pd^{II}-CO_3. This intermediate forms the organopalladium species (R_2-Pd^{II}-R_1) via transmetalation with the boron-ate complex. At the final step, reductive elimination of the desired product R_1-R_2 restores the original palladium catalyst Pd^o.
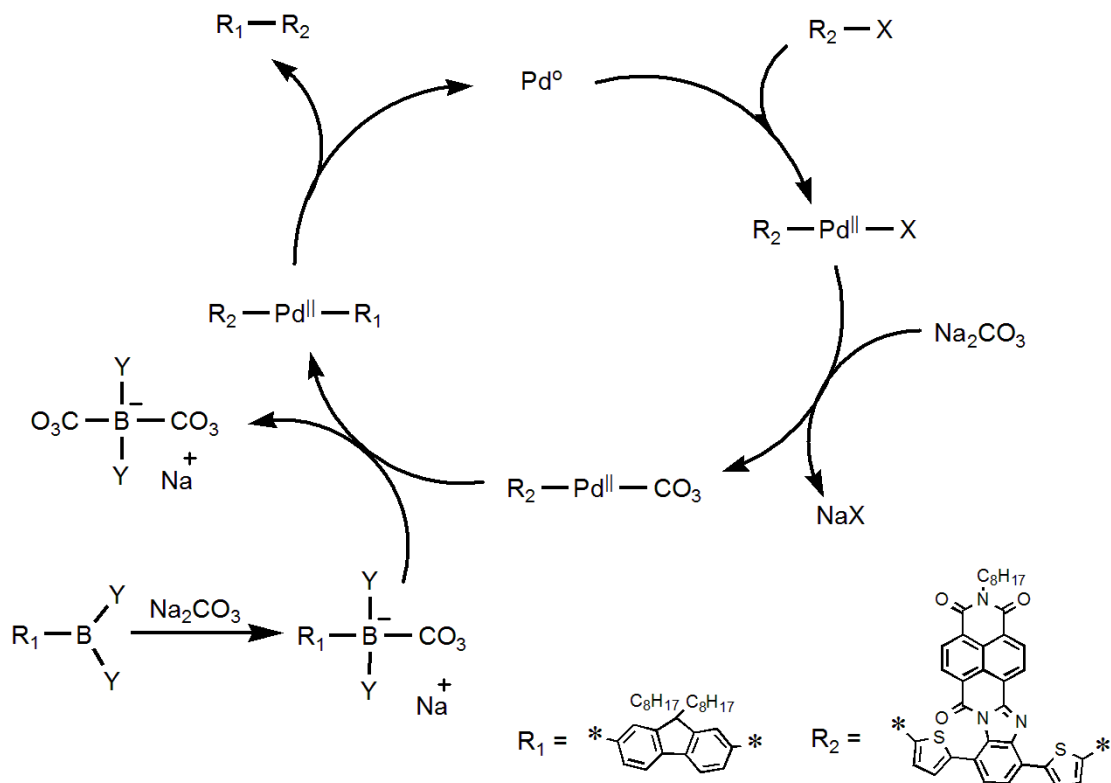
Scheme 6-18. Mechanism for synthesising polymer **311**.

6.3.2 Spectroscopic studies

The spectroscopic data of all derivatives are compatible with the proposed structures. Compounds **296**, **297**, **302**, **303**, **306**, **307**, **308** and polymer **311** and the key compounds that lead to their synthesis were characterized by ^{1}H, ^{13}C NMR, mass spectrometry, and FTIR spectroscopy and they are agreement with the proposed structures.

The ^{1}H NMR spectra confirmed the expected signals of the anthraquinone protons at 9.32, 8.98, 8.86, and 8.56 ppm for compound **296** respectively. Moreover, the infrared spectra data for compound **296** shows the (C=O) absorption at 1704 and 1680 cm^{-1}. The ^{1}H NMR spectra of compound **297** showed the expected signals for the naphthalene, N-CH$_2$ and alkyl group. The infrared spectra data for compound **297** showed the (C≡N) absorption at 2360 cm^{-1}. The ^{1}H NMR spectra of compound **303** confirmed the expected signals of the

thiophene protons at 7.67, 7.13, and 6.81 ppm respectively. Furthermore, the infrared spectra data for compound **303** showed the (C-Br) absorption at 645 cm^{-1}. Compounds **307** and **308** showed the expected signals in ^{1}H NMR spectra for the phenyl protons at 8.39, 8.04, and 7.63 ppm respectively, and the infrared spectra data shows the (C-Br) absorption at 601cm^{-1}. For compound **306**, the expected signals of the EDOT unit in the ^{1}H NMR spectra at 4.13, and 3.91 ppm were observed. Moreover, it shows the phenyl protons at 7.71, and 7.43 ppm and thiophene proton at 6.53 ppm. Also, the infrared spectra data shows the (C-Br) absorption at 640 cm^{-1}.

The ^{1}H NMR spectra for polymer **311** displayed the expected signals as it consisted of very broad overlapping signals, especially for the naphthalene, thiophene, and phenyl units at 8.36, 8.01-7.18, 6.90 and 6.77 ppm respectively. The average molecular weight was determined by gel permeation chromatography in THF using polystyrene standards, and gave an average molecular weight *(Mw)* = 42469 *g/mol* and the polydispersity index (*PDI*) = 1.28 (Figure 6-11).
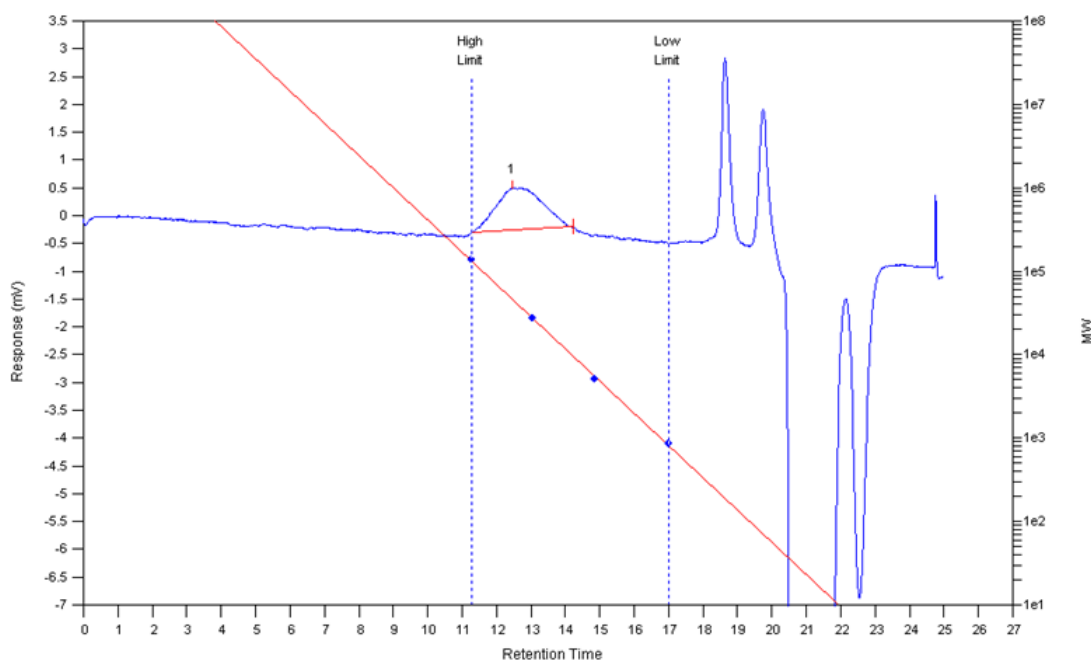
Figure 6-11. Molecular weight determination of polymer **311** by GPC.

The UV-vis spectra of polymer **311** recorded in CH$_2$Cl$_2$ was investigated (Figure 6-12, Table 6-1). Polymer **311** UV-vis spectroscopy displayed a broad band absorption near to IR region at λ_{max}= 588 nm. In addition, it shows high absorption at 430 nm and a small shoulder at 351 nm. Inset shows λ_{max} absorption extent at 500-750 nm.
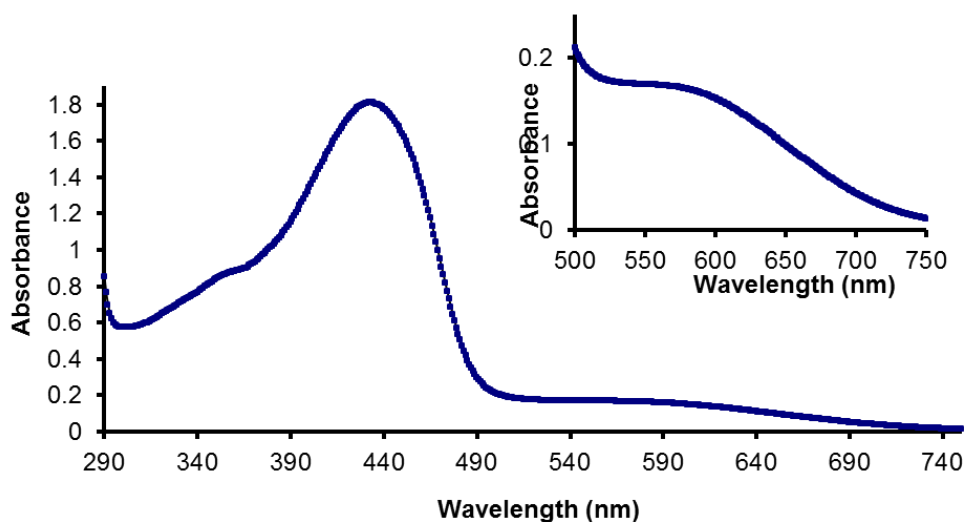
Figure 6-12. UV-visible spectra of polymer **311** recorded in CH_2Cl_2 (1×10^{-4} M).Showing inset 500-750 nm.

Table 6-1. UV-visible spectra data of polymer **311** recorded in CH_2Cl_2 (1×10^{-4} M). Where the λ_{abs} is absorption wavelength (nm), λ_{Max} is maximum absorption wavelength (nm), and E_g^{opt} is optically determined band gap energy (eV).

Compounds	λ_{abs1} (nm)	λ_{abs2} (nm)	λ_{max} (nm)	Band gap (eV)
311	351	430	588	2.11

The photophysical behavior of polymer **311** was investigated by fluorescence spectroscopy recorded as a 10^{-5} M solution in CH_2Cl_2. Inset shows a fluorescence extent at 550-750 nm (Figure 6-13).
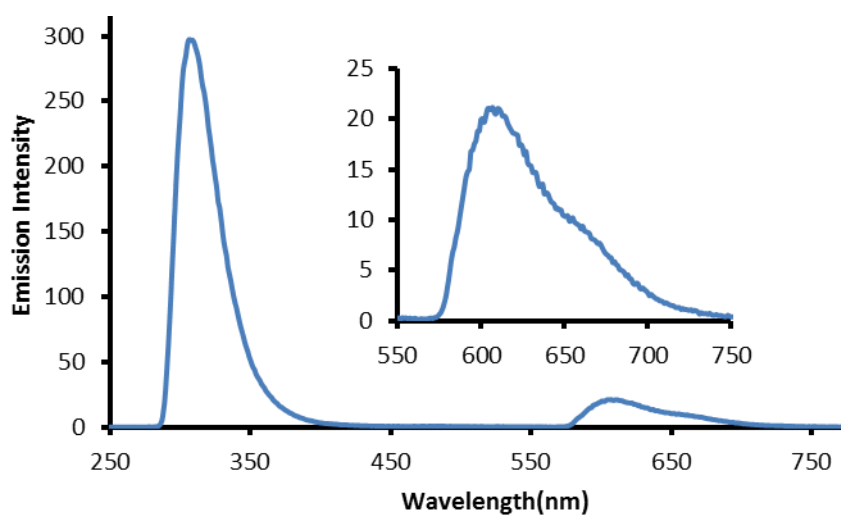
Figure 6-13. Fluorescence spectra recorded for polymer **311** in CH_2Cl_2 (1×10^{-5} M) at excitation wavelength = 287 nm. Inset shows 550-750 nm region.

6.3.3 Electrochemical Studies of the polymer 311

The redox properties of the new polymer **311** were investigated by cyclic voltammetry (CV) using tetrabutylammonium hexafluorophosphate (n-Bu$_4$NPF$_6$) as supporting electrolyte and ferrocene (Fc$^+$/Fc) as internal reference in CH$_2$Cl$_2$. Polymer **311** was reduced in two well-defined reversible one-electron reduction steps (Figure 6-14).
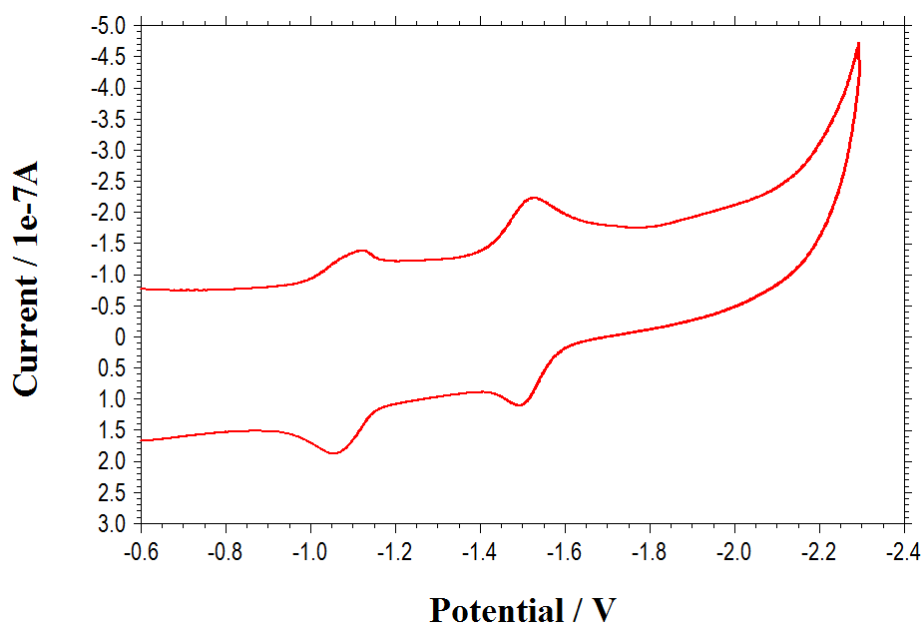
Figure 6-14. Cyclic voltammogramms of polymer **311** recorded using a glassy working electrode, an Ag wire as a reference electrode and a Pt wire as a counter electrode. Recorded in CH$_2$Cl$_2$ (1x 10^{-4} M) with 0.1M (n-Bu$_4$NPF$_6$) as a supporting electrolyte at 20 ^{0}C, and a scan rate of 0.1 Vs^{-1}.

Polymer **311** displayed reversible redox waves at E$_{1/2}$= -1.10 V and E$_{1/2}$= -1.51 V for the reduction of NDI-thiophene and fluorene moieties. This corresponds to a LUMO energy of = -3.70 eV. This should be related to the stronger electron-donating ability of the thiophene and fluorene units. Also, the planarity between the thiophene and fluorene plays an important role on the delocalization of the LUMO.

6.3.4 Electrochemical polymerisation of 302
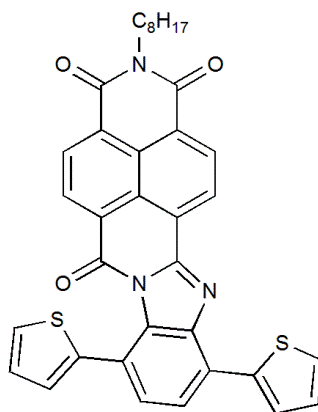
Figure 6-15. Structure of compound **302**.

The electrochemical polymerisation of the monomer **302** (Figure 6-15) on to a glassy carbon working electrode surface was achieved. The absorption spectrum of monomer **302** shows three peaks at 342 nm and 424 nm and 508 nm, the onset of absorption edge of this compound (597 nm) gives the optically determined band gap energy of 2.08 eV (Figure 6-16).
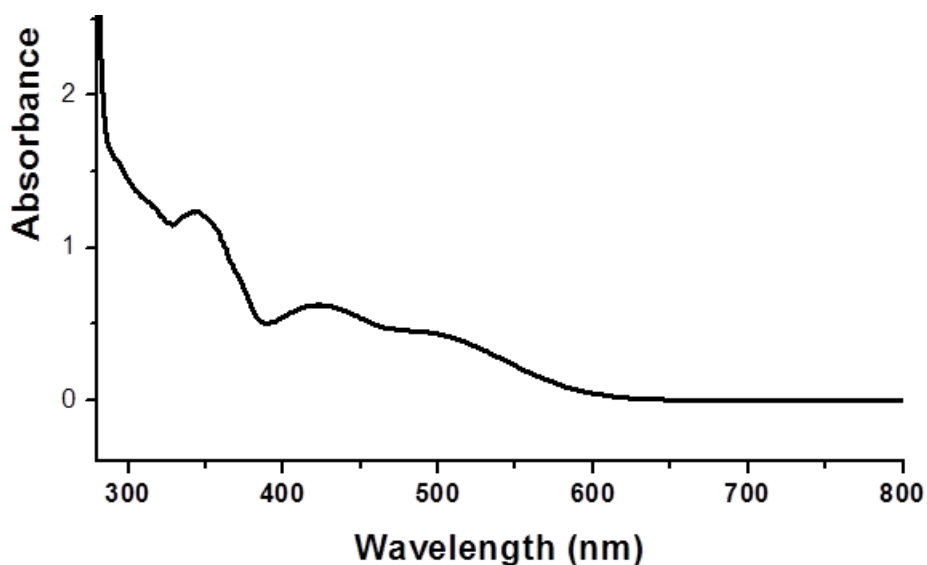
Figure 6-16. UV- Vis spectra of compound **302** measured in acetonitrile and toluene solution (1:1).

The oxidation of monomer **302** shows two quasi-reversible waves at + 1.0 and +1.33 V (Figure 6-17). The reduction process gives clear reversible waves at $E_{1/2}$= -1.11 and at $E_{1/2}$= -1.93 V (Figure 6-18).
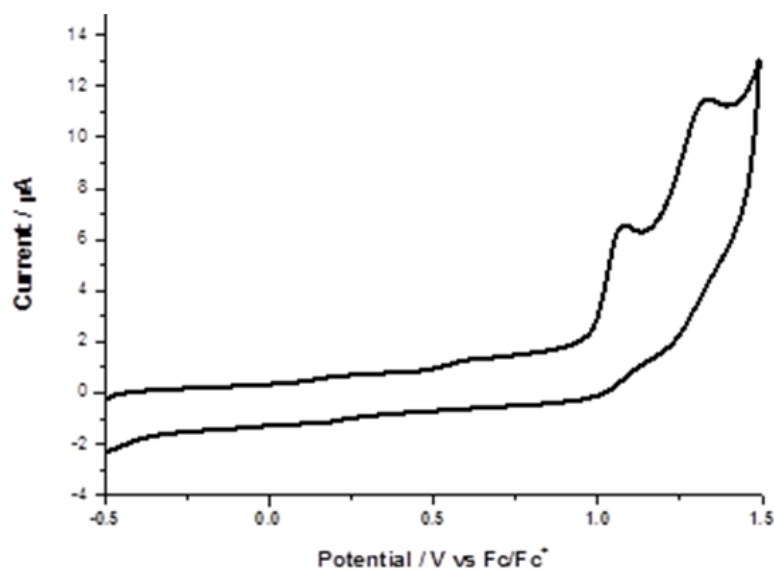
Figure 6-17. Oxidation of compound **302** recorded using a glassy carbon working electrode, an Ag wire as a reference electrode and a Pt wire as a counter electrode. Recorded in acetonitrile and toluene solution (1:1), (1×10^{-4} M) with 0.1M (n-Bu$_4$NPF$_6$) as a supporting electrolyte at 20 °C, and a scan rate of 0.1 Vs^{-1}.
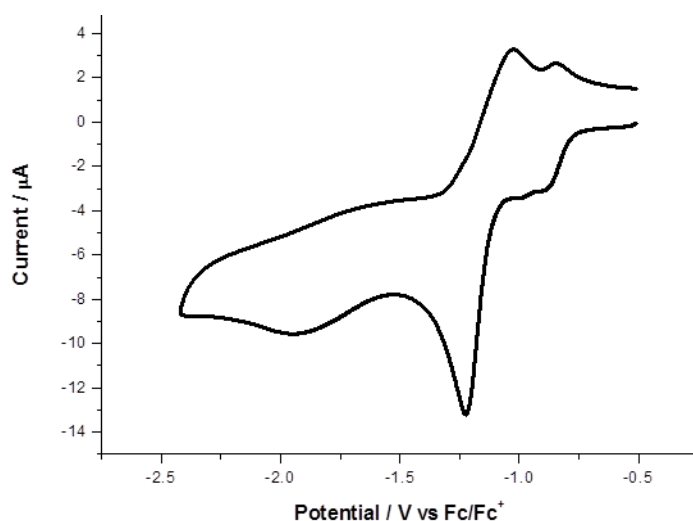
Figure 6-18. Reduction of compound **302** recorded using a glassy carbon working electrode, an Ag wire as a reference electrode and a Pt wire as a counter electrode. Recorded in acetonitrile and toluene solution (1:1), (1×10^{-4} M) with 0.1M (n-Bu$_4$NPF$_6$) as a supporting electrolyte at 20 °C, and a scan rate of 0.1 Vs^{-1}.

The oxidation-reduction of monomer **302** shows the onset of oxidation = +0.97 V which gives HOMO = -5.77 eV, and the onset of reduction = -1.07 V which gives LUMO = -3.73 eV. The electrochemically determined HOMO-LUMO gap energy (2.04 eV) is similar to the optically determined band gap energy (2.08 eV) of the monomer.

A number of attempts were made to find conditions for growing films of polymer **312** on large electrodes such as ITO coated glass. Best results were obtained by cycling over -0.5V to +1.5V (Figure 6-19).
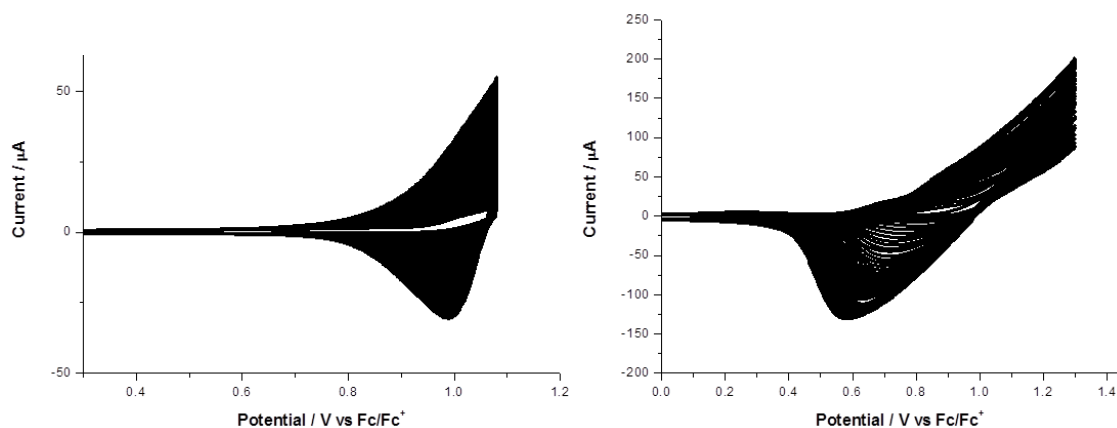
Figure 6-19. Polymer **312** growth on glassy carbon (left) and ITO slides (right), an Ag wire as a reference electrode and a Pt wire as a counter electrode. Recorded in acetonitrile and toluene solution (1:1), (1x10^{-4} M) over 200 segments at scan rate 0.1 Vs^{-1}.
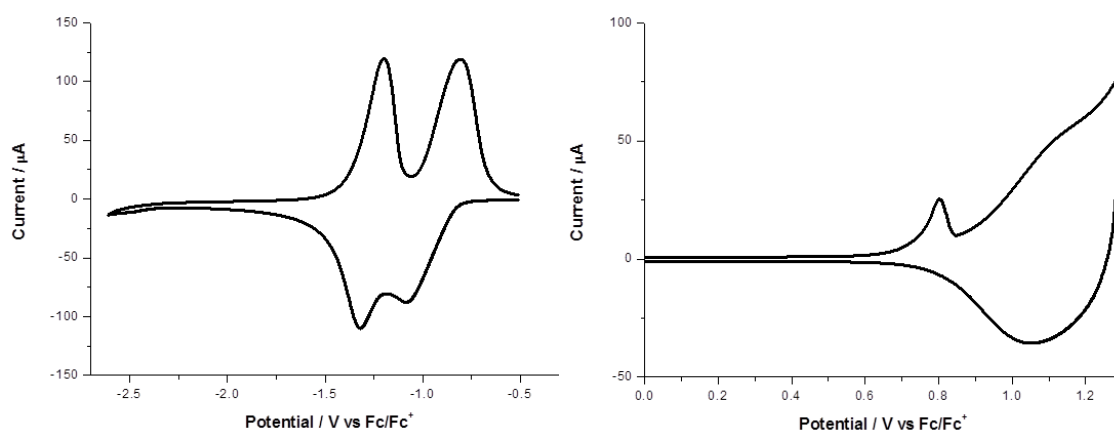
Figure 6-20. Oxidation (left) and Reduction (right) of polymer **312** on glassy carbon (left) and ITO slides (right), an Ag wire as a reference electrode and a Pt wire as a counter electrode. Recorded in acetonitrile solution (1x10^{-4} M) at scan rate 0.1 Vs^{-1}.

The oxidation of polymer **312** displays irreversible waves at + 0.80 V and broad wave at +1.06 V. The reduction process gives two reversible waves at $E_{1/2}$= -1.26 and at $E_{1/2}$= -0.94 V. The CV of polymer **312**, shows that the onset of oxidation = +0.72 V which gives HOMO= -5.52 eV, and the onset of reduction = -0.84 V which gives LUMO= -3.96 eV. The electrochemically determined HOMO-LUMO gap energy = 1.56 eV (Figure 6-20).

The stability of the polymer films was investigated using CV, which indicated that the polymer **312** possessed good oxidative stability (Figure 6-21).
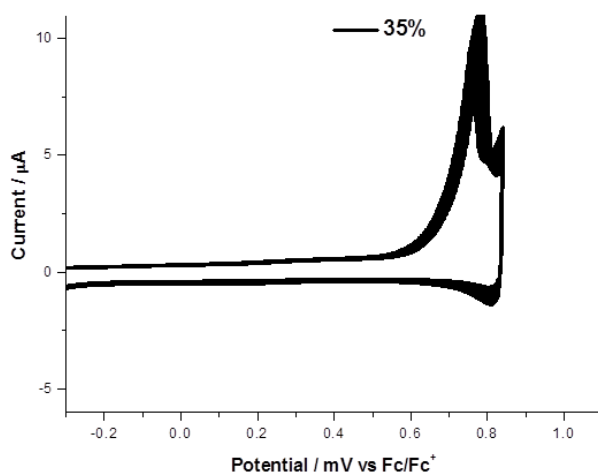
Figure 6-21. Oxidation stability of polymer **312** over 100 segments.

The absorption spectroscopy of the polymer provides information on the π–π∗ transition which is normally associated with the band gap of a conjugated polymer. It shows that the onset of the longest wavelength absorption band in polymer is hardly shifted compared to the monomer (Figure 6-22). The absorption spectra of polymer **312** displays two peaks at 410 nm and 567 nm, the onset of absorption edge (771 nm) of this polymer gives the optically determined band gap energy of 1.61 eV, which is slightly higher compared to electrochemically determined band gap energy (1.56 eV).
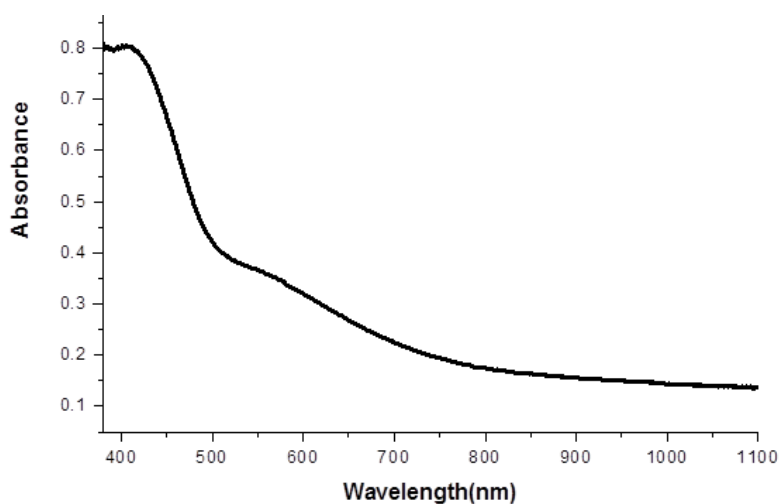
Figure 6-22. UV- vis spectra of polymer **312** on ITO slide.

6.4 Conclusion

Naphthalene diimides (NDIs) are excellent electron acceptors and have been used in many applications. A range of new systems have successfully been synthesised based on reacting the NDI core with different diamine molecules such as 1,2-diaminoanthraquinone; diaminomalonitrile; 3,6-dibromo-1,2-phenylenediamine; and 4-bromo-1,2-diaminobenzene respectively, to yield a series of naphthaleneamidinemonoimide-fused rings. All these derivatives were characterised using different techniques ^{1}H NMR, ^{13}C NMR, I.R, mass, fluorescence, UV-vis spectroscopies, and cyclic voltammetry. Unfortunately, all attempts to crystallise these derivatives for X-ray analysis proved unsuccessful.

These NDI compounds were alternated with electron-rich units such as thiophene and EDOT and electron-deficient units such as anthraquinone to furnish low band gap materials. Compound **303** was used as a monomer for the synthesis of the conjugated polymer by Suzuki cross-coupling reactions. This polymer has a high molecular weight and green colour with an optically determined band gap of 1.75 eV. On the other hand, compound **302** was polymerised by electropolymerisation to provide a polymer with an optically determined band gap of 1.61 eV, which is slightly higher compared to the electro-chemically determined band gap (1.56 eV).

For future work, naphthaleneamidinemonoimide-fused rings derivatives can be used as a precursor for new acceptor-acceptor systems. Also, they can be used as a monomer for polymerisation.

7. Chapter 7

Synthesis of new naphthalenediimide-based phthalocyanines

7.1. Introduction

7.1.1. Phthalocyanines

Phthalocyanines (Pcs) were accidentally discovered in the early 1900s[274] at Scottish dyes Ltd. Insoluble blue material was observed by Dandridge and co-workers during the manufacture of phthalimide from phthalic anhydride (both of which are white solids). Linstead *et al.*[275-277] proved the structure of this material to be an iron containing organic compound. Then, they conceived the term 'phthalocyanine' from two Greek terms relating to the compound: naphtha (rock oil) to give emphasis to the Pc association with its various phthalic acid derived precursors, and cyanine (blue). Later, Linstead and co-workers elucidated the structure of phthalocyanines as well as procedures for obtaining several metal and metal free Pcs.

The formal name for phthalocyanines is tetrabenzo[5,10,15,20]-tetraazaporphyrin. Pcs **313** are closely related to the naturally occurring porphyrin ring system **314**. The differences between them being the four benzo-subunits and the nitrogen atoms at each of the four *meso* positions (Figure 7-1). Pcs are more stable derivatives than porphyrins.[278]
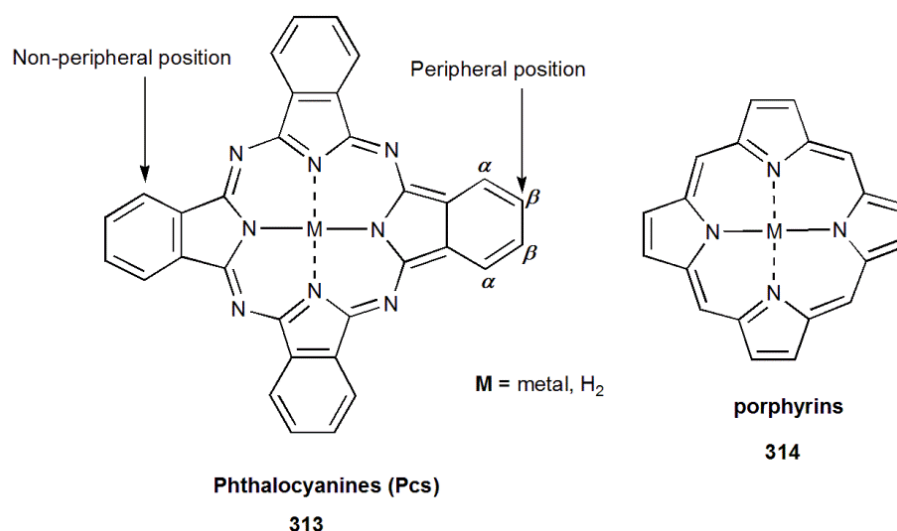
Figure 7-1. General structure of phthalocyanines **313** and porphyrins **314**.

Figure 7-2 shows the accepted numbering system for the phthalocyanines ring. The Pcs can be named using the formula a-(L)$_n$MPc-*n&p*-S. There are sixteen possible sites for macrocycle substitution associated with the four benzo-subunits. The 2,3,9,10,16,17,23,24 carbon atoms are termed the *peripheral* (*p*) sites and the 1,4,8,11,15,18,22,25 carbon atoms are symbolised the *non-peripheral* (*np*) sites.[279]
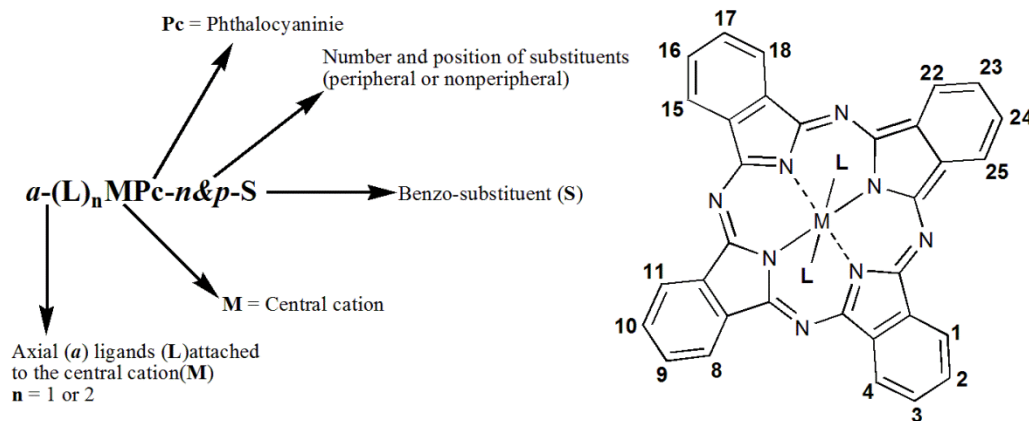
Figure 7-2. Nomenclature of phthalocyanine

Phthalocyanines are planar macrocyclic aromatic compounds consisting of four isoindoline units linked together by nitrogen atoms. Phthalocyanines have a great structural flexibility, and the central cavity of phthalocyanines can host ~70 different elemental ions including hydrogens (metal-free phthalocyanine, H_2Pc). Moreover, the variation in the central metal, type, number and position of substituents on the α-non-peripheral substitution, β-peripheral substitution or axial substitution attached to the phthalocyanine, can have a significant influence on their chemical properties.[280]

Peripheral substituents of phthalocyanines are usually introduced to improve the poor solubility of unsubstituted phthalocyanine. Introduction of bulky or long chain substituents in the periphery of macrocycle (peripheral substitution) increases the solubility in common organic solvents. The coordination of the central metal with additional axial ligands (axial substitution) also will increase the solubility. Introduction of substituents on Pc will increase the distance between the stacked molecules which enables phthalocyanine solvation. Un-substituted phthalocyanines commonly exhibit poor solubility in most organic solvents and water due to the molecular interactions between their π-systems. Due to these interactions, the Pcs stack upon themselves to form a strong and hydrophobic crystal lattice and this insolubility significantly limits their usefulness.[281, 282]

The standard oxidation state of phthalocyanine is -2, so it can coordinate a central atom M with oxidation state +2. Also, the coordination number of the square-planar phthalocyanine is four, for that reason many of the metals, having higher coordination numbers, can bond with a variety of axial ligands.[283]

Pc molecules have a conjugated system of 18 π-electrons and possess very high thermal and chemical stability. Also, they may exhibit a series of electrochemical processes and

can consequently be used as efficient electron mediators. These properties make phthalocyanines applicable in a diverse range of fields. Phthalocyanines have numerous applications in various disciplines. The original and most widely used application is that of dyes and pigments in textiles, polymers and paints. Other applications are in nonlinear optics (including optical limitation), xerography (as photoconductors), optical data storage (as the laser absorption layer within recordable compact discs), molecular electronics, photovoltaic and solar cells, catalysis, semiconductors, gas sensors, as photosensitizers, liquid crystals, in cancer therapy, and in fuel cells. Scheme 7-1 shows some applications of phthalocyanines.[283-285]
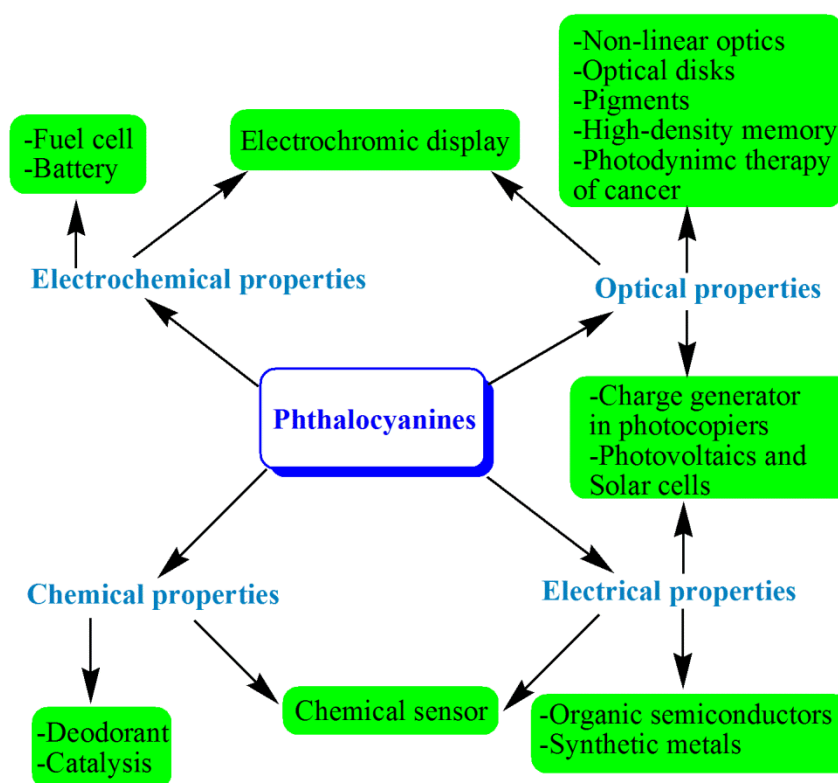
Scheme 7-1. Some applications of phthalocyanines.

7.1.2. UV-vis absorption spectra of phthalocyanines

UV-vis spectroscopy of phthalocyanines provides a very intense absorption band in the far red end of the visible spectrum around λ_{max}= 650-720 nm which is known as the Q-band region. This has been attributed to the $\pi \rightarrow \pi*$ electronic transition from the HOMO to the LUMO of the Pc^{-2} ring. A second band called B-(or Soret) Band appears between 300-400 nm in the blue end of the UV region. Generally, B-band absorptions are much less intense than the Q-band absorption. The B-bands have been attributed to the deeper π levels $\rightarrow$ LUMO transitions.[286] The extended π-conjugation of the phthalocyanine causes the

maximum absorption in the Q-band region to be shifted to longer wavelengths relative to porphyrins. The positions of the phthalocyanines spectral absorption bands, especially the Q-band, are affected by factors such as central metal, symmetry, substituents, aggregation, and solvents. Figure 7-3 shows the UV visible spectra of non-metallated (H_2Pc) (solid line), metallated (MPc) (dashed line) phthalocyanines and Q-band and B-band positions.[287]
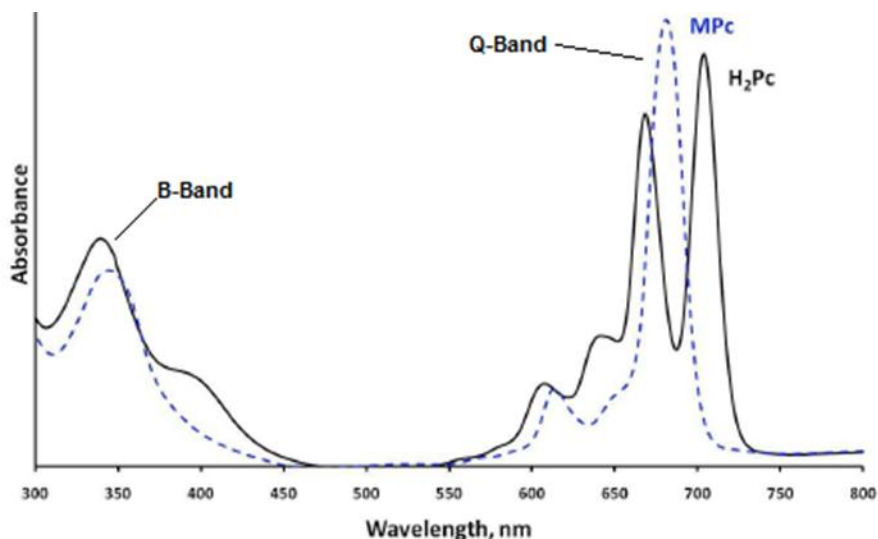
Figure 7-3. UV-vis spectra of non-metallated (H_2Pc) (solid line) and metallated (MPc) (dashed line).

7.1.3. Synthesis of phthalocyanines

There are many methods that can be used for the preparation of phthalocyanines. These methods depend on the availability of the precursors involved, the cost of the synthesis and the substituents on the starting materials. Generally, the synthesis of phthalocyanines results from a single step reaction that is called cyclotetramerisation. Typical precursor units of Pc are benzoic acid or its derivatives, (e.g. phthalic anhydride **316**, phthalonitrile **320**, phthalimide **323**, *o*-cyanobenzamide **315**, and isoindoline-diimine **318**) (Scheme 7-2). Substituted phthalonitrile and isoindolinediimines are the most common precursors used for substituted phthalocyanine synthesis.

The metal-free phthalocyanines can be easily synthesised from these precursors by heating in high boiling alcohols (e.g. pentanol, octanol) in the presence of nucleophilic hindered strong organic bases (e.g. 1,8-diazabicylo-[5,4,0]-undec-7-ene (DBU), 1,5-diazabicyclo [4.3.0]non-5-ene (DBN) or NH_3) used as powerful catalysts for the cyclotetramerisation of phthalonitriles. Also, the metal free phthalocyanine can be formed by treatment of the MPc with concentrated sulphuric acid.[288]

Several different ways can be used for synthesis of metal containing phthalocyanine complexes. Most of MPcs can be obtained from phthalonitrile or diiminoisoindoline in addition of a metal ion in high-boiling solvents such as Dimethylethanolamine (DMAE), DMF, and quinoline or 1-chloronaphthalene. Phthalimide and phthalic acid anhydride can be used for synthesis of MPcs in presence of urea as a source of nitrogen and catalysts such as ammonium molybdate or boric acid to promote the cyclization. The variety of starting materials for phthalocyanine synthesis and the varied methods for their preparation, allow Pcs to achieve their potential.[280, 289, 290]

Phthalocyanine complexes with axial ligands can be synthesised directly by reacting the precursors with a metal salt containing an anion that can ligate to the central metal. Refluxing MPc in coordinating solvents, such as dimethylsulfoxide (DMSO) and pyridine or in the presence of the axial ligand, have also resulted in axially ligated phthalocyanines. Microwave methods have been used for the solvent-free synthesis of axially substituted MPcs.[291]
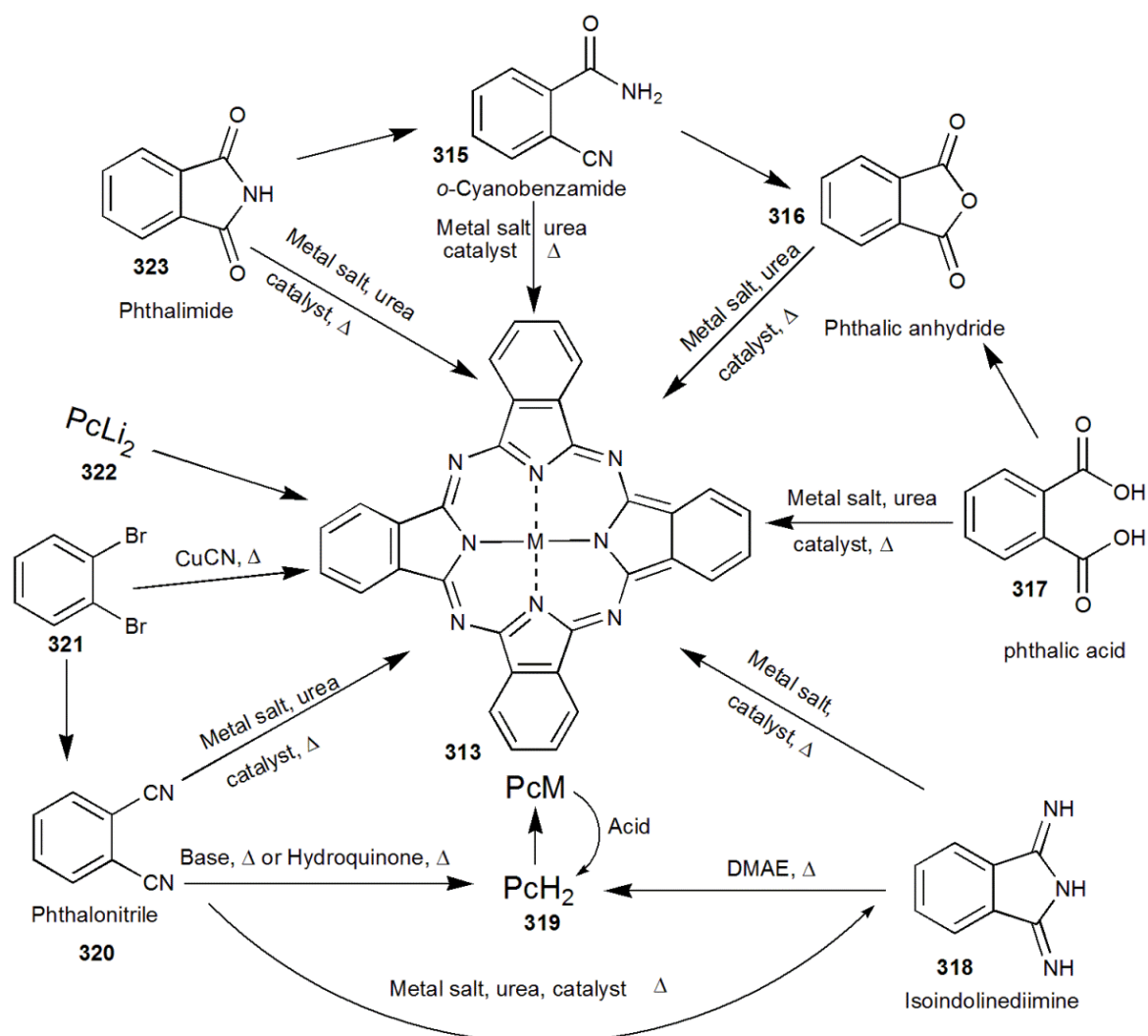
Scheme 7-2. Synthetic routes to phthalocyanine.

7.1.4. The mechanism of phthalocyanine formation

In 1989, Leznoff[280] proposed a mechanism in Pc formation involving organic bases such as DBU and DBN or alkali metalalkoxides in alcohol. He suggested that the alkoxide can act as nucleophile; also in metal containing Pc synthesis the counter anion can play the same role as the nucleophile (Scheme 7-3). The cyclotetramerisation of phthalonitrile can occur even without the concurrent complexation of a metal ion. It is clear that both the electronic and steric effects of substituents can have a significant influence on the mechanism and outcome of cyclotetramerisation reactions.[289]
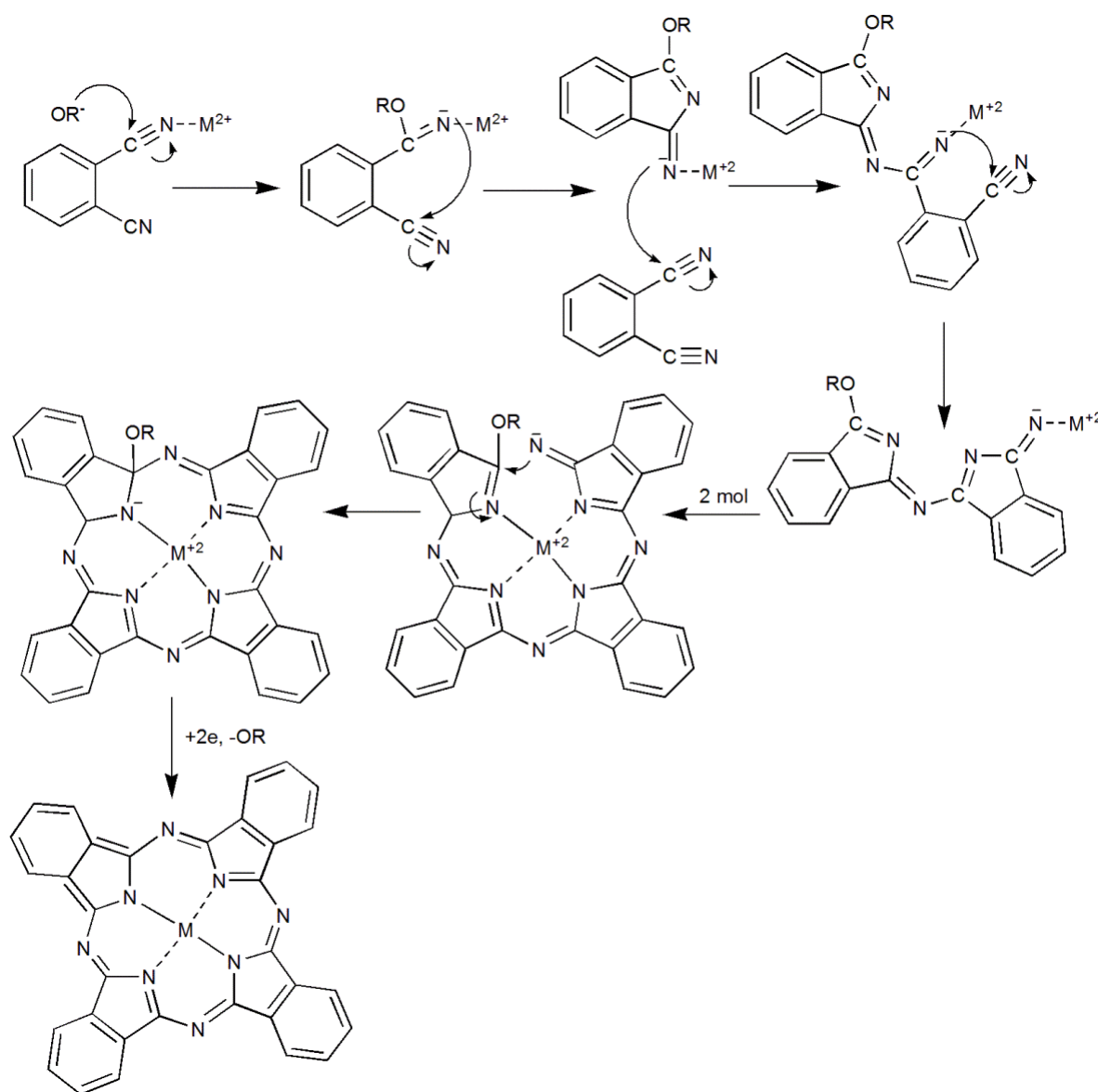
Scheme 7-3. Proposition of a reaction mechanism for a MPc.

7.1.5. NDI-Phthalocyanines

Phthalocyanines have a variety of excellent properties which are promising for different applications. Pcs have excellent light-harvesting properties. Also, phthalocyanines exhibit rich redox chemistry, characteristic electrical, thermal, optical, light stability, semi-conducting and catalytic properties.

Fukuzumi et al.[292] reported the integration of silicon phthalocyanine with two different electron acceptors, 1,4,5,8-naphthalenenediimide (NDI) and fullerene (C_{60}), through the axial position to form the SiPc-(NDI)$_2$-(C_{60})$_2$ pentad **324** (Figure 7-4). Here, the SiPc was expected to act as a photosensitizing electron donor and NDI and C_{60} act as planar and spherical electron acceptors, respectively. Photoinduced electron-transfer experiments suggested the usefulness of **324** and **325** as light-harvesting systems.
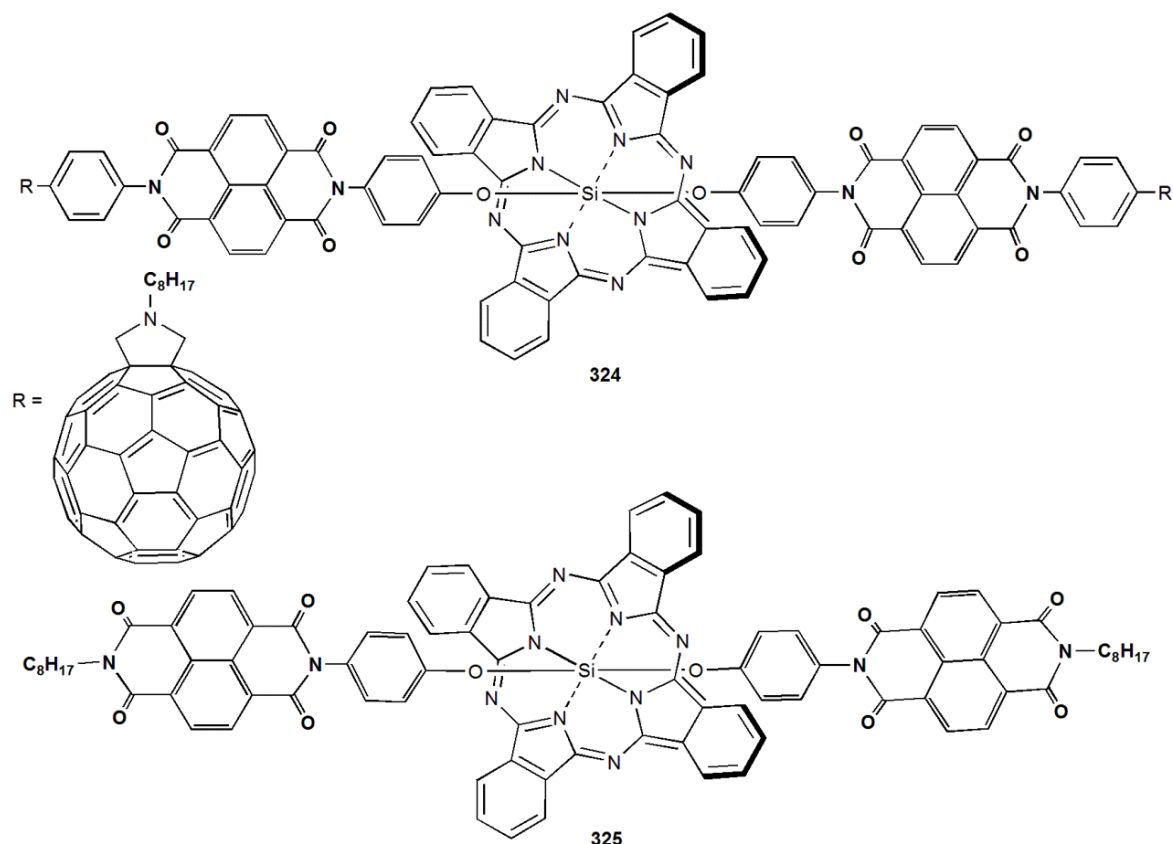
Figure 7-4. Structure of compounds **324** and **325**.

The use of non-covalent binding (such as metal-ligand) has recently merited increasing attention as a simpler but more elegant way to construct electron donor-acceptor assemblies. Two novel self-assembled donor-acceptor dyads formed by axial units coordination to pyridine attached to naphthalenediimide (NDI) acted as an electron

acceptor to zinc naphthalocyanine (ZnNc) donor.[293] Self-assembled dyads **326** and **327** absorb light over a wide region of the UV/Vis/near infrared (NIR) spectrum. Their absorption over a wide portion of the solar spectrum suggests that **326** and **327** are useful as photosynthetic models.
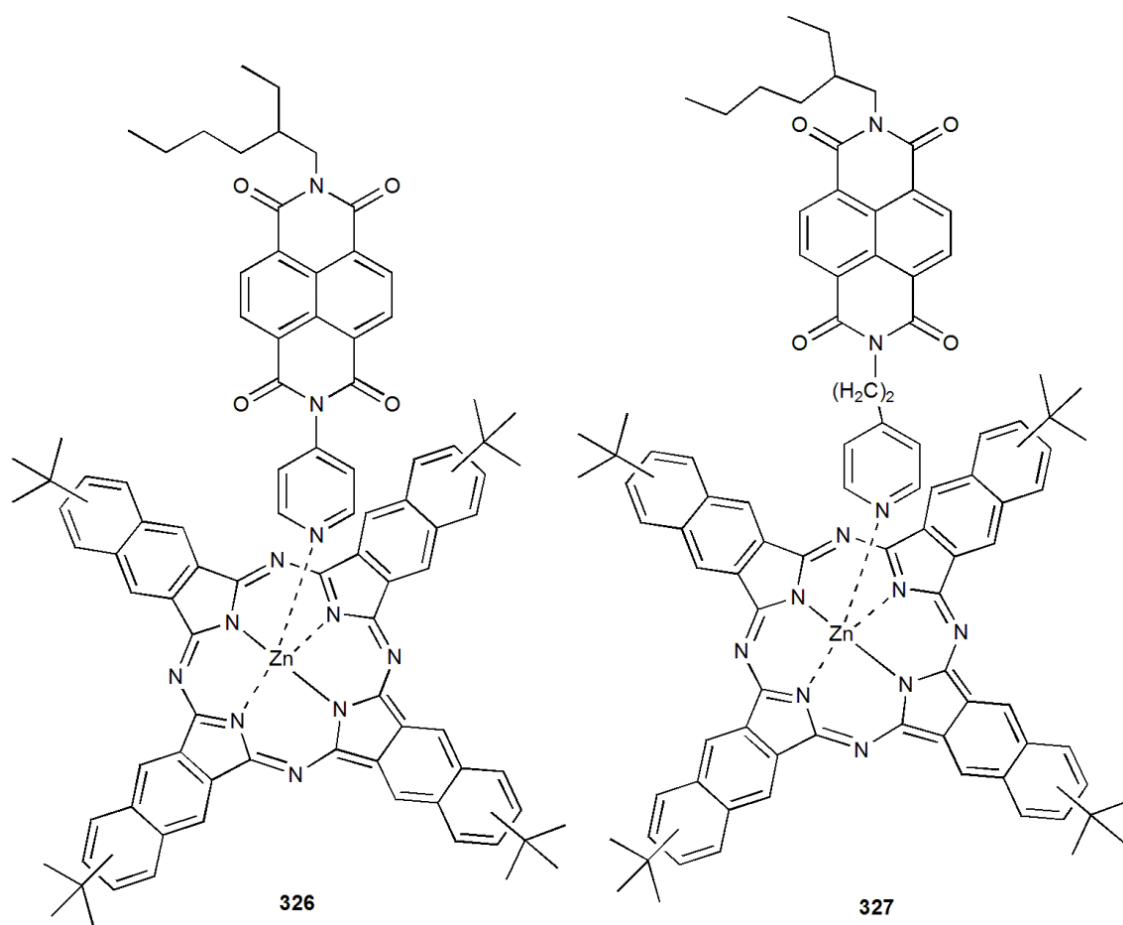
Figure 7-5. Structure of compounds **326** and **327**.

Recently, El-Khouly and co-workers[294] synthesised covalent organic frameworks (COFs) **328** which are crystalline molecular skeletons that allow atomically precise integration of building blocks into periodic array structures (Figure 7-6). They show that both solvated and solid-state COFs absorb light over a broad visible and near-infrared region up to 1100 nm. They found that the donor-acceptor COFs are promising high performance semi-conducting materials.
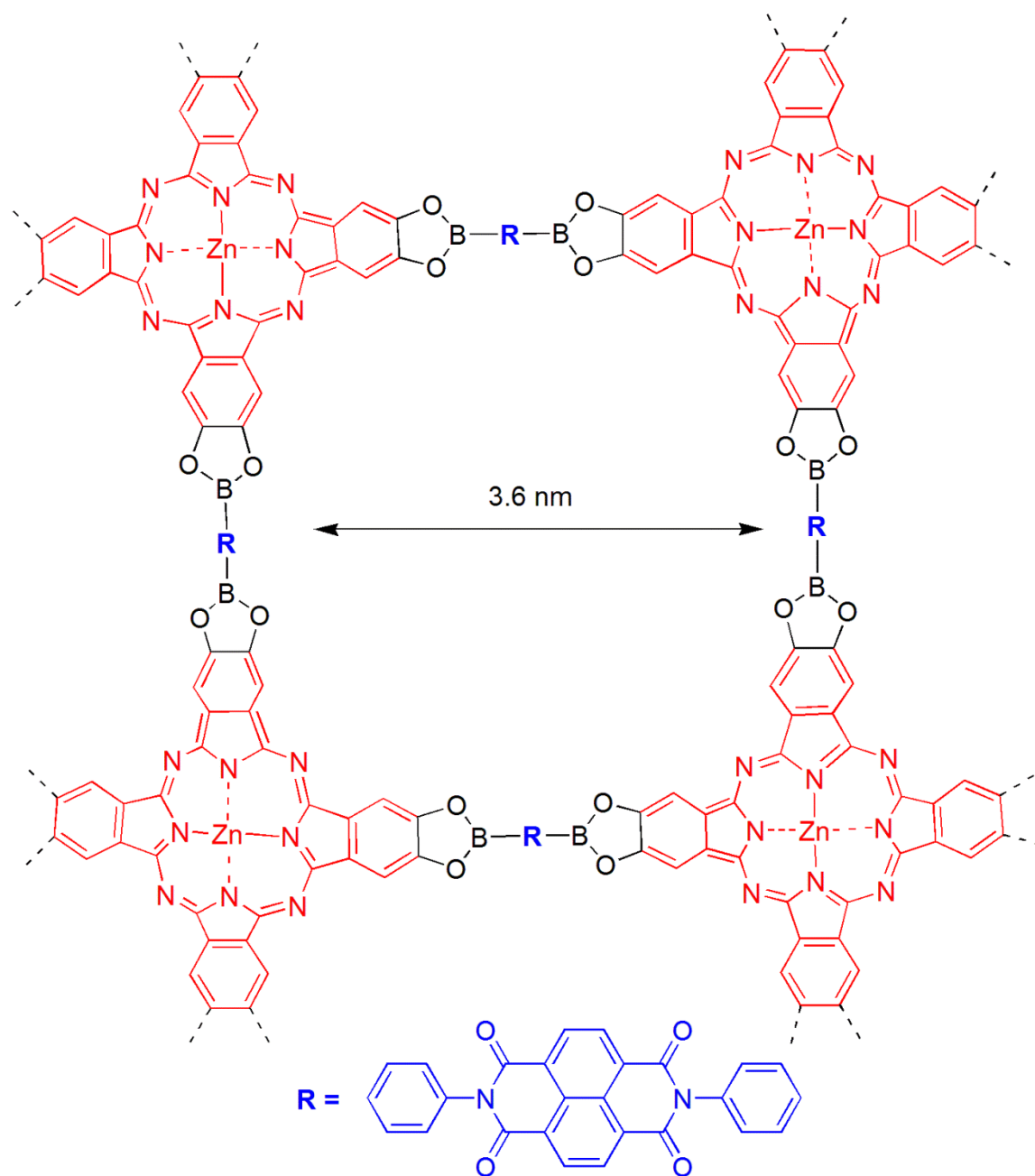
Figure 7-6. Compound **328,** donor and acceptor units are shown in red and blue, respectively. The dotted black lines suggest the extension of periodic structures.

Latterly, Sforazzini *et al.*[295] reported the synthesis of multicomponent surface architectures composed of phthalocyanines, porphyrins and naphthalenediimides. Naphthalenediimide stacks are grown first by self-organizing surface initiated disulphide-exchange polymer-isations. Then the lateral stacks of porphyrins and phthalocyanines were added by template stack exchange. The compatibility of this technology with porphyrins and phthalocyanines could lead to the development of materials with interesting molecular electronics applications.

7.2. The aim of the project

The objective of this work is the synthesis and characterisation of novel substituted phthalocyanines featuring naphthalenediimide as represented in Figure 7-7. MPcs carrying electroactive metals like Cu, Zn, Ni, and Co have disparate redox properties and therefore could lead to Pcs with interesting electrochemical properties. Also, the aim of this chapter was to use axial ligation to increase the solubility and activity of zinc phthalocyanine using a NDI-pyridine **334** (Page 212) as axial ligands.
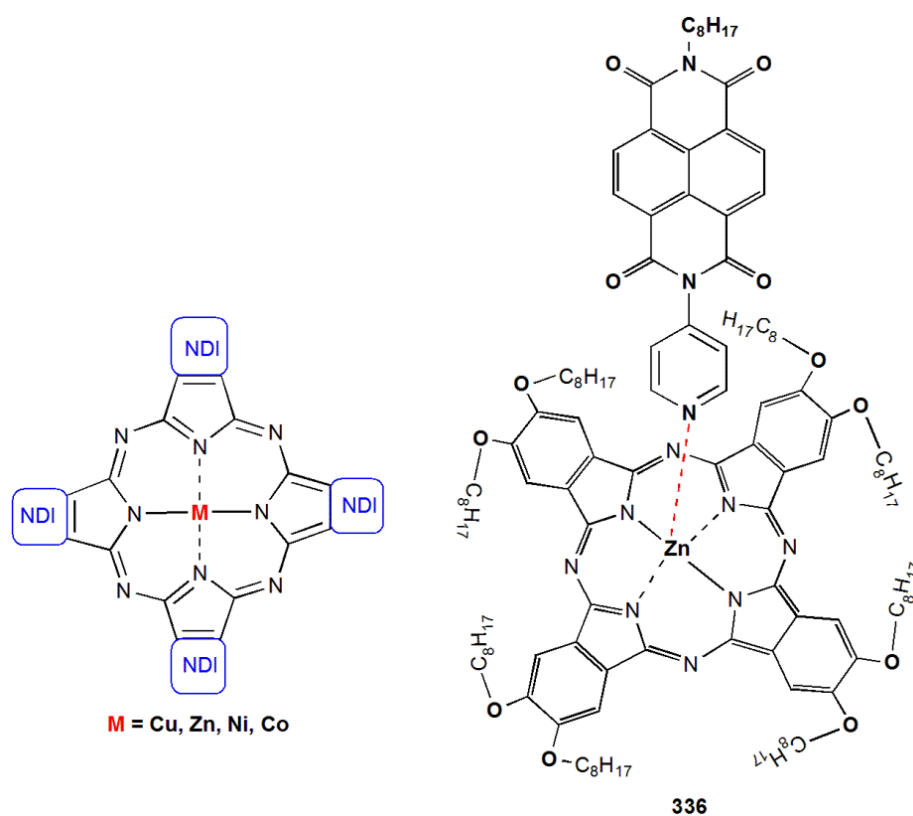
Figure 7-7. New phthalocyanines based on NDI.

7.3. Results and Discussion

7.3.1. Synthesis

7.3.1.1 Synthesis of compounds 329,330,331,332, and 333

Due to the success of using phthalic anhydride as a precursor to Pcs,[296, 297] we decided to investigate whether naphthalic anhydride could also be used as a starting material for Pc synthesis. Several attempts were made to prepare a metal phthalocyanine **337** and **338** from compound **293** (previously synthesised) by using copper and zinc salts respectively under different conditions (Scheme 7-4). However, each method proved to be unsuccessful and this route was abandoned.
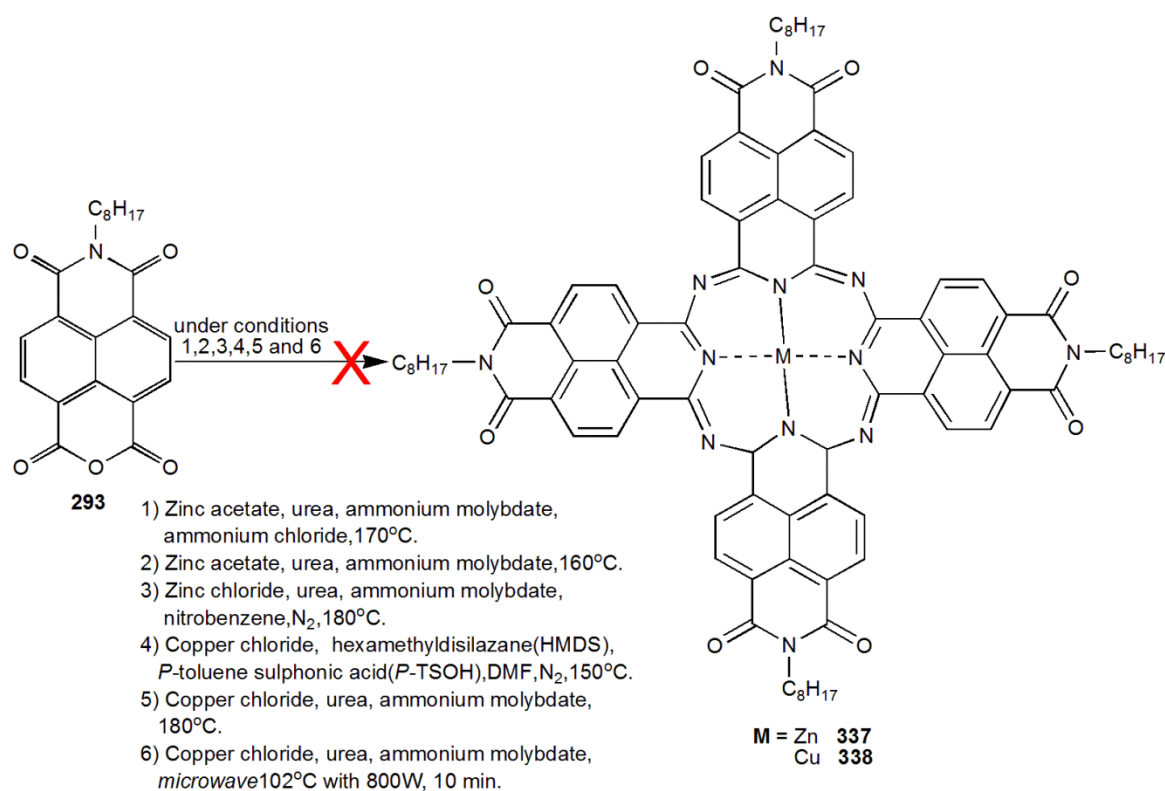
Scheme 7-4. Attempts to synthesise of compounds **337** and **338**.

The naphthalenediimide monomer bearing phthalonitrile **329** was targeted as a potential precursor for the formation of the new phthalocyanines. The precursor NDI-phthalonitrile molecule **329** was synthesised by reaction of naphthalene-1,4,5,8-tetracarboxylic di-anhydride **27** with octylamine and 4-aminophthalonitrile in a one-pot, two-step reaction in DMF at 140 °C under N_2 (Scheme 7-5). This one-pot process affords compound **329** in (30%) yield.
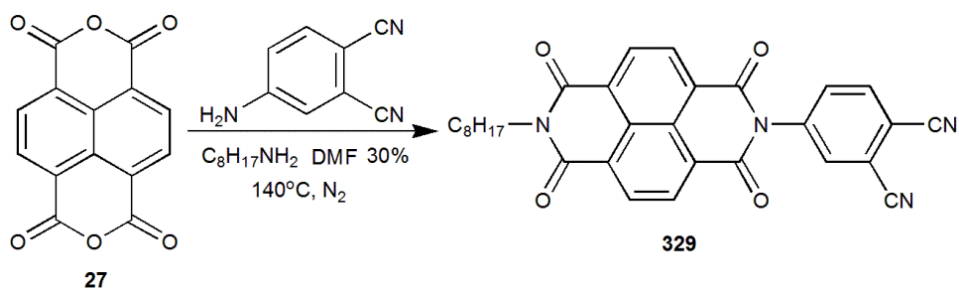
Scheme 7-5. Synthesis of compound **329**.

Several attempts were made to prepare copper and zinc phthalocyanine targets **330** and **331** by using compound **329** with DBU or HMDS in melt reaction or in different organic solvents such as DMF, pentanol, and dichlorobenzene under different conditions. However, each method proved to be unsuccessful. Compounds **330**, **331**, **332**, and **333** were synthesised by reacting compound **329** with zinc chloride, copper chloride, nickel chloride, and cobalt chloride respectively in presence of dimethylaminoethanol (DMEA) under N_2 (Scheme 7-6, Figure 7-8).

Figure 7-8. Photographs of solutions of compounds **330**, **331**, **332**, and **333** in CH_2Cl_2 (1×10^{-4} M).
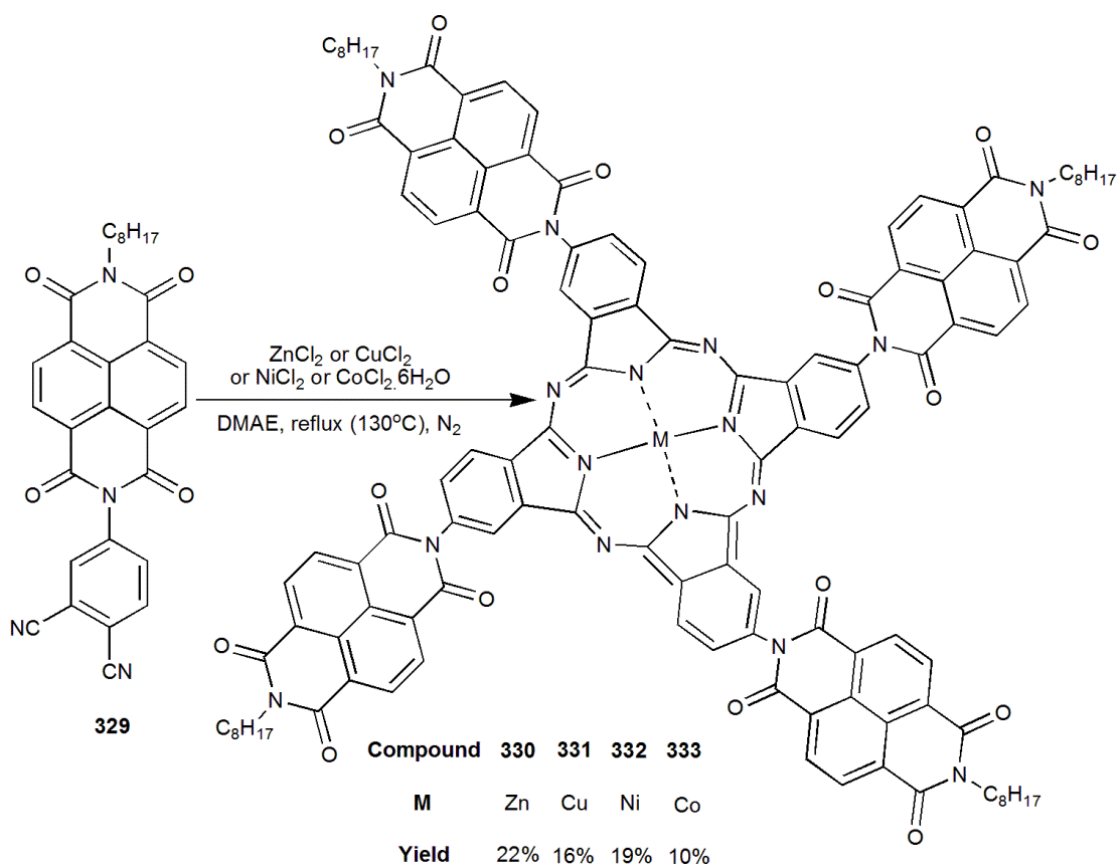
Scheme 7-6. Synthesis of compounds **330**, **331**, **332**, and **333**.

7.3.1.2 Synthesis of compounds 334, and 336

Axial ligand coordination complex **336** was achieved by coordinating the pyridine entity of pyridylnaphthalenediimide **334** with the zinc ion of ZnPc **335** (Scheme 7-8). 1,4,5,8-Naphthalenediimide was chosen as the electron acceptor because of its tendency to form n-type over p-type semiconductor materials. Naphthalenediimide has been functionalized with a pyridine entity to afford **334**. ZnPc **335** was chosen as a potential electron donor due to its rich redox behavior and strong absorption in the visible and near infrared (NIR) regions. Compound **334** was synthesised by reacting compound **27** with octylamine and 4-aminopyridine at 180 °C under N_2 in 37% yield (Scheme 7-7). Octyl groups were introduced to the naphthalenediimide and zinc phthalocyanine to improve their solubility.
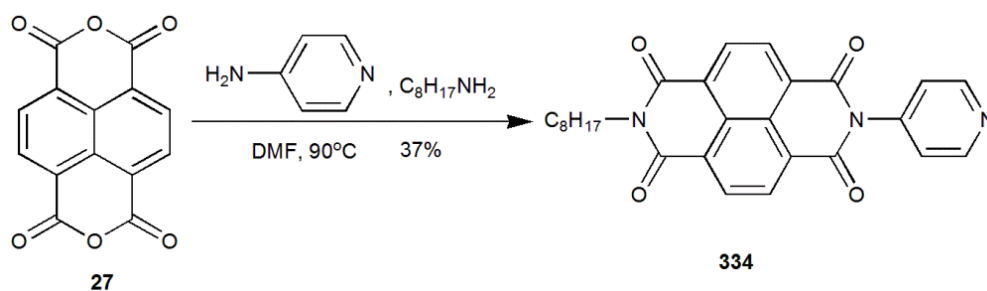
Scheme 7-7. Synthesis of compound **334**.
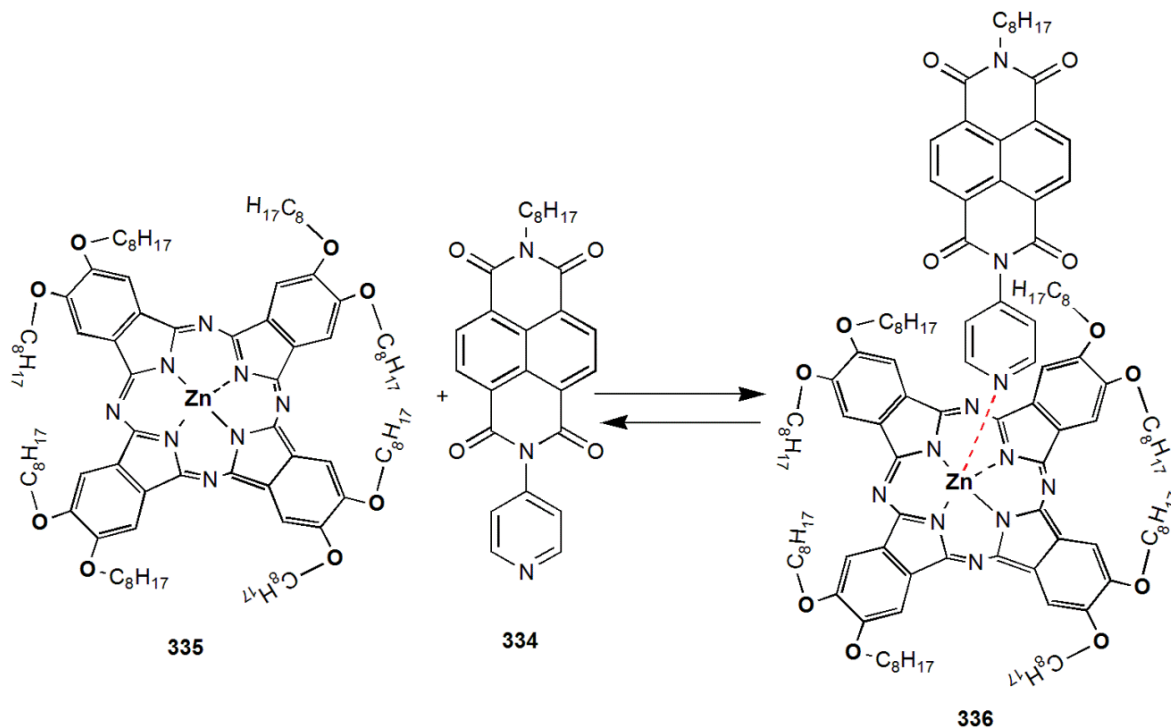
Scheme 7-8. Fabrication of complex **336**.

7.3.2. Spectroscopic studies 329, 330, 331, 332, and 333

^{1}H, ^{13}C NMR, mass spectrometry, and FTIR spectra, were consistent with the structures of **329**, **330**, **331**, **332**, and **333**. The ^{1}H NMR and ^{13}C NMR displayed the expected signals for these compounds.

The UV-vis spectra generally show that the electronic properties of the phthalonitrile-NDI **329** and Pc derivatives **330**, **331**, **332**, and **333** indicate that there is a systematic change in the spectral range of absorption and energy gaps. The UV-vis spectra of **329** recorded in CH$_2$Cl$_2$ (1 x 10^{-4} M) displayed broad absorption bands with end-absorptions reaching into the visible region. Compound **329** displayed the maximum absorption at λ_{max}= 380 nm and

an onset wavelength at λ_{onset}= 396 nm. Other absorptions occurred at 240 nm, 297 nm, 344 nm and 362 nm, respectively (Figure 7-9, Table 7-1).
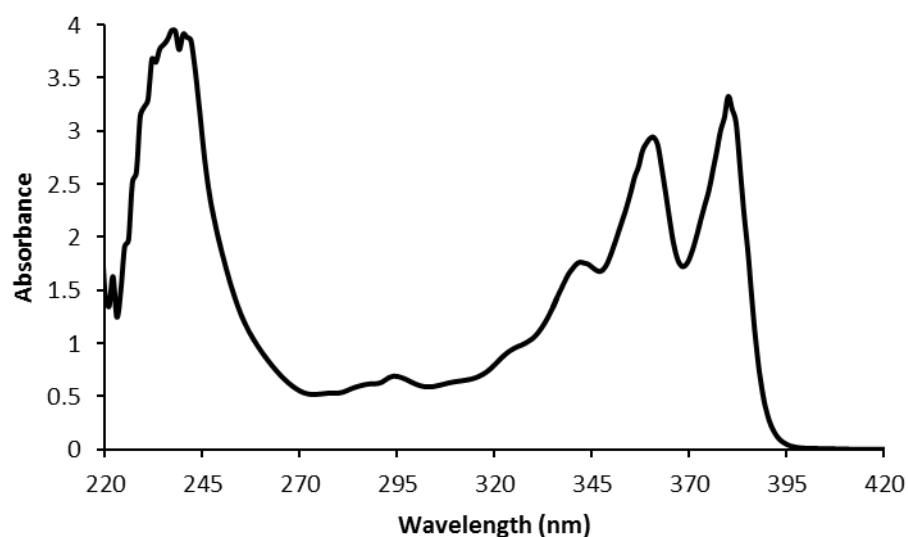
Figure 7-9. UV-vis spectra of compound **329** recorded in CH_2Cl_2 ($1x10^{-4}$ M)

The UV-vis spectra of compounds **330**, **331**, **332**, and **333** are shown in Figure 7-10. These compounds have strong absorptions near to the near-IR region between 675 and 690 nm. These strong absorptions (675, 677, 682 and 690 nm) are identified as the "Q-band". The Q-band absorption is particularly sensitive to both the central metals and the peripheral substitution of the PC macrocycle. The Q-band is caused by a π-π* transition from the excited highest occupied molecular orbital (HOMO) to the lowest unoccupied molecular orbital (LUMO). The Q-band absorptions of zinc Pc **330**, cobalt Pc **333**, nickel Pc **332** are at 675 nm, 677 nm, 682 nm respectively, but copper Pc **331** has a maximum absorption at 690 nm, which is 15 nm red-shifted (Table 7-1). There is another strong absorption near the ultra-violet (UV) region (328-380 nm), which is referred to as the "B-band". Also compounds **330**, **331**, **332**, and **333** shows end-absorption λ_{onset} at 750,760, 740, and 752 nm, respectively.
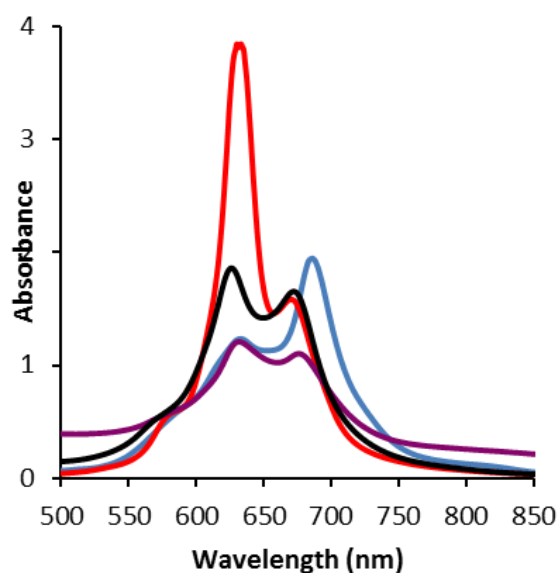
Figure 7-10. UV-vis spectra of compounds **330** (red line),**331** (blue line),**332** (purple line) and **333** (black line) recorded in CH_2Cl_2 (1×10^{-4} M).

Table 7-1. UV-vis spectra data of compounds **329**, **330**, **331**, **332** and **333** recorded in CH_2Cl_2 (1×10^{-4} M). Where the λ_{abs} is absorption wavelength (nm), λ_{onset} is end-absorption, λ_{Max} is maximum absorption wavelength (nm), and Eg^{opt} is optically determined band gap energy (eV).

Compounds	λ_{abs1} (nm)	λ_{abs2} (nm)	λ_{abs3} (nm)	λ_{abs4} (nm)	λ_{abs5} (nm)	Band gap (eV)
329	240	297	344	362	380	3.27
330	635	675	----	----	----	1.84
331	637	690	----	----	----	1.80
332	636	682	----	----	----	1.82
333	630	677	----	----	----	1.83

The fluorescence properties of compounds **330**, **331**, **332**, and **333** were investigated by fluorescence spectroscopy (recorded in 10^{-5} M solution in CH_2Cl_2). It can be seen that the macrocycle plays an important role in modulating the fluorescence properties of the phthalonitrile NDI unit **329** as shown in Figure 7-11. The fluorescence of compounds **330**, **331**, **332**, and **333** is significantly quenched compared to the **329**, and ZnPc **330** shows strong quenching compared to **331**, **332**, and **333**.
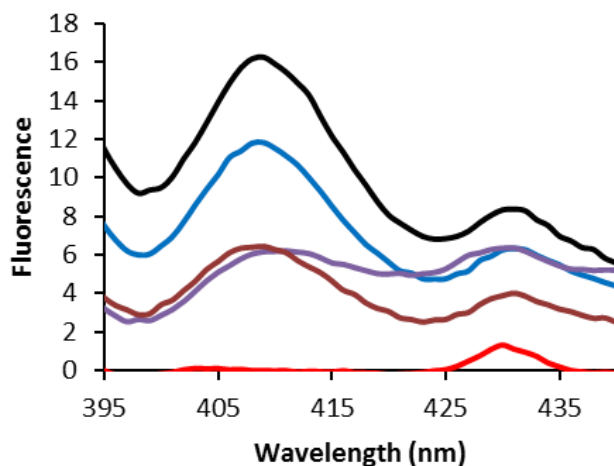
Figure 7-11. Fluorescence spectra recorded for compounds **329** (black), **330** (red), **331** (blue), **332** (purple), and **333** (brown) in CH$_2$Cl$_2$ (1x10^{-5} M) at excitation wavelength = 380 nm.

7.3.3. Electrochemical Studies of 329, 330, 331, 332, and 333

The redox properties of the new compounds **329**, **330**, **331**, **332**, and **333** were investigated by cyclic voltammetry (CV) using tetrabutylammonium hexafluorophosphate (nBu$_4$NPF$_6$) as a supporting electrolyte and ferrocene (Fc$^+$/Fc) as internal reference in CH$_2$Cl$_2$. As shown in Figure 7-12 the compounds **329** and **331** were reduced in two well-defined reversible one-electron reduction steps.

Compound **329** displayed reversible redox waves at E$_{1/2}$= -0.98 V and at E$_{1/2}$= -1.40 V which corresponds to a LUMO energy of E$_{LUMO}$= -3.82 eV. Compound **331** displayed reversible redox waves at E$_{1/2}$= -1.03 V and at E$_{1/2}$= -1.44 V which corresponds to a LUMO energy of E$_{LUMO}$ = -3.77 eV (Table 7-2).
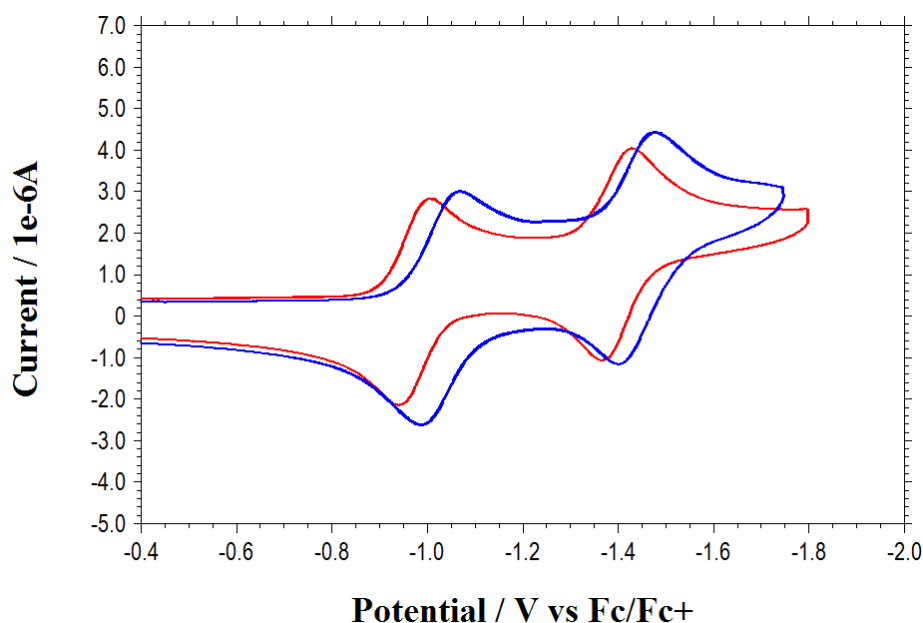
Figure 7-12. Cyclic voltammogramms of compounds **329** (red line), and **331** (blue line), recorded using a glassy carbon working electrode, an Ag wire as a reference electrode and a Pt wire as a counter electrode. Recorded in CH_2Cl_2 (1×10^{-4}M) with 0.1M (n-Bu$_4$NPF$_6$) as a supporting electrolyte at 20 ºC, and a scan rate of 0.1 Vs^{-1}.

As shown in Figure 7-13 the compounds **330**, **332**, and **333** were reduced in two well-defined reversible one-electron reduction steps. Compound **330** displayed two reversible redox waves at $E_{1/2}$= -1.15 V and at $E_{1/2}$= -1.50 V. This corresponds to a LUMO energy of E_{LUMO}= -3.65 eV. Compound **332** displayed two reversible redox waves at $E_{1/2}$= -1.05 V and at $E_{1/2}$= -1.47 V. This corresponds to a LUMO energy of E_{LUMO}= -3.75 eV. Compound **333** displayed two reversible redox waves at $E_{1/2}$= -1.03 V and at $E_{1/2}$= -1.47 V. This corresponds to a LUMO energy of E_{LUMO}= -3.77 eV (Table 7-2).
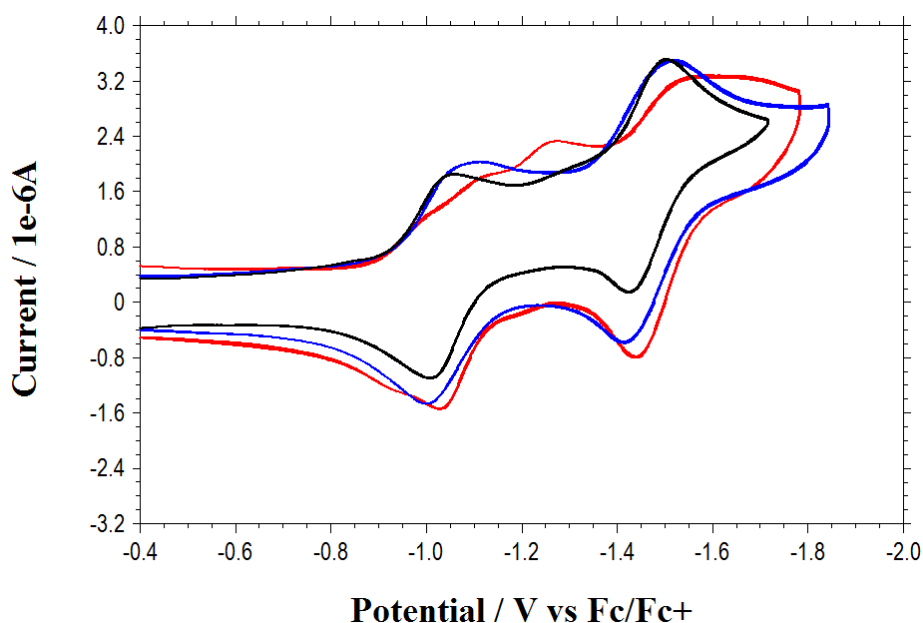
Figure 7-13. Cyclic voltammogramms of compounds **330** (red line), **332** (blue line) and **333** (black line), recorded using a glassy carbon working electrode, an Ag wire as a reference electrode and a Pt wire as a counter electrode. Recorded in CH_2Cl_2 ($1x10^{-4}$M) with 0.1M (n-Bu4NPF$_6$) as a supporting electrolyte at 20 ºC, and a scan rate of 0.1 Vs^{-1}.

Table 7-2. Electrochemical data (CV) of compounds **329**, **330**, **331**, **332**, and **333** recorded in CH_2Cl_2 ($+0.1M$ n-Bu$_4$NPF$_6$) vs.Fc$^+$/Fc at scan rate v = 0.1 V s^{-1}.

Compounds	$E^1_{1/2}$ [V]	$E^2_{1/2}$ [V]	E_{LUMO} [eV]
329	-0.98	-1.40	-3.82
330	-1.15	-1.50	-3.65
331	-1.03	-1.44	-3.77
332	-1.05	-1.47	-3.75
333	-1.03	-1.47	-3.77

7.3.4. Spectroscopic studies 334,335, and 336

The spectroscopic data of all derivatives are compatible with the proposed structures. Compounds **334** and **336** and the key precursor compounds were characterized by ^{1}H, ^{13}C NMR, mass spectrometry, and FTIR spectroscopy and they are agreement with the proposed structures.

The UV-vis spectra generally show that the electronic properties of **334**, **335**, and **336** have a systematic change in the spectral range of absorption and energy gaps (Figure 7-14). The UV-vis spectra of **335** and **336** recorded in CH_2Cl_2 (1 x 10^{-4} M) displayed broad bands with end-absorptions reaching into the NIR region.

The absorption spectrum of ZnPc **335** shows a strong absorption band in the NIR region at 776 nm (1.84 eV) and onset wavelength at λ_{onset} = 705 nm. In addition, weak absorptions were observed at 643, 608, 342 and 289 nm. In contrast, the main absorption bands of compound **334** were in the in UV-vis region. For example, the λ_{max} occurred at 377 nm (3.29 eV) and had an onset wavelength at λ_{onset} = 393 nm. Other absorptions were observed at 241 nm, 337 nm, and 358 nm. This observation indicates that the absorption bands of the NDI **334** and ZnPc **335** are well separated, providing the possibility for selective excitation of either moiety. Complex **336** had almost similar absorption spectra of **335**, however **336** had a λ_{max} = 679 nm (1.83 eV) which is shifted (3 nm) to higher wavelength (Table 7-3). This indicates that Py-NDI **334** forms a 1:1 complex with ZnPc **335**. It is well known that such nitrogenous bases readily bind to ZnPc **335** with a 1:1 stoichiometry (Scheme 7-8).
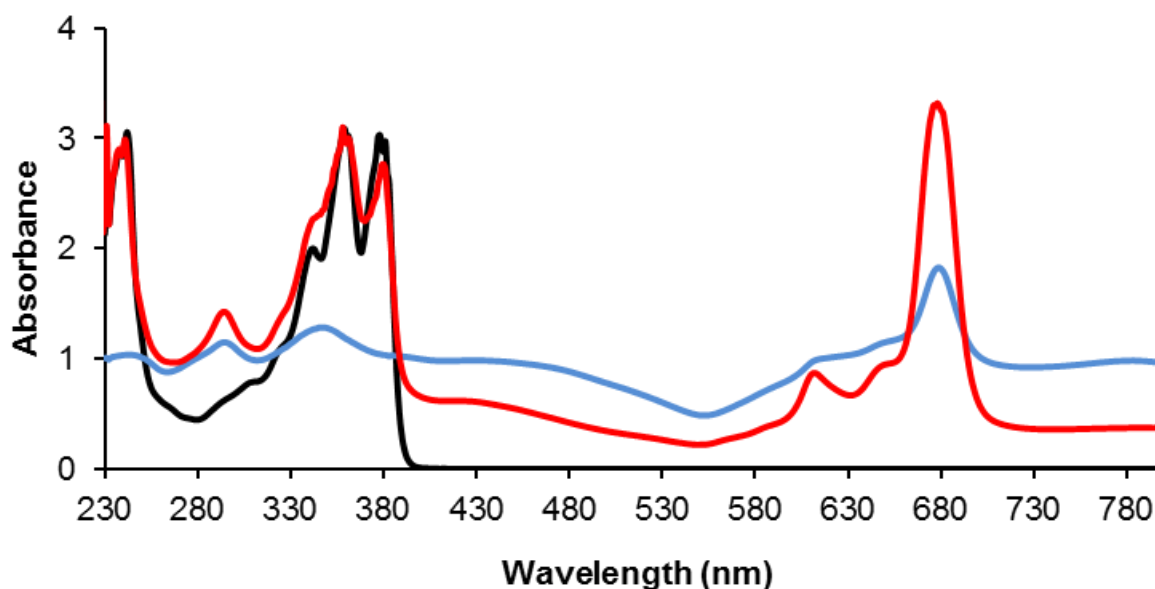
Figure 7-14. UV-vis spectra of compounds **334** (black line), **335** (blue line), and **336** (red line) recorded in CH_2Cl_2 ($1x10^{-4}$ M).

Table 7-3. UV-visible spectra data of compounds **334**, **335**, and **336** recorded in CH_2Cl_2 ($1x10^{-4}$ M). Where the λ_{abs} is absorption wavelength (nm), λ_{Max} is maximum absorption wavelength (nm), and Eg^{opt} is the optically determined band gap energy (eV).

Compounds	λ_{abs1} (nm)	λ_{abs2} (nm)	λ_{abs3} (nm)	λ_{abs4} (nm)	λ_{abs5} (nm)	λ_{abs6} (nm)	λ_{abs7} (nm)	λ_{abs8} (nm)	Band gap (eV)
334	241	337	358	377	---	---	---	---	3.29
335	289	342	608	643	676	---	---	---	1.84
336	240	290	341	358	379	608	644	679	1.83

The photophysical behavior of **334**, **335**, and **336** was investigated by fluorescence spectroscopy recorded as a 10^{-5} M solution in CH_2Cl_2 (excitation wavelength = 361 nm) (Figure 7-15). It can be seen that the NDI units play an important role in modulating the fluorescence properties of the ZnPc **335**. As shown in Figure 7-15, the fluorescence emission of **335** is quenched strongly compared to **336**.
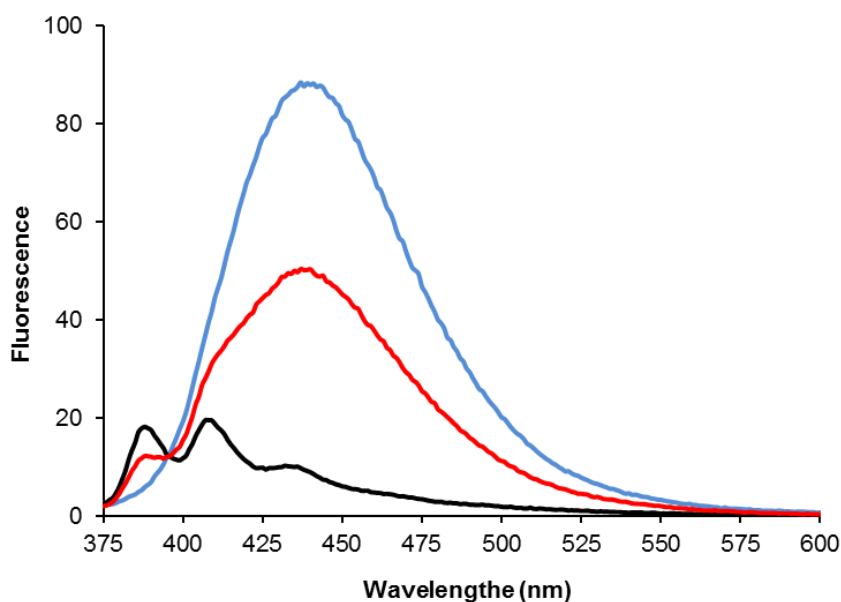
Figure 7-15. Fluorescence spectra recorded for compounds **334** (black line), **335** (blue line), and **336** (red line) in CH_2Cl_2 ($1x10^{-5}$ M) at excitation wavelength = 361 nm.

7.3.5. Electrochemical Studies of 334, 335 and 336

The redox properties of the compounds **334, 335** and **336** were investigated by cyclic voltammetry (CV) using tetrabutylammonium hexafluorophosphate (n-Bu$_4$NPF$_6$) as a supporting electrolyte and ferrocene (Fc$^+$/Fc) as internal reference in CH$_2$Cl$_2$. Compounds **334** and **336** were reduced in two well-defined reversible one-electron reduction steps. As shown in Figure 7-16(b) compounds **334** and **336** displayed a reversible redox wave at E$_{1/2}$ = -1.01 V and E$_{1/2}$= -1.43 V which corresponds to a LUMO energy of E$_{LUMO}$= -3.78 eV. Figure 7-16(a) shows no oxidation process for compound **335**.
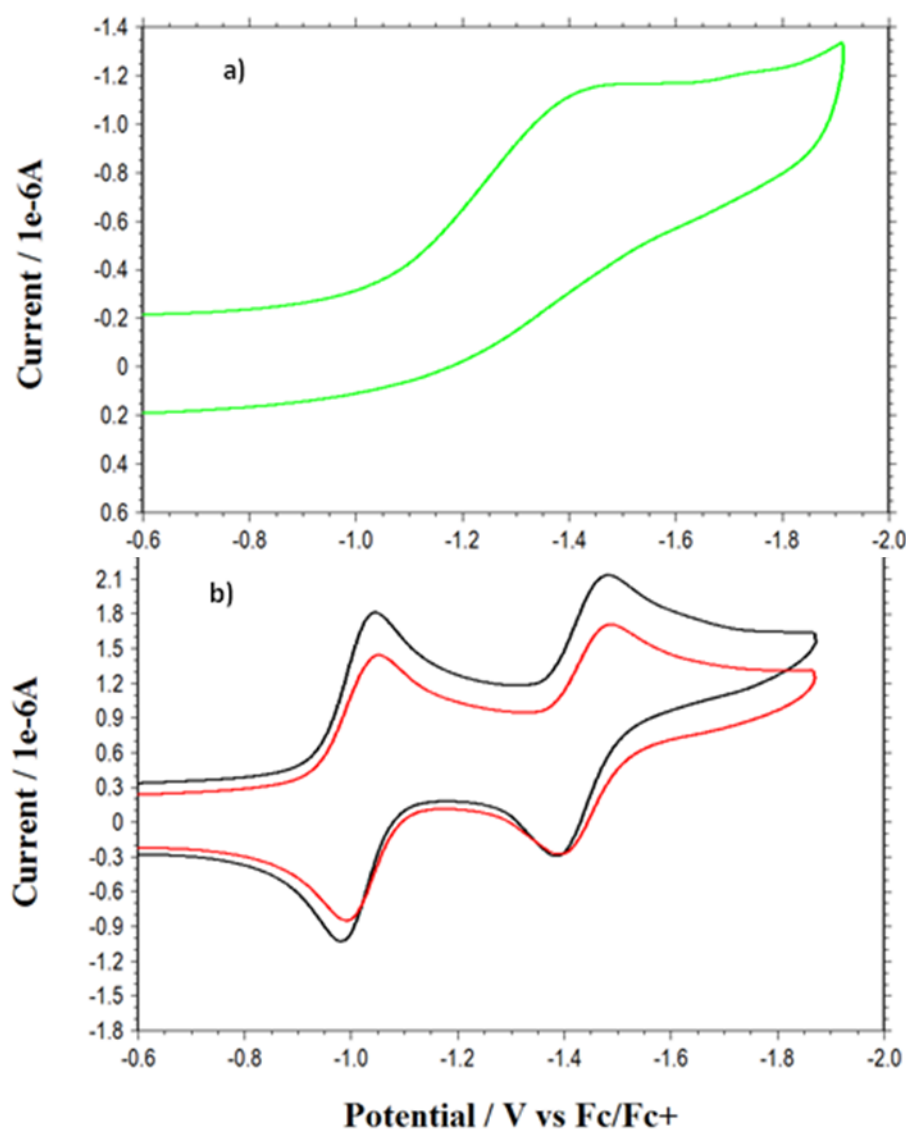
Figure 7-16. Cyclic voltammogramms of compounds a) **335** (green line), b) **334** (black line), and **336** (12:13 (1:1 red line)) recorded using a glassy working electrode, an Ag wire as a reference electrode and a Pt wire as a counter electrode. Recorded in CH$_2$Cl$_2$ (1x10^{-4}M) with 0.1M (n-Bu$_4$NPF$_6$) as a supporting electrolyte at 20 ºC, and a scan rate of 0.1 Vs^{-1}.

Figure 7-17 shows that the reduction-oxidation behavior of compound **336** with increasing addition of ZnPc **335** concentration. No significant change occurred which indicates that metal-ligand coordination in complex **336** does not modulate the redox properties of either component.
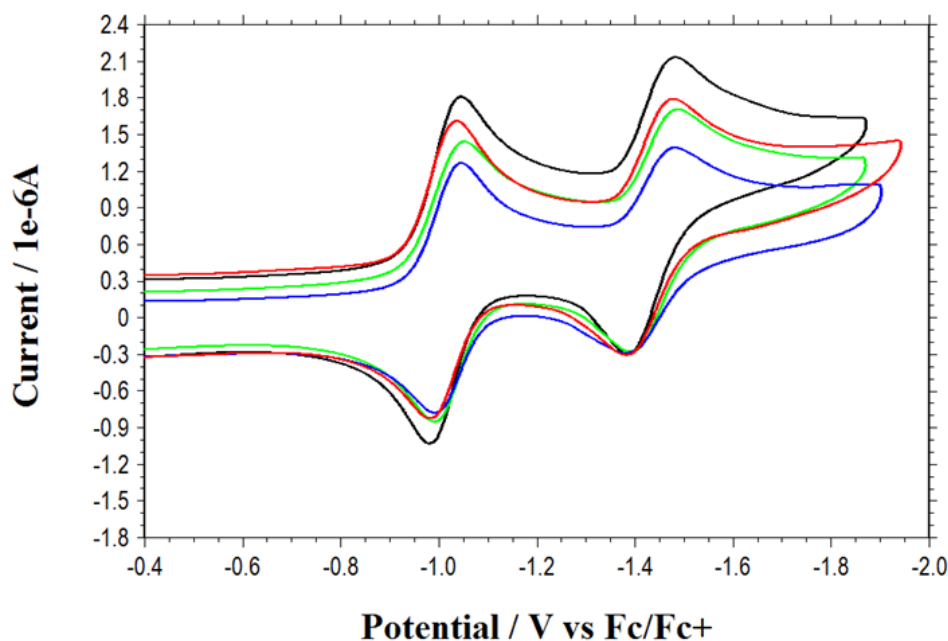
Figure 7-17. Cyclic voltammogramms of compounds **334** (black line), **336** (**334**:**335** (1:1 green line)), (**334**:**335** (1:5 blue line)), and (**334**:**335** (1:10 red line)), recorded using a glassy working electrode, an Ag wire as a reference electrode and a Pt wire as a counter electrode. Recorded in CH_2Cl_2 (1x 10^{-4} M) with 0.1M (n-Bu$_4$NPF$_6$).

7.3.6. NMR Studies of 334, 335 and 336

Complex formation between the pyridyl-NDI **334** and **335** can be monitored by solution NMR spectroscopy using the deshielding effect of the phthalocyanine ring. The ^{1}H NMR signals of free NDI-Py **334** exhibit upfield shifts upon complexation with addition of increasing quantities of ZnPc **335** as shown in Figure 7-18. The pyridyl signals of **334**, which appear initially at 8.86 and 7.32 ppm, are shifted upfield to 3.75 and 5.75 ppm, respectively, upon the addition of increasing quantities of **335**. This indicates that the complexation occurs fast on the NMR time scale. The upfield shift of the pyridyl aromatic α and β protons of **334** (induced by the complexation) is due to the large phthalocyanine aromatic ring current. This result clearly indicates that the pyridyl group of **334** coordinates axially to the central zinc ion of **335**. d_8-Toluene and d_6-THF also used as a solvent in this study and the results shows that the CDCl$_3$ provides the largest shift in resonances.
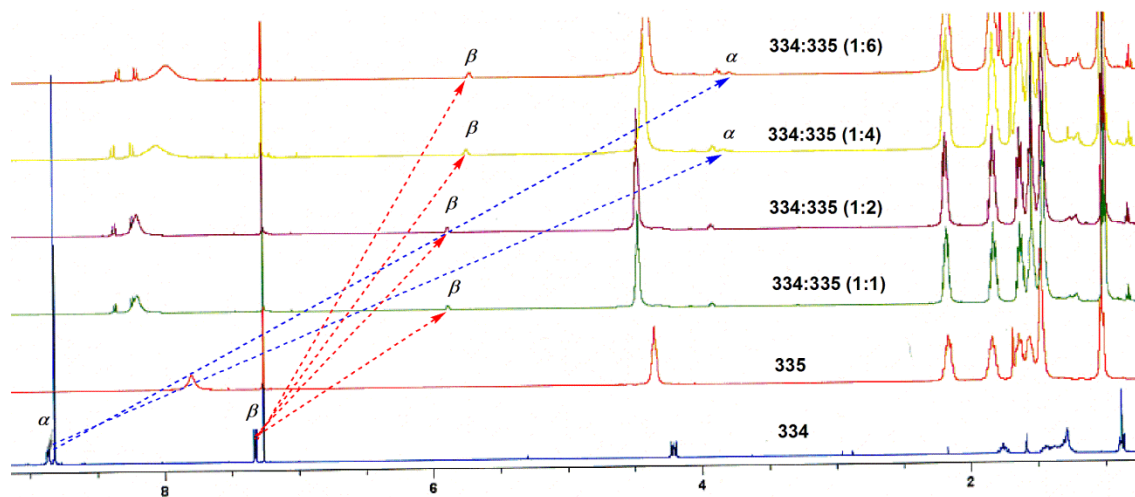
Figure 7-18. ^{1}HNMR spectra of **334** and **335** and **336** in the presence of various concentrations of **335** in CDCl$_3$.

7.3.7. Molecular Modelling of compound 336

The electron distribution was calculated using density functional theory (DFT) in order to study the electron delocalization in molecule **336**. In order to simplify the calculation, the long alkyl chain (octyl) was replaced by a methyl group in the molecules. The MO electron density plots reveal that the LUMO is completely delocalized across the naphthalenedi‑imide core and the computed LUMO energy for **336** was E_{LUMO}= -3.74 eV (Figure 7-19). Inspection of the HOMO densities for this system showed that π-orbitals were delocalized along the phthalocyanine molecule and the computed HOMO energy for **336** was E_{HOMO}= -4.42 eV (Figure 7-20).
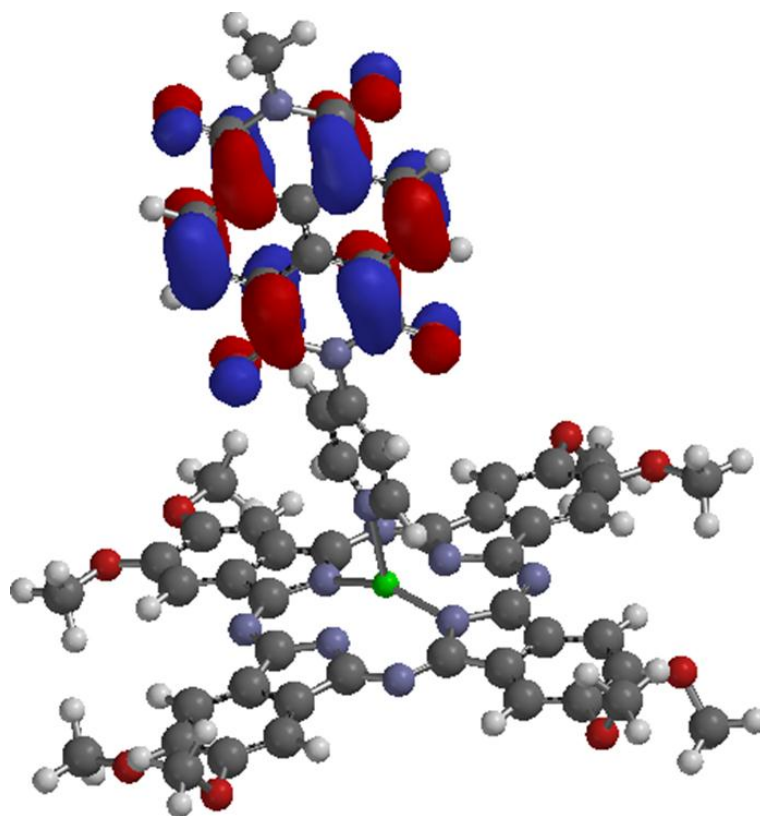
Figure 7-19. DFT B3LYP 6-311G calculation of **336** showing LUMO location.
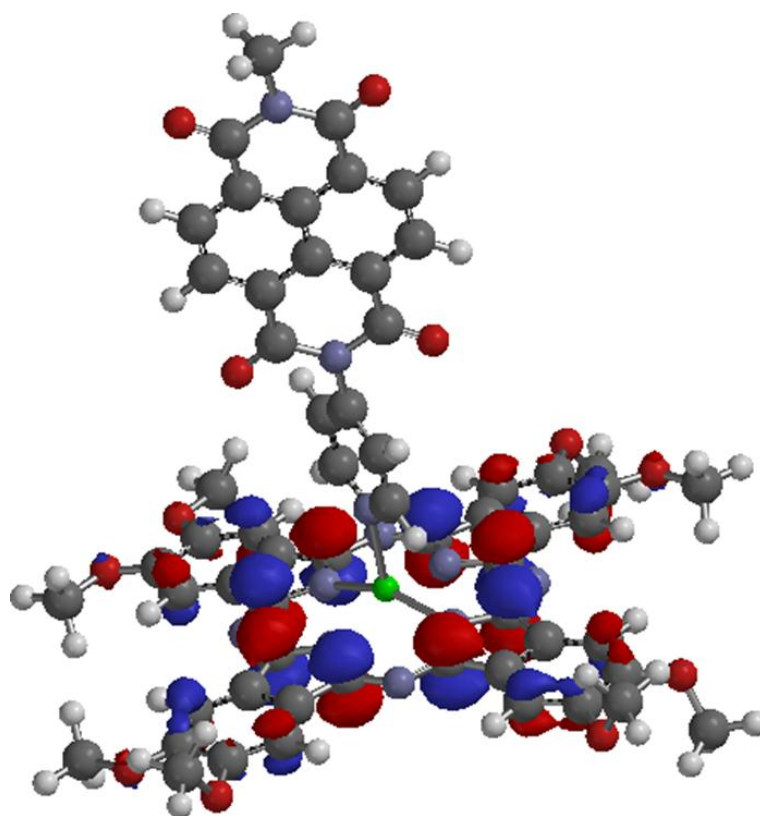
Figure 7-20. DFT B3LYP 6-311G calculation of **366** showing HOMO location.

7.4. Conclusion

Zinc, copper, nickel and cobalt phthalocyanines have been successfully synthesised using a new phthalonitrile-NDI precursor **329**. The photophysical and photochemical properties associated with the molecules synthesised in this work have been determined. All the phthalocyanines are soluble in common organic solvents such as DMF, DMSO, $CHCl_3$, THF and DCM.

The NMR and infrared spectra of all the synthesised phthalocyanines displayed characteristic bands proving the formation of the desired Pc from the starting material. The UV-vis spectra of compounds **330**, **331**, **332**, and **333** shows, that these compounds have strong absorptions towards the NIR region between 675 and 690 nm. Also, it can be seen that the macrocycle unit of **330**, **331**, **332**, and **333** plays an important role in modulating the fluorescence properties of the phthalonitrile NDI unit **329**.

The UV-vis spectra of the complexes displayed metal-dependent wavelength maxima, showing the effect of the central Pc metal on the absorption maxima. The commercially available ZnPc **335** was used as an example to study the possibility of using axial ligands to increase the solubility and photochemical activity. New compound **334** featuring a pyridyl ligand has been synthesised. The choice of the axial ligand **334** as well as the solvent $CDCl_3$ has been optimized to achieve efficient complexation between **335** and **334**. Future work will involve full photophysical characterisation of these materials and incorporation into photovoltaic devices.

8. **Chapter 8**

Experimental

8.1. General Experimental and Materials

All reagents were purchased from Sigma/Aldrich and TCI, and were used as received without further purification. All solvents were used without drying unless stated. Melting points were determined using a Steward Scientific melting point apparatus and are uncorrected.

^{1}H-NMR and ^{13}C NMR spectra were recorded on a Bruker AC 400 NMR spectrometer, operating at 400 MHz for ^{1}H-NMR and 100 MHz for ^{13}C NMR. All chemical shifts (δ) are reported in ppm relative to tetramethylsilane (TMS) as reference (δ = 0.0 ppm). Coupling constants (J) are reported in Hertz.

All infrared spectra were recorded on a Perkin-Elmer RX FT-IR spectrophotometer. All UV-Vis spectra were recorded on a Perkin-Elmer Lambda 25 UV-Vis spectrophotometer. UV-Vis-NIR spectra were recorded on a SHIMADZU UV-3600 spectrophotometer. Fluorescence measurements were run on Shimadzu RF 3501PC spectrofluorimeter.

MS spectra were obtained from the Mass Spectrometry laboratory in the school of chemistry - University of Glasgow. Measurements were run on a JEOL JMS 700 Mass Spectrometer [FAB, EI, CI, and Accurate Mass].

All cyclic voltammogramms were recorded on a CH Instruments electrochemical workstation,440 a EC Analyser., with a 0.1M solution of tetrabutylammonium hexafluoro-phosphate (n-TBAPF$_6$) as a supporting electrolyte in dry dichloromethane or THF as a solvent and Fc/Fc$^+$ for calibration.

The polymer molecular weights were characterised by Gel Permeation Chromatography (GPC) using a Polymer Lab GPC50 instrument from Varian Inc. The recording time was set to 25 minutes under a flow rate of 1 ml/min and the oven temperature was set to 30 °C.

Particle sizing was carried out using a Zetasizer Nano (Malvern Instruments Ltd) and Zetasizer software was used to collect and analyse the data. Theoretical calculations are performed on using Spartan 08 computational programs windows version software.

8.2. Synthetic experimental - Chapter 2

8.2.1. *N*-Octyl-*N'*-(4-iodophenyl) naphthalene-1,4,5,8-tetracarboxylic acid diimide (62)
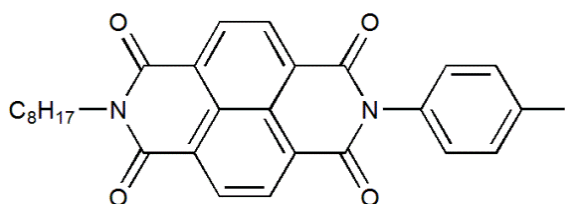
Naphthalene-1,4,5,8-tetracarboxylic dianhydride **27** (2.5 g, 9.30 mmol) was stirred in a freshly distilled DMF (20 ml) and the slurry was heated to about 140 °C under a N_2 atmosphere. Octylamine (1.54 ml, 9.30 mmol) was added dropwise to the mixture over 10 minutes and the reaction mixture was heated under reflux overnight. After complete consumption of naphthalene dianhydride, 4-iodoaniline (2.0 g, 9.30 mmol) was added and the mixture was left under reflux overnight. After the completion of the reaction, the mixture was allowed to cool and DMF was evaporated under vacuum. The residue was partitioned using DCM/water, and the organic layer was dried over $MgSO_4$. The solution was filtered and the filtrate was evaporated in vacuum. The product was purified by silica gel column chromatography eluting with DCM then DCM: Acetone (90:10, v/v) to afford **62** as a yellow solid in 64% (3.45 g) yield. M.p. 249-251 °C. ^{1}H-NMR (δ/ppm, 400 MHz, $CDCl_3$): 8.80 (s, 4H, naphthalene); 7.91 (d, 2H, *J* = 8.5 Hz, phenyl); 7.10 (d, 2H, *J* = 8.5 Hz, phenyl); 4.21 (t, 2H, *J* = 7.6 Hz, CH_2); 1.76 (m, 2H, CH_2); 1.42 (m, 2H, CH_2); 1.27 (m, 8H, CH_2); 0.88 (t, 3H, *J* = 6.9 Hz, CH_3). ^{13}CNMR (δ/ppm, 100 MHz, $CDCl_3$): 162.9 (C=O), 162.8 (C=O), 162.8 (C=O), 162.7 (C=O), 138.8, 134.3, 131.5, 131.0, 130.9, 130.4, 127.1, 127, 126.8, 126.7, 126.6, 126.4, 95.0, 41.1, 41 (N-CH_2), 31.8, 29.3, 29.2, 28.1, 27.1, 22.6, 14.1 (CH_3). FTIR (ν, cm^{-1}): 3090-3040 (m, C-H aromatic), 2924-2855 (s, C-H alkane), 1780-1663 (s, C=O), 1580-1454 (m, C=C aromatic), 1371-1348 (C-H), 1247 (C-N), 766-724 (benzene ring). Anal.calcd. for $C_{28}H_{25}IN_2O_4$: C, 57.89; H, 4.34; N, 4.82, Found C, 57.69; H, 4.06; N, 4.76. Mass spectrum [M + H$^+$]= 580.15 .

8.2.2. *N*-Octyl-*N'*-(4-(4-ethynyl-*N,N*-dimethylaniline)phenyl)naphthalene-1,4,5,8-tetracarboxylic acid diimide (63)
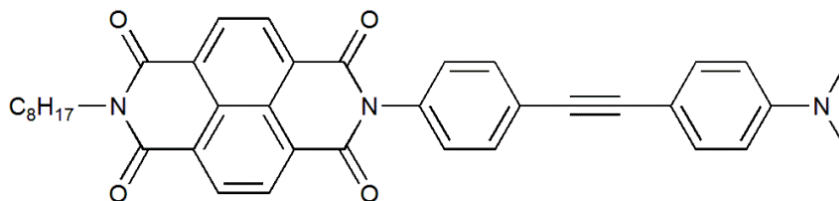
N-Octyl-*N'*-(4'-iodophenyl) naphthalene-1,4,5,8-tetracarboxylic acid diimide **62** (300 mg, 0.52 mmol), 10% Pd/C (11.0 mg, 0.10 mmol), CuI (39.0 mg, 0.21 mmol), Ph$_3$P (108 mg, 0.41 mmol), and K$_2$CO$_3$ (178 mg, 1.29 mmol) were mixed in a 1:1 solution of water and dimethoxyethane (10 mL). The mixture was degassed with N$_2$ for 5 minutes and stirred for 30 minutes under N$_2$. 4-Ethynyl-*N,N*-dimethylaniline (106 mg, 0.73 mmol) was then added, and the mixture was heated to 80 ºC for overnight. After cooling, the reaction mixture was extracted with DCM (5 x 20 ml). The organic extracts were combined and dried over MgSO$_4$. The solution was filtered and the filtrate was evaporated in vacuum. The product was purified by silica gel column chromatography eluting with DCM/Pet. Ether (80:20, v/v) to afford **63** as a violet solid in 88% (270 mg) yield. M.p. 257-259 ºC. ^{1}H-NMR (δ/ppm, 400 MHz, CDCl$_3$): 8.80 (s, 4H, naphthalene); 7.68 (d, 2H, *J* = 8.6 Hz, ArH) ;7.43 (d, 2H, *J* = 9.2 Hz, ArH); 7.28 (d, 2H, *J* = 8.6 Hz, ArH); 6.67 (d, 2H, *J* = 9.2 Hz ,ArH); 4.21 (t, 2H, *J* = 8.0 Hz, CH$_2$); 3.01 (s, 6H, N-CH$_3$); 1.76 (m, 2H, CH$_2$); 1.42 (m, 2H, CH$_2$); 1.27 (m, 8H, CH$_2$); 0.88 (t, 3H, *J* = 7.0 Hz, CH$_3$). ^{13}CNMR (δ/ppm, 100 MHz, CDCl$_3$): 162.9 (C=O), 162.8 (C=O), 150.3 (C), 133.4, 132.9, 132.3, 131.4, 131.0, 128.5, 127.1, 127.0, 126.9, 126.6, 125.4, 111.8 (CH), 109.7, 92.0, 86.7, 41.1, 40.2 (CH$_2$), 31.8, 29.3, 29.2, 28.1, 27.1, 22.6, 14.1 (CH$_3$). FTIR (ν, cm^{-1}): 3080-3076 (m, C-H aromatic), 2925-2853 (s, C-H alkane), 2213 very weak (C≡C), 1715, 1659 (s, C=O), 1522, 1484, 1451, 1440 (m, C=C aromatic), 1371, 1343 (C-H), 1252, 1241 (C-N), 751, 695 (benzene ring). HRMS (ES$^+$): *m/z* 598.2706 [M + H$^+$], calculated 598.2708.

8.2.3. *N*-Octyl-*N'*-(4-(4-(tetracyanobutadiene)-*N,N*-dimethylaniline)phenyl) naphthalene-1,4,5,8-tetracarboxylic acid diimide (64)
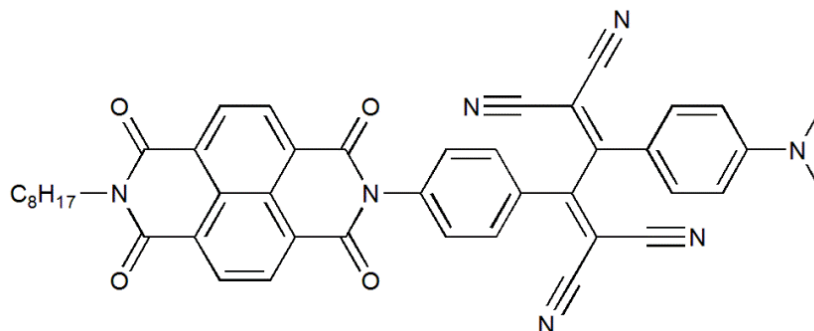
Tetracyanoethene (TCNE) (51.0 mg, 0.40 mmol) was added to solution of *N*-octyl-*N'*- (4-(4-ethynyl-*N,N*-dimethylaniline) phenyl) naphthalene-1,4,5,8-tetracarboxylic acid diimide **63** (200 mg, 0.33 mmol) in THF (25 mL), and the mixture was stirred for 4 h. at 66 °C. The THF was evaporated in vacuum and the product was dissolved in the minimum amount of DCM and precipitated by adding petroleum ether. The solution was filtered to afford a red product. The product was purified by recrystallization from DCM/methanol to afford **64** as a red solid in 66 % (160 mg) yield. M.p. 307- 309 °C. ^{1}H-NMR (δ/ppm, 400 MHz, CDCl$_3$): δ =8.81 (s, 4H, naphthalene); 7.92 (d, *J* = 8.7 Hz, 2H, phenyl); 7.84 (d, *J* = 9.3, 2H, phenyl); 7.52 (d, *J* = 8.7 Hz, 2H, phenyl); 6.77 (d, *J* = 9.3 Hz, 2H, phenyl); 4.21 (t, *J* = 7.6 Hz, 2H, CH$_2$); 3.20 (s, 6H, CH$_3$); 1.76 (m, 2H, CH$_2$); 1.44 (m, 2H, CH$_2$); 1.28 (m, 8H, CH$_2$); 0.88 (t, *J* = 6.6 Hz, 3H, CH$_3$) . ^{13}CNMR (δ/ppm, 100 MHz, CDCl$_3$): 168.0, 162.6, 162.6, 154.5, 139.6, 132.5, 132.2, 131.7, 131.1, 130.4, 130.3, 127.3, 127.1, 126.9, 126.2, 117.7, 114.2, 113.3, 112.4, 111.7, 111.1, 88.4, 74.5, 41.1, 40.2, 31.8, 29.3, 29.2, 28.1, 27.1, 22.6, 14.1. FTIR (ν, cm^{-1}): 3050 (m, C-H aromatic), 2930-2812 (m, C-H alkane), 2209 (v.weak, C≡N), 1705 (s, C=O), 1680-1667 (m, C=C alkene), 1603, 1581, 1478 (m, C=C aromatic), 1385, 1342 (C-H), 1247- 1215 (C-N), 770 (benzene ring). HRMS (ES$^+$): *m/z* 726.2828 [M + H$^+$], calculated 726.2829.

8.2.4. *N*-Octyl-*N'*-(4-(4-(7,7,8,8-tetracyanoquinodimethane)-*N,N*-dimethyl aniline)phenyl)naphthalene-1,4,5,8-tetracarboxylic acid diimide (65)
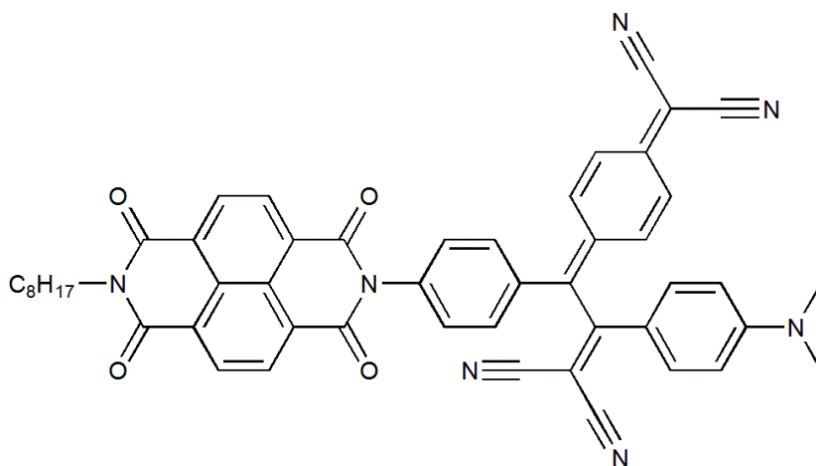
7,7,8,8-Tetracyanoquinodimethane (TCNQ) (68.0 mg, 0.33 mmol) was added to solution of *N*-octyl-*N'*-(4-(4-ethynyl-*N,N*-dimethylaniline) phenyl) naphthalene-1,4,5,8-tetra-carbo-xylic acid diimide **63** (200 mg, 0.33 mmol) in THF (20 mL) and the mixture was stirred under reflux for 6 hr. at 66 ºC. The THF was evaporated in vacuum and the product was dissolved in the minimum amount of DCM and precipitated by adding petroleum ether. The solution was filtered to afford a blue product. The product was purified by recrystallization from DCM/methanol to afford **65** as a blue solid in 64% (170 mg). M.p. 299-301 ºC. ^{1}H-NMR (δ/ppm, 400 MHz, CDCl$_3$): 8.80 (m, 4H, naphthalene); 7.88 (d, J = 8.6 Hz, 2H, phenyl) ; 7.53 (dd, J = 9.6, 2.0 Hz, 2H, phenyl); 7.47 (d, J= 8.6 Hz, 2H, phenyl); 7.32 (d, J = 9.2 Hz, 2H, phenyl); 7.21 (dd, J = 9.6, 2.0 Hz, 1H, phenyl); 7.03 (dd, J = 9.5, 2.0 Hz, 1H, phenyl); 6.75 (d, J = 9.2 Hz, 2H, phenyl); 4.20 (t, J = 7.6 Hz, 2H, CH$_2$), 3.16 (s, 6H, CH$_3$); 1.75 (m, 2H, CH$_2$); 1.43 (m, 2H, CH$_2$) ;1.28 (m, 8H, CH$_2$) ; 0.87 (t, J = 6.6 Hz, 3H, CH$_3$).^{13}CNMR (δ/ppm, 100 MHz, CDCl$_3$): 171.2, 162.7, 162.6, 154.1, 153.0, 151, 139.1, 135.7, 134.9, 134.4, 134.2, 131.7, 131.7, 131.2, 131.1, 130.6, 130.2, 127.4, 127.1, 126.9, 126.1, 125.5, 125.3, 123.1, 114.7, 114.6, 112.7, 112.1, 88.4, 72.3, 41.2, 40.2, 31.8, 29.3, 29.2, 28.1, 27.1, 22.7, 14.1. FTIR (ν, cm^{-1}): 3030 (m, C-H aromatic), 2924-2859 (m, C-H alkane), 2202 (v.weak, C≡N), 1707 (s, C=O), 1668 (m, C=C alkene), 1580, 145 (m, C=C aromatic), 1369, 1343 (C-H), 12461, 1168 (C-N), 768-667 (benzene ring). HRMS (ES$^+$): *m/z* 802.3142 [M + H$^+$], calculated 802.3148.

8.2.5. *N*-Octyl-*N'*-(4-(3-ethynyl-ferrocene) phenyl) naphthalene-1,4,5,8-tetra-carboxylic acid diimide (66)
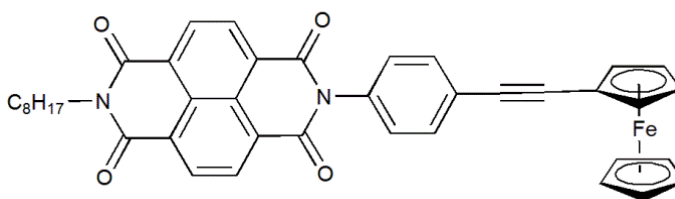
N-Octyl-*N'*-(4'-iodophenyl)naphthalene-1,4,5,8-tetracarboxylic acid diimide **62** (400 mg, 0.68 mmol), 10% Pd/C (13.0 mg, 0.13 mmol), CuI (52.0 mg, 0.26 mmol), Ph$_3$P (144 mg, 0.55 mmol) and K$_2$CO$_3$ (237 mg, 1.72 mmol) were mixed in a 1:1 solution of water: DME (14 mL) at room temperature. The mixture was degassed with N$_2$ for 5 min. and stirred for 30 min under N$_2$. 3-Ethynylferrocene (200 mg, 0.98 mmol) was then added and the mixture was heated to 80 ºC overnight. After cooling, the reaction mixture was extracted with DCM (5 x 20 mL). The organic extracts were combined and dried over MgSO$_4$. The solution was filtered and the filtrate was evaporated in vacuum. The product was purified by silica gel column chromatography eluting with DCM/Pet. Ether (80:20, v/v) to afford **66** as a green solid in 92% (420 mg) yield. M.p. 205-307 ºC. ^{1}H-NMR (δ/ppm, 400 MHz, CDCl$_3$): 8.81 (s, 4H, naphthalene); 7.67 (d, 2H, *J* = 4.2 Hz, phenyl); 7.28 (d, 2H, *J* = 4.2 Hz, phenyl); 4.54 (t, 2H, *J* = 1.8 Hz, ferrocene); 4.26 (m, 7H, ferrocene); 4.21 (t, 2H, *J* = 7.8 Hz, CH$_2$); 1.76 (m, 2H, CH$_2$CH$_3$); 1.48-1.22 (m, 10H, CH$_2$); 0.88 (t, 3H, *J* = 6.8 Hz, CH$_3$). ^{13}CNMR (δ/ppm, 100 MHz, CDCl$_3$): 162.9 (C=O), 162.8 (C=O), 133.6 (C), 132.4, 131.4, 131, 128.5, 127.1, 127, 126.9, 126.6, 125.2, 90 (CH), 85, 71.6, 70, 69, 64.8, 41.1 (CH$_2$), 31.8, 29.3, 29.2, 28.1, 27.1, 22.6, 14.1 (CH$_3$). FTIR (ν, cm^{-1}): 3051 (m, C-H aromatic), 2922-2854 (m, C-H alkane), 2190 (v.weak, C≡N), 1716-1705 (s, C=O), 1662-1582 (C=C, aromatic), 1513-1434 (C-C), 1371-1347 (C-H), 1246, 1190 (C-N), 746-692 (benzene ring). HRMS (ES$^+$): *m/z* 662.1869 [M + H$^+$], calculated 662.1867.

8.2.6. *N*-Octyl-*N'*-(4-(3(tetracyanobutadiene)ferrocene)phenyl)naphthalene-1,4,5,8-tetracarboxylic acid diimide (67)
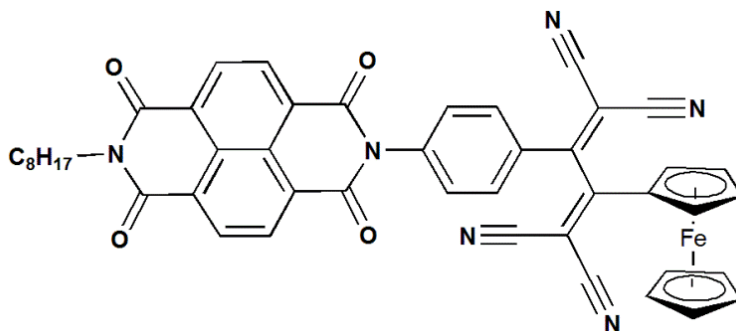
Tetracyanoethene (23.0 mg, 0.18 mmol) was added to solution of *N*-octyl-*N'*-(4-(3-ethynyl -ferrocene)phenyl)naphthalene-1,4,5,8-tetracarboxylic acid diimide **66** (100 mg, 0.15 mmol) in dry CH_2Cl_2 (9.0 mL) under nitrogen. The mixture was stirred at 20 °C for overnight. The DCM was evaporated under vacuum and the product was dissolved in the minimum amount of DCM and precipitated by adding petroleum ether. The solution was filtered to afford a blue product. The product was purified by recrystallization from DCM / methanol to afford **67** as a blue solid in 93% (110 mg) yield. M.p. 246-248 °C. ^{1}H-NMR (δ/ppm, 400 MHz, CDCl$_3$): 8.81 (s, 4H, naphthalene); 7.82 (d, 2H, *J* = 8.6 Hz, phenyl); 7.54 (d, 2H, *J* = 8.6 Hz, phenyl); 5.29 (s, H, ferrocene); 5.05 (s, H, ferrocene); 4.94 (s, 2H, ferrocene); 4.75 (s, 2H, ferrocene); 4.42 (s, 3H, ferrocene); 4.21 (t, 2H, *J* = 7.7 Hz ,CH_2); 1.75 (m, 2H, CH_2CH_3); 1.46-1.25 (m, 10H, CH_2); 0.87 (m, 3H, CH_3). ^{13}C NMR (δ/ppm, 100 MHz, CDCl$_3$): 162.6 (C=O), 162.6 (C=O), 150.1 (C), 141.1 (C), 131.7 (C), 131.1, 130.4, 129.6, 127.4, 126.1, 113.0, 88.8 (CH), 78.4, 75.4, 72.8, 72.7, 72.7, 71.2 (CH_2), 31.8, 29.3, 29.2, 28.7, 27.8, 27.1, 22.6, 14.1 (CH_3). FTIR (v, cm[-1]): 3105 (m, C-H aromatic), 2927-2857 (m, C-H alkane), 2223 (C≡N), 1708, 1666 (s, C=O) 1651, 1582 (C=C aromatic), 1518, 1449 (C=C alkene), 1412, 1340, 1371 (C-H), 1245, 1189 (C-N), 768 (benzene ring). HRMS (ES$^+$): *m/z* 813.1866 [M + H$^+$], calculated 813.1883.

8.2.7. *N*-Octyl-*N'*-(4-(3- (7,7,8,8-tetracyanoquinodimethane) ferrocene) phenyl) naphthalene-1,4,5,8-tetracarboxylic acid diimide (68)
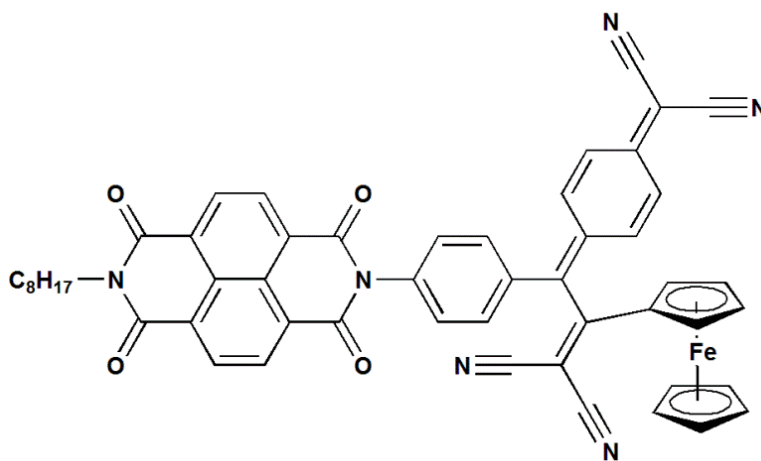
To solution of *N*-octyl-*N'*-(4-(3-ethynyl-ferrocene) phenyl) naphthalene-1,4,5,8-tetracarbo-xylic acid diimide **66** (100 mg, 0.15 mmol) in 1,2-dichloroethane (DCE) (8 mL), 7,7,8,8-tetracyanoquinodimethane (61 mg, 0.3 mmol) was added under dry nitrogen. The mixture was stirred at 70 ºC for 72 hrs. and the DCE was evaporated under vacuum .The product was purified by silica gel column chromatography eluting with DCM to afford **68** as a brown solid in 77% (100 mg) yield. M.p.> 310 ºC. ^{1}H-NMR (δ/ppm, 400 MHz, CDCl$_3$): 8.81 (s, 4H, naphthalene); 7.68 (m, 4H, phenyl); 7.55 (s, 2H, phenyl); 7.28 (d, 2H, J = 3.9 Hz, phenyl); 4.54 (t, 2H, J = 1.9 Hz, ferrocene); 4.26 (m, 7H, ferrocene); 4.21 (t, 2H, J= 7.7 Hz, CH$_2$); 1.76 (m, 2H, CH$_2$CH$_3$); 1.48-1.25 (m, 10H, CH$_2$); 0.88 (m, 3H, CH$_3$). ^{13}C NMR (δ/ppm, 100 MHz, CDCl$_3$): 162.7 (C=O), 162.6 (C=O), 154.1 (C), 153.0, 151.0, 139.1 (C),135.7, 134.9, 134.4, 134.1, 131.8, 131.7 (C), 131.2, 131.1, 130.6, 130.2, 127.9, 126.9, 126.1 (CH), 125.5, 125.3, 123.1, 114.6, 112.7, 112.1, 88.4 (CH) ,72.3 (CH), 41.2 (CH$_2$),, 40.2, 31.81, 29.3, 29.2, 28.1, 27.1, 22.7 (CH$_2$), 14.1(CH$_3$). FTIR (ν, cm^{-1}): 3105 (m, C-H aromatic), 2927-2857 (m, C-H alkane), 2223 (C≡N), 1708, 1666 (s, C=O) 1651, 1582 (C=C aromatic), 1518, 1449 (C=C alkene), 1412, 1340, 1371 (C-H), 1245, 1189 (C-N), 768 (benzene ring). HRMS (ES^{+}): *m/z* 889.2146 [M + H^{+}], calculated 889.2196.

8.2.8. *N*-Octyl-*N'*-(4-(3-thynyl-thiophene)phenyl)naphthalene-1,4,5,8-tetracarboxy-lic acid diimide (69)

N-Octyl-*N'*-(4'-iodophenyl) naphthalene-1,4,5,8-tetracarboxylic acid diimide **62** (300 mg, 0.51 mmol), 10% Pd/C (11.0 mg, 0.10 mmol), CuI (39.0 mg, 0.20 mmol), Ph$_3$P (108 mg, 0.41 mmol) and K$_2$CO$_3$ (178 mg, 1.29 mmol) were mixed in a 1:1 solution of water: DME (10 mL)   and stirred at room temperature. The mixture was degassed with N$_2$ for 5 min and stirred for 30 min under N$_2$. 3-Ethynylthiophene (0.07 mL, 0.73 mmol) was then added and the mixture was heated to 80 ºC overnight. After cooling, the reaction mixture was extracted with DCM (5 x 20 mL). The organic extracts were combined and dried over MgSO$_4$. The solution was filtered and the filtrate was evaporated under vacuum. The product was purified by silica gel column chromatography eluting with DCM/pet.ether (80:20, v/v) to afford **69** as a yellow solid in 61% (176 mg) yield. M.p. 243-245 ºC. ^{1}H-NMR (δ/ppm, 400 MHz, CDCl$_3$): 8.80 (s, 4H, naphthalene); 7.60 (d, 2H, *J* = 4.4 Hz, phenyl); 7.57 (dd, 1H, *J* = 1.6 Hz, phenyl); 7.32 (m, 2H, phenyl); 7.30 (s, 1H, thiophene); 7.23 (dd, 1H, *J* = 2.5, 1.2 Hz, thiophene); 4.21 (t, 2H, *J* = 7.6 Hz ,CH$_2$); 1.76 (m, 2H, CH$_2$CH$_3$); 1.48-1.25 (m, 10H, CH$_2$); 0.88 (t , 3H, *J* = 7.1 Hz, CH$_3$). ^{13}C NMR (δ/ppm, 100 MHz, CDCl$_3$): 162.9 (C=O), 162.7 (C=O), 134.2 (C), 132.6 (C), 131.5, 131.0, 129.9, 129.1, 128.6, 127.1, 126.9, 126.5, 125.5, 124.4, 122, 88.0 (CH), 85.8, 41.1 (CH$_2$), 31.8, 30.9, 29.3, 29.2, 28.1, 27.1, 22.6, 14.1 (CH$_3$). FTIR (ν, cm^{-1}): 3066 (m, C-H aromatic), 2919-2853 (C-H alkane), 2250 (v.weak, C≡C), 1717 (s, C=O) ,1655, 1623, 1579 (C=C, aromatic), 1502, 1450 (ring thiophene stretching), 1369, 1342 (C-H), 1244, 1189 (C-N), 1088 (C-H thiophene ring), 779 (benzene ring). HRMS (ES$^+$): *m/z* 583.1642 [M + H$^+$], calculated 583.1662.

8.2.9. [2,5-(3-(*N*-Octyl-*N'*-ethynylphenyl-naphthalenediimides) thiophene,3-hexyl-2,5-thiophene] polymer (73)
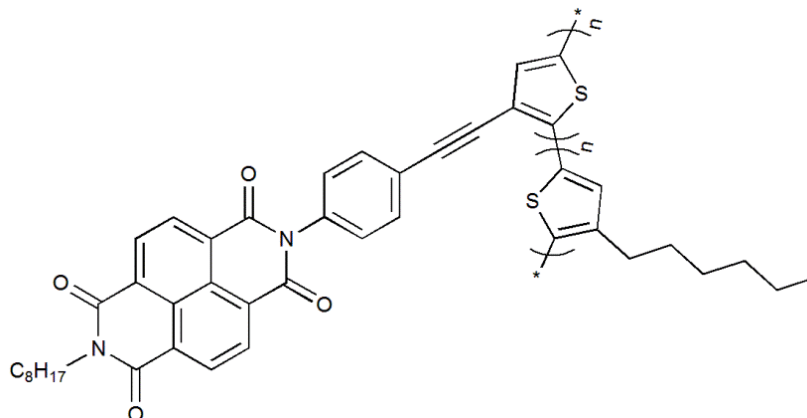
The co-monomer *N*-octyl-*N'*-(4-(3-ethynyl-thiophene) phenyl) naphthalene-1,4,5,8-tetra-carboxylic acid diimide **69** (200 mg, 0.55 mmol) and 3-hexylthiophene (239 mg, 1.42 mmol) were stirred under dry nitrogen. Nitromethane (40 mL) was added to the mixture with stirring. Solid $FeCl_3$ (1154 mg, 7.12 mmol) was added to the solution all at once and the reaction was allowed to proceed for 1 hr. and CCl_4 (160 mL) was added to the system, and the mixture was kept under stirring for an additional 3 hr. The reaction was then quenched by adding CH_3OH/HCl 5% (761 mL/40 mL) solution. The solid co-polymer was filtered off and washed with CH_3OH until no iron (III) was detectable by means of the NH_4SCN test. The material was then extracted by Soxhlet apparatus with (CH_3OH, CH_3CH_2OH, and petroleum ether respectively) until washings became colourless. The material was extracted in Soxhlet apparatus with DCM until no further colour was detected in the thimble. The DCM was evaporated under vacuum and the product was dissolved in the minimum amount of DCM and precipitated by adding petroleum ether to give the polymer. The polymer was then dried under high vacuum for 24 hours to yield polymer **73** as a red powder in 95% (190 mg) yield. ^{1}H-NMR (δ/ppm, 400 MHz, $CDCl_3$): 8.80 (s, br, 4H, naphthalene); 8.10 (m, br, phenyl); 7.70 (s, br, thiophene); 7.51 (s, br, thiophene); 6.97 (m, br, ArH); 4.20 (m, br, CH_2); 3.48 (m, br, CH_2); 2.67 (d, br, J = 45.4 Hz, CH_2); 1.69 (m, br, CH_2); 1.48-1.25 (m, br, CH_2); 0.88 (m, br, CH_3). FTIR (v, cm^{-1}): 3100 (m, br, C-H aromatic), 2953-2852 (m, C-H alkane), 2150 (v.weak, C≡C), 1707 (s, C=O), 1668, 1579 (C=C, aromatic), 1510, 1450 (ring thiophene stretching), 1371, 1338 (C-H), 1244, 1209 (C-N), 1088 (C-H thiophene ring), 768 (benzene ring). GPC: (THF, 40 ^{o}C, 1mL/min), *Mn* = 10035 *g/mol*, *Mw* = 24972 *g/mol*, *PDI* = 2.4885.

8.3. Synthetic experimental - Chapter 3

8.3.1. Synthesis of 1,4-di(thiophen-2-yl)butane-1,4-dione (82)[150]
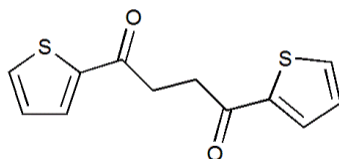
To a suspension of AlCl$_3$ (16.0 g, 120 mmol) in CH$_2$Cl$_2$ (15 mL) a solution of thiophene **80** (9.6 mL, 120 mmol) and succinyl chloride **81** (5.5 mL, 50.0 mmol) in CH$_2$Cl$_2$ was added dropwise. The red mixture was stirred at room temperature for 20 hours. The reaction was then quenched with water. After intensive stirring for 2 hours the dark green organic phase was separated. After evaporation of the solvent a blue-green solid remained, which was suspended in ethanol. Filtration and washing with ethanol and diethyl ether provided green solid. The product was purified by silica gel column chromatography eluting with CH$_2$Cl$_2$ /hexane (1:1, v/v) and recrystallization from ethanol gave 1,4-di(thiophen-2-yl)butane-1,4-dione **82** as a white solid in 80% (10 g) yield. M.p. 129-130 °C , (lit [2] 130-131 °C) ; ^{1}H-NMR (δ/ppm, 400 MHz, CDCl$_3$): 3.38 (s, 4H*, -CO-CH2-*); 7.13 (dd, 2H, *J* = 3.8, 1.1 Hz, 4,4′- thienyl); 7.63 (dd, 2H, *J* = 3.8, 5.0 Hz, 3,3′- thienyl); 7.80 (dd, 2H, *J* = 1.1, 5.0 Hz, 5,5′- thienyl). FTIR (ν, cm^{-1}): 3101, 3083, 2918, 1651. Mass spectrum [M + H$^+$] = 251.

8.3.2. 3-(2,5-Di(thiophen-2-yl)-1H-pyrrol-1-yl)benzoic acid (104)[298]
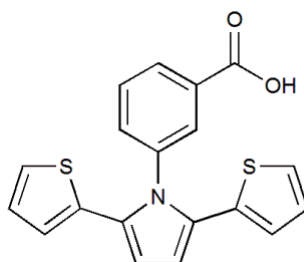
A mixture 1,4-dithiophen-2-yl-butatane-1,4dione **82** (1.50 g, 5.8 mmol). 3-Aminobenzoic acid **103** (0.8 g, 5.80 mmol) and *para*-toluenesulfonic acid (0.15 g, 0.58 mmol) in dry toluene (180 mL) was heated to reflux using a Dean-Stark apparatus for 12 hours. The toluene was removed using a rotary evaporator, and water (100 ml) was added. The crude product was removed by filtration, and purified on a slice gel column eluting first with CH_2Cl_2 to remove the unreacted dione and then with CH_2Cl_2 /ethyl acetate (80:20, v/v) to afford **104** as an white powder in 28% (0.57 g, 1.62 mmol) yield. M.p. 268-269 °C (lit[3] 268-269 °C); ^{1}H-NMR (δ/ppm, 400 MHz, DMSO-d_6) : 13.35 (s, br, 1H, OH); 8.09-8.12 (m, 1H); 7.76 (m, 1H); 7.67 (m, 2H); 7.32 (dd, 2H, *J* = 2.6, 1.1 Hz); 6.88-6.90 (m, 2H); 6.90 (s, 2H); 6.70 (dd, 2H, *J* = 2.6, 1.1 Hz) . FTIR (*v*, cm[-1]): 3065, 2958, 2843, 2646, 2532, 2843, 1700, 1588, 1487, 1454, 1294, 1196, 1046, 933, 826, 763, 698, 558. Mass spectrum [M + H^{+}] = 352.0458.

8.3.3. 2-[[2-Nitro-4-(trifluoromethyl)phenyl]amino]-ethanol (106)[151]
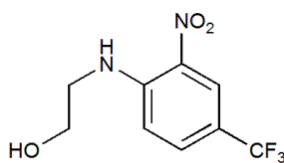
A solution of ethanolamine (3.0 mg, 51.11 mmol), triethylamine (14 mL, 102 mmol) and 1-chloro-4-(trifluoromethyl)-2-nitrobenzene **105** (15 mL, 102 mmol) were stirred in THF (100 mL). The solution was heated under reflux for 4 hours. After cooling to room temperature, the solvent was evaporated under vacuum, and the residue was dissolved in DCM (100 mL), and washed with water (50 mL). The aqueous layer was further extracted with DCM (3 x 100 mL). The combined organic extracts were dried over MgSO$_4$. The solution was filtered and the filtrate was evaporated under vacuum. The product was purified by silica gel column chromatography eluting with hexane/acetone (40:60, v/v) to afford the **106** as a yellow solid in 40 % (9.3 g) yield. M.p. 76-77 °C (lit[4] 76 °C); ^{1}H-NMR (δ/ppm, 400 MHz, CDCl$_3$) : 8.52 (s, br, 1H, NH); 8.50 (s, 1H); 7.63 (dd, 1H, J =9.0, 2.2 Hz); 7.01 (d, 1H, J = 9.0 Hz); 4.0 (t, 2H, J = 5.2 Hz); 3.57 (m, 2H, J = 5.2 Hz); 1.73 (m, br, 1H, OH). FTIR (v, cm^{-1}): 3371 (OH), 3283 (NH), 3118 (CH aromatic), 2952 - 2885(CH alkane), 1635, 1573 (aromatic C=C), 1532 (C-NO$_2$), 761 (aromatic ring) .Mass spectrum [M + H$^+$] = 251.1.

8.3.4. 2-(2-Amino-4-(trifluoromethyl)phenyl amino) ethanol (107)[299]
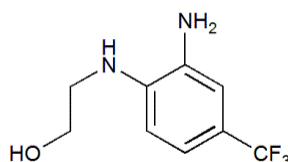
2-(2-Nitro-4-trifluoromethyl-phenylamino)-ethanol **106** (5.0 g, 20 mmol) was dissolved in methanol (120 mL). The solution was quickly purged with N_2, and 10% Pd/C (0.50 g) was charged to the solution. Ammonium formate (7.6 g, 120 mmol) was then added to the vigorously stirred solution. After quick purge with N_2, the reaction was stirred for 2 hours at room temperature. The solution was filtered and the solvent was evaporated under vacuum. The residue was dissolved in DCM (100 mL) and washed with water (50 mL). The aqueous layer was further extracted with DCM (2 x 100 mL). The combined organic extracts were dried over $MgSO_4$. The solution was filtered and the filtrate was evaporated in vacuum to afford **107** as red oil in 98% (4.9 g) yield. No further purification undergoes due to the instability of the compound. The product was taken on to react with alloxan monohydrate and boron oxide. ^{1}H-NMR (δ/ppm, 400 MHz, DMSO-d_6): 6.84 (d, 2H, $J = 8.3$ Hz); 6.50 (d, 1H, $J = 8.3$ Hz); 4.99 (t, br, H, NH); 4.92 (s, br, 2H, NH_2); 4.78 (m, br, 1H, OH); 3.65 (t, 2H, $J = 5.4$ Hz), 3.19 (t, 2H, $J = 5.4$ Hz).

8.3.5. 10-(2-Hydroxyethyl)-7-(trifluoromethyl)-benzo[*g*]pteridine-2,4(3*H*,10*H*)-dione (108)[151]
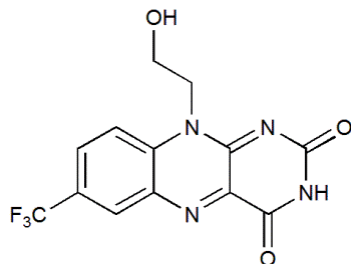
2-(2-Amino-4-(trifluoromethyl) phenyl amino) ethanol **107** (4.50 g, 20.45 mmol) was dissolved in acetic acid (105 mL). Alloxan monohydrate (3.30 g, 20.45 mmol) and boron oxide (2.90 g, 40.94 mmol) were then added. The mixture was heated under reflux for 2 hours. The solvent was then evaporated under vacuum. The product was purified by silica gel column chromatography eluting with hexane/acetone (80:20, v/v) to afford **108** as a yellow powder in 93% (4.2 g) yield. M.p. > 290 ℃ (Dec.) (lit[4] 297-281 ℃ (Dec.)). ^{1}H-NMR (δ/ppm, 400 MHz, DMSO-d_6): 11.42 (s, 1H, NH); 8.55 (s, 1H); 8.39 (d, 1H, J = 8.6 Hz); 8.22 (dd, H, J = 6.8, 8.6 Hz); 4.89 (t, 1H, J = 5.5 Hz, OH); 4.42 (t, 2H, J = 5.5 Hz, CH$_2$-N); 3.36 (dd, 4H, J = 5.5, 11.0 Hz).^{13}C NMR (δ/ppm, 100 MHz, DMSO-d_6): 207.9 (C=O) , 206.7 (C=O), 170.8, 170.3, 150, 69.2, 48.7, 30.7, 29.2. FTIR (ν, cm^{-1}): 3300 (OH), 3100 (NH), 2998 (CH-aromatic), 2805 (CH-alkane), 1690, 1590 (aromatic C=C), 1557, 1446, 1406, 1322, 1293, 1231, 1180, 766 (aromatic ring). Mass spectrum [M + H$^+$]= 326.9.

8.3.6. 3-(2,5-Di-2-thienyl-1*H*-pyrrol-1-yl)-benzoicacid-2-(3,4-dihydro-7-trifluoromethyl -2,4-dioxobenzo[*g*]pteridin-10(2*H*)-yl) ethyl ester (109)
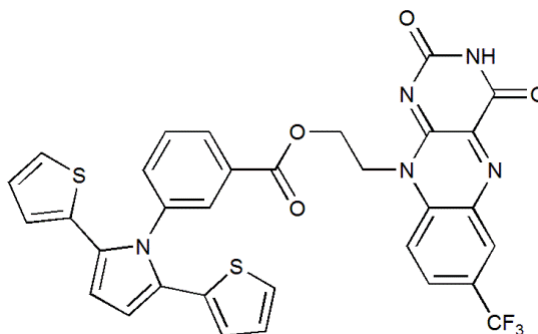
To a solution of compound 7-(trifluoromethyl)-10-(2-hydroxyethyl) benzo[g]pteridine-2,4 (3H,10H)-dione **108** (446 mg, 1.37 mmol) and 3-(2,5-di(thiophen-2-yl)-1H-pyrrol-1-yl) benzoic acid **104** (480 mg, 1.37 mmol) in DMF (25 mL) were added 1-(3-dimethyl-aminopropyl)-3-ethylcarbodiimide hydrochloride (EDCI) (22.0 mg, 0.11 mmol) and 4-dimethylaminopyridine (DMAP) (14.0 mg, 0.11 mmol). The resulting solution was stirred at room temperature for 3 days. The solvent was evaporated under reduced pressure. The residue was dissolved in DCM (100 mL) and washed with water (50 mL). The aqueous layer was further extracted with DCM (2 x 100 mL). The combined organic extracts were dried over MgSO$_4$. The solution was filtered and the filtrate was evaporated in vacuum. The product was purified by silica gel column chromatography eluting with DCM/acetone (90:10, v/v) to afford **109** as green powder in 64% (280 mg) yield. M.p. 222-223 ℃. ^{1}H-NMR (δ/ppm, 400 MHz, CDCl$_3$): 8.59 (s, 1H, NH); 8.47 (s, 1H, phenyl); 7.95 (m, 4H); 7.90 (dd, H, *J* = 9.1, 1.8 Hz, ArH); 7.85 (s, 1H, phenyl); 7.57 (d, 1H, *J* = 8.1 Hz, thiophene); 7.50 (t, *J* = 8.1 Hz, ArH); 7.08 (dd, H, *J* = 4.4, 0.9 Hz, thiophene); 6.84 (m, 2H); 6.59 (s, 1H, ArH); 6.57 (dd, H, *J* = 4.4, 0.9 Hz, thiophene); 5.10 (t , *J* = 5.6 Hz, CH$_2$-N); 4.85 (t, *J* = 5.6 Hz, CH$_2$-CH$_2$-N). ^{13}C NMR (δ/ppm, 100 MHz, CDCl$_3$): 206.9 (C=O), 200 (C=O), 165.4, 158.0, 150.8, 144.8, 139.1 (CH), 139.0, 135.4, 134.7, 134.4, 131.8, 131.1, 130.8, 130.2, 130.1, 129.8, 129.5, 127.0, 125.0, 124.5, 116.4, 110.5, 60.9 (CH$_2$), 44.3 (CH$_2$), 30.9. FTIR (ν,cm^{-1}):3200 (m, N-H), 3100-3045 (C-H aromatic), 2823 (C-H alkane), 1716 (s) (C=O), 1663 (C=N), 1594, 1555, 1521 (C-C aromatic), 1446 (C=C), 1358, 1324 (C-H), 1250, 1231(C-N), 1118 (C-F), 923 (N-H, wag) 763, 697 (benzene ring). HRMS (ES$^+$): *m/z* 660. 0987 [M + H$^+$], calculated 660.0990.

8.3.7. 3-(2,5-Di-2- thienyl-1*H*-pyrrol-1-yl)-benzoic acid 2-(3-methyl-3,4-dihydro -7-trifluoromethyl-2,4-dioxobenzo[*g*]pteridin-10-(2*H*)-yl)ethyl ester (112)
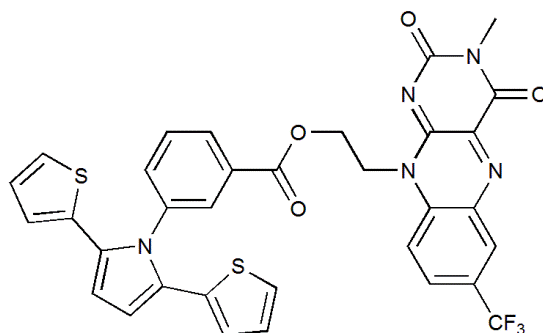
To a solution of 3-(2,5-di-2-thienyl-1*H*-pyrrol-1-yl)-benzoic acid-2-(3,4-dihydro-7-tri-fluoromethyl-2,4-dioxobenzo[*g*]pteridin-10-(2*H*)-yl) ethyl ester **109** (200 mg, 0.30 mmol) and K$_2$CO$_3$ (168 mg, 1.21 mmol) in DMF (10 mL) at room temperature, methyl iodide (129 mg, 0.91 mmol) was added. The reaction was allowed to proceed overnight. The solvent was evaporated under vacuum. The crude product was then purified using flash silica gel column chromatography eluting with hexane / ethyl acetate (1:1, v/v) to afford **112** as green solid in 92% (180 mg) yield. M.p. 195-197 ºC. ^{1}H-NMR (δ/ppm, 400 MHz, CDCl$_3$): 8.60 (s, 1H, ArH); 7.90 (m, 4H, ArH); 7.52 (m, 2H, ArH); 7.10 (d, 2H, *J* = 4.5 Hz, thiophene); 6.84 (t, 2H, *J* = 4.5 Hz, thiophene); 6.57 (t, 4H, *J* = 3.4 Hz thiophene and pyrrole); 5.10 (t, 2H, *J* = 5.6 Hz, CH$_2$); 4.84 (t, 2H, *J* = 5.6 Hz, CH$_2$); 3.55 (s, 3H, CH$_3$). ^{13}C NMR (δ/ppm, 100 MHz, CDCl$_3$): 165.4 (C), 158.8 (C), 155.2 (C), 149.2 (C), 139.0 (C), 138.4 (CF$_3$), 135.3 (C), 135.0 (C), 134.7 (C), 134.4 (CH), 131.4, 130.8, 129.9, 127.0, 124.2, 121.5, 116.2, 110.5, 61.0 (CH$_2$), 43.8 (CH$_2$), 28.9 (CH$_3$). FTIR (ν, cm^{-1}): 3112 (m) ,(C-H aromatic), 2918, 2851 (C-H alkane), 1732, 1761(s) (C=O), 1663 (C=N), 1592, 1558, 1534 (C=C aromatic), 1439, 1429 (C=C), 1354, 1318 (C-H), 1293, 1272, 1237 (C-N), 1159, 1210 (s) (C-O), 1139 (s) (C-F), 746-718 (benzene ring). HRMS (ES$^+$): *m/z* 674.0684 [M + H$^+$], calculated 674.0687.

8.3.8. 3-(2,5-Di-(5-bromo-2-thienyl)-1*H*-pyrrol-1-yl)-benzoic acid 2-(3-methyl-3,4-dihydro-7-trifluoromethyl2,4-dioxobenzo[*g*]pteridin-10(2*H*)-yl)ethyl ester (113)
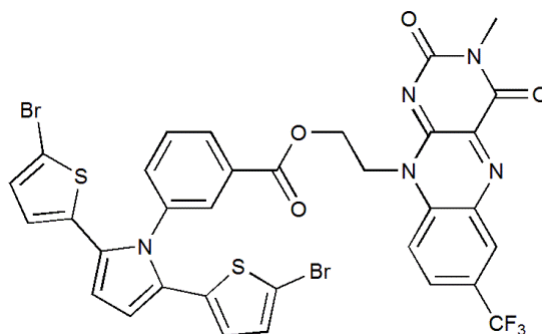
A solution of 3-(2,5-di-2- thienyl-1*H*-pyrrol-1-yl)-benzoic acid 2-(3-methyl-3,4-dihydro-7-trifluoromethyl-2,4-dioxobenzo[*g*]pteridin-10-(2*H*)-yl)ethyl ester **112** (100 mg, 0.15 mmol) and DMF (3 mL) was prepared and protected from light. The mixture was cooled to -10 ºC and N-bromosuccinimide (62 mg, 0.35 mmol) was added. The mixture was stirred for 6 hrs. at room temperature. The solution was treated with 2N HCl and was extracted with ether. The ether extracts was washed with 2N HCl and water (3 x 100 mL). The combined organic extracts were dried over Na_2SO_4. The solution was filtered and the filtrate was evaporated under vacuum. The product was purified by silica gel column chromatography eluting with DCM/petroleum ether (80:20, v/v) to afford **113** as a yellow solid in 48 % (60 mg) yield. M.p. 203-205 ºC, ^{1}H-NMR (δ/ppm, 400 MHz, CDCl$_3$): 8.61 (s, 1H, ArH); 7.95 (m, 2H, ArH); 7.85 (m, 1H, ArH); 7.75 (d, 2H, *J* = 1.9 Hz, ArH); 7.41 (m, 2H, pyrrole); 6.86 (m, 1H, thiophene); 6.79 (d, 1H, *J* = 3.9 Hz, thiophene); 6.66 (d, 1H, *J* = 3.9 Hz, thiophene); 6.58 (s, 1H, ArH); 6.37 (d, 1H, *J* = 3.9 Hz, thiophene); 5.08 (t, 2H, *J* = 6.1 Hz, CH$_2$); 4.80 (t, 2H, *J* = 6.1 Hz, CH$_2$); 3.53 (s, 3H, N-CH$_3$). ^{13}C NMR (δ/ppm, 100 MHz, CDCl$_3$): 165.2 (C), 158.5 (C), 155.8 (C), 149.2 (C), 138.9 (C), 135.4 (C), 134.7 (CH), 131.1, 130.6, 130.0, 129.8, 129.7, 126.2, 124.6, 124.5, 116.4, 113.2, 110.3, 60.8, 43.7, 42.3 (CH$_2$), 31.7, 30.9, 29.0, 27.7, 26.9, 22.6, 14.1 (CH$_3$). FTIR (ν, cm^{-1}): 3089 (m)(C-H aromatic), 2924-2885(C-H alkane), 1715 (s) (C=O), 1664 (C=N), 1596, 1560, 1537, 151 7(C=C aromatic), 1500, 1447, 1431, 1410 (C-C aromatic), 1324 (C-H), 1284, 1261 (C-O), 1250, 1216 (C-N), 1131, 1116 (C-F$_3$), 645 (C-Br). HRMS (ES$^+$): *m/z* 851.9192 [M + H$^+$], calculated 851.9168.

8.3.9. 3-(2,5-Di-2- thienyl-1*H*-pyrrol-1-yl)-benzoic acid 2-(3-heptyl-3,4-dihydro -7-trifluoromethyl-2,4-dioxobenzo[*g*]pteridin-10(2*H*)-yl)ethyl ester (110)
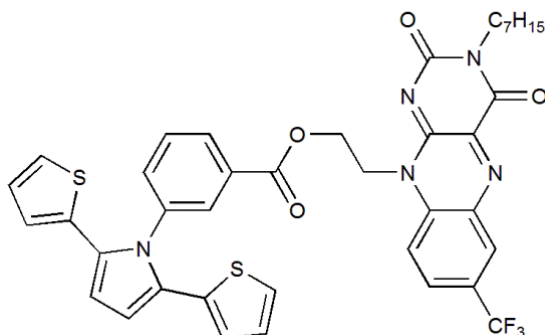
To a solution of 3-(2,5-di-2-thienyl-1*H*-pyrrol-1-yl)-benzoicacid-2-(3,4-dihydro-7-tri-fluoromethyl -2,4-dioxobenzo[*g*]pteridin-10(2*H*)-yl) ethyl ester **109** (1.0 g, 1.52 mmol) and sodium carbonate (0.67 g, 4.86 mmol) in dry DMF (50 mL), iodoheptane (0.75 mL, 4.56 mmol) was added. The reaction mixture was allowed to proceed overnight at room temperature. Upon cooling, the solvent was evaporated under vacuum. The crude product was then purified using flash silica gel column chromatography eluting with DCM/acetone (80:20, v/v) to afford **110** as green solid in 42% (0.50 g) yield. M.p. 95-97 ℃. ^{1}H-NMR (δ/ppm, 400 MHz, CDCl$_3$): 8.52 (s, 1H, phenyl); 7.91 (t, 2H, *J* = 7.8 Hz, phenyl); 7.83 (m, 2H, phenyl); 7.53 (d, 1H, *J* = 4.2 Hz, phenyl); 7.45 (m, 1H, phenyl); 7.0 (d, 2H, *J* = 2.6 Hz, pyrrole); 6.78 (m, 2H, thiophene); 6.50 (m, 4H, thiophene); 5.03 (t, 2H, *J* = 5.9 Hz, CH$_2$); 4.80 (t, 2H, *J* = 5.9 Hz, CH$_2$); 4.0 (t, 2H, *J* = 7.5 Hz, N-CH$_2$); 1.68 (m, 2H, CH$_2$-CH$_3$); 1.42-1.26 (m, 8H, CH$_2$); 0.87 (t, 3H, *J* = 6.9 Hz, CH$_3$). ^{13}C NMR (δ/ppm, 100 MHz, CDCl$_3$): 165.4 (C), 158.5 (C), 154.8 (C), 149.2 (C), 138.9 (C), 138.5 (C), 135.3 (C), 135.0 (C), 134.7 (CH), 134.3, 131.1, 130.6, 130.2, 130.0, 129.9, 129.6, 127.0, 124.6, 124.4, 116.3, 110.3, 61.1, 43.7, 42.3 (CH$_2$), 31.7, 30.9, 29.0, 27.7, 26.9, 22.6, 22.4, 14.1 (CH$_3$). FTIR (v, cm^{-1}): 3100 (m) (C-H aromatic), 2924-2885 (C-H alkane), 1716 (s)(C=O), 1661 (C≡N), 1596, 1559, 1537 (C=C aromatic), 1214, 1271 (C-O), 1323 (C-H), 1448, 1430 (C-C aromatic), 1130, 1156 (C-F$_3$), 759-688 (benzene ring). Anal.calcd. for C$_{39}$H$_{34}$F$_3$N$_5$O$_4$S$_2$: C, 61.75; H, 4.51; N, 9.24, Found C, 61.48; H, 4.65; N, 9.17. HRMS (ES$^+$): *m/z* 758.2083 [M + H$^+$], calculated 758.2085.

8.3.10. 3-(2,5-Di-(5,5'-dibromo)-2- thienyl-1*H*-pyrrol-1-yl)-benzoic acid 2-(3-heptyl-3,4-dihydro -7-trifluoromethyl-2,4-dioxobenzo[*g*]pteridin-10(2*H*)-yl) ethyl ester (111)
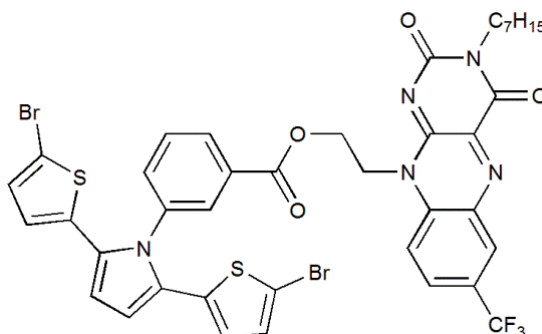
A solution of 3- (2,5-di-2-thienyl-1*H*-pyrrol-1-yl)-benzoic acid-2-(3-heptyl-3,4-dihydro-7-trifluoromethyl-2,4-dioxobenzo[*g*]pteridin-10-(2*H*)-yl) ethyl ester **110** (100 mg, 0.13 mmol) and DMF (30 mL) was prepared and protected from the light. The mixture was cooled to 0 °C and N-bromosuccinimide (48 mg, 0.26 mmol) in DMF (10 mL) was added drop wise to the solution. The mixture was stirred for 5hrs. The solvent was concentrated in vacuum and the solid was dissolved in CHCl$_3$ (50 mL). The organic solution was washed well with brine solution and water and dried over anhydrous MgSO$_4$. The solution was filtered and the filtrate was evaporated under vacuum. The product was purified by silica gel column chromatography eluting with DCM/acetone (90:10, v/v) to afford **111** as yellow powder in 58% (70 mg) yield. M.p.106-108 °C. ^{1}H-NMR (δ/ppm, 400MHz, CDCl$_3$): 8.6 (s, 1H, phenyl); 7.94 (m, 2H, pyrrole); 7.85 (d, 1H, *J* = 7.2 Hz, phenyl); 7.75 (s, 1H, phenyl); 7.50 (m, 1H, phenyl); 7.41 (m, 1H, phenyl); 6.85 (d, 1H, *J* = 4.1 Hz, thiophene); 6.8 (d, 1H, *J* = 4.1 Hz, thiophene); 7.50 (m, 1H, phenyl); 6.66 (d, 1H, *J* = 4.1 Hz, thiophene); 6.58 (s, 1H, phenyl); 6.37 (d, 1H, *J* = 4.1 Hz ,thiophene); 5.1 (t, 2H, *J* = 6.0 Hz, CH$_2$); 4.79 (t, 2H, *J* = 6.0 Hz, CH$_2$); 4.08 (t, 2H, *J* =7.6 Hz, N-CH$_2$); 1.71 (m, 2H, CH$_2$-CH$_3$); 1.44-1.27 (m, 8H, CH$_2$); 0.88 (t, *J* = 7.0 Hz, CH$_3$). ^{13}C NMR (δ/ppm, 100 MHz, CDCl$_3$): 165.2 (C), 158.5 (C), 155.8 (C), 149.2 (C), 138.9 (C), 135.4 (C), 134.7 (CH), 131.1, 130.6, 130.0, 129.8, 129.7, 126.2, 124.6, 124.5, 116.4, 113.2, 110.3, 60.9, 43.7, 42.3 (CH$_2$), 31.7, 30.9, 29.0, 27.7, 26.9, 22.6, 14.1 (CH$_3$). FTIR (ν, cm^{-1}): 3089 (m) (C-H aromatic), 2924-2885(C-H alkane), 1715 (s) (C=O), 1664 (C=N), 1596, 1560, 1537, 1517 (C=C aromatic), 1500, 1447, 1431, 1410 (C-C aromatic), 1324 (C-H), 1284, 1261 (C-O), 1250, 1216 (C-N), 1131, 1116 (C-F$_3$), 645 (C-Br). HRMS (ES$^+$): *m/z* 914.0241 [M + H$^+$], calculated 914.0215.

8.3.11. 3-(2,5-Di-2-thienyl-1*H*-pyrrol-1-yl)-benzoicacid-6-(3,4-di-hydro-7-tri-fluoromethyl-2,4-dioxobenzo[*g*]pteridin-10(2*H*)-yl)ethyl ester (115)
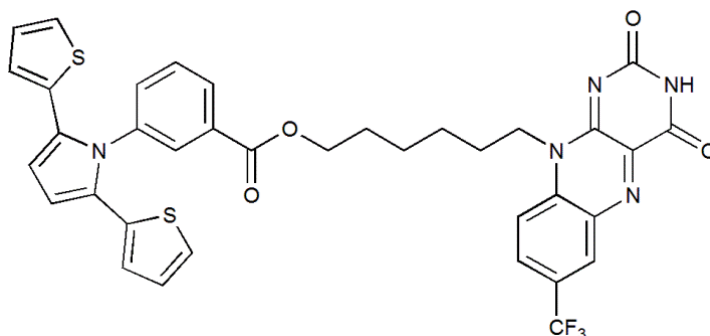
To solution of 3-(2,5-di(thiophen-2-yl)-1H-pyrrol-1-yl)benzoic acid **104** (300 mg, 0.85 mmol), and 7-(trifluoromethyl)-10-(6-hydroxyhexyl)benzo[g]pteridine-2,4-(3H,10H)dione **114** (320 mg, 0.85 mmol) in DMF (25 mL) were added EDCI (160 mg, 0.85 mmol) and DMAP (100 mg, 0.85 mmol). The resulting solution was stirred at room temperature for 7 days. The solvent was evaporated under reduced pressure, and the residue was dissolved in DCM (100 mL) and washed with water (50 mL). The aqueous layer was further extracted with DCM (2 x 100 mL). The combined organic extracts were dried over anhydrous MgSO$_4$. The solution was filtered and the filtrate was evaporated under vacuum. The product was purified by silica gel column chromatography eluting with DCM/acetone (90:10, v/v) to afford **115** as green powder in 74% (450 mg) yield. M.p. 101-103 ºC. ^{1}H-NMR (δ/ppm, 400 MHz, CDCl$_3$): 8.55 (1H, s, NH); 8.15 (d, 1H, J = 1.7 Hz, phenyl); 8.13 (d, 1H, J = 1.7 Hz, phenyl); 8.0 (m, 1H, phenyl); 7.74 (d, 1H, J = 4.6 Hz, thiophene); 7.50 (m, 1H, thiophene); 7.33 (s, 1H, phenyl); 7.0 (dd, 2H, J = 2.6, 1.0 Hz, thiophene); 6.76 (m, 1H, thiophene); 6.48 (d, 1H, J = 2.6 Hz, thiophene); 4.46 (m, 2H, CH$_2$); 4.31 (t, 2H, J = 6.5 Hz, OCH$_2$); 1.91-1.75 (m, 2H, CH$_2$); 1.63-1.47 (m, 6H, CH$_2$). ^{13}C NMR (δ/ppm, 100 MHz, CDCl$_3$): 165.6 (C), 158.4 (C), 154.7 (C), 150.5 (C), 139.0 (C), 134.8 (C), 134.6 (CH), 134.5, 134.4, 131.8, 130.9, 130.3, 129.5, 127.0, 124.5, 124.2, 116.3, 110.1, 73.9, 65.9, 65.0, 60.8, 45.5 (CH$_2$) 28.3, 28.2, 26.7, 26.3, 25.5, 22.4. FTIR (ν, cm^{-1}): 3400 (N-H), 3071 (C-H aromatic), 2940 (C-H alkane), 1716 (C=O), 1649 (C=N), 1559, 1555, 1518, 1450, (C=C aromatic), 1406, 1448 (C=C), 1326 (C-H), 1240, 1286 (C-O), 1119 (CF$_3$), 695, 762 (Benzene ring). HRMS (ES$^+$): *m/z* 738.1412 [M + H$^+$], calculated 738.1427.

8.3.12. [5,5'(3-(2,5-Di-2-thienyl-1*H*-pyrrol-1-yl)-benzoicacid-6-(3,4-dihydro-7-trifluoromethyl-2,4-dioxobenzo[*g*]pteridin-10(2*H*)-yl) ethyl ester) thiophene-3-hexyl-2,5-thiophene]polymer (116)
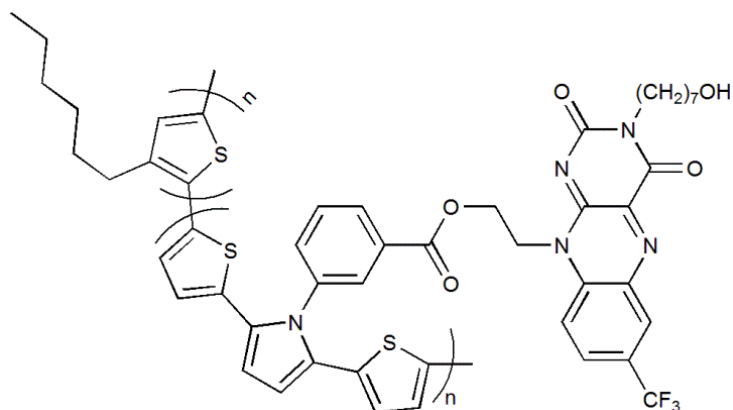
The co-monomer 3-(2,5-di-(5-bromo)-2-thienyl-1H-pyrrol-1-yl)-benzoic acid-2-(3-heptyl-3,4-dihydro-7-trifluoromethyl-2,4-dioxobenzo[g]pteridin-10-(2H)-yl) ethyl ester **110** (200 mg, 0.26 mmol) and 3-hexylthiophene **72** (178 mg, 1.0 mmol) were stirred under dry nitrogen. Nitromethane (30 mL) was added to the mixture with stirring. Solid FeCl$_3$ (856 mg, 5.27 mmol) was added to the solution all at once and the reaction was allowed to proceed for 1 hr. and CCl$_4$ (119 mL) was added to the system, and the mixture was kept under stirring for an additional 3 hr. The reaction was quenched with of CH$_3$OH/HCl 5% (600 mL/30mL) solution. The solid co-polymer was filtered off and washed with CH$_3$OH until no iron (ш) was detectable by means of the NH$_4$SCN test. The material was then extracted by Soxhlet apparatus with (CH$_3$OH, CH$_3$CH$_2$OH, and petroleum ether respectively) until washings became colourless. The material was extracted in Soxhlet apparatus with DCM until no further colour was detected in the thimble. The DCM was evaporated under vacuum and the product was dissolved in the minimum amount of DCM and precipitated by adding petroleum ether to give the polymer. The polymer was then dried under high vacuum for 24 hours to yield polymer **116** as a red powder in 86% (172 mg) yield. ^{1}H-NMR (δ/ppm, 400 MHz, CDCl$_3$): 8.08 (m, br, phenyl); 7.91 (m, br, thiophene); 7.55 (m, thiophene); 7.51 (m, br, phenyl); 6.99 (s, br, thiophene); 6.97 (s, br, phenyl); 6.63 (s, br, phenyl); 6.42 (d, br, J = 2.5 Hz); 5.02 (m, br, CH$_2$); 4.78 (m, br, CH$_2$); 4.25 (m, br, CH$_2$); 4.05 (m, br, N-CH$_2$); 3.73 (m, br, CH$_2$); 2.79 (m, br, CH$_2$); 1.85 (m, br, CH$_2$); 1.68 (m, br, CH$_2$-CH$_3$); 1.47-1.23 (m, br, CH$_2$); 0.87(m, br, CH$_3$). FTIR (ν, cm^{-1}): 3100 (m, br, C-H aromatic), 2953-2854 (C-H alkane), 1722 (s) (C=O), 1668 (C=N), 1597, 1562, 1539 (C=C aromatic), 1454, 1408 (C-C aromatic), 1377, 1325 (C-H), 1284, 1217

(C-O), 1167 (C-F$_3$), (795-725, benzene ring). GPC: (THF, 40 ^{o}C, 1mL/min), *Mn* = 15631 *g/mol*, *Mw* = 21351 *g/mol*, *PDI* = 1.3659.

8.3.13. Electrochemical polymerisation of the compound (115)
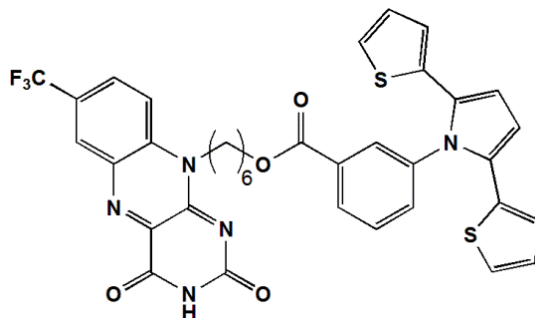
The electrochemical polymerisation of the compound **115** on to a glassy carbon working electrode surface was achieved. The conditions are describes briefly below.

The electrolyte solutions (0.1M) were prepared from n-Bu$_4$NPF$_6$ and dry toluene and acetonitrile. A three-electrode configuration was used with a glassy carbon disc working electrode, a silver wire reference electrode and a platinum wire as the counter electrode. Cyclic voltammetry of the compound **115** and polymer **120** films grown on the carbon electrode were measured using 0.4 g/L solution of monomer **115** in acetonitrile. The electrochemical experiments were referenced to ferrocene, which has a HOMO of -4.8 eV, and the HOMO and LUMO of the polymer has been estimated from the onset of the corresponding reduction/oxidation waves. The onset of absorption edge of compound 3 at 481 nm gives the optically determined band gap energy of 2.58 eV.

8.3.14. Electrochemical polymerisation of compounds (109)
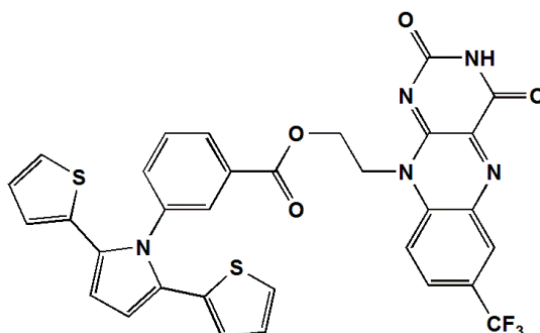
The electrochemical polymerisation of the compound **109** on to a glassy carbon working electrode surface was achieved. The conditions are describes briefly below.

The electrolyte solutions (0.1M) were prepared from Bu_4NPF_6 and dry toluene and acetonitrile. A three-electrode configuration was used with a glassy carbon disc working electrode, a silver wire reference electrode and a platinum wire as the counter electrode. Cyclic voltammetry of the compound **109** and polymer **121** films grown on the carbon electrode were measured using 0.4 g/L solution of monomer **109** in acetonitrile. The electrochemical experiments were referenced to ferrocene, which has a HOMO of -4.8 eV, and the HOMO and LUMO of the polymer has been estimated from the onset of the corresponding reduction/oxidation waves. The onset of absorption edge of compound **109** at 480 nm gives the optically determined band gap energy of 2.59 eV.

8.4. Synthetic experimental - Chapter 4

8.4.1. Ferrocenecarboxylic acid chloride (175) [200]
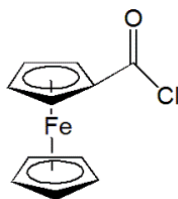
To a solution of ferrocene carboxylic acid **174** (1.0 g, 4.30 mmol) in dry toluene (100 mL), oxalyl chloride (0.50 mL, 6.0 mmol) was added dropwise. Then, two drops of DMF were added. The reaction mixture was heated under reflux at 60 ºC for one hour. The mixture was allowed to cool and the solvent was removed under vacuum to yield a dark red solid. The solid was taken up into DCM and impurities were precipitated out by the addition of hexane. Then, the mixture was filtered and washed with hexane. The resulting liquid was collected and the solvent was evaporated under vacuum to yield dark red oil. No further purification was attempted due to the instability of the compound **175**. The product was taken on to react with 2,2′-(ethylenedioxy)bis(ethylamine). Assumed 100% yield. ^{1}H-NMR (δ/ppm, 400 MHz, CDCl$_3$): 4.35 (s, 5H, C5$H5$); 4.66 (s, 2H, Cp ring, CH); 4.94 (s, 2H, Cp ring, CH).

8.4.2. *N*-(2-(2-(2-Aminoethoxy)ethoxy)ethylamido)ferrocene (176) [200]

176

+

177
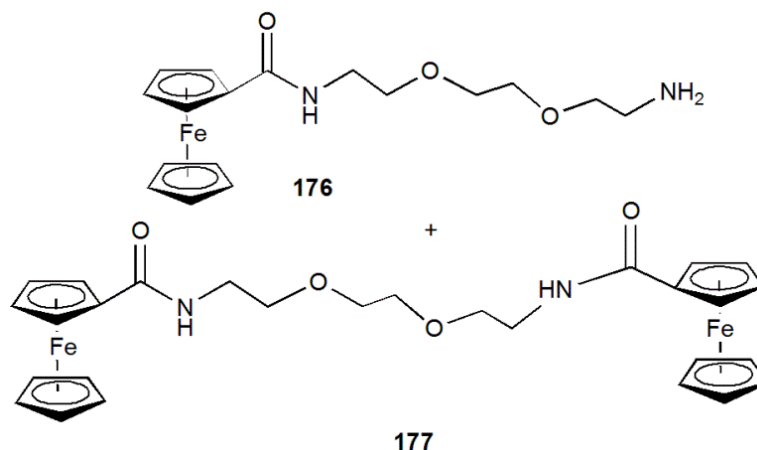
To a solution of 2,2′-(ethylenedioxy)bis(ethylamine) (1.20 mL, 8.70 mmol) and triethyl-amine (1.20 mL, 8.70 mmol) in DCM (125 mL) was added the ferrocene acid chloride **175** (1.0 g, 4.35 mmol) in DCM (125 mL) *via* a pressure equalising dropping funnel over a period of 30 minutes. The reaction mixture was stirred for 16 hrs. at room temperature. The reaction mixture was partitioned between DCM and water; the organic layer was washed with water (3 x 100 mL) and then dried with $MgSO_4$. The organic layer was collected after filtration and the solvent was evaporated under vacuum. Flash silica column chromate-graphy eluting with 0-20% MeOH in DCM with 3% triethylamine to yield products **176** and **177** in a 70% (1.70 g) and 30% (0.74 g) yield respectively. ^{1}H-NMR (δ/ppm, 400 MHz, CDCl₃) of ferrocene amine **176** : 6.53 (s, br, 1H, NH amide); 4.73 (s, 2H, Cp ring, CH); 4.33 (s, 2H, Cp ring CH); 4.20 (s, 5H, Cp ring CH); 3.69-3.63 (m, 6H, m, CH_2); 3.59 (t, 2H, J = 5.0 Hz, CH_2); 3.54 (t, 2H, J = 5.0 Hz, CH_2); 2.90 (t, 2H, J = 5.0 Hz, CH_2); 1.69 (s, br, 2H, NH_2). ^{13}C NMR (δ/ppm, 100 MHz, CDCl₃) of ferrocene amine **176**: 170.4 (QC), 73.3 (QC), 70.4 (CH), 70.3 (CH_2), 70.2 (CH_2), 69.8 (CH), 68.2 (CH), 41.7 (CH_2), 39.3 (CH_2), 31.0 (CH_2). FTIR (ν, cm^{-1}): 3384, 3321, 3074, 2929, 2914, 2893, 2884, 2850, 1643, 1629, 1542, 1103. Mass spectrum [M+H]$^+$ = 361.2. ^{1}H-NMR (δ/ppm, 400 MHz, CDCl₃) of ferrocene dimer **177** : 6.17 (s, br, 2H, NH amide); 4.67 (s, 4H, Cp ring CH); 4.34 (s, 4H, Cp ring CH); 4.22 (s, 10 H, 2 Cp ring CH); 3.69 (s, 4H, CH_2); 3.66 (t, 4H, J = 5.0 Hz, CH_2); 3.60 (t, 4H, J = 5.0 Hz, CH_2) , Mass spectrum [M + H$^+$] = 573.1.

8.4.3. *N*-(2-(2-(2-Bromoisobutyrylamino)ethoxy)ethoxy)ethyl-amido) ferrocene (179)
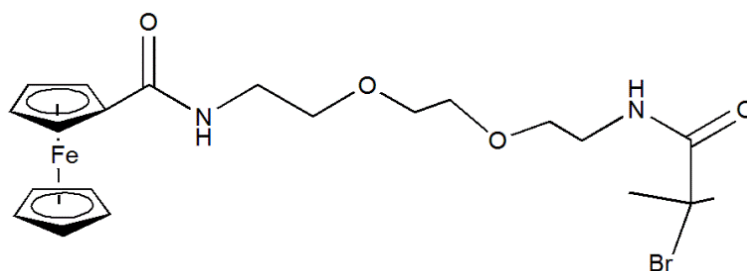
To a solution of triethylamine (0.44 mL, 3.12 mmol) in THF (25 mL) was added ferrocene amine **176** (1.0 g, 2.60 mmol) followed by 2-bromoisobutyryl bromide (0.30 mL, 2.60 mmol). The mixture was stirred at room temperature overnight. The solution was filtered and the filtrate was evaporated under vacuum. The product was purified by silica gel column chromatography eluting with DCM: acetone (80:20, v/v) to afford **179** as a red product in 49% (0.65 g) yield. M.p. 111-113 °C. ^{1}H-NMR (δ/ppm, 400 MHz, CDCl$_3$): 7.1 (s, br, 1H, NH amide); 6.16 (s, br, 1H, NH amide); 4.69 (s, 2H, Cp ring, CH); 4.23 (s, 2H, Cp ring, CH); 4.20 (s, 5H, Cp ring CH); 3.67 (m, 6H, CH$_2$); 3.61 (m, 4H, CH$_2$); 3.50 (t, 2H); 1.98 (s, br, 6H, CH$_3$). ^{13}C NMR (δ/ppm, 100 MHz, CDCl$_3$): 170.4 (amide carbonyl), 70.5 (QC), 70.4 (QC), 70.3 (CH), 69.8 (CH), 69.5 (CH), 68.2 (CH), 40.1 (CH$_2$), 39.3 (CH$_2$), 32.5 (CH$_2$), 14.5 (CH$_3$). FTIR (ν, cm^{-1}): 3298 (m, HN-C=O), 2932, 2889, 2866 (m, C-H), 1622, 1652 (s, C=O), 1530, 1490 (m, C=C aromatic), 1302 (s), 1128 (s, C-O, ether), 601(m, C-Br). HRMS (ES$^+$): *m/z* 531.0556 [M + H$^+$], calculated 531.0552.

8.4.4. *N*-(2-(2-(2-(Methacryloyl amino)ethoxy)ethoxy)ethylamido) ferrocene (178)
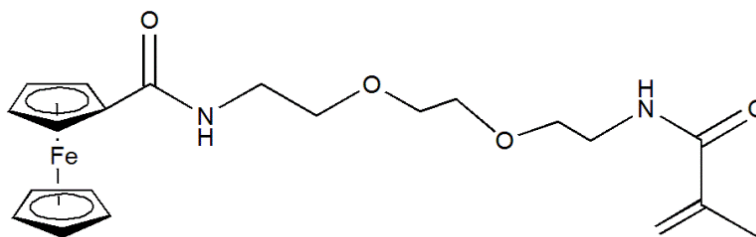
To a solution of triethylamine (0.75 mL, 5.38 mmol) in THF (25 mL) was added ferrocene amine **176** (1.70 g, 4.48 mmol) followed by methacryloyl chloride (0.45 mL, 4.48 mmol) dropwise. The mixture was stirred at room temperature overnight. The solution was filtered and the filtrate was evaporated under vacuum. The product was purified by silica gel column chromatography eluting with DCM/ acetone (80:20, v/v) to afford **178** as an oily red product in 44% (0.84 g) yield. ^{1}H-NMR (δ/ppm, 400 MHz, CDCl$_3$): 6.26 (s, br, 2H, NH amide); 5.34 (s, 1H); 4.70 (s, 2H, Cp ring CH); 4.22 (s, 5H, Cp ring CH); 3.73-3.53 (m, 6H, CH$_2$); 3.59 (t, 2H, *J* = 5.0 Hz, CH$_2$); 3.54 (t, 2H, *J* = 5.0 Hz, CH$_2$); 2.90 (t, 2H, *J* = 5.0 Hz, CH$_2$); 1.79 (s, br, 3H, CH$_3$). ^{13}C NMR (δ/ppm, 100 MHz, CDCl$_3$): 170.7 (QC), 168.6 (QC), 130.9 (QC), 128.8 (QC), 119.7 (CH), 70.5 (CH), 70.4 (CH), 70.3 (CH$_2$), 69.9 (CH$_2$), 69.8 (CH), 68.2 (CH), 39.4 (CH$_2$), 39.3 (CH$_2$), 30.4 (CH$_2$), 32.5 (CH), 28.9 (CH), 23.7 (CH$_2$), 23 (CH$_2$), 18.7 (CH$_3$) .FTIR (ν, cm^{-1}): 3316 (s, br, N-H), 3010-3070 (s) (C-H aromatic), 2930-2861 (C-H alkane), 1731 (s) (C=O), 1592 (C=C), 1530, 1454 (m) (C=C aromatic), 1415 C-C (m) (stretch (in-ring) aromatic), 720(m) (C-H (rock) alkane). HRMS (ES$^+$): *m/z* 451.1276 [M + H$^+$], calculated 451.1291.

8.4.5. Ferrocenemethacrylate-PEG co-polymer (181)
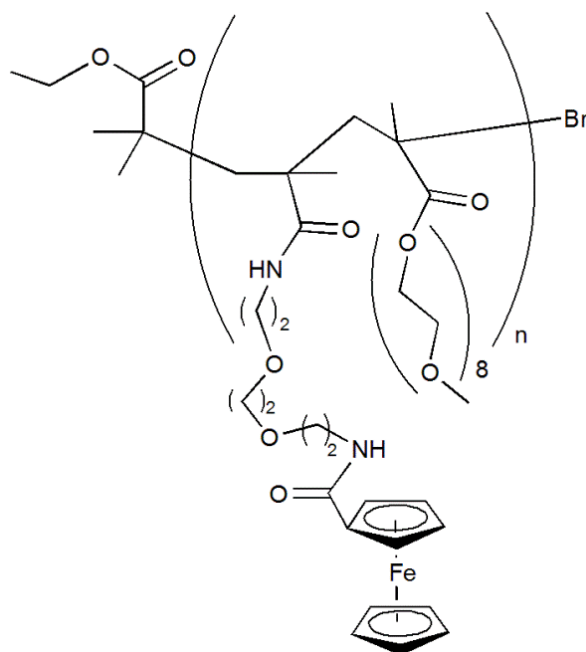
CuCl (3.30 mg, 0.03 mmol), CuBr$_2$ (3.20 mg, 0.01 mmol) were mixed together. DMSO (1 mL) was added and followed by PMDETA (8.30 mg, 0.05 mmol). The mixture was stirred at room temperature to form solution 1. Ferrocenemethacrylate **178** (200 mg, 0.48 mmol) and polyethylene glycol **180** (2.05 g, 4.32 mmol) were dissolved in DMSO (5.0 mL) to form solution 2. Both of solutions were mixed together, and then the reaction system was degassed with three (freeze-pump-thaw) cycles. The ethyl-2-bromo-2-methylpropanoate (EBIB) (7.0 μl, 0.048 mmol) was added to above mixture and stirred under nitrogen gas at 40 °C for four hours. Monomer conversion was determined via the GPC response of samples withdrawn periodically during the reaction. The mixture was cooled to room temperature and poured into a vigorously stirred diethyl ether (400 mL) for one hour. The resulting mixture was put in fridge overnight. Then, the diethyl ether was removed by decantation and the result oil was dissolved in a minimum quantity of chloroform and then purified using a column chromatography with aluminum oxide to remove traces of the copper catalyst. The filtrate was reduced in volume under vacuum to approximately 20 mL and the polymer was re-precipitated and collected in the same manner as before to provide the polymer as a red solid. The polymer was then dried under high vacuum for 24 hours to yield polymer **181** in 94% (0.44 g) yield. ^{1}H-NMR (δ/ppm, 400 MHz, CDCl$_3$): 4.87 (s, 2H, Cp ring CH); 4.22-4.10 (s, 2H, Cp ring CH); 4.20 (s, 5H, Cp ring CH); 3.67 (s, CH$_2$); 3.59 (m, CH$_2$); 3.40 (t, CH$_3$); 1.27 (s, br, NH); 0.87 (b, CH$_3$); 0.40 (b, CH$_3$). FTIR (ν, cm^{-1}): 3550 (N-H, b), 3100 (C-H aromatic), 2868 (C-H alkane), 1726 (s)(C=O), 1452 (C=C

aromatic), 1350 C-C (stretch (in-ring) aromatic), 1095 (C-N, stretch), 731 (C-H (rock) alkane), 586 (C-Br, stretch). GPC: (THF, 40 °C, 1mL/min), $Mn = 10928$ g/mol, $Mw = 11579$ g/mol, $PDI = 1.059$.

8.4.6. Ferrocenemethacrylate-DMAEMA co-polymer (183)
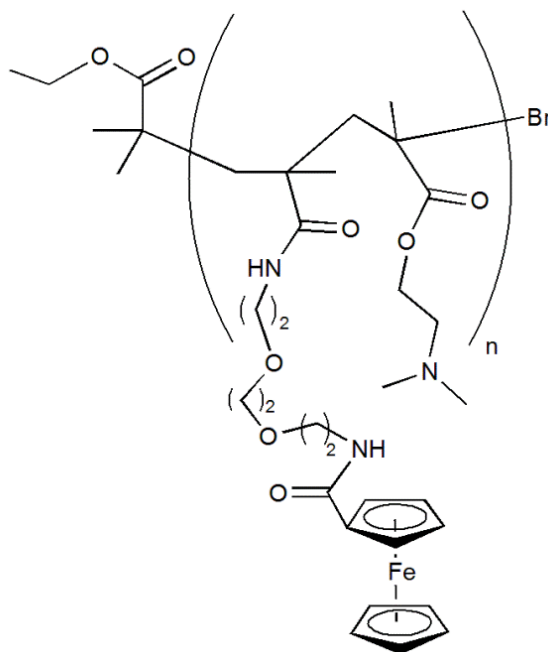
CuCl (1.70 mg, 0.02 mmol), CuBr$_2$ (1.60 mg, 0.01 mmol) were mixed together. DMSO (1 mL) was added, followed by PMDETA (4.20 mg, 0.02 mmol) to form solution 1. 2-(Dimethyl amino) ethyl methacrylate (DMAEMA) **182** (302 mg, 1.92 mmol) and ferrocene methacrylate **178** (200 mg, 0.48 mmol) were dissolved in DMSO (0.50 mL) to form solution 2. Both solutions were mixed and the reaction system was degassed with three (freeze-pump-thaw) cycles. EBIB (3.50 mL, 0.02 mmol) was added to mixture and stirred under nitrogen gas at 60 °C for 2 hours. The mixture was cooled to room temperature and poured into vigorously stirred hexane (400 mL). The solution was then put in the fridge overnight. The solvent was decanted and the resulting oil was dissolved in a minimum quantity of THF and then purified using a column with aluminium oxide to remove traces of the copper catalyst. The filtrate was reduced in volume under vacuum to approximately 20 mL and the polymer was re-precipitated and collected in the same manner as before to provide the polymer as bright yellow syrup. The polymer was then dried under high vacuum for 24 hours to yield polymer **183** in 97% (0.51 g) yield. ^{1}H-NMR (δ/ppm, 400 MHz, CDCl$_3$): 7.01 (d, br, N-H); 6.22 (d, br, N-H); 4.71 (t, br, Cp ring, CH, $J = 1.8$ Hz); 4.37 (t, br, Cp ring, CH, $J = 1.8$ Hz); 4.23 (s, 5H, Cp ring CH); 3.69 (m, br, CH$_2$); 2.65 (s,

br, CH$_2$); 2.30 (s, br, CH$_2$); 1.98 (t, br, CH$_3$); 1.66 (s, br, CH$_3$); 1.46 (s, br, CH$_3$). FTIR (v, cm^{-1}): 3550 (N-H, b), 3100 (C-H aromatic), 2868 (C-H alkane), 1726 (s) (C=O), 1452 (C=C aromatic), 1350 C-C (stretch (in-ring) aromatic), 1095 (C-N, stretch), 731 (C-H (rock) alkane), 586 (C-Br, stretch). GPC: (THF, 40 ^{o}C, 1mL/min), Mn = 17109 g/mol, Mw = 17127 g/mol, PDI = 1.00.

8.4.7. Ferrocene-DMAEMA co-polymer (184)
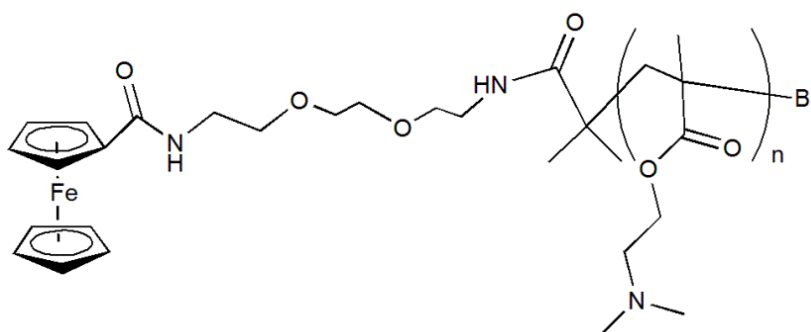
CuCl (8.90 mg, 0.09 mmol), CuBr$_2$ (8.60 mg, 0.04 mmol) were mixed together. DMSO (1.0 ml) was added, followed by PMDETA (22.0 mg, 0.13 mmol). The mixture was stirred at room temperature to form solution1. DMAEMA **182** (2.01 g, 12.81 mmol) was dissolved in DMSO (1.0 mL) to form solution 2. Both of solutions were mixed together and the mixture was degassed with three (freeze-pump-thaw) cycles. Ferrocene initiator **179** (65 mg, 0.12 mmol) was added to the mixture and stirred under nitrogen gas at 60 ºC for 2 hours. The mixture was cooled to room temperature and poured into vigorously stirred hexane (400 ml) for one hour. The resulting mixture was put in fridge for overnight. The solvent was decanted and the resulting oil was dissolved in a minimum quantity of THF and then purified using column with aluminium oxide to remove traces of the copper catalyst. The filtrate was reduced in volume under vacuum to approximately 20 mL and the polymer was re-precipitated and collected in the same manner as before to provide the polymer as clear red syrup. The polymer was then dried under high vacuum for 24 hours to yield polymer **184** in 100% (0.71 g) yield. ^{1}H-NMR (δ/ppm, 400 MHz, CDCl$_3$): 4.5 (s, 2H, Cp ring CH), 4.22- 4.10 (s, 2H, Cp ring CH); 4.20 (s, 5H, Cp ring CH); 4.05 (s, br, 2H, CH$_2$); 3.62 (t, 2H, CH$_2$); 2.59 (s, 3H, CH$_3$); 2.20 (s, 3H, CH$_3$); 1.76 (s, br, 2H, NH); 0.97- 0.82 (br, CH$_3$). FTIR (v, cm^{-1}): 3400 (HN-C=O), 2980 - 2781(m)(C-H), 1751, 1703 (s) (C=O), 1389 (C-H rock), 1280 (s), 1265 (s) (C-O ether), 1199 (C-N stretch), 601(m)(C-Br).GPC: (THF, 40 ^{o}C, 1mL/min), Mn = 29098 g/mol, Mw = 33183 g/mol, PDI = 1.14.

8.4.8. *N*-Octyl-*N'*-(propan-1-ol) naphthalene-1,4,5,8 -tetracarboxylic acid diimide (187)
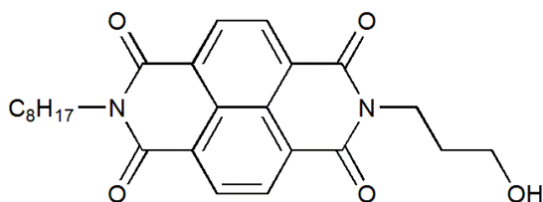
Naphthalene dianhydride **27** (5.0 g, 18.60 mmol) was a stirred in freshly distilled DMF (20 mL) and the slurry was heated to about 140 ℃ under a N_2 atmosphere. Octylamine (3.0 mL, 18.60 mmol) was added dropwise to the mixture over 10 minutes and the reaction mixture was heated under reflux overnight. After complete consumption of naphthalene di-anhydride, 3-amino-1-propanol (1.40 mL, 18.60 mmol) was added and the mixture was left under reflux overnight. After the completion of the reaction, the mixture was allowed to cool and DMF was evaporated under vacuum. The residue was partitioned using DCM/water, and the organic layer was dried over $MgSO_4$. The solution was filtered and the filtrate was evaporated under vacuum. The product was purified by silica gel column chromatography eluting with DCM then DCM:acetone (90:10, v/v) to afford **185** as a white solid in 28 % (2.30 g) yield. M.p. 197-198 ℃. ^{1}H-NMR (δ/ppm, 400 MHz, CDCl$_3$): 8.81 (s, 4H, naphthalene); 4.41 (t, 2H, J = 6.5 Hz, CH$_2$OH); 4.23 (t, 2H, J = 7.6 Hz, CH$_2$); 3.67 (m, 2H, CH$_2$); 2.65 (t, H, J = 6.5 Hz, OH); 2.05 (m, 2H, CH$_2$); 1.77 (m, 2H, CH$_2$); 1.48- 1.27 (m, 10H, CH$_2$); 0.91 (t, 3H, J = 7.0 Hz, CH$_3$). ^{13}C NMR (δ/ppm, 100 MHz, CDCl$_3$): 162.9 (C), 162.8 (C), 162.8 (C), 162.7 (C), 131.3 (CH), 131.0, 130.9, 130.4, 127.1, 127.0, 126.8, 126.7, 126.6, 126.4, 41.1 (CH$_2$), 41.0 (N-CH$_2$), 37.6, 36.4, 31.8, 31.4, 31.0, 29.3, 29.2, 28.1, 27.1, 22.6, 14.1 (CH$_3$). FTIR (ν, cm^{-1}): 3513 (s, sharp, O-H), 3079 (m, C-H aromatic),2923-2853 (s, C-H alkane), 1696 (s, C=O), 1648, 1580 (C=C aromatic), 1454, 1375, 1339 (C-H bending), 1243 (s, C-N), 1084 (s, C-O), 722 (m, C-H rock alkane), 770 (benzene ring). HRMS (ES$^+$): *m/z* 459.1879 [M + H$^+$], calculated 459.1890.

8.4.9. *N*-Octyl-*N'*-(propan-1-methacrylate)naphthalene-1,4,5,8-tetra carboxylic acid diimide (186)
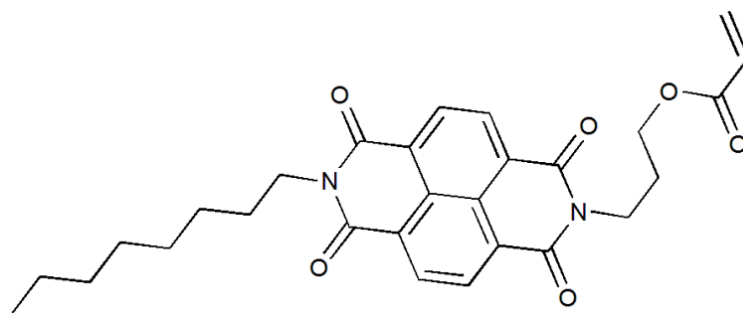
To solution of *N*-octyl-*N'*-(propan-1-ol) naphthalene-1,4,5,8-tetracarboxylic acid diimide **185** (0.70 g, 1.6 mmol) and acrylic acid (0.10 mL, 1.6 mmol) in dry DCM (20 mL) were added 1-ethyl-3-(3-dimethylaminopropyl)carbodiimide (EDCI) (0.30 g, 1.6 mmol) and 4-dimethylaminopyridine (DMAP) (0.20 g, 1.6 mmol). The resulting solution was stirred at room temperature for 24 hrs. The solvent was evaporated under vacuum and the product was purified by silica gel column chromatography eluting with DCM to afford **186** as a white solid in 22% (0.17g) yield. M.p. 137-139 °C. ^{1}H-NMR (δ/ppm, 400 MHz, CDCl$_3$): 8.79 (s, 4H, naphthalene); 6.42 (dd, 1H, *J* = 6.3, 0.7 Hz, CH$_2$=CH); 6.10 (m, 1H, CH$_2$=CH); 5.82 (dd, 1H, *J* = 6.3, 0.7 Hz, CH$_2$=CH); 4.38 (t, 2H, *J* = 7.4 Hz, CH$_2$); 4.33 (t, 2H, *J* = 6.3 Hz, CH$_2$); 4.22 (t, 2H, *J* = 7.4 Hz, CH$_2$); 2.20 (m, 2H, CH$_2$); 1.77 (m, 2H, CH$_2$); 1.50- 1.28 (m, 8H, CH$_2$); 0.90 (t, 3H, *J* = 7.1 Hz, CH$_3$). ^{13}C NMR (δ/ppm, 100 MHz, CDCl$_3$): 166.1, 162.9 (C), 162.8 (C), 131.1 (CH), 131 (CH$_2$), 130.9 (CH), 128.3, 126.8 (CH$_2$), 126.7, 126.4, 62.3 (CH$_2$), 41.1 (CH$_2$), 38.1, 31.8, 29.3, 29.2, 28.1, 27.3, 27.1, 22.7, 14.1 (CH$_3$). FTIR (v, cm^{-1}): 3075-3060 (m, C-H aromatic), 2920-2854 (s, C-H alkane), 1738, 1699 (s, C=O), 1652, 1579 (C=C, aromatic), 1455, 1403, 1374, 1339 (C-H bending), 1247, 1241 (C-N), 1194, 1173, 1074, 1053 (C-O), 770 (benzene ring). HRMS (ES^{+}): *m/z* 491.2182 [M + H^{+}], calculated 491.2183.

8.4.10. *N*-Octyl-*N'*-(propan-1-methacrylate)naphthalene-1,4,5,8-tetra carboxylic acid diimide (186)
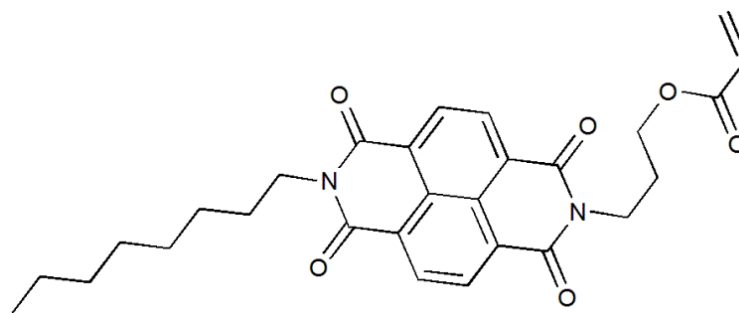
A mixture of *N*-octyl-*N'*-(propan-1-ol) naphthalene-1,4,5,8-tetracarboxylic acid diimide **185** (0.70g, 1.6 mmol), DMAP (0.2 g, 1.6 mmol) and dry THF (150 mL) were stirred at 0 ºC. Triethylamine (0.45 mL, 3.20 mmol) was added followed by acryloyl chloride (0.26 mL, 13.20 mmol) and the resulting solution was stirred at room temperature overnight. The reaction mixture was partitioned between DCM and water; the organic layer was washed with water (3 x 100 mL) and dried over MgSO$_4$. The organic layer was collected and filtrated and the solvent was evaporated under vacuum. The product was purified by silica gel column chromatography eluting with DCM to afforded **186** as a white solid in 57% (0.45 g) yield. M.p. 137-139 ºC. ^{1}H-NMR (δ/ppm, 400 MHz, CDCl$_3$): 8.79 (s, 4H, naphthalene); 6.42 (dd, 1H, *J* = 6.3, 0.7 Hz, CH$_2$=CH); 6.10 (m, 1H, CH$_2$=CH); 5.82 (dd, 1H, *J* = 6.3, 0.7 Hz, CH$_2$=CH); 4.38 (t, 2H, *J* = 7.4 Hz, CH$_2$); 4.33 (t, 2H, *J* = 6.3 Hz, CH$_2$); 4.22 (t, 2H, *J* = 7.4 Hz, CH$_2$); 2.20 (m, 2H, CH$_2$); 1.77 (m, 2H, CH$_2$); 1.50-1.28 (m, 8H, CH$_2$); 0.90 (t, 3H, *J* = 7.1 Hz, CH$_3$). ^{13}C NMR (δ/ppm, 100 MHz, CDCl$_3$): 166.1, 162.9 (C), 162.8 (C), 131.1 (CH), 131 (CH$_2$), 130.9 (CH), 128.3, 126.8 (CH$_2$), 126.7, 126.4, 62.3 (CH$_2$), 41.1 (CH$_2$), 38.1, 31.8, 29.3, 29.2, 28.1, 27.3, 27.1, 22.7, 14.1 (CH$_3$). FTIR (v, cm^{-1}): 3075-3060 (m, C-H aromatic), 2920-2854 (s, C-H alkane), 1738, 1699 (s, C=O), 1652, 1579 (C=C, aromatic), 1455, 1403, 1374, 1339 (C-H bending), 1247, 1241 (C-N), 1194, 1173, 1074, 1053 (C-O), 770 (benzene ring). HRMS (ES$^+$): *m/z* 491.2182 [M + H$^+$], calculated 491.2183.

8.4.11. *N*-Octyl-*N'*-(propan-1-methylmethacrylate)naphthalene-1,4,5,8-tetra-carboxylic acid diimide (187)
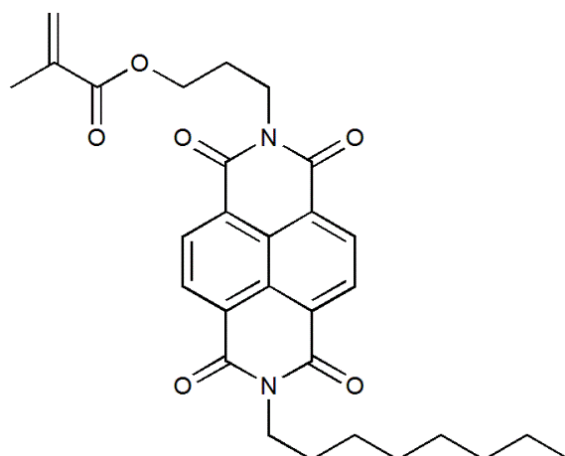
Methacryloyl chloride (0.7 mL, 7.1 mmol) was added dropwise to a stirring solution of *N*-octyl-*N'*-(propan-1-ol)naphthalene-1,4,5,8-tetracarboxylic acid diimide **185** (2.8 g, 6.4 mmol), DMAP (0.8 g, 6.4 mmol) and triethylamine (8.9 mL, 64 mmol) in DCM (50 mL) kept at 0 °C. The reaction was gradually allowed to warm to r.t over 4h, before diluting with DCM (50 mL) and partitioned against distilled water (3 x 100 mL). The organic layer was dried over $MgSO_4$. The organic layer was collected and filtrated and the solvent evaporated under vacuum. The product was purified by silica gel column chromatography eluting with DCM/hexanes/EtOAc (50:50:5) to afforded **187** as a white solid in 65% (2.1 g) yield. M.p. 141-143 °C. ^{1}H-NMR (δ/ppm, 400 MHz, $CDCl_3$): 8.76 (s, 4H, naphthalene), 6.10 (s, 1H), 5.50 (m, 1H), 4.35 (t, *J* = 7.4 Hz, 2H), 4.28 (t, *J* = 6.5 Hz, 2H), 4.19 (t, *J* = 7.4 Hz, 2H), 2.17 (m, 2H), 1.92 (s, 3H), 1.74 (m, 2H), 1.48-1.22 (m, 10H), 0.87 (t, *J* = 6.8 Hz, 3H). ^{13}C NMR (δ/ppm, 100 MHz, $CDCl_3$): 167.5 (C=O methacrylate), 163.0 (C=O x2), 162.9 (C=O x2), 136.6 (C=CH_2), 131.0 (C), 130.9 (C), 127.0 (C x2), 126.9 (C x2), 126.9 (CH x2), 126.7 (CH x2), 125.5 (C=CH_2), 62.6 (OCH_2), 41.3 (CH_2), 38.4 (CH_2), 32.0 (CH_2), 29.5 (CH_2), 29.4 (CH_2), 28.3 (CH_2), 27.8 (CH_2), 27.3 (CH_2), 22.9 (CH_2), 18.4 (CH_3), 14.3 (CH_3). HRMS (ES$^+$): *m/z* 504.2263 [M + H$^+$], calculated 504.2260.

8.4.12. NDI-mono-block polymer (188)
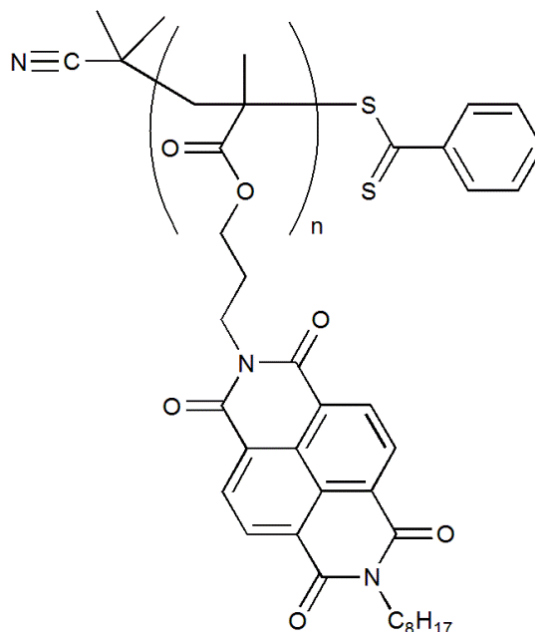
NDI methacrylate **187** (650 mg, 1.3 mmol), AIBN (1.8 mg, 11 μmol) and 2-cyano-2-propyl benzodithioate (9.5 mg, 43 μmol) were added to a flask containing 1,2-dichloro-benzene (2.0 mL). Oxygen was removed from the reaction mixture by freeze-pump-thaw (3 cycles) before sealing under nitrogen gas and placing in an oil bath thermostatically controlled at 70 °C. The reaction was terminated after 1.5h by precipitation into vigorously stirring methanol (250 mL). The pink precipitate was collected by filtration and dried under vacuum before subjecting to Soxhlet extraction in hexane for 4h. The polymer was then extracted using DCM after which the organic solvent was removed by evaporation under vacuum. A second precipitated into methanol (250 mL) afforded the polymer **188** as a pink solid. Yield = 550 mg (84%). GPC results determined the polymer Mw = 10785 g/mol, Mn = 9986 g/mol with PDI = 1.08.

8.5. Synthetic experimental - Chapter 5

8.5.1. *N*-Octyl-*N'*-(anthraquinone) naphthalene-1,4,5,8-tetra carboxylic acid diimide (227)
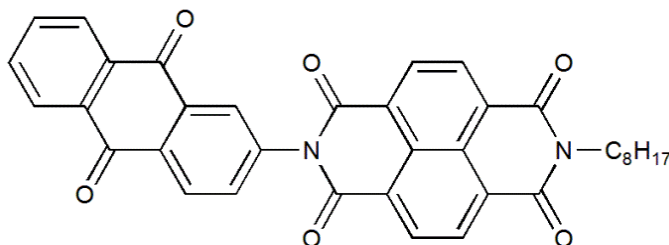
Naphthalene-1,4,5,8-tetracarboxylic dianhydride **27** (5.0 g, 18.60 mmol) was a stirred in freshly distilled DMF (20 mL) and the slurry was heated to about 140 ºC under a N_2 atmosphere. Octylamine (3.0 mL, 18.60 mmol) was added dropwise to the mixture over 10 minutes and the reaction mixture was heated under reflux overnight. After complete consumption of naphthalene dianhydride, 2-aminoanthraquinone **226** (4.15 g, 18.60 mmol) was added and the mixture was left under reflux overnight. After the completion of the reaction, the mixture was allowed to cool and DMF was evaporated under vacuum. The residue was partitioned using DCM/water, and the organic layer was dried over $MgSO_4$. The solution was filtered and the filtrate was evaporated under vacuum. The product was purified by silica gel column chromatography eluting with DCM then DCM:acetone (90:10, v/v) to afford **227** as a brown solid in 1 % (75 mg) yield. M.p. > 300 ºC, ^{1}H-NMR (δ/ppm, 400 MHz, CDCl$_3$): 8.80 (s, 1H, anthraquinone); 8.75 (d, 1H, J = 3.8 Hz, anthra-quinone); 8.64 (t, 1H, J = 7.4 Hz, anthraquinone); 8.28 (m, 2H, anthraquinone); 8.13 (d, 1H, J = 8.2 Hz, naphthalene); 8.0 (s, 1H, naphthalene); 7.8 (m, 1H, naphthalene); 7.74 (m, 1H, naphthalene); 7.43 (d, 1H, J = 2.5 Hz, naphthalene); 6.95 (dd, 1H, J = 8.2, 2.50 Hz, naphthalene); 4.19 (m, 2H, N-CH$_2$); 1.74 (m, 2H, CH$_2$); 1.46-1.25 (m, 10H, CH$_2$); 0.87 (t, 3H, J = 7.0 Hz, CH$_3$). ^{13}C NMR (δ/ppm, 100 MHz, CDCl$_3$): 182.0 (C), 172.2 (C), 165.5 (C), 165.0 (C), 162.8 (C), 154.5 (C), 153.5 (C), 149.7 (C), 142.9 (C), 141.9 (C), 132.9 (CH), 132.2 (C), 130.0 (CH), 127.9 (C), 126.2 (CH), 102 (CH), 99.9 (CH), 96.8 (CH), 94.6 (C), 93.0 (C), 65.8 (C), 45.6 (C), 41.0 (CH), 37.1 (CH$_2$), 33.6 (CH$_2$), 31.8 (CH$_2$), 29.3 (CH$_2$), 28.1 (CH$_2$), 26.5 (CH$_2$), 23.3 (CH$_2$), 14.1 (CH$_3$). FTIR (ν, cm^{-1}): 3074 (m, C-H aromatic), 2959-2851 (C-H, alkane), 1709, 1659 (C=O), 1581 (C=C, m, aromatic), 1338 (C-H), 1290, 1242 (C-N), 1192-1124 (C-O), 769 (C-H benzene ring). HRMS (ES$^+$): *m/z* 607.1817 [M + H$^+$], calculated 607.1840.

8.5.2. *N*-Octyl-*N'*-(propan-1-anthraquinonecarboxylate)naphthal-ene-1,4,5,8-tetracarboxylic acid diimide (229)
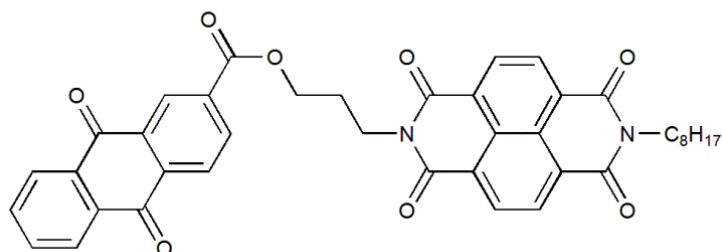
To solution of *N*-octyl-*N'*-(propan-1-ol) naphthalene-1,4,5,8-tetracarboxylic acid diimide **185** (1.0 g, 2.30 mmol) and anthraquinone 2- carboxylic acid **228** (0.57 g, 2.30 mmol) in DMF (50 mL) were added EDCI (0.44 g, 2.30 mmol) and DMAP (0.28 g, 2.30 mmol). The resulting solution was stirred at room temp for 7 days. The solvent was evaporated under vacuum. The product was dissolved in DCM (100 mL) and washed with water (50 mL). The aqueous layer was further extracted with DCM (2 x 100 mL). The organic extracts were combined and dried over $MgSO_4$. The solution was filtered and the filtrate was evaporated under vacuum. The product was purified by silica gel column chromatography eluting with DCM/acetone (90:10, v/v) to afford **229** as a pale yellow solid in 55% (0.84 g) yield. M.p. 198-200 ºC. ^{1}H-NMR (δ/ppm, 400 MHz, $CDCl_3$): 8.63 (m, 4H, naphthalene); 8.54 (s, 1H, anthraquinone); 8.30 (m, 2H, anthraquinone); 8.20 (m, 2H, anthraquinone); 7.83 (m, 2H, anthraquinone); 4.57 (t, 2H, *J* = 6.6 Hz, CH_2); 4.47 (t, 2H, *J* = 6.6 Hz, CH_2); 3.99 (t, 2H, *J* = 6.6 Hz, CH_2); 2.37 (m, 2H, CH_2); 1.64 (m, 2H, CH_2CH_3); 1.39-1.27 (m, 10H, CH_2); 0.87 (t, 3H, *J* = 7.1 Hz, CH_3). ^{13}C NMR (δ/ppm, 100 MHz, $CDCl_3$): 182.1 (C), 181.6 (C), 164.7 (C), 162.9 (C), 162.5 (C), 135.8 (C), 135 (C), 134.5 (CH), 134.5 (CH), 134.4 (CH), 133.2 (C), 133.1 (C), 132.9 (C), 131.0 (CH), 130.8 (CH), 128.0 (CH), 127.5 (CH), 127.4 (CH), 127.3 (CH), 127.0 (C), 126.5 (C), 126.3 (C), 64.5 (CH_2), 40.9 (CH_2), 38.6 (CH_2), 31.8 (CH_2), 29.3 (CH_2), 29.2 (CH_2), 28.0 (CH_2), 27.1 (CH_2), 22.6 (CH_2), 14.1 (CH_3). FTIR (ν, cm^{-1}): 3076-3062 (m, C-H aromatic), 2923, 2852 (s, C-H alkane), 1731, 1702 (s, C=O), 1655, 1594, 1582 (C=C, aromatic), 1454, 1377, 1341 (C-H bending), 1260, 1240 (C-N), 1185, 1166, 1075, 1037 (C-O), 769, 704 (benzene ring). HRMS (ES$^+$): *m/z* 671.2393 [M + H$^+$], calculated 671.2398.

8.5.3. 9,10-Dioxo-9,10-dihydro-2-anthracenecarbonylchloride (231) [229]
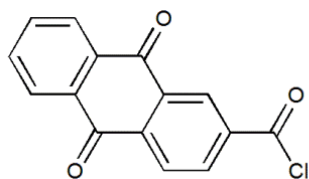
Anthraquinone carboxylic acid **230** (1.0 g, 4 mmol) and (10 mL, 140 mmol) thionyl chloride were heated under reflux for 6 h. The mixture was cooled to room temperature and the excess thionyl chloride was evaporated in vacuum. The residue was dried for 3 h under vacuum and used without further purification to afford **231** as yellow solid in 97% (1.0 g) yield. M.p. 141-143 ºC (lit[5] 143 ºC). ^{1}H-NMR (δ/ppm, 400 MHz, DMSO-d_6): 8.58 (s, 1H, anthraquinone); 8.32 (m, 1H, anthraquinone); 8.24 (m, 1H, anthraquinone); 8.2 (m, 2H, anthraquinone); 7.91 (m, 2H, anthraquinone).

8.5.4. *N*-Octyl-*N'*-(propan-1-anthraquinonecarboxylate)naphthal-ene-1,4,5,8-tetracarboxylic acid diimide (229)
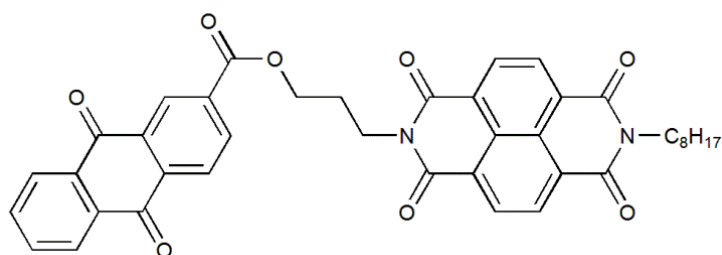
A mixture of *N*-octyl-*N'*-(propan-1-ol) naphthalene-1,4,5,8-tetracarboxylic acid diimide **185** (0.60 g, 1.40 mmol), DMAP (0.17 g, 1.4 mmol) and dry THF (150 mL) was stirred at 0 °C. Triethylamine (0.4 mL, 2.8 mmol) was added followed by 9,10-dioxo-9,10-dihydro-2-anthracenecarbonylchloride **231** (0.75 g, 2.8 mmol) and the resulting solution was stirred at room temperature overnight. The reaction mixture was partitioned between DCM and water; the organic layer was washed with water (3 x 100 mL) and dried over MgSO$_4$. The organic layer was collected, filtrated and the solvent was evaporated under vacuum. The product was purified by silica gel column chromatography eluting with DCM/acetone (90:10, v/v) to afford **229** as a pale yellow solid in 91% (0.85 g) yield. M.p. 198-200 °C. ^{1}H-NMR (δ/ppm, 400 MHz, CDCl$_3$): 8.63 (m, 4H, naphthalene); 8.54 (s, 1H, anthra-quinone); 8.30 (m, 2H, anthraquinone); 8.20 (m, 2H, anthraquinone); 7.83 (m, 2H, anthraquinone); 4.57 (t, 2H, *J* = 6.1 Hz, CH$_2$); 4.47 (t, 2H, *J* = 6.1 Hz, CH$_2$); 3.99 (t, 2H, *J* = 7.7 Hz, CH$_2$); 2.37 (m, 2H, CH$_2$); 1.64 (m, 2H, CH$_2$CH$_3$); 1.39-1.27 (m, 10H, CH$_2$); 0.87 (t, 3H, *J* = 7.1 Hz, CH$_3$). ^{13}C NMR (δ/ppm, 100 MHz, CDCl$_3$): 182.1 (C), 181.6 (C), 164.7 (C), 162.9 (C), 162.4 (C), 135.7 (C), 135 (C), 134.6 (CH), 134.5 (CH), 134.4 (CH), 133.2 (C), 133.1 (C), 132.9 (C), 131 (CH), 130.8 (CH), 128.0 (CH), 127.5 (CH), 127.4 (CH), 127.3 (CH), 126.6 (C), 126.5 (C), 126.3 (C), 64.5 (CH$_2$), 40.9 (CH$_2$), 38.6 (CH$_2$), 31.8 (CH$_2$), 29.3 (CH$_2$), 29.2 (CH$_2$), 28.0 (CH$_2$), 27.1 (CH$_2$), 22.6 (CH$_2$), 14.1 (CH$_3$). FTIR (ν, cm^{-1}): 3076-3062 (m, C-H aromatic), 2923, 2852 (s, C-H alkane), 1731, 1702 (s, C=O), 1655, 1594, 1582 (C=C, aromatic), 1454, 1377, 1341 (C-H bending), 1260, 1240 (C-N), 1185, 1166, 1075, 1037 (C-O), 769, 704 (benzene ring). HRMS (ES$^+$): *m/z* 671.2393 [M + H$^+$], calculated 671.2398.

8.5.5. *N*-Octyl-*N'*-(propan-1-anthraquinonecarboxylate)naphthal-ene-1,4,5,8-tetracarboxylic acid diimide (232)
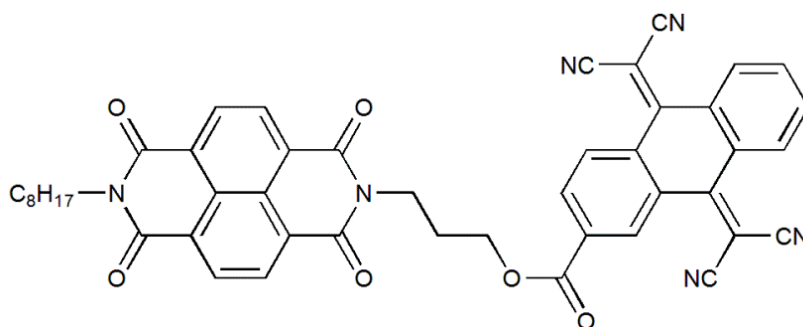
A mixture of *N*-octyl-*N'*-(propan-1-anthraquinonecarboxylate)naphthalene-1,4,5,8-tetra-carboxylic acid diimide **229** (200 mg, 0.30 mmol) and malonitrile (295 mg, 4.50 mmol) in dry CH_2Cl_2 (30 mL) was stirred at 0 °C. Titanium tetrachloride ($TiCl_4$) (0.40 mL) was added followed by pyridine (0.50 mL) and the resulting solution was heated under reflux for 24hrs. After cooling to room temperature, the reaction mixture was added into a large amount of aqueous hydrochloric acid (5%). The product was extracted with $CHCl_3$, and the organic layer was washed with an aqueous $NaHCO_3$ brine and water, separated and dried over Na_2SO_4. The organic layer was collected, filtered and the solvent was evaporated under vacuum. The product was purified by silica gel column chromatography eluting with acetone/petroleum ether (40:60, v/v) to afford **232** as a bright orange solid in 74% (0.17 g) yield. M.p. 190-192 °C. ^{1}H-NMR (δ/ppm, 400 MHz, $CDCl_3$): 9.0 (s, H, anthraquinone); 8.76 (s, 4H, naphthalene); 8.39 (m, 1H ,anthraquinone); 8.30 (m, 3H, anthraquinone); 7.79 (m, 2H, anthraquinone); 4.51 (t, 2H, $J = 6.3$ Hz, CH_2); 4.45 (t, 2H, $J = 6.3$ Hz, CH_2); 4.19 (t, 2H, $J = 7.6$ Hz ,CH_2); 2.30 (m, 2H, CH_2); 1.74 (m, 2H, CH_2CH_3); 1.47-1.26 (m, 10H, CH_2); 0.87 (t, 3H, $J = 7.1$ Hz, CH_3). ^{13}C NMR (δ/ppm, 100 MHz, $CDCl_3$): 162.9 (C), 159.2 (C), 132.9 (CH), 132.8 (CH), 131.2 (CH), 131.0 (CH), 128.6 (CH), 128.0 (C), 127.9 (CH), 127.8 (C), 127.7 (CH), 126.3 (CH), 112.7 (C), 108.8 (CH), 105.3 (C), 98.4 (C), 84.4 (C), 69.7 (C), 63.7 (CH_2), 41.1 (CH_2), 31.8 (CH_2), 29.3 (C), 29.2 (CH_2), 28.1 (C), 27.4 (CH_2), 27.1 (CH_2), 22.7 (CH_2), 14.1 (CH_3). FTIR (ν, cm^{-1}): 3050 (m, C-H aromatic), 2926-2851 (m, C-H, alkane), 2357 (C≡N), 1653, 1594, 1582 (C=C aromatic), 1455, 1377, 1338 (C=H bending), 1260, 1241 (C-N), 1185, 1167, 1075 (C-O), 769-703 (benzene ring). HRMS (ES$^+$): *m/z* 789.2394 [M + H$^+$], calculated 789.2432.

8.6. Synthetic experimental - Chapter 6

8.6.1. *N*-Octyl-naphthalene-1,4,5,8-tetracarboxylic acid diimide (293) [269,300]
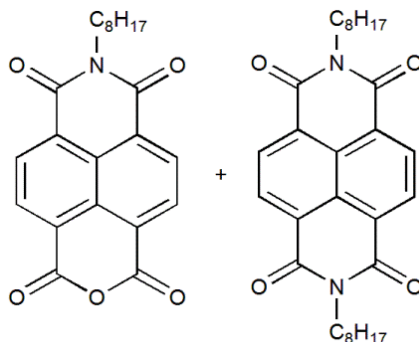
Naphthalene-1,4,5,8-tetracarboxylic dianhydride **27** (10 g, 0.037 mol) was stirred in a freshly distilled DMF (100 mL) and the brownish slurry was heated to about 140 $^{\circ}$C under a N_2 atmosphere. Octylamine (4.82 g, 0.037 mol) was added dropwise to the mixture over 10 minutes and the reaction mixture was heated under reflux for 15 hr and then cooled in the refrigerator at 4 $^{\circ}$C for 2hrs. The white precipitate of diimide was filtered, washed with methanol and dried under vacuum. The oily DMF filtrate was evaporated to near dryness on a rotary evaporator to yield 13.0 g of crude naphthalene-monoimide and dianhydride. The oily residue was purified by silica gel column chromatography eluting with DCM to afford naphthalene-monoimide **293** as a purple solid in 29% (4.0 g) yield. M.p. 172-174 $^{\circ}$C (lit[7] 173-175 $^{\circ}$C). ^{1}H-NMR (δ/ppm, 400 MHz, CDCl$_3$): 8.82 (s, 4H, naphthalene ring); 4.20 (t, 2H, CH$_2$); 1.44-1.22 (m, 12H, CH$_2$, octyl chain); 0.88 (t, 3H, J = 6.6 Hz, CH$_3$). Mass spectrum [M + H]$^+$ = 380.8. Naphthalene-diimide **294** was afforded as a white solid in 21% (3.80 g) yield. M.p.184-186 $^{\circ}$C (lit[7-8] 184-187 $^{\circ}$C). ^{1}H-NMR (δ/ppm, 400 MHz, CDCl$_3$): 8.81 (s, 8H, naphthalene ring); 4.20 (t, 4H, CH$_2$); 1.42-1.28 (m, 24H, CH$_2$, octyl chain); 0.88 (t, 6H, J = 6.6 Hz, CH$_3$). Mass spectrum [M + H$^+$] = 491.3.

8.6.2. 2-Octyl-anthraquinone-benzimidazo[2,1-*b*]benzo[*lmn*][3,8] phenan-throline-1,3,6(2*H*)-trione (296)
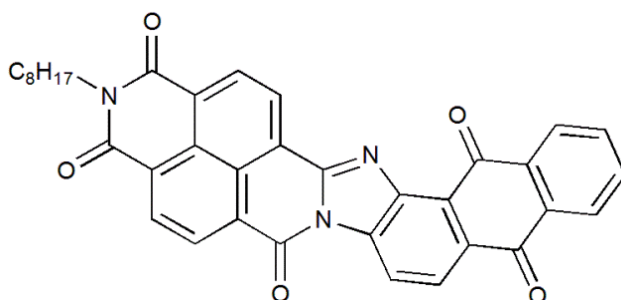
A mixture of *N*-octyl-naphthalene-1,4,5,8-tetracarboxylic acid diimide **293** (200 mg, 0.53 mmol), 1,2-diaminoanthraquinone **295** (300 mg, 1.26 mmol), and imidazole (3.0 g, 45.60 mmol) was heated under reflux at 180 ℃ for 2hrs under an nitrogen atmosphere. The crude mixture was cooled to room temperature and washed out of reaction vessel with ethanol (200 mL). Then, 2N HCl solution (100 mL) was slowly added and the solution was stirred at room temperature for 1 hr. The reaction mixture was extracted with DCM (5 x 25 mL). The organic extracts were combined and dried over $MgSO_4$. The solution was filtered and the filtrate was evaporated under vacuum. The product was purified by silica gel column chromatography eluting with DCM then DCM/ethyl acetate (9.5:0.5,v/v) to afford **296** as an black solid in 59% (180 mg) yield. M.p. > 300 ℃. ^{1}H-NMR (δ/ppm, 400 MHz, $CDCl_3$): 9.32 (d, 1H, *J* = 7.7 Hz, anthraquinone); 8.8 (dd, 2H, *J* = 8.1, 1.8 Hz, anthra-quinone); 8.86 (m, 2H, anthraquinone); 8.56 (d, 1H, *J* = 8.8 Hz, anthraquinone); 8.41 (dd, 1H, *J* = 6.6, 1.8 Hz, naphthalene); 8.34 (dd, 1H, *J* = 6.6, 1.8 Hz, naphthalene); 7.85 (m, 2H, naphthalene); 4.21 (t, 2H, *J* = 7.8 Hz, N-CH_2); 1.76 (m, 2H, CH_2); 1.45-1.24 (m, 10H, CH_2); 0.88 (m, 3H,CH_3). ^{13}C NMR (δ/ppm, 100 MHz, $CDCl_3$): 185.0 (C), 179.2 (C), 164.8 (C), 163.0 (C), 161.4 (C), 154.5 (C), 152.5 (C), 152.2 (C), 146.8 (C), 144.2 (C), 134.6 (CH), 132.0 (C) , 123.3 (CH), 111.5 (C), 107.5 (CH), 97.1 (CH), 95.3 (CH), 93.5 (CH), 92.4 (C), 83.4 (C), 65.3 (C), 42.7 (C), 41.9 (CH), 35.5 (CH_2), 34.5 (CH_2), 32.9 (CH_2), 31.2 (CH_2), 27.0 (CH_2), 25.6 (CH_2), 23.5 (CH_2), 14.1 (CH_3). FTIR (v, cm^{-1}): 3057 (m, C-H aromatic), 2922-2848 (C-H, alkane), 1709, 1666 (C=O), 1639-1587 (C=C, m, aromatic), 1485-1360 (C-H), 1282, 1220 (C-N), 1192-1124 (C-O), 735 (C-H benzene ring). HRMS (ES$^+$): *m/z* 604.1825 [M + H$^+$], calculated 604.1843.

8.6.3. 2-Octyl-malonitrile-benzimidazo[2,1-*b*]benzo[*lmn*] [3,8] phenan-throline-1,3,6(2*H*)-trione (297)
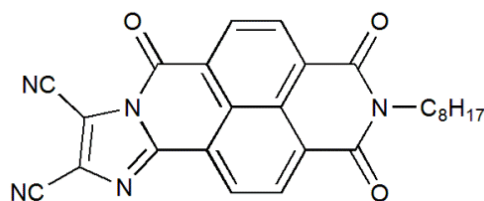
A mixture of *N*-octyl-naphthalene-1,4,5,8-tetracarboxylic acid diimide **293** (500 mg, 1.31 mmol), diaminomalonitrile (143 mg, 1.32 mmol), and imidazole (2.35 g) was heated under reflux at 180 ℃ for 2 hrs. under a nitrogen atmosphere. The crude mixture was cooled to room temperature and 18% HCl solution was slowly added. The reaction mixture was extracted with DCM (3 x 100 mL). The organic extracts were combined and dried over MgSO$_4$, filtered and the filtrate was evaporated under vacuum. The product was purified by silica gel column chromatography eluting with DCM to afford **297** as an orange solid in 5% (30 mg) yield. M.p. 252-254 ℃. ^{1}H-NMR (δ/ppm, 400 MHz, CDCl$_3$): 9.03 (s, 1H, naphthalene); 8.94 (d, 1H, *J* = 6.8 Hz, naphthalene); 8.77 (d, 1H, *J* = 6.8 Hz, naphthalene); 8.47 (s, 1H, naphthalene); 4.20 (m, 2H, N-CH$_2$); 1.74 (m, 2H, CH$_2$); 1.45-1.23 (m, 10H, CH$_2$); 0.88 (t, 3H, *J* = 6.8 Hz, CH$_3$). ^{13}C NMR (δ/ppm, 100 MHz, CDCl$_3$): 184.0 (C), 165.1 (C), 162.9 (C), 158.5 (C), 146.6 (C), 143.8 (C), 142.8 (C), 141.9 (C), 139.9 (CH), 138.8 (CH), 135.2 (C), 135.0 (CH), 130.0 (C), 128.9 (C), 128.0 (C), 126.2 (C), 122.0 (C), 121.8 (C), 111.0 (C), 102.3 (C), 41.5 (CH$_2$), 32.1 (CH$_2$), 29.4 (CH$_2$), 28.8 (CH$_2$), 27.7 (CH$_2$), 26.7 (CH$_2$), 23.3 (CH$_2$), 14.1 (CH$_3$). FTIR (ν, cm^{-1}): 3080 (m, C-H aromatic), 2927-2855 (s, C-H alkane), 2241 (m, C≡N), 1709, 1664 (s, C=O), 1581-1452 (C=C, aromatic), 1373, 1348 (C-H), 1246 (C-N), 739 (benzene ring).Mass spectrum [M + H$^+$] = 452.3.

8.6.4. 2,1,3-Benzothiadiazole (298)[270]
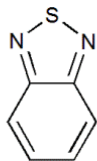
Phenylenediamine (5.0 g, 46.25 mmol), triethylamine (18.7 g, 185 mmol) and dry CH_2Cl_2 (150 mL) was stirred and thionyl chloride (92.45 mmol, 7.0 mL) was added dropwise very slowly. The mixture was heated under reflux for 5 hr. The solvent was removed under vacuum, and water (350 mL) was added. Concentrated HCl was added until the pH of solution was reached to 1, and water was added to the reaction mixture. The product was extracted with CH_2Cl_2 (5 x 100 mL), and the organic layer was washed with aqueous $NaHCO_3$ brine and water and dried over $MgSO_4$. The organic layer was collected, filtrated and the solvent was evaporated under vacuum to afford **298** as a brown solid in 93% (5.80 g) yield. M.p. 43-45 °C (lit.[9] 43.6-44.4 °C). ^{1}H-NMR (δ/ppm, 400 MHz, CDCl$_3$): 7.99 (dd, 2H, $J = 3.2$, 5.7 Hz); 7.57 (dd, 2H, $J = 3.2$, 5.7 Hz).

8.6.5. 4,7-Dibromo-2,1,3-benzothiadiazole (299) [270]
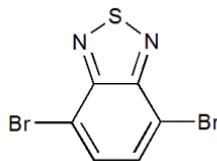
Benzothiadiazole **298** (5.0 g, 36.70 mmol) and HBr (75 mL) was stirred and a solution containing Br_2 (17.6 g, 110.2 mmol) in HBr (100 mL) was added dropwise very slowly. The solution was heated under reflux for 6 hr. The mixture was cooled to room temperature; and the resulting solid was filtered under vacuum. The product was washed with water and diethyl ether. The product was dried under vacuum for 20 hrs. to afford **299** as a light brown solid in a 95% (10.20 g) yield. M.p. 188-189 °C (lit[9] 189-190 °C). ^{1}H-NMR (δ/ppm, 400 MHz, DMSO-d_6): 7.74 (s, 2 H).

8.6.6. 3,6-Dibromo-1,2-phenylenediamine (300)[271]
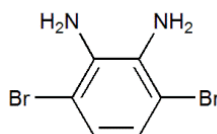
To a mixture of acetic acid (14 mL) and water (6.0 mL) and 4,7-dibromobenzothadiazole **299** (2.0 g , 6.8 mmol), Zn dust (4.0 g, 61.2 mmol) was added at once and stirred for 3hrs. at 60 °C. After filtration, the brown solution was poured into Aqueous NaOH- solution (50%) (60 mL) and cooled. The solution was extracted with diethyl ether and dried over $MgSO_4$. The organic layer was collected and filtrated and the solvent was evaporated under vacuum to afford **300** as white needles in 69% (1.24 g) yield. M.p. 88-90 °C (lit[10] 92-94 °C). ^{1}H-NMR (δ/ppm, 400 MHz, $CDCl_3$): 6.88 (s, 2H, CH aromatic), 3.92 (s, 4H, NH_2).

8.6.7. 8,11-Dibromo-2-octyl-benzimidazo[2,1-*b*]benzo[*lmn*][3,8] phenanthroline-1,3,6(2*H*)-trione (301)
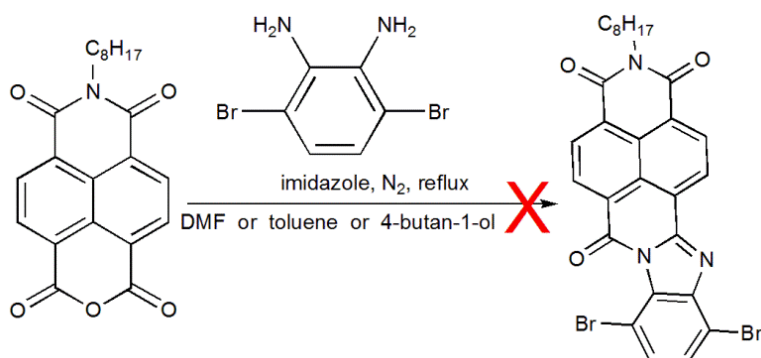
A mixture of 3,6-dibromo-1,2-phenylenediamine **300** (600 mg, 2.25 mmol), *N*-octyl-naphthalene-1,4,5,8-tetracarboxylic acid diimide **293** (940 mg, 2.5 mmol) and imidazole (4.44 g) was dissolved in DMF or toluene or 4-butan-1-ol (50 mL) . The mixture reaction was heated under reflux for 2 hrs under a nitrogen atmosphere. The crude mixture was cooled to room temperature and 18% HCl solution was slowly added. The reaction mixture was extracted with DCM (5 x 50 mL). The organic extracts were combined and dried over MgSO$_4$. The solution was filtered and the filtrate was evaporated under vacuum. The product was purified by silica gel column chromatography eluting with DCM to afford orange solid. TLC, mass spectrum and ^{1}H NMR showed no reaction.

8.6.8. 8,11-Dibromo-2-octyl-benzimidazo[2,1-*b*]benzo[*lmn*][3,8] phenan-throline-1,3,6(2*H*)-trione (301)[260]
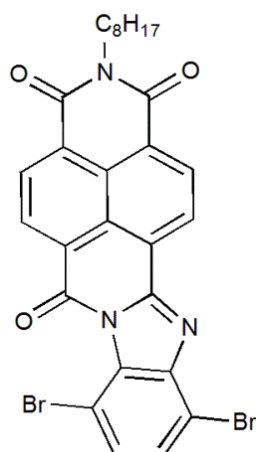
A mixture of 3,6-dibromo-1,2-phenylenediamine **300** (420 mg, 1.6 mmol), *N*-octyl-naphthalene-1,4,5,8 -tetracarboxylic acid diimide **293** (660 mg, 1.74 mmol) and imidazole (3.11 g) was heated under reflux at 180 ℃ for 2hrs under an nitrogen atmosphere. The crude mixture was cooled to room temperature and 18 % HCl solution was slowly added. The reaction mixture was extracted with DCM (5 x 50 mL). The organic extracts were combined and dried over $MgSO_4$. The solution was filtered and the filtrate was evaporated under vacuum. The product was purified by silica gel column chromatography eluting with DCM to afford **301** as an orange solid in 45% (0.45 g) yield. M.p. 247-249 ℃ (lit[11] 247-248 ℃). ^{1}H-NMR (δ/ppm, 400 MHz, CDCl$_3$): 9.04 (d, 1H, *J* = 7.8 Hz, naphthalene); 8.89 (d, 1H, *J* = 7.8 Hz, naphthalene); 8.80 (m, 2H, naphthalene); 7.62 (d, 1H, *J* = 8.4 Hz, phenyl); 7.55 (d, 1H, *J* = 8.4 Hz, phenyl); 4.23 (t, 2H, *J* = 7.6 Hz, N-CH$_2$); 1.79 (m, 2H, CH$_2$); 1.52-1.28 (m, 10H, CH$_2$); 0.91 (t, 3H, *J* = 7.1 Hz, CH$_3$). HRMS (ES$^+$): *m/z* 610.0166 [M + H$^+$], calculated 610.0171.

8.6.9. 2-Octyl-8,11-di-2-thienyl-benzimidazo[2,1*b*]benzo[*lmn*][3,8] phenan-throline-1,3,6(2*H*)-trione (302)[260]
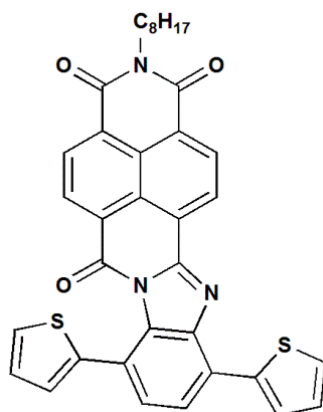
A mixture of 8,11-dibromo-2-octyl-benzimidazo [2,1b] benzo [*lmn*] [3,8] phenanthroline-1,3,6 (2H)- trione **301** (250 mg, 0.40 mmol), 2-(tributylstannyl) thiophene (368 mg, 0.98 mmol), $PdCl_2(PPh_3)_2$ (10 mg) and dry THF (25 mL) was heated under reflux for 24 hrs. under an nitrogen atmosphere. Upon cooling, the solvent was evaporated under vacuum. The crude product was purified by flash silica gel column chromatography eluting with DCM to afford **302** as a deep brown solid in 73% (190 mg) yield. M.p. 242-244 °C (lit[11] 242-243 °C). ^{1}H-NMR (δ/ppm, 400 MHz, CDCl$_3$): 8.90 (d, 1H, *J* = 7.8 Hz, naphthalene); 8.69 (d, 1H, *J* = 7.8 Hz, naphthalene); 8.63 (s, 2H, naphthalene); 8.1 (dd, 1H, *J* = 3.8, 1.0 Hz, thiophene); 7.71 (d, 1H, *J* = 8.0 Hz, thiophene); 7.49 (m, 3H, *Ph and Th*); 7.20 (m, 2H, thiophene); 7.1 (dd, 1H, *J* = 3.8 Hz, 1.0 Hz, thiophene); 4.19 (t, 2H, *J* = 7.4 Hz, N-CH$_2$); 1.76 (m, 2H, CH$_2$); 1.50-1.26 (m, 10H, CH$_2$); 0.88 (t, 3H, *J* = 6.79 Hz, CH$_3$). Mass spectrum [M + H$^+$] = 616.1.

8.6.10. 2-Octyl-8,11-di-2-(5-dibromo)thienyl-benzimidazo[2,1*b*] benzo[*lmn*] [3,8]phenanthroline-1,3,6(2*H*)-trione (303)
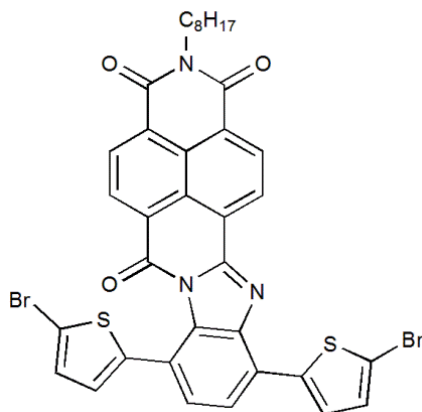
2-Octyl-8,11-di-2-thienyl-benzimidazo[2,1b]benzo[*lmn*][3,8]phenanthroline-1,3,6-(2H)-trione **302** (150 mg, 0.24 mmol) and *N*-bromosuccinimide (173 mg, 0.97 mmol) were dissolved in dry THF (25 mL). The mixture was stirred under reflux overnight. Upon cooling, the solvent was evaporated under vacuum. The crude product was purified by flash silica gel column chromatography eluting with DCM to afford **303** as a dark red solid in 97% (195 mg) yield. M.p. 262-264 ºC. ^{1}H-NMR (δ/ppm, 400 MHz, CDCl$_3$): 8.86 (d, 1H, J = 7.4 Hz, naphthalene); 8.68 (d, 3H, J = 7.4 Hz, naphthalene); 7.67 (d, 1H, J = 4.0 Hz, thiophene); 7.61 (d, 1H, J = 8.0 Hz, phenyl); 7.43 (d, 1H, J = 8.0 Hz, phenyl); 7.13 (dd, 2H, J = 3.8, 0.8 Hz, thiophene); 6.81 (d, 1H, J = 3.8 Hz, thiophene); 4.19 (t, 2H, J = 7.8 Hz, N-CH$_2$); 1.77 (m, 2H, CH$_2$); 1.47-1.25 (m, 10H, CH$_2$); 0.88 (m, 3H, CH$_3$). ^{13}C NMR (δ/ppm, 100 MHz, CDCl$_3$): 172.3 (C), 162.9 (C), 162.9 (C), 162.7 (C), 157.6 (C), 148.8 (C), 143.6 (C), 141.0 (C), 140.0 (C), 131.4 (CH), 130.9 (CH), 130.7 (CH), 130.3 (CH), 129.7 (CH), 128.6 (CH), 127.3 (C), 127.1 (CH), 126.9 (CH), 126.7 (C), 124.6 (CH), 122.1 (CH), 115.5 (C), 113.6 (C), 110.9 (C), 97.1 (C), 91.3, 81.8 (C), 61.6 (C), 41.0 (CH$_2$), 31.8 (CH$_2$), 29.3 (CH$_2$), 29.2 (CH$_2$), 28.2 (CH$_2$), 27.2 (CH$_2$), 22.7 (CH$_2$), 14.1 (CH$_3$). FTIR (ν, cm^{-1}): 3074 (m, C-H aromatic), 2959-2853 (C-H, alkane), 1719, 1705 (C=O), 1666, 1580 (C=C, m, aromatic), 1376-1305 (C-H), 1296 (C-N), 1168, 1084 (C-O), 758 (benzene ring), 733 (C-Br). HRMS (ES$^+$): *m/z* 773.9921 [M + H$^+$], calculated 773.9945.

8.6.11. Poly–((2,'2-(5,'5-(phenylene-naphthalenediimide)thienyl-ene))-2,7-(9,'9-dioctylflurene)) (311)
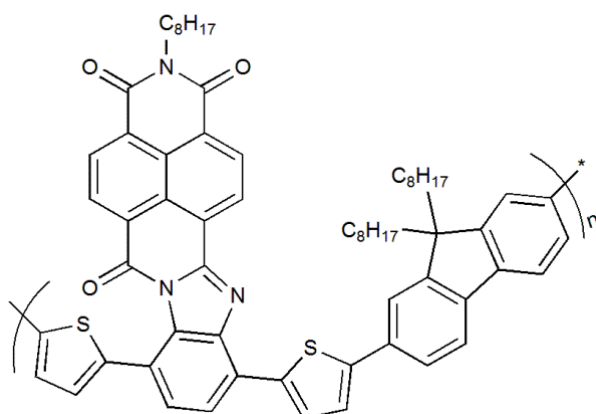
2-Octyl-8,11-di-2-(5-dibromo)thienyl-benzimidazo[2,1b]benzo[*lmn*][3,8]phenanthroline-1,3,6 (2H)-trione **303** (300 mg, 0.38 mmol), 9,9-dioctylfluorene-2,7-bis (trimethylborate) **309** (239 mg, 0.43 mmol) and Pd(PPh$_3$)$_4$ (20 mg, 0.02 mmol) were dissolved in a degassed mixture of aqueous Na$_2$CO$_3$ (430 mg, in 2.0 mL of water), n-butanol (2.0 mL), toluene (10 mL) and THF (10 mL). The mixture was stirred under reflux for 3 days. After cooling to room temperature 2N aqueous HCl (20 mL) was added. The reaction mixture was extracted with CH$_3$Cl (5 x 50 mL). The organic extracts were combined and washed with 2N aqueous HCl and saturated NaHCO$_3$ solution respectively. The organic layers were combined and dried over Na$_2$SO$_4$. The solution was filtered and the filtrate was evaporated in vacuum. The polymer was dissolved in CH$_3$Cl and then precipitated into mixture of methanol and 2N aqueous HCl (10:1, v/v). The polymer was collected by filtration and extracted in a Soxhlet apparatus with methanol, acetone, CH$_3$Cl, and toluene to remove the impurities and oligomers. The resulting polymer was dissolved in the minimum amount of THF and precipitated in methanol to give the pure product. The polymer was then dried under high vacuum for 24 hours to yielded polymer **311** as a green powder in 17% (50 mg) yield. ^{1}H-NMR (δ/ppm, 400 MHz, CDCl$_3$): 8.36 (m, br, naphthalene); 8.01-7.18 (m, br, phenyl and thiophene); 6.90 (s, br, thiophene); 6.77 (m, br, thiophene); 4.19 (m, N-CH$_2$); 1.73 (m, br, CH$_2$); 1.43-0.99 (m, br, CH$_2$); 0.89 (m, br, CH$_3$); 0.79 (m, br, CH$_3$). GPC: (THF, 40 °C, 1mL/min), *Mn* = 33015 *g/mol*, *Mw* = 42469 *g/mol*, *PDI* = 1.28.

8.6.12. 10-Bromo-2-octyl-benzimidazo[2,1-b]benzo[*lmn*][3,8] phenanthroline-1,3,6(2H)-trione (307 and 308)
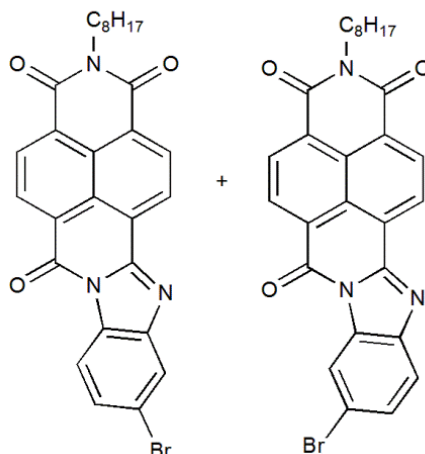
A mixture of 4-bromo-1, 2-diaminobenzene (0.50 g, 2.66 mmol), *N*-octyl- naphthalene-1,4,5,8 -tetracarboxylic acid diimide **293** (1.0 g, 2.63 mmol) and imidazole (4.70 g) were heated under reflux at 180 ºC for 2 hrs. under an nitrogen atmosphere. The crude mixture was cooled to room temperature and a 18 % HCl solution was slowly added. The reaction mixture was extracted with DCM (3 x 100 mL). The organic extracts were combined and dried over $MgSO_4$. The solution was filtered and the filtrate was evaporated under vacuum. The product was purified by silica gel column chromatography eluting with DCM to afford **308** as an orange solid in 10% (0.16 g) yield, M.p. 212-214 ºC, and **307** as a yellow solid in 8% (0.11 g) yield, M.p. 212-213 ºC. For both isomer, ^{1}H-NMR (δ/ppm, 400 MHz, CDCl$_3$): 8.93 (t, 2H, *J* = 9.6 Hz, naphthalene); 8.81 (t, 2H, *J* = 9.6 Hz, naphthalene); 8.39 (d, 1H, *J* = 8.5 Hz, phenyl); 8.0 (s, 1H, phenyl); 7.63 (d, 1H, *J* = 8.5 Hz, phenyl); 4.21 (t, 2H, *J* = 7.2 Hz, N-CH$_2$); 1.76 (m, 2H, CH$_2$); 1.48-1.22 (m, 10H, CH$_2$); 0.88 (m, 3H, CH$_3$). ^{13}C NMR (δ/ppm, 100 MHz, CDCl$_3$): 182.0 (C), 162.8 (C), 162.6 (C), 131.6 (CH), 131.4 (CH), 131.0 (C), 130.9 (CH), 129.9 (C), 129.8 (CH), 127.1 (CH), 123.7 (CH), 116.9 (CH), 98.4 (C), 83.4 (C), 65.3 (C), 41.2 (C), 41.1 (CH), 31.9 (CH$_2$), 31.8 (CH$_2$), 29.7 (CH$_2$), 29.3 (CH$_2$), 28.1 (CH$_2$), 27.1 (CH$_2$), 22.6 (CH$_2$), 14.1 (CH$_3$). FTIR (ν, cm^{-1}): 3072 (m, C-H aromatic), 2930-2850 (C-H, alkane), 1704, 1661 (C=O), 1576-1418 (C=C, m, aromatic), 1376-1305 (C-H), 1239-1254 (C-N), 1168, 1084 (C-O), 1616 (C=N), 601 (C-Br), 722 (C-H benzene ring). MS (MALDI) = *m/z* 531.425 [M + H$^+$], calculated 531.420.

8.6.13. 10-(4-Ethynyl-*N,N*-dimethylaniline)-2-octyl-benzimidazo[2,1*b*]benzo [*lmn*][3,8]phenanthroline-1,3,6(2*H*)-trione
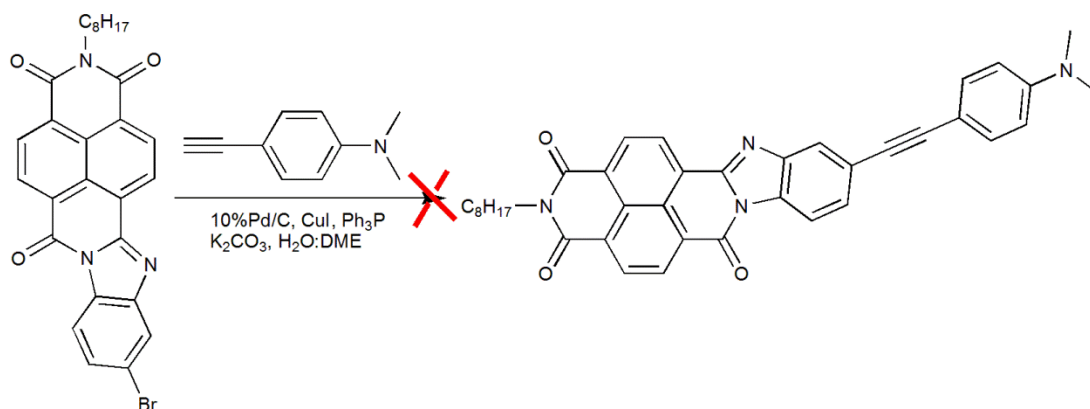
10-Bromo-2-octyl-benzimidazo[2,1-b]benzo[*lmn*][3,8]phenanthroline-1,3,6(2H)-trione **307** or **308** (220 mg, 0.38 mmol), 10% Pd/C (8.0 mg, 0.75 mmol), CuI (29 mg, 0.15 mmol), Ph$_3$P (79 mg, 0.30 mmol), and K$_2$CO$_3$ (130 mg, 0.094 mmol) were mixed in a 1:1 solution of water and dimethoxymethane (15 mL).The mixture was degassed with N$_2$ for 5 minutes and stirred for 30 minutes under N$_2$. 4-Ethynyl-*N,N*-dimethylaniline (78 mg, 0.53 mmol) was then added, and the mixture was heated to 80 °C for 5 hrs. After cooling, the reaction mixture was extracted with DCM (3 x 100 mL). The organic extracts were combined and dried over MgSO$_4$. The solution was filtered and the filtrate was evaporated under vacuum. The product was purified by silica gel column chromatography eluting with DCM/pet.ether (80:20,v/v) to afford a yellow solid. TLC, mass spectrum and ^{1}H NMR showed no reaction.

8.6.14. 2-Octyl-8-bromo,11-2-(3,4-ethylenedioxythiophene)-benz-imidazo[2, 1*b*]benzo[3,8]phenanthroline-1,3,6(2*H*)-trione (306)
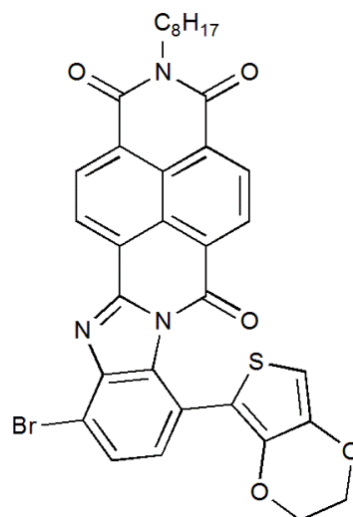
A mixture of 8,11-dibromo-2-octyl-benzimidazo[2,1b]benzo[3,8]phenanthroline-1,3,6 (2H)-trione **301** (100 mg, 0.16 mmol), 2-(tributylstannyl)3,4-ethylenedioxythiophene (167 mg, 0.41 mmol), PdCl$_2$(PPh$_3$)$_2$ (5 mg) and dry THF (25 mL) was heated under reflux for 24 hrs. under an nitrogen atmosphere. Upon cooling, the solvent was evaporated under vacuum. The crude product was purified by flash silica gel column chromatography eluting with DCM/petroleum ether (80:20, v/v) to afford **306** as a brown solid in 14 % (20 mg) yield. M.p 267-269 °C. ^{1}H-NMR (δ/ppm, 400 MHz, CDCl$_3$): 9.1 (d, 1H, J = 7.8 Hz, naphthalene); 8.75 (m, 3H, naphthalene); 7.71 (d, 1H, J = 8.2 Hz, phenyl); 7.43 (d, 1H, J = 8.2 Hz, phenyl); 6.53 (s, 1H, thiophene); 4.21 (t, 2H, J = 7.8 Hz, N-CH$_2$); 4.13 (m, 2H, CH$_2$, EDOT); 3.91 (m, 2H, CH$_2$, EDOT); 1.75 (m, 2H, CH$_2$); 1.47-1.25 (m, 10H, CH$_2$); 0.87 (t, 3H, J = 7.0 Hz, CH$_3$). ^{13}C NMR (δ/ppm, 100 MHz, CDCl$_3$): 178.5 (C), 162.8 (C), 162.9 (C), 160.7 (C), 144.0 (C), 141.1 (C), 134.5 (C), 134.0 (C), 131.7 (C), 131.0 (CH), 130.4 (CH), 130.4 (CH), 130.2 (CH), 129.5 (CH), 127.6 (CH), 127.4 (C) ,125.7 (CH), 124.8 (CH), 114.0 (C), 108.2 (C), 101.8 (C), 99.1 (C), 92.6, 64.9 (CH), 40.9 (CH$_2$), 31.8 (CH$_2$), 29.3 (CH$_2$), 29.2 (CH$_2$), 28.2 (CH$_2$), 27.1 (CH$_2$), 22.6 (CH$_2$), 14.1 (CH$_3$). FTIR (ν, cm^{-1}): 3106 (m, C-H aromatic), 2953-2853 (C-H, alkane), 1705, 1663 (C=O), 1581, 1506 (C=C, m, aromatic), 1302-1244 (C-N), 1171, 1067 (C-O), 756 (C-H benzene ring), 601 (C-Br). HRMS (ES$^+$): m/z 692.0792 [M + H$^+$], calculated 692.0825.

8.6.15. Electrochemical polymerisation of compound (302)
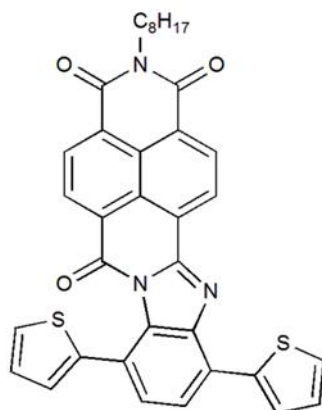
The electrochemical polymerisation of the monomer **302** on to a glassy carbon working electrode surface was achieved. The conditions are described briefly below.

The electrolyte solutions (0.1M) were prepared from Bu_4NPF_6 and dry toluene and acetonitrile. A three-electrode configuration was used with a glassy carbon disc working electrode, a silver wire reference electrode and a platinum wire as the counter electrode. Cyclic voltammetry of the monomer **302** and polymer **312** films grown on the carbon electrode were measured using 0.4 g/L solution of monomer **302** in acetonitrile: toluene (1:1) solution. The electrochemical experiments were referenced to ferrocene, which has a HOMO of -4.8 eV, and the HOMO and LUMO of the polymer has been estimated from the onset of the corresponding reduction/oxidation waves.

8.7. Synthetic experimental - Chapter 7

8.7.1. *N*-Octyl-*N'*-(pyridyl)naphthalene-1,4,5,8-tetracarboxylic acid diimide (334)
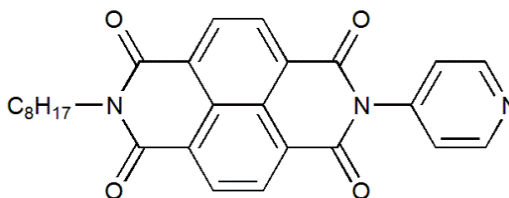
A mixture of naphthalene-1,4,5,8-tetracarboxylic dianhydride **27** (3.0 g, 11.2 mmol), 4-aminopyridine (2.1 g, 22.3 mmol) and octylamine (1.8 mL, 11.2 mmol) was a stirred in freshly distilled DMF (400 mL) and the slurry was heated to about 90 ºC under a N_2 atmosphere for 12 hrs. The reaction mixture was precipitated into water (1 L). The solution was filtered to afford a pink solid. The resulting product was dispersed in minimum DCM and filtered. The filtered solution was purified by silica gel column chromatography eluting with DCM, then DCM:acetone (90:10, v/v) to afford **334** as a white solid in 37% (1.9 g) yield. M.p. 250-252 ºC. ^{1}H-NMR (δ/ppm, 400 MHz, CDCl$_3$): 8.86 (dd, 2H, J = 4.5, 1.5 Hz, pyridine); 8.82 (s, 4H, naphthalene); 7.32 (dd, 2H, J = 4.5, 1.5 Hz, pyridine); 4.21 (t, 2H, J = 7.7 Hz, CH$_2$); 1.76 (m, 2H, CH$_2$); 1.48-1.25 (m , 10H, CH$_2$); 0.88 (t, 3H, J = 7.1 Hz, CH$_3$). ^{13}C NMR (δ/ppm, 100 MHz, CDCl$_3$): 162.6 (C), 162.3 (C), 151.3 (CH), 142.5 (C), 131.6 (CH), 131.1 (CH), 127.3 (C), 127.1 (C), 126.9 (C), 126.2 (C), 123.8 (CH), 41.1 (CH$_2$), 31.8 (CH$_2$), 29.3 (CH$_2$), 29.2 (CH$_2$), 28.1 (CH$_2$), 27.1 (CH$_2$), 22.6 (CH$_2$), 14.1 (CH$_3$). FTIR (v, cm^{-1}): 3655, 3371 (H-C=N and H-C=C), 3076 (m, C-H aromatic), 2924-2852 (s, C-H alkane), 1722-1656 (m, C=O), 1581-1452 (m, C=C aromatic), 1371-1346 (C-H), 1244 (C-N), 767 (benzene ring). HRMS (ES$^+$): *m/z* 456.1923 [M + H$^+$], calculated 456.1919.

8.7.2. *N*-Octyl-*N'*-(phthalonitrile) naphthalene-1,4,5,8-tetra-carboxylic acid diimide (329)
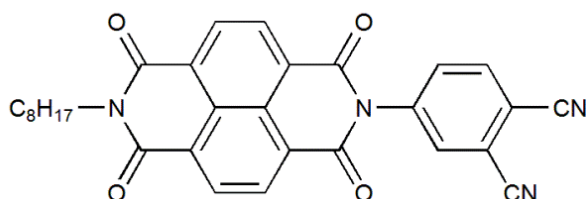
Naphthalene-1,4,5,8-tetracarboxylic dianhydride **27** (10 g, 37.3 mmol) was a stirred in freshly distilled DMF (25 mL) and the slurry was heated to about 140 ℃ under a N_2 atmosphere. Octylamine (6.0 mL, 37.3 mmol) was added dropwise to the mixture over 10 minutes and the reaction mixture was heated under reflux overnight. After complete consumption of naphthalene dianhydride, 4-aminophthalonitrile (5.34 g, 37.3 mmol) was added and the mixture was left under reflux overnight. After the completion of the reaction, the mixture was allowed to cool and DMF was evaporated under vacuum. The residue was partitioned using DCM/water, and the organic layer was dried over $MgSO_4$. The solution was filtered and the filtrate was evaporated under vacuum. The product was purified by silica gel column chromatography eluting with DCM then DCM:acetone (90:10, v/v) to afford **329** as a yellow solid in 30% (5.60 g) yield. M.p. 289-291 ℃. ^{1}H-NMR (δ/ppm, 400 MHz, $CDCl_3$): 8.83 (s, 4H, naphthalene); 8.83 (d, 1H, *J* = 8.5 Hz, phenyl); 7.84 (d, 1H, *J* = 1.8 Hz, phenyl); 7.76 (dd, 1H, *J* = 4.1, 1.8 Hz, phenyl); 4.21 (t, 2H, *J* = 7.7 Hz, CH_2) 1.76 (m, 2H, CH_2); 1.47-1.25 (m, 10H, CH_2); 0.88 (t, 3H, *J* = 7.0 Hz, CH_3). ^{13}C NMR (δ/ppm, 100 MHz, $CDCl_3$): 162.4 (C=O), 162.3 (C=O), 139 (C) , 134.5 (CH), 134.4 (CH), 134.2 (CH), 132.0 (CH), 131.1 (CH), 127.7 (C), 127.0 (C), 126.9 (C), 125.6 (C), 117.3 (C), 116.4 (C), 114.7 (C), 114.4 (C), 41.2 (N-CH_2), 31.8 (CH_2), 31.0 (CH), 29.3 (CH_2), 29.2 (CH_2), 28.1 (CH_2), 27.1 (CH_2), 22.6 (CH_2), 14.1 (CH_3). FTIR (v, cm^{-1}): 3080, 3050 (m, C-H aromatic), 2927, 2855 (s, C-H alkane), 2241 (m, C≡N), 1709-1658 (s, C=O), 1581, 1429, 1452 (C=C, aromatic), 1373, 1348 (C-H), 1246 (C-N), 770-715 (benzene ring). HRMS (ES$^+$): *m/z* 527.1664 [M + H$^+$], calculated 527.1690.

8.7.3. *N*-Octyl-naphthalene-1,4,5,8-tetracarboxylic acid diimide zinc phthalo-cyanine (330)
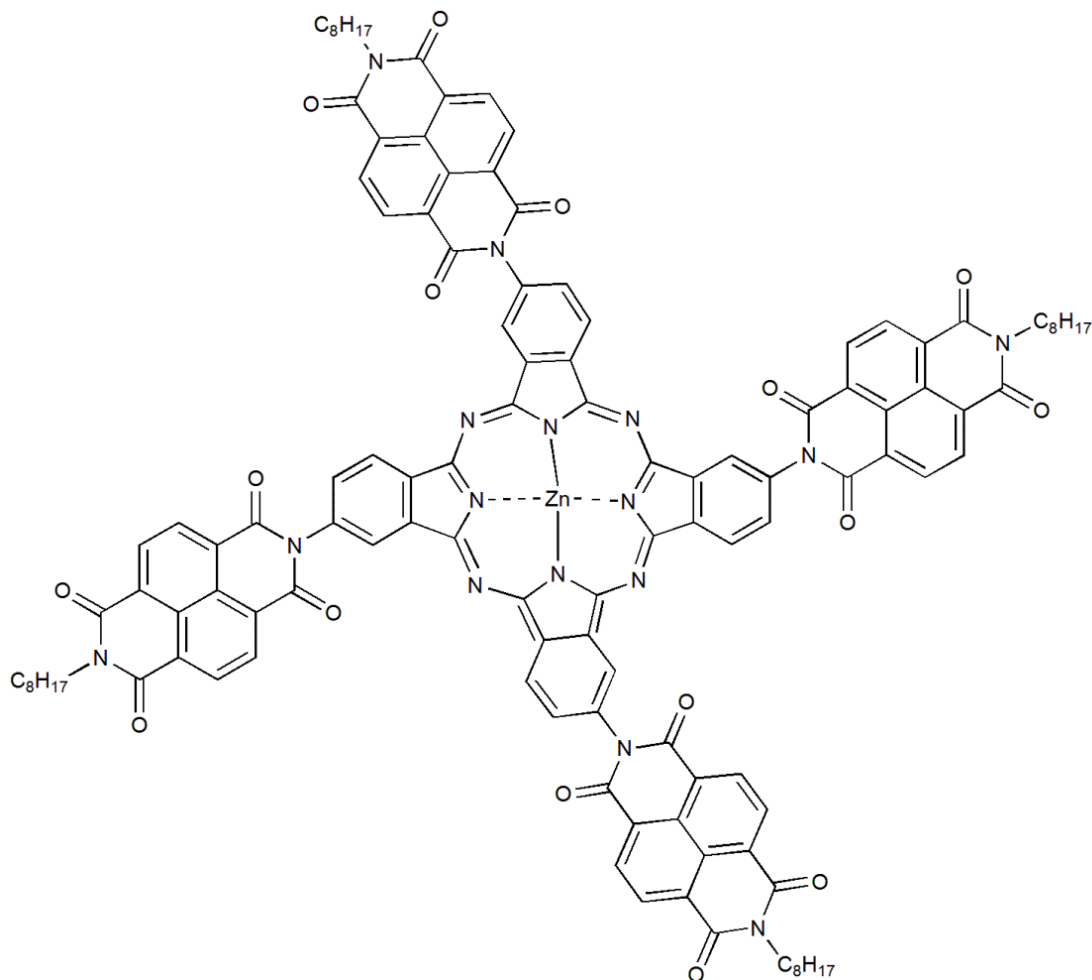
A mixture of *N*-octyl-*N'*-(phthalonitrile)naphthalene-1,4,5,8-tetracarboxylic acid diimide **329** (100 mg, 0.20 mmol), anhydrous zinc chloride (35 mg, 0.25 mmol), and DMEA (3.0 mL) was placed in schlenk tube and heated at 130 ºC for 24 hours under a N_2 atmosphere. The reaction mixture was cooled to room temperature. Ethanol (20 mL) was added and heated under reflux for 1 hr. to precipitate the product. During this time the mixture turns yellow and brown before turning deep blue. The reaction mixture was cooled to room temperature; water (10 mL) was added to dissolve the unreacted $ZnCl_2$ and DMEA. The reaction mixture was filtered and the blue solid product was washed with ethanol to remove the residual phthalonitrile. The product was purified by silica gel column chromatography eluting with DCM then DCM: acetone (90:10, v/v) to afford **330** as a deep blue solid in 22% (90 mg) yield. M.p. > 300 ºC. ^{1}H-NMR (δ/ppm, 400 MHz, $CDCl_3$): 8.84 (s, 16H, naphthalene); 8.1 (d, 4H, *J* = 6.6 Hz, phenyl); 7.87 (d, 4H, *J* = 6.6 Hz, phenyl); 4.24 (m, 8H, CH_2); 1.78 (m, 8H, CH_2); 1.44-1.24 (m, 40H, CH_2); 0.91 (m, 12H, CH_3). ^{13}C NMR (δ/ppm, 100 MHz, $CDCl_3$): 185.5 (C=O), 178.9 (C=O), 165.9 (C=O), 161.5 (C=O),

154 (C), 147.4 (CH), 144.3 (CH), 136.9 (CH), 131.9 (CH), 130.6 (CH), 128.1 (CH), 127.7 (C), 127.0 (C), 126.9 (C), 121.3 (C), 118.5 (C), 117.1 (C), 107.2 (C), 105.0 (C), 104.0 (C), 102.0 (C), 99.2 (C), 96.5 (C), 65.9 (C), 42.6 (N-CH$_2$), 39.5 (CH$_2$), 33.5 (CH), 31.9 (CH), 29.3 (CH$_2$), 22.8 (CH$_2$), 22.4 (CH$_2$), 21.4 (CH$_2$), 20.9 (CH$_2$), 14.1 (CH$_3$). FTIR (v, cm^{-1}): 3063 (m, C-H, Pc), 2955-2855 (C-H,alkane), 1709, 1668 (C=O), 1581 (C=C, m, aromatic), 1489, 1452 (C-N, Pc), 1376-1305 (C-H), 1239-1254 (C-N), 1194, 1168 (C-C), 1165 (C-O), 1093, 1060 (C-N, Pc), 739 (C-H benzene ring). MS (MALDI) = m/z 2084.543 [M + H$^+$], calculated 2084.541.

8.7.4. *N*-Octyl-naphthalene-1,4,5,8-tetracarboxylic acid diimide copper phthalocyanine (331)
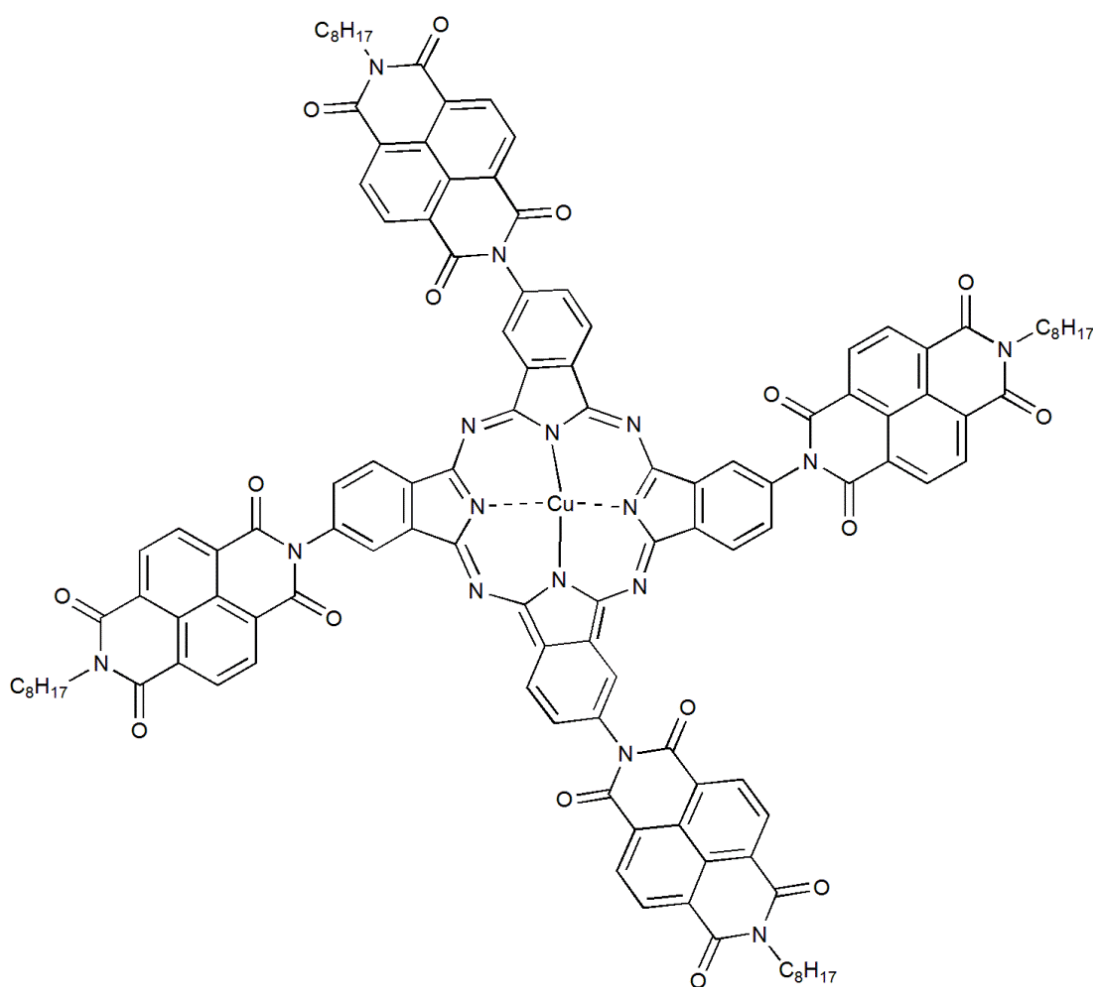
A mixture of *N*-octyl-*N'*-(phthalonitrile) naphthalene-1,4,5,8-tetracarboxylic acid diimide **329** (100 mg, 0.20 mmol), copper chloride (10 mg, 0.07 mmol), and dimethylamino-ethanol (DMEA) (3.0 mL) was placed in schlenk tube and heated at 130 ºC for 24 hours under a N$_2$ atmosphere. The reaction mixture was cooled to room temperature. Ethanol (20 mL) was added and heated under reflux for 1 hr. to precipitate the product. During this

time the mixture turned yellow and brown before turning deep blue. The reaction mixture was cooled to room temperature; water (10 mL) was added to dissolve the unreacted copper chloride and DMEA. The reaction mixture was filtered and the blue solid product was washed with ethanol to remove the residual phthalonitrile. The product was purified by flash silica gel column chromatography eluting with DCM/acetone (80:20,v/v) to afford **331** as a deep blue in 16% (65 mg). M.p. > 300 ºC. ^{1}H-NMR (δ/ppm, 400 MHz, CDCl$_3$): 8.84 (s, 16H, naphthalene); 8.1 (d, 4H, J = 6.6 Hz, phenyl); 7.87 (d, 4H, J = 6.6 Hz, phenyl); 4.24 (m, 8H, CH$_2$); 1.78 (m, 8H, CH$_2$); 1.44-1.24 (m, 40H, CH$_2$); 0.91 (m, 12H, CH$_3$). ^{13}C NMR (δ/ppm, 100 MHz, CDCl$_3$): 187.3 (C=O), 184.6 (C=O), 173.9 (C=O), 172.0 (C=O), 170.0 (C=O), 169.6 (C=O), 165.9 (C=O), 154.0 (C), 147.4 (CH), 144.3 (CH), 135.8 (CH), 134.6 (CH), 130.9 (CH), 129.7 (CH), 126.6 (CH), 126.0 (CH), 121.1 (C), 113.8 (C), 102.7 (C), 102.3 (C), 99.2 (C), 93.1 (C), 81.6 (C) 70.6 (C), 42.5 (N-CH$_2$), 39.7 (CH$_2$), 31.5 (CH), 30.9 (CH), 28.7 (CH$_2$), 28.1 (CH$_2$), 27.2 (CH$_2$), 27.1 (CH$_2$), 26.85 (CH$_2$), 23.2 (CH$_2$), 22.7 (CH$_2$), 22.6 (CH$_2$), 22.4 (CH$_2$), 14.1 (CH$_3$). FTIR (ν, cm^{-1}): 3073 (m, C-H, Pc), 2957-2853 (C-H, alkane), 1709, 1664 (C=O), 1581 (C=C, m, aromatic), 1452, 1371 (C-N, Pc), 1376-1305 (C-H), 1239-1254 (C-N), 1194, 1171 (C-C), 1168 (C-O), 1093 (C-N, Pc), 739 (C-H benzene ring). MS (MALDI) = m/z 2082.698 [M + H$^+$], calculated 2082.697.

8.7.5. *N*-Octyl-naphthalene-1,4,5,8-tetracarboxylic acid diimide nickel phthalo-cyanine (332)
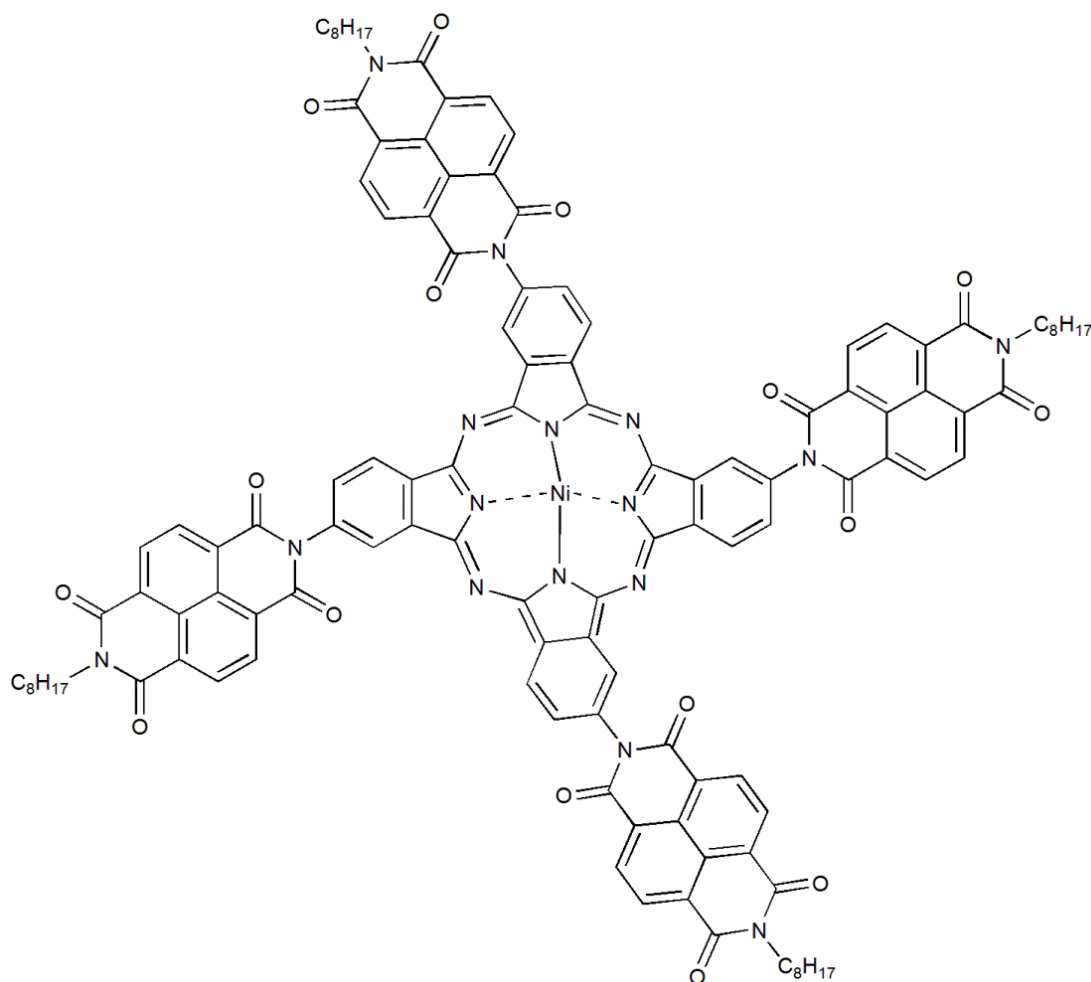
A mixture of *N*-octyl-*N'*-(phthalonitrile) naphthalene-1,4,5,8-tetracarboxylic acid diimide **329** (100 mg, 0.20 mmol), anhydrous NiCl$_2$ (32 mg, 0.25 mmol), and DMEA (3.0 mL) was placed in Schlenk tube and heated at 130 ºC for 24 hours under a N$_2$ atmosphere. The reaction mixture was cooled to room temperature; ethanol (20 mL) was added and heated under reflux for 1 hr. to precipitate the product. During this time the mixture turns yellow and brown before turning deep blue. The reaction mixture was cooled to room temperature and water (10 mL) was added to dissolve the unreacted NiCl$_2$ and DMEA. The reaction mixture was filtered and the blue solid product was washed with ethanol to remove the residual phthalonitrile. The product was purified by silica gel column chromatography eluting with DCM then DCM/acetone (90:10, v/v) to afford **332** as a deep blue solid in 19% (80 mg) yield. M.p. > 300 ºC. ^{1}H-NMR (δ/ppm, 400 MHz, CDCl$_3$): 8.82 (s, 16H, naphthalene); 8.1 (d, 4H, *J* = 7.6 Hz, phenyl); 7.86 (s, 4H, phenyl); 7.73 (d, 4H, *J* = 7.6 Hz, phenyl); 4.21 (m, 8H, CH$_2$); 1.76 (m, 8H, CH$_2$); 1.47-1.25 (m, 40H, CH$_2$); 0.88 (m, 12H, CH$_3$). ^{13}C NMR (δ/ppm, 100 MHz, CDCl$_3$): 167.5 (C=O), 167.3 (C=O), 162.7 (C=O),

162.6 (C=O), 139.8 (C), 134.5 (CH), 132.6 (CH), 131.7 (CH), 131.1 (C), 130.9 (CH), 127.4 (CH), 127.1 (CH), 126.1 (CH), 124.4 (C), 124.2 (C), 61.1 (C), 44.1 (C), 43.5 (C) 43.1 (C), 41.2 (N-CH$_2$), 37.4 (CH$_2$), 36.4 (C), 35.3 (CH$_2$), 31.8 (CH), 29.7 (CH), 29.4 (CH$_2$), 29.3 (C), 28.1 (CH$_2$), 27.3 (CH$_2$), 27.1 (CH$_2$), 26.4 (CH$_2$), 25.3 (CH$_2$), 22.7 (CH$_2$), 22.5 (CH$_2$), 19.3 (CH$_2$), 14.1 (CH$_3$). FTIR (ν, cm^{-1}): 3071 (m, C-H, Pc), 2955-2855 (C-H, alkane), 1709, 1666 (C=O), 1581 (C=C, m, aromatic), 1452 (C-N, Pc), 1376-1305 (C-H), 1239-1254 (C-N), 1192, 1170 (C-C), 1168 (C-O), 1096 (C-N, Pc), 732 (C-H benzene ring). MS (MALDI)= *m/z* 2077.759 [M + H$^+$], calculated 2077.845.

8.7.6. *N*-Octyl-naphthalene-1,4,5,8-tetracarboxylic acid diimide cobalt phthalocyanine (333)
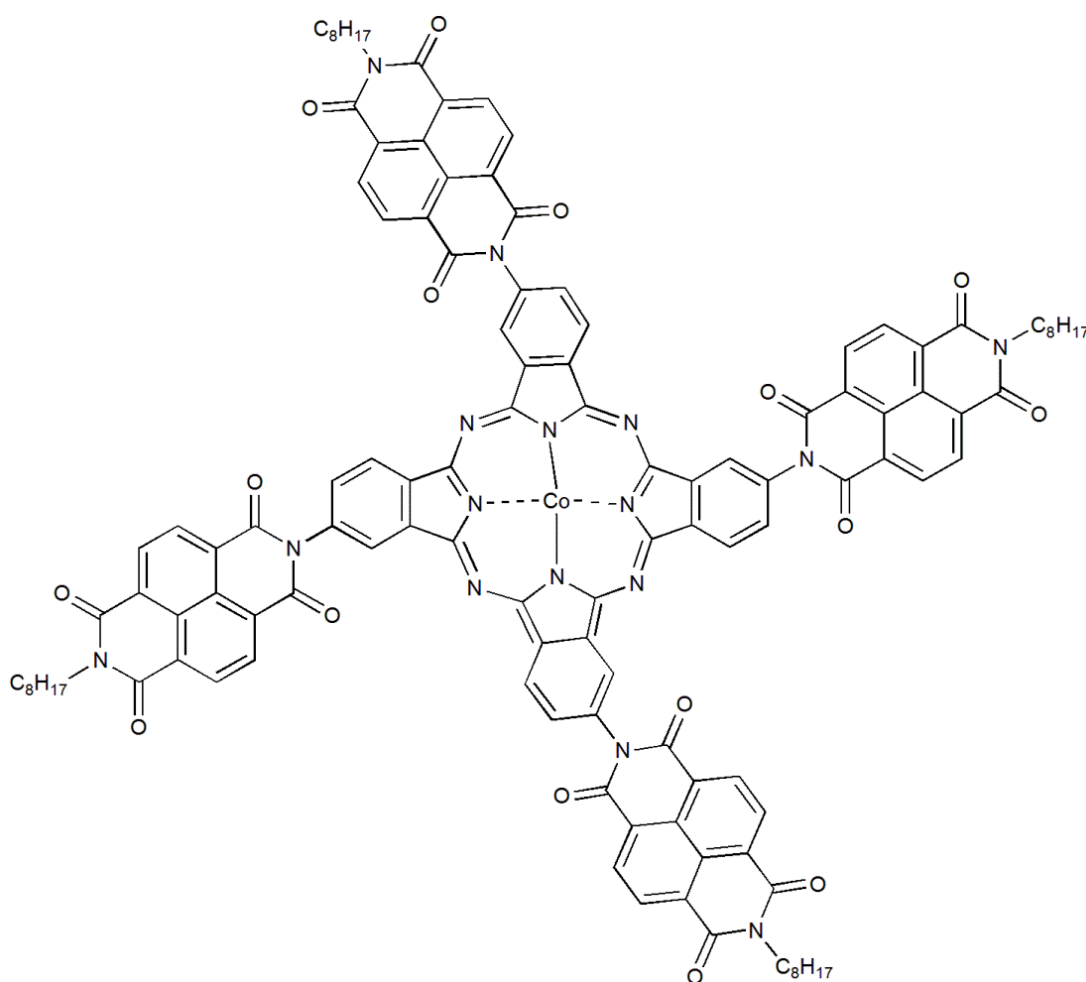
A mixture of *N*-octyl-*N'*-(phthalonitrile) naphthalene-1,4,5,8-tetracarboxylic acid diimide **329** (100 mg, 0.20 mmol), anhydrous CoCl$_2$.6H$_2$O (59 mg, 0.25 mmol), and DMEA (3.0 mL) was placed in Schlenk tube and heated at 130 ºC for 24 hours under a N$_2$ atmosphere. The reaction mixture was cooled to room temperature; ethanol (20 mL) was added and heated under reflux for 1 hr. to precipitate the product. During this time the mixture turns

yellow and brown before turning deep blue. The reaction mixture was cooled to room temperature; water (10 mL) was added to dissolve the unreacted nickel chloride and DMEA. The reaction mixture was filtered and the blue solid product was washed with ethanol to remove the residual phthalonitrile. The product was purified by silica gel column chromatography eluting with DCM then DCM/acetone (90:10, v/v) to afford **333** as a blue solid in 10% (40 mg). M.p. > 300 ℃. ^{1}H-NMR (δ/ppm, 400 MHz, CDCl$_3$): 8.86 (s, 16H, naphthalene); 8.0 (s, 4H, phenyl); 7.73 (d, 8H, J = 6.6 Hz, phenyl); 4.15 (m, 8H, CH$_2$); 1.69 (m, 8H, CH$_2$); 1.57-1.25 (m, 40H, CH$_2$); 0.87 (m, 12H, CH$_3$). ^{13}C NMR (δ/ppm, 100 MHz, CDCl$_3$): 178.9 (C=O), 176.9 (C=O), 176.8 (C=O), 174.9 (C=O), 174.2 (C=O), 166.4 (C=O), 165.8 (C=O), 164.4 (C=O), 159.3 (C), 158.1 (C), 157.0 (C), 156.7 (C), 156.7 (C), 148.3 (C), 140.7 (C), 135.0 (C), 134.7 (CH), 128.0 (CH), 127.3 (CH), 126.3 (C), 124.9 (CH), 119.5 (CH), 118.6 (CH), 118.5 (CH), 118.2 (C), 113.7 (C), 112.7 (C), 111.0 (CH), 107.7 (C), 96.8 (C), 86.5 (C), 69.0 (CH), 60.6 (C), 58.3 (C), 43.6 (C) 41.1 (N-CH$_2$), 37.1 (CH$_2$), 35.6 (CH$_2$), 33.1 (CH$_2$), 31.2 (CH), 30.2 (CH$_2$), 29.7 (CH), 27.3 (CH$_2$), 26.5 (CH$_2$), 25.9 (CH$_2$), 16.44 (CH$_2$), 16.1 (CH$_2$), 14.1 (CH$_3$). FTIR (ν, cm^{-1}): 3073 (m, C-H, Pc), 2957-2855 (C-H, alkane), 1709, 1669 (C=O), 1581 (m, C=C, aromatic), 1452, 1342 (C-N, Pc), 1376-1305 (C-H), 1239-1254 (C-N), 1192, 1170 (C-C), 1168 (C-O), 1096 (C-N, Pc), 737 (C-H benzene ring). MS (MALDI)= m/z 2078.032 [M + H$^+$], calculated 2078.085.

9. **Chapter 9**

Appendices

9.1. Calculation for optical band gap energy value

Optical band gap energy ($Eg^{opt} = 1242 / \lambda_{onset}$) calculated from the definition, $Eg^{opt} = hc / \lambda_{onset}$ with h being Planck's constant (6.626×10^{-34} Js), C being the speed of light (3.0×10^{8} m/s), and λ_{onset} being the onset wavelength.

9.2. Cyclic Voltammetry for polymers 181,183 and 184

Voltammetry experiments for polymers **181,183** and **184** were performed in aqueous media using 0.01 mM solutions of the conjugates with 0.1 M NaCl as the supporting electrolyte. Cyclic voltammograms (CV) were recorded using a glassy carbon (GC) electrode (diameter 3.1 mm). Voltammograms were referenced against an Ag/AgCl electrode.

9.3. X-ray crystallography of 64
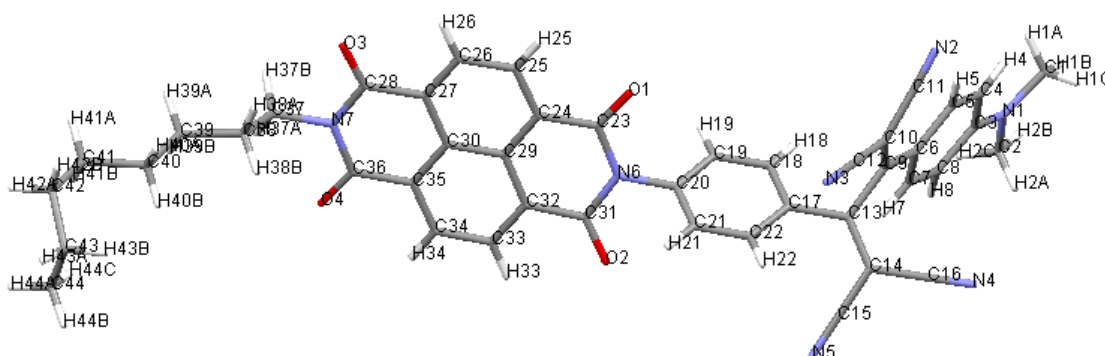
Figure 9-1. X-ray crystal structure of **64**.

Table 9-1. Crystal data and structure refinement for **64**

Identification code	mkm4te
Empirical formula	$C_{44} H_{35} N_7 O_4$
Formula weight	725.79
Temperature	150(2) K
Wavelength	1.54178 Å
Crystal system	Monoclinic
Space group	P2(1)/c
Unit cell dimensions	a = 8.4810(5) Å $\alpha = 90^o$.
	b= 23.3297(10) Å $\beta = 92.104(5)^o$.
	c = 18.5166(13) Å $\gamma = 90^o$.
Volume	3661.2(4) $Å^3$
Z	4
Density (Calculated)	1.317 Mg/m^3
Absorption coefficient	0.700 mm^{-1}
F(000)	1520
Crystal size	0.30 x 0.07 x 0.05 mm^3
Theta range for data collection	3.05 to 59.99^o.
Limiting indices	-8<=h<=9, -22<=k<=26, -20<=l<=20
Reflections collected	24327
unique	5446 [R(int) = 0.0629]
Completeness to theta= 59.99^o	100.0 %
Absorption correction	Analytical
Max. and min. transmission	0.9658 and 0.8175
Refinement method	Full-matrix least squares on F^2
Data / /	5446
restraints	9
parameters	503
Goodness-of-fit on F^2	1.025
Final R indices [I>2sigma(I)]	R1 = 0.0642, wR2 = 0.1776
R indices (all data)	R1 = 0.0894, wR2 = 0.2081
Largest diff. peak and hole	0.51 and -0.35 $e.Å^{-3}$

Table 9-2. Atomic coordinates (x 10^4) and equivalent isotropic displacement parameters (Å^2 x 10^3) for **64**. U(eq) is defined as one third of the trace of the orthogonalized Uij tensor.

	x	y	z	U(eq)
C(1)	3019(5)	9508(2)	2725(3)	89(1)
C(2)	1849(6)	9314(2)	1494(3)	103(2)
C(3)	3651(4)	8629(1)	2084(2)	61(1)
C(4)	4646(4)	8444(1)	2659(2)	60(1)
C(5)	5501(4)	7955(1)	2625(2)	54(1)
C(6)	5442(4)	7600(1)	2008(2)	50(1)
C(7)	4403(4)	7775(1)	1441(2)	64(1)
C(8)	3529(5)	8268(2)	1467(2)	72(1)
C(9)	6354(4)	7078(1)	1933(2)	51(1)
C(10)	7381(4)	6824(1)	2427(2)	52(1)
C(11)	7744(4)	7019(1)	3147(2)	57(1)
C(12)	8200(4)	6311(2)	2231(2)	59(1)
C(13)	6133(4)	6755(1)	1228(2)	51(1)
C(14)	6848(4)	6939(1)	631(2)	57(1)
C(15)	6496(4)	6697(2)	-76(2)	61(1)
C(16)	7958(5)	7403(2)	656(2)	66(1)
C(17)	5112(4)	6244(1)	1234(2)	48(1)
C(18)	3692(4)	6254(1)	1591(2)	53(1)
C(19)	2733(4)	5777(1)	1594(2)	52(1)
C(20)	3203(4)	5282(1)	1252(2)	49(1)
C(21)	4635(4)	5257(1)	917(2)	54(1)
C(22)	5586(4)	5736(1)	904(2)	54(1)
C(23)	2112(4)	4491(1)	1932(2)	53(1)
C(24)	1125(4)	3973(1)	1938(2)	51(1)
C(25)	1026(4)	3660(2)	2560(2)	59(1)
C(26)	102(4)	3163(2)	2572(2)	60(1)
C(27)	-718(4)	2986(1)	1967(2)	54(1)
C(28)	-1640(4)	2445(2)	1979(2)	60(1)
C(29)	295(3)	3799(1)	1301(2)	48(1)
C(30)	-642(4)	3298(1)	1317(2)	50(1)
C(31)	1488(4)	4597(1)	610(2)	49(1)
C(32)	434(4)	4094(1)	643(2)	50(1)
C(33)	-361(4)	3904(1)	31(2)	57(1)
C(34)	-1325(4)	3420(1)	53(2)	61(1)
C(35)	-1470(4)	3118(1)	684(2)	54(1)
C(36)	-2477(4)	2596(1)	701(2)	60(1)

C(37)	-3403(4)	1756(2)	1369(2)	66(1)
C(38)	-2367(6)	1233(2)	1251(3)	101(2)
C(39)	-3337(9)	678(3)	1118(4)	85(2)
C(40)	-2482(10)	157(3)	823(5)	113(2)
C(41)	-3563(9)	-382(3)	730(4)	101(2)
C(42)	-2682(10)	-888(4)	470(4)	91(2)
C(43)	-1761(11)	-843(4)	-200(4)	86(2)
C(44)	-2828(15)	-733(6)	-856(7)	107(4)
N(1)	2815(4)	9121(1)	2120(2)	78(1)
N(2)	8065(4)	7157(1)	3728(2)	74(1)
N(3)	8859(4)	5899(1)	2083(2)	72(1)
N(4)	8884(5)	7765(2)	690(2)	86(1)
N(5)	6202(4)	6510(1)	-636(2)	67(1)
N(6)	2210(3)	4780(1)	1269(1)	50(1)
N(7)	-2488(3)	2294(1)	1350(1)	59(1)
O(1)	2836(3)	4670(1)	2460(1)	68(1)
O(2)	1760(3)	4846(1)	50(1)	55(1)
O(3)	-1648(3)	2142(1)	2510(1)	76(1)
O(4)	-3265(3)	2438(1)	178(1)	77(1)
C(39')	-1320(11)	1198(4)	720(5)	67(2)
C(42')	-4046(19)	-829(7)	819(8)	73(4)
C(43')	-4260(40)	-850(17)	41(12)	117(11)
C(44')	-2760(40)	-698(15)	-340(20)	119(9)
C(41")	-2800(30)	-438(8)	647(9)	66(5)
C(42")	-2150(30)	-358(10)	-58(11)	94(6)
C(43")	-940(20)	-839(8)	-75(10)	95(6)
C(44")	-6(16)	-790(6)	-796(7)	106(4)

Table 9-3. Bond lengths [Å] and angles [°] for **64**

C(1)-N(1)	1.445(6)
C(2)-N(1)	1.465(6)
C(3)-N(1)	1.352(4)
C(3)-C(4)	1.401(5)
C(3)-C(8)	1.419(5)
C(4)-C(5)	1.355(5)
C(5)-C(6)	1.410(4)
C(6)-C(7)	1.405(4)
C(6)-C(9)	1.452(4)

C(7)-C(8)	1.371(5)
C(9)-C(10)	1.375(5)
C(9)-C(13)	1.513(4)
C(10)-C(11)	1.432(5)
C(10)-C(12)	1.436(5)
C(11)-N(2)	1.145(4)
C(12)-N(3)	1.151(4)
C(13)-C(14)	1.350(5)
C(13)-C(17)	1.474(4)
C(14)-C(16)	1.434(5)
C(14)-C(15)	1.446(5)
C(15)-N(5)	1.144(4)
C(16)-N(4)	1.153(5)
C(17)-C(18)	1.394(4)
C(17)-C(22)	1.399(4)
C(18)-C(19)	1.379(4)
C(19)-C(20)	1.382(4)
C(20)-C(21)	1.385(4)
C(20)-N(6)	1.444(4)
C(21)-C(22)	1.379(5)
C(23)-O(1)	1.210(4)
C(23)-N(6)	1.406(4)
C(23)-C(24)	1.470(5)
C(24)-C(25)	1.370(5)
C(24)-C(29)	1.411(4)
C(25)-C(26)	1.399(5)
C(26)-C(27)	1.363(5)
C(27)-C(30)	1.410(4)
C(27)-C(28)	1.486(5)
C(28)-O(3)	1.212(4)
C(28)-N(7)	1.390(4)
C(29)-C(32)	1.408(4)
C(29)-C(30)	1.413(4)
C(30)-C(35)	1.407(4)
C(31)-O(2)	1.217(4)
C(31)-N(6)	1.411(4)
C(31)-C(32)	1.479(4)
C(32)-C(33)	1.370(4)
C(33)-C(34)	1.397(5)

C(34)-C(35)	1.373(5)
C(35)-C(36)	1.490(5)
C(36)-O(4)	1.214(4)
C(36)-N(7)	1.392(4)
C(37)-N(7)	1.477(4)
C(37)-C(38)	1.523(6)
C(38)-C(39)	1.548(8)
C(39)-C(40)	1.526(10)
C(40)-C(41)	1.562(9)
C(41)-C(42)	1.486(10)
C(42)-C(43)	1.494(10)
C(43)-C(44)	1.510(12)
C(42')-C(43')	1.447(19)
C(43')-C(44')	1.513(19)
C(41")-C(42")	1.446(18)
C(42")-C(43")	1.524(18)
C(43")-C(44")	1.581(16)
N(1)-C(3)-C(4)	121.8(3)
N(1)-C(3)-C(8)	121.3(3)
C(4)-C(3)-C(8)	116.9(3)
C(5)-C(4)-C(3)	122.2(3)
C(4)-C(5)-C(6)	121.9(3)
C(7)-C(6)-C(5)	116.0(3)
C(7)-C(6)-C(9)	119.5(3)
C(5)-C(6)-C(9)	124.5(3)
C(8)-C(7)-C(6)	122.8(3)
C(7)-C(8)-C(3)	120.1(3)
C(10)-C(9)-C(6)	128.7(3)
C(10)-C(9)-C(13)	114.5(3)
C(6)-C(9)-C(13)	116.8(3)
C(9)-C(10)-C(11)	126.3(3)
C(9)-C(10)-C(12)	119.5(3)
C(11)-C(10)-C(12)	114.2(3)
N(2)-C(11)-C(10)	177.5(4)
N(3)-C(12)-C(10)	179.2(4)
C(14)-C(13)-C(17)	123.1(3)
C(14)-C(13)-C(9)	120.1(3)
C(17)-C(13)-C(9)	116.8(2)
C(13)-C(14)-C(16)	121.8(3)

C(13)-C(14)-C(15)	122.2(3)
C(16)-C(14)-C(15)	116.0(3)
N(5)-C(15)-C(14)	179.2(4)
N(4)-C(16)-C(14)	177.8(4)
C(18)-C(17)-C(22)	119.2(3)
C(18)-C(17)-C(13)	120.6(3)
C(22)-C(17)-C(13)	120.1(3)
C(19)-C(18)-C(17)	120.5(3)
C(18)-C(19)-C(20)	119.5(3)
C(19)-C(20)-C(21)	120.8(3)
C(19)-C(20)-N(6)	119.3(3)
C(21)-C(20)-N(6)	119.9(3)
C(22)-C(21)-C(20)	119.9(3)
C(21)-C(22)-C(17)	120.0(3)
O(1)-C(23)-N(6)	119.7(3)
O(1)-C(23)-C(24)	123.4(3)
N(6)-C(23)-C(24)	116.9(3)
C(25)-C(24)-C(29)	120.4(3)
C(25)-C(24)-C(23)	119.8(3)
C(29)-C(24)-C(23)	119.9(3)
C(24)-C(25)-C(26)	120.5(3)
C(27)-C(26)-C(25)	120.5(3)
C(26)-C(27)-C(30)	120.5(3)
C(26)-C(27)-C(28)	119.9(3)
C(30)-C(27)-C(28)	119.5(3)
O(3)-C(28)-N(7)	120.9(3)
O(3)-C(28)-C(27)	121.8(3)
N(7)-C(28)-C(27)	117.3(3)
C(32)-C(29)-C(24)	121.9(3)
C(32)-C(29)-C(30)	119.1(3)
C(24)-C(29)-C(30)	119.0(3)
C(35)-C(30)-C(27)	121.3(3)
C(35)-C(30)-C(29)	119.5(3)
C(27)-C(30)-C(29)	119.2(3)
O(2)-C(31)-N(6)	120.2(3)
O(2)-C(31)-C(32)	123.2(3)
N(6)-C(31)-C(32)	116.6(3)
C(33)-C(32)-C(29)	120.3(3)
C(33)-C(32)-C(31)	120.1(3)

C(29)-C(32)-C(31)	119.6(3)
C(32)-C(33)-C(34)	120.5(3)
C(35)-C(34)-C(33)	120.7(3)
C(34)-C(35)-C(30)	119.9(3)
C(34)-C(35)-C(36)	120.4(3)
C(30)-C(35)-C(36)	119.7(3)
O(4)-C(36)-N(7)	120.9(3)
O(4)-C(36)-C(35)	122.1(3)
N(7)-C(36)-C(35)	117.0(3)
N(7)-C(37)-C(38)	111.8(3)
C(37)-C(38)-C(39)	112.7(4)
C(40)-C(39)-C(38)	117.8(6)
C(39)-C(40)-C(41)	113.3(6)
C(42)-C(41)-C(40)	112.0(7)
C(41)-C(42)-C(43)	119.9(7)
C(42)-C(43)-C(44)	111.3(9)
C(3)-N(1)-C(1)	121.4(3)
C(3)-N(1)-C(2)	120.1(4)
C(1)-N(1)-C(2)	117.9(3)
C(23)-N(6)-C(31)	125.0(3)
C(23)-N(6)-C(20)	117.5(2)
C(31)-N(6)-C(20)	117.4(2)
C(28)-N(7)-C(36)	125.1(3)
C(28)-N(7)-C(37)	116.8(3)
C(36)-N(7)-C(37)	118.1(3)
C(42')-C(43')-C(44')	112(2)
C(41")-C(42")-C(43")	101.6(16)
C(42")-C(43")-C(44")	108.9(14)

Symmetry transformations used to generate equivalent atoms

Table 9-4. Anisotropic displacement parameters ($\mathring{A}^2$ x 10^3) for **64**. The anisotropic displacement factor exponent takes the form: -2 pi^2 [h^2 a^{*2} U11 + ... + 2 h k a* b* U12]

	U11	U22	U33	U23	U13	U12
C(1)	83(3)	53(2)	132(4)	-15(2)	18(3)	8(2)
C(2)	100(3)	86(3)	124(4)	40(3)	5(3)	33(3)
C(3)	69(2)	45(2)	69(2)	6(2)	0(2)	6(2)
C(4)	70(2)	50(2)	58(2)	-6(2)	1(2)	-3(2)
C(5)	64(2)	52(2)	45(2)	-1(1)	-4(1)	-1(2)
C(6)	63(2)	49(2)	39(2)	0(1)	-3(1)	0(1)
C(7)	89(2)	57(2)	45(2)	-2(2)	-14(2)	6(2)
C(8)	85(3)	69(2)	60(2)	7(2)	-17(2)	11(2)
C(9)	64(2)	50(2)	39(2)	-2(1)	3(1)	-6(1)
C(10)	63(2)	50(2)	42(2)	-1(1)	-4(1)	1(1)
C(11)	68(2)	54(2)	50(2)	5(2)	-7(2)	1(2)
C(12)	61(2)	57(2)	58(2)	-2(2)	-1(2)	0(2)
C(13)	63(2)	48(2)	41(2)	-2(1)	0(1)	5(1)
C(14)	72(2)	57(2)	42(2)	-4(1)	-2(2)	-1(2)
C(15)	70(2)	65(2)	48(2)	-2(2)	6(2)	4(2)
C(16)	92(3)	64(2)	42(2)	1(2)	2(2)	-10(2)
C(17)	60(2)	50(2)	34(2)	-5(1)	-1(1)	2(1)
C(18)	61(2)	49(2)	48(2)	-12(1)	1(1)	4(1)
C(19)	54(2)	57(2)	45(2)	-9(1)	3(1)	4(1)
C(20)	58(2)	50(2)	39(2)	-6(1)	0(1)	-1(1)
C(21)	67(2)	48(2)	48(2)	-11(1)	8(2)	6(2)
C(22)	64(2)	55(2)	43(2)	-8(1)	8(1)	2(2)
C(23)	60(2)	57(2)	41(2)	-7(1)	1(1)	2(2)
C(24)	55(2)	58(2)	41(2)	-5(1)	3(1)	1(1)
C(25)	63(2)	70(2)	43(2)	-1(2)	-1(1)	-6(2)
C(26)	66(2)	69(2)	44(2)	8(2)	1(2)	-6(2)
C(27)	60(2)	59(2)	43(2)	0(1)	2(1)	-1(2)
C(28)	63(2)	64(2)	51(2)	5(2)	2(2)	-4(2)
C(29)	53(2)	49(2)	43(2)	-4(1)	1(1)	6(1)
C(30)	56(2)	48(2)	45(2)	-4(1)	1(1)	3(1)
C(31)	61(2)	44(2)	40(2)	-6(1)	2(1)	9(1)
C(32)	62(2)	44(2)	43(2)	-3(1)	0(1)	6(1)
C(33)	78(2)	48(2)	44(2)	1(1)	-7(2)	2(2)

C(34)	83(2)	52(2)	48(2)	-3(2)	-12(2)	-3(2)
C(35)	68(2)	49(2)	44(2)	-3(1)	-4(1)	-1(2)
C(36)	74(2)	53(2)	51(2)	-2(2)	-5(2)	-2(2)
C(37)	73(2)	64(2)	62(2)	0(2)	2(2)	-17(2)
C(38)	93(3)	60(2)	151(5)	7(3)	15(3)	-14(2)
N(1)	81(2)	52(2)	101(2)	3(2)	-1(2)	10(2)
N(2)	98(2)	69(2)	53(2)	1(2)	-15(2)	3(2)
N(3)	66(2)	65(2)	86(2)	-11(2)	2(2)	6(2)
N(4)	123(3)	82(2)	53(2)	0(2)	4(2)	-31(2)
N(5)	80(2)	78(2)	42(2)	-7(1)	1(1)	5(2)
N(6)	62(2)	47(1)	42(1)	-7(1)	3(1)	0(1)
N(7)	68(2)	58(2)	50(2)	0(1)	-1(1)	-10(1)
O(1)	84(2)	72(2)	47(1)	-3(1)	-6(1)	-16(1)
O(2)	70(1)	50(1)	44(1)	-2(1)	3(1)	2(1)
O(3)	90(2)	85(2)	54(1)	16(1)	-4(1)	-28(1)
O(4)	100(2)	71(2)	58(2)	0(1)	-19(1)	-22(1)

9.4. X-ray crystallography of 109
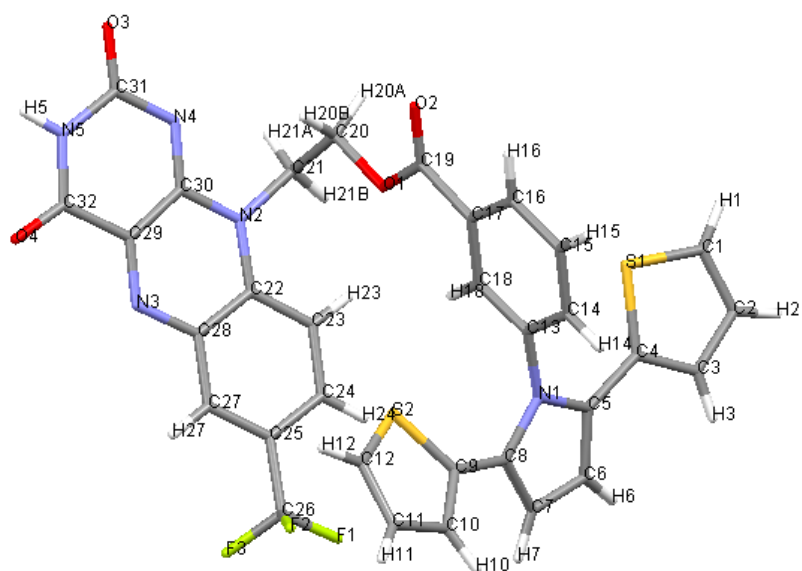
Figure 9-2. X-ray crystal structure of **109**.

Table 9-5. Crystal data and structure refinement for **109**.

Identification code	mksnsf2
Empirical formula	$C_{32}H_{22}F_3N_5O_5S_2$
Formula weight	677.67
Temperature	150(2) K
Wavelength	0.71073 Å
Crystal system	Triclinic
space group	P-1
Unit cell dimensions	a = 9.7255(5) Å α = 82.482(3)
	b = 10.0305(6) Å β = 74.732(3)
	c = 16.8016(8) Å γ = 65.680(3)
Volume	1440.39(13) Å^3
Z	2
Calculated density	1.562 Mg/m^3
Absorption coefficient	0.258 mm^{-1}
F(000)	696
Crystal size	0.20 x 0.10 x 0.03 mm
Theta range for data collection	2.23 to 26.00º
Limiting indices	-11<=h<=11, -12<=k<=11, -20<=l<=20
Reflections collected	19747
unique	5632 [R(int) = 0.0420]
Completeness to theta = 26.00º	99.60%
Absorption correction	Empirical
Max. and min. transmission	0.9923 and 0.9501
Refinement method	Full-matrix least-squares on F^2
Data	5632
restraints	10
parameters	444
Goodness-of-fit on F^2	1.083
Final R indices [I>2sigma(I)]	R1 = 0.0537, wR2 = 0.1332
R indices (all data)	R1 = 0.0800, wR2 = 0.1465
Extinction coefficient	none
Largest diff. peak and hole	0.28 and -0.40 e.Å^{-3}

Table 9-6. Atomic coordinates (x 10^4) and equivalent isotropic displacement parameters ($Å^2$ x 10^3) for **109**. U(eq) is defined as one third of the trace of the orthogonalized Uij tensor.

	x	y	z	U(eq)
C(1)	7717(3)	7986(4)	2716(2)	31(1)
C(2)	8991(4)	6812(4)	2853(2)	38(1)
C(3)	8700(4)	5537(4)	3092(2)	34(1)
C(4)	7210(3)	5726(3)	3131(2)	26(1)
C(5)	6652(3)	4558(3)	3329(2)	25(1)
C(6)	7527(4)	3080(3)	3311(2)	30(1)
C(7)	6526(4)	2348(3)	3581(2)	32(1)
C(8)	5028(4)	3387(3)	3775(2)	27(1)
C(9)	3605(4)	3164(3)	4164(2)	29(1)
C(10)	3391(17)	2094(19)	4749(11)	96(7)
C(10')	2010(20)	3930(30)	4111(16)	122(12)
C(11)	1883(5)	2114(5)	5014(3)	54(1)
C(12)	1025(5)	3201(4)	4586(2)	48(1)
C(13)	3823(3)	6138(3)	3735(2)	21(1)
C(14)	3354(3)	6820(3)	4481(2)	28(1)
C(15)	2193(4)	8205(4)	4579(2)	32(1)
C(16)	1497(4)	8900(3)	3942(2)	30(1)
C(17)	1941(3)	8205(3)	3198(2)	23(1)
C(18)	3126(3)	6817(3)	3087(2)	22(1)
C(19)	1152(3)	9013(3)	2529(2)	25(1)
C(20)	934(3)	9001(3)	1172(2)	24(1)
C(21)	1503(3)	7948(3)	488(2)	22(1)
C(22)	1561(3)	5453(3)	996(2)	20(1)
C(23)	3067(3)	4962(3)	1121(2)	24(1)
C(24)	3746(3)	3581(3)	1447(2)	27(1)
C(25)	2942(3)	2655(3)	1657(2)	27(1)
C(26)	3637(4)	1191(4)	2066(2)	34(1)
C(27)	1479(3)	3099(3)	1523(2)	26(1)
C(28)	776(3)	4496(3)	1189(2)	22(1)
C(29)	-1397(3)	6241(3)	834(2)	23(1)
C(30)	-709(3)	7312(3)	629(2)	22(1)
C(31)	-2901(3)	9121(3)	317(2)	27(1)
C(32)	-3027(3)	6723(3)	735(2)	26(1)
N(1)	5107(3)	4743(3)	3613(1)	23(1)
N(2)	789(3)	6852(3)	696(1)	21(1)
N(3)	-710(3)	4911(3)	1089(1)	24(1)

N(4)	-1409(3)	8669(3)	390(2)	25(1)
N(5)	-3625(3)	8144(3)	469(2)	27(1)
O(1)	1648(2)	8236(2)	1848(1)	22(1)
O(2)	155(3)	10226(2)	2591(2)	43(1)
O(3)	-3624(2)	10390(2)	110(2)	36(1)
O(4)	-3716(2)	5921(2)	864(1)	33(1)
F(1)	5132(2)	807(2)	2045(2)	57(1)
F(2)	2897(3)	1142(2)	2850(1)	50(1)
F(3)	3572(2)	117(2)	1692(1)	40(1)
S(1)	6157(1)	7521(1)	2871(1)	34(1)
S(2)	1910(2)	4133(3)	3939(2)	44(1)
S(2')	3668(5)	1827(6)	4870(3)	48(1)
O(5)	-2491(4)	2729(4)	1400(2)	63(1)

Table 9-7. Bond lengths [Å] and angles [deg] for **109**.

C(1)-C(2)	1.361(5)
C(1)-S(1)	1.712(3)
C(2)-C(3)	1.407(5)
C(3)-C(4)	1.367(4)
C(4)-C(5)	1.450(4)
C(4)-S(1)	1.730(3)
C(5)-C(6)	1.372(4)
C(5)-N(1)	1.392(4)
C(6)-C(7)	1.400(5)
C(7)-C(8)	1.379(4)
C(8)-N(1)	1.381(4)
C(8)-C(9)	1.460(4)
C(9)-C(10)	1.400(13)
C(9)-S(2)	1.649(4)
C(10)-C(11)	1.409(13)
C(11)-C(12)	1.328(6)
C(12)-S(2)	1.643(4)
C(13)-C(14)	1.382(4)
C(13)-C(18)	1.387(4)
C(13)-N(1)	1.436(4)
C(14)-C(15)	1.380(4)
C(15)-C(16)	1.373(4)
C(16)-C(17)	1.389(4)

C(17)-C(18)	1.391(4)
C(17)-C(19)	1.489(4)
C(19)-O(2)	1.200(3)
C(19)-O(1)	1.334(4)
C(20)-O(1)	1.453(3)
C(20)-C(21)	1.497(4)
C(21)-N(2)	1.488(4)
C(22)-N(2)	1.390(4)
C(22)-C(23)	1.405(4)
C(22)-C(28)	1.415(4)
C(23)-C(24)	1.376(4)
C(24)-C(25)	1.402(4)
C(25)-C(27)	1.376(4)
C(25)-C(26)	1.500(4)
C(26)-F(2)	1.330(4)
C(26)-F(1)	1.334(4)
C(26)-F(3)	1.345(4)
C(27)-C(28)	1.397(4)
C(28)-N(3)	1.380(4)
C(29)-N(3)	1.295(4)
C(29)-C(30)	1.448(4)
C(29)-C(32)	1.503(4)
C(30)-N(4)	1.309(4)
C(30)-N(2)	1.367(4)
C(31)-O(3)	1.229(4)
C(31)-N(4)	1.365(4)
C(31)-N(5)	1.389(4)
C(32)-O(4)	1.211(4)
C(32)-N(5)	1.363(4)
C(2)-C(1)-S(1)	111.0(3)
C(1)-C(2)-C(3)	112.9(3)
C(4)-C(3)-C(2)	113.8(3)
C(3)-C(4)-C(5)	123.9(3)
C(3)-C(4)-S(1)	109.7(2)
C(5)-C(4)-S(1)	126.4(2)
C(6)-C(5)-N(1)	107.0(3)
C(6)-C(5)-C(4)	127.3(3)
N(1)-C(5)-C(4)	125.6(3)
C(5)-C(6)-C(7)	108.4(3)

C(8)-C(7)-C(6)	108.0(3)
C(7)-C(8)-N(1)	107.3(3)
C(7)-C(8)-C(9)	128.2(3)
N(1)-C(8)-C(9)	124.2(3)
C(10)-C(9)-C(8)	129.0(7)
C(10)-C(9)-S(2)	106.4(6)
C(8)-C(9)-S(2)	124.5(2)
C(9)-C(10)-C(11)	117.3(10)
C(12)-C(11)-C(10)	105.5(6)
C(11)-C(12)-S(2)	116.7(3)
C(14)-C(13)-C(18)	121.0(3)
C(14)-C(13)-N(1)	119.6(3)
C(18)-C(13)-N(1)	119.3(3)
C(15)-C(14)-C(13)	119.6(3)
C(16)-C(15)-C(14)	120.2(3)
C(15)-C(16)-C(17)	120.3(3)
C(16)-C(17)-C(18)	120.1(3)
C(16)-C(17)-C(19)	117.9(3)
C(18)-C(17)-C(19)	122.0(3)
C(13)-C(18)-C(17)	118.7(3)
O(2)-C(19)-O(1)	122.9(3)
O(2)-C(19)-C(17)	124.1(3)
O(1)-C(19)-C(17)	112.9(2)
O(1)-C(20)-C(21)	108.0(2)
N(2)-C(21)-C(20)	111.1(2)
N(2)-C(22)-C(23)	123.0(3)
N(2)-C(22)-C(28)	118.0(2)
C(23)-C(22)-C(28)	119.1(3)
C(24)-C(23)-C(22)	120.1(3)
C(23)-C(24)-C(25)	120.3(3)
C(27)-C(25)-C(24)	120.6(3)
C(27)-C(25)-C(26)	119.0(3)
C(24)-C(25)-C(26)	120.3(3)
F(2)-C(26)-F(1)	107.8(3)
F(2)-C(26)-F(3)	106.0(3)
F(1)-C(26)-F(3)	106.0(3)
F(2)-C(26)-C(25)	112.4(3)
F(1)-C(26)-C(25)	112.5(3)
F(3)-C(26)-C(25)	111.7(3)

C(25)-C(27)-C(28)	119.7(3)
N(3)-C(28)-C(27)	117.7(3)
N(3)-C(28)-C(22)	122.1(3)
C(27)-C(28)-C(22)	120.1(3)
N(3)-C(29)-C(30)	124.8(3)
N(3)-C(29)-C(32)	118.4(3)
C(30)-C(29)-C(32)	116.8(3)
N(4)-C(30)-N(2)	118.3(3)
N(4)-C(30)-C(29)	125.2(3)
N(2)-C(30)-C(29)	116.5(2)
O(3)-C(31)-N(4)	120.9(3)
O(3)-C(31)-N(5)	118.8(3)
N(4)-C(31)-N(5)	120.3(3)
O(4)-C(32)-N(5)	124.0(3)
O(4)-C(32)-C(29)	123.3(3)
N(5)-C(32)-C(29)	112.7(3)
C(8)-N(1)-C(5)	109.2(2)
C(8)-N(1)-C(13)	126.4(2)
C(5)-N(1)-C(13)	124.3(2)
C(30)-N(2)-C(22)	121.0(2)
C(30)-N(2)-C(21)	116.8(2)
C(22)-N(2)-C(21)	122.1(2)
C(29)-N(3)-C(28)	117.5(3)
C(30)-N(4)-C(31)	118.2(3)
C(32)-N(5)-C(31)	126.7(2)
C(19)-O(1)-C(20)	114.7(2)
C(1)-S(1)-C(4)	92.65(15)
C(12)-S(2)-C(9)	94.0(2)

Symmetry transformations used to generate equivalent atoms:

Table 9-8. Anisotropic displacement parameters (A^2 x 10^3) for **109**. The anisotropic displacement factor exponent takes the form: $-2\,pi^2\,[\,h^2\,a^{*2}\,U11 + ... + 2\,h\,k\,a^*\,b^*\,U12\,]$.

	U11	U22	U33	U23	U13	U12
C(1)	25(2)	35(2)	33(2)	8(1)	-8(1)	-15(2)
C(2)	27(2)	46(2)	41(2)	1(2)	-8(2)	-16(2)
C(3)	24(2)	36(2)	34(2)	3(2)	-8(1)	-5(2)
C(4)	22(2)	29(2)	19(1)	0(1)	-5(1)	-2(1)
C(5)	23(2)	22(2)	21(2)	-1(1)	-5(1)	-1(1)
C(6)	27(2)	23(2)	28(2)	-5(1)	-3(1)	1(1)
C(7)	39(2)	17(2)	30(2)	-1(1)	-9(1)	-1(1)
C(8)	36(2)	20(2)	23(2)	2(1)	-11(1)	-9(1)
C(9)	37(2)	20(2)	31(2)	0(1)	-12(1)	-11(1)
C(10)	94(11)	90(13)	102(11)	10(9)	-67(8)	-11(8)
C(11)	68(3)	49(3)	53(2)	10(2)	-13(2)	-36(2)
C(12)	41(2)	54(3)	55(2)	0(2)	-6(2)	-26(2)
C(13)	19(1)	18(2)	24(2)	1(1)	-4(1)	-5(1)
C(14)	26(2)	28(2)	24(2)	0(1)	-7(1)	-6(1)
C(15)	31(2)	31(2)	26(2)	-9(1)	-3(1)	-4(1)
C(16)	26(2)	23(2)	33(2)	-7(1)	-2(1)	-2(1)
C(17)	17(1)	19(2)	32(2)	0(1)	-6(1)	-5(1)
C(18)	21(2)	21(2)	26(2)	-1(1)	-6(1)	-8(1)
C(19)	20(2)	21(2)	33(2)	0(1)	-7(1)	-5(1)
C(20)	22(2)	21(2)	28(2)	8(1)	-12(1)	-6(1)
C(21)	18(1)	23(2)	26(2)	8(1)	-9(1)	-9(1)
C(22)	18(1)	19(2)	20(1)	0(1)	-6(1)	-3(1)
C(23)	22(2)	24(2)	28(2)	0(1)	-8(1)	-8(1)
C(24)	21(2)	24(2)	34(2)	0(1)	-13(1)	-2(1)
C(25)	28(2)	19(2)	31(2)	1(1)	-11(1)	-5(1)
C(26)	32(2)	24(2)	49(2)	2(2)	-20(2)	-9(2)
C(27)	26(2)	23(2)	29(2)	0(1)	-8(1)	-8(1)
C(28)	20(2)	22(2)	25(2)	-2(1)	-6(1)	-6(1)
C(29)	20(2)	26(2)	22(2)	-1(1)	-7(1)	-7(1)
C(30)	17(1)	26(2)	20(1)	3(1)	-8(1)	-6(1)
C(31)	19(2)	31(2)	30(2)	8(1)	-10(1)	-8(1)

C(32)	18(2)	31(2)	26(2)	1(1)	-7(1)	-7(1)
N(1)	23(1)	18(1)	22(1)	0(1)	-6(1)	-2(1)
N(2)	16(1)	22(1)	23(1)	3(1)	-7(1)	-6(1)
N(3)	20(1)	24(1)	26(1)	0(1)	-7(1)	-7(1)
N(4)	18(1)	26(1)	31(1)	10(1)	-12(1)	-7(1)
N(5)	14(1)	30(2)	37(2)	6(1)	-12(1)	-7(1)
O(1)	21(1)	16(1)	27(1)	5(1)	-10(1)	-3(1)
O(2)	40(1)	25(1)	49(2)	-11(1)	-23(1)	11(1)
O(3)	23(1)	30(1)	54(2)	17(1)	-20(1)	-10(1)
O(4)	24(1)	33(1)	45(1)	5(1)	-14(1)	-14(1)
F(1)	43(1)	33(1)	103(2)	24(1)	-47(1)	-12(1)
F(2)	76(2)	32(1)	38(1)	10(1)	-19(1)	-16(1)
F(3)	40(1)	20(1)	57(1)	-3(1)	-16(1)	-6(1)
S(1)	26(1)	27(1)	45(1)	6(1)	-9(1)	-8(1)
S(2)	31(1)	44(1)	62(1)	10(1)	-12(1)	-20(1)
S(2')	37(2)	45(2)	59(2)	24(2)	-16(2)	-18(1)
O(5)	95(2)	65(2)	50(2)	5(2)	-25(2)	-47(2)

References:

1.   J. C. Cuevas and E. Scheer, *Molecular Electronics : an Introduction to Theory and Experiment*, New Jersey: World Scientific, 2010.

2.   A. Aviram and M. A. Ratner, *Chem. Phys. Lett.*, 1974, **29**, 277-283.

3.   F. L. Carter, in *Progress in concepts of conformational switching and molecular electronic devices*, ed. N. R. Lab, Washington DC. 24, 1982.

4.   N. S. Hush, *Ann. N.Y. Acad. Sci.*, 2003, **1006**, 1-20.

5.   J. E. McGinness, *Science*, 1972, **177**, 896-897.

6.   A. J. Heeger, *Reviews of Modern Physics*, 2001, **73**, 681-700.

7.   J. R. Heath and M. A. Ratner, *Physics Today*, 2003, **56**, 43-49.

8.   B. G. Levi, *Physics Today*, 2000, **53**, 19-22.

9.   H. Shirakawa, E. J. Louis, A. G. MacDiarmid, C. K. Chiang and A. J. Heeger, *J. Chem. Soc., Chem. Commun.*, 1977, **0**, 578-580.

10.   M. G. Kanatzidis, *Chemical & Engineering News Archive*, 1990, **68**, 36-50.

11.   X. Li, Y. Jiao and S. Li, *Eur. Polym. J.*, 1991, **27**, 1345-1351.

12.   Y.-J. Cheng, S.-H. Yang and C.-S. Hsu, *Chem. Rev.*, 2009, **109**, 5868-5923.

13.   P. Reiss, E. Couderc, J. De Girolamo and A. Pron, *Nanoscale*, 2011, **3**, 446-489.

14.   M. A. Green, *Solar cells : operating principles, technology and system applications / Martin A. Green*, University of New South Wales, Kensington, N.S.W. :, 1992.

15.   S. S. Hegedus and A. Luque, in *Handbook of Photovoltaic Science and Engineering*, John Wiley & Sons, Ltd, 2005, pp. 1-43.

16.   A. Becquerel, *Comptes Rendus de L´Academie des Sciences*, 1839, **9**, 145-149.

17.   W. Smith, *Nature*, 1873, **7**, 303-303.

18.   W. G. Adams and R. E. Day, *Proceedings of the Royal Society of London*, 1876, **25**, 113-117.

19.   A. Pochettino, *Acad. Lincei Rend.*, 1906, **15**, 355.

20.   M. Volmer, *Annalen der Physik*, 1913, **40**, 775-796.

21.   H. Spanggaard and F. C. Krebs, *Sol. Energy Mater. Sol. Cells*, 2004, **83**, 125-146.

22.   D. K. Emily, H. A. Jackson, P. James, P. Albert and A. A. Harry, *Light: Science & Applications*, 2013, **2**.

23.   A. K. Ghosh, D. L. Morel, T. Feng, R. F. Shaw and J. C. A. Rowe, *J. Appl. Phys.*, 1974, **45**, 230-236.

24.   M. A. Green, K. Emery, Y. Hishikawa and W. Warta, *Prog. Photovolt: Res. Appl.*, 2011, **19**, 84-92.

25. M. A. Green, K. Emery, Y. Hishikawa, W. Warta and E. D. Dunlop, *Prog. Photovolt: Res. Appl.*, 2011, **19**, 565-572.

26. K. Zweibel, P. Hersch and S. E. R. Institute, *Basic photovoltaic principles and methods*, Van Nostrand Reinhold, 1984.

27. D. Fuchs and H. Sigmund, *Solid-State Electronics*, 1986, **29**, 791-795.

28. P. N. Rivers, *Leading edge research in solar energy*, Nova Science Publishers, 2007.

29. C. J. Brabec, *Organic Photovoltaics: Concepts and Realization*, Springer, 2003.

30. B. R. Weinberger, M. Akhtar and S. C. Gau, *Synth. Met.*, 1982, **4**, 187-197.

31. S. Glenis, G. Tourillon and F. Garnier, *Thin Solid Films*, 1986, **139**, 221-231.

32. N. S. Sariciftci, D. Braun, C. Zhang, V. I. Srdanov, A. J. Heeger, G. Stucky and F. Wudl, *Appl. Phys. Lett.*, 1993, **62**, 585-587.

33. J. J. M. Halls, K. Pichler, R. H. Friend, S. C. Moratti and A. B. Holmes, *Appl. Phys. Lett.*, 1996, **68**, 3120-3122.

34. G. Yu, J. Gao, J. C. Hummelen, F. Wudl and A. J. Heeger, *Science*, 1995, **270**, 1789-1791.

35. W. Ma, C. Yang, X. Gong, K. Lee and A. J. Heeger, *Adv. Funct. Mater.*, 2005, **15**, 1617-1622.

36. Y. Liang, Z. Xu, J. Xia, S.-T. Tsai, Y. Wu, G. Li, C. Ray and L. Yu, *Adv. Mater.*, 2010, **22**, E135-E138.

37. A. C. Arango, L. R. Johnson, V. N. Bliznyuk, Z. Schlesinger, S. A. Carter and H. H. Hörhold, *Adv. Mater.*, 2000, **12**, 1689-1692.

38. I. F. Perepichka and D. F. Perepichka, *Handbook of Thiophene-Based Materials: Applications in Organic Electronics and Photonics, 2 Volume Set*, Wiley, 2009.

39. W.-H. Baek, H. Yang, T.-S. Yoon, C. J. Kang, H. H. Lee and Y.-S. Kim, *Sol. Energ. Mat. Sol.* , 2009, **93**, 1263-1267.

40. B. J. Worfolk, D. A. Rider, A. L. Elias, M. Thomas, K. D. Harris and J. M. Buriak, *Adv. Funct. Mater.*, 2011, **21**, 1816-1826.

41. J. O. Jeppesen, M. B. Nielsen and J. Becher, *Chem. Rev.*, 2004, **104**, 5115-5132.

42. S. Wenger, P.-A. Bouit, Q. Chen, J. Teuscher, D. D. Censo, R. Humphry-Baker, J.-E. Moser, J. L. Delgado, N. Martín, S. M. Zakeeruddin and M. Grätzel, *J. Am. Chem. Soc.*, 2010, **132**, 5164-5169.

43. M. Bendikov, F. Wudl and D. F. Perepichka, *Chem. Rev.*, 2004, **104**, 4891-4946.

44. P. Frere and P. J. Skabara, *Chem. Soc. Rev.*, 2005, **34**, 69-98.

45. L. Huchet, S. Akoudad and J. Roncali, *Adv. Mater.*, 1998, **10**, 541-545.

46. F. Langa, J. F. Nierengarten and R. S. o. Chemistry, *Fullerenes: Principles and Applications*, Rsc Publishing, 2007.

47. S. Yoo, W. J. Potscavage, B. Domercq, J. Kim, J. Holt and B. Kippelen, *Appl. Phys. Lett.*, 2006, **89**, 233516-233513.

48. D. H. K. Murthy, M. Gao, M. J. W. Vermeulen, L. D. A. Siebbeles and T. J. Savenije, *J. Phys. Chem. C*, 2012, **116**, 9214-9220.

49. J. Y. Kim, K. Lee, N. E. Coates, D. Moses, T.-Q. Nguyen, M. Dante and A. J. Heeger, *Science*, 2007, **317**, 222-225.

50. F. Yang, R. R. Lunt and S. R. Forrest, *Appl. Phys. Lett.*, 2008, **92**, 053310-053313.

51. C.-F. Lin, M. Zhang, S.-W. Liu, T.-L. Chiu and J.-H. Lee, *Int. J. Mol. Sci.*, 2011, **12**, 476-505.

52. Z.-X. Xu, V. A. L. Roy, K.-H. Low and C.-M. Che, *Chem. Commun.*, 2011, **47**, 9654-9656.

53. T. L. Benanti, P. Saejueng and D. Venkataraman, *Chem. Commun.*, 2007, 692-694.

54. D. Venkataraman, S. Yurt, B. H. Venkatraman and N. Gavvalapalli, *J. Phys. Chem. Lett.*, 2010, **1**, 947-958.

55. L. Schmidt-Mende, A. Fechtenkotter, K. Mullen, E. Moons, R. H. Friend and J. D. MacKenzie, *Science*, 2001, **293**, 1119-1122.

56. M. R. Molla, A. Das and S. Ghosh, *Chem. Eur. J.*, 2010, **16**, 10084-10093.

57. P. Jonkheijm, N. Stutzmann, Z. Chen, D. M. de Leeuw, E. W. Meijer, A. P. H. J. Schenning and F. Wuerthner, *J. Am. Chem. Soc.*, 2006, **128**, 9535-9540.

58. G. Koshkakaryan, L. M. Klivansky, D. Cao, M. Snauko, S. J. Teat, J. O. Struppe and Y. Liu, *J. Am. Chem. Soc.*, 2009, **131**, 2078-2079.

59. V. J. Bradford and B. L. Iverson, *J. Am. Chem. Soc.*, 2008, **130**, 1517-1524.

60. B. C. Thompson and J. M. J. Frechet, *Angew. Chem. Int. Ed.*, 2008, **47**, 58-77.

61. S. V. Bhosale, C. H. Jani and S. J. Langford, *Chem. Soc. Rev.*, 2008, **37**, 331-342.

62. H. E. Katz, A. J. Lovinger, J. Johnson, C. Kloc, T. Siegrist, W. Li, Y. Y. Lin and A. Dodabalapur, *Nature*, 2000, **404**, 478-481.

63. P. Mukhopadhyay, Y. Iwashita, M. Shirakawa, S. Kawano, N. Fujita and S. Shinkai, *Angew. Chem. Int. Ed.*, 2006, **45**, 1592-1595.

64. W. W. Stewart, *Nature*, 1981, **292**, 17-21.

65. F. Wurthner, S. Ahmed, C. Thalacker and T. Debaerdemaeker, *Chem. Eur. J.*, 2002, **8**, 4742-4750.

66. H. Vollmann, H. Becker, M. Corell and H. Streeck, *Liebigs Ann.*, 1937, **531**, 1-159.

67. K. D. Johnstone, N. Bampos, J. K. M. Sanders and M. J. Gunter, *New J. Chem.*, 2006, **30**, 861-867.

68. H. Shiratori, T. Ohno, K. Nozaki, I. Yamazaki, Y. Nishimura and A. Osuka, *J. Org. Chem.*, 2000, **65**, 8747-8757.

69. S. Alp, Ş. Erten, C. Karapire, B. Köz, A. O. Doroshenko and S. İçli, *J. Photochem. Photobiol.*, 2000, **135**, 103-110.

70. M. Licchelli, A. Orbelli Biroli and A. Poggi, *Org. Lett.*, 2006, **8**, 915-918.

71. L. L. Miller, R. G. Duan, Y. Hong and I. Tabakovic, *Chem. Mater.*, 1995, **7**, 1552-1557.

72. G. Andric, J. F. Boas, A. M. Bond, G. D. Fallon, K. P. Ghiggino, C. F. Hogan, J. A. Hutchison, M. A. Lee, S. J. Langford, J. R. Pilbrow, G. J. Troup and C. P. Woodward, *Aust. J. Chem.*, 2004, **57**, 1011-1019.

73. M. Bauscher and W. Maentele, *J. Phys. Chem.*, 1992, **96**, 11101-11108.

74. Ş. Erten, Y. Posokhov, S. Alp and S. İçli, *Dyes Pigments*, 2005, **64**, 171-178.

75. C. J. Zhong, W. S. V. Kwan and L. L. Miller, *Chem. Mater.*, 1992, **4**, 1423-1428.

76. P. Pengo, G. D. Pantoş, S. Otto and J. K. M. Sanders, *J. Org. Chem.*, 2006, **71**, 7063-7066.

77. W. S. Horne, N. Ashkenasy and M. R. Ghadiri, *Chem. Eur. J.*, 2005, **11**, 1137-1144.

78. B. A. Jones, A. Facchetti, T. J. Marks and M. R. Wasielewski, *Chem. Mater.*, 2007, **19**, 2703-2705.

79. H. E. Katz, J. Johnson, A. J. Lovinger and W. Li, *J. Am. Chem. Soc.*, 2000, **122**, 7787-7792.

80. T. C. Barros, S. Brochsztain, V. G. Toscano, P. B. Filho and M. J. Politi, *J. Photochem. Photobiol.*, 1997, **111**, 97-104.

81. M. Borgström, N. Shaikh, O. Johansson, M. F. Anderlund, S. Styring, B. Åkermark, A. Magnuson and L. Hammarström, *J. Am. Chem. Soc.*, 2005, **127**, 17504-17515.

82. O. Johansson, H. Wolpher, M. Borgstrom, L. Hammarstrom, J. Bergquist, L. Sun and B. Akermark, *Chem. Commun.*, 2004, 194-195.

83. Y. Ofir, A. Zelichenok and S. Yitzchaik, *J. Mater. Chem.*, 2006, **16**, 2142-2149.

84. G. P. Wiederrecht and M. R. Wasielewski, *J. Am. Chem. Soc.*, 1998, **120**, 3231-3236.

85. M. R. Wasielewski, *J. Org. Chem*, 2006, **71**, 5051-5066.

86. P. Ganesan, X. Yang, J. Loos, T. J. Savenije, R. D. Abellon, H. Zuilhof and E. J. R. Sudhölter, *J. Am. Chem. Soc.*, 2005, **127**, 14530-14531.

87. S. Brochsztain, M. A. Rodrigues, G. J. F. Demets and M. J. Politi, *J. Mater. Chem.*, 2002, **12**, 1250-1255.

88. S. Takenaka, Y. Uto, H. Saita, M. Yokoyama, H. Kondo and W. David Wilson, *Chem. Commun.*, 1998, 1111-1112.

89. S. Sato, S. Fujii, K. Yamashita, M. Takagi, H. Kondo and S. Takenaka, *J. Organomet. Chem.*, 2001, **637–639**, 476-483.

90. M. Tomasulo, D. M. Naistat, A. J. P. White, D. J. Williams and F. M. Raymo, *Tetrahedron Lett.*, 2005, **46**, 5695-5698.

91. J. Jazwinski, A. J. Blacker, J.-M. Lehn, M. Cesario, J. Guilhem and C. Pascard, *Tetrahedron Lett.*, 1987, **28**, 6060.

92. G. D. Fallon, M. A. P. Lee, S. J. Langford and P. J. Nichols, *Org. Lett.*, 2004, **6**, 655-658.

93. A. J. Taylor, E. S. Davies, J. A. Weinstein, I. V. Sazanovich, O. V. Bouganov, S. A. Tikhomirov, M. Towrie, J. McMaster and C. D. Garner, *Inorg. Chem.*, 2012.

94. A. M. Scott, T. Miura, A. B. Ricks, Z. E. X. Dance, E. M. Giacobbe, M. T. Colvin and M. R. Wasielewski, *J. Am. Chem. Soc.*, 2009, **131**, 17655-17666.

95. A. B. Ricks, K. E. Brown, M. Wenninger, S. D. Karlen, Y. A. Berlin, D. T. Co and M. R. Wasielewski, *J. Am. Chem. Soc.*, 2012, **134**, 4581-4588.

96. I. V. Sazanovich, M. A. H. Alamiry, J. Best, R. D. Bennett, O. V. Bouganov, E. S. Davies, V. P. Grivin, A. J. H. M. Meijer, V. F. Plyusnin, K. L. Ronayne, A. H. Shelton, S. A. Tikhomirov, M. Towrie and J. A. Weinstein, *Inorg. Chem.*, 2008, **47**, 10432-10445.

97. D. S. Acker and W. R. Hertler, *J. Am. Chem. Soc.*, 1962, **84**, 3370-3374.

98. R. N. Compton and C. D. Cooper, *J. Chem. Phys*, 1977, **66**, 4325-4329.

99. S. Chowdhury and P. Kebarle, *J. Am. Chem. Soc.*, 1986, **108**, 5453-5459.

100. J. C. May, J. H. Lim, I. Biaggio, N. N. P. Moonen, T. Michinobu and F. Diederich, *Opt. Lett.*, 2005, **30**, 3057-3059.

101. M. I. Bruce, J. R. Rodgers, M. R. Snow and A. G. Swincer, *J. Am. Chem. Soc.*, 1981, 271-272.

102. R. García, M. Á. Herranz, M. R. Torres, P.-A. Bouit, J. L. Delgado, J. Calbo, P. M. Viruela, E. Ortí and N. Martín, *J. Org. Chem.*, 2012.

103. D. Gust, T. A. Moore and A. L. Moore, *Acc. Chem. Res.*, 2000, **34**, 40-48.

104. P. J. Bracher and D. I. Schuster, *KAP (Dordrecht, The Netherlands)* 2002, **6**, 163-212.

105. F. Chaignon, M. Falkenstrom, S. Karlsson, E. Blart, F. Odobel and L. Hammarstrom, *Chem. Commun.*, 2007, 64-66.

106. K. Sonogashira, *J. Organomet. Chem.*, 2002, **653**, 46-49.

107. P. Karrer, K. Schöpp and F. Benz, *Helv. Chim. Acta.*, 1935, **18**, 426-429.

108. F. Müller, *Free Radic. Biol.* , 1987, **3**, 215-230.

109. H. Theorell, *Biochem Z.*, 1935, **275**, 344-346.

110. P. Galland, in *Comprehensive Series in Photosciences*, eds. P. H. Donat and A. M. Breure, Elsevier, 2001, vol. Volume 1, pp. 621-657.

111. H. A. Krebs, *Biochem. J.*, 1935, **29**, 1620-1644.

112. O. Warburg and W. Christian, *Biochem Z.*, 1933, **266**, 377-411.

113. D. Clerin and T. C. Bruice, *J. Am. Chem. Soc.*, 1974, **96**, 5571-5573.

114. P. Macheroux, 1999, vol. 131, pp. 1-7.

115. S. D. M. Islam, T. Susdorf, A. Penzkofer and P. Hegemann, *J. Chem. Phys*, 2003, **295**, 137-149.

116. W. Holzer, J. Shirdel, P. Zirak, A. Penzkofer, P. Hegemann, R. Deutzmann and E. Hochmuth, *J. Chem. Phys*, 2005, **308**, 69-78.

117. P. F. Heelis, *Chem. Soc. Rev.*, 1982, **11**, 15-39.

118. V. Massey and G. Palmer, *Biochemistry*, 1966, **5**, 3181-3189.

119. V. Massey, *Biochem. Soc. Trans.*, 2000, **28**, 283-296.

120. R. Miura, *Chem. Rec.*, 2001, **1**, 183-194.

121. A. Niemz and V. M. Rotello, *Acc. Chem. Res.*, 1998, **32**, 44-52.

122. A. Niemz, J. Imbriglio and V. M. Rotello, *J. Am. Chem. Soc.*, 1997, **119**, 887-892.

123. D. Edmondson and S. Ghisla, 1999, vol. 131, pp. 157-179.

124. M. M. Oliva, T. M. Pappenfus, J. H. Melby, K. M. Schwaderer, J. C. Johnson, K. A. McGee, D. A. da Silva Filho, J.-L. Bredas, J. Casado and J. T. López Navarrete, *Chem. Eur. J.*, 2010, **16**, 6866-6876.

125. L. I. Belen'kii, G. P. Gromova and V. I. Smirnov, *Chem. Heterocycl. Compd.*, 2008, **44**, 1092-1100.

126. W.-T. Guo, Z.-M. Miao and Y.-L. Wang, *Acta Crystallogr. Sect. E*, 2012, **68**, o689-o690.

127. G. G. McLeod, M. G. B. Mahboubian-Jones, R. A. Pethrick, S. D. Watson, N. D. Truong, J. C. Galin and J. François, *Polymer*, 1986, **27**, 455-458.

128. V. Amarnath, D. C. Anthony, K. Amarnath, W. M. Valentine, L. A. Wetterau and D. G. Graham, *J. Org. Chem.*, 1991, **56**, 6924-6931.

129. R. Kiebooms, R. Menon and K. Lee, in *Handbook of Advanced Electronic and Photonic Materials and Devices*, eds. N. Hari Singh, M.Sc and M. S. P. D. Ph.D.A2 - Hari Singh Nalwa, Academic Press, Burlington, 2001, pp. 1-102.

130. C. Alemán, V. M. Domingo, L. Fajarí, L. Juliá and A. Karpfen, *J. Org. Chem.*, 1998, **63**, 1041-1048.

131. P. E. Just, K. I. Chane-Ching and P. C. Lacaze, *Tetrahedron*, 2002, **58**, 3467-3472.

132. N. A. Lengkeek, J. M. Harrowfield and G. A. Koutsantonis, *Synt. Met.*, 2010, **160**, 72-75.

133. Z. Kaleta, B. T. Makowski, T. Soós and R. Dembinski, *Org. Lett.*, 2006, **8**, 1625-1628.

134. R. E. Niziurski-Mann, C. Scordilis-Kelley, T. L. Liu, M. P. Cava and R. T. Carlin, *J. Am. Chem. Soc.*, 1993, **115**, 887-891.

135. J. P. Ferraris and T. R. Hanlon, *Polymer*, 1989, **30**, 1319-1327.

136. J. P. Ferraris and G. D. Skiles, *Polymer*, 1987, **28**, 179-182.

137. S. Tuncagil, D. Odaci, E. Yildiz, S. Timur and L. Toppare, *Sensor Actust B-Chem*, 2009, **137**, 42-47.

138. S. Tuncagil, S. Varis and L. Toppare, *J. Mol. Catal. B: Enzym.*, 2010, **64**, 195-199.

139. A. Cihaner and F. Algı, *J. Electroanal. Chem.*, 2008, **614**, 101-106.

140. G. R. Kiani, N. Arsalani, M. G. Hosseini and A. A. Entezami, *J. Appl. Polym. Sci.*, 2008, **108**, 2700-2706.

141. G. R. Kiani, N. Arsalani, A. M. Goganian, M. G. Hosseini and A. A. Entezami, *Electropolymerization*, 2011, **1**, 119-130.

142. J. Carrasco, A. Figueras, T. F. Otero and E. Brillas, *Synt. Met.*, 1993, **61**, 253-258.

143. Y. H. Kim, J. Hwang, J. I. Son and Y.-B. Shim, *Synt. Met.*, 2010, **160**, 413-418.

144. P. Camurlu and C. Gültekin, *Sol. Energ. Mat. Sol.* , 2012, **107**, 142-147.

145. F. Algı and A. Cihaner, *Tetrahedron Lett.*, 2008, **49**, 3530-3533.

146. Y. Liu, M. A. Summers, C. Edder, J. M. J. Fréchet and M. D. McGehee, *Adv. Mater.*, 2005, **17**, 2960-2964.

147. G. Cooke, J. F. Garety, S. Mabruk, G. Rabani, V. M. Rotello, G. Surpateanu and P. Woisel, *Tetrahedron Lett.*, 2006, **47**, 783-786.

148. G. Cooke, J. Garety, S. Mabruk, V. Rotello, G. Surpateanu and P. Woisel, *Chem. Commun.*, 2004, **0**, 2722-2723.

149. G. Cooke, J. F. Garety, B. Jordan, N. Kryvokhyzha, A. Parkin, G. Rabani and V. M. Rotello, *Org. Lett.*, 2006, **8**, 2297-2300.

150. A. Merz and F. Ellinger, *Synthesis-Stuttgart*, 1991, 462-464.

151. G. A. Vavilov, Z. V. Pushkareva and V. S. Mokrushin, *Khim Geterotsikl Soedin*, 1970, **6**, 111-113.

152. Vivek Mishra and R. Kumar, *J. Sci. Res.*, 2012, **56**, 141-176.

153. D. Braun, *Int. J. Polymer.Sci.*, 2009, **2009**.

154. G. Moad, J. Chiefari, R. T. A. Mayadunne, C. L. Moad, A. Postma, E. Rizzardo and S. H. Thang, *Macromol. Symp.*, 2002, **182**, 65-80.

155. G. G. Odian, *Principles of polymerization*, Wiley, 1984.

156. T. Otsu and M. Yoshida, *Macromol. Chem.* , 1982, **3**, 127-132.

157. K. Matyjaszewski, in *Controlled/Living Radical Polymerization*, American Chemical Society, 2000, vol. 768, pp. 2-26.

158. K. Matyjaszewski and J. Spanswick, *Mater. Today*, 2005, **8**, 26-33.

159. M. S. Kharasch, B. M. Kuderna and W. Urry, *J. Org. Chem.*, 1948, **13**, 895-902.

160. D. P. Curran, *Synthesis*, 1988, **7**, 489-513.

161. H. Fischer, *Chem. Rev.*, 2001, **101**, 3581-3610.

162. M. Szwarc, *Nature*, 1956, **178**, 1168 - 1169.

163. K. Matyjaszewski and C.-H. Lin, *Macromol. Symp.*, 1991, **47**, 221-237.

164. G. Litvinenko and A. H. E. Müller, *Macromolecules*, 1997, **30**, 1253-1266.

165. T. Otsu, *J. Polym. Sci. A Polym.* , 2000, **38**, 2121-2136.

166. B. Boutevin, *J. Polym. Sci. A Polym.* , 2000, **38**, 3235-3243.

167. C. H. Bamford, N. S. Allen and J. C. Bevington, *In Comprehensive Polymer Science,(eds.), Elsevier*, 1992, **3**.

168. M. Kamigaito, T. Ando and M. Sawamoto, *Chem. Rec.*, 2004, **4**, 159-175.

169. S. Edmondson, V. L. Osborne and W. T. S. Huck, *Chem. Soc. Rev.*, 2004, **33**, 14-22.

170. *Advances in Controlled/Living Radical Polymerization*, American Chemical Society, 2003.

171. J.-S. Wang and K. Matyjaszewski, *J. Am. Chem. Soc.*, 1995, **117**, 5614-5615.

172. M. Kato, M. Kamigaito, M. Sawamoto and T. Higashimura, *Macromolecules*, 1995, **28**, 1721-1723.

173. S. S. Sheiko, B. S. Sumerlin and K. Matyjaszewski, *Prog. Polym. Sci.*, 2008, **33**, 759-785.

174. K. Matyjaszewski, M. Wei, J. Xia and S. G. Gaynor, *Macromol. Chem. Phys.*, 1998, **199**, 2289-2292.

175. F. di Lena and K. Matyjaszewski, *Prog. Polym. Sci.*, 2010, **35**, 959-1021.

176. J.-S. Wang and K. Matyjaszewski, *Macromolecules*, 1995, **28**, 7572-7573.

177. K. A. Davis, H.-j. Paik and K. Matyjaszewski, *Macromolecules*, 1999, **32**, 1767-1776.

178. K. Matyjaszewski and J. Xia, *Chem. Rev.*, 2001, **101**, 2921-2990.

179. J. Xia, X. Zhang, and K. Matyjaszewski, *Transition Metal Catalysis in Macromolecular Design*, Amer. Chem. Soc., 2000.

180. Y. Shen, S. Zhu, F. Zeng and R. H. Pelton, *Macromol. Chem. Phys.*, 2000, **201**, 1169-1175.

181. J. Xia, X. Zhang and K. Matyjaszewski, *Macromolecules*, 1999, **32**, 3531-3533.

182. J. Xia, S. G. Gaynor and K. Matyjaszewski, *Macromolecules*, 1998, **31**, 5958-5959.

183. A. Mühlebach, S. G. Gaynor and K. Matyjaszewski, *Macromolecules*, 1998, **31**, 6046-6052.

184. K. Matyjaszewski, *Macromolecules*, 2012, **45**, 4015-4039.

185. V. Percec and B. Barboiu, *Macromolecules*, 1995, **28**, 7970-7972.

186. V. Percec, H. J. Kim and B. Barboiu, *Macromolecules*, 1997, **30**, 8526-8528.

187. T. E. Patten and K. Matyjaszewski, *Acc. Chem. Res.*, 1999, **32**, 895-903.

188. T. E. Patten and K. Matyjaszewski, *Adv. Mater.*, 1998, **10**, 901-915.

189. K. Matyjaszewski, T. E. Patten and J. Xia, *J. Am. Chem. Soc.*, 1997, **119**, 674-680.

190. V. Percec, B. Barboiu, A. Neumann, J. C. Ronda and M. Zhao, *Macromolecules*, 1996, **29**, 3665-3668.

191. X. S. Wang and S. P. Armes, *Macromolecules*, 2000, **33**, 6640-6647.

192. K. Matyjaszewski, S. Coca, S. G. Gaynor, M. Wei and B. E. Woodworth, *Macromolecules*, 1997, **30**, 7348-7350.

193. J. Chiefari, Y. K. Chong, F. Ercole, J. Krstina, J. Jeffery, T. P. T. Le, R. T. A. Mayadunne, G. F. Meijs, C. L. Moad, G. Moad, E. Rizzardo and S. H. Thang, *Macromolecules*, 1998, **31**, 5559-5562.

194. G. Moad, M. Chen, M. Haussler, A. Postma, E. Rizzardo and S. H. Thang, *Poly. Chem.*, 2011, **2**, 492-519.

195. M. Chen, M. Haussler, G. Moad and E. Rizzardo, *Org. Biomol. Chem.*, 2011, **9**, 6111-6119.

196. J. Levillain, S. Masson, A. Hudson and A. Alberti, *J. Am. Chem. Soc.*, 1993, **115**, 8444-8446.

197. J. Zhang, L. Ren, C. G. Hardy and C. Tang, *Macromolecules*, 2012, **45**, 6857-6863.

198. G. R. Whittell and I. Manners, *Adv. Mater.*, 2007, **19**, 3439-3468.

199. Y. Yang, Z. Xie and C. Wu, *Macromolecules*, 2002, **35**, 3426-3432.

200. S. Mehdipour-Ataei and S. Babanzadeh, *Appl. Organomet. Chem.*, 2007, **21**, 360-367.

201. M. A. Gouda, M. A. Berghot, A. Shoeib and A. E.-G. M. Khalil, *Turk. J. Chem.*, 2010, **34**, 651-709.

202. S. K. Varshney, H. Monobe, Y. Shimizu, H. Takezoe and V. Prasad, *Liq. Cryst.*, 2010, **37**, 607-615.

203. A. Schultz, S. Laschat, S. Diele and M. Nimtz, *Eur. J. Org. Chem.*, 2003, 2829-2839.

204. M. Sing, U. Schwingenschlogl, R. Claessen, P. Blaha, J. M. P. Carmelo, L. M. Martelo, P. D. Sacramento, M. Dressel and C. S. Jacobsen, *Phys. Rev. B*, 2003, **68**.

205. S. Yamaguchi, H. Tatemitsu, Y. Sakata and S. Misumi, *Chem. Lett.*, 1983, 1229-1230.

206. B. S. Ong and B. Keoshkerian, *J. Org. Chem.*, 1984, **49**, 5002-5003.

207. A. M. Kini, D. O. Cowan, F. Gerson and R. Möckel, *Mol. Cryst. Liq. Cryst.*, 1985, **120**, 299-303.

208. A. M. Kini, D. O. Cowan, F. Gerson and R. Mockel, *J. Am. Chem. Soc.*, 1985, **107**, 556-562.

209. F. Giacalone, J. L. Segura, N. Martín, M. Catellani, S. Luzzati and N. Lupsac, *Org. Lett.*, 2003, **5**, 1669-1672.

210. K. Isoda, T. Yasuda and T. Kato, *J. Mater. Chem.*, 2008, **18**, 4522-4528.

211. F. Bures, W. B. Schweizer, C. Boudon, J.-P. Gisselbrecht, M. Gross and F. Diederich, *Eur. J. Org. Chem.*, 2008, 994-1004.

212. T. Suzuki, K. Ichioka, H. Higuchi, H. Kawai, K. Fujiwara, M. Ohkita, T. Tsuji and Y. Takahashi, *J. Org. Chem.*, 2005, **70**, 5592-5598.

213. W. Huang and C. D. Han, *Macromolecules*, 2012, **45**, 4425-4428.

214. G. Zerza, M. C. Scharber, C. J. Brabec, N. S. Sariciftci, R. Gomez, J. L. Segura, N. Martin and V. I. Srdanov, *J. Phys. Chem. A*, 2000, **104**, 8315-8322.

215. A. Aumuller and S. Hunig, *Liebigs Ann.*, 1984, 618-621.

216. D. H. Evans and K. Hu, *J. Chem. Soc., Faraday Trans.*, 1996, **92**, 3983-3990.

217. J. Li, Y. Xiong, Q. Wu, S. Wang, X. Gao and H. Li, *Eur. J. Org. Chem.*, 2012, **2012**, 6136-6139.

218. T. Yanagimoto, K. Takimiya, T. Otsubo and F. Ogura, *J. Chem. Soc.Chem.Commun*, 1993, **0**, 519-520.

219. S. L. Vorobeva and T. S. Berzina, *J. Chem. Soc.-Perkin Trans. 2*, 1992, 1133-1136.

220. N. Martín, I. Pérez, L. Sánchez and C. Seoane, *J. Org. Chem.*, 1997, **62**, 870-877.

221. W. Lehnert, *Synthesis-Stuttgart*, 1974, 667-669.

222. A. Aumuller and S. Hunig, *Angew. Chem. Int. Ed.*, 1984, **23**, 447-448.

223. B. Illescas, N. Martin and C. Seoane, *Tetrahedron Lett.*, 1997, **38**, 2015-2018.

224. B. M. Illescas and N. Martin, *J. Org. Chem.*, 2000, **65**, 5986-5995.

225. M. Prato and M. Maggini, *Acc. Chem. Res.*, 1998, **31**, 519-526.

226. J. L. Segura and N. Martin, *Chem. Rev.*, 1999, **99**, 3199-3246.

227. Y. A. Cao, Y. B. Bai, Q. J. Men, C. H. Chen, J. H. Yang, X. D. Chai, W. S. Yang, Z. W. Wu and T. J. Li, *Synt. Met.*, 1997, **85**, 1267-1268.

228. N. Martin, I. Perez, L. Sanchez and C. Seoane, *J. Org. Chem.*, 1997, **62**, 5690-5695.

229. M.-H. David-Cordonnier, M.-P. Hildebrand, B. Baldeyrou, A. Lansiaux, C. Keuser, K. Benzschawel, T. Lemster and U. Pindur, *Eur. J. Med. Chem.*, 2007, **42**, 752-771.

230. H. Ishikawa, K. Amano, A. Kobayashi, M. Satoh and E. Hasegawa, *Synt. Met.*, 1994, **64**, 49-52.

231. N. K. Guimard, N. Gomez and C. E. Schmidt, *Prog. Polym. Sci.*, 2007, **32**, 876-921.

232. X.-G. Li, A. Li and M.-R. Huang, *Chem. A Europ. J.*, 2008, **14**, 10309-10317.

233. X.-G. Li, Q.-F. Lü and M.-R. Huang, *Small*, 2008, **4**, 1201-1209.

234. D. Triantou, S. Soulis, S. Koureli, A. De Sio and E. von Hauff, *J. Appl. Polym. Sci.*, 2013, **127**, 585-592.

235. F. S. Kim, G. Ren and S. A. Jenekhe, *Chem. Mater.*, 2010, **23**, 682-732.

236. H. Shirakawa, E. J. Louis, A. G. MacDiarmid, C. K. Chiang and A. J. Heeger, *J. Chem. Soc.Chem.Commun*, 1977, **0**, 578-580.

237. U. Lange, N. V. Roznyatovskaya and V. M. Mirsky, *Anal. Chim. Acta*, 2008, **614**, 1-26.

238. T. Yamamoto, K. Sanechika and A. Yamamoto, *J. Polym. Sci*, 1980, **18**, 9-12.

239. J. W. P. Lin and L. P. Dudek, *J. Polym. Sci*, 1980, **18**, 2869-2873.

240. G. Koßmehl and G. Chatzitheodorou, *Makromol. Chem.*, 1981, **2**, 551-555.

241. M. Leclerc, F. M. Diaz and G. Wegner, *Makromol. Chem.*, 1989, **190**, 3105-3116.

242. G. Daoust and M. Leclerc, *Macromolecules*, 1991, **24**, 455-459.

243. M. R. Andersson, D. Selse, M. Berggren, H. Jaervinen, T. Hjertberg, O. Inganaes, O. Wennerstroem and J. E. Oesterholm, *Macromolecules*, 1994, **27**, 6503-6506.

244. A. Diaz, *Chemica Scripta*, 1981, **17**, 145-148.

245. J. Roncali, *Chem. Rev.*, 1992, **92**, 711-738.

246. G. Tourillon and F. Garnier, *J Electroanal Chem Interfacial Elechochem*, 1982, **135**, 173-178.

247. A. Yassar, J. Roncali and F. Garnier, *Macromolecules*, 1989, **22**, 804-809.

248. B. AG, *Eur. Patent*, 1988, 339-340.

249. M. M. de Kok, M. Buechel, S. I. E. Vulto, P. van de Weijer, E. A. Meulenkamp, S. H. P. M. de Winter, A. J. G. Mank, H. J. M. Vorstenbosch, C. H. L. Weijtens and V. van Elsbergen, *Phys. Status Solidi A*, 2004, **201**, 1342-1359.

250. L. Groenendaal, G. Zotti, P. H. Aubert, S. M. Waybright and J. R. Reynolds, *Adv. Mater.*, 2003, **15**, 855-879.

251. M. Leclerc, *J. Polym. Sci. A Polym.* , 2001, **39**, 2867-2873.

252. E. Bundgaard and F. C. Krebs, *Sol. Energ. Mat. Sol.* , 2007, **91**, 954-985.

253. S. Kobayashi, T. Takenobu, S. Mori, A. Fujiwara and Y. Iwasa, *Appl. Phys. Lett.*, 2003, **82**, 4581-4583.

254. M. L. Tang, J. H. Oh, A. D. Reichardt and Z. Bao, *J. Am. Chem. Soc.*, 2009, **131**, 3733-3740.

255. H. Vogel and C. S. Marvel, *J. Polym. Sci.*, 1961, **50**, 511-539.

256. E. C. Wagner and W. H. Millett, *Org. Synth.*, 1943, **2**, 65-65.

257. H. D. Burks, *An annotated bibliography of Pyrrone and BBB publications*, National Aeronautics and Space Administration, 1972.

258. R. J. Kline, M. D. McGehee, E. N. Kadnikova, J. Liu and J. M. J. Fréchet, *Adv. Mater.*, 2003, **15**, 1519-1522.

259. C. W. Tang, *Appl. Phys. Lett.*, 1986, **48**, 183-185.

260. R. Ponce Ortiz, H. Herrera, R. Blanco, H. Huang, A. Facchetti, T. J. Marks, Y. Zheng and J. L. Segura, *J. Am. Chem. Soc.*, 2010, **132**, 8440-8452.

261. A. Babel and S. A. Jenekhe, *J. Am. Chem. Soc.*, 2003, **125**, 13656-13657.

262. H. Langhals and H. Jaschke, *Chem. Eur. J.*, 2006, **12**, 2815-2824.

263. D. J. McConnell, B. T. P.;, V. Cuong; and G. J. F., *USP Application,20070134572*, 2007, 1-14.

264. C. Tozlu, S.Ertenela, TH. B. Singh, N.S. Sariciftci, S. Icli and S. Oktik, *Ba.Ph.L*, 2009, **16**, 161010-161014.

265. P. Deng, Y. Yan, S.-D. Wang and Q. Zhang, *Chem. Commun.*, 2012, **48**, 2591-2593.

266. S. R. González, J. Casado, J. T. L. p. Navarrete, R. l. Blanco and J. L. Segura, *J. Phys. Chem. A*, 2008, **112**, 6732-6740.

267. T. F. Otero, J. Arias-Pardilla, H. Herrera, J. L. Segura and C. Seoane, *Phys. Chem. Chem. Phys.*, 2011, **13**, 16513-16515.

268. R. P. Ortiz, H. Herrera, C. Seoane, J. L. Segura, A. Facchetti and T. J. Marks, *Chem. Eur. J.*, 2012, **18**, 532-543.

269. S. R. Greenfield, W. A. Svec, D. Gosztola and M. R. Wasielewski, *J. Am. Chem. Soc.*, 1996, **118**, 6767-6777.

270. F. S. Mancilha, B. A. DaSilveira Neto, A. S. Lopes, P. F. Moreira, Jr., F. H. Quina, R. S. Goncalves and J. Dupont, *Eur. J. Org. Chem.*, 2006, 4924-4933.

271. R. Naef and H. Balli, *Helv. Chim. Acta.*, 1978, **61**, 2958-2973.

272. A. L. Casado and P. Espinet, *Organometallics*, 1998, **17**, 954-959.

273. N. Miyaura and A. Suzuki, *Chem. Rev.*, 1995, **95**, 2457-2483.

274. A. G. Dandridge, S. W. Dunworth, H. A. E. Drescher and A. L. Thomas, *GB, ICI, 322169*, 1928.

275. R. P. Linstead, *J. Chem. Soc.*, 1934, **0**, 1016-1017.

276. R. P. Linstead and A. R. Lowe, *J. Chem. Soc.*, 1934, **0**, 1022-1027.

277. C. E. Dent and R. P. Linstead, *J. Am. Chem. Soc.*, 1934, **0**, 1027-1031.

278. M. J. Cook, *Angew. Chem. Int. Ed.*, 1994, **33**, 236-237.

279. McKeown and N. B., *Phthalocyanine materials : synthesis, structure, and function* Cambridge University, Cambridge, U.K., 1998.

280. C. C. Leznoff and A. B. P. Lever, *Phthalocyanines: properties and applications*, VCH, 1989.

281. B. J. Kennedy, K. S. Murray, P. R. Zwack, H. Homborg and W. Kalz, *Inorg. Chem.*, 1986, **25**, 2539-2545.

282. C. G. Claessens, U. Hahn and T. Torres, *TCR*, 2008, **8**, 75-97.

283. M. A. Dahlen, *Ind. Eng. Chem. Res.*, 1939, **31**, 839-847.

284. M. G. Walter, A. B. Rudine and C. C. Wamser, *JPP*, 2010, **14**, 759-792.

285. D. J. Sandman, *Mol. Cryst. Liq. Cryst. Sci. Technol., Sect. A*, 1999, **333**, 285-286.

286. T. Nyokong and H. Isago, *JPP*, 2004, **08**, 1083-1090.

287. M. Durmuş and T. Nyokong, *Tetrahedron*, 2007, **63**, 1385-1394.

288. H. Kliesch, A. Weitemeyer, S. Müller and D. Wöhrle, *Liebig's Ann. Chem.*, 1995, **1995**, 1269-1273.

289. H. Tomoda, S. Saito, S. Ogawa and S. Shiraishi, *Chem. Lett.*, 1980, **9**, 1277-1280.

290. S. W. Oliver and T. D. Smith, *J. Chem. Soc. Perkin Trans II*, 1987, **0**, 1579-1582.

291. M. D. Maree and T. Nyokong, *J. Chem. Research (S)*, 2001, **2001**, 68-69.

292. M. E. El-Khouly, J. H. Kim, K.-Y. Kay, C. S. Choi, O. Ito and S. Fukuzumi, *Chem. Eur. J.*, 2009, **15**, 5301-5310.

293. M. E. El-Khouly, A. G. Moiseev, A. van der Est and S. Fukuzumi, *Chem. Phys. Chem*, 2012, **13**, 1191-1198.

294. S. Jin, X. Ding, X. Feng, M. Supur, K. Furukawa, S. Takahashi, M. Addicoat, M. E. El-Khouly, T. Nakamura, S. Irle, S. Fukuzumi, A. Nagai and D. Jiang, *Angew. Chem. Int. Ed.*, 2013, **52**, 2017-2021.

295. G. Sforazzini, R. Turdean, N. Sakai and S. Matile, *Chem. Sci.*, 2013, **4**, 1847-1851.

296. J. Chen, N. Chen, J. Huang, J. Wang and M. Huang, *Inorg. Chem. Commun.*, 2006, **9**, 313-315.

297. J. Alzeer, P. J. C. Roth and N. W. Luedtke, *Chem. Commun.*, 2009, **0**, 1970-1971.

298. G. Cooke, J. Garety, S. Mabruk, V. Rotello, G. Surpateanu and P. Woisel, *Chem. Commun.*, 2004, 2722-2723.

299. W. S. Li, N. J. Zhang and L. M. Sayre, *Tetrahedron*, 2001, **57**, 4507-4522.

300. P. M. Alvey, J. J. Reczek, V. Lynch and B. L. Iverson, *J. Org. Chem.*, 2010, **75**, 7682-7690.